frontiers | Research Topics

# Novel regulatory mechanisms behind thermogenesis of brown and beige adipocytes

**Edited by**
Rubén Cereijo and Endre Károly Kristóf

**Coordinated by**
Abhirup Shaw

**Published in**
Frontiers in Endocrinology
Frontiers in Cell and Developmental Biology

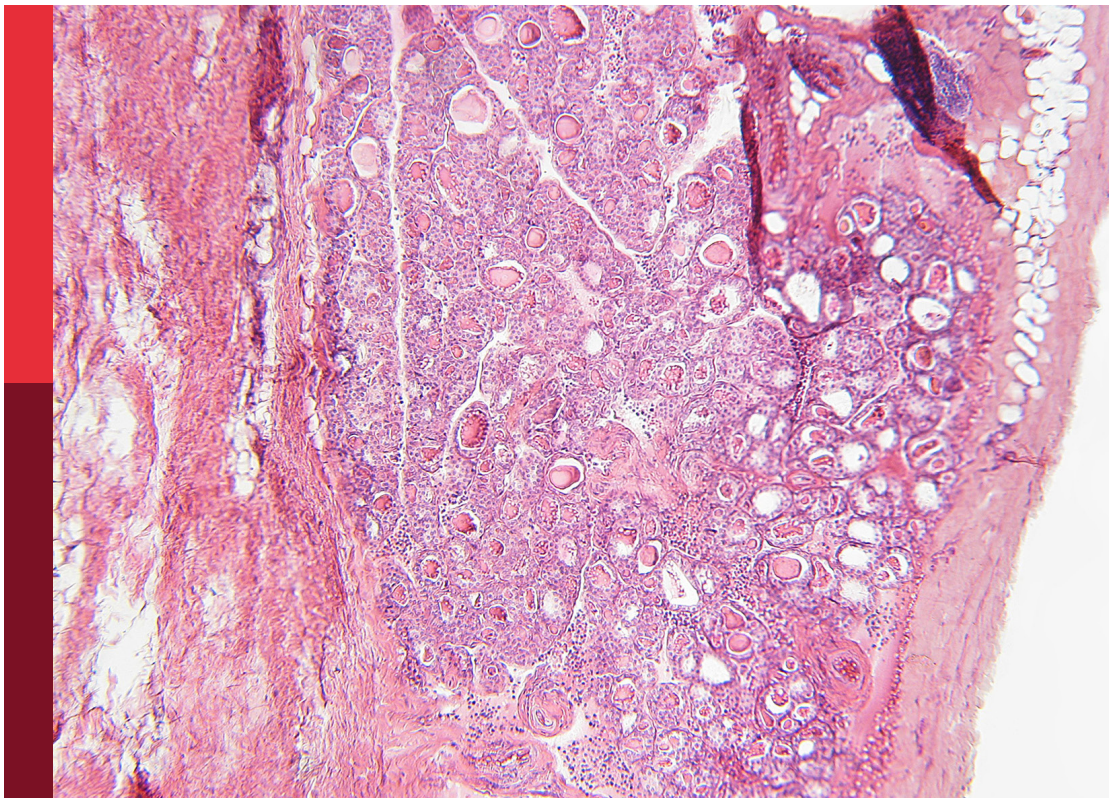

FRONTIERS EBOOK COPYRIGHT STATEMENT

The copyright in the text of individual articles in this ebook is the property of their respective authors or their respective institutions or funders. The copyright in graphics and images within each article may be subject to copyright of other parties. In both cases this is subject to a license granted to Frontiers.

The compilation of articles constituting this ebook is the property of Frontiers.

Each article within this ebook, and the ebook itself, are published under the most recent version of the Creative Commons CC-BY licence. The version current at the date of publication of this ebook is CC-BY 4.0. If the CC-BY licence is updated, the licence granted by Frontiers is automatically updated to the new version.

When exercising any right under the CC-BY licence, Frontiers must be attributed as the original publisher of the article or ebook, as applicable.

Authors have the responsibility of ensuring that any graphics or other materials which are the property of others may be included in the CC-BY licence, but this should be checked before relying on the CC-BY licence to reproduce those materials. Any copyright notices relating to those materials must be complied with.

Copyright and source acknowledgement notices may not be removed and must be displayed in any copy, derivative work or partial copy which includes the elements in question.

All copyright, and all rights therein, are protected by national and international copyright laws. The above represents a summary only. For further information please read Frontiers' Conditions for Website Use and Copyright Statement, and the applicable CC-BY licence.

ISSN 1664-8714
ISBN 978-2-8325-3400-7
DOI 10.3389/978-2-8325-3400-7

## About Frontiers

Frontiers is more than just an open access publisher of scholarly articles: it is a pioneering approach to the world of academia, radically improving the way scholarly research is managed. The grand vision of Frontiers is a world where all people have an equal opportunity to seek, share and generate knowledge. Frontiers provides immediate and permanent online open access to all its publications, but this alone is not enough to realize our grand goals.

## Frontiers journal series

The Frontiers journal series is a multi-tier and interdisciplinary set of open-access, online journals, promising a paradigm shift from the current review, selection and dissemination processes in academic publishing. All Frontiers journals are driven by researchers for researchers; therefore, they constitute a service to the scholarly community. At the same time, the *Frontiers journal series* operates on a revolutionary invention, the tiered publishing system, initially addressing specific communities of scholars, and gradually climbing up to broader public understanding, thus serving the interests of the lay society, too.

## Dedication to quality

Each Frontiers article is a landmark of the highest quality, thanks to genuinely collaborative interactions between authors and review editors, who include some of the world's best academicians. Research must be certified by peers before entering a stream of knowledge that may eventually reach the public - and shape society; therefore, Frontiers only applies the most rigorous and unbiased reviews. Frontiers revolutionizes research publishing by freely delivering the most outstanding research, evaluated with no bias from both the academic and social point of view. By applying the most advanced information technologies, Frontiers is catapulting scholarly publishing into a new generation.

## What are Frontiers Research Topics?

Frontiers Research Topics are very popular trademarks of the *Frontiers journals series*: they are collections of at least ten articles, all centered on a particular subject. With their unique mix of varied contributions from Original Research to Review Articles, Frontiers Research Topics unify the most influential researchers, the latest key findings and historical advances in a hot research area.

Find out more on how to host your own Frontiers Research Topic or contribute to one as an author by contacting the Frontiers editorial office: frontiersin.org/about/contact

# Novel regulatory mechanisms behind thermogenesis of brown and beige adipocytes

**Topic editors**
Rubén Cereijo— University of Barcelona, Spain
Endre Károly Kristóf — University of Debrecen, Hungary

**Topic coordinator**
Abhirup Shaw — McGill University, Canada

**Citation**
Cereijo, R., Kristóf, E. K., Shaw, A., eds. (2023). *Novel regulatory mechanisms behind thermogenesis of brown and beige adipocytes*. Lausanne: Frontiers Media SA.
doi: 10.3389/978-2-8325-3400-7

# Table of contents

frontiers | Frontiers in Endocrinology

TYPE Editorial
PUBLISHED 18 August 2023
DOI 10.3389/fendo.2023.1268299

Check for updates

OPEN ACCESS

EDITED AND REVIEWED BY
Ralf Jockers,
Université Paris Cité, France

*CORRESPONDENCE
Endre Kristóf
kristof.endre@med.unideb.hu
Rubén Cereijo
rcereijo@ub.edu

†These authors have contributed equally to this work and shared last authorship

RECEIVED 27 July 2023
ACCEPTED 09 August 2023
PUBLISHED 18 August 2023

CITATION
Shaw A, Kristóf E and Cereijo R (2023) Editorial: Novel regulatory mechanisms behind thermogenesis of brown and beige adipocytes. *Front. Endocrinol.* 14:1268299. doi: 10.3389/fendo.2023.1268299

COPYRIGHT
© 2023 Shaw, Kristóf and Cereijo. This is an open-access article distributed under the terms of the Creative Commons Attribution License (CC BY). The use, distribution or reproduction in other forums is permitted, provided the original author(s) and the copyright owner(s) are credited and that the original publication in this journal is cited, in accordance with accepted academic practice. No use, distribution or reproduction is permitted which does not comply with these terms.

# Editorial: Novel regulatory mechanisms behind thermogenesis of brown and beige adipocytes

Abhirup Shaw[1,2], Endre Kristóf[1*†] and Rubén Cereijo[3,4*†]

[1]Laboratory of Cell Biochemistry, Department of Biochemistry and Molecular Biology, Faculty of Medicine, University of Debrecen, Debrecen, Hungary, [2]Rosalind & Morris Goodman Cancer Institute, McGill University, Montreal, QC, Canada, [3]Departament de Bioquímica i Biomedicina Molecular, Institut de Biomedicina de la Universitat de Barcelona (IBUB), and Institut de Recerca de Sant Joan de Déu, Universitat de Barcelona, Barcelona, Spain, [4]CIBER Fisiopatología de la Obesidad y Nutrición, Madrid, Spain

KEYWORDS

**obesity, brown adipocytes, beige adipocytes, UCP1, thermogenesis, beiging, browning**

Editorial on the Research Topic
Novel regulatory mechanisms behind thermogenesis of brown and beige adipocytes

## Introduction

Brown adipose tissue (BAT) has emerged as a pivotal organ in the field of metabolic research due to its unique properties. Unlike white adipose tissue (WAT), which predominantly stores energy in the form of triglycerides, BAT possesses a remarkable capacity to dissipate energy as heat through the process of non-shivering thermogenesis (1). This specialized function is primarily attributed to a high abundance of mitochondria and the expression of uncoupling protein (UCP) 1 within brown and beige adipocytes - a subpopulation of thermogenic cells that can originate from WAT depots in response to certain stimuli (1). Over the past decade, there has been a resurgence of interest in BAT as a potential therapeutic target for the rising global epidemic of obesity and related metabolic disorders, since the (re)discovery of active BAT in adult humans overturned the conventional belief that BAT exclusively existed in newborns to regulate body temperature (2). The identification and understanding of key regulators and molecular pathways governing BAT have provided exciting prospects for the development of new approaches to combat obesity and concomitant metabolic diseases (1, 2). However, despite such significant advancements, numerous questions regarding its precise regulatory

mechanisms, interactions with other organs, and potential long-term effects on overall metabolic health remain unanswered. This Research Topic aimed to comprehensively integrate original studies and state-of-the-art knowledge on BAT and its physiological role in energy expenditure, as well as the underlying molecular pathways and potential therapeutic implications.

## Regulatory mechanisms in brown/beige adipocytes

Wang et al. comprehensively reviewed the transcriptional cascades, epigenetic modifications, non-coding RNAs, and endogenous or exogenous metabolites which can regulate brown/beige adipocyte differentiation from preadipocytes or white to beige transdifferentiation. The paracrine and endocrine factors that mediate the communication between either different cell types of BAT or distinct organs are also discussed.

Mitochondrial biogenesis, clearance, and dynamics are key processes in maintaining the proper functions of adipocytes (3). Brown/beige adipocytes convert the subtracted energy of nutrient molecules into heat (1, 4). In the mini review written by Chang, the regulation of how the heterogeneous mitochondrial populations of thermogenic adipocytes select distinct nutrient molecules was discussed. Moreover, Zheng et al. systematically reviewed how these processes contribute to the regulation of thermogenesis, browning, beige to white transition, and glucolipid metabolism. Furthermore, the potential applications of compounds present in herbal extracts in the treatment of obesity by the induction of mitochondrial functions of adipocytes are also summarized.

The circadian clock is maintained by self-sustained transcription-translation feedback loops by which organisms anticipate and adapt to the regular daily environmental cues, such as light (5). The circadian oscillation of clock genes also contribute to the regulation of adipocyte browning and thermogenesis reviewed by Peng and Chen. This is underlined by epidemiologic studies and laboratory interventions which provided evidence that reduced sleep duration and quality represent risk factors for the development of obesity and type 2 diabetes (6).

Metabolites generated from nutrients also contribute to the replenishment of vital macromolecules within adipocytes. Vámos et al. modelled thermogenic differentiation and conversion into the inactive state of human subcutaneous adipocytes. By global gene expression and metabolomics analyses, the critical importance of single nucleotide polymorphism at fat mass and obesity-associated *(FTO)* rs1421085 locus was revealed in the aforementioned processes most prominently by the regulation of several metabolic pathways, including amino acid utilization *via* alanine-serine-cysteine (ASC) transporter 1, which was postulated to support β-adrenergic-driven thermogenic activation (7).

On the other hand, proteostasis has also been shown to be a mechanism relevant in thermogenic adipocytes (8). In this regard, Koçberber et al. explored the role of two proteasome activators, PA28αβ (*Psme1*) and PA200 (*Psme4*), in brown adipocyte differentiation and function. Interestingly, siRNA-mediated studies revealed a dispensable role on murine brown adipocyte proteostasis, adipogenesis, and thermogenesis, prospecting further research on protein turnover complex regulation in BAT.

## Non-sympathetic molecular induction of beiging

Beyond classic β-adrenergic stimulation, some non-sympathetic mechanisms can physiologically regulate BAT functions (9). In this Research Topic, several authors also aimed to describe novel molecules capable of inducing human brown/beige adipocyte recruitment. By differentiating adipocytes from individuals with obesity, Coulter et al. showed that β–carotene can act synergistically with naringenin to induce expression of UCP1 and glucose metabolism-associated genes *in vitro*, as well as inducing lipase-mediated triglyceride hydrolysis in beige adipocytes. Ali et al. also demonstrated that another diet-derived bioactive compound, allicin, can also trigger a beigeing transcriptomic program in human adipocytes, with rearrangements in mitochondrial morphology and lipid droplet dynamics. Beyond dietary nutrients, Nagy et al. reported that nicotinamide-riboside, a $NAD^+$ precursor, can also induce a respiration uncoupling-based beige phenotype both at the transcriptional and functional level in human primary adipocytes, a process mediated *via* sirtuin-1.

## Novel insights on the endocrine role of human BAT

Beyond its energy-dissipating functions, a secretory endocrine role has currently been well-established for BAT. Analogously to WAT-derived adipokines, BAT can communicate with distant organs by releasing so-called brown adipokines (or batokines) to orchestrate beneficial systemic metabolic actions (10). While this has been extensively explored in experimental models, batokine studies in humans are still scarce. In this topic, Garcia-Beltran et al. shed some light into this question by assessing expression and circulating levels of a batokine, meteorin-like (METRNL) (11), in human newborns. They demonstrated that METRNL is highly expressed in neonatal interscapular BAT, and that its circulating levels correlate to those of chemokine (C-X-C) motif ligand (CXCL) 14, another known batokine (12). Moreover, they were also associated with infrared-assessed BAT thermogenic activation, indicating METRNL is a new biomarker of BAT activity in early life.

## Closing remarks and future perspectives

The contributions to this Research Topic have remarkably bestowed to elucidate the intricate biology of BAT, adding novel

insight to the growing body of evidence supporting its role in human metabolic homeostasis. While further research is needed, fully ascertaining the regulatory mechanisms ruling brown/beige adipocyte differentiation, especially in human models, will ultimately provide new avenues for therapeutic intervention against obesity and associated metabolic disorders in the pursuit of improved public health.

## Author contributions

AS: Writing – original draft, Writing – review & editing. EK: Writing – original draft, Writing – review & editing. RC: Writing – original draft, Writing – review & editing.

## Funding

EK was funded by the National Research, Development and Innovation Office (NKFIH-FK131424) of Hungary. RC is a Serra Húnter Fellow (Generalitat de Catalunya).

## Acknowledgments

We are very grateful to all participating authors for their contributions and to all reviewers for their altruistic constructive comments to this Research Topic.

## Conflict of interest

The authors declare that the research was conducted in the absence of any commercial or financial relationships that could be construed as a potential conflict of interest.

## Publisher's note

All claims expressed in this article are solely those of the authors and do not necessarily represent those of their affiliated organizations, or those of the publisher, the editors and the reviewers. Any product that may be evaluated in this article, or claim that may be made by its manufacturer, is not guaranteed or endorsed by the publisher.

## References

1. Cohen P, Kajimura S. The cellular and functional complexity of thermogenic fat. *Nat Rev Mol Cell Biol* (2021) 22:393–409. doi: 10.1038/s41580-021-00350-0

2. Blondin DP. Human thermogenic adipose tissue. *Curr Opin Genet Dev* (2023) 80:102054. doi: 10.1016/j.gde.2023.102054

3. Altshuler-Keylin S, Kajimura S. Mitochondrial homeostasis in adipose tissue remodeling. *Sci Signal* (2017) 10:eaai9248. doi: 10.1126/scisignal.aai9248

4. Sakers A, De Siqueira MK, Seale P, Villanueva CJ. Adipose-tissue plasticity in health and disease. *Cell* (2022) 185:419–46. doi: 10.1016/j.cell.2021.12.016

5. Ruan W, Yuan X, Eltzschig HK. Circadian rhythm as a therapeutic target. *Nat Rev Drug Discov* (2021) 20:287–307. doi: 10.1038/s41573-020-00109-w

6. Broussard JL, Van Cauter E. Disturbances of sleep and circadian rhythms: novel risk factors for obesity. *Curr Opin Endocrinol Diabetes Obes* (2016) 23:353–9. doi: 10.1097/MED.0000000000000276

7. Arianti R, Vinnai BÁ, Tóth BB, Shaw A, Csősz É, Vámos A, et al. ASC-1 transporter-dependent amino acid uptake is required for the efficient thermogenic response of human adipocytes to adrenergic stimulation. *FEBS Lett* (2021) 595:2085–98. doi: 10.1002/1873-3468.14155

8. Bartelt A, Widenmaier SB, Schlein C, Johann K, Goncalves RLS, Eguchi K, et al. Brown adipose tissue thermogenic adaptation requires Nrf1-mediated proteasomal activity. *Nat Med* (2018) 24:292–303. doi: 10.1038/nm.4481

9. Cereijo R, Villarroya J, Villarroya F. Non-sympathetic control of brown adipose tissue. *Int J Obes Suppl* (2015) 5:S40–44. doi: 10.1038/ijosup.2015.10

10. Gavaldà-Navarro A, Villarroya J, Cereijo R, Giralt M, Villarroya F. The endocrine role of brown adipose tissue: An update on actors and actions. *Rev Endocr Metab Disord* (2022) 23:31–41. doi: 10.1007/s11154-021-09640-6

11. Rao RR, Long JZ, White JP, Svensson KJ, Lou J, Lokurkar I, et al. Meteorin-like is a hormone that regulates immune-adipose interactions to increase beige fat thermogenesis. *Cell* (2014) 157:1279–91. doi: 10.1016/j.cell.2014.03.065

12. Cereijo R, Gavaldà-Navarro A, Cairó M, Quesada-López T, Villarroya J, Morón-Ros S, et al. CXCL14, a brown adipokine that mediates brown-fat-to-macrophage communication in thermogenic adaptation. *Cell Metab* (2018) 28:750–763.e6. doi: 10.1016/j.cmet.2018.07.015

frontiers | Frontiers in Cell and Developmental Biology

TYPE Original Research
PUBLISHED 22 August 2022
DOI 10.3389/fcell.2022.979330

Check for updates

OPEN ACCESS

EDITED BY
Endre Károly Kristóf,
University of Debrecen, Hungary

REVIEWED BY
Monica Colitti,
University of Udine, Italy
Tibor Pankotai,
University of Szeged, Hungary

*CORRESPONDENCE
Péter Bai,
baip@med.unideb.hu

SPECIALTY SECTION
This article was submitted to Signaling, a section of the journal Frontiers in Cell and Developmental Biology

RECEIVED 27 June 2022
ACCEPTED 28 July 2022
PUBLISHED 22 August 2022

CITATION
Nagy L, Rauch B, Szerafin T, Uray K, Tóth A and Bai P (2022), Nicotinamide-riboside shifts the differentiation of human primary white adipocytes to beige adipocytes impacting substrate preference and uncoupling respiration through SIRT1 activation and mitochondria-derived reactive species production.
*Front. Cell Dev. Biol.* 10:979330.
doi: 10.3389/fcell.2022.979330

COPYRIGHT
© 2022 Nagy, Rauch, Szerafin, Uray, Tóth and Bai. This is an open-access article distributed under the terms of the Creative Commons Attribution License (CC BY). The use, distribution or reproduction in other forums is permitted, provided the original author(s) and the copyright owner(s) are credited and that the original publication in this journal is cited, in accordance with accepted academic practice. No use, distribution or reproduction is permitted which does not comply with these terms.

# Nicotinamide-riboside shifts the differentiation of human primary white adipocytes to beige adipocytes impacting substrate preference and uncoupling respiration through SIRT1 activation and mitochondria-derived reactive species production

Lilla Nagy[1], Boglárka Rauch[1], Tamás Szerafin[2], Karen Uray[1], Attila Tóth[3,4,5] and Péter Bai[1,5,6,7]*

[1]Department of Medical Chemistry, Faculty of Medicine, University of Debrecen, Debrecen, Hungary, [2]Department of Cardiology and Heart Surgery, Faculty of Medicine, University of Debrecen, Debrecen, Hungary, [3]Section of Clinical Physiology, Department of Cardiology and Heart Surgery, Faculty of Medicine, University of Debrecen, Debrecen, Hungary, [4]HAS-UD Vascular Biology and Myocardial Pathophysiology Research Group, Hungarian Academy of Sciences, Budapest, Hungary, [5]Research Center for Molecular Medicine, Faculty of Medicine, University of Debrecen, Debrecen, Hungary, [6]MTA-DE Lendület Laboratory of Cellular Metabolism, Debrecen, Hungary, [7]MTA-DE Cell Biology and Signaling Research Group ELKH, Debrecen, Hungary

Beige adipocytes play key roles in organismal energy and metabolic balance. In this study, we assessed whether the supplementation of human white adipocytes, differentiated from human adipose tissue-derived stem cells, with nicotinamide riboside (NR), a potent NAD + precursor, can shift differentiation to beige adipocytes (beiging). NR induced mitochondrial biogenesis and the expression of beige markers (TBX1 and UCP1) in white adipocytes demonstrating that NR can declutch beiging. NR did not induce PARP activity but supported SIRT1 induction, which plays a key role in beiging. NR induced etomoxir-resistant respiration, suggesting increases in the oxidation of carbohydrates, carbohydrate breakdown products, or amino acids. Furthermore, NR boosted oligomycin-resistant respiration corresponding to uncoupled respiration. Enhanced etomoxir and oligomycin-resistant respiration were dependent on mitochondrial reactive-species production. Taken together, NR supplementation can induce beiging and uncoupled respiration, which are beneficial for combatting metabolic diseases.

KEYWORDS

**beige adipocyte, mitochondrial oxidation, nicotinamide riboside, uncoupled respiration, adipocyte differentiation**

# 1 Introduction

Altered organismal energy homeostasis contributes to the induction of metabolic diseases, such as obesity (Hall et al., 2022). Adipocytes play a major role in organismal energy homeostasis by storing or oxidizing fatty acids (Giordano et al., 2014; Cohen and Spiegelman, 2016). Both brown and beige adipocytes have considerable oxidative phosphorylation (OXPHOS) capacity (Wu et al., 2012). White adipocytes are responsible for lipid storage and lipid clearance from the circulation. Uncoupling between the OXPHOS and ATP production yields heat in brown and beige cells due to the overexpression of uncoupling protein-1 (UCP1). Brown cells have multiple lipid droplets in the cytoplasm and are often called multilocular adipocytes. Brown cells enshroud major arteries in adults, and newborns have extra brown cell-rich adipose tissue localized in the interscapular region (Lidell et al., 2013; Nedergaard and Cannon, 2018). Unstimulated, resting beige adipocytes can be found in regular adipose tissues and have similar unilocular morphology as white adipocytes (Altshuler-Keylin et al., 2016). Without stimulation the expression of thermogenic genes is low in beige cells (Petrovic et al., 2010; Waldén et al., 2012; Shabalina et al., 2013). Beige cells induce mitochondrial biogenesis in response to adrenergic stimulus and are very efficient in fatty acid oxidation (Wu et al., 2012; Harms and Seale, 2013). Beige adipocyte dysfunction is a serious risk factor for developing obesity and type II diabetes (Claussnitzer et al., 2015; Alcala et al., 2019; Scherer, 2019).

NAD+ is a central molecule in biochemistry that is often referred to as the NAD + -node. NAD + has a redox cycle (NAD+ ↔ NADH) and a non-redox cycle in which NAD+ is cleaved into nicotinamide (NA) and ADP-ribose (ADPR) and then resynthesized (NAD+ ↔ NA + ADPR) (Houtkooper et al., 2010). NAD+ is cleaved by sirtuins (SIRTs), PARPs, and CD38, while the resynthesis involves members of the enzyme machinery of NAD + salvage (Houtkooper et al., 2010; Nikiforov et al., 2011; Cantó et al., 2013). Increases in NAD + levels induce pathways that upregulate mitochondrial biogenesis and, consequently, alleviate insulin resistance and obesity (Houtkooper et al., 2010; Nikiforov et al., 2011; Cantó et al., 2013). NAD + precursors can efficiently boost NAD + levels (Canto et al., 2012; Giroud-Gerbetant et al., 2019). NAD + metabolism is linked to adipocyte differentiation (Luo et al., 2017; Ryu et al., 2018; Huang et al., 2020; Szanto and Bai, 2020; Szanto et al., 2021)

Nicotinamide-riboside (NR) is an NAD + precursor that efficiently induces cellular NAD + levels and mitochondrial biogenesis (Canto et al., 2012). NR supplementation efficiently induced mitochondrial biogenesis in models of obesity (Canto et al., 2012; Jukarainen et al., 2016; Rappou et al., 2016; Jokinen et al., 2017; Asnani-Kishnani et al., 2019; Vannini et al., 2019; Nascimento et al., 2021), inflammatory diseases (Wu et al., 2022), Parkinson's (Brakedal et al., 2022), non-alcoholic fatty liver disease (Dall et al., 2021), and aging (Sun et al., 2021). The objective of this study was to assess the effects of NR on the induction of shift of differentiation of white adipocytes to beige adipocytes (beiging) in a human adipose tissue-derived mesenchymal stem cell (hADMSC) model.

# 2 Materials and methods

## 2.1 Chemicals

Chemicals were purchased from Sigma-Aldrich (St. Louis, MO, United States) unless stated otherwise. NR was a generous gift from ChromaDex (Los Angeles, CA, United States). NR concentration was selected based on literature search [e.g., (Canto et al., 2012; Ryu et al., 2016)]. Mito-TEMPO, a mitochondrial antioxidant (Jankó et al., 2021; Kacsir et al., 2021) was from Sigma-Aldrich (St. Louis, MO, United States).

## 2.2 Ethical statement

The study protocol was approved by the Ethics Committee of the University of Debrecen (Hungary) and the National Medical Research Council Committee of Human Reproduction (ETT TUKEB). All experiments were carried out in accordance with the Declaration of Helsinki and the approved ethical guidelines and regulations. Written informed consent was obtained from all participants before the surgical procedure.

## 2.3 Isolation, culture, and differentiation of hADMSCs

Human ADMSCs, also called stromal-vascular fraction (SVF) cells, were isolated from pericardial adipose tissue specimens as described in (Kristof et al., 2015; Abdul-Rahman et al., 2016). The hADMSCs were maintained and differentiated to white or beige adipocytes as described in (Nagy et al., 2019). Primary human adipose tissue-derived stem cells (hADMSC) were cultured in DMEM F-12 HAM containing 10% FBS, 1% penicillin/streptomycin, 33 μM Biotion and 17 μM Pantothenic acid. Before the induction of differentiation cells were grown to confluency then the following media were applied. For the differentiation of white adipocytes during the 1st–3rd days of differentiation serum-free DMEM HAM-F12 supplemented with 1% Penicilline- streptomycin, 33 μM Biotin, 17 μM Pantothenic acid, 10 μg/ml Apotransferrin, 200 p.m. 3,3′,5-Triiodo-L-thyronine sodium salt, 20 nM Human Insulin, 100 nM Hydrocortisone, 2 μM Rosiglitazone, 25 nM Dexamethasone, 500 μM 3-Isobutyl-1-methylxanthine that is exchanged for serum-free DMEM HAM-F12 supplemented with 1% Penicilline- streptomycin, 33 μM Biotin, 17 μM Pantothenic

acid, 10 μg/ml Apotransferrin, 200 p.m. 3,3′,5-Triiodo-L-thyronine sodium salt, 20 nM Human Insulin, 100 nM Hydrocortisone between the 4th–14th day of differentiation. For the induction of the differentiation of beige adipocytes serum-free DMEM HAM-F12 supplemented with 1% Penicilline- streptomycin, 33 μM Biotin, 17 μM Pantothenic acid, 10 μg/ml Apotransferrin, 200 p.m. 3,3′,5-Triiodo-L-thyronine sodium salt, 850 nM Human Insulin, 1 μM Dexamethasone, 500 μM 3-Isobutyl-1-methylxanthine was used. From day 4$^{th}$ to day 14 serum-free DMEM HAM-F12 supplemented with 1% Penicilline- streptomycin, 33 μM Biotin, 17 μM Pantothenic acid, 10 μg/ml Apotransferrin, 200 p.m. 3,3',5-Triiodo-L-thyronine sodium salt, 850 nM Human Insulin and 500 nM Rosiglitazone was applied. Medium was changed every 2 days. A subset of white adipocytes was treated with 500 μM NR for 14 days during the differentiation process.

## 2.4 Immunofluorescence and confocal microscopy

Mitochondrial structure was determined by staining differentiated hADMSCs with TOMM20 immunohistochemistry similar to (Jankó et al., 2021). The hADMSCs were seeded on glass coverslips and differentiated as described in 2.3. To detect TOMM20, differentiated cells were washed with PBS, fixed with 4% paraformaldehyde for 10 min at 37°C, and permeabilized with 1% Triton X-100 in PBS for 10 min. Between each step, cells were rinsed twice with PBS. Cells were blocked with 1% bovine serum albumin (BSA) in PBS for 1 h at room temperature. TOMM20 primary antibody was applied overnight (4°C, humidified chamber, diluted in blocking buffer). The next day, cells were washed and probed with Alexa Fluor 647-conjugated secondary antibody (Goat anti-Mouse IgG (H + L), Thermo Fisher Scientific, Waltham, MA, United States; excitation: 651 nm, emission: 667 nm). The pictures were taken with the ×40 objective of the system. Cell nuclei were visualized with DAPI (NucBlue Fixed Cell ReadyProbes Reagent, Thermo Fisher Scientific, Waltham, MA, United States). Confocal images were acquired with a Leica TCS SP8 confocal microscope (Leica, Wetzlar, Germany) and LAS X 3.5.5.19976 software (Leica, Wetzlar, Germany). Nonspecific binding of secondary antibodies was checked in control experiments (not shown). Processed images were analyzed using the ImageJ software Mito-Morphology Macro (Dagda et al., 2009; Dagda, 2019). Mitochondrial content, perimeter, circularity, and form factor were calculated from confocal microscopic images.

## 2.5 Gene expression and RT-qPCR

Reverse transcription-coupled real-time quantitative PCR (RT-qPCR) reactions were performed as described in (Bai et al., 2007). Primers are summarized in Table 1. Expression was normalized to the geometric mean of β-actin and 36B4 genes and was expressed as fold change.

## 2.6 Protein extraction and western blotting

The hADMSCs were seeded, differentiated, and treated in 10 cm Petri dishes. Cell were rinsed with PBS 2 times, scraped, centrifuged, and lysed in RIPA lysis buffer (50 mM Tris, 150 mM NaCl, 0.1% SDS, 1% Triton X 100, 0.5% sodium deoxycholate, 1 mM EDTA, 1 mM Na3VO4, 1 mM NaF, and protease inhibitor cocktail). Western blotting was performed as described by (Nagy et al., 2018). Blots were probed with the antibodies summarized in Table 2. Signals were detected using enhanced chemiluminescence (ECL) and were captured by ChemiDoc Touch (Bio-Rad Laboratories, CA, United States).

## 2.7 Determination of differentiation rate

The rate of differentiation was determined as described in (Bai et al., 2007). The hADMSC cells were seeded, differentiated, and treated in 24-well plates. On the day of the experiment, cells were stained with Nile Red dye (10 μg/ml) in medium and incubated for 30 min at 37°C. Cells were rinsed with PBS 3 times, digested with Trypsin-EDTA, suspended in PBS, and pipetted in FACS tubes. The differentiation rate was determined using a NovoCyte Flow Cytometer (NovoCyte 3000, Acea Biosciences Inc., San Diego, United States) and analyzed using NovoExpress 1.2.5 Software. Differentiation rate was expressed as a percent of all cells.

## 2.8 Determination of oxygen consumption

Oxygen consumption rate (OCR) was determined using an XF96 Flux Analyzer using the assay plates designed for the instrument (Agilent Technologies, CA, United States). The hADMSCs were seeded in 96-well assay plates, then differentiated as described above. After recording the baseline oxygen consumption, cells were treated with a single bolus dose of dibutyril-cAMP (500 μM final concentration) to simulate adrenergic stimulation and OCR was recorded in 30 min intervals 5 times. Next, etomoxir (50 μM final concentration) was applied and OCR was recorded every 5 times for 3 min. Etomoxir is an inhibitor of mitochondrial fatty acid import (Declercq et al., 1987), etomoxir-sensitive respiration corresponds to fatty acid oxidation, while etomoxir-resistant respiration corresponds to the oxidation of other, non-fatty acid substrates. The cells were then treated with oligomycin (2.5 μM final concentration), and OCR was recorded every 5 times for 3 min.

TABLE 1 Human primers used in RT-qPCR reactions.

| Gene | Forward | Reverse |
|---|---|---|
| 36B4 | 5′-CCATTGAAATCCTGAGTGATGTG-3′ | 5′-GTCGAACACCTGCTGGATGAC-3′ |
| β-actin | 5′-GACCCAGATCATGTTTGAGACC-3′ | 5′-CATCACGATGCCAGTGGTAC -3′ |
| UCP1 | 5′-AACGAAGGACCAACGGCTTTC-3′ | 5′-GGCACAGTCCATAGTCTGCCTTG -3′ |
| TBX1 | 5′-TCCCACCTTCCAAGTGAAGCTC -3′ | 5′-CACGATTTGCTTCATCCACTGC -3′ |
| PRDM16 | 5′-CACTGTGCAGGCAGGCTAAGAA-3′ | 5′-AGAGGTGGTTGATGGGGTGAAA-3′ |
| COX7A1 | 5′-ATACGGAAACAGGCTCGGAGGT-3′ | 5′-ATCCGTTTCGGTCTCGGAATTT-3′ |
| CIDEA | 5′-TCTCCAACCATGACAGGAGCAG-3′ | 5′-AATGCGTGTTGTCTCCCAAGGT-3′ |
| TMEM26 | 5′-ACCTCCCATGTGTGGACATCCT-3′ | 5′-ACCAACAGCACCAACAACCTCA -3′ |
| SIRT1 | 5′-TGGCAAAGGAGCAGATTAGTAGGC-3′ | 5′-TGGACTCTGGCATGTCCCACT-3′ |
| PGC1α | 5′-TTCCTCTGACCCCAGAGTCACC-3′ | 5′-TTGCAAGAGGACTTCAGCTTTGG-3′ |
| PPARγ1 | 5′-GTGGCCGCAGATTTGAAAGAAG-3′ | 5′-CCATGGTCATTTCGTTAAAGGCTG-3′ |
| PPARγ2 | 5′-CAGCAAACCCCTATTCCATGC-3′ | 5′-GGGAGTGGTCTTCCATTACGG-3′ |
| ADIPOQ | 5′-TTAAAACCTCCCCCAAGCAGA-3′ | 5′-GCCTTGAGGAACAGGGATGAG-3′ |
| FAS | 5′-GCAGGAGCTCAAGAAGGTGATC-3′ | 5′-ACCAGGTTGTTGACATTGTACTCG-3′ |
| FABP4 | 5′-GGAAAGTCAAGAGCACCATAACC-3′ | 5′-GCTCTCTCATAAACTCTCGTGGAAG-3′ |
| HSL | 5′-GAAGCCTTTGAGATGCCACTG-3′ | 5′-CTCACTGTCCTGTCCTTCACG-3′ |
| leptin | 5′-CACACACGCAGTCAGTCTCCTC-3′ | 5′-GTATGCCTTCCAGAAACGTGATCC-3′ |
| LPL | 5′-CTGGATGGAGGAGGAGTTTAACTACC-3′ | 5′-CTGCATCATCAGGAGAAAGACG-3′ |
| PLIN1/2 | 5′-GAACAAGTTCAGTGAGGTAGCAGC-3′ | 5′-CTTGGTTGAGGAGACAGCAGG-3′ |
| TNFa | 5′-GCAGTCAGATCATCTTCTCGAAC-3′ | 5′-GAAGAGGACCTGGGAGTAGATGAG-3′ |
| PARP1 | 5′-CACTGGTACCACTTCTCCTGCTTC-3′ | 5′-CTTTGCCTGTCACTCCTCCAG-3′ |
| PARP2 | 5′-GCTAAATCAGACCAATCTCC-3′ | 5′-CAGGCTGTGCTGTCCCATTT-3′ |
| PARP3 | 5′- CTTCCTGGGCCTCATCCTCTG-3′ | 5′- CAACCGCTTCTTCACCTGCTG-3′ |
| PARP5a | 5′- AACATCCTTCCTTCCAAAACCT-3′ | 5′- GGCAAACGTAAATGCAAAGG-3′ |
| PARP5b | 5′- AAGGTTACCCGGCAAAAGA-3′ | 5′- TGGGTGTCCAGTTCACAAAG-3′ |
| PARP10 | 5′-CTGTGGACCTGCTGTTGCTG-3′ | 5′-GGATGTCGTAGTGGGGGACA-3′ |

TABLE 2 Primary antibodies used in the study.

| Target | Type | Company | Dilution |
|---|---|---|---|
| TOMM20 | monoclonal | Abcam, Cambridge UK | 1:200 |
| UCP1 | monoclonal | Cell Signaling, Danvers MA, United States | 1:1000 |
| TBX1 | polyclonal | GeneTex, Irvine, CA, United States | 1:500 |
| PGC1a | polyclonal | Thermo Fisher Scientific, Waltham, MA, United States | 1:1000 for WB<br>1:200 for IP |
| acetyl-lysine antibody | polyclonal | Cell Signaling, Danvers MA, United States | 1:500 |
| Poly (ADP-ribose) (10H) | monoclonal | Sigma aldrich | 1:500 |
| Mono(ADP-ribose) | monoclonal | Sigma aldrich | 1:1000 |
| β-Actin–Peroxidase | polyclonal | Sigma aldrich | 1:20000 |

Oligomycin blocks the F1/F0 ATP synthase. Therefore, etomoxir-resistant respiration corresponds to uncoupled respiration. Finally, cells were treated with a single bolus dose of antimycin A (10 μM) and rotenone (5 μM) and OCR was recorded every 5 times for 3 min. These drugs completely block mitochondrial respiration and can be used to determine the baseline fluorescence intensity (i.e., background). After the measurement, XF96 cell plates were stained with Nile Red dye, and cell number and differentiation rate were determined using a Novocyte Flow cytometer (NovoCyte 3000, Acea Biosciences Inc., San Diego, United States) and

analyzed using NovoExpress 1.2.5 Software. OCR values were normalized to the differentiation rate for each well and normalized readings were analyzed and plotted. The calculation and measurement procedure are published in (Miko et al., 2017).

## 2.9 Immunoprecipitation

Cells were lysed in RIPA lysis buffer as described in 2.6. PGC1α acetylation levels were analyzed by immunoprecipitating lysates with anti-PGC1α antibodies followed by Western blotting using an acetyl-lysine antibody and normalization to total PGC1α levels similar to (Bai et al., 2011a; Bai et al., 2011b).

## 2.10 Statistical analysis

Data were analyzed using GraphPad Prism nine software. The modified Thompson Tau test was used to identify outlier data points that were removed from the analysis. Normality was tested using D'Agonstino and Pearson tests. Statistical tests are stated in the figure legends. All data is represented as average ±SD, unless stated otherwise. All experiments were repeated at least three times.

# 3 Results

## 3.1 NR treatment induces mitochondrial biogenesis and mitochondrial oxidation in human primary white adipocytes

First, we measured mitochondrial content by immunofluorescently labeling TOMM20, a mitochondrial marker protein, followed by image analysis. Mitochondrial content was higher in beige cells compared with white adipocytes, similar to NR-treated white adipocytes (Figure 1A). Furthermore, beige and NR-treated adipocytes had a more fused mitochondrial network compared with the network of white adipocytes, marked by increases in the form factor (Figure 1A). These changes resulted in increases in mitochondrial oxidative activity upon cAMP stimulation. (Figure 1B). Furthermore, the substrates for mitochondrial oxidation were altered. In beige adipocytes, etomoxir-resistant respiration, representing carbohydrate and amino acid oxidation, decreased, while etomoxir-sensitive respiration, representing fatty acid oxidation, increased (Figure 1B) compared with respiration in white adipocytes. In NR-treated cells, etomoxir-resistant respiration was similar to white adipocytes, while, fatty acid oxidation was higher in beige adipocytes (Figure 1B), highlighting the robust increases in fatty acid oxidation in response to NR treatment. Oligomycin-resistant respiration, a proxy for uncoupled respiration, increased in beige adipocytes compared with white and beige cells (Figure 1B). Furthermore, oligomycin-sensitive respiration, representing coupled-respiration, increased both in beige and NR-treated cells (Figure 1B).

NR treatment reduced the rate of differentiation in adipocytes compared with white adipocytes (Figure 1C), similar to treatment of cells with olaparib, a PARP inhibitor (Nagy et al., 2019). The mRNA and protein expression levels of a brown and beige marker gene, *uncoupling protein-1* (*UCP1*), which drives uncoupled respiration and heat generation (Cinti, 2017), and *T-Box Transcription Factor* (*TBX1*), a beige-specific marker. The mRNA expression levels of *UCP1* and *TBX1* were higher in beige and NR-treated cells compared with white adipocytes (Figure 1D). Furthermore, higher UCP1 mRNA expression was translated to higher UCP1 protein levels in beige and NR-treated cells (Figure 1E). Finally, we assessed the mRNA expression of adipogenic marker genes. The expression of peroxisome proliferator activated receptor- γ1 (PPARγ1), fatty acid binding protein-4 (FABP4), fatty acid synthase (FAS), perilipin, and tumor necrosis factor α (TNFα) increased, while lipoprotein lipase (LPL) decreased in beige adipocytes compared with expression levels in white adipocytes (Figure 1F). NR-treatment of white adipocytes did not elicit identical changes to gene expression as beige differentiation. NR treatment induced the expression of *perilipin* and decreased the expression of *LPL* and *FABP4* but did not alter the expression of *PPARγ*, *FAS,* and *TNFα,* suggesting that NR-treated cells have a different adipogenic enzyme composition and, therefore, different function.

## 3.2 NR treatment induces SIRT1 activation but not excess PARP1 activation

NR is a precursor of NAD + salvage and can support the activity of NAD + -dependent enzymes, such as PARPs or sirtuins (Canto et al., 2012). First, we assessed the mRNA expression of PARP enzymes known to be involved in regulating mitochondrial metabolism, including PARP1 (Virag et al., 1998; Bai et al., 2011b), PARP2 (Bai et al., 2011a; Mohamed et al., 2014), PARP3 (Rodriguez-Vargas et al., 2020), PARP5a (TNKS1), PARP5b (TNKS2) (Yeh et al., 2009; Wang et al., 2020), and PARP10 (Marton et al., 2018). The activity of PARP1 and PARP2, the enzymes responsible for the bulk of cellular PARP activity (Schreiber et al., 2002; Szanto et al., 2011), and PARP10 did not change in response to NR supplementation (Figure 2A). However, the mRNA levels of PARP3, PARP5a, and PARP5b were slightly increased by NR (Figure 2A). Of note, the mRNA expression levels of PARP3, PARP5a, and PARP5b were also elevated upon differentiation of hADMSCs into beige adipocytes (Figure 2A). These findings prompted us to assess poly- and mono-ADP-ribosylation in cells.

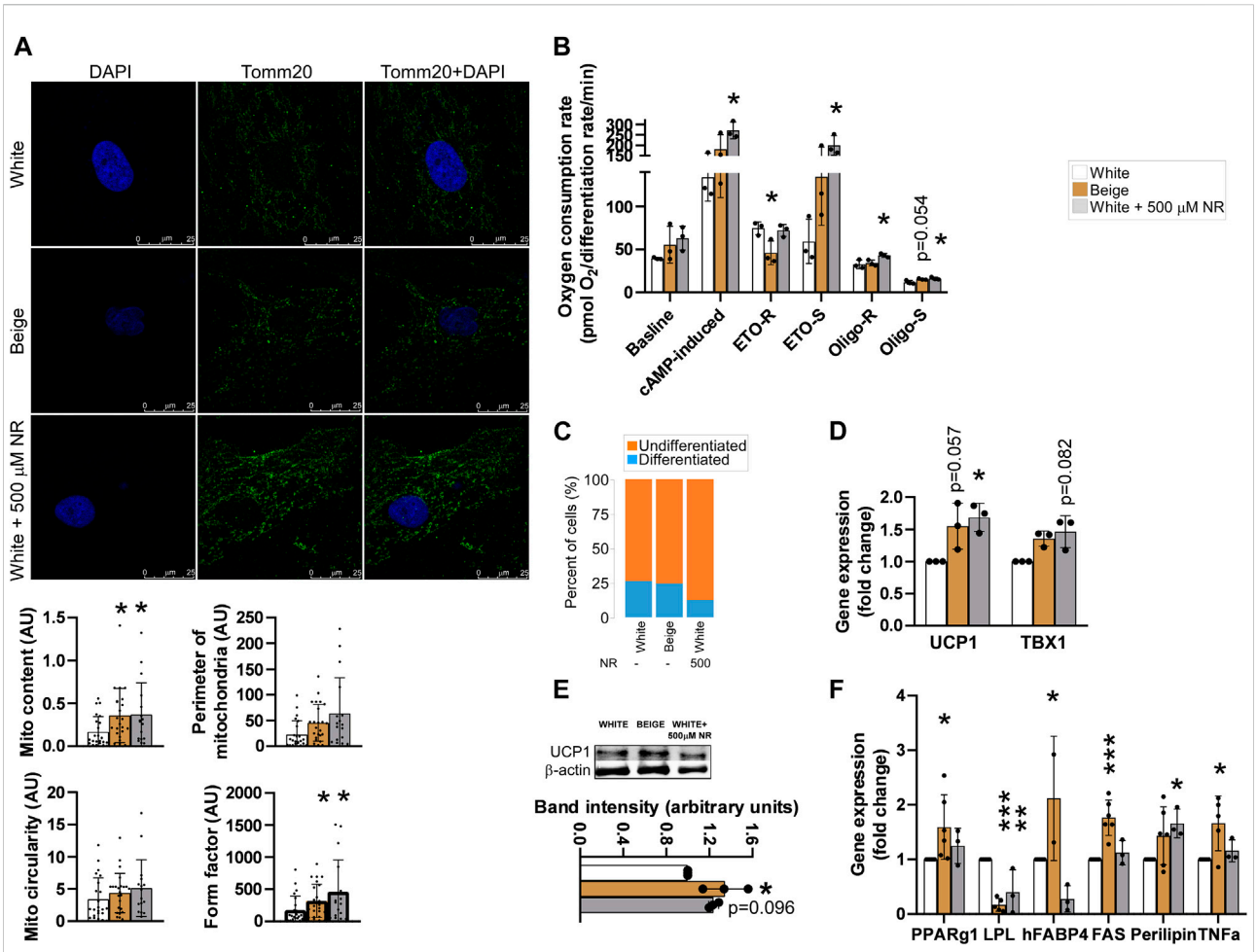


FIGURE 1
NR-treatment shifts the differentiation of white adipocytes to beige-like cells. The hADMSCs cells from three donors were seeded and differentiated to mature adipocytes. Cells were treated with NR (500 μM) throughout the differentiation process. **(A)** Differentiated cells were stained with TOMM20 antibody, then mitochondrial quantity and morphology were evaluated **(B)** Human adipose tissue-derived mesenchymal stem cells were seeded into Seahorse assay plates and assayed after differentiation. Mitochondrial oxygen consumption was assessed as described in Materials and Methods. **(C)** Adipocyte differentiation rate was determined as described in Materials and Methods **(D)** The expression levels of the indicated genes were measured by RT-qPCR in differentiated human adipose tissue-derived mesenchymal stem cells. **(E)** UCP1 protein expression was measured by Western blot in differentiated human adipose tissue-derived mesenchymal stem cells **(F)** The expression levels of the indicated genes were measured by RT-qPCR in differentiated human adipose tissue-derived mesenchymal stem cells. Normality was checked. Statistical significance was assessed by One-way ANOVA test followed by a post-hoc test versus white adipocytes. *, **, *** indicate significant differences between groups at $p < 0.05$, $p < 0.01$ or $p < 0.001$, respectively. Data are represented as means ± SD. Data are expressed as fold change normalized to white adipocytes. Abbreviations: ETO-S, etomoxir sensitive; ETO-R, etomoxir-resistant; hADMSC, human adipose tissue-derived mesenchymal stem cell; NR, nicotinamide-riboside; PAR, poly (ADP-ribose); UCP, uncoupling protein-1.

No differences in cellular levels of poly-ADP-ribose or mono-ADP-ribose were detected (Figure 2B), suggesting that NR supplementation did not induce PARP activity.

Sirtuins are also major NAD + consumers in cells and SIRT1 is a major driver of beige differentiation (Fu et al., 2014; Khanh et al., 2018; Liao et al., 2021). Therefore, we assessed SIRT1 activity in differentiated cells. Peroxisome proliferator-activated receptor gamma coactivator-1α (PGC1α) is a target of SIRT1 deacetylation (Nemoto et al., 2005). Hence, determining changes in PGC1α acetylation is a good proxy for SIRT1 activity. In addition, PGC1α is a key element in beige differentiation (Yan et al., 2016). PGC1α acetylation levels decreased in beige cells compared with white adipocytes, similar to NR-treated cells (Figure 2C), suggesting the SIRT1 activity increased during beige differentiation and upon NR-induced shift in differentiation.

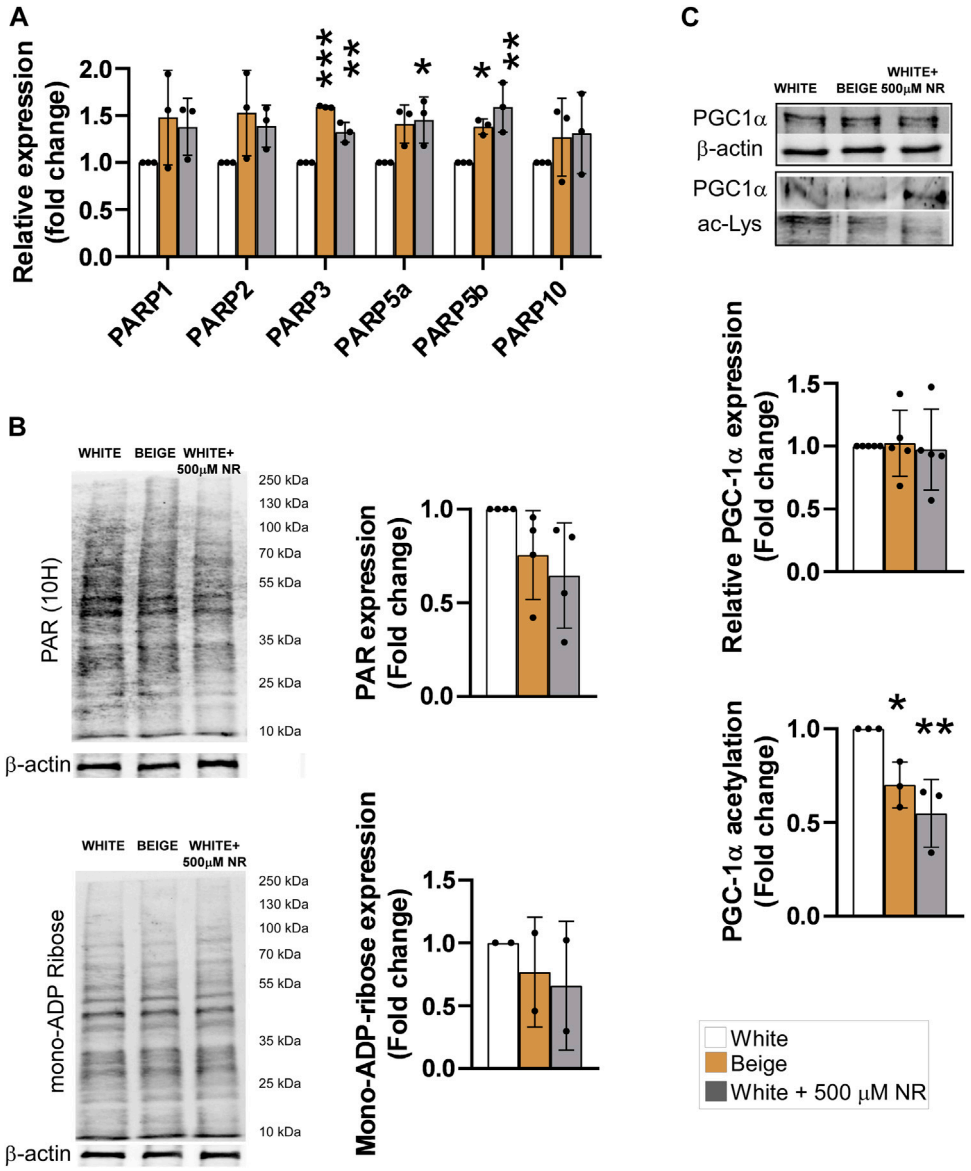


FIGURE 2
NR supplementation does not induce PARP activity but induces SIRT1 in hADMSC-derived adipocytes. Human adipose tissue-derived mesenchymal stem cells from three different controls were differentiated to adipocytes as described in Materials and Methods. **(A)** The expression levels of the indicated genes were determined using RT-qPCR **(B)** Poly (ADP-ribose) and mono-ADP-ribose levels were determined by Western blot. **(C)** PGC-1α was immunoprecipitated and acetylation levels were determined in the immunprecipitates. Normality was checked. Statistical significance was assessed by One-way ANOVA test followed by a post-hoc test versus white adipocytes. *, **, *** indicate significant differences between groups at $p < 0.05$, $p < 0.01$ or $p < 0.001$, respectively. Data are represented as means ± SD. Data are expressed as fold change normalized to white adipocytes. Abbreviations: hADMSC, human adipose tissue-derived mesenchymal stem cell; NR, nicotinamide-riboside; PAR, poly (ADP-ribose); PGC1α, peroxisome proliferator-activated receptor gamma coactivator-1α.

## 3.3 NR treatment supports uncoupled respiration through mitochondrial reactive species production

Mitochondrial reactive species play a fundamental role in inducing mitochondrial biogenesis (Valero, 2014; Fu et al., 2018; Ryoo and Kwak, 2018; Palmeira et al., 2019; Jankó et al., 2021). We tested whether reactive species were produced in our system by supplementing the differentiation medium with Mito-TEMPO, a mitochondrial-targeted antioxidant, during the differentiation process. Mito-TEMPO treatment did not influence baseline, cAMP-induced, or etomoxir-sensitive (representing fatty acid

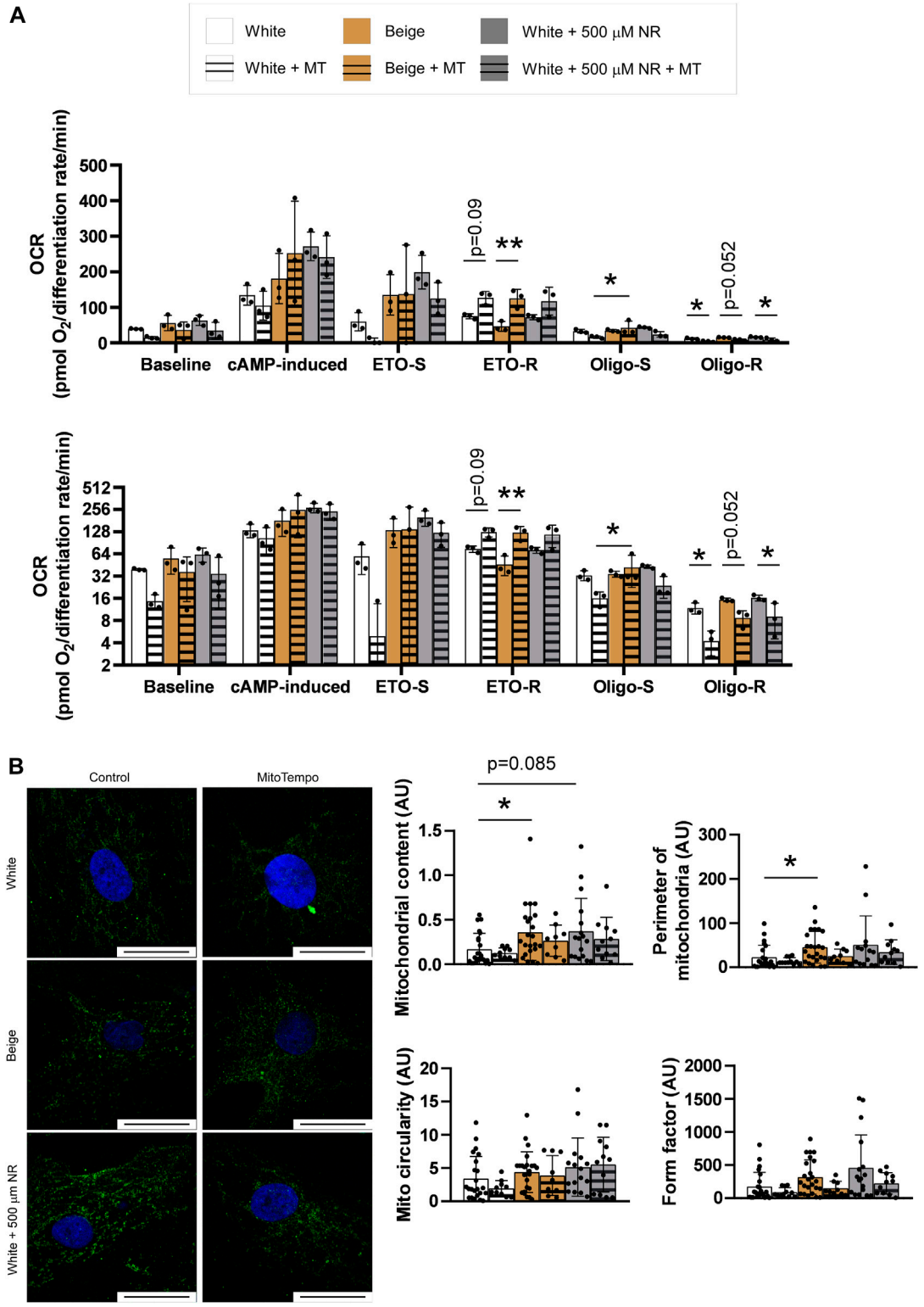


FIGURE 3
Mitochondria-derived reactive species production supports a switch towards uncoupled respiration. **(A)** Human adipose tissue-derived mesenchymal stem cells from three different donors were seeded in Seahorse plates and differentiated to adipocytes and mitochondrial oxidation was determined as described in Materials and Methods. The bottom graph depicts the same data on a log2-scale for better visibility **(B)** Human adipose tissue-derived mesenchymal stem cells from three different donors were seeded on coverslips, differentiated, stained with a

(*Continued*)

FIGURE 3
TOMM20 antibody, and mitochondrial morphology was assessed as described in Materials and Methods. The bar equals to 25 μm. Normality was checked. Statistical significance was assessed by Two-way ANOVA test followed by a post-hoc test that compares all possible combinations. * and ** symbolize significant differences between groups at $p < 0.05$ or $p < 0.01$, respectively. Data are represented as means ± SD. Data are expressed as fold change, where white adipocytes were considered as 1. Abbreviations: ETO-S, etomoxir sensitive; ETO-R, etomoxir-resistant; hADMSC, human adipose tissue-derived mesenchymal stem cell; Mito, mitochondria; MT, Mito-TEMPO; NR, nicotinamide-riboside; Oligo-S, oligomycin sensitive; Oligo-R, oligomycin resistant.

oxidation) mitochondrial oxidation rates (Figure 3A). However, etomoxir-resistant rates (representing amino acid and carbohydrate oxidation) were increased in response to Mito-TEMPO treatment in white and beige adipocytes, suggesting that reactive species production is important in driving fatty acid oxidation (Figure 3A). A similar trend was observed in NR-treated cells; however, the changes were not statistically significant (Figure 3A). No differences in the oligomycin-sensitive fraction of mitochondrial oxidation, corresponding to coupled-respiration, were detected. Nevertheless, Mito-TEMPO suppressed oligomycin-resistant (uncoupled) respiration in white and beige adipocytes and NR-treated white adipocytes (Figure 3A). These results highlight the key role of reactive species production in uncoupling. Mito-TEMPO treatment did not influence mitochondrial morphology (Figure 3B).

# 4 Discussion

In this study, we assessed the applicability of an NAD + precursor, NR, in shifting the differentiation of human adipose-derived pluripotent cells differentiated to white adipocytes. NR supplementation induced mitochondrial biogenesis and, consequently, increased mitochondrial oxidative capacity. These changes coincided with increased expression of UCP1, a marker of uncoupled mitochondrial oxidation, and TBX1, a beige marker gene. NR suppressed the rate of differentiation, similar to olaparib, a PARP inhibitor that induces NAD + -sparing and declutches beige transdifferentiation in the same model system (Nagy et al., 2019).

Previous studies identified NAD + as a key player in the induction of thermogenesis (Yamaguchi et al., 2019) and NR supplementation induces NAD + levels (Canto et al., 2012). NAD + interacts with a plethora of enzymes (Ziegler, 2000; Houtkooper et al., 2010; Nikiforov et al., 2011; Chiarugi et al., 2012; Bai et al., 2015), some of which are involved in intermediary metabolism and higher order metabolic regulation in beige or brown adipose tissue differentiation and function. These enzymes include AMP-activated protein kinase (AMPK) (Shan et al., 2013; Abdul-Rahman et al., 2016; Mottillo et al., 2016; Zhu et al., 2016; Desjardins and Steinberg, 2018; Imran et al., 2018; Wu et al., 2018; Serrano et al., 2020), PGC1α (Shan et al., 2013; Nagy et al., 2019), and SIRT1 (Qiang et al., 2012; Khanh et al., 2018; Asnani-Kishnani et al., 2019). Serrano and colleagues showed that NR also induces epigenetic changes (Serrano et al., 2020). We observed the activation of SIRT1 in response to NR treatment, which is consistent with previous studies (Qiang et al., 2012; Khanh et al., 2018). PARP enzymes are major consumers of NAD+ and can degrade NAD+ and limit NAD + availability to sirtuins (Bai et al., 2011a; Bai et al., 2011b; Cantó et al., 2013). However, we did not detect PARP activation in response to NR supplementation, suggesting that increases in NAD + support SIRT1 but not activation of PARP enzymes.

We observed changes in substrate preferences in NR-treated cells that were dependent on mitochondria-derived reactive species. Mito-TEMPO, a mitochondrial reactive species scavenger, induced etomoxir-resistant respiration in adipocytes but did not affect etomoxir-sensitive respiration (Figure 3A). Etomoxir is an inhibitor of mitochondrial fatty acid import (Declercq et al., 1987). Hence, etomoxir-sensitive respiration corresponds to fatty acid oxidation, while etomoxir-resistant respiration corresponds to the oxidation of carbohydrates, carbohydrate degradation products (e.g., pyruvate), and other substrates (e.g., amino acids). Thus, our data suggest that increased mitochondrial oxidation upon cAMP stimulation is dependent on increased carbohydrate and amino acid oxidation. Our observations are consistent with Dall et al. (Dall et al., 2019), who showed that the beneficial effects of NR treatment in liver mitochondria were dependent on glutamine and pyruvate oxidation. Pyruvate oxidation was implicated in modulating obesity and adipose tissue function (Ingram and Roth, 2021). However, our findings conflict with the findings of Canto et al. (Canto et al., 2012), who reported increases in fatty acid oxidation in NR-treated C57/Bl6 mice. Shi et al. (Shi et al., 2017) reported that NR administration to mice supported metabolic flexibility marked by large changes in respiratory quotient (or respiratory exchange ratio) values between the fed and fasted states compared with vehicle-fed animals.

Another important finding of this study is the key role that mitochondria-derived reactive species play in setting the ratio of coupled to uncoupled respiration. Mito-TEMPO treatment decreased the oligomycin-resistant fraction of respiration, indicating decreased uncoupled respiration in white, beige, and NR-treated adipocytes, while Mito-TEMPO had no effect on oligomycin-sensitive, coupled respiration. In other words, mitochondrial reactive species production is needed to support uncoupled respiration. Consistent with this conclusion, Chouchani and colleagues showed that the addition of the general thiol reductant, N-acetyl-cysteine (NAC), reduced UCP1-mediated uncoupling in mitochondria (Chouchani et al.,

2016). NAC is a general thiol reducing agent and may affect thiols and redox-labile groups outside the mitochondria. Mito-TEMPO is specific for the mitochondria. Hence, our results consolidate the role of mitochondrial reactive species production in inducing uncoupled respiration. In addition, these data highlight the role of reactive species in regulating mitochondrial oxidation. The accepted view is that reactive species inhibit mitochondrial respiration by oxidizing components of the electron transport chain (Wang et al., 2010). Our results indicate that reactive species overproduction can induce uncoupling that spares destructive oxidation of mitochondrial oxidative phosphorylation machinery. Nevertheless, in human subjects, NR had no impact on thermogenesis (Nascimento et al., 2021), leaving the question open about how these findings can be translated to humans.

In this study, we showed that the application of NR to hADMSCs shifted the differentiation of white adipocytes to beige. Furthermore, we showed that SIRT1 induction and reactive species production play key roles in differentiation, mitochondrial biogenesis, substrate preference, and the induction of uncoupled respiration. These results have implications for understanding organismal energy balance mechanisms and may have implications in the metabolic arena.

## Data availability statement

The datasets presented in this study can be found in online repositories. The names of the repository/repositories and accession number(s) can be found below: https://figshare.com/s/b553ecd08aca5c0b1347.

## Ethics statement

The studies involving human participants were reviewed and approved by the Ethics Committee of the University of Debrecen (Hungary) and the National Medical Research Council Committee of Human Reproduction (ETT TUKEB). The patients/participants provided their written informed consent to participate in this study.

## Author contributions

LN and BR performed experiments; TS and AT supplied human samples; PB, KU, and AT conceptualized and supervised research, wrote the paper, and contributed to the manuscript editing.

## Funding

The work was supported by grants from the NKFIH (K123975, K142141, TKP2021-EGA-19, TKP2021-EGA-20). The Project nos. TKP2021-EGA-19 and TKP2021-EGA-20, K132623 were implemented with the support provided by the National Research, Development and Innovation Fund of Hungary, financed under the TKP2021-EGA funding scheme. The POST-COVID2021-33 grant to PB was from the Hungarian Academy of Sciences. The research was financed by the Thematic Excellence Program of the Ministry for Innovation and Technology in Hungary (TKP2020-IKA-04, TKP2020-NKA-04).

## Conflict of interest

The authors declare that the research was conducted in the absence of any commercial or financial relationships that could be construed as a potential conflict of interest. ChromaDex had no impact on the study design and interpretation.

## Publisher's note

All claims expressed in this article are solely those of the authors and do not necessarily represent those of their affiliated organizations, or those of the publisher, the editors and the reviewers. Any product that may be evaluated in this article, or claim that may be made by its manufacturer, is not guaranteed or endorsed by the publisher.

## References

Abdul-Rahman, O., Kristof, E., Doan-Xuan, Q. M., Vida, A., Nagy, L., Horvath, A., et al. (2016). AMP-activated kinase (AMPK) activation by AICAR in human white adipocytes derived from pericardial white adipose tissue stem cells induces a partial beige-like phenotype. *PLoS One* 11 (6), e0157644. doi:10.1371/journal.pone.0157644

Alcala, M., Calderon-Dominguez, M., Serra, D., Herrero, L., and Viana, M. (2019). Mechanisms of impaired Brown adipose tissue recruitment in obesity. *Front. Physiol.* 10, 94. doi:10.3389/fphys.2019.00094

Altshuler-Keylin, S., Shinoda, K., Hasegawa, Y., Ikeda, K., Hong, H., Kang, Q., et al. (2016). Beige adipocyte maintenance is regulated by autophagy-induced mitochondrial clearance. *Cell Metab.* 24 (3), 402–419. doi:10.1016/j.cmet.2016.08.002

Asnani-Kishnani, M., Rodriguez, A. M., Serrano, A., Palou, A., Bonet, M. L., and Ribot, J. (2019). Neonatal resveratrol and nicotinamide riboside supplementations sex-dependently affect beige transcriptional programming of preadipocytes in mouse adipose tissue. *Front. Physiol.* 10, 83. doi:10.3389/fphys.2019.00083

Bai, P., Canto, C., Brunyánszki, A., Huber, A., Szántó, M., Cen, Y., et al. (2011a). PARP-2 regulates SIRT1 expression and whole-body energy expenditure. *Cell Metab.* 13 (4), 450–460. doi:10.1016/j.cmet.2011.03.013

Bai, P., Cantó, C., Oudart, H., Brunyánszki, A., Cen, Y., Thomas, C., et al. (2011b). PARP-1 inhibition increases mitochondrial metabolism through SIRT1 activation. *Cell Metab.* 13 (4), 461–468. doi:10.1016/j.cmet.2011.03.004

Bai, P., Houten, S. M., Huber, A., Schreiber, V., Watanabe, M., Kiss, B., et al. (2007). Poly(ADP-ribose) polymerase-2 [corrected] controls adipocyte

differentiation and adipose tissue function through the regulation of the activity of the retinoid X receptor/peroxisome proliferator-activated receptor-gamma [corrected] heterodimer. *J. Biol. Chem.* 282 (52), 37738–37746. doi:10.1074/jbc.M701021200

Bai, P., Nagy, L., Fodor, T., Liaudet, L., and Pacher, P. (2015). Poly(ADP-ribose) polymerases as modulators of mitochondrial activity. *Trends Endocrinol. Metab.* 26 (2), 75–83. doi:10.1016/j.tem.2014.11.003

Brakedal, B., Dölle, C., Riemer, F., Ma, Y., Nido, G. S., Skeie, G. O., et al. (2022). The NADPARK study: A randomized phase I trial of nicotinamide riboside supplementation in Parkinson's disease. *Cell Metab.* 34 (3), 396–407.e6. e396. doi:10.1016/j.cmet.2022.02.001

Canto, C., Houtkooper, R. H., Pirinen, E., Youn, D. Y., Oosterveer, M. H., Cen, Y., et al. (2012). The NAD(+) precursor nicotinamide riboside Enhances oxidative metabolism and Protects against high-fat diet-induced obesity. *Cell Metab.* 15 (6), 838–847. doi:10.1016/j.cmet.2012.04.022

Cantó, C., Sauve, A., and Bai, P. (2013). Crosstalk between poly(ADP-ribose) polymerase and sirtuin enzymes. *Mol. Asp. Med.* 34 (6), 1168–1201. doi:10.1016/j.mam.2013.01.004

Chiarugi, A., Dolle, C., Felici, R., and Ziegler, M. (2012). The NAD metabolome - a key determinant of cancer cell biology. *Nat. Rev. Cancer* 12 (11), 741–752. doi:10.1038/nrc3340

Chouchani, E. T., Kazak, L., Jedrychowski, M. P., Lu, G. Z., Erickson, B. K., Szpyt, J., et al. (2016). Mitochondrial ROS regulate thermogenic energy expenditure and sulfenylation of UCP1. *Nature* 532 (7597), 112–116. doi:10.1038/nature17399

Cinti, S. (2017). UCP1 protein: The molecular hub of adipose organ plasticity. *Biochimie* 134, 71–76. doi:10.1016/j.biochi.2016.09.008

Claussnitzer, M., Dankel, S. N., Kim, K. H., Quon, G., Meuleman, W., Haugen, C., et al. (2015). FTO obesity variant circuitry and adipocyte browning in humans. *N. Engl. J. Med.* 373 (10), 895–907. doi:10.1056/NEJMoa1502214

Cohen, P., and Spiegelman, B. M. (2016). Cell biology of fat storage. *Mol. Biol. Cell* 27 (16), 2523–2527. doi:10.1091/mbc.E15-10-0749

Dagda, R. K., Cherra, S. J., 3rd, Kulich, S. M., Tandon, A., Park, D., and Chu, C. T. (2009). Loss of PINK1 function promotes mitophagy through effects on oxidative stress and mitochondrial fission. *J. Biol. Chem.* 284 (20), 13843–13855. doi:10.1074/jbc.M808515200

Dagda, R. K. (2019). Mito-morphology macro [online]. Available at: https://imagejdocu.tudor.lu/plugin/morphology/mitochondrial_morphology_macro_plug-in/start (Accessed 06 24, 2020).

Dall, M., Hassing, A. S., Niu, L., Nielsen, T. S., Ingerslev, L. R., Sulek, K., et al. (2021). Hepatocyte-specific perturbation of NAD(+) biosynthetic pathways in mice induces reversible nonalcoholic steatohepatitis-like phenotypes. *J. Biol. Chem.* 297 (6), 101388. doi:10.1016/j.jbc.2021.101388

Dall, M., Trammell, S. A. J., Asping, M., Hassing, A. S., Agerholm, M., Vienberg, S. G., et al. (2019). Mitochondrial function in liver cells is resistant to perturbations in NAD(+) salvage capacity. *J. Biol. Chem.* 294 (36), 13304–13326. doi:10.1074/jbc.RA118.006756

Declercq, P. E., Falck, J. R., Kuwajima, M., Tyminski, H., Foster, D. W., and McGarry, J. D. (1987). Characterization of the mitochondrial carnitine palmitoyltransferase enzyme system. I. Use of inhibitors. *J. Biol. Chem.* 262 (20), 9812–9821. doi:10.1016/s0021-9258(18)48006-4

Desjardins, E. M., and Steinberg, G. R. (2018). Emerging role of AMPK in Brown and beige adipose tissue (BAT): Implications for obesity, insulin resistance, and type 2 diabetes. *Curr. Diab. Rep.* 18 (10), 80. doi:10.1007/s11892-018-1049-6

Fu, M. H., Wu, C. W., Lee, Y. C., Hung, C. Y., Chen, I. C., and Wu, K. L. H. (2018). Nrf2 activation attenuates the early suppression of mitochondrial respiration due to the alpha-synuclein overexpression. *Biomed. J.* 41 (3), 169–183. doi:10.1016/j.bj.2018.02.005

Fu, T., Seok, S., Choi, S., Huang, Z., Suino-Powell, K., Xu, H. E., et al. (2014). MicroRNA 34a inhibits beige and brown fat formation in obesity in part by suppressing adipocyte fibroblast growth factor 21 signaling and SIRT1 function. *Mol. Cell. Biol.* 34 (22), 4130–4142. doi:10.1128/MCB.00596-14

Giordano, A., Smorlesi, A., Frontini, A., Barbatelli, G., and Cinti, S. (2014). White, brown and pink adipocytes: the extraordinary plasticity of the adipose organ. *Eur. J. Endocrinol.* 170 (5), R159–R171. doi:10.1530/EJE-13-0945

Giroud-Gerbetant, J., Joffraud, M., Giner, M. P., Cercillieux, A., Bartova, S., Makarov, M. V., et al. (2019). A reduced form of nicotinamide riboside defines a new path for NAD(+) biosynthesis and acts as an orally bioavailable NAD(+) precursor. *Mol. Metab.* 30, 192–202. doi:10.1016/j.molmet.2019.09.013

Hall, K. D., Farooqi, I. S., Friedman, J. M., Klein, S., Loos, R. J. F., Mangelsdorf, D. J., et al. (2022). The energy balance model of obesity: beyond calories in, calories out. *Am. J. Clin. Nutr.* 115 (5), 1243–1254. doi:10.1093/ajcn/nqac031

Harms, M., and Seale, P. (2013). Brown and beige fat: development, function and therapeutic potential. *Nat. Med.* 19 (10), 1252–1263. doi:10.1038/nm.3361

Houtkooper, R. H., Canto, C., Wanders, R. J., and Auwerx, J. (2010). The secret life of NAD+: an old metabolite controlling new metabolic signaling pathways. *Endocr. Rev.* 31 (2), 194–223. doi:10.1210/er.2009-0026

Huang, D., Camacho, C. V., Setlem, R., Ryu, K. W., Parameswaran, B., Gupta, R. K., et al. (2020). Functional interplay between histone H2B ADP-ribosylation and phosphorylation controls adipogenesis. *Mol. Cell* 79 (6), 934–949. doi:10.1016/j.molcel.2020.08.002

Imran, K. M., Yoon, D., and Kim, Y. S. (2018). A pivotal role of AMPK signaling in medicarpin-mediated formation of brown and beige. *Biofactors* 44 (2), 168–179. doi:10.1002/biof.1392

Ingram, D. K., and Roth, G. S. (2021). Glycolytic inhibition: an effective strategy for developing calorie restriction mimetics. *GeroScience* 43 (3), 1159–1169. doi:10.1007/s11357-020-00298-7

Jankó, L., Kovács, T., Laczik, M., Sári, Z., Ujlaki, G., Kis, G., et al. (2021). Silencing of poly(ADP-ribose) polymerase-2 induces mitochondrial reactive species production and mitochondrial fragmentation. *Cells* 10 (6), 1387. doi:10.3390/cells10061387

Jokinen, R., Pirnes-Karhu, S., Pietiläinen, K. H., and Pirinen, E. (2017). Adipose tissue NAD(+)-homeostasis, sirtuins and poly(ADP-ribose) polymerases -important players in mitochondrial metabolism and metabolic health. *Redox Biol.* 12, 246–263. doi:10.1016/j.redox.2017.02.011

Jukarainen, S., Heinonen, S., Ramo, J. T., Rinnankoski-Tuikka, R., Rappou, E., Tummers, M., et al. (2016). Obesity is associated with low NAD(+)/SIRT pathway expression in adipose tissue of BMI-discordant monozygotic twins. *J. Clin. Endocrinol. Metab.* 101 (1), 275–283. doi:10.1210/jc.2015-3095

Kacsir, I., Sipos, A., Ujlaki, G., Buglyo, P., Somsak, L., Bai, P., et al. (2021). Ruthenium half-sandwich type complexes with bidentate monosaccharide ligands show antineoplastic activity in ovarian cancer cell models through reactive oxygen species production. *Int. J. Mol. Sci.* 22 (19), 10454. doi:10.3390/ijms221910454

Khanh, V. C., Zulkifli, A. F., Tokunaga, C., Yamashita, T., Hiramatsu, Y., and Ohneda, O. (2018). Aging impairs beige adipocyte differentiation of mesenchymal stem cells via the reduced expression of Sirtuin 1. *Biochem. Biophys. Res. Commun.* 500 (3), 682–690. doi:10.1016/j.bbrc.2018.04.136

Kristof, E., Doan-Xuan, Q. M., Bai, P., Bacso, Z., and Fesus, L. (2015). Laser-scanning cytometry can quantify human adipocyte browning and proves effectiveness of irisin. *Sci. Rep.* 5, 12540. doi:10.1038/srep12540

Liao, Z. M., Li, A. N., Cai, Y., Chen, J. J., Xu, Y., Sui, L. H., et al. (2021). Skip participates in formation and lipid metabolism of beige adipose and might mediate the effects of SIRT1 activator BTM-0512 on beige remodeling. *Biochem. Biophys. Res. Commun.* 537, 109–117. doi:10.1016/j.bbrc.2020.12.058

Lidell, M. E., Betz, M. J., Dahlqvist Leinhard, O., Heglind, M., Elander, L., Slawik, M., et al. (2013). Evidence for two types of brown adipose tissue in humans. *Nat. Med.* 19 (5), 631–634. doi:10.1038/nm.3017

Luo, X., Ryu, K. W., Kim, D. S., Nandu, T., Medina, C. J., Gupte, R., et al. (2017). PARP-1 controls the adipogenic transcriptional Program by PARylating C/EBPβ and modulating its transcriptional activity. *Mol. Cell* 65 (2), 260–271. doi:10.1016/j.molcel.2016.11.015

Marton, J., Fodor, T., Nagy, L., Vida, A., Kis, G., Brunyanszki, A., et al. (2018). PARP10 (ARTD10) modulates mitochondrial function. *PLoS One* 13 (1), e0187789. doi:10.1371/journal.pone.0187789

Miko, E., Kovacs, T., Fodor, T., and Bai, P. (2017). Methods to assess the role of poly(ADP-ribose) polymerases in regulating mitochondrial oxidation. *Methods Mol. Biol.* 1608, 185–200. doi:10.1007/978-1-4939-6993-7_13

Mohamed, J. S., Hajira, A., Pardo, P. S., and Boriek, A. M. (2014). MicroRNA-149 inhibits PARP-2 and promotes mitochondrial biogenesis via SIRT-1/PGC-1α network in skeletal muscle. *Diabetes* 63 (5), 1546–1559. doi:10.2337/db13-1364

Mottillo, E. P., Desjardins, E. M., Crane, J. D., Smith, B. K., Green, A. E., Ducommun, S., et al. (2016). Lack of adipocyte AMPK exacerbates insulin resistance and hepatic steatosis through brown and beige adipose tissue function. *Cell Metab.* 24 (1), 118–129. doi:10.1016/j.cmet.2016.06.006

Nagy, L., Marton, J., Vida, A., Kis, G., Bokor, E., Kun, S., et al. (2018). Glycogen phosphorylase inhibition improves beta cell function. *Br. J. Pharmacol.* 175 (2), 301–319. doi:10.1111/bph.13819

Nagy, L., Rauch, B., Balla, N., Ujlaki, G., Kis, G., Abdul-Rahman, O., et al. (2019). Olaparib induces browning of *in vitro* cultures of human primary white adipocytes. *Biochem. Pharmacol.* 25 (19), 76–85. doi:10.1016/j.bcp.2019.06.022

Nascimento, E. B. M., Moonen, M. P. B., Remie, C. M. E., Gariani, K., Jörgensen, J. A., Schaart, G., et al. (2021). Nicotinamide riboside Enhances *in vitro* beta-adrenergic brown adipose tissue activity in humans. *J. Clin. Endocrinol. Metab.* 106 (5), 1437–1447. doi:10.1210/clinem/dgaa960

Nedergaard, J., and Cannon, B. (2018). Brown adipose tissue as a heat-producing thermoeffector. *Handb. Clin. Neurol.* 156, 137–152. doi:10.1016/B978-0-444-63912-7.00009-6

Nemoto, S., Fergusson, M. M., and Finkel, T. (2005). SIRT1 functionally interacts with the metabolic regulator and transcriptional coactivator PGC-1{alpha}. *J. Biol. Chem.* 280 (16), 16456–16460. doi:10.1074/jbc.M501485200

Nikiforov, A., Dolle, C., Niere, M., and Ziegler, M. (2011). Pathways and subcellular compartmentation of NAD biosynthesis in human cells: from entry of extracellular precursors to mitochondrial NAD generation. *J. Biol. Chem.* 286 (24), 21767–21778. doi:10.1074/jbc.M110.213298

Palmeira, C. M., Teodoro, J. S., Amorim, J. A., Steegborn, C., Sinclair, D. A., and Rolo, A. P. (2019). Mitohormesis and metabolic health: The interplay between ROS, cAMP and sirtuins. *Free Radic. Biol. Med.* 141, 483–491. doi:10.1016/j.freeradbiomed.2019.07.017

Petrovic, N., Walden, T. B., Shabalina, I. G., Timmons, J. A., Cannon, B., and Nedergaard, J. (2010). Chronic peroxisome proliferator-activated receptor gamma (PPARgamma) activation of epididymally derived white adipocyte cultures reveals a population of thermogenically competent, UCP1-containing adipocytes molecularly distinct from classic brown adipocytes*. *J. Biol. Chem.* 285 (10), 7153–7164. doi:10.1074/jbc.M109.053942

Qiang, L., Wang, L., Kon, N., Zhao, W., Lee, S., Zhang, Y., et al. (2012). Brown remodeling of white adipose tissue by SirT1-dependent deacetylation of Pparγ. *Cell* 150 (3), 620–632. doi:10.1016/j.cell.2012.06.027

Rappou, E., Jukarainen, S., Rinnankoski-Tuikka, R., Kaye, S., Heinonen, S., Hakkarainen, A., et al. (2016). Weight loss is associated with increased NAD(+)/SIRT1 expression but reduced PARP activity in white adipose tissue. *J. Clin. Endocrinol. Metab.* 101 (3), 1263–1273. doi:10.1210/jc.2015-3054

Rodriguez-Vargas, J. M., Martin-Hernandez, K., Wang, W., Kunath, N., Suganthan, R., Amé, J. C., et al. (2020). Parp3 promotes astrocytic differentiation through a tight regulation of Nox4-induced ROS and mTorc2 activation. *Cell Death Dis.* 11 (11), 954. doi:10.1038/s41419-020-03167-5

Ryoo, I. G., and Kwak, M. K. (2018). Regulatory crosstalk between the oxidative stress-related transcription factor Nfe2l2/Nrf2 and mitochondria. *Toxicol. Appl. Pharmacol.* 359, 24–33. doi:10.1016/j.taap.2018.09.014

Ryu, D., Zhang, H., Ropelle, E. R., Sorrentino, V., Mázala, D. A., Mouchiroud, L., et al. (2016). NAD+ repletion improves muscle function in muscular dystrophy and counters global PARylation. *Sci. Transl. Med.* 8 (361), 361ra139. doi:10.1126/scitranslmed.aaf5504

Ryu, K. W., Nandu, T., Kim, J., Challa, S., DeBerardinis, R. J., and Kraus, W. L. (2018). Metabolic regulation of transcription through compartmentalized NAD(+) biosynthesis. *Science* 360 (6389), eaan5780. doi:10.1126/science.aan5780

Scherer, P. E. (2019). The many secret lives of adipocytes: implications for diabetes. *Diabetologia* 62 (2), 223–232. doi:10.1007/s00125-018-4777-x

Schreiber, V., Ame, J. C., Dolle, P., Schultz, I., Rinaldi, B., Fraulob, V., et al. (2002). Poly(ADP-ribose) polymerase-2 (PARP-2) is required for efficient base excision DNA repair in association with PARP-1 and XRCC1. *J. Biol. Chem.* 277 (25), 23028–23036. doi:10.1074/jbc.M202390200

Serrano, A., Asnani-Kishnani, M., Couturier, C., Astier, J., Palou, A., Landrier, J.-F., et al. (2020). DNA methylation changes are associated with the programming of white adipose tissue browning features by resveratrol and nicotinamide riboside neonatal supplementations in mice. *Nutrients* 12 (2), 461. doi:10.3390/nu12020461

Shabalina, I. G., Petrovic, N., de Jong, J. M., Kalinovich, A. V., Cannon, B., and Nedergaard, J. (2013). UCP1 in brite/beige adipose tissue mitochondria is functionally thermogenic. *Cell Rep.* 5 (5), 1196–1203. doi:10.1016/j.celrep.2013.10.044

Shan, T., Liang, X., Bi, P., and Kuang, S. (2013). Myostatin knockout drives browning of white adipose tissue through activating the AMPK-PGC1α-Fndc5 pathway in muscle. *FASEB J.* 27 (5), 1981–1989. doi:10.1096/fj.12-225755

Shi, W., Hegeman, M. A., van Dartel, D. A. M., Tang, J., Suarez, M., Swarts, H., et al. (2017). Effects of a wide range of dietary nicotinamide riboside (NR) concentrations on metabolic flexibility and white adipose tissue (WAT) of mice fed a mildly obesogenic diet. *Mol. Nutr. Food Res.* 61 (8), 1600878. doi:10.1002/mnfr.201600878

Sun, X., Cao, B., Naval-Sanchez, M., Pham, T., Sun, Y. B. Y., Williams, B., et al. (2021). Nicotinamide riboside attenuates age-associated metabolic and functional changes in hematopoietic stem cells. *Nat. Commun.* 12 (1), 2665. doi:10.1038/s41467-021-22863-0

Szanto, M., and Bai, P. (2020). The role of ADP-ribose metabolism in metabolic regulation, adipose tissue differentiation, and metabolism. *Genes. Dev.* 34 (5-6), 321–340. doi:10.1101/gad.334284.119

Szanto, M., Gupte, R., Kraus, W. L., Pacher, P., and Bai, P. (2021). PARPs in lipid metabolism and related diseases. *Prog. Lipid Res.* 84, 101117. doi:10.1016/j.plipres.2021.101117

Szanto, M., Rutkai, I., Hegedus, C., Czikora, A., Rozsahegyi, M., Kiss, B., et al. (2011). Poly(ADP-ribose) polymerase-2 depletion reduces doxorubicin-induced damage through SIRT1 induction. *Cardiovasc. Res.* 92 (3), 430–438. doi:10.1093/cvr/cvr246

Valero, T. (2014). Mitochondrial biogenesis: pharmacological approaches. *Curr. Pharm. Des.* 20 (35), 5507–5509. doi:10.2174/1381612820351409111421 18

Vannini, N., Campos, V., Girotra, M., Trachsel, V., Rojas-Sutterlin, S., Tratwal, J., et al. (2019). The NAD-booster nicotinamide riboside potently stimulates hematopoiesis through increased mitochondrial clearance. *Cell Stem Cell* 24 (3), 405–418. e407. doi:10.1016/j.stem.2019.02.012

Virag, L., Salzman, A. L., and Szabo, C. (1998). Poly(ADP-ribose) synthetase activation mediates mitochondrial injury during oxidant-induced cell death. *J. Immunol.* 161 (7), 3753–3759.

Waldén, T. B., Hansen, I. R., Timmons, J. A., Cannon, B., and Nedergaard, J. (2012). Recruited vs. nonrecruited molecular signatures of brown, "brite, " and white adipose tissues. *Am. J. Physiol. Endocrinol. Metab.* 302 (1), E19–E31. doi:10.1152/ajpendo.00249.2011

Wang, H., Kuusela, S., Rinnankoski-Tuikka, R., Dumont, V., Bouslama, R., Ramadan, U. A., et al. (2020). Tankyrase inhibition ameliorates lipid disorder via suppression of PGC-1α PARylation in db/db mice. *Int. J. Obes.* 44 (8), 1691–1702. doi:10.1038/s41366-020-0573-z

Wang, T., Si, Y., Shirihai, O. S., Si, H., Schultz, V., Corkey, R. F., et al. (2010). Respiration in adipocytes is inhibited by reactive oxygen species. *Obesity* 18 (8), 1493–1502. doi:10.1038/oby.2009.456

Wu, J., Bostrom, P., Sparks, L. M., Ye, L., Choi, J. H., Giang, A. H., et al. (2012). Beige adipocytes are a distinct type of thermogenic fat cell in mouse and human. *Cell* 150 (2), 366–376. doi:10.1016/j.cell.2012.05.016

Wu, J., Singh, K., Lin, A., Meadows, A. M., Wu, K., Shing, V., et al. (2022). Boosting NAD+ blunts TLR4-induced type I IFN in control and systemic lupus erythematosus monocytes. *J. Clin. Invest.* 132 (5), e139828. doi:10.1172/jci139828

Wu, L., Zhang, L., Li, B., Jiang, H., Duan, Y., Xie, Z., et al. (2018). AMP-activated protein kinase (AMPK) regulates energy metabolism through modulating thermogenesis in adipose tissue. *Front. Physiol.* 9, 122. doi:10.3389/fphys.2018.00122

Yamaguchi, S., Franczyk, M. P., Chondronikola, M., Qi, N., Gunawardana, S. C., Stromsdorfer, K. L., et al. (2019). Adipose tissue NAD(+) biosynthesis is required for regulating adaptive thermogenesis and whole-body energy homeostasis in mice. *Proc. Natl. Acad. Sci. U. S. A.* 116 (47), 23822–23828. doi:10.1073/pnas.1909917116

Yan, M., Audet-Walsh, E., Manteghi, S., Dufour, C. R., Walker, B., Baba, M., et al. (2016). Chronic AMPK activation via loss of FLCN induces functional beige adipose tissue through PGC-1α/ERRα. *Genes. Dev.* 30 (9), 1034–1046. doi:10.1101/gad.281410.116

Yeh, T. Y., Beiswenger, K. K., Li, P., Bolin, K. E., Lee, R. M., Tsao, T. S., et al. (2009). Hypermetabolism, hyperphagia, and reduced adiposity in tankyrase-deficient mice. *Diabetes* 11, 2476–2485. doi:10.2337/db08-1781

Zhu, Q., Ghoshal, S., Rodrigues, A., Gao, S., Asterian, A., Kamenecka, T. M., et al. (2016). Adipocyte-specific deletion of Ip6k1 reduces diet-induced obesity by enhancing AMPK-mediated thermogenesis. *J. Clin. Invest.* 126 (11), 4273–4288. doi:10.1172/JCI85510

Ziegler, M. (2000). New functions of a long-known molecule. Emerging roles of NAD in cellular signaling. *Eur. J. Biochem.* 267 (6), 1550–1564. doi:10.1046/j.1432-1327.2000.01187.x

frontiers | Frontiers in Endocrinology

TYPE Mini Review
PUBLISHED 21 February 2023
DOI 10.3389/fendo.2023.1106544

Check for updates

OPEN ACCESS

EDITED BY
Endre Károly Kristóf,
University of Debrecen, Hungary

REVIEWED BY
Rosemari Otton,
Universidade Cruzeiro do Sul, Brazil

*CORRESPONDENCE
Ji Suk Chang
jisuk.chang@pbrc.edu

SPECIALTY SECTION
This article was submitted to Cellular Endocrinology, a section of the journal Frontiers in Endocrinology

RECEIVED 23 November 2022
ACCEPTED 10 February 2023
PUBLISHED 21 February 2023

CITATION
Chang JS (2023) Recent insights into the molecular mechanisms of simultaneous fatty acid oxidation and synthesis in brown adipocytes.
*Front. Endocrinol.* 14:1106544.
doi: 10.3389/fendo.2023.1106544

COPYRIGHT
© 2023 Chang. This is an open-access article distributed under the terms of the Creative Commons Attribution License (CC BY). The use, distribution or reproduction in other forums is permitted, provided the original author(s) and the copyright owner(s) are credited and that the original publication in this journal is cited, in accordance with accepted academic practice. No use, distribution or reproduction is permitted which does not comply with these terms.

# Recent insights into the molecular mechanisms of simultaneous fatty acid oxidation and synthesis in brown adipocytes

Ji Suk Chang*

Gene Regulation and Metabolism Laboratory, Pennington Biomedical Research Center, Baton Rouge, LA, United States

Brown adipocytes is a specialized fat cell that dissipates nutrient-derived chemical energy in the form of heat, instead of ATP synthesis. This unique feature provides a marked capacity for brown adipocyte mitochondria to oxidize substrates independent of ADP availability. Upon cold exposure, brown adipocytes preferentially oxidize free fatty acids (FFA) liberated from triacylglycerol (TAG) in lipid droplets to support thermogenesis. In addition, brown adipocytes take up large amounts of circulating glucose, concurrently increasing glycolysis and *de novo* FA synthesis from glucose. Given that FA oxidation and glucose-derived FA synthesis are two antagonistic mitochondrial processes in the same cell, it has long been questioned how brown adipocytes run FA oxidation and FA synthesis simultaneously. In this review, I summarize mechanisms regulating mitochondrial substrate selection and describe recent findings of two distinct populations of brown adipocyte mitochondria with different substrate preferences. I further discuss how these mechanisms may permit a concurrent increase in glycolysis, FA synthesis, and FA oxidation in brown adipocytes.

KEYWORDS

**brown adipocytes, fatty acid oxidation, *de novo* fatty acid synthesis, mitochondrial substrate utilization, uncoupled respiration**

## Introduction

While white adipocytes primarily store excess energy in the form of triacylglycerol (TAG), brown adipocytes located in the interscapular brown adipose tissue (BAT) have a marked capacity to oxidize nutrients and dissipate energy as heat (1). Brown-like beige adipocytes also emerge within white adipose tissue (WAT) during prolonged cold exposure or pharmacological stimulation of $\beta_3$-adrenergic receptors (2–5). Notably, activation of brown and beige adipocytes in rodents (6, 7) and humans (8–14) increases energy expenditure and improves systemic glucose and lipid homeostasis. Thus, brown/beige adipocytes have emerged as an appealing target against obesity and its related metabolic disorders, such as type 2 diabetes, insulin resistance, and dyslipidemia.

Upon activation, brown adipocytes simultaneously increase glycolysis, glucose-derived *de novo* fatty acid synthesis (FAS), and fatty acid oxidation (FAO) (15–19), which are mutually exclusive pathways in the same cell (20). In most mammalian cells, elevated glycolysis and subsequent pyruvate oxidation in the mitochondria block mitochondrial FAO. Conversely, elevated FAO decreases the activity of glycolytic enzymes in the cytosol and pyruvate dehydrogenase (PDH) within the mitochondrial matrix, thus leading to inhibition of pyruvate production, oxidation, and *de novo* FAS. It is not fully understood how brown adipocytes simultaneously increase glycolysis and FAS while primarily oxidizing FA in the mitochondria. To target brown adipocytes therapeutically, it is important to understand the underlying mechanism responsible for this unique phenomenon. This mini review will focus on recent advances in our understanding of substrate utilization in brown adipocytes and discuss molecular mechanisms that may permit the concurrence of glycolysis, FAS, and FAO in brown adipocytes.

## UCP1-mediated proton leak: A mechanism for high substrate oxidation in brown adipocytes

In mammalian cells, oxidation pathways of glucose, FA, and amino acids converge onto a common pathway, the tricarboxylic acid (TCA) cycle, which generates NADH and $FADH_2$ in the mitochondrial matrix. These reduced electron carriers donate their electrons to the electron transport chain (ETC) system, which is composed of four multi-subunit complexes (I-IV) located in the inner mitochondrial membrane (IMM) and two mobile electron carriers coenzyme Q and cytochrome c (21, 22). Subsequent electron transfer through the ETC leads to pumping of protons ($H^+$ ions) from the mitochondrial matrix to the intermembrane space, creating an electrochemical proton gradient, also known as the proton motive force (PMF). The PMF is a form of potential energy composed of an electrical charge gradient ($\Delta\Psi_m$) and a chemical gradient ($\Delta$pH) across the IMM (23). The resulting PMF is used by $F_0F_1$-ATP synthase (Figure 1A; coupled respiration). The protons pass from the intermembrane space into the matrix through the $F_0$ component, causing a conformational change in $F_0F_1$-ATP synthase so that ATP is produced from ADP and inorganic phosphate (24). For the coupling of ETC-mediated proton pumps to the ATP synthesis, the rate of substrate oxidation and electron flow is highly dependent on the availability of ADP (25). Fluctuations in coupling between ETC activity and ATP production can cause electron leak from the ETC onto oxygen, resulting in production of reactive oxygen species (ROS) (26).

Brown adipocytes contain a large number of mitochondria that uniquely express uncoupling protein 1 (UCP1) in the IMM (27, 28) along with abundant expression of TCA cycle enzymes and ETC complexes (I-IV) (1). Membrane-bound UCP1, an $H^+$ transport protein, allows the re-entry of protons into the mitochondrial matrix independent of ATP synthesis (Figure 1B; uncoupled respiration) (29, 30). Thus, UCP1-mediated proton leak causes a

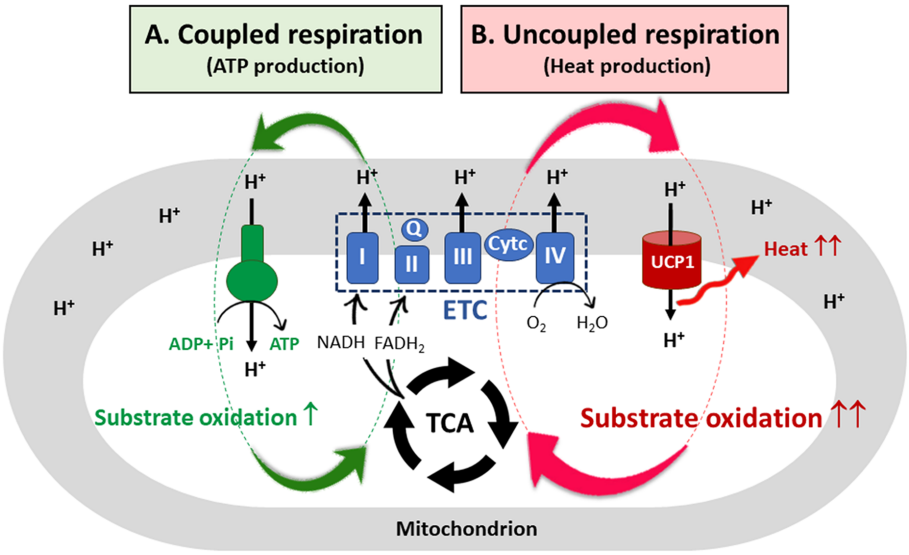


FIGURE 1
UCP1-mediated uncoupled respiration and its contribution to substrate oxidation. **(A)** In most mammalian cells, a proton motive force (PMF) created by the electron transfer chain (ETC) system is used by ATP synthase, resulting in ATP production (coupled respiration). To re-establish the electrochemical proton gradient across the inner mitochondrial membrane (IMM), the cells increase substrate oxidation, generating more NADH and $FADH_2$ needed by the ETC. However, for coupled respiration, the rate of substrate oxidation and electron flow through the ETC is highly dependent on ADP availability. **(B)** In brown adipocytes, the protons pass from the intermembrane space into the mitochondrial matrix through the membrane bound UCP1. The resulting proton leak causes a drop in the PMF, releasing heat but not ATP synthesis (uncoupled respiration). The futile cycle of ETC-mediated proton pumps and UCP1-mediated proton leak provides a marked capacity for brown adipocyte mitochondria to oxidize substrates independent of ADP availability. TCA, the tricarboxylic acid cycle; I, II, III, IV, ETC multi-subunit complexes I through IV; Q, coenzyme Q; Cyt c, cytochrome c; UCP1, uncoupled protein 1.

drop in the PMF, and energy is lost as heat. As a mechanism to re-establish the electrochemical proton gradient (ΔpH) across the IMM, brown adipocytes increase the rate of substrate oxidation, generating more NADH and $FADH_2$ needed by the ETC. Consequently, the futile cycle of ETC-mediated proton pumps and UCP1-mediated proton leak provides a marked capacity for brown adipocyte mitochondria to oxidize substrates without being affected by ADP availability. In addition, dissipation of the PMF by UCP1 has been shown to reduce mitochondrial ROS production, contributing to an increase in ETC complexes (31–33).

## Mitochondrial substrate utilization in brown adipocytes: Fatty acids vs glucose?

Brown adipocytes oxidize substantial amounts of substrates due to high ETC activity (proton pumping) and UCP1 activity (proton leak) in the IMM. Upon adrenergic stimulation of the cell by cold-dependent activation of the sympathetic nervous system or $\beta_3$-adrenergic receptor agonists, brown adipocytes liberate free fatty acids (FFA) by lipolysis of TAG stored in lipid droplets as well as take up extracellular nonesterified fatty acids (NEFA) from the circulation (1, 34–38). FFA released from the intracellular TAG is the main source of FA for thermogenesis. Circulating NEFA is directed toward TAG replenishment in brown adipocytes although a portion of NEFA contributes to thermogenesis (35, 39). These FAs are ligated to CoA groups before being converted to acyl-carnitine for mitochondrial import through carnitine palmitoyltransferase 1 (CPT1) located in the outer mitochondrial membrane (OMM). Subsequent FA β-oxidation in the matrix produces acetyl-CoA, which then enters the TCA cycle as citrate after condensation with oxaloacetate (OAA). FAO results in a larger increase in acetyl-CoA levels per molecule of nutrient than glucose-derived pyruvate oxidation (i.e., 1 $C_{16}$-palmitic acid generates 8 acetyl-CoA; 1 glucose generates 2 acetyl-CoA). Accordingly, FAO is more efficient in generating NADH and $FADH_2$ and FA has been viewed as the primary substrate for energy-demanding brown adipocyte mitochondria (1, 6). Moreover, it is interesting to note that FA is not only the energy substrate for thermogenesis but also activates the UCP1-mediated proton leak across the IMM (29, 40).

Surprisingly, activated brown adipocytes also take up large amounts of glucose from the circulation while primarily utilizing FA to fuel thermogenesis (19, 41–45). However, recent studies have further found that the primary function of this glucose is not to support thermogenesis (<15%) but instead fuel *de novo* lipogenesis (DNL) through multiple mechanisms (16, 17, 19, 38, 42, 46–49): i) Pyruvate-derived citrate serves as the precursor for *de novo* FA synthesis (FAS); ii) Glucose-derived glycerol-3-phosphate serves as the structural backbone for TAG synthesis; iii) Glycolytic intermediates support the pentose phosphate pathway generating NADPH needed for DNL; and iv) Cytosolic ATP production during glycolysis meets energy requirement for DNL as well as compensates for the loss of mitochondrial ATP synthesis. Therefore, it has been suggested that, while oxidizing FA to fuel thermogenesis, brown adipocytes concurrently increase glycolysis and *de novo* FAS to replenish intracellular TAG pool in lipid droplets (15–19). However, it is currently unclear how brown adipocytes concurrently perform FAO and FAS in the same cell because these processes are two mutually exclusive pathways in healthy cells.

More interestingly, recent studies have shown that cold-activated BAT in rodents and humans utilizes additional substrates such as branched-chain amino acids (BCAA) (50, 51), glutamate (44), and succinate (52) to support thermogenesis. Extracellular succinate contributes to thermogenic respiration in BAT by the succinate dehydrogenase (SDH)-mediated oxidation in the TCA cycle (52), although its relative contribution to thermogenesis is unclear. Similarly, BCAAs and glutamate enter the TCA cycle as acetyl-CoA/succinyl-CoA and α-ketoglutarate, respectively, to generate more reducing equivalents in BAT (44, 50, 51). It is also possible that carbons from these additional substrates replenish TCA cycle intermediates that leave the cycle for biosynthetic pathways (e.g., citrate for *de novo* FA synthesis).

## Molecular mechanisms regulating mitochondrial substrate selection

In most mammalian cells, mitochondrial FAO suppresses glycolysis, pyruvate oxidation, and *de novo* FAS (20). FAO-induced increases in acetyl-CoA/CoA, NADH/$NAD^+$, and ATP/ADP ratios inhibit the activity of pyruvate dehydrogenase (PDH) that catalyzes the conversion of glucose-derived pyruvate to acetyl-CoA in the mitochondria (53, 54). The resulting decrease in acetyl-CoA reduces the production of pyruvate-derived citrate that exits the mitochondria to serve as the precursor for FAS. Thus, FAO-dependent inhibition of PDH activity in the mitochondria is the primary mechanism preventing both pyruvate oxidation and *de novo* FAS from glucose. Additionally, FAO can inhibit glycolysis. A portion of excess citrate produced from FA-derived acetyl-CoA is exported to the cytosol, where it in turn inhibits glycolytic enzymes, such as phosphofructokinases (PFK1, PFK2) and pyruvate kinase (PK) (20, 55–57).

Conversely, when extracellular glucose increases, enhanced glycolysis provides more pyruvate to the mitochondria. The conversion of pyruvate to acetyl-CoA by PDH and to OAA by pyruvate carboxylase (PC) increases citrate production in the mitochondria. Under high glucose, excess citrate is exported to the cytosol and hydrolyzed back to acetyl-CoA and OAA by ATP-citrate lyase (ACLY). Acetyl-CoA is then carboxylated to malonyl-CoA by two acetyl-CoA carboxylases, ACC1 and ACC2 (58). Malonyl-CoA is the precursor of *de novo* synthesized FA. Remarkably, malonyl-CoA produced by ACC2 allosterically inhibits CPT1 (59, 60) that controls the entry of long-chain fatty acids from the cytosol into mitochondria. By this mechanism, glucose-derived malonyl-CoA prevents the oxidation of newly synthesized and pre-existing FAs. Thus, malonyl-CoA is a key metabolite regulating the balance between FAS and FAO.

Although ACC1 and ACC2 have same enzyme activity with over 70% protein sequence similarity, they play distinct roles in the control of FAS and FAO (58, 61, 62). ACC1 is cytosolic and directs malonyl-CoA toward *de novo* FA synthesis catalyzed by fatty acid synthase (FAS). In contrast, ACC2 is associated with the OMM and regulates FAO through malonyl-CoA-mediated CPT1 inhibition (59–61, 63). While lipogenic WAT predominantly expresses ACC1, BAT expresses similar amounts of ACC1 and ACC2 (64). In addition, BAT expresses CPT1β, an isoform with high sensitivity to malonyl-CoA (65–67). Despite the expression of ACC2 and CPT1β, BAT mitochondria have the highest CPT1 activity among the tissues expressing CPT1β (65–67). High FAO in BAT is surprising in light of the inhibitory effect of malonyl-CoA produced by ACC2 on CPT1β-mediated FA transport. It is unclear whether ACC2 activity or association to the mitochondria is negatively regulated by cold in brown adipocytes.

It is interesting to note that concurrent FAO and FAS have also been observed in a subset of cancer cells (68–70). Glycolytic colorectal cancer cells recruit FAO as an adaptive response to extracellular acidification associated with increased pyruvate to lactate conversion (68). A selective decrease in the transcription of *ACACB* gene under acidosis was in part the mechanism permitting mitochondrial FAO. However, it is unlikely that the selective decrease in *ACACB* gene expression provides a mechanism by which brown adipocytes concurrently perform FAO and FAS because BAT upregulates the expression of both *ACACA* and *ACACB* genes encoding ACC1 and ACC2, respectively, in response to cold (17). As another example, a subset of highly proliferating B-cell lymphomas concurrently stimulates mitochondrial FAO while increasing glycolysis and FAS (69); however, the underlying mechanism remains unknown.

## Heterogeneity of brown adipocytes in BAT

Single-cell and single-nucleus RNA sequencing of BAT has uncovered the existence of multiple brown adipocyte subpopulations with large variability in their transcriptomes and with different degrees of thermogenic capacities (71–73). Compared with the high-thermogenic brown adipocytes, low-thermogenic brown adipocytes express lower levels of Ucp1 along with reduced mitochondrial respiration (71). It is considered that these subpopulations are derived from distinct precursor cells and/or represent different cell states acquired during environmental temperature changes (71–73). The co-existence of functionally different brown adipocytes within the BAT may in part explain how BAT performs FAO and FAS simultaneously. Further studies are required to delineate the location, functional specialization, and substrate utilization of these brown adipocyte subpopulations and their ratios in response to environmental stimuli.

## Heterogeneity of mitochondria within the brown adipocyte: FA-oxidizing vs lipogenic mitochondria

In addition to heterogeneity of brown adipocytes, recent studies have demonstrated the presence of metabolically distinct populations of mitochondria within the same brown adipocyte: cytosolic mitochondria (CM) and peridroplet mitochondria (PDM) (74–78). PDM are found to be anchored to the lipid droplets and have reduced motility and fusion-fission dynamics that segregate PDM from the rest of the mitochondrial population (79, 80). While CM preferentially oxidize FA for theromgenesis, PDM have a higher capacity for pyruvate oxidation and ATP synthesis (74) (Figure 2). In line with increased oxidative phosphorylation, PDM is enriched with ATP synthase compared to CM (74) although UCP1 levels are comparable in PDM and CM (74, 78). More interestingly, an increase in PDM is associated with lipid droplet expansion in brown adipocytes (74). Given that coupled respiration is dependent on ADP availability, excess citrate produced from pyruvate-derived acetyl-CoA in the PDM may exit the mitochondria and be converted to malonyl-CoA by ACC1 and ACC2, thus contributing to *de novo* FAS for TAG synthesis and concurrently preventing FA entry into these specific subpopulations of mitochondria (Figure 2). On the contrary, in CM preferentially oxidizing FA (74), FA-derived acetyl-CoA could inhibit PDH activity, resulting in a decrease in pyruvate-derived citrate production and subsequent malonyl-CoA accumulation in close vicinity of CM (Figure 2). It is unclear whether there is a difference in ACC2 levels between PDM and CM. CM could maximize UCP1-mediated thermogenesis by producing high levels of NADH and $FADH_2$ from FAO. The resulting rapid oxidation of FA-derived citrate through the TCA cycle may prevent citrate export to the cytosol for inhibition of glycolytic enzymes.

The association between mitochondria and lipid droplets has been overserved in other tissue/cell types including skeletal muscle, heart, and adipocytes (77, 81–83). In contrast to the lipogenic role of PDM in brown adipocytes, several studies reported conflicting results that PDM promotes the oxidation of FA released from lipid droplets (77, 81). This discrepancy may imply that the role of PDM is differently regulated by the cell type, nutritional status, or cellular stress. Proteome profiling of PDM and CM in BAT has identified a subset of mitochondrial proteins differentially expressed between PDM and CM although their impact on the functional difference has not been explored (78). Additional studies are required to quantitatively characterize PDM and CM mitochondrial proteins (e.g., MPC1/2, ACC2, CPT1β) and understand the significance of relative PDM/CM ratio and the mechanism controlling this ratio in brown adipocytes.

## Conclusion

Brown adipocytes have two unique features: (1) UCP1-mediated dissipation of the PMF, which provides a mechanism for maximal substrate oxidation in the mitochondria and (2)

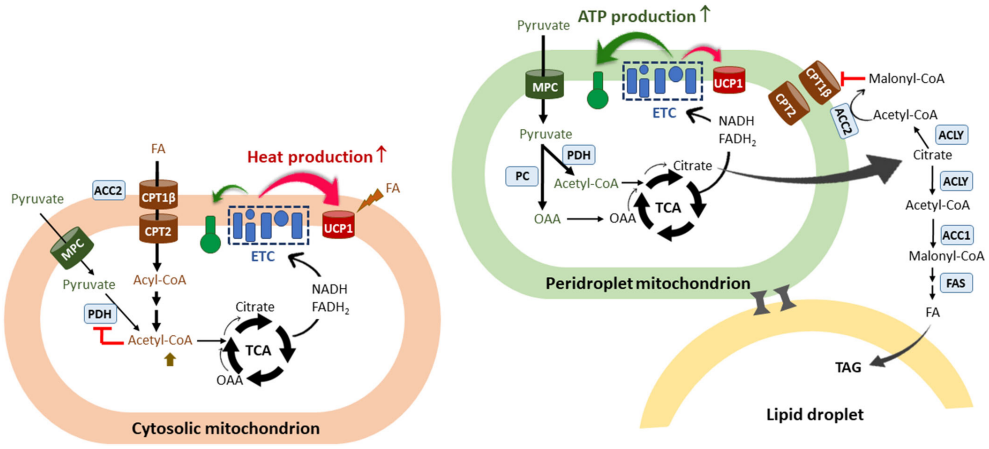


FIGURE 2
The co-existence of two functionally different mitochondria within the brown adipocyte. A scheme of two types of mitochondria identified in the brown adipocyte: cytosolic mitochondria (CM) and peridroplet mitochondria (PDM) (74–78). PDM are anchored to the lipid droplets and segregated from the pool of CM. CM preferentially oxidize FA and are more thermogenic compared to PDM. FAO-induced increases in acetyl-CoA/CoA and NADH/NAD$^+$ ratios would inhibit PDH in the matrix, resulting in a decrease in pyruvate-derived citrate production and subsequent malonyl-CoA accumulation in close vicinity of CM. FA-derived citrate would be rapidly oxidized through the TCA cycle to support UCP1-mediated thermogenesis. On the contrary, PDM have a higher capacity for pyruvate oxidation and ATP synthesis compared to CM. Given that coupled respiration is dependent on ADP availability, excess citrate would escape from the mitochondria and be converted to malonyl-CoA by ACC1 and ACC2, thus contributing to *de novo* lipogenesis and simultaneously preventing CPT1β-mediated FA entry into PDM. The co-existence of two functionally different mitochondria within the brown adipocyte may in part explain the concurrence of glycolysis, FA synthesis, and FA oxidation in brown adipocytes. FA, fatty acids; ETC, electron transport chain; CPT, carnitine palmitoyltransferase; UCP1, uncoupled protein 1; TCA, the tricarboxylic acid cycle; OAA, oxaloacetate; MPC, mitochondrial pyruvate carrier; PDH, pyruvate dehydrogenase; PC, pyruvate carboxylase; ACLY, ATP-citrate lyase; ACC, acetyl-CoA carboxylases; FAS, fatty acid synthase; TAG, triacylglycerol.

concurrence of glycolysis, *de novo* FAS, and FAO. Upon activation, brown adipocytes increase glycolysis and *de novo* FAS to replenish intracellular TAG pools that are depleted due to increased lipolysis and FAO. The co-existence of FA-oxidizing and lipogenic mitochondria within the brown adipocyte in addition to heterogeneity of brown adipocytes may in part explain the unique capacity of brown adipocytes to be involved simultaneously in FAO and FAS.

## Author contributions

The author confirms being the sole contributor of this work and has approved it for publication.

## Conflict of interest

The author declares that the research was conducted in the absence of any commercial or financial relationships that could be construed as a potential conflict of interest.

## Publisher's note

All claims expressed in this article are solely those of the authors and do not necessarily represent those of their affiliated organizations, or those of the publisher, the editors and the reviewers. Any product that may be evaluated in this article, or claim that may be made by its manufacturer, is not guaranteed or endorsed by the publisher.

## References

1. Cannon B, Nedergaard J. Brown adipose tissue: Function and physiological significance. *Physiol Rev* (2004) 84(1):277–359. doi: 10.1152/physrev.00015.200384/1/277[pii]

2. Wu J, Bostrom P, Sparks LM, Ye L, Choi JH, Giang AH, et al. Beige adipocytes are a distinct type of thermogenic fat cell in mouse and human. *Cell* (2012) 150(2):366–76. doi: 10.1016/j.cell.2012.05.016S0092-8674(12)00595-8[pii]

3. Himms-Hagen J, Cui J, Danforth EJr., Taatjes DJ, Lang SS, Waters BL, et al. Effect of cl-316,243, a thermogenic beta 3-agonist, on energy balance and brown and white adipose tissues in rats. *Am J Physiol* (1994) 266(4 Pt 2):R1371–82. doi: 10.1152/ajpregu.1994.266.4.R1371

4. Himms-Hagen J, Melnyk A, Zingaretti MC, Ceresi E, Barbatelli G, Cinti S. Multilocular fat cells in wat of cl-316243-Treated rats derive directly from white adipocytes. *Am J Physiol Cell Physiol* (2000) 279(3):C670–81. doi: 10.1152/ajpcell.2000.279.3.C670

5. Granneman JG, Li P, Zhu Z, Lu Y. Metabolic and cellular plasticity in white adipose tissue I: Effects of Beta3-adrenergic receptor activation. *Am J Physiol Endocrinol Metab* (2005) 289(4):E608–16. doi: 10.1152/ajpendo.00009.2005

6. Townsend KL, Tseng YH. Brown fat fuel utilization and thermogenesis. *Trends Endocrinol Metab* (2014) 25(4):168–77. doi: 10.1016/j.tem.2013.12.004

7. Stanford KI, Middelbeek RJ, Townsend KL, An D, Nygaard EB, Hitchcox KM, et al. Brown adipose tissue regulates glucose homeostasis and insulin sensitivity. *J Clin Invest* (2013) 123(1):215–23. doi: 10.1172/JCI62308

8. van Marken Lichtenbelt WD, Vanhommerig JW, Smulders NM, Drossaerts JM, Kemerink GJ, Bouvy ND, et al. Cold-activated brown adipose tissue in healthy men. *N Engl J Med* (2009) 360(15):1500–8. doi: 10.1056/NEJMoa0808718360/15/1500[pii]

9. Chondronikola M, Volpi E, Borsheim E, Porter C, Annamalai P, Enerback S, et al. Brown adipose tissue improves whole-body glucose homeostasis and insulin sensitivity in humans. *Diabetes* (2014) 63(12):4089–99. doi: 10.2337/db14-0746

10. Ouellet V, Labbe SM, Blondin DP, Phoenix S, Guerin B, Haman F, et al. Brown adipose tissue oxidative metabolism contributes to energy expenditure during acute cold exposure in humans. *J Clin Invest* (2012) 122(2):545–52. doi: 10.1172/JCI6043360433[pii]

11. Hanssen MJ, Hoeks J, Brans B, van der Lans AA, Schaart G, van den Driessche JJ, et al. Short-term cold acclimation improves insulin sensitivity in patients with type 2 diabetes mellitus. *Nat Med* (2015) 21(8):863–5. doi: 10.1038/nm.3891

12. Cypess AM, Weiner LS, Roberts-Toler C, Franquet Elia E, Kessler SH, Kahn PA, et al. Activation of human brown adipose tissue by a Beta3-adrenergic receptor agonist. *Cell Metab* (2015) 21(1):33–8. doi: 10.1016/j.cmet.2014.12.009

13. O'Mara AE, Johnson JW, Linderman JD, Brychta RJ, McGehee S, Fletcher LA, et al. Chronic mirabegron treatment increases human brown fat, hdl cholesterol, and insulin sensitivity. *J Clin Invest* (2020) 130(5):2209–19. doi: 10.1172/JCI131126

14. Cypess AM, Lehman S, Williams G, Tal I, Rodman D, Goldfine AB, et al. Identification and importance of brown adipose tissue in adult humans. *N Engl J Med* (2009) 360(15):1509–17. doi: 10.1056/NEJMoa0810780360/15/1509[pii]

15. Buckley MG, Rath EA. Regulation of fatty acid synthesis and malonyl-coa content in mouse brown adipose tissue in response to cold-exposure, starvation or re-feeding. *Biochem J* (1987) 243(2):437–42. doi: 10.1042/bj2430437

16. Mottillo EP, Balasubramanian P, Lee YH, Weng C, Kershaw EE, Granneman JG. Coupling of lipolysis and *De novo* lipogenesis in brown, beige, and white adipose tissues during chronic Beta3-adrenergic receptor activation. *J Lipid Res* (2014) 55(11):2276–86. doi: 10.1194/jlr.M050005

17. Yu XX, Lewin DA, Forrest W, Adams SH. Cold elicits the simultaneous induction of fatty acid synthesis and beta-oxidation in murine brown adipose tissue: Prediction from differential gene expression and confirmation *in vivo*. *FASEB J* (2002) 16(2):155–68. doi: 10.1096/fj.01-0568com16/2/155[pii]

18. Mccormack JG, Denton RM. Evidence that fatty-acid synthesis in interscapular brown adipose-tissue of cold-adapted rats is increased invivo by insulin by mechanisms involving parallel activation of pyruvate-dehydrogenase and acetyl-coenzyme-a carboxylase. *Biochem J* (1977) 166(3):627–30. doi: 10.1042/bj1660627

19. Jung SM, Doxsey WG, Le J, Haley JA, Mazuecos L, Luciano AK, et al. *In vivo* isotope tracing reveals the versatility of glucose as a brown adipose tissue substrate. *Cell Rep* (2021) 36(4):109459. doi: 10.1016/j.celrep.2021.109459

20. Hue L, Taegtmeyer H. The randle cycle revisited: A new head for an old hat. *Am J Physiol Endocrinol Metab* (2009) 297(3):E578–91. doi: 10.1152/ajpendo.00093.2009

21. Cogliati S, Frezza C, Soriano ME, Varanita T, Quintana-Cabrera R, Corrado M, et al. Mitochondrial cristae shape determines respiratory chain supercomplexes assembly and respiratory efficiency. *Cell* (2013) 155(1):160–71. doi: 10.1016/j.cell.2013.08.032

22. Zhao RZ, Jiang S, Zhang L, Yu ZB. Mitochondrial electron transport chain, ros generation and uncoupling (Review). *Int J Mol Med* (2019) 44(1):3–15. doi: 10.3892/ijmm.2019.4188

23. Mitchell P. Coupling of phosphorylation to electron and hydrogen transfer by a chemi-osmotic type of mechanism. *Nature* (1961) 191:144–8. doi: 10.1038/191144a0

24. Jonckheere AI, Smeitink JA, Rodenburg RJ. Mitochondrial atp synthase: Architecture, function and pathology. *J Inherit Metab Dis* (2012) 35(2):211–25. doi: 10.1007/s10545-011-9382-9

25. Leverve X, Sibille B, Devin A, Piquet MA, Espie P, Rigoulet M. Oxidative phosphorylation in intact hepatocytes: Quantitative characterization of the mechanisms of change in efficiency and cellular consequences. *Mol Cell Biochem* (1998) 184(1-2):53–65. doi: 10.1023/A:1006810209531

26. Wong HS, Dighe PA, Mezera V, Monternier PA, Brand MD. Production of superoxide and hydrogen peroxide from specific mitochondrial sites under different bioenergetic conditions. *J Biol Chem* (2017) 292(41):16804–9. doi: 10.1074/jbc.R117.789271

27. Golozoubova V, Hohtola E, Matthias A, Jacobsson A, Cannon B, Nedergaard J. Only Ucp1 can mediate adaptive nonshivering thermogenesis in the cold. *FASEB J* (2001) 15(11):2048–50. doi: 10.1096/fj.00-0536fje00-0536fje[pii]

28. Nedergaard J, Golozoubova V, Matthias A, Asadi A, Jacobsson A, Cannon B. Ucp1: The only protein able to mediate adaptive non-shivering thermogenesis and metabolic inefficiency. *Biochim Biophys Acta* (2001) 1504(1):82–106. doi: 10.1016/S0005-2728(00)00247-4

29. Fedorenko A, Lishko PV, Kirichok Y. Mechanism of fatty-Acid-Dependent Ucp1 uncoupling in brown fat mitochondria. *Cell* (2012) 151(2):400–13. doi: 10.1016/j.cell.2012.09.010

30. Nicholls DG. The physiological regulation of uncoupling proteins. *Biochim Biophys Acta* (2006) 1757(5-6):459–66. doi: 10.1016/j.bbabio.2006.02.005

31. Dlaskova A, Clarke KJ, Porter RK. The role of ucp 1 in production of reactive oxygen species by mitochondria isolated from brown adipose tissue. *Biochim Biophys Acta* (2010) 1797(8):1470–6. doi: 10.1016/j.bbabio.2010.04.008

32. Oelkrug R, Kutschke M, Meyer CW, Heldmaier G, Jastroch M. Uncoupling protein 1 decreases superoxide production in brown adipose tissue mitochondria. *J Biol Chem* (2010) 285(29):21961–8. doi: 10.1074/jbc.M110.122861

33. Kazak L, Chouchani ET, Stavrovskaya IG, Lu GZ, Jedrychowski MP, Egan DF, et al. Ucp1 deficiency causes brown fat respiratory chain depletion and sensitizes mitochondria to calcium overload-induced dysfunction. *Proc Natl Acad Sci U.S.A.* (2017) 114(30):7981–6. doi: 10.1073/pnas.1705406114

34. Bartelt A, Bruns OT, Reimer R, Hohenberg H, Ittrich H, Peldschus K, et al. Brown adipose tissue activity controls triglyceride clearance. *Nat Med* (2011) 17(2):200–5. doi: 10.1038/nm.2297nm.2297[pii]

35. Wu Q, Kazantzis M, Doege H, Ortegon AM, Tsang B, Falcon A, et al. Fatty acid transport protein 1 is required for nonshivering thermogenesis in brown adipose tissue. *Diabetes* (2006) 55(12):3229–37. doi: 10.2337/db06-0749

36. Chondronikola M, Volpi E, Borsheim E, Porter C, Saraf MK, Annamalai P, et al. Brown adipose tissue activation is linked to distinct systemic effects on lipid metabolism in humans. *Cell Metab* (2016) 23(6):1200–6. doi: 10.1016/j.cmet.2016.04.029

37. Zechner R, Kienesberger PC, Haemmerle G, Zimmermann R, Lass A. Adipose triglyceride lipase and the lipolytic catabolism of cellular fat stores. *J Lipid Res* (2009) 50(1):3–21. doi: 10.1194/jlr.R800031-JLR200

38. Li Y, Fromme T, Schweizer S, Schottl T, Klingenspor M. Taking control over intracellular fatty acid levels is essential for the analysis of thermogenic function in cultured primary brown and Brite/Beige adipocytes. *EMBO Rep* (2014) 15(10):1069–76. doi: 10.15252/embr.201438775

39. Heine M, Fischer AW, Schlein C, Jung C, Straub LG, Gottschling K, et al. Lipolysis triggers a systemic insulin response essential for efficient energy replenishment of activated brown adipose tissue in mice. *Cell Metab* (2018) 28(4):644–55.e4. doi: 10.1016/j.cmet.2018.06.020

40. Bertholet AM, Kirichok Y. Ucp1: A transporter for h(+) and fatty acid anions. *Biochimie* (2017) 134:28–34. doi: 10.1016/j.biochi.2016.10.013

41. Labbe SM, Caron A, Bakan I, Laplante M, Carpentier AC, Lecomte R, et al. *In vivo* measurement of energy substrate contribution to cold-induced brown adipose tissue thermogenesis. *FASEB J* (2015) 29(5):2046–58. doi: 10.1096/fj.14-266247

42. Ma SW, Foster DO. Uptake of glucose and release of fatty acids and glycerol by rat brown adipose tissue *in vivo*. *Can J Physiol Pharmacol* (1986) 64(5):609–14. doi: 10.1139/y86-101

43. Olsen JM, Aslund A, Bokhari MH, Hutchinson DS, Bengtsson T. Acute beta-adrenoceptor mediated glucose clearance in brown adipose tissue; a distinct pathway independent of functional insulin signaling. *Mol Metab* (2019) 30:240–9. doi: 10.1016/j.molmet.2019.10.004

44. Weir G, Ramage LE, Akyol M, Rhodes JK, Kyle CJ, Fletcher AM, et al. Substantial metabolic activity of human brown adipose tissue during warm conditions and cold-induced lipolysis of local triglycerides. *Cell Metab* (2018) 27(6):1348–55.e4. doi: 10.1016/j.cmet.2018.04.020

45. Virtanen KA, Lidell ME, Orava J, Heglind M, Westergren R, Niemi T, et al. Functional brown adipose tissue in healthy adults. *N Engl J Med* (2009) 360(15):1518–25. doi: 10.1056/NEJMoa0808949360/15/1518[pii]]

46. Winther S, Isidor MS, Basse AL, Skjoldborg N, Cheung A, Quistorff B, et al. Restricting glycolysis impairs brown adipocyte glucose and oxygen consumption. *Am J Physiol Endocrinol Metab* (2018) 314(3):E214–E23. doi: 10.1152/ajpendo.00218.2017

47. Hao Q, Yadav R, Basse AL, Petersen S, Sonne SB, Rasmussen S, et al. Transcriptome profiling of brown adipose tissue during cold exposure reveals extensive regulation of glucose metabolism. *Am J Physiol Endocrinol Metab* (2015) 308(5):E380–92. doi: 10.1152/ajpendo.00277.2014ajpendo.00277.2014[pii]

48. Hankir MK, Klingenspor M. Brown adipocyte glucose metabolism: A heated subject. *EMBO Rep* (2018) 19(9). doi: 10.15252/embr.201846404

49. Isler D, Hill HP, Meier MK. Glucose metabolism in isolated brown adipocytes under beta-adrenergic stimulation. quantitative contribution of glucose to total thermogenesis. *Biochem J* (1987) 245(3):789–93. doi: 10.1042/bj2450789

50. Yoneshiro T, Wang Q, Tajima K, Matsushita M, Maki H, Igarashi K, et al. Bcaa catabolism in brown fat controls energy homeostasis through Slc25a44. *Nature* (2019) 572(7771):614–9. doi: 10.1038/s41586-019-1503-x

51. Lopez-Soriano FJ, Fernandez-Lopez JA, Mampel T, Villarroya F, Iglesias R, Alemany M. Amino acid and glucose uptake by rat brown adipose tissue. effect of cold-exposure and acclimation. *Biochem J* (1988) 252(3):843–9. doi: 10.1042/bj2520843

52. Mills EL, Pierce KA, Jedrychowski MP, Garrity R, Winther S, Vidoni S, et al. Accumulation of succinate controls activation of adipose tissue thermogenesis. *Nature* (2018) 560(7716):102–6. doi: 10.1038/s41586-018-0353-2

53. Patel MS, Korotchkina LG. Regulation of the pyruvate dehydrogenase complex. *Biochem Soc Trans* (2006) 34(Pt 2):217–22. doi: 10.1042/BST20060217

54. Sugden MC, Holness MJ. Recent advances in mechanisms regulating glucose oxidation at the level of the pyruvate dehydrogenase complex by pdks. *Am J Physiol Endocrinol Metab* (2003) 284(5):E855–62. doi: 10.1152/ajpendo.00526.2002

55. Garland PB, Randle PJ, Newsholme EA. Citrate as an intermediary in the inhibition of phosphofructokinase in rat heart muscle by fatty acids, ketone bodies, pyruvate, diabetes, and starvation. *Nature* (1963) 200:169–70. doi: 10.1038/200169a0

56. Newsholme EA, Randle PJ, Manchester KL. Inhibition of the phosphofructokinase reaction in perfused rat heart by respiration of ketone bodies, fatty acids and pyruvate. *Nature* (1962) 193:270–1. doi: 10.1038/193270a0

57. Cheema-Dhadli S, Robinson BH, Halperin ML. Properties of the citrate transporter in rat heart: Implications for regulation of glycolysis by cytosolic citrate. *Can J Biochem* (1976) 54(6):561–5. doi: 10.1139/o76-082

58. Munday MR. Regulation of mammalian acetyl-coa carboxylase. *Biochem Soc Trans* (2002) 30(Pt 6):1059–64. doi: 10.1042/bst0301059

59. Alam N, Saggerson ED. Malonyl-coa and the regulation of fatty acid oxidation in soleus muscle. *Biochem J* (1998) 334(Pt 1):233–41. doi: 10.1042/bj3340233

60. McGarry JD, Leatherman GF, Foster DW. Carnitine palmitoyltransferase i. the site of inhibition of hepatic fatty acid oxidation by malonyl-coa. *J Biol Chem* (1978) 253 (12):4128–36. doi: 10.1016/S0021-9258(17)34693-8

61. Abu-Elheiga L, Matzuk MM, Abo-Hashema KA, Wakil SJ. Continuous fatty acid oxidation and reduced fat storage in mice lacking acetyl-coa carboxylase 2. *Science* (2001) 291(5513):2613–6. doi: 10.1126/science.1056843

62. Abu-Elheiga L, Matzuk MM, Kordari P, Oh W, Shaikenov T, Gu Z, et al. Mutant mice lacking acetyl-coa carboxylase 1 are embryonically lethal. *Proc Natl Acad Sci U.S.A.* (2005) 102(34):12011–6. doi: 10.1073/pnas.0505714102

63. Abu-Elheiga L, Brinkley WR, Zhong L, Chirala SS, Woldegiorgis G, Wakil SJ. The subcellular localization of acetyl-coa carboxylase 2. *Proc Natl Acad Sci U.S.A.* (2000) 97(4):1444–9. doi: 10.1073/pnas.97.4.1444

64. Bianchi A, Evans JL, Iverson AJ, Nordlund AC, Watts TD, Witters LA. Identification of an isozymic form of acetyl-coa carboxylase. *J Biol Chem* (1990) 265 (3):1502–9. doi: 10.1016/S0021-9258(19)40045-8

65. Esser V, Brown NF, Cowan AT, Foster DW, McGarry JD. Expression of a cdna isolated from rat brown adipose tissue and heart identifies the product as the muscle isoform of carnitine palmitoyltransferase I (M-cpt i). m-cpt I is the predominant cpt I isoform expressed in both white (Epididymal) and brown adipocytes. *J Biol Chem* (1996) 271(12):6972–7. doi: 10.1074/jbc.271.12.6972

66. Yamazaki N, Shinohara Y, Shima A, Terada H. High expression of a novel carnitine palmitoyltransferase I like protein in rat brown adipose tissue and heart: Isolation and characterization of its cdna clone. *FEBS Lett* (1995) 363(1-2):41–5. doi: 10.1016/0014-5793(95)00277-g

67. Doh KO, Kim YW, Park SY, Lee SK, Park JS, Kim JY. Interrelation between long-chain fatty acid oxidation rate and carnitine palmitoyltransferase 1 activity with different isoforms in rat tissues. *Life Sci* (2005) 77(4):435–43. doi: 10.1016/j.lfs.2004.11.032

68. Corbet C, Pinto A, Martherus R, Santiago de Jesus JP, Polet F, Feron O. Acidosis drives the reprogramming of fatty acid metabolism in cancer cells through changes in mitochondrial and histone acetylation. *Cell Metab* (2016) 24(2):311–23. doi: 10.1016/j.cmet.2016.07.003

69. Caro P, Kishan AU, Norberg E, Stanley IA, Chapuy B, Ficarro SB, et al. Metabolic signatures uncover distinct targets in molecular subsets of diffuse Large b cell lymphoma. *Cancer Cell* (2012) 22(4):547–60. doi: 10.1016/j.ccr.2012.08.014

70. De Oliveira MP, Liesa M. The role of mitochondrial fat oxidation in cancer cell proliferation and survival. *Cells* (2020) 9(12). doi: 10.3390/cells9122600

71. Song A, Dai W, Jang MJ, Medrano L, Li Z, Zhao H, et al. Low- and high-thermogenic brown adipocyte subpopulations coexist in murine adipose tissue. *J Clin Invest* (2020) 130(1):247–57. doi: 10.1172/JCI129167

72. Sun W, Dong H, Balaz M, Slyper M, Drokhlyansky E, Colleluori G, et al. Snrna-seq reveals a subpopulation of adipocytes that regulates thermogenesis. *Nature* (2020) 587(7832):98–102. doi: 10.1038/s41586-020-2856-x

73. Spaethling JM, Sanchez-Alavez M, Lee J, Xia FC, Dueck H, Wang W, et al. Single-cell transcriptomics and functional target validation of brown adipocytes show their complex roles in metabolic homeostasis. *FASEB J* (2016) 30(1):81–92. doi: 10.1096/fj.15-273797

74. Benador IY, Veliova M, Mahdaviani K, Petcherski A, Wikstrom JD, Assali EA, et al. Mitochondria bound to lipid droplets have unique bioenergetics, composition, and dynamics that support lipid droplet expansion. *Cell Metab* (2018) 27(4):869–85.e6. doi: 10.1016/j.cmet.2018.03.003

75. Yu J, Zhang S, Cui L, Wang W, Na H, Zhu X, et al. Lipid droplet remodeling and interaction with mitochondria in mouse brown adipose tissue during cold treatment. *Biochim Biophys Acta* (2015) 1853(5):918–28. doi: 10.1016/j.bbamcr.2015.01.020

76. Benador IY, Veliova M, Liesa M, Shirihai OS. Mitochondria bound to lipid droplets: Where mitochondrial dynamics regulate lipid storage and utilization. *Cell Metab* (2019) 29(4):827–35. doi: 10.1016/j.cmet.2019.02.011

77. Cui L, Mirza AH, Zhang S, Liang B, Liu P. Lipid droplets and mitochondria are anchored during brown adipocyte differentiation. *Protein Cell* (2019) 10(12):921–6. doi: 10.1007/s13238-019-00661-1

78. Mirza AH, Cui L, Zhang S, Liu P. Comparative proteomics reveals that lipid droplet-anchored mitochondria are more sensitive to cold in brown adipocytes. *Biochim Biophys Acta Mol Cell Biol Lipids* (2021) 1866(10):158992. doi: 10.1016/j.bbalip.2021.158992

79. Wang H, Sreenivasan U, Gong DW, O'Connell KA, Dabkowski ER, Hecker PA, et al. Cardiomyocyte-specific perilipin 5 overexpression leads to myocardial steatosis and modest cardiac dysfunction. *J Lipid Res* (2013) 54(4):953–65. doi: 10.1194/jlr.M032466

80. Twig G, Elorza A, Molina AJ, Mohamed H, Wikstrom JD, Walzer G, et al. Fission and selective fusion govern mitochondrial segregation and elimination by autophagy. *EMBO J* (2008) 27(2):433–46. doi: 10.1038/sj.emboj.7601963

81. Rambold AS, Cohen S, Lippincott-Schwartz J. Fatty acid trafficking in starved cells: Regulation by lipid droplet lipolysis, autophagy, and mitochondrial fusion dynamics. *Dev Cell* (2015) 32(6):678–92. doi: 10.1016/j.devcel.2015.01.029

82. Cui L, Liu P. Two types of contact between lipid droplets and mitochondria. *Front Cell Dev Biol* (2020) 8:618322. doi: 10.3389/fcell.2020.618322

83. Olzmann JA, Carvalho P. Dynamics and functions of lipid droplets. *Nat Rev Mol Cell Biol* (2019) 20(3):137–55. doi: 10.1038/s41580-018-0085-z

frontiers | Frontiers in Endocrinology

TYPE Original Research
PUBLISHED 01 March 2023
DOI 10.3389/fendo.2023.1141303

Check for updates

OPEN ACCESS

EDITED BY
Endre Károly Kristóf,
University of Debrecen, Hungary

REVIEWED BY
Stefania Carobbio,
Principe Felipe Research Center (CIPF), Spain
Rosalba Senese,
University of Campania Luigi Vanvitelli, Italy

*CORRESPONDENCE
Monica Colitti
monica.colitti@uniud.it

SPECIALTY SECTION
This article was submitted to Cellular Endocrinology, a section of the journal Frontiers in Endocrinology

RECEIVED 10 January 2023
ACCEPTED 17 February 2023
PUBLISHED 01 March 2023

CITATION
Ali U, Wabitsch M, Tews D and Colitti M (2023) Effects of allicin on human Simpson-Golabi-Behmel syndrome cells in mediating browning phenotype. *Front. Endocrinol.* 14:1141303. doi: 10.3389/fendo.2023.1141303

COPYRIGHT
© 2023 Ali, Wabitsch, Tews and Colitti. This is an open-access article distributed under the terms of the Creative Commons Attribution License (CC BY). The use, distribution or reproduction in other forums is permitted, provided the original author(s) and the copyright owner(s) are credited and that the original publication in this journal is cited, in accordance with accepted academic practice. No use, distribution or reproduction is permitted which does not comply with these terms.

# Effects of allicin on human Simpson-Golabi-Behmel syndrome cells in mediating browning phenotype

Uzair Ali[1], Martin Wabitsch[2], Daniel Tews[2] and Monica Colitti[1]*

[1]Department of Agricultural, Food, Environmental and Animal Sciences, University of Udine, Udine, Italy, [2]Division of Pediatric Endocrinology and Diabetes, Department of Pediatrics and Adolescent Medicine, Ulm University Medical Center, Ulm, Germany

**Introduction:** Obesity is a major health problem because it is associated with increased risk of cardiovascular disease, diabetes, hypertension, and some cancers. Strategies to prevent or reduce obesity focus mainly on the possible effects of natural compounds that can induce a phenotype of browning adipocytes capable of releasing energy in the form of heat. Allicin, a bioactive component of garlic with numerous pharmacological functions, is known to stimulate energy metabolism.

**Methods:** In the present study, the effects of allicin on human Simpson-Golabi-Behmel Syndrome (SGBS) cells were investigated by quantifying the dynamics of lipid droplets (LDs) and mitochondria, as well as transcriptomic changes after six days of differentiation.

**Results:** Allicin significantly promoted the reduction in the surface area and size of LDs, leading to the formation of multilocular adipocytes, which was confirmed by the upregulation of genes related to lipolysis. The increase in the number and decrease in the mean aspect ratio of mitochondria in allicin-treated cells indicate a shift in mitochondrial dynamics toward fission. The structural results are confirmed by transcriptomic analysis showing a significant arrangement of gene expression associated with beige adipocytes, in particular increased expression of T-box transcription factor 1 (TBX1), uncoupling protein 1 (UCP1), PPARG coactivator 1 alpha (PPARGC1A), peroxisome proliferator-activated receptor alpha (PPARA), and OXPHOS-related genes. The most promising targets are nuclear genes such as retinoid X receptor alpha (RXRA), retinoid X receptor gamma (RXRG), nuclear receptor subfamily 1 group H member 3 (NR1H3), nuclear receptor subfamily 1 group H member 4 (NR1H4), PPARA, and oestrogen receptor 1 (ESR1).

**Discussion:** Transcriptomic data and the network pharmacology-based approach revealed that genes and potential targets of allicin are involved in ligand-activated transcription factor activity, intracellular receptor signalling, regulation of cold-induced thermogenesis, and positive regulation of lipid metabolism. The present study highlights the potential role of allicin in triggering browning in human SGBS cells by affecting the LD dynamics, mitochondrial morphology, and expression of brown marker genes. Understanding the potential targets through which allicin promotes this effect may reveal the underlying signalling pathways and support these findings.

KEYWORDS

**SGBS cells, allicin, lipid droplets, mitochondria, thermogenesis**

# Introduction

Obesity is a complex multifactorial disease that presents a risk of death as it is associated with many noncommunicable diseases such as cardiovascular diseases, type 2 diabetes, and cancer. Since the discovery of brown adipose tissue (BAT) in the adult human body and its ability to dissipate energy, it has been of particular interest to exploit the activity of BAT as a therapeutic option to counteract obesity. In addition, the formation of thermogenic or beige adipocytes in white adipose tissue (e.g., adipocyte browning) may represent another option to increase energy expenditure (1). In both brown and beige adipocytes oxidative phosphorylation is uncoupled from ATP production, which is due to up-regulation of uncoupling protein-1 (UCP1) (2). To date, *in vitro* and *in vivo* studies have identified a considerable number of browning agents, such as capsaicin, resveratrol, caffeine, and fucoxanthin (3, 4). Garlic (*Allium sativum* L.) is a popular species rich in organosulfur compounds that are useful for medicinal purposes. When garlic is chopped or crushed, alliin is released and then hydrolyzed into allicin by allicinase. Allicin *in vitro* breaks down into a variety of fat-soluble organosulfur compounds, including diallyl trisulfide (DATS), diallyl disulfide (DADS), and diallyl sulfide (DAS) (5–7). The high permeability of allicin through cell membranes and rapid reaction with free thiol groups promote its diverse biological and therapeutic functions (8). Allicin is known for its antibacterial, antifungal, and antiparasitic activities (9), as well as its anticarcinogenic (10, 11) and anti-inflammatory functions (12, 13). Allicin has also been shown to suppress cholesterol biosynthesis by inhibiting squalene monooxygenase and acetyl-CoA synthetase (14). Methanolic extract of black garlic containing alliin, upregulated the expression of genes related to adipokines, lipolysis, and fatty acid oxidation in adipose tissue of rats fed a high-fat diet (15).

Recently, allicin was reported to promote browning in differentiated 3T3-L1 adipocytes and white inguinal adipose tissue of mice through extracellular signal regulated kinase 1/2 (ERK1/2) and KLF Transcription Factor 15 (KLF15) pathways, which stimulates the expression of UCP1 through interaction with its promoter (16). It has also been suggested that the Sirt1-PGC1α-Tfam pathway plays a role in promoting allicin-mediated BAT activity (17).

Although several mouse cell lines are available to understand the adipogenic and thermogenic regulatory networks *in vitro*, human cell lines are of interest to explore the molecular mechanism of browning and to identify potential dietary supplements and nutraceuticals that could induce browning. The Simpson-Golabi-Behmel Syndrome (SGBS) cell strain is commonly used as a model for the differentiation of human white adipocytes (18). These cells retain their differentiation ability up to several generations when provided with the appropriate adipogenic differentiation medium. Based on the effect of rosiglitazone (19), a browning phenotype was observed in SGBS cells during differentiation, and RNA sequencing revealed an increase in genes involved in extracellular matrix organization and oxidative stress that may regulate adaptive thermogenesis, with an increased percentage of brown phenotype, confirming that differentiated SGBS cells gradually acquire BAT-like function from day 4 to day 10 (20).

After stimulation of browning, the formation of micro lipid droplets (LDs) has been demonstrated in response to lipolytic release of fatty acids (21). This enables efficient intracellular lipolysis from the LD surface and subsequent promotion of free fatty acid transport to mitochondria for β-oxidation in BAT (22). Consistent with this property, both cold exposure and adrenergic stimulation induce rapid mitochondrial fragmentation, which synergistically promote uncoupling and thus heat production (23).

Using RNAseq and quantifying the dynamics of LDs and mitochondrial morphology, the current study aims to evaluate the browning effect of allicin *in vitro* using the SGBS cell strain as a human primary adipocyte model in comparison to the control and cells treated with dibutyryl cAMP sodium salt (cAMP) as a positive control. To clarify the potential browning effect of allicin, a network pharmacology strategy was also performed based on the identification of potential targets.

# Materials and methods

## Chemicals and culture media

Dulbecco's modified Eagle medium (DMEM)/F-12 medium (1:1) enriched with L-glutamine and 15 mM 4-(2-hydroxyethyl)-1-piperazineethanesulfonic acid (HEPES), fetal bovine serum (FBS) and penicillin streptomycin solution were purchased from Gibco by Life Technologies (Thermo Fisher Scientific Inc., Waltham, Massachusetts). TRIzol reagent, PureLink™ RNA Mini Kit and SuperScript™ III one-step RT-PCR system with Platinum™ *Taq* DNA polymerase were purchased from Invitrogen (Thermo Fisher Scientific Inc., Waltham, Massachusetts). Rosiglitazone was purchased from Cayman Chemical (Ann Arbor, Michigan). Allicin was purchased from Solarbio Life Sciences® (Beijing, China).

All other chemicals used in the experiment and not listed above were purchased from Sigma-Aldrich (Darmstadt, Germany).

## Cell culture and treatments

Human SGBS cells were grown Dulbecco's Modified Eagle Medium Nutrient Mixture F-12 (DMEM/F-12) supplemented with 10% fetal bovine serum (FBS), 3.3 mM biotin, 1.7 mM panthotenate and 1% penicillin/streptomycin solution, at 37°C, 5% $CO_2$ and 95% relative humidity. Cells were platted in Petri dishes (100mm) in duplicate. Once the cells reached approximately 90% confluence, differentiation was induced by feeding the cells with serum-free growth medium supplemented with 10 µg/ml transferrin, 0.2 nM triiodothyronine ($T_3$), 250 nM hydroxycortisone, 20 nM human insulin, 25 nM dexamethasone, 250 µM 3-isobutyl-1-methylxanthine (IBMX) and 2 µM rosiglitazone (day 0 of differentiation). After 4 days, the

differentiation medium was replaced with maintenance medium composed by serum-free growth medium supplemented with 10 µg/ml transferrin, 0.2 nM $T_3$, 250 nM hydroxycortisone and 20 nM human insulin. Fresh maintenance medium was added every 2 days.

Treatment with allicin began on day 0 of differentiation (D0), and continued until analysis on day six (D06) of differentiation (Figure 1). Allicin concentrations of 5, 12.5, 25, and 50 µM were tested. Prior to treatment, allicin was diluted in dimethyl sulfoxide (DMSO) and a stock solution was prepared. Stock solutions were prepared so that the volume of DMSO in the treatment medium did not exceed 0.5%. Control cells (CTRL) were incubated with the same volume of 0.5% DMSO in the differentiation medium for 6 days. As a positive control (cAMP), SGBS cells were treated with 500 µM dibutyryl cAMP sodium salt (a cyclic nucleotide derivative that mimics endogenous cAMP) for 24 hours before the sixth day of differentiation (24) (Figure 1).

## Cell viability assay

Cell viability was determined using the 3-(4,5-dimethylthiazol-2-yl)-2,5-diphenyltetrazolium bromide (MTT) assay. Cells were plated in a 96-well plate and treated with 5.0, 12.5, 25.0, and 50 µM allicin (25). Before incubation with 5 mg/mL MTT in HBSS, cells were rinsed with 1X phosphate buffer saline (PBS) 1X. Incubation with the MTT solution was performed at 37°C for 4 hours. The resulting formazan was dissolved in dimethyl sulfoxide (DMSO) and incubated overnight (O/N) at 37°C. Optical density was used as an indicator of cell viability and was measured at 590 nm.

## BODIPY staining and confocal imaging

Cells for BODIPY™ staining and subsequent confocal imaging were cultured on ibiTreat 8-well µ-slides (Ibidi GmbH, Planegg/Martinsried, Germany). Cells were fixed in a 2% formalin solution diluted in PBS 1X at room temperature (RT) for 15 minutes. Subsequently, after washing three times in PBS 1X, the cells were incubated in a solution of BODIPY™ 493/503 in PBS 1X to fluorescently label the lipid droplets. Incubation was performed for 45 minutes in the dark at RT. The slides were then washed three times in PBS 1X.

Fluorescence images were acquired using a Leica SP8 confocal microscope (Leica Microsystems Srl, Milan, Italy) and LAS X 3.1.5.16308 software. Slides were viewed with the HCX PL APO lambda blue 63x/1.40 OIL objective. DAPI fluorescence was detected with a 405 diode laser (410/480 nm), while BODIPY fluorescence was detected with a white light laser (503/588 nm). Images were acquired using a photomultiplier tube (PMT) that allowed point scanning of the region of interest (ROI) with the selected laser and produced 1024 × 1024 px images.

## Morphology of LDs

The MRI_Lipid Droplets Tool (http://dev.mri.cnrs.fr/projects/imagej-macros/wiki/LipidDroplets_Tool), a macro in the ImageJ 1.50b software (http://rsb.info.nih.gov/ij/), was used to measure LD area (26). Individual cells were defined by regions of interest (ROIs) and images were analyzed as previously described (27). For each cell, the LD area (in $\mu m^2$), maximum Feret diameter (MFD, in µm), and integrated optical density (IOD, dimensionless) were measured. The MDF is used as a measure of the diameter of irregularly shaped objects, whereas the IOD is related to both triglyceride accumulation and the size of LDs (28).

## MitoTracker® staining

SGBS cells cultured on ibiTreat 8-well µ-slides (Ibidi GmbH, Germany) were incubated at 37°C with 100 nM MitoTracker® Orange CMTMRos (Thermo Fisher Scientific, USA) for 30 minutes. The stained cells were washed with PBS 1X and fixed with 2% formalin at RT for 15 minutes. After fixation, cells were rinsed three times with PBS 1X, mounted in DAPI-containing mounting medium (Cayman Chemical Company, USA), and imaged using a Leica SP8 confocal microscope (Leica Microsystems, Germany) and LAS X 3.1.5.16308 software. Slides were viewed with the HCX PL APO lambda blue 63x/1.40 OIL objective. DAPI fluorescence was detected with a 405 diode laser (410/480 nm), while MitoTracker® fluorescence was detected with a white light laser (550/605 nm). Images were acquired using a photomultiplier tube (PMT) that allowed point-by-point scanning of the region of interest (ROI) with the selected laser and produced images with a resolution of 1024 x 1024 px.

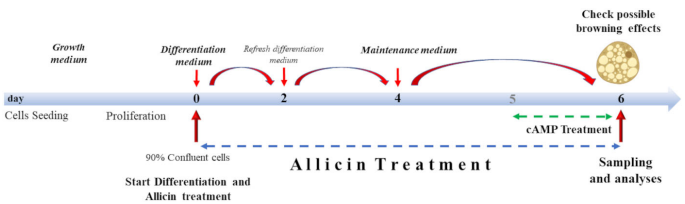


FIGURE 1
Cell culture treatment protocol. Cells were grown to 90% confluence. Differentiation lasted 6 days supplemented with allicin treatment. From day 4, cells were incubated with allicin in maintenance medium. Cells were incubated with cAMP for 24 hours (from day 5 to day 6 of differentiation). Sampling and analyses were performed on day 6.

## Mitochondrial morphology analyses

To quantify mitochondrial morphology on standard confocal fluorescence microscopy images of CTRL, ALLI, and cAMP-treated cells, the Mitochondrial Analyzer based on adaptive thresholding and the ImageJ/Fiji open-source image analysis platform were used (29). Scale was set for magnification and the global check box in the Set Scale dialog box was selected. After 2D threshold optimization, the images were thresholded with a block size of 1,350µm and a C-value of 5. Subsequently, the images were also processed using the MiNa (30) and Micro2P (31) tools.

The Mitochondria Analyzer tool was used to measure counts (number of mitochondria in the image), total area (sum of the area of all mitochondria in the image), mean area (total area/mitochondria number), total perimeter (sum of perimeter of all mitochondria in the image), mean perimeter (total perimeter/mitochondria number), mean aspect ratio (shape descriptor measuring elongation), and mean form factor (shape descriptor measuring round to filamentous shape). In addition, parameters describing the connectivity of the mitochondrial network were calculated, including the number of branches, the total length of branches, the mean length of branches, the branch junctions, the end points of branches, and the mean diameter of branches. The branches consist of point-shaped objects without branching junctions and minimal length, long single tubular objects without branching junctions, but the highest branch length and complex objects with multiple branches and junctions. The number of branches, total branch length, branch junctions and branch end points were also expressed as normalization to either the number of mitochondria or total area (29).

The MiNa tool, a macro of the ImageJ1.53o software (http://rsb.info.nih.gov/ij/), was also used to quantify mitochondrial morphology (30). Threshold images were processed using the Tophat option (32), as was the MiNa interface. The macro detected 'individual' mitochondrial structures in a skeletonized image, such as punctate, rod-shaped, and large/round structures without branching, and 'networks' identified as mitochondrial structures with a single node and three branches. All parameters were used in the discriminant analysis. Among the nine parameters calculated by MiNa, the number of individuals (punctate, rod-shaped, and large/round mitochondria), the number of networks (objects with at least one branch), and the mean rod/branch length, which refers to the average length of all mitochondrial rods/branches, were considered for statistical comparisons. Other parameters such as the mean number of branches per network, i.e., the mean number of mitochondrial branches per network, the mean length of branches, and the mitochondrial footprint, which refers to the total area of mitochondria, were included in the discriminant analysis.

Mitochondria were also analyzed and classified using MicroP software, a useful tool validated in CHO-K1 cells (31). The software classifies six morphological types of mitochondria, such as small globules, round-shaped mitochondria, that may have arisen by fission; large globules with a larger area; simple tubules, i.e. straight, elongated mitochondria without branches; twisted tubules, elongated tubular mitochondria with a non-linear development; donuts, like elongated tubules mitochondria but with fused ends; branched tubules, complex interconnected mitochondria with a network-like structure. On each image, the total number of mitochondria and their area were calculated as the ratio of mitochondria and area for each subtype in the different SGBS cells treated. These data with the number of objects and total area were used for discriminant analysis.

## RNA extraction and sequencing

The experiment was set up with 2 biological replicates for the 3 experimental conditions.

After removing the culture medium from the Petri dishes, 1ml/10cm$^2$ of TRIzol reagent was added to each plate and repeatedly pipetted to induce a severe breakdown of the cell structures. These samples were immediately processed further using the PureLink™ RNA Mini Kit according to the manufacturer's instructions.

The concentration of extracted total RNA was quantified using a spectrophotometer (NanoDrop 1000 Spectrophotometer, ThermoScientific, Wilmington, Delaware), and the purity of the RNA samples ranged from 1.8 to 1.9. RNA integrity was assessed by observing the 18S and 28S ribosomal bands after electrophoresis on 1% agarose gel, in the presence of GelRed. β-actin expression was used as an internal control, and confirmed the complete integrity of the RNA.

The purified total RNA was subjected to deep sequencing analysis. First, the isolated RNA was quantified using Agilent Bioanalyzer 2100 with the RNA integrity number (RIN) greater than 8.0 before sequencing using Illumina Genome Analyzer (GA). Generally, 2-4 ug of the total RNA was used for library construction. Total RNA was reverse transcribed into double-stranded cDNA, digested with NlaIII and ligated to an Illumina specific adapter containing a recognition site of MmeI. After MmeI digestion, a second Illumina adapter, containing a 2-bp degenerate 3' overhang was ligated. The obtained sequences were aligned on GRCh38 human genome (https://www.ncbi.nlm.nih.gov/assembly/GCF_000001405.39) using STAR software (33).

## Data processing

Raw data were uploaded to the R package (v0.92) Differential Expression and Pathway analysis (iDEP951) that is a web-based tool available at http://bioinformatics.sdstate.edu/idep/(34, 35). In the pre-processing step, genes expressed at very low levels across samples were filtered out, and genes expressed at a minimum of 0.5 counts per million (CPM) in a library were further analyzed. To reduce variability and normalizecount data, EdgeR log2(CPM+c) was chosen with pseudocount c = 4 transformation,. Next, the DESeq2 package in the R language was used to identify differentially expressed genes (DEG) between ALLI_ cAMP, ALLI_CTRL and cAMP_CTRL using a of false discovery rate (FDR) threshold ≤ 0.05 and fold-change > |1.0|. Heatmaps, principal component analysis

(PCA), k-means cluster and enrichment analyses were also performed in iDEP951.

Gene set enrichment analysis to determine the shared biological functions of differentially regulated genes based on significant GO terms (36), Kyoto Encyclopedia of Genes and Genomes (KEGG) pathway (37) and TF. target.TRED analyses were performed (38).

Venn diagrams were created by web tool available at http://bioinformatics.psb.ugent.be/webtools/Venn/.

## Protein-protein interaction Network construction and hub genes analysis

On the basis of the online tool Search Tool for the Retrieval of Interacting Genes (STRING; https://string-db.org/), PPI networks of the up regulated and the down regulated DEGs in each comparison were generated with a confidence level of ≥ 0.4, and the PPI network was visualized using Cytoscape software (version 3.9.1, https://cytoscape.org/). Then, the PPI networks of DEGs in each comparison were analyzed using the Cytoscape CytoHubba plugin to select the top 10 hub nodes according to the Degree algorithm (39). The Molecular Complex Detection (MCODE) plug-in (40) in the Cytoscape suite was used to examine the significant modules in the PPI network of overlapping DEGs that are the target ofshared TF networks between comparisons. Degree cutoff = 2, K-core = 2, and node score cutoff = 0.2 were set as options. Enrichment analysis of DEGs in modules with a score ≥ 5 was then performed.

## PROFAT webtool analysis

Estimation of the proportion of brown adipocytes in each sample was analyzed based on read counts using the PROFAT tool, which automatically performs hierarchical cluster analysis to predict the browning capacity of mouse and human RNA-seq datasets (41).

## Targets prediction of allicin, DAS, DADS, DATS

To identify a larger number of potential targets, PharmMapper (http://www.lilab-ecust.cn/pharmmapper/; 42, 43), the similarity ensemble approach (SEA, https://sea.bkslab.org/), the STITCH database (http://stitch.embl.de/; 44), Swiss Target Prediction (http://www.swisstargetprediction.ch/; 45), and GeneCard (https://www.genecards.org/) were used. The 2D structure and canonical SMILES of allicin (CID_65036), diallyl sulphide (CID_11617), diallyl disulfide (CID_16590), and diallyl trisulfide (CID_16315) were obtained from the PubChem database (https://pubchem.ncbi.nlm.nih.gov/). The sdf files were uploaded to the PharmMapper server, and the search was started using the maximum generated conformations of 300 by selecting the option 'Human Protein Targets Only (v2010, 2241)' and the default value of 300 for the number of reserved matching targets. for the other parameters, the 'default mode' was selected. Canonical SMILES were uploaded to the other tools. The predicted targets were entered into the UniProt database (https://www.uniprot.org/) with the species set to *Homo sapiens* to determine their gene IDs. A Venn diagram was used to find common targets among the allicin compounds. Genes related to 'adipocyte', 'browning', 'non shivering thermogenesis', 'cold-induced thermogenesis', 'brown adipose thermogenesis,' and 'adaptive thermogenesis' were downloaded from GeneCard, and the intersection of the targets was determined using the Venn tool. The resulting common genes associated with browning and adipocytes were then crossed with common putative targets of allicin, and a Venn diagram was generated. Subsequently, the overlapping targets were uploaded to GeneMANIA (https://genemania.org/) (46) to perform functional gene analysis and generate a PPI network.

CytoNCA, another Cytoscape plugin, was applied to the network to perform topological analysis evaluating the centrality measures of the network (47). Then, the Cytoscape intersectional merge function was used to isolate the PPI subnetworks. Key node functions were determined by analyzing GO terms, KEGG and Reactome pathways.

By entering the screened key nodes into the online tool VarElect (48), the correlation between nodes and 'cold induced thermogenesis' was investigated.

## Statistical analysis

All measurement results are given as means ± SD and were analyzed with XLSTAT (49). Measurements of LD area surface/cell, MFD/cell, and IOD/cell obtained from 15 biological replicates were compared along with Mitochondrial Analyzer, MiNa, and Micro2P results using the Kruskal-Wallis statistical test, followed by pairwise comparisons using the Mann-Whitney approach with Bonferroni correction ($p < 0.0167$).

All Mitochondrial Analyzer and MiNa parameters, as well as ratios of parameters obtained with the Micro2P tool, were calculated together to perform a canonical discriminant analysis (DA) that integrates morphological mitochondrial parameters into a single multivariate model with the aim of maximizing differences between treatments and calculating the best discriminant components between treatments (49).

# Results

## Cell viability

To investigate possible adverse effects of allicin, a viability assay was used to investigate possible adverse effects of ALLI extract on SGBS cells treated with doses of 5, 12.5, 25, and 50 µM. In particular, the analysis showed that the viability of cells treated with ALLI extract decreased significantly ($p < 0.001$) in a dose-dependent manner (Figure S1), with the 50 µM dose always significantly different from the other doses. Nevertheless, viability remained above 85% up to 25 µM and 12.5 µM ALLI and did not

10.3389/fendo.2023.1141303

differ from 5 and 25 μM. Based on these findings, 12.5 μM ALLI was selected for further experiments.

## Allicin treatment affects the number of lipid droplets and their maximum diameter

Next, We investigated whether allicin has an effect on early adipogenic differentiation. Thus, we performed LD analysis in SGBS cells after ALLI treatment during the induction of adipogenesis. Figure 1 shows statistically significant differences in area of LDs/cell, MFD/cell, and IOD/cell between treatments and illustrates Bodipy staining in SGBS cells after 6 days of treatment with allicin (ALLI), CTRL, and dibutyryl cAMP (cAMP). The area of LDs/cell was significantly lower in cells treated with cAMP and ALLI compared with cells from CTRL ($p < 0.0001$). No significant differences were observed between cAMP- and ALLI-treated cells (Figure 2A). A significant ($p < 0.0001$) decrease in MDF/cell was observed in cells treated with cAMP and ALLI compared with CTRL ($p < 0.0001$) (Figure 2B), while IOD/cell was significantly lower in cells treated with cAMP compared with cells treated with ALLI ($p = 0.016$) and CTRL ($p = 0.0001$) (Figure 2C). A significant increase in the number of LDs/cell ($p = 0.015$) was observed between ALLI treated cells and CTRL cells (Figure 2D).

## Allicin increases the number and area of small round mitochondria

Accurate analysis of mitochondria is critical for determining mitochondrial dynamics, so three different tools were used to characterize mitochondrial morphology. Figure S2 shows the identification and classification of objects using adaptive thresholding (radius = 1.350 μm, C = 5) on images of ALLI- and cAMP-treated cells and CTRL. Figures S2A, B show the effects of the different treatments measured with the three tools, on the total number and area of mitochondria in SGBS cells. No statistical differences in mitochondrial distribution patterns were detected between treatments, although treatments with allicin and cAMP caused a shift toward a greater number of mitochondria (Figure S2A) and a greater total area of mitochondria compared with cells from CTRL (Figure S2B). These results suggest that ALLI treatment increases the number of mitochondria by inducing mitochondrial fission or biogenesis and thus also increases the total area of mitochondria.

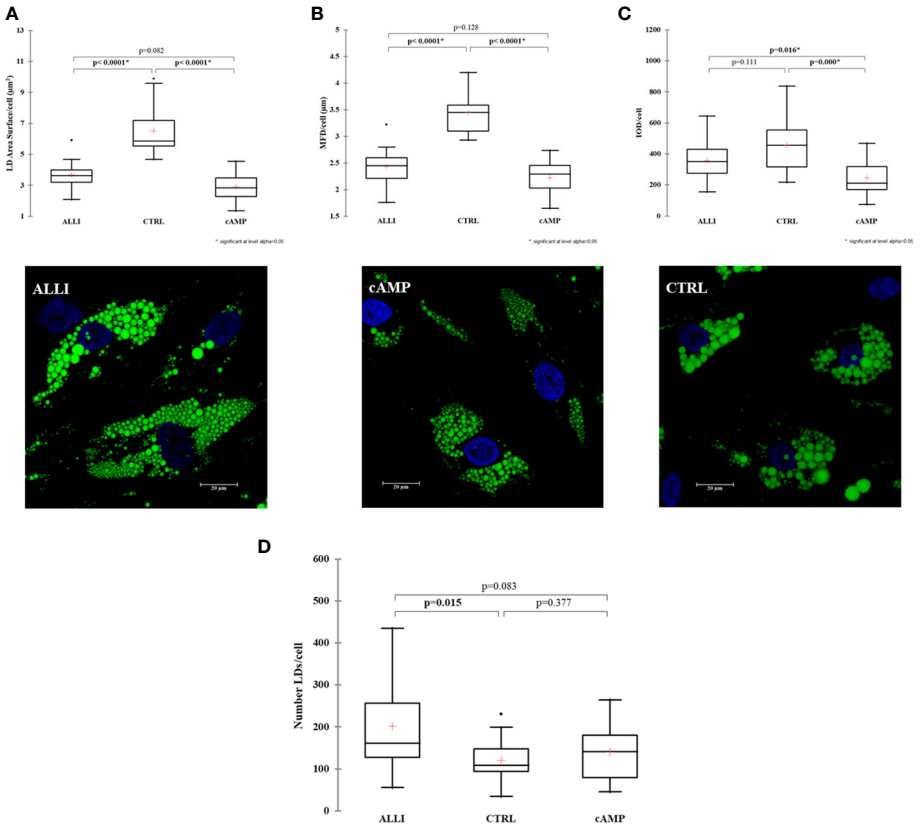


FIGURE 2
Results of lipid droplet analysis performed on SGBS cells. Boxplots show the median (horizontal lines), the first to third quartiles (box), and the most extreme values with the interquartile range (vertical lines). For all comparisons, differences between treatments on SGBS cells were statistically significant using the Kruskal-Wallis test and Bonferroni correction. **(A)** LD area per cell; **(B)** Maximum Feret Diameter (MFD) per cell; **(C)** Optical Density Intensity (IOD) per cell; **(D)** number of lipid droplets per cell in treated and CTRL cells.Representative confocal images of SGBS cells treated with allicin (ALLI), dibutyryl cAMP (cAMP), or control (CTRL) 6 days after differentiation and stained with BODIPY. Nuclear staining, DAPI. Images are representative of n. 15 biological replicates. ALLI, 12.5 μg/mL allicin-treated cells; CTRL, control cells; cAMP, 500 μM dibutyryl cAMP-treated cells.

Therefore, more than 26000 mitochondria were analysed using Micro2P software to classify six morphological subtypes and calculate the average proportion of mitochondrial subtypes within each treatment (Figure 3A, B). ALLI and cAMP treatments resulted in 13.6% ($p < 0.01$) and 11.5% ($p < 0.05$) more small globules, respectively, compared with CTRL. ALLI treatment reduced the percentage of mitochondria with large globules to 32.5% and that of the simple tube subtype to 19.5% compared with CTRL ($p < 0.01$) (Figure 3A). Accordingly, the ratio of surface area was significantly higher ($p < 0.05$) in ALLI- and cAMP-treated cells compared with CTRL at 30.3 and 31.7%, respectively, whereas the area of large globules in ALLI-treated cells decreased significantly ($p < 0.05$) (Figure 3B).

Specifically, the average ratio of mitochondrial amount in the different treatments was 53.4% in ALLI-treated cells, 28.6% in cAMP-treated cells, and 18.02% in CTRL. The relative percent area of total mitochondrial content between treatments was 51.9% in ALLI-treated cells, 27.8% in cAMP-treated cells, and 20.3% in cells from CTRL. Considering all treatments together, small globules (65.7%) and simple tubules (23.3%) were the most representative subtypes, followed by branched tubules (5.42%), large globules (2.3%), donuts (1.7%), and twisting tubules (1.6%). Accordingly, the percentage area of mitochondrial subtypes was 34.9% for small globules, 33.9.8% for simple tubules, 16.67% in branching tubules, 7.4% for donuts, 3.6% for large globules, and 3.5% for twisting tubules.

Mitochondrial Analyzer detected significantly higher numbers of mitochondria in ALLI-treated cells (Figure 3C), whereas the mean perimeter and area (Figure 3D) were significantly lower compared with cells from CTRL. No statistical differences were observed in the cells treated with cAMP. The shape of mitochondria, characterized by aspect ratio and form factor, decreased significantly under ALLI and cAMP compared with cells from CTRL (Figures 3E, F). Mitochondria Analyser tool was also used to quantify the morphological complexity of mitochondria. The mean length of branches and the total number of branches per mitochondrion were lowest in cells treated with ALLI and showed a significant difference in cells treated with cAMP (data not shown).

Network parameters calculated with MiNa confirmed a significant ($p < 0.05$) increase in the number of individuals (puncta, rods and large) in ALLI-treated cells compared with CTRL cells (Figure 4A). The number of networks showed no significant differences between treatments (Figure 4B), but the mean value of rod/branch length significantly decreased in cells treated with ALLI ($p < 0.05$) and cAMP ($p < 0.05$) (Figure 4C).

## Mitochondrial analysis results classify treatments into non-overlapping groups

To determine the extent of treatment-specific variation in an unbiased manner, all Mitochondrial Analyzer measurements, six MiNa measurements from, and the percentage of the number and area of each mitochondrial subtype, number of objects, and total area calculated by Micro2P were integrated into a single

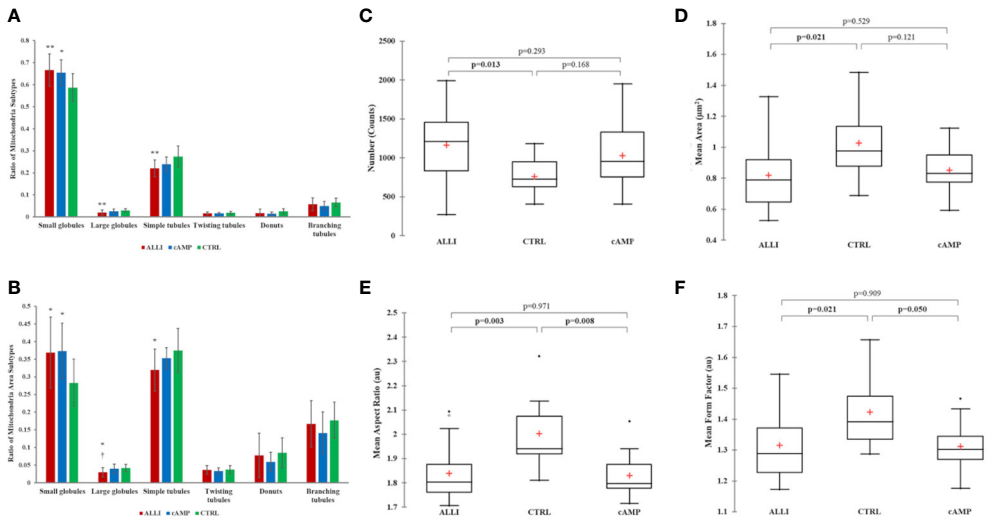


FIGURE 3
Mitochondrial analyses. Differences in the distribution of mitochondrial morphological characteristics were analysed between cells incubated with ALLI and cAMP compared with cells from CTRL. **(A)** Average ratio of mitochondrial subtypes within each treatment. The Kruskal-Wallis test was performed between ALLI-treated cells compared with CTRL (**$p < 0.01$) and cAMP-treated cells compared with CTRL (*$p < 0.05$). Differences between ALLI-treated cells and cAMP were also detected († $p < 0.05$). **(B)** The ratio of the surface area was significantly higher in ALLI- and cAMP-treated cells compared with CTRL by 30.3 and 31.7%, respectively ($p < 0.05$). The average ratio surface area of large globules showed a significant (* † $p < 0.05$) decrease in ALLI-treated cells by 24.9 and 28.6% compared with cAMP-treated and CTRL cells, respectively. Mitochondria features determined using the Mitochondria Analyser tool. **(C)** Number of mitochondria. **(D)** Mitochondrial size measured by mean area. **(E, F)** Mitochondrial shape measured by mean aspect ratio and mean form factor. Boxplots showed the difference between medians (horizontal lines), first to third quartiles (box), and the most extreme values within the interquartile range (vertical lines) between treatments. Statistical significance in the boxplots was determined by the Kruskal-Wallis statistical test with Bonferroni correction ($p < 0.0167$). ALLI, 12.5 µg/mL allicin-treated cells; CTRL, control cells; cAMP, 500 µM dibutyryl cAMP-treated cells.

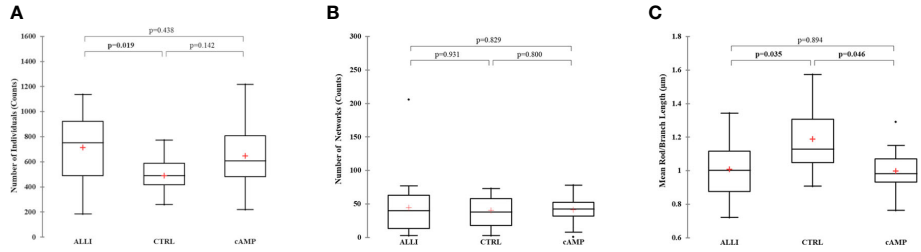


FIGURE 4
Summary statistics of mitochondrial network analysis performed with the MiNa tool on SGBS cells for each treatment. **(A)** Number of individual mitochondria. **(B)** Number of networks. **(C)** Mean value of rod/branch length. Boxplots show the median (horizontal lines), first through third quartiles (box), and the most extreme values with the interquartile range (vertical lines). The number of individual counts was statistically different in ALLI-treated SGBS cells from CTRL cells, using the Kruskal-Wallis test and Bonferroni correction ($p < 0.0167$). The number of networks showed no statistical difference. The mean length of rod/branch mitochondria significantly decreased in ALLI- ($p = 0.035$) and cAMP-treated cells ($p < 0.046$) compared with CTRL. ALLI, 12.5 µg/mL allicin-treated cells; CTRL, control cells; cAMP, 500 µM dibutyryl cAMP-treated cells.

multivariate model (DA) that maximized differences between treatments (Figure 5).

The model achieved clear separation of samples. With few exceptions, the treatments were grouped and divided into 3 clusters. Mitochondrial values of ALLI-treated cells were projected in the quadrant with a positive value for the F1 and F2 components, CTRL was projected in the quadrant with a negative value for F1 and a positive value for the F2 component. The projection of cAMP-treated cells was observed in the quadrant with negative value for F1 and positive value for F2. The significant morphological characteristics that distinguished the different experimental groups are shown in Table 1. This analysis showed that most of the variance between treatments in mitochondrial dynamics was based on elongation index, area of small globes, solidity of simple tubes, number of punctate and rod-shaped mitochondria (individuals), and number of simple tubes (Table 1). Discriminant functions were used to classify the treatments into the correct groups. To check the functionality and robustness of the classification model, a cross-validation test was performed, in which the success rate of correctly classified samples was 88.6%.

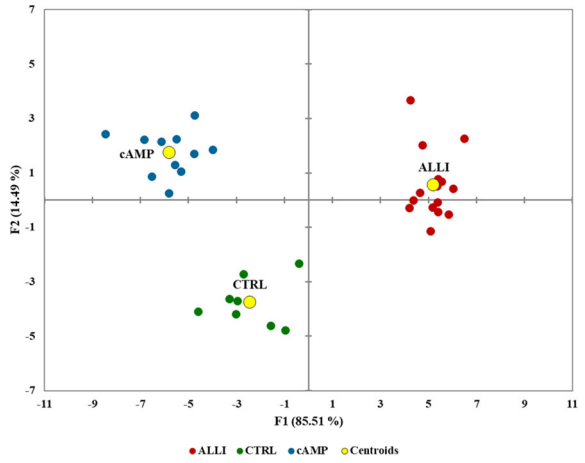


FIGURE 5
Biplot of canonical discriminant analysis to visualize the information of the whole mitochondrial dataset in the treatments and controls. F1 and F2 are canonical discriminant functions, and the two-component model separated the treatments. Centroids are shown as yellow circles. ALLI, 12.5 µg/mL allicin-treated cells; CTRL, control cells; cAMP, 500 µM dibutyryl cAMP-treated cells.

## RNAseq analysis

After removal of low abundance reads, the final mapping rate of the filtered transcript reads was 71.2%. Hierarchical clustering was performed on the initial analysis of the RNAseq results, that showed that the transcriptomic data was well-clustered according to the treatment. In addition, PCA showed the overall variability in the expression profile of the samples and treatments. Overall, there was a significant difference between CTRL and the treatments with cAMP and ALLI along the first principal component, which explained 61% of the variance, with smaller differences 28% along the second component (Figure S3).

Analysis of DEGs was performed between cells treated with allicin and cAMP compared to control cells and between allicin and cAMP treatments, based on a $\log_2$fold change of $|1|$ and an FDR adjusted $p$ value of $\leq 0.05$.

iDEP951 expression analysis significantly identified ($p < 0.05$) 820 up regulated genes between cells treated with ALLI *vs* cAMP, 1417 up regulated genes between cells treated with ALLI *vs* CTRL and 1647 between cells treated with cAMP *vs* CTRL cells. Significantly down regulated ($p < 0.05$) genes were 640 between cells treated with ALLI compared with cAMP, 1085 genes between cells treated with ALLI *vs* CTRL and 1521 between cells treated with cAMP compared with CTRL cells (Supplementary Table 1).

## GO term and KEGG analysis enriches genes of treated cells in cellular respiration, mitochondrial organization, and thermogenesis

To further investigate the function of the DEGs, GO term enrichment analysis was performed. The up- and down regulated DEGs were significantly enriched in biological processes (BP), molecular functions (MF) and cellular components (CC).

TABLE 1 Unidimensional test of equality of the means of the classes illustrating the contribution of different morphological features to the separation of differentially treated cells.

| Variable | Wilk's Lambda | F | p-value |
|---|---|---|---|
| Mean Aspect Ratio (au) | 0.746 | 5.795 | 0.007 |
| Simple tubules (%) | 0.765 | 5.224 | 0.011 |
| Mean Branch Length (µm) | 0.779 | 4.817 | 0.014 |
| Total Branch Length/area | 0.789 | 4.533 | 0.018 |
| Median Branch Length (µm) | 0.802 | 4.205 | 0.023 |
| Mean Network Size (Branches) (µm) | 0.805 | 4.115 | 0.025 |
| Mean Branch Length (µm) | 0.808 | 4.050 | 0.026 |
| Mean Form Factor (au) | 0.815 | 3.863 | 0.031 |
| Area_Large globules (%) | 0.834 | 3.392 | 0.045 |
| Mean Perimeter (µm) | 0.834 | 3.381 | 0.046 |

The most discriminant parameters have a low Wilk's lambda and a high F.

In all comparisons, 30 BP, CC and MF GO terms were found to be significantly enriched (Supplementary Tables 2–4). Notably, BP terms such as 'Oxoacid metabolic process', 'Small molecule metabolic process', 'Fatty acid metabolic process', 'Cellular respiration', 'Cellular lipid metabolic process', 'Energy derivation by oxidation of organic compounds', 'Monocarboxylic acid metabolic process' were down regulated in the ALLI_cAMP comparison, but up regulated in the ALLI_CTRL and cAMP_ CTRL comparisons (Supplementary Table 2). Interestingly 'Mitochondrion', 'Mitochondrial matrix', 'Mitochondrial inner membrane', 'Mitochondrial membrane', 'Mitochondrial envelope', 'Mitochondrial protein-containing complex' CC terms were down regulated in ALLI_cAMP comparison, but up regulated in ALLI_CTRL and in cAMP_ CTRL comparisons (Supplementary Table 3).

In contrast, significantly enriched MF terms such as 'Calcium ion binding', 'Cell adhesion molecule binding', 'Collagen binding', 'Extracellular matrix structural constituent', 'Glycosaminoglycan binding', 'Growth factor binding', 'Heparin binding', 'Integrin binding' and 'Signalling receptor binding' were up regulated in the ALLI_cAMP comparison, but down regulated in the ALLI_CTRL and in the cAMP_CTRL comparisons (Supplementary Table 4). Interestingly, significantly enriched MF terms such as 'Active transmembrane transporter activity', 'Electron transfer activity', 'Oxidoreductase activity' and 'Transmembrane transporter activity' were up regulated in the ALLI_CTRL and in the cAMP_CTRL comparisons (Supplementary Table 4).

Figure 6 shows the results of the KEGG analysis in the form of a graphical representation of the scatter plots. Each figure shows the KEGG enrichment of 15 identified pathways for each treatment comparison with the corresponding GeneRatio, adjusted *p*-value, and number of enriched genes in the corresponding pathways. The GeneRatio is defined as the number of enriched candidate genes compared with the total number of annotated genes included in the corresponding pathway in the KEGG analysis. Therefore, a higher GeneRatio indicates a higher enrichment of candidate genes in the corresponding pathway. KEGG analysis showed that DEGs were significantly down regulated within the 'PPAR pathway,' Fatty acid metabolism, elongation and degradation, and in 'Citrate cycle (TCA cycle)' in ALLI_cAMP comparison. Of note, DEGs were over-expressed in pathways such as 'cAMP signalling pathway,' 'Calcium signalling pathway,' and 'CGMP-PKG signalling pathway' in ALLI_cAMP comparison (Figure 6). ALLI_CTRL and cAMP_CTRL had common DEGs significantly enriched in 'Oxidative phosphorylation' and 'Thermogenesis', whereas DEGs within the 'PPAR signalling pathway' were down regulated in ALLI *vs* cAMP and up regulated only in cells under cAMP treatment (Figure 6).

These results suggest that the browning effect of ALLI is only evident when compared with CTRL cells, so the ALLI-cAMP contrast was not discussed further.

## Construction of PPI networks and module analysis of DEGs in cells treated with allicin and positive control indicate brown adipocyte differentiation associated with an increase in AMPK and PPARA signalling through downregulation of extracellular matrix organization

The PPIs of all up regulated and down regulated DEGs with combined scores greater than 0.4 were constructed from the three comparisons, and each entire PPI network was analysed using Cytohubba. The ten most highly regulated hub genes with a high degree of connectivity between nodes are listed in Table 2. The highly regulated hub genes in the ALLI_CTRL and cAMP_CTRL comparisons shared 6 genes such as PPARG, FASN, SREBF1, SCD, PPARGC1A, and ACLY. Both comparisons, referring to CTRL, were similarly enriched in 'Fatty acid synthase complex,' 'acetyl-CoA carboxylase complex,' 'AMPK signalling pathway,' 'PPARA activates gene


FIGURE 6
KEGG pathway enrichment analysis. Dot size represents the number of genes in each KEGG pathway; p.val (adjusted p-value): Red < orange < green. ALLI_cAMP = 12.5 μg/mL allicin-treated cells *vs* cAMP = 500 μM dibutyryl cAMP-treated cells; ALLI_CTRL = 12.5 μg/mL allicin-treated cells *vs* control cells; cAMP_CTRL =500 μM dibutyryl cAMP-treated cells *vs* control cells. Scatter plot was drawn by http://www.bioinformatics.com.cn/srplot.

expression,' 'Regulation of small molecule metabolic process,' and 'Thermogenesis'.

Four down regulated hub genes, such as FN1, THBS1, COL1A2, and CCN2, are common between ALLI- and cAMP-treated cells compared with CTRL cells (Table 3). Enrichment of both comparisons included 'AGE-RAGE signalling pathway in diabetic complications', 'PI3K-Akt signalling pathway', 'Focal adhesion', 'ECM-receptor interaction', and 'TGF-beta signalling pathway'.

TABLE 2 Top 10 hub genes from up regulated DEGs calculated by Degree topological algorithm of Cytohubba plugin.

| ALLI_CTRL | | | cAMP_CTRL | | |
|---|---|---|---|---|---|
| ank | Gene | Score | Rank | Gene | Score |
| 1 | PPARG | 100 | 1 | FASN | 100 |
| 2 | IL1B | 87 | 2 | PPARG | 97 |
| 3 | FASN | 86 | 3 | CS | 96 |
| 4 | SREBF1 | 84 | 3 | ACLY | 96 |
| 5 | EGF | 78 | 5 | SREBF1 | 94 |
| 5 | SCD | 78 | 6 | SCD | 89 |
| 7 | APOE | 74 | 7 | PPARGC1A | 87 |
| 7 | PPARGC1A | 74 | 8 | ACADM | 86 |
| 9 | CD4 | 73 | 9 | ACACA | 79 |
| 10 | ACLY | 69 | 9 | ACO2 | 79 |

ALLI_CTRL, 12.5 μg/mL allicin-treated cells vs control cells; cAMP_CTRL, 500 μM dibutyryl cAMP-treated cells vs control cells.

TABLE 3 Top 10 hub genes from down regulated DEGs calculated by Degree topological algorithm of Cytohubba plugin.

| ALLI_CTRL | | | cAMP_CTRL | | |
|---|---|---|---|---|---|
| Rank | Gene | Score | Rank | Gene | Score |
| 1 | FN1 | 96 | 1 | FN1 | 179 |
| 2 | MYC | 61 | 2 | IL6 | 130 |
| 3 | CD34 | 45 | 3 | CD44 | 104 |
| 4 | THBS1 | 39 | 4 | COL1A1 | 103 |
| 5 | COL1A2 | 38 | 5 | MMP2 | 99 |
| 5 | THY1 | 38 | 6 | ERBB2 | 83 |
| 5 | HGF | 38 | 7 | THBS1 | 82 |
| 8 | LOX | 36 | 7 | CCN2 | 82 |
| 8 | DCN | 36 | 7 | CCND1 | 82 |
| 8 | CCN2 | 36 | 10 | COL1A2 | 79 |

ALLI_CTRL, 12.5 μg/mL allicin-treated cells vs control cells; cAMP_CTRL, 500 μM dibutyryl cAMP-treated cells vs control cells.

## Genes upregulated by allicin and cAMP are enriched in the target genes of AR and PPARG, which are involved in the positive regulation of cold-induced thermogenesis and fatty acid metabolism

TRED analysis (http://rulai.cshl.edu/TRED) allows to know interaction data between transcription factors (TFs) and the promoters of their target genes, including binding motifs (38). In the ALLI_cAMP comparison, the target genes of only 1 TF (c-MYC) were down regulated and 15 were up regulated; in the ALLI_CTRL comparison, 4 TFs were down regulated and 3 (AR, PPARA, PPAG) were up regulated; in the cAMP_CTRL, 15 were down regulated and the same 3 of the ALLI_CTRL comparison were up regulated (Supplementary Table 5).

The up regulated genes were enriched in the target of AR in all comparisons (14 genes), whereas genes enriched in the target of PPARG (37 genes) and PPARA (18 genes) were enriched only in the ALLI_CTRL and cAMP_ CTRL comparisons (Supplementary Table 5). The target genes of JUN, SP1, and TP53 were significantly down regulated in the ALLI_CTRL and cAMP_CTRL comparisons but up regulated in the ALLI_cAMP comparison (Supplementary Table 5). Down regulated DEGs were enriched in target genes of EGR1, ETS1, SMAD1, SMAD3, SMAD4, and TFAP2A in the cAMP_CTRL comparison, but up regulated in ALLI_cAMP (Supplementary Table 5).

Enrichment analysis of the 14 genes targeting to AR and common to all comparisons showed significant up-regulation of 'Response to hormone, 'Regulation of lipid metabolic process', 'Regulation of small molecule metabolic process', 'Cellular response to hormone stimulus', 'Zinc finger nuclear hormone receptor-type' and 'PPARA activates gene expression'. The MCODE plugin cluster analysis did not filter any cluster with a score ≥ 5 for these genes.

The 37 DEGs targeting AR that were common only between ALLI and cAMP treatments compared with CTRL cells and the 51 common DEGs targeting PPARG resulted in only one MCODE cluster. No cluster with a score ≥ 5 was found for common DEGs targeting PPARA.

Enrichment analysis revealed the potential function of genes in each module. Shared DEGs targeted by AR and PPARG and over-expressed in ALLI_CTRL and cAMP_CTRL were enriched, among others, in 'PPARG signalling pathway' (Figures 7A, B red), 'Positive regulation of cold-induced thermogenesis' (Figures 7A, B, brown), 'Fatty acid metabolic process', 'AMPK signalling pathway' (Figures 7A, B, green), 'AMPK signalling pathway' (Figure 7A, blue) and 'PPARA activates gene expression' (Figure 7B, blue).

DEGs targeted by TP53, JUN and SP1 were down regulated in both ALLI_CTRL and cAMP_CTRL comparisons, but up regulated in ALLI_cAMP comparison. Shared DEGs targeted by SP1 and down-expressed in ALLI_CTRL and cAMP_CTRL were enriched in 'Interleukin-4 and Interleukin-13 signalling' (Figure 7C, red), and in 'Extracellular matrix organization' (Figure 7C, red). Interestingly, DEGs targeted by SP1 were found over-expressed in ALLI_cAMP comparison. Down regulated DEGs targeted by TP53 and JUN common to ALLI_CTRL and cAMP_CTRL were enriched in 'Interleukin-4 and Interleukin-13 signalling' and 'IL-18 signalling pathway' (data not shown).

## Allicin stimulation favors the differentiation into brown adipocyte

Allicin stimulation favors the differentiation into beige adipocyte The PROFAT tool (41) generated the heatmap of marker expression starting from normalized reads counts of SGBS cells. The estimation of BAT phenotype in ALLI- and cAMP-treated cells increased significantly ($p < 0.0001$) in comparison to CTRL cells. In contrast, WAT phenotype decreased significantly ($p < 0.0001$) in ALLI- and cAMP-treated cells compared with CTRL (Figure 8). These results evidenced that SGBS cells exhibit a gene expression pattern

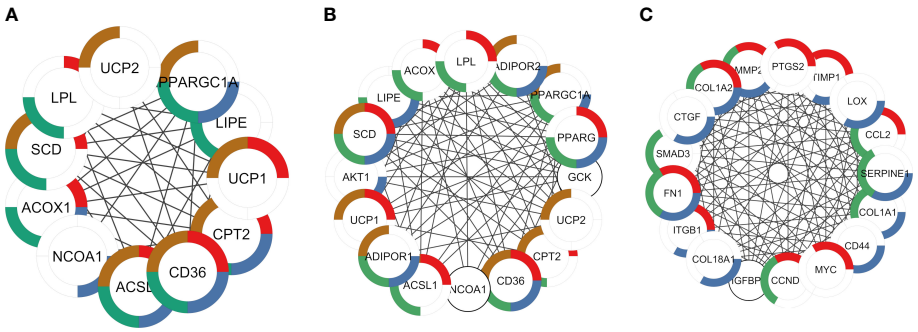


FIGURE 7
PPI networks identified by cluster functional analysis constructed with up- and down regulated DEG targets to TFs and overlapping to ALLI and cAMP treatments *vs* CTRL. The enriched pathways are marked in different colors. **(A)** Cluster 1 with a MCODE score of 7.83 achieved from up regulated genes target of AR. Red: genes enriched in 'PPARG signalling pathway' (FDR $1.82^{-12}$); brown: 'Positive regulation of cold-induced thermogenesis' (FDR $4.05^{-10}$); green: 'Fatty acid metabolic process' (FDR $3.08^{-09}$); and blue: 'PPARA activates gene expression (FDR $4.59^{-08}$). **(B)** Cluster 1 with a MCODE score of 10.47 achieved from up regulated genes target of PPARG. Red: genes enriched in 'PPARG signalling pathway' (FDR $3.10^{-13}$); brown: 'Positive regulation of cold-induced thermogenesis' (FDR $4.02^{-13}$); green: 'Fatty acid metabolic process' (FDR $5.23^{-13}$); and blue: 'AMPK signalling pathway' (FDR $5.53^{-12}$). **(C)** Cluster 1 with a MCODE score of 13.67 achieved from down regulated genes target of SP1. Red: genes enriched in 'Interleukin-4 and Interleukin-13 signalling (FDR $3.32^{-13}$); green: AGE-RAGE signalling pathway in diabetic complications (FDR $4.42^{-12}$); blue: 'Extracellular matrix organization' (FDR $7.12^{-12}$).

similar to that of brown cells during 6 days of differentiation under allicin treatment.

## Identification of common candidate targets among allicin, their organosulfur compounds and browning target genes

Because allicin is rapidly converted *in vitro* to its related fat-soluble organosulfur compounds such as DATS, DADS and DAS, the potential targets of these compounds and of allicin were screened by computational target fishing from the PharmMapper, STITCH, Swiss Target Prediction and GeneCard databases. By overlapping the highest ranked common targets of allicin and related organosulfur compounds with the 315 overlapped 'adipocyte-browning' genes, 26 common targets between allicin compounds and adipocyte-browning were used to create a GeneMania network (Supplementary Table 5). The results of the analysis showed that these 26 targets correlated with 20 others and a total of 407 different links were predicted to construct a network linking these 46 genes (Figure 9A). The constructed network had 33.99% physical interactions and 23.56% predicted functional relationships between genes. In addiction 20.58% shared the same protein domain and 13.85% shared similar co-expression characteristics, other results were pathways (5.24%) and colocalization (2.77%) as shown in Figure 9A. The molecular functions of the top ranked targets, filtered by their FDR score, were reported as GO categories. The preliminary network illustrated that the genes, depicted by different colours in Figure 9A, were involved in 'ligand-activated transcription factor activity', 'intracellular receptor signalling pathway', 'temperature homeostasis', 'regulation of cold induced thermogenesis', 'reactive

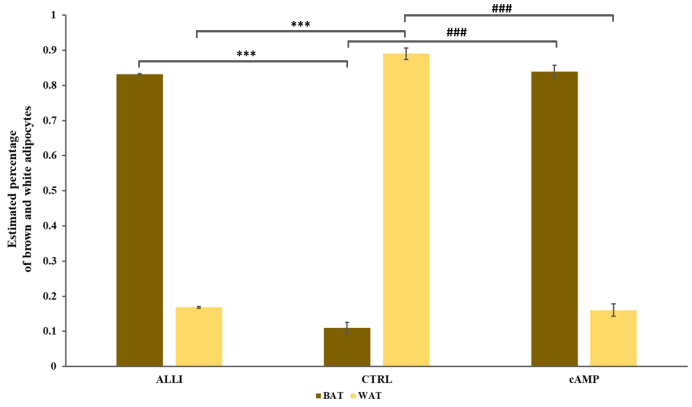


FIGURE 8
Statistical significance of PROFAT prediction percentage of brown and white adipocytes was determined using Euclidean distance and complete linkage on normalized gene expression values and analyzed by statistical test-t. *** = $p < 0.0001$ between estimated percentage of brown cells; ### = $p < 0.0001$ between estimated percentage of white cells. ALLI, 12.5 µg/mL allicin-treated cells; cAMP, 500 µM dibutyryl cAMP-treated cells; CTRL, control cells.

10.3389/fendo.2023.1141303

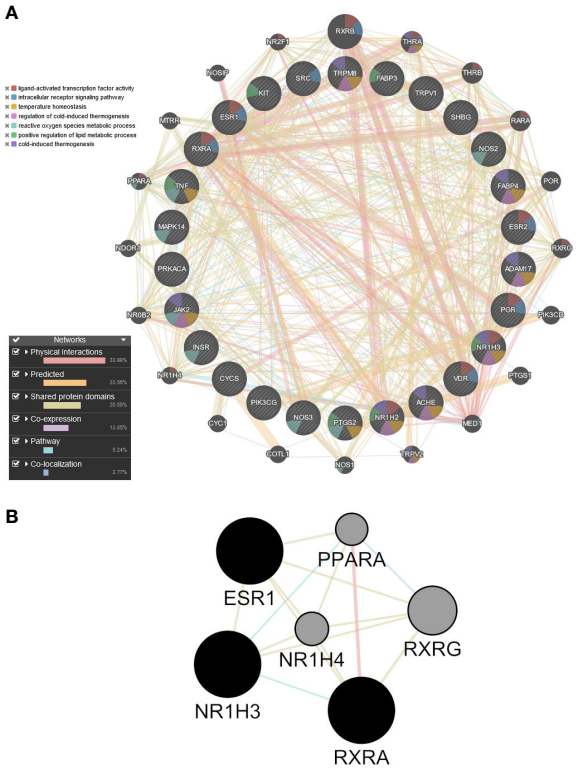


FIGURE 9
Preliminary PPI network constructed with GeneMANIA. **(A)** Twenty-six common targets between allicin, related fat-soluble organosulfur compounds and adipocytes-browning were built as assigned based on query gene. Genes are linked by functional associated networks filtered on their FDR score. Black nodes are the query targets and the larger the node, the higher degree of the node. The stronger interaction between node, the ticker and deeper colour of the edge. **(B)** Core PPI subnetwork generated by intersectional merge of PPI subnetworks according to the calculated degree, betweenness, closeness, eigenvector, LAC and network average values. ESR1, Estrogen Receptor 1; PPARA,Peroxisome Proliferator Activated Receptor Alpha; NR1H3, Nuclear Receptor Subfamily 1 Group H Member 3; NR1H4, Nuclear Receptor Subfamily 1 Group H Member 4; RXRA, Retinoid X Receptor Alpha; RXRG, Retinoid X Receptor Gamma.

oxygen species metabolic process', 'positive regulation of lipid metabolic process', and 'cold-induced thermogenesis'.

## PPI subnetwork construction and identification of core targets

A topological analysis of the preliminary network was performed using the CytoNCA plugin in Cytoscape to find the core proteins that form the preliminary network. The mean the degree (17.70), betweenness (48.96), closeness (0.49), eigenvector (0.106), LAC (12.40), network (10.95) values of the preliminary network was calculated, and the nodes of the preliminary PPI network that were above this mean were sorted out to build the corresponding subnetworks. Using the intersectional merge function in Cytoscape a core PPI subnetwork was extracted (Figure 9B) containing 6 key nodes (ESR1, NR1H3, NR1H4, PPARA, RXRA, RXRG) and 15 edges. Among these genes, Nuclear Receptor Subfamily 1 Group H Member 4 (NR1H4) and PPARA were significantly up regulated in the ALLI_CTRL comparison of SGBS cells (Supplementary Table 1), whereas estrogen receptor 1 (ESR1), Nuclear Receptor Subfamily 1 Group H Member 3 (NR1H3) and Retinoid X receptor alpha (RXRA) are common targets of allicin and related fat-soluble organosulfur compounds.

## The effects of allicin are related to mitochondrial biogenesis and lipid catabolism through the activation of core targets transcription factors

GO terms from biological process, cellular component, and molecular functions were examinedand the most enriched GO terms from biological process were 'intracellular receptor signalling pathway', 'cellular response to lipid', 'hormone-mediated signalling pathway', 'response to steroid hormone', 'response to lipid', whereas the most enriched GO terms from cellular component and molecular functions were 'transcription regulator complex', 'nuclear receptor activity', and ligand-activated transcription factor activity, respectively (data not shown).

KEGG pathways were analysed with a redundancy cut-off of 0.7, 17 pathways were statistically significant (FDR < 0.05) 'PPAR signalling pathway', 'Adipocytokine signalling pathway', 'Thyroid hormone signalling pathway', 'Non-alcoholic fatty liver disease, 'Insulin resistance' and 'Lipid and atherosclerosis'(data not shown).

The pathways enriched by Reactome analysis were 'Nuclear Receptor transcription pathway', 'PPARA activates gene expression', 'SUMOylation of intracellular receptors', Regulation of lipid metabolism by PPARalpha' and 'Mitochondrial biogenesis', which were shown as bubble plot combined with a Sankey diagram (Figure 10).

In addition, the score of the 6 key nodes identified by the topological analysis was scored using VarElect. The score indicates the strength of the association between the target and the 'cold induced thermogenesis' phenotype (Table 4). ESR1, PPARA, NR1H3, and NR1H4 scored > 6.

# Discussion

As a thermogenic organ, BAT is known to enhance energy metabolism and weight loss (50), so promoting mass and activity of BAT is one of the most promising strategies against obesity. Treatment of white adipose cells with rosiglitazone or with other β-adrenergic agonists induces beige cells with similar properties as BAT (51). Induction of the beige/brown fat cell phenotype leads not only to thermogenesis, but also to lipolysis, which facilitates energy metabolism, and mitochondrial dynamics, which precede the depolarization associated with heat dissipation (23). A high rate of mitochondrial fragmentation and free fatty acid release promote mitochondrial uncoupling and energy expenditure (52). Knowledge of the signalling pathways that stimulate the transition from white

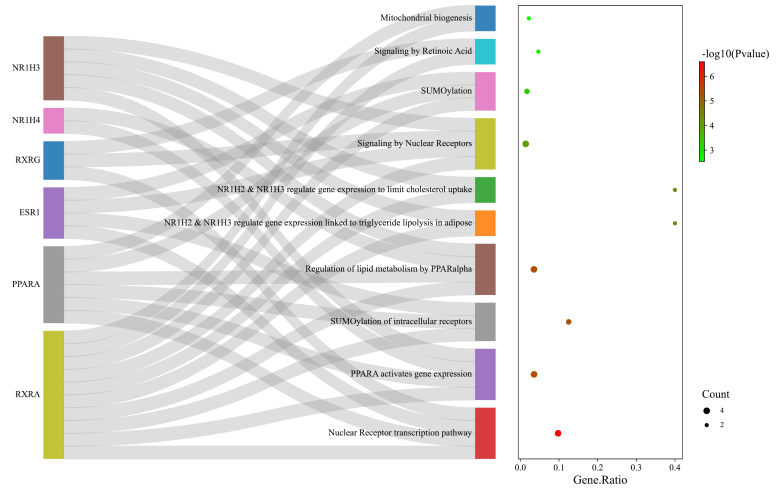


FIGURE 10
Bubble plot combined with Sankey diagram showing statistically significant Reactome pathways and the genes within each pathway. Figure was plotted by http://www.bioinformatics.com.cn/srplot.

to beige adipocytes, could help identify effective therapeutic strategies against obesity.

The discovery of functionally active BAT in adult humans and the possible recruitment of beige adipocytes by browning of WAT have introduced the way for new potential strategies for anti-obesity agents (53).

Previous studies have shown that SGBS cells gradually acquire BAT-like function in the absence of external stimulation during different days of differentiation, suggesting that lipid droplets t dynamics, and mitochondrial morphology (27) together with a differential expression of genes involved in extracellular matrix organization and oxidative stress are related to the brown fat phenotype (20). While it has been clearly demonstrated that the β3-adrenergic receptor (β3-AR) mediates thermogenesis in rodents (54), BAT is activated in humans by β2-AR signalling (55). Therefore, to bypass the ADRBs receptors dibutyryl-cAMP was chosen as a positive control.

The present study demonstrated that allicin supported the transition from white to beige adipocytes in SGBS after 6 days of differentiation and that the transformation of structural cell phenotype was evidenced by the dynamic changes in the size of LDs and the shape of mitochondria similar to those observed in the positive control.Lipolysis is generally considered an essential requirement for thermogenesis in brown and beige adipocytes, and any lipolytic compound could be a potential activator of thermogenesis (56). In HepG2 cells, allicin reduces lipid accumulation either by regulating AMPK-SREBPs and PKA-CREB signalling pathways (57) or by activating PPARA and FABP6 gene expression (58). The effect of allicin on lipid reduction argues for PPARγ/LXRα signalling in THP-1 macrophage foam cells (59). In the present work, ALLI and cAMP treatments decreased the area and diameter of LDs, but because the number of LDs/cell increased significantly with ALLI treatment, the lipolytic activity of allicin may have led to the formation of multilocular adipocytes, a feature of WAT browning. This is confirmed by the increased number of differentially expressed genes related to lipolysis, such as DNA fragmentation factor subunit alpha (DFFA), monoglyceride lipase (MGLL), perilipin 1 (PLIN1), patatin like phospholipase domain containing 2 (PNPLA2), lipoprotein lipase (LPL) and hormone-sensitive lipase (LIPE) in ALLI- and cAMP-treated cells (Supplementary Table 1). However, a thermogenic futile cycle of lipolysis/lipogenesis has been claimed to explain the unilocular to multilocular transformation during WAT browning (21). In 3T3-L1 cells exposed to β-adrenergic stimulation, remodelling of LDs involves first their reduction into small LDs and then their new

TABLE 4 Score of the six key nodes evaluated by VarElect.

| Gene Symbol | Description | -Log10(*P*) | Score |
|---|---|---|---|
| ESR1 | Estrogen Receptor 1 | 2.35 | 14.91 |
| PPARA | Peroxisome Proliferator Activated Receptor Alpha | 2.07 | 11.56 |
| NR1H3 | Nuclear Receptor Subfamily 1 Group H Member 3 | 1.49 | 6.30 |
| NR1H4 | Nuclear Receptor Subfamily 1 Group H Member 4 | 1.63 | 6.09 |
| RXRA | Retinoid X Receptor Alpha | 1.44 | 5.89 |
| RXRG | Retinoid X Receptor Gamma | 0.55 | 0.56 |

formation and subsequent enlargement (21). Indeed, significant expression of negative regulators of lipolysis such as G0/G1 switch gene 2 (G0S2) and patatin like phospholipase domain containing 3 (PNPLA3) were also found in ALLI-treated SBGS cells as well as the mRNA levels of the perilipin 4 (PLIN4), diacylglycerol o-acyltransferase 1 (DGAT1), diacylglycerol o-acyltransferase 2 (DGAT2) and adipocyte glycerol transporter aquaporin7 (AQP7), (Supplementary Table 1), indicating that the cells store and export metabolites released during lipolysis. Moreover, other studies have shown that triglyceride lipolysis catalysed by PNPLA2 in mice brown adipocytes is not required to maintain body temperature during cold exposure (60, 61) and that other sources such as circulating glucose and fatty acids can balance thermogenesis (62).

During cold exposure mitochondrial reorganization and free fatty acid release synergize to facilitate uncoupling and thereby heat production (23). Concomitantly, mitochondria acquire a spheroid morphology driven by increased fission (63). Present results show an increased in number and area of mitochondria in cells treated with allicin, and the data was also confirmed by the reduction of elongation (mean aspect ratio) and by the change from round to filamentous shape (mean form factor) in ALLI- and cAMP-treated cells. Network parameters obtained by MiNa also show a significant decrease in mean rod/branch length in both treatments compare to CTRL cells. According to the Micro2P plugin, six different subtypes of mitochondria with the highest proportion of small globules were classified in ALLI- and cAMP-treated cells. Canonical DA further evidenced that mitochondrial parameters specifically those related to mean aspect ratio, percentage of simple tubules, mean branch length, accurately clustered differentially treated cells and CTRL cells.

The high content of organosulfur compounds in garlic suggests that many of its active compounds may have anti-adipogenic effects by promoting the expression of genes specific for brown adipocytes (64). Recent data showed that allicin promotes browning of 3T3-L1 mouse adipocytes and iWAT by inducing the expression of brown marker genes through KLF15 signalling (16) or through the SIRT1-PGC1α-TFAM pathway (17).

PCA analysis based on reads clearly grouped the data set on the first component between CTRL cells and cells treated with ALLI or cAMP. On the second component, the treatments are separated, but the replicates of the same point were very close, indicating robust reproducibility of the data.

Classical thermogenesis is activated by adrenoreceptors that promote cAMP synthesis for PKA activation and expression of downstream targets (65). Intracellular cAMP levels are maintained by a balance between the rate of synthesis mediated by adenylate cyclase and the rate of degradation regulated by cAMP phosphodiesterase 3 (PDE3). Allicin is known to increase intracellular cAMP by inhibiting phosphodiesterase activity in isolated human platelets (66, 67) or by increasing adenylate cyclase activity in the human bronchial epithelial cell line (68). In adipose tissue, PDE3 inhibitors increase intracellular cAMP levels, thereby enhancing lipolysis (69). The present results showed a significant up-regulation of PDE3B in ALLI_CTRL and cAMP_CTRL (Supplementary Table 1), resulting in an increase in intracellular cAMP and downstream genes involved in lipolysis, such as LIPE and PLIN1, and in browning, such as TBX1 and UCP1 (Supplementary Table 1). This is consistent with the results obtained in adipose tissue of mice fed a high-fat diet when treated with cilostazol, a selective inhibitor of phosphodiesterase III with multiple effects on metabolism (70). In addition, cilostazol, which has antiplatelet, antithrombotic, and vasodilatory properties similar to allicin, increased the intracellular concentration of cAMP, which stimulated the expression of thermogenic and brown specific genes (70). The BP GO terms enrichment, such as cellular respiration and cellar lipid metabolic process as well as CC GO terms related to mitochondria were significantly up regulated in ALLI- and cAMP-treated cells compared with CTRL cells, suggesting similar activity in cells with different treatments, but was opposite when ALLI-treated cells were compared with cAMP-treated cells. MF GO terms, such as oxidoreductase activity, were up regulated in ALLI- and cAMP-treated cells compared with CTRL cells, but down regulated in ALLI-treated and cAMP-treated cells. Therefore, the positive browning effect of ALLI treatment was evident only in comparison with CTRL cells, but not in comparison with cAMP incubation. However, ALLI and cAMP treatments shared the most up regulated hub genes such as PPARG, FASN, SREBF1, SCD, PPARGC1A, and ACLY, which are related to fatty acid metabolic process, fatty acid oxidation and response to cold. The lowest down regulated hub genes common to ALLI and cAMP treatments FN1, THBS, COL1A2 and CCN2 were enriched in ECM receptor interactions, integrin cell surface interactions and focal adhesion. This is consistent with the down regulation of collagen, integrin and laminin genes (COL1A1, COL1A2, ITGA2, ITGA3, ITGA4, ITGA5, LAMA1, LAMA2, LAMA3; Supplementary Table 1) observed in SGBS cells during differentiation (20) demonstrating their ability to adjust cytoskeletal reorganization according to their size, LDs dynamics and thermogenesis (71).

KEGG pathway enrichment confirmed that oxidative phosphorylation, thermogenesis, and fatty acid metabolism were the most significantly up-regulated pathways in the ALLI_CTRL and cAMP_CTRL comparisons, whereas ECM-receptor interaction, PI3K-Akt signalling pathway and Focal adhesion were downregulated. In contrast, pathways related to PPAR and fatty acid metabolism were significantly downregulated in the ALLI_ cAMP comparison.

Interestingly, an *in vivo* study suggests that the allyl-containing sulphides of garlic significantly enhance thermogenesis and increase epinephrine and norepinephrine levels in rat plasma (72), which is why allicin may interact with the adrenergic receptor (AR), which is one of the most effective mechanisms to deplete excess energy through cAMP/PKA-dependent signal transduction (73). In the present study, up regulated DEGs common to ALLI_CTRL and cAMP_CTRL comparisons and the targets of transcription factor AR were significantly associated with 'PPARG signalling pathway', 'positive regulation of cold-induced thermogenesis', 'fatty acid metabolic process' and 'PPARA activates gene expression'. All of these metabolic pathways and processes share the genes for fatty acid translocase (FATP or CD36), acyl-coA synthetase long chain family member 1 (ACSL1) and carnitine palmitoyltransferase II (CPT2), each of which is involved in the storage and recycling of

fatty acids, their conversion to acyl-CoA and transport to mitochondria (74). Their co-expression is clearly part of the thermogenesis programme. In 3T3-L1 adipocytes, CD36 has been found to play an important lipolytic role (75) and its translocation from the cell membrane to lipid droplets mediates the release of long-chain fatty acids by exocytosis (76). In human macrophages aged garlic extract inhibits CD36 expression through modulation of the PPARγ pathway (77), but in SGBS cells, its over expression together with that of LPL, and aquaporin 7 (AQP7) (Supplementary Table 1) can lead to triglycerides uptake and then lipolysis associated with heat production (78). In addition, CD36 has been found to be a scavenger receptor required for coenzyme Q (CoQ10) uptake in BAT and therefore essential for adaptive thermogenesis and BAT morphology, (79). Of note, CoQ10 is up regulated in ALLI-treated SGBS cells (Supplementary Table 1).

ACSL1 and CPT2 have been shown to be required for fatty acid oxidation for cold-induced thermogenesis (80). Interestingly, all of these genes are downstream targets of the nuclear transcription factor PPARA, which is expressed in metabolically active tissues such as brown adipose tissue (81). In contrast, down regulated DEGs targets of SP1 and other TFs, such as TP53 and JUN, were involved in 'Interleukin-4 and Interleukin-13 signalling' and 'Extracellular matrix organization', 'Cytokine-mediated signalling pathways' and 'IL-18 signalling pathways', as previously described in SGBS cells (20). In particular, the down regulation of fibronectin (FN1), collagen type I alpha 1 chain (COL1A1), collagen type I alpha 2 chain (COL1A2) is associated with that of the zinc finger transcription factor early growth response-1 (EGR1) (Supplementary Table 1) and, in mice, with a concomitant increase of beige cells differentiation and a decrease in genes encoding the extracellular matrix proteins (82). The down regulations of cell-surface glycoprotein CD44 and its receptor ONP in SGBS cells treated with allicin and cAMP (Supplementary Table 1) further confirms the browning activity of the compounds present in garlic. CD44 was recently recognized as a major receptor for an extracellular matrix component that plays an essential role in promoting obesity and diabetes (83).

Brown features were also confirmed by PROFAT analysis, which revealed a significant increase in 80% of genes related to BAT phenotype.

Using open-source tools, computational target fishing facilitates the investigation of biological targets of bioactive molecules using the reverse pharmacophore mapping approach (84) (Supplementary Table 6). To understand potential targets involved in the browning process six major targets ESR1, NR1H3, RXRA, PPARA, NR1H4, and RXRG were extracted from the comparison of targets of allicin and related organosulfur compounds with browning genesafter topological analysis. The targets were strongly associated, and enrichment analysis confirmed the involvement of these genes in limiting cholesterol uptake, lipolysis and mitochondrial biogenesis, all processes in which allicin plays a role. The lipolytic role of allicin may be related to the activation of PPARA through the release of fatty acids. RXRA forms heterodimers with PPARA to regulate the expression of genes involved in fatty acid oxidation (ACOX1, ACADM, CYP4A1, HMGCS2), fatty acid transport (CD36, SLC27A1, CPT2), and lipid storage (PLIN) (85), that were over expressed by ALLI treatment (Supplementary Table 1). This is consistent with the activation of PPARA promoted by allicin in palmitic acid-loaded HepG2 cells (58). Again, garlic essential oil significantly up regulated PPARA expression level in the liver of HFD-fed mice compared with control mice (86). Moreover, PPARA was found to be associated with the expression of superoxide dismutase (CuZn-SOD) in human aortic endothelial cells (87), a scavenger of ROS, which is consistent with the antioxidant properties of allicin. Of note, ESR1 is known to induce a selective beiging in 3T3-L1 cells leading to ATGL-mediated lipolysis (88). Moreover, in human and mouse adipocytes ESR1 promotes mitochondrial remodelling and thermogenesis through uncoupled respiration by regulating the mitochondrial gene POLG1 (89). All of downstream genes of these metabolic pathways, such as SOD1, ATGL, and POLG were significantly expressed in SGBS cells (Supplementary Table 1).

## Conclusion

Overall, this study supports the modulatory role of allicin in stimulating the brown phenotype of SGBS cells, which is associated with an increase in mitochondrial biogenesis and lipid catabolism. The possible mechanism of this interesting process may be based on the partial interaction of allicin within the regulatory steps of cAMP signalling and PPARA signalling.

However, the study has some limitations, because neither down-regulation of SIRT5 nor significant up-regulation of KLF15, as recently reported, was detected in SGBS cells. The mechanism by which allicin promotes browning and induces mitochondrial biogenesis is not yet fully elucidated, and functional studies could be performed to further investigate the browning effect.

## Data availability statement

The original contributions presented in the study are included in the article/Supplementary Material. Further inquiries can be directed to the corresponding author.

## Author contributions

UA and MC designed the study. UA performed the experiments and collected data. MC collected data measurements, performed statistical analyses prepared the figures and wrote the manuscript. MW and DT provided SGBS cells and were involved in the revision of the paper. All authors read and approved the manuscript. All authors contributed to the article and approved the submitted version.

## Funding

This research did not receive any specific grant from funding agencies in the public, commercial, or not-for-profit sectors.

## Conflict of interest

The authors declare that the research was conducted in the absence of any commercial or financial relationships that could be construed as a potential conflict of interest.

The handling editor EKK declared a past co-authorship with the author MW.

## Publisher's note

All claims expressed in this article are solely those of the authors and do not necessarily represent those of their affiliated organizations, or those of the publisher, the editors and the reviewers. Any product that may be evaluated in this article, or claim that may be made by its manufacturer, is not guaranteed or endorsed by the publisher.

## Supplementary material

The Supplementary Material for this article can be found online at: https://www.frontiersin.org/articles/10.3389/fendo.2023.1141303/full#supplementary-material

## References

1. Oliver P, Lombardi A, De Matteis R. Editorial: Insights into brown adipose tissue functions and browning phenomenon. *Front Physiol* (2020) 11:219. doi: 10.3389/fphys.2020.00219

2. Wu J, Boström P, Sparks LM, Ye L, Choi JH, Giang AH, et al. Beige adipocytes are a distinct type of thermogenic fat cell in mouse and human. *Cell* (2012) 150:366–76. doi: 10.1016/j.cell.2012.05.016

3. Montanari T, Pošćić N, Colitti M. Factors involved in white-to-brown adipose tissue conversion and in thermogenesis: A review. *Obes Rev* (2017) 18:495–513. doi: 10.1111/obr.12520

4. Manríquez-Núñez J, Ramos-Gómez M. Bioactive compounds and adipocyte browning phenomenon. *Curr Issues Mol Biol* (2022) 44:3039–52. doi: 10.3390/cimb44070210

5. Amagase H. Clarifying the real bioactive constituents of garlic. *J Nutr* (2006) 136 (3 Suppl):716S–25S. doi: 10.1093/jn/136.3.716S

6. Borlinghaus J, , (Née Reiter) FJ, Kappler U, Antelmann H, Ulrike Noll U, Gruhlke MCH, et al. Allicin, the odor of freshly crushed garlic: A review of recent progress in understanding allicin's effects on cells. *Molecules* (2021) 26:1505. doi: 10.3390/molecules26061505

7. Hu Y, Xu J, Gao R, Xu Y, Huangfu B, Asakiya C, et al. Diallyl trisulfide prevents adipogenesis and lipogenesis by regulating the transcriptional activation function of KLF15 on PPARγ to ameliorate obesity. *Mol Nutr Food Res* (2022) 66:e2200173. doi: 10.1002/mnfr.202200173

8. Miron T, Listowsky I, Wilchek M. Reaction mechanisms of allicin and allyl-mixed disulfides with proteins and small thiol molecules. *Eur J Med Chem* (2010) 45:1912–8. doi: 10.1016/j.ejmech.2010.01.031

9. Ankri S, Mirelman D. Antimicrobial properties of allicin from garlic. *Microbes Infect* (1999) 1:125–9. doi: 10.1016/s1286-4579(99)80003-3

10. Oommen S, Anto RJ, Srinivas G, Karunagaran D. Allicin (from garlic) induces caspase-mediated apoptosis in cancer cells. *Eur J Pharmacol* (2004) 485:97–103. doi: 10.1016/j.ejphar.2003.11.059

11. Bat-Chen W, Golan T, Peri I, Ludmer Z, Schwartz B. Allicin purified from fresh garlic cloves induces apoptosis in colon cancer cells *via* Nrf2. *Nutr Cancer* (2010) 62:947–57. doi: 10.1080/01635581.2010.509837

12. Arreola R, Quintero-Fabián S, López-Roa RI, Flores-Gutiérrez EO, Reyes-Grajeda JP, Carrera-Quintanar L, et al. Immunomodulation and anti-inflammatory effects of garlic compounds. *J Immunol Res* (2015) 2015:401630. doi: 10.1155/2015/401630

13. Tedeschi P, Nigro M, Travagli A, Catani M, Cavazzini A, Merighi S, et al. Therapeutic potential of allicin and aged garlic extract in alzheimer's disease. *Int J Mol Sci* (2022) 23:6950. doi: 10.3390/ijms23136950

14. Gupta N, Porter TD. Garlic and garlic-derived compounds inhibit human squalene monooxygenase. *J Nutr* (2001) 131:1662–7. doi: 10.1093/jn/131.6.1662

15. Chen YC, Kao TH, Tseng CY, Chang WT, Hsu CL. Methanolic extract of black garlic ameliorates diet-induced obesity *via* regulating adipogenesis, adipokine biosynthesis, and lipolysis. *J Funct Food* (2014) 9:98–108. doi: 10.1016/j.jff.2014.02.019

16. Lee CG, Rheea DK, Kimb BO, Umc SH, Pyo S. Allicin induces beige-like adipocytes *via* KLF15 signal cascade. *J Nutr Biochem* (2019) 64:13–24. doi: 10.1016/j.jnutbio.2018.09.014

17. Zhang C, He X, Sheng Y, Xu J, Yang C, Zheng S, et al. Allicin regulates energy homeostasis through brown adipose tissue. *iScience* (2020) 23:101113. doi: 10.1016/j.isci.2020.101113

18. Wabitsch. M, Brenner. RE, Melzner. I, Braun. M, Möller. P, Heinze E, et al. Characterization of a human preadipocyte cell strain with high capacity for adipose differentiation. *Int J Obes Relat Metab Disord* (2001) 25:8–15. doi: 10.1038/sj.ijo.0801520

19. Halbgebauer D, Dahlhaus M, Wabitsch M, Fischer-Posovszky P, Tews. D. Browning capabilities of human primary adipose-derived stromal cells compared to SGBS cells. *Sci Rep* (2020) 10:9632. doi: 10.1038/s41598-020-64369-7

20. Colitti M, Ali U, Wabitsch M, Tews D. Transcriptomic analysis of Simpson golabi behmel syndrome cells during differentiation exhibit BAT-like function. *Tissue Cell* (2022) 77:101822. doi: 10.1016/j.tice.2022.101822

21. Barneda D, Frontini A, Cinti S, Christian M. Dynamic changes in lipid droplet-associated proteins in the "browning" of white adipose tissues. *Biochim Biophys Acta* (2013) 1831:924–33. doi: 10.1016/j.bbalip.2013.01.015

22. Nishimoto Y, Tamori YJ. CIDE family-mediated unique lipid droplet morphology in white adipose tissue and brown adipose tissue determines the adipocyte energy metabolism. *Atheroscler. Thromb* (2017) 24:989–98. doi: 10.5551/jat.RV17011

23. Wikstrom JD, Mahdaviani K, Liesa M, Sereda SB, Si Y, Las G, et al. Hormone-induced mitochondrial fission is utilized by brown adipocytes as an amplification pathway for energy expenditure. *EMBO J* (2014) 33:418–36. doi: 10.1002/embj.201385014

24. Klusóczki Á., Veréb Z, Vámos A, Fischer-Posovszky P, Wabitsch M, Bacso Z, et al. Differentiating SGBS adipocytes respond to PPARγ stimulation, irisin and BMP7 by functional browning and beige characteristics. *Sci Rep* (2019) 9:5823. doi: 10.1038/s41598-019-42256-0

25. Hirsch K, Danilenko M, Giat J, Miron T, Rabinkov A, Wilchek M, et al. Effect of purified allicin, the major ingredient of freshly crushed garlic, on cancer cell proliferation. *Nutr Canc.* (2009) 38:245–54. doi: 10.1207/S15327914NC382_14

26. Bäcker V. (2012). ImageJ macro tool sets for biological image analysis, in: *ImageJ User and Developer Conference 2012*, Luxembourg. doi: 10.13140/RG.2.1.2868.9446

27. Montanari T, Colitti M. Simpson-Golabi-Behmel syndrome human adipocytes reveal a changing phenotype throughout differentiation. *Histochem Cell Biol* (2018) 149:593–605. doi: 10.1007/s00418-018-1663-z

28. Boschi F, Rizzatti V, Zoico E, Montanari T, Zamboni M, Sbarbati A, et al. Relationship between lipid droplets size and integrated optical density. *Eur J Histochem* (2019) 63:3017. doi: 10.4081/ejh.2019.3017

29. Chaudhry A, Shi R, Luciani DS. A pipeline for multidimensional confocal analysis of mitochondrial morphology, function, and dynamics in pancreatic β-cells. *Am J Physiol Endocrinol Metab* (2020) 318:E87–E101. doi: 10.1152/ajpendo.00457.2019

30. Valente AJ, Maddalena LA, Robb WL, Moradi F, Stuart JA. A simple ImageJ macro tool for analyzing mitochondrial network morphology in mammalian cell culture. *Acta Histochem* (2017) 119:315–26. doi: 10.1016/j.acthis.2017.03.001

31. Peng JY, Lin CC, Chen YJ, Kao LS, Liu YC, Chou CC, et al. Automatic morphological subtyping reveals new roles of caspases in mitochondrial dynamics. *PloS Comput Biol* (2011) 7:e1002212. doi: 10.1371/journal.pcbi.1002212

32. Iannetti EF, Smeitink JAM, Beyrath J, Willems PHGM, Koopman WJH. Multiplexed high-content analysis of mitochondrial morphofunction using live-cell microscopy. *Nat Protoc* (2016) 11:1693–710. doi: 10.1038/nprot.2016.094

33. Dobin A, Davis CA, Schlesinger F, Drenkow J, Zaleski C, Jha S, et al. STAR: Ultrafast universal RNA-seq aligner. *Bioinformatics* (2013) 29:15–21. doi: 10.1093/bioinformatics/bts635

34. Ge SX, Son EW, Yao R. iDEP: an integrated web application for differential expression and pathway analysis of RNA-seq data. *BMC Bioinf* (2018) 19:534. doi: 10.1186/s12859-018-2486-6

35. Ge X. iDEP web application for RNA-seq data analysis. *Methods Mol Biol* (2021) 2284:417–43. doi: 10.1007/978-1-0716-1307-8_22

36. Ashburner M, Ball CA, Blake JA, Botstein D, Butler H, Cherry JM, et al. Gene ontology: Tool for the unification of biology. *Nat Genet* (2000) 25:25–9. doi: 10.1038/75556

37. Kanehisa M, Goto S. KEGG: Kyoto encyclopedia of genes and genomes. *Nucleic Acids Res* (2000) 28:27–30. doi: 10.1093/nar/28.1.27

38. Jiang C, Xuan Z, Zhao F, Zhang MQ. TRED: A transcriptional regulatory element database, new entries and other development. *Nucleic Acids Res* (2007) 35:137–40. doi: 10.1093/nar/gkl1041

39. Chin CH, Chen SH, Wu HH, Ho CW, Ko MT, Lin CY. CytoHubba: Identifying hub objects and sub-networks from complex interactome. *BMC Syst Biol* (2014) 8 (Suppl 4):S11. doi: 10.1186/1752-0509-8-S4-S11

40. Bader GD, Hogue CW. An automated method for finding molecular complexes in large protein interaction networks. *BMC Bioinf* (2003) 4:2. doi: 10.1186/1471-2105-4-2

41. Cheng Y, Jiang L, Keipert S, Zhang S, Hauser A, Graf E, et al. Prediction of adipose browning capacity by systematic integration of transcriptional profiles. *Cell Rep* (2018) 23:3112–25. doi: 10.1016/j.celrep.2018.05.021

42. Liu X, Ouyang S, Yu B, Huang K, Liu Y, Gong J, et al. PharmMapper server: A web server for potential drug target identification *via* pharmacophore mapping approach. *Nucleic Acids Res* (2010) 38:W609–14. doi: 10.1093/nar/gkq300

43. Wang X, Shen Y, Wang S, Li S, Zhang W, Liu X, et al. PharmMapper 2017 update: a web server for potential drug target identification with a comprehensive target pharmacophore database. *Nucleic Acids Res* (2017) 45:W356–60. doi: 10.1093/nar/gkx374

44. Szklarczyk D, Santos A, von Mering C, Jensen LJ, Bork P, Kuhn M. STITCH 5: augmenting protein-chemical interaction networks with tissue and affinity data. *Nucleic Acids Res* (2016) 44:D380–384. doi: 10.1093/nar/gkv1277

45. Daina A, Michielin O, Vincent Z. SwissTargetPrediction: Updated data and new features for efficient prediction of protein targets of small molecules. *Nucleic Acids Res* (2019) 47:W357–64. doi: 10.1093/nar/gkz382

46. Warde-Farley D, Donaldson SL, Comes O, Zuberi K, Badrawi R, Chao P, et al. The GeneMANIA prediction server: biological network integration for gene prioritization and predicting gene function. *Nucleic Acids Res* (2010) 38 Suppl: W214–220. doi: 10.1093/nar/gkq537

47. Tang Y, Li M, Wang J, Pan Y, Wu FX. CytoNCA: a cytoscape plugin for centrality analysis and evaluation of protein interaction networks. *Biosystems* (2015) 127:67–72. doi: 10.1016/j.biosystems.2014.11.005

48. Stelzer G, Plaschkes I, Oz-Levi D, Alkelai A, Olender T, Zimmerman S, et al. VarElect: the phenotype-based variation prioritizer of the GeneCards suite. *BMC Genomics* (2016) 17(Suppl 2):444. doi: 10.1186/s12864-016-2722-2

49. Addinsoft. *XLSTAT statistical and data analysis solution*. USA: New York (2022). Available at: https://www.xlstat.com/en.

50. Harms M, Seale P. Brown and beige fat: development, function and therapeutic potential. *Nat Med* (2013) 19:1252–63. doi: 10.1038/nm.3361

51. Cheng L, Wang J, Dai H, Duan Y, An Y, Shi L. Brown and beige adipose tissue: a novel therapeutic strategy for obesity and type 2 diabetes mellitus. *Adipocyte* (2021) 10:48–65. doi: 10.1080/21623945.2020.1870060

52. Gao AW, Houtkooper RH. Mitochondrial fission: Firing up mitochondria in brown adipose tissue. *EMBO J* (2014) 33:401–2. doi: 10.1002/embj.201487798

53. Murugan DD, Balan D, Wong PF. Adipogenesis and therapeutic potentials of antiobesogenic phytochemicals: Insights from preclinical studies. *Phytother Res* (2021) 35:5936–60. doi: 10.1002/ptr.7205

54. Cypess AM, Weiner LS, Roberts-Toler C, Franquet EE, Kessler SH, Kahn PA, et al. Activation of human brown adipose tissue by a β3-adrenergic receptor agonist. *Cell Metab* (2015) 21:33–8. doi: 10.1016/j.cmet.2014.12.009

55. Blondin DP, Nielsen S, Kuipers EN, Severinsen MC, Jensen VH, Miard S, et al. Human brown adipocyte thermogenesis is driven by β2-AR stimulation. *Cell Metab* (2020) 32:287–300. doi: 10.1016/j.cmet.2020.07.005

56. Braun K, Oeckl J, Westermeier J, Li Y, Klingenspor M. Non-adrenergic control of lipolysis and thermogenesis in adipose tissues. *J Exp Biol* (2018) 221(Pt Suppl 1): jeb165381. doi: 10.1242/jeb.165381

57. Lu J, Cheng C, Fang B, Meng Z, Zheng Y, Tian X, et al. Protective effects of allicin on 1,3-DCP-induced lipid metabolism disorder in HepG2 cells. *Biomed Pharmacother.* (2017) 96:1411–7. doi: 10.1016/j.biopha.2017.10.125

58. Cheng B, Li T, Li F. Use of network pharmacology to investigate the mechanism by which allicin ameliorates lipid metabolism disorder in HepG2 cells. *Evid. Based Complement. Alternat. Med* (2021) 12:3956504. doi: 10.1155/2021/3956504

59. Lin XL, Hu HJ, Liu YB, Hu XM, Fan XJ, Zou WW, et al. Allicin induces the upregulation of ABCA1 expression *via* PPARγ/LXRα signaling in THP-1 macrophage-derived foam cells. *Int J Mol Med* (2017) 39:1452–60. doi: 10.3892/ijmm.2017.2949

60. Schreiber R, Diwoky C, Schoiswohl G, Feiler U, Wongsiriroj N, Abdellatif M. Cold-induced thermogenesis depends on ATGL-mediated lipolysis in cardiac muscle, but not brown adipose tissue. *Cell Metab* (2017) 26:753–763.e7. doi: 10.1016/j.cmet.2017.09.004

61. Shin H, Ma Y, Chanturiya T, Cao Q, Wang Y, Kadegowda AKG, et al. Lipolysis in brown adipocytes is not essential for cold-induced thermogenesis in mice. *Cell Metab* (2017) 26:764–777.e5. doi: 10.1016/j.cmet.2017.09.002

62. Chitraju C, Fischer AW, Farese R, Walther. TC. Lipid droplets in brown adipose tissue are dispensable for cold-induced thermogenesis. *Cell Rep* (2020) 33:108348. doi: 10.1016/j.celrep.2020.108348

63. Von Bank H, Hurtado-Thiele M, Oshimura N, Simcox J. Mitochondrial lipid signaling and adaptive thermogenesis. *Metabolites* (2021) 11:124. doi: 10.3390/metabo11020124

64. Quesada I, de Paola M, Torres-Palazzolo C, Camargo A, Ferder L, Manucha W, et al. Effect of garlic's active constituents in inflammation, obesity and cardiovascular disease. *Curr Hypertens Rep* (2020) 22:6. doi: 10.1007/s11906-019-1009-9

65. Tabuchi C, Sul HS. Signaling pathways regulating thermogenesis. *Front Endocrinol* (2021) 12:595020. doi: 10.3389/fendo.2021.595020

66. Agarwal KC. Therapeutic actions of garlic constituents. *Med Res Rev* (1996) 16:111–24. doi: 10.1002/(SICI)1098-1128(199601)16:1<111::AID-MED4>3.0.CO;2-5

67. Allison GL, Lowe GM, Rahman K. Aged garlic extract inhibits platelet activation by increasing intracellular cAMP and reducing the interaction of GPIIb/IIIa receptor with fibrinogen. *Life Sci* (2012) 91:1275–80. doi: 10.1016/j.lfs.2012.09.019

68. Qiu ZR, Xu JB, Chen L, Huang ZX, Lei TL, Huang ZY. Allicin facilitates airway surface liquid hydration by activation of CFTR. *Front Pharmacol* (2022) 13:890284. doi: 10.3389/fphar.2022.890284

69. Chaves VE, Frasson D, Kawashita NH. Several agents and pathways regulate lipolysis in adipocytes. *Biochimie* (2011) 93:1631–40. doi: 10.1016/j.biochi.2011.05.018

70. Seo DH, Shin E, Lee YH, Park SE, Nam KT, Kim JW, et al. Effects of a phosphodiesterase inhibitor on the browning of adipose tissue in mice. *Biomedicines* (2022) 10:1852. doi: 10.3390/biomedicines10081852

71. Gonzalez Porras MA, Stojkova K, Vaicik MK, Pelowe A, Goddi A, Carmona A, et al. Integrins and extracellular matrix proteins modulate adipocyte thermogenic capacity. *Sci Rep* (2021) 11:5442. doi: 10.1038/s41598-021-84828-z

72. Oi Y, Kawada T, Shishido C, Wada K, Kominato Y, Nishimura S, et al. Allyl-containing sulfides in garlic increase uncoupling protein content in brown adipose tissue, and noradrenaline and adrenaline secretion in rats. *J Nutr* (1999) 129:336–42. doi: 10.1093/jn/129.2.336

73. Cannon B, Nedergaard JAN. Brown adipose tissue: Function and physiological significance. *Physiol Rev* (2004) 84:277–359. doi: 10.1152/physrev.00015.2003

74. Hankir MK, Klingenspor M. Brown adipocyte glucose metabolism: A heated subject. *EMBO Rep* (2018) 19:e46404. doi: 10.15252/embr.201846404

75. Zhou D, Samovski D, Okunade AL, Stahl PD, Abumrad NA, Su X. CD36 level and trafficking are determinants of lipolysis in adipocytes. *FASEB J* (2012) 26:4733–42. doi: 10.1096/fj.12-206862

76. Daquinag AC, Gao Z, Fussell C, Immaraj L, Pasqualini R, Arap W, et al. Fatty acid mobilization from adipose tissue is mediated by CD36 posttranslational modifications and intracellular trafficking. *JCI Insight* (2021) 6:e147057. doi: 10.1172/jci.insight.147057

77. Morihara N, Ide N, Weiss N. Aged garlic extract inhibits CD36 expression in human macrophages *via* modulation of the PPARgamma pathway. *Phytother Res* (2010) 24:602–8. doi: 10.1002/ptr.3008

78. van der Vaart JI, Boon MR, Houtkooper RH. The role of AMPK signaling in brown adipose tissue activation. *Cells* (2021) 10:1122. doi: 10.3390/cells10051122

79. Anderson CM, Kazantzis M, Wang J, Venkatraman S, Goncalves RL, Quinlan CL, et al. Dependence of brown adipose tissue function on CD36-mediated coenzyme q uptake. *Cell Rep* (2015) 10:505–15. doi: 10.1016/j.celrep.2014.12.048

80. Lee J, Ellis JM, Wolfgang MJ. Adipose fatty acid oxidation is required for thermogenesis and potentiates oxidative stress-induced inflammation. *Cell Rep* (2015) 10:266–79. doi: 10.1016/j.celrep.2014.12.023

81. Grygiel-Górniak B. Peroxisome proliferator-activated receptors and their ligands: nutritional and clinical implications – a review. *Nutr J* (2014) 13:17. doi: 10.1186/1475-2891-13-17

82. Milet C, Bléher M, Allbright K, Orgeur M, Coulpier F, Duprez D, et al. Egr1 deficiency induces browning of inguinal subcutaneous white adipose tissue in mice. *Sci Rep* (2017) 7:16153. doi: 10.1038/s41598-017-16543-7

83. Weng X, Maxwell-Warburton S, Hasib A, Ma L, Kang L. The membrane receptor CD44: Novel insights into metabolism. *Trends Endocrinol Metab* (2022) 33:318–32. doi: 10.1016/j.tem.2022.02.002

84. Forouzesh A, Samadi Foroushani S, Forouzesh F, Zand E. Reliable target prediction of bioactive molecules based on chemical similarity without employing statistical methods. *Front Pharmacol* (2019) 10:835. doi: 10.3389/fphar.2019.00835

85. Rakhshandehroo M, Knoch B, Müller M, Kersten S. Peroxisome proliferator-activated receptor alpha target genes. *PPAR Res* (2010) 2010:612089. doi: 10.1155/2010/612089

86. Lai YS, Chen WC, Ho CT, Lu KH, Lin SH, Tseng HC, et al. Garlic essential oil protects against obesity-triggered nonalcoholic fatty liver disease through modulation of lipid metabolism and oxidative stress. *J Agric Food Chem* (2014) 62:5897–906. doi: 10.1021/jf500803c

87. Inoue I, Goto S, Matsunaga T, Nakajima T, Awata T, Hokari S, et al. The ligands/activators for peroxisome proliferator-activated receptor alpha (PPARalpha) and PPARgamma increase Cu2+, Zn2+-superoxide dismutase and decrease p22phox message expressions in primary endothelial cells. *Metabolism* (2001) 50:3–11. doi: 10.1053/meta.2001.19415

88. Santos RS, Frank AP, Fatima LA, Palmer BF, Oz OK, Clegg DJ. Activation of estrogen receptor alpha induces beiging of adipocytes. *Mol Metab* (2018) 18:51–9. doi: 10.1016/j.molmet.2018.09.002

89. Zhou Z, Moore TM, Drew BG, Ribas V, Wanagat J, Civelek M, et al. Estrogen receptor α controls metabolism in white and brown adipocytes by regulating Polg1 and mitochondrial remodeling. *Sci Transl Med* (2020) 12:eaax8096. doi: 10.1126/scitranslmed.aax8096

frontiers | Frontiers in Endocrinology

TYPE Original Research
PUBLISHED 02 March 2023
DOI 10.3389/fendo.2023.1136245

Check for updates

OPEN ACCESS

EDITED BY
Endre Károly Kristóf,
University of Debrecen, Hungary

REVIEWED BY
Naresh Chandra Bal,
KIIT University, India
Daniel Tews,
University of Ulm, Germany

*CORRESPONDENCE
Francesc Villarroya
fvillarroya@ub.edu
Lourdes Ibáñez
lourdes.ibanez@sjd.es

†These authors have contributed equally to this work

SPECIALTY SECTION
This article was submitted to Cellular Endocrinology, a section of the journal Frontiers in Endocrinology

RECEIVED 02 January 2023
ACCEPTED 20 February 2023
PUBLISHED 02 March 2023

CITATION
Garcia-Beltran C, Navarro-Gascon A, López-Bermejo A, Quesada-López T, de Zegher F, Ibáñez L and Villarroya F (2023) Meteorin-like levels are associated with active brown adipose tissue in early infancy.
*Front. Endocrinol.* 14:1136245.
doi: 10.3389/fendo.2023.1136245

COPYRIGHT
© 2023 Garcia-Beltran, Navarro-Gascon, López-Bermejo, Quesada-López, de Zegher, Ibáñez and Villarroya. This is an open-access article distributed under the terms of the Creative Commons Attribution License (CC BY). The use, distribution or reproduction in other forums is permitted, provided the original author(s) and the copyright owner(s) are credited and that the original publication in this journal is cited, in accordance with accepted academic practice. No use, distribution or reproduction is permitted which does not comply with these terms.

# Meteorin-like levels are associated with active brown adipose tissue in early infancy

Cristina Garcia-Beltran[1,2†], Artur Navarro-Gascon[3,4†], Abel López-Bermejo[5,6], Tania Quesada-López[3,4], Francis de Zegher[7], Lourdes Ibáñez[1,2*] and Francesc Villarroya[1,3,4*]

[1]Research Institute Sant Joan de Déu, University of Barcelona, Barcelona, Spain, [2]Centro de Investigación Biomédica en Red de Diabetes y Enfermedades Metabólicas Asociadas (CIBERDEM), Health Institute Carlos III, Madrid, Spain, [3]Biochemistry and Molecular Biomedicine Department, Biomedicine Institute, University of Barcelona, Barcelona, Spain, [4]Network Biomedical Research Center of Physiopathology of Obesity and Nutrition (CIBEROBN), Health Institute Carlos III, Madrid, Spain, [5]Department of Pediatrics, Dr. Josep Trueta Hospital, Girona, Spain, [6]Department of Medical Sciences, Faculty of Medicine, University of Girona, Girona, Spain, [7]Leuven Research and Development, University of Leuven, Leuven, Belgium

**Introduction:** Meteorin-like (METRNL) is a hormonal factor released by several tissues, including thermogenically active brown and beige adipose tissues. It exerts multiple beneficial effects on metabolic and cardiovascular systems in experimental models. However, the potential role of METRNL as brown adipokine in humans has not been investigated previously, particularly in relation to the metabolic adaptations taking place in early life, when brown adipose tissue (BAT) is particularly abundant.

**Methods and materials:** METRNL levels, as well as body composition (DXA) and circulating endocrine-metabolic variables, were assessed longitudinally in a cohort of infants at birth, and at ages 4 and 12 months. BAT activity was measured by infrared thermography at age 12 months. METRNL levels were also determined cross-sectionally in adults; *METRNL* gene expression (qRT-PCR) was assessed in BAT and liver samples from neonates, and in adipose tissue and liver samples form adults. Simpson-Golabi-Behmel Syndrome (SGBS) adipose cells were thermogenically activated using cAMP, and *METRNL* gene expression and METRNL protein released were analysed.

**Results:** Serum METRNL levels were high at birth and declined across the first year of life albeit remaining higher than in adulthood. At age 4 and 12 months, METRNL levels correlated positively with circulating C-X-C motif chemokine ligand 14 (CXCL14), a chemokine released by thermogenically active BAT, but not with parameters of adiposity or metabolic status. METRNL levels also correlated positively with infrared thermography-estimated posterior-cervical BAT activity in girls aged 12 months. Gene expression analysis indicated high levels of *METRNL* mRNA in neonatal BAT. Thermogenic stimulus of brown/beige adipocytes led to a significant increase of *METRNL* gene expression and METRN protein release to the cell culture medium.

10.3389/fendo.2023.1136245

**Conclusion:** Circulating METRNL levels are high in the first year of life and correlate with indices of BAT activity and with levels of an established brown adipokine such as CXCL14. These data, in addition with the high expression of *METRNL* in neonatal BAT and in thermogenically-stimulated brown/beige adipocytes, suggest that METRNL is actively secreted by BAT and may be a circulating biomarker of BAT activity in early life.

KEYWORDS

**meteorin-like (METRNL), brown adipose tissue (BAT), brown adipokine, infancy, thermogenesis**

# 1 Introduction

Meteorin-like protein (METRNL), also known as Meteorin-β, interleukin-41 and subfatin, is a recently identified hormone involved in metabolic regulation and considered a candidate biomarker of metabolic syndrome (1). In rodent models, METRNL is highly expressed in brown adipose tissue (BAT) upon thermogenic activation and also in skeletal muscle after exercise (2). METRNL was found to promote energy expenditure and glucose tolerance through the induction of alternatively activated macrophages at adipose depots and by promoting the browning of adipose tissue. Further research showed that peroxisome proliferator–activated receptor-γ (PPARγ) enhances the capacity of METRNL to antagonize insulin resistance in adipose tissue (3). METRNL also attenuates inflammation and insulin resistance in skeletal muscle *via* AMP-activated protein kinase and PPARδ-dependent pathways (4, 5). The beneficial effects of METRNL have been associated with innate immunity (6, 7), and protection against cardiac dysfunction (8, 9). In adult humans, METRNL levels are low in patients with obesity and diabetes and correlate negatively with glucose levels and markers of insulin resistance (10–13).

Metabolic and nutritional alterations in the early postnatal life are not only relevant for health during infancy but may also contribute to the development of metabolic syndrome in later life. In recent years, the activity of thermogenic (brown/beige) adipose tissues in adult humans has gained attention as a protective factor against obesity, type 2 diabetes and cardiovascular disease (14). This is attributed to the capacity of BAT to both drain glucose and lipids for adaptive thermogenesis and to secrete adipokines with healthy effects on metabolism (15). However, despite the existing awareness that BAT size and activity are particularly relevant in infants (16), the pathophysiological consequences of distinct BAT activities early after birth have not been studied. The identification of BAT-derived adipokines in infants and their capacity to be used as biomarkers of metabolic health has also been scarcely undertaken, and only a few circulating molecules, such as bone morphogenetic protein-8B (BMP8B) and C-X-C motif chemokine ligand 14 (CXCL14), have respectively been associated with BAT activity in newborns and in one-year-old infants (17–19).

Here we determined for the first time the circulating levels of METRNL across the first year of life and disclosed a significant association between this variable and the extent of BAT activity.

# 2 Materials and methods

## 2.1 Study population and ethics

The primary study cohort consisted of 50 infants (27 girls and 23 boys) who were enrolled prenatally during the customary third trimester visit among Caucasian pregnant mothers consecutively seen in the outpatient clinics of Hospital Sant Joan de Déu and Hospital de Sant Boi – Parc Sanitari Sant Joan de Déu (Barcelona, Spain) (Supplementary Figure 1). These infants had previously participated in a longitudinal study assessing BAT activity and circulating levels of CXCL14 and BMP8B in the first year of life (18, 19).

Inclusion criteria were: maternally uncomplicated, singleton pregnancy with delivery at term (37-42 weeks), exclusive breastfeeding or formula-feeding in the first 4 months, postnatal follow-up completed (at 15 days, 4 and 12 months) and written informed consent. Exclusion criteria were maternal disease, alcohol or drug abuse, congenital malformations and complications at birth. Birth weight was not considered as inclusion or exclusion criterium; accordingly, the study population included infants with a wide range of birth weight Z-scores (between −2.9 and +1.0).

Circulating METRNL was exclusively measured in a subset of infants who had spare serum sample available at birth (20 girls and 18 boys), and at age 4 and 12 months (26 girls and 16 boys). Serum METRNL was also measured in 30 mothers of those infants (age, 33.6 ± 0.9 years) during the third trimester of pregnancy (Supplementary Figure 1). In addition, serum METRNL concentrations were analyzed cross-sectionally in healthy adult women (N= 10; age, 38.7 ± 1.9 years)

*METRNL* mRNA gene expression was assessed in dorso-interscapular BAT (N= 5) and liver (N= 6) post-mortem samples obtained on occasion of autopsies (2–3 h after the death) of Caucasian newborns with a gestational age of 28–36 weeks who survived, at most, 3 days post-partum, supplied by the Academy of

Sciences of the Czech Republic as previously described (20) (Supplementary Table 1). For comparison, *METRNL* mRNA gene expression was also determined in adult liver samples (obtained from hepatic biopsies performed when a hepatic tumor was suspected, with a negative ultimate result), deltoid muscle samples (from adult individuals who underwent skeletal muscle biopsy because of muscle complaint in whom skeletal muscle histology was thereafter normal) and subcutaneous adipose tissue samples (obtained from volunteers), as described (8, 21).

The study was approved by the Institutional Review Board of the University of Barcelona, Sant Joan de Déu University Hospital; all participating mothers signed the informed consent at recruitment.

## 2.2 Clinical and endocrine-metabolic assessments

Maternal data were retrieved from hospital clinical records. Gestational age was calculated according to the last menses and validated by first-trimester ultrasound. Weight and length of the newborns were measured immediately after delivery, and again at age 4 months and 12 months.

Maternal venous samples were obtained during the third trimester of gestation, between week 28 and delivery. Neonatal blood samples were obtained at birth from the umbilical cord before placenta separation (22). At age 4 and 12 months, venous samples were obtained during the morning in the fasting state. Adult venous samples were also obtained after overnight fasting. The serum fraction of the samples was separated by centrifugation and stored at -80°C until analysis.

Serum glucose, insulin, insulin-like growth factor (IGF)-I, high-molecular-weight (HMW) adiponectin, CXCL14 and BMP8B were assessed as previously reported (18, 19). Serum METRNL levels were determined in serum and cell culture media with a specific human enzyme-linked immunosorbent assay kit [R&D Systems, Minneapolis, MN, USA; sensitivity: 0.64 ng/mL; intra-assay coefficient of variation (CV) <10%; inter-assay CV < 12%].

## 2.3 Body composition and BAT activity assessment

Body composition was assessed at age 15 days, 4 months and 12 months by dual-energy X-ray absorptiometry (DXA) with a Lunar Prodigy and Lunar software (version 3.4/3.5; Lunar Corp., Madison, WI, USA) adapted for infants (22).

As previously described (18), BAT activity at age 12 months was estimated through the infrared thermography-based measurement of the skin temperature overlying BAT depots. The parameters assessed included the maximal temperature at the posterior cervical ($T_{PCR}$) and supraclavicular ($T_{SCR}$) regions, and the extent of active BAT in these regions ($Area_{PCR}$ and $Area_{SCR}$).

## 2.4 Cell cultures of neonatal beige adipocytes

Pre-adipocyte cells obtained post-mortem from a 3-month-old infant with Simpson Golabi Behmel Syndrome (SGBS cells) (23), capable to differentiate into adipocytes bearing a beige phenotype (24, 25) were used. SGBS pre-adipocytes were maintained in Dulbecco's modified Eagle's (DMEM)/F12 medium, 10% fetal bovine serum (FBS). Beige adipogenic differentiation was initiated by incubating confluent cell cultures for 4 days in serum-free medium plus 20 nM insulin, 0.2 nM triiodothyronine, 100 nM cortisol, 25 nM dexamethasone, 500 µM 3-isobutyl-1-methyl-xanthine, and 2 µM rosiglitazone. Subsequently, cells were switched to DMEM/F12, 20 nM insulin, 0.2 nM triiodothyronine, and 100 nM cortisol and maintained for up to 10 days, when more than 90% cells have acquired differentiated adipocyte morphology. To induce thermogenic activation of adipocytes, differentiated cells were treated with 1mM dibutyril-cAMP for 24 hours. All cell culture reagents and drugs were from Sigma-Aldrich (St Louis, Missouri, USA). Cells were collected for RNA isolation and the cell culture medium, corresponding to 24 h before harvest, was also collected for measurement of METRNL levels.

## 2.5 RNA isolation and qRT-PCR analyses

RNA was extracted from tissues and cells using an affinity-based method (NucleoSpin, Macherey-Nagel, Germany). *METRNL, UCP1, PPARGC1A, DIO2 and BMP8B* transcript levels were determined by qRT-PCR using TaqMan technology (Thermo Fisher Scientific, Waltham, MA, USA). 0.5 µg RNA were retrotranscribed using random hexamer primers (Thermo Fisher Scientific, Waltham, MA, USA). For qRT-PCR, the *METRNL* (Hs00417150), *UCP1* (Hs00222453*), PPARGC1A* (Hs00173304), *DIO2* (Hs00255341), *BMP8B* (Hs01629120) TaqMan Gene Expression assay probes were used, with reaction mixtures containing 1 µL cDNA, 10 µL TaqMan Universal PCR Master Mix (Thermo Fisher Scientific, Waltham, MA, USA), 250 nM probes and 900 nM of primers from the Assays-on-Demand Gene Expression Assay Mix (Thermo Fisher Scientific, Waltham, MA, USA). The 18S rRNA transcript (Hs99999901) was measured as housekeeping reference gene. The mRNA level of *METRNL* and *UCP1*: PGC1a, Dio2, Bmp8b in tissues and cells sample was normalized to that of the reference control using the comparative ($2^{-\Delta CT}$) method.

## 2.6 Statistics

Statistical analyses were implemented in SPSS version 27.0 (SPSS software, IBM, Armonk, NY, USA), GraphPad Prism 5 (GraphPad Software, CA, USA) and R Project version 4.2.2 (RStudio, MA, USA). Results are shown as mean ± standard error of the mean (SEM). Variables with normal distribution were compared with two-tailed Student's t-test. Chi-square test was used to compare qualitative variables. Correlation and stepwise multi-regression analysis were used to study associations between circulating METRNL levels and the assessed variables; outliers were detected using a studentized residual outlier test and excluded from further analyses; this approach did not modify the statistical significance of any analysis. Covariance analysis was used to

adjust for ponderal index and breastfeeding. A P-value < 0.05 was considered statistically significant.

# 3 Results

## 3.1 METRNL levels in the first year of life

Supplementary Table 2 shows the longitudinal data from infants over the first year of life and from their mothers in late pregnancy in the cohort in which serum METRNL assessment was performed. As previously reported (18, 19), girls had less lean mass, higher levels of circulating CXCL14 and higher posterior BAT activity.

When splitting METRNL levels by sex, or by type of early feeding, no differences were found at any study time; accordingly, the results were pooled. Circulating METRNL concentrations in infants at birth were higher than at the postnatal ages of 4 and 12 months, and higher than in non-pregnant women (Figure 1).

## 3.2 Correlations between METRNL levels and clinical, endocrine-metabolic and body composition variables

The associations between circulating levels of METRNL and anthropometric, adiposity-related, and endocrine-metabolic parameters, including some putative brown adipokines (CXCL14, BMP8B), throughout follow-up are shown in Supplementary Table 3. At birth, circulating METRNL levels were negatively related to abdominal fat only in girls (R= -0.678; P= 0.013, Supplementary Table 3). At age 4 months, circulating METRNL showed a strong positive correlation with circulating CXCL14 concentrations in the entire population (R= 0.648; P= 0.002) (Figure 2A). At age 12 months, METRNL concentrations were also positively correlated with CXCL14 levels (R= 0.693, P= 0.001) (Figure 2B). This correlation was maintained when girls were analyzed separately (R= 0.698; P= 0.012).

## 3.3 Correlations between METRNL concentrations and parameters of BAT activity

BAT activity at the posterior cervical and supraclavicular regions at age 12 months was analyzed in a subset of infants of the study cohort by using infrared thermography-based procedures, as previously described (18). Correlations between circulating METRNL levels at all time points and indicators of BAT activity at age 12 months are summarized in Supplementary Table 4. Significant positive correlations between posterior-cervical BAT activity and METRNL levels at 4 months (R= 0.400; P= 0.047; Figure 3A) and at 12 months (R= 0.432; P= 0.006; Figure 3B) were disclosed. Separate analyses by sex revealed a significant correlation between BAT activity and METRNL levels at 12 months only in girls (R= 0.426; P= 0.004).

## 3.4 *METRNL* expression in neonatal and adult tissues

*METRNL* expression levels in human neonatal post-mortem samples were significantly higher in dorso-interscapular BAT than in the liver. In addition, *METRNL* expression in neonatal BAT was much higher than in adult adipose tissue, skeletal muscle, and liver (Figure 4).

## 3.5 Activation of neonatal brown/beige adipocytes leads to increased *METRNL* expression and secretion of METRNL

Neonatal adipocytes differentiated into beige phenotype (SGBS cells) were thermogenically activated using cAMP (26). *METRNL* gene expression was dramatically induced, similarly to the thermogenic biomarker *UCP1* (Figure 5A) and other marker genes of brown/beige phenotype such as peroxisome proliferator-activated receptor-γ coactivator-1α (*PPARGC1A*), iodothyronine 5'-deiodinase (*DIO2*) and *BMP8B* (Supplementary Figure 2).

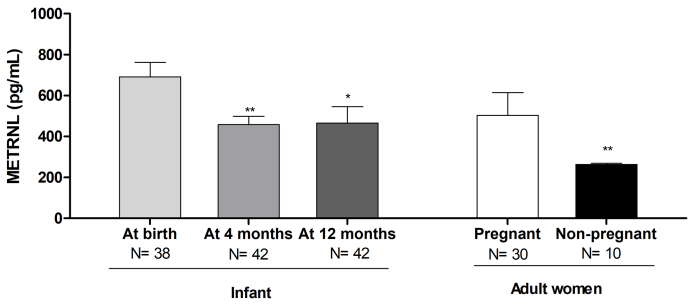


FIGURE 1
Serum Meteorin-like (METRNL) concentrations in human infants at birth and at age 4 and 12 months, in the mothers of those infants during the third trimester of pregnancy, and in healthy adult women. *P<0.05, **P<0.01 vs at birth. P values are adjusted for ponderal index and breastfeeding.

10.3389/fendo.2023.1136245

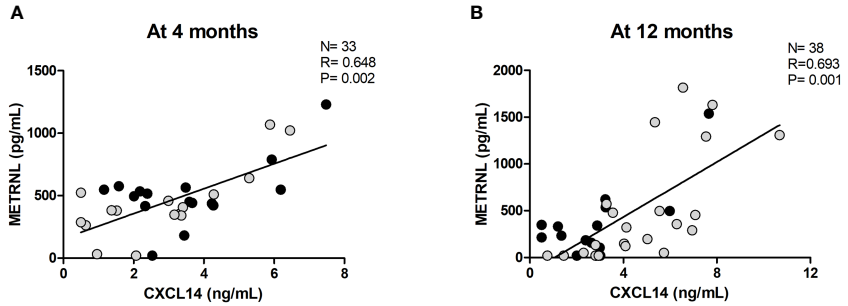


FIGURE 2
Correlation between circulating Meteorin-like (METRNL) and C-X-C motif chemokine ligand 14 (CXCL14) at age 4 months **(A)** and 12 months **(B)**. Grey dots correspond to girls and black dots represent boys. P values are adjusted for ponderal index and breastfeeding.

Moreover, thermogenic activation of the cells also induced a significant increase in the release of METRNL protein to the culture medium (Figure 5B).

## 4 Discussion

The present study is, to our knowledge, the first to have assessed the circulating concentrations of METRNL in human infants, and to have related METRNL levels to BAT activity.

Our study demonstrates that circulating levels of METRNL – a novel adipokine that promotes browning of white adipocytes upon thermogenic stimulus (2) – is high at birth as compared to adult values and decreases over the first year of human life, although remaining higher than in adults. These findings are in line with those recently reported on circulating BMP8B – another brown adipokine involved in thermoregulation and metabolic homeostasis – that shows a similar decreasing trend from birth to age 12 months (19). Moreover, our data also disclosed a high expression of *METRNL* in neonatal human BAT and in thermogenic activated neonatal brown/beige adipocytes, as well as an increased secretion of METRNL in thermogenically activated cells, which confirms the capacity of human neonatal brown adipocytes to secrete this adipokine. Altogether, these data highlight the elevated activity of BAT after birth, when the demands for thermogenesis and risks for hypothermia can be especially high (16), and the concomitant production of BAT-secreted adipokines such as METRNL.

Circulating METRNL concentrations displayed a positive association with posterior-cervical BAT activity, as well as with circulating levels of CXCL14 – a chemokine secreted by active brown/beige adipose tissue (27). These data fit well with previous studies reporting a positive correlation between circulating CXCL14 levels and BAT activity in early life (18), and also between CXCL14 and METRNL expression in adult adipose tissue (28). Interestingly, CXCL14 and METRNL have emerged as circulating factors that modulate M2 macrophage activation playing a role in brown/beige thermogenic regulation (2, 27).

There is evidence of an interplay between BAT and skeletal muscle development in large mammalian species, which is characterized by a progressive decline in BAT after birth concomitant with skeletal muscle maturation, and this may affect BAT and muscle secretome (29). In rodents, skeletal muscle is a relevant site of *METRNL* gene expression (2) whereas in adult humans *METRNL* expression is low (8) but induced after exercise (2, 30). Lack of availability of muscle samples -or tissues other than BAT and liver- from neonates and young infants is a limitation of our study on *METRL* expression, and thus we cannot exclude a role of muscle or other tissues in influencing systemic METRNL levels in early development. Given the developmental overlap between BAT and muscle (29), it can't be excluded that the correlation between

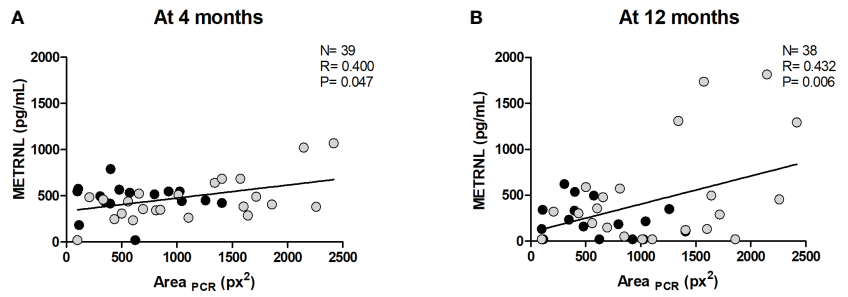


FIGURE 3
Correlation between the area of active brown adipose tissue at the posterior cervical region, as determined by infrared thermography ($Area_{PCR}$), at age 12 months, and circulating Meteorin-like (METRNL) concentrations at age 4 months **(A)** and at age 12 months **(B)**. Grey dots correspond to girls and black dots represent boys. P values are adjusted for ponderal index and breastfeeding.

10.3389/fendo.2023.1136245

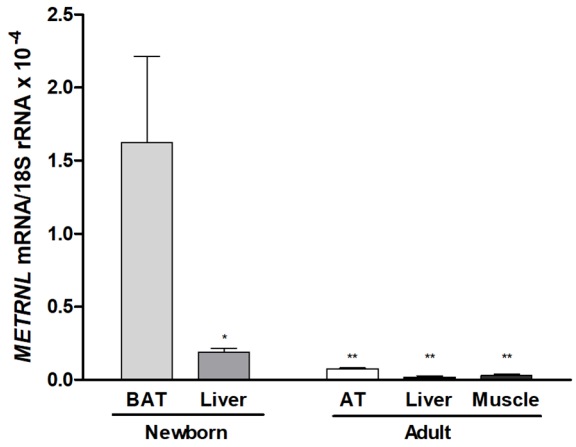


FIGURE 4
Meteorin-like (*METRNL*) gene expression levels in dorso-interscapular brown adipose tissue (BAT, N= 5) and liver (N= 6) obtained from post-mortem autopsies of newborns with a gestational age of 28–36 weeks who survived, at most, 3 days post-partum, and samples from subcutaneous adipose tissue (AT, N= 5), skeletal muscle (N = 5) and liver (N= 5) from healthy adults. Data are mean ± SEM of relative levels of *METRNL* mRNA (*METRNL* mRNA/18S rRNA). *P<0.05; **P<0.01 *vs* neonatal BAT.

METRNL levels and BAT activity in early infancy is indeed an indirect reflection of METRNL release by muscle. In any case, data retrieved from the transcriptomics database in muscle from infants in the first year of life and elderly adults does not indicate relevant differences in *METRNL* gene expression (31). Further studies would be required to establish the relative contribution of BAT and muscle to METRNL level changes in the first year of life.

Although METRNL levels were not different between girls and boys, the above-mentioned associations of METRNL levels in relation to BAT activity and CXCL14 levels at age 12 months were only maintained in girls. This finding may fit with the previously reported observation that BAT activity at that age is higher in girls than in boys (18) and with prior data reporting sex-based differences in the levels of other putative batokines such as CXCL14 and BMP8B (18, 19). There is extensive evidence of sex-based differences in BAT thermogenic activity due to direct and indirect hormonal mechanisms (32) and it is likely that sex-based differences occur also for the BAT secretome.

The distinct prevalence of "classic brown" versus "beige" adipocytes at specific anatomical BAT depots in humans (33, 34) may explain why circulating METRNL levels correlate with measures of posterior-cervical – but not supraclavicular – BAT activity. Differential secretory properties of brown-versus-beige cells have not yet been reported (even in experimental models) but a distinct capacity for METRNL secretion by different types of thermogenic adipocytes could account for the preferential association between METRNL levels and posterior-cervical BAT. On the other hand, high METRNL levels in early life, released by BAT and perhaps also by other tissues may promote a "browned" phenotype in white adipose depots in infants, given the known effects of METRNL in inducing the browning of adipose tissue (8), which would be especially adaptive to the thermally challenging conditions occurring in early infancy.

Circulating METRNL levels did not show significant correlations with systemic parameters of endocrine-metabolic status or adiposity in our cohort. This indicates that, although

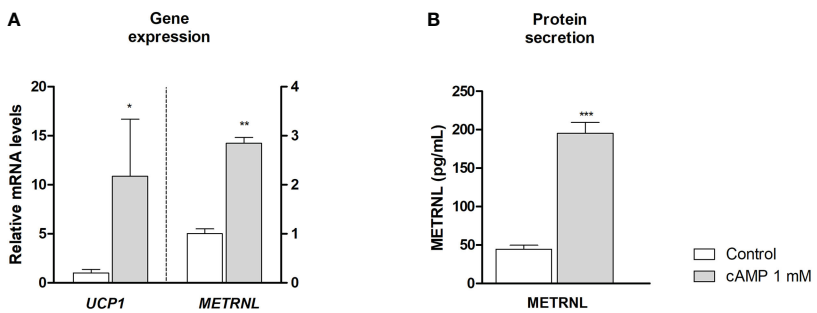


FIGURE 5
Meteorin-like (*METRNL*) gene expression **(A)** and METRNL protein secretion **(B)** by neonatal SGBS beige adipocytes. *METRNL* and uncoupling protein-1 (*UCP1*) transcript level **(A)** and METRNL protein levels **(B)** accumulating in cell culture medium after 24 h treatment of cell with 1 mM dibutyril-cAMP and untreated controls. Data mean ± SEM, N= 3 each condition. *P<0.05; **P<0.01; ***P<0.001 *vs* control.

METRNL concentrations appear to be a potential indicator of the extent of BAT activity in one-year-old infants, they are poorly informative about their general endocrine-metabolic status. Possibly, the fact that our cohort involved apparently healthy children exhibiting no major differences in metabolic or adiposity parameters among individuals, precluded the identification of meaningful associations. Along these lines, the only significant correlation was the negative association between METRNL levels and abdominal fat in girls, present only at birth. Although this finding is reminiscent of the negative correlations between METRNL levels and visceral adiposity found in adults with obesity and/or type 2 diabetes (12, 13), the fact that it occurs only at birth indicates the need for future studies to explore a possible involvement of METRNL in the fat accretion occurring during late fetal development, something totally unknown to date.

Our study has several limitations, among them the relatively low number of serum samples available for METRNL assessment, the lack of tissue samples for *METRNL* mRNA gene expression from infants of the studied cohort due to obvious ethical reasons, and the lack of follow-up beyond age 1 year. Moreover, the lack of availability of neonatal samples from additional tissues (e.g. muscle) for gene expression analysis limited our capacity to infer whether, in addition to BAT, other tissue sources may be relevant contributors to systemic METRNL levels in infants, as in rodent models. Moreover, high levels of METRNL in blood from pregnant mothers, which may be caused by the high *METRNL* gene expression in placenta [data accessible at GEO profile database; GEO accession GDS3113, symbol 197624 (35)], may influence the high levels of METRNL in neonates at birth. On the other hand, further studies would be particularly interesting to assess in early infancy the potential relationship of METRNL levels with those of other secreted factors for which there is experimental evidence of involvement in BAT development, such as fibroblast growth factor (FGF)-9 or FGF21 (36). It should be also mentioned that our data on BAT activity were obtained by infrared methodology, which is minimally invasive but does not allow to assess the actual BAT mass which would require water-fat magnetic resonance imaging or quantification of the proton density fat fraction using magnetic resonance imaging (MRI) (37, 38). The strengths of our study include being the first assessment of METRNL levels in humans in early life and the co-availability of a large set of endocrine-metabolic, body composition and BAT activity data.

In summary, early life is associated with higher levels of circulating METRNL. The progressive reduction of METRNL concentrations in the first year of life -albeit maintained above those in adults- might reflect overall changes in BAT activity during early development. In addition, circulating METRNL concentrations associate with BAT activity and with CXCL14 levels, particularly in girls, supporting a role for METRNL as a brown adipokine and novel biomarker for BAT activity in early life.

## Data availability statement

The raw data supporting the conclusions of this article will be made available by the authors, without undue reservation.

## Ethics statement

The studies involving human participants were reviewed and approved by Institutional Review Board of the University of Barcelona, Sant Joan de Déu University Hospital, Spain. Written informed consent to participate in this study was provided by the participants' legal guardian/next of kin.

## Author contributions

CG-B contributed to literature research, design of figures and tables, data collection, data analysis and interpretation. AN-G contributed to the analysis of circulating parameters and interpretation of data. TQ-L performed gene expression and cell culture-based studies. AL-B and FZ contributed to data interpretation, and reviewed/edited the manuscript. LI and FV contributed to study design, data interpretation, reviewed/edited the manuscript and wrote the manuscript. All authors contributed to the article and approved the submitted version.

## Funding

This work was supported by the Ministerio de Ciencia e Innovacion, Instituto de Salud Carlos III and by the Fondo Europeo de Desarrollo Regional (FEDER) (PI18/00109), Ministerio de Ciencia e Innovación, Agencia Estatal de Investigación (MICIN/AEI/10.13039/50110 0011033), (PID2020-114112RB-100), Spain; and by a grant PERIS-SLT017/20/000228 from the AQU, Generalitat de Catalunya, Spain.

## Acknowledgments

CG-B and LI are investigators of CIBERDEM (Centro de Investigación Biomédica en Red de Diabetes y Enfermedades Metabólicas Asociadas, ISC III, Madrid, Spain). AL-B is a Clinical Investigator of the I3 Fund for Scientific Research (Ministry of Science and Innovation, Spain). FV is an ICREA Academia Researcher (Generalitat de Catalunya) and TQ-L is a "Juan de la Cierva-Incorporación" researcher (Ministry of Science and Innovation, Spain). We thank Merche Morales for technical support. We acknowledge Dr. J. Kopecky, Academy of Sciences of the Czech Republic, for providing access to neonatal necropsy samples.

## Conflict of interest

The authors declare that the research was conducted in the absence of any commercial or financial relationships that could be construed as a potential conflict of interest.

## Publisher's note

All claims expressed in this article are solely those of the authors and do not necessarily represent those of their affiliated organizations, or those of the publisher, the editors and the reviewers. Any product that may be evaluated in this article, or claim that may be made by its manufacturer, is not guaranteed or endorsed by the publisher.

## Supplementary material

The Supplementary Material for this article can be found online at: https://www.frontiersin.org/articles/10.3389/fendo.2023.1136245/full#supplementary-material

## References


1. Alizadeh H. Meteorin-like protein (Metrnl): A metabolic syndrome biomarker and an exercise mediator. *Cytokine* (2022) 157:155952. doi: 10.1016/j.cyto.2022.155952

2. Rao RR, Long JZ, White JP, Svensson KJ, Lou J, Lokurkar I, et al. Meteorin-like is a hormone that regulates immune-adipose interactions to increase beige fat thermogenesis. *Cell* (2014) 157:1279–91. doi: 10.1016/j.cell.2014.03.065

3. Li ZY, Song J, Zheng SL, Fan MB, Guan YF, Qu Y, et al. Adipocyte metrnl antagonizes insulin resistance through PPARγ signaling. *Diabetes* (2015) 64:4011–22. doi: 10.2337/db15-0274

4. Jung TW, Lee SH, Kim HC, Bang JS, Abd El-Aty AM, Hacımüftüoğlu A, et al. METRNL attenuates lipid-induced inflammation and insulin resistance *via* AMPK or PPARδ-dependent pathways in skeletal muscle of mice. *Exp Mol Med* (2018) 50:1–11. doi: 10.1038/s12276-018-0147-5

5. Lee JO, Byun WS, Kang MJ, Han JA, Moon J, Shin MJ, et al. The myokine meteorin-like (metrnl) improves glucose tolerance in both skeletal muscle cells and mice by targeting AMPKα2. *FEBS J* (2020) 287:2087–104. doi: 10.1111/febs.15301

6. Ushach I, Arrevillaga-Boni G, Heller GN, Pone E, Hernandez-Ruiz M, Catalan-Dibene J, et al. Meteorin-like/Meteorin-β is a novel immunoregulatory cytokine associated with inflammation. *J Immunol* (2018) 201:3669–76. doi: 10.4049/jimmunol.1800435

7. Ushach I, Burkhardt AM, Martinez C, Hevezi PA, Gerber PA, Buhren BA, et al. METEORIN-LIKE is a cytokine associated with barrier tissues and alternatively activated macrophages. *Clin Immunol* (2015) 156:119–27. doi: 10.1016/j.clim.2014.11.006

8. Rupérez C, Ferrer-Curriu G, Cervera-Barea A, Florit L, Guitart-Mampel M, Garrabou G, et al. Meteorin-like/Meteorin-β protects heart against cardiac dysfunction. *J Exp Med* (2021) 218:e20201206. doi: 10.1084/jem.20201206

9. Reboll MR, Klede S, Taft MH, Cai CL, Field LJ, Lavine KJ, et al. Meteorin-like promotes heart repair through endothelial KIT receptor tyrosine kinase. *Science* (2022) 376:1343–7. doi: 10.1126/science.abn3027

10. Lee JH, Kang YE, Kim JM, Choung S, Joung KH, Kim HJ, et al. Serum meteorin-like protein levels decreased in patients newly diagnosed with type 2 diabetes. *Diabetes Res Clin Pract* (2018) 135:7–10. doi: 10.1016/j.diabres.2017.10.005

11. Pellitero S, Piquer-Garcia I, Ferrer-Curriu G, Puig R, Martínez E, Moreno P, et al. Opposite changes in meteorin-like and oncostatin m levels are associated with metabolic improvements after bariatric surgery. *Int J Obes (Lond)* (2018) 42:919–22. doi: 10.1038/ijo.2017.268

12. Du Y, Ye X, Lu A, Zhao D, Liu J, Cheng J, et al. Inverse relationship between serum metrnl levels and visceral fat obesity (VFO) in patients with type 2 diabetes. *Diabetes Res Clin Pract* (2020) 161:108068. doi: 10.1016/j.diabres.2020.108068

13. Schmid A, Karrasch T, Schäffler A. Meteorin-like protein (Metrnl) in obesity, during weight loss and in adipocyte differentiation. *J Clin Med* (2021) 10:4338. doi: 10.3390/jcm10194338

14. Becher T, Palanisamy S, Kramer DJ, Eljalby M, Marx SJ, Wibmer AG, et al. Brown adipose tissue is associated with cardiometabolic health. *Nat Med* (2021) 27:58–65. doi: 10.1038/s41591-020-1126-7

15. Villarroya F, Cereijo R, Villarroya J, Giralt M. Brown adipose tissue as a secretory organ. *Nat Rev Endocrinol* (2017) 13:26–35. doi: 10.1038/nrendo.2016.136

16. Lidell ME. Brown adipose tissue in human infants. In: Pfeifer A, Klingenspor M, Herzig S, editors. *Brown adipose tissue. handbook of experimental pharmacology*, vol. 251 . Heidelberg: Springer (2019). p. 107–23. doi: 10.1007/164_2018_118

17. Urisarri A, González-García I, Estévez-Salguero Á, Pata MP, Milbank E, López N, et al. BMP8 and activated brown adipose tissue in human newborns. *Nat Commun* (2021) 12:5274. doi: 10.1038/s41467-021-25456-z

18. Garcia-Beltran C, Cereijo R, Plou C, Gavaldà-Navarro A, Malpique R, Villarroya J, et al. Posterior cervical brown fat and CXCL14 levels in the first year of life: Sex differences and association with adiposity. *J Clin Endocrinol Metab* (2022) 107:e1148–58. doi: 10.1210/clinem/dgab761

19. Garcia-Beltran C, Villarroya J, Plou C, Gavaldà-Navarro A, Casano P, Cereijo R, et al. Bone morphogenetic protein-8B levels at birth and in the first year of life: Relation to metabolic-endocrine variables and brown adipose tissue activity. *Front Pediatr* (2022) 10:869581. doi: 10.3389/fped.2022.869581

20. Hondares E, Gallego-Escuredo JM, Flachs P, Frontini A, Cereijo R, Goday A, et al. Fibroblast growth factor-21 is expressed in neonatal and pheochromocytoma-induced adult human brown adipose tissue. *Metabolism* (2014) 63:312–7. doi: 10.1016/j.metabol.2013.11.014

21. Gallego-Escuredo JM, Gómez-Ambrosi J, Catalan V, Domingo P, Giralt M, Frühbeck G, et al. Opposite alterations in FGF21 and FGF19 levels and disturbed expression of the receptor machinery for endocrine FGFs in obese patients. *Int J Obes (Lond)* (2015) 39:121–9. doi: 10.1038/ijo.2014.76

22. Díaz M, García C, Sebastiani G, de Zegher F, López-Bermejo A, Ibáñez L. Placental and cord blood methylation of genes involved in energy homeostasis: Association with fetal growth and neonatal body composition. *Diabetes* (2017) 66:779–84. doi: 10.2337/db16-0776

23. Wabitsch M, Brenner RE, Melzner I, Braun M, Möller P, Heinze E, et al. Characterization of a human preadipocyte cell strain with high capacity for adipose differentiation. *Int J Obes Relat Metab Disord* (2001) 25:8–15. doi: 10.1038/sj.ijo.0801520

24. Yeo CR, Agrawal M, Hoon S, Shabbir A, Shrivastava MK, Huang S, et al. SGBS cells as a model of human adipocyte browning: A comprehensive comparative study with primary human white subcutaneous adipocytes. *Sci Rep* (2017) 7:4031. doi: 10.1038/s41598-017-04369-2

25. Klusóczki Á, Veréb Z, Vámos A, Fischer-Posovszky P, Wabitsch M, Bacso Z, et al. Differentiating SGBS adipocytes respond to PPARγ stimulation, irisin and BMP7 by functional browning and beige characteristics. *Sci Rep* (2019) 9:5823. doi: 10.1038/s41598-019-42256-0

26. Szatmári-Tóth M, Shaw A, Csomós I, Mocsár G, Fischer-Posovszky P, Wabitsch M, et al. Thermogenic activation downregulates high mitophagy rate in human masked and mature beige adipocytes. *Int J Mol Sci* (2020) 21:6640. doi: 10.3390/ijms21186640

27. Cereijo R, Gavaldà-Navarro A, Cairó M, Quesada-López T, Villarroya J, Morón-Ros S, et al. CXCL14, a brown adipokine that mediates brown-Fat-to-Macrophage communication in thermogenic adaptation. *Cell Metab* (2018) 28:750–763.e6. doi: 10.1016/j.cmet.2018.07.015

28. Cereijo R, Quesada-López T, Gavaldà-Navarro A, Tarascó J, Pellitero S, Reyes M, et al. The chemokine CXCL14 is negatively associated with obesity and concomitant type-2 diabetes in humans. *Int J Obes (Lond)* (2021) 45:706–10. doi: 10.1038/s41366-020-00732-y

29. Pani S, Dey S, Pati B, Senapati U, Bal NC. Brown to white fat transition overlap with skeletal muscle during development of larger mammals: Is it a coincidence? *J Endocr Soc* (2022) 6:bvac151. doi: 10.1210/jendso/bvac151

30. Eaton M, Granata C, Barry J, Safdar A, Bishop D, Little JP. Impact of a single bout of high-intensity interval exercise and short-term interval training on interleukin-6, FNDC5, and METRNL mRNA expression in human skeletal muscle. *J Sport Health Sci* (2018) 7:191–6. doi: 10.1016/j.jshs.2017.01.003

31. Kang PB, Kho AT, Sanoudou D, Haslett JN, Dow CP, Han M, et al. Variations in gene expression among different types of human skeletal muscle. *Muscle Nerve* (2005) 32:483–91. doi: 10.1002/mus.20356

32. Kaikaew K, Grefhorst A, Visser JA. Sex differences in brown adipose tissue function: Sex hormones, glucocorticoids, and their crosstalk. *Front Endocrinol (Lausanne)* (2021) 12:652444. doi: 10.3389/fendo.2021.652444

33. Lidell ME, Betz MJ, Enerbäck S. Two types of brown adipose tissue in humans. *Adipocyte* (2014) 3:63–6. doi: 10.4161/adip.26896

34. Pilkington AC, Paz HA, Wankhade UD. Beige adipose tissue identification and marker specificity-overview. *Front Endocrinol (Lausanne)* (2021) 12:599134. doi: 10.3389/fendo.2021.599134

35. Dezso Z, Nikolsky Y, Sviridov E, Shi W, Serebriyskaya T, Dosymbekov D, et al. A comprehensive functional analysis of tissue specificity of human gene expression. *BMC Biol* (2008) 6:49. doi: 10.1186/1741-7007-6-4

36. Sahu B, Tikoo O, Pati B, Senapati U, Bal NC. Role of distinct fat depots in metabolic regulation and pathological implications. *Rev Physiol Biochem Pharmacol* (2023) 186:135–76. doi: 10.1007/112_2022_73

37. Andersson J, Roswall J, Kjellberg E, Ahlström H, Dahlgren J, Kullberg J. MRI Estimates of brown adipose tissue in children - associations to adiposity, osteocalcin, and thigh muscle volume. *Magn Reson Imaging* (2019) 58:135–42. doi: 10.1016/j.mri.2019.02.001

38. Drabsch T, Junker D, Bayer S, Wu M, Held C, Karampinos DC, et al. Association between adipose tissue proton density fat fraction, resting metabolic rate and FTO genotype in humans. *Front Endocrinol (Lausanne)* (2022) 13:804874. doi: 10.3389/fendo.2022.804874

frontiers | Frontiers in Endocrinology

TYPE Original Research
PUBLISHED 17 April 2023
DOI 10.3389/fendo.2023.1148954

Check for updates

OPEN ACCESS

EDITED BY
Rubén Cereijo,
University of Barcelona, Spain

REVIEWED BY
Alexander Bartelt,
Ludwig Maximilian University of Munich, Germany
Andrea Galmozzi,
University of Wisconsin-Madison, United States

*CORRESPONDENCE
Candida J. Rebello
candida.rebello@pbrc.edu

†Deceased

SPECIALTY SECTION
This article was submitted to a section of the journal Obesity, Frontiers in Endocrinology

RECEIVED 20 January 2023
ACCEPTED 20 March 2023
PUBLISHED 17 April 2023

CITATION
Coulter AA, Greenway FL, Zhang D, Ghosh S, Coulter CR, James SL, He Y, Cusimano LA and Rebello CJ (2023) Naringenin and β-carotene convert human white adipocytes to a beige phenotype and elevate hormone- stimulated lipolysis. *Front. Endocrinol.* 14:1148954. doi: 10.3389/fendo.2023.1148954

COPYRIGHT
© 2023 Coulter, Greenway, Zhang, Ghosh, Coulter, James, He, Cusimano and Rebello. This is an open-access article distributed under the terms of the Creative Commons Attribution License (CC BY). The use, distribution or reproduction in other forums is permitted, provided the original author(s) and the copyright owner(s) are credited and that the original publication in this journal is cited, in accordance with accepted academic practice. No use, distribution or reproduction is permitted which does not comply with these terms.

# Naringenin and β-carotene convert human white adipocytes to a beige phenotype and elevate hormone-stimulated lipolysis

Ann A. Coulter[1], Frank L. Greenway[2], Dachuan Zhang[3], Sujoy Ghosh[4], Cathryn R. Coulter[1], Sarah L. James[1†], Yanlin He[5], Luke A. Cusimano[6] and Candida J. Rebello[7*]

[1]Computational Biology, Pennington Biomedical Research Center, Baton Rouge, LA, United States, [2]Clinical Trials, Pennington Biomedical Research Center, Baton Rouge, LA, United States, [3]Biostatistics, Pennington Biomedical Research Center, Baton Rouge, LA, United States, [4]Adjunct Faculty, Pennington Biomedical Research Center, Baton Rouge, LA, United States, [5]Brain Glycemic and Metabolism Control, Pennington Biomedical Research Center, Baton Rouge, LA, United States, [6]Cusimano Plastic and Reconstructive Surgery, Baton Rouge, LA, United States, [7]Nutrition and Chronic Disease, Pennington Biomedical Research Center, Baton Rouge, LA, United States

**Introduction:** Naringenin, a peroxisome proliferator-activated receptor (PPAR) activator found in citrus fruits, upregulates markers of thermogenesis and insulin sensitivity in human adipose tissue. Our pharmacokinetics clinical trial demonstrated that naringenin is safe and bioavailable, and our case report showed that naringenin causes weight loss and improves insulin sensitivity. PPARs form heterodimers with retinoic-X-receptors (RXRs) at promoter elements of target genes. Retinoic acid is an RXR ligand metabolized from dietary carotenoids. The carotenoid β-carotene reduces adiposity and insulin resistance in clinical trials. Our goal was to examine if carotenoids strengthen the beneficial effects of naringenin on human adipocyte metabolism.

**Methods:** Human preadipocytes from donors with obesity were differentiated in culture and treated with 8μM naringenin + 2μM β-carotene (NRBC) for seven days. Candidate genes involved in thermogenesis and glucose metabolism were measured as well as hormone-stimulated lipolysis.

**Results:** We found that β-carotene acts synergistically with naringenin to boost UCP1 and glucose metabolism genes including GLUT4 and adiponectin, compared to naringenin alone. Protein levels of PPARα, PPARγ and PPARγ-coactivator-1α, key modulators of thermogenesis and insulin sensitivity, were also upregulated after treatment with NRBC. Transcriptome sequencing was conducted and the bioinformatics analyses of the data revealed that NRBC induced enzymes for several non-UCP1 pathways for energy expenditure including triglyceride cycling, creatine kinases, and Peptidase M20 Domain Containing 1 (PM20D1). A comprehensive analysis of changes in receptor expression showed that NRBC upregulated eight receptors that have been linked to lipolysis or thermogenesis including the β1-adrenergic receptor and the parathyroid hormone receptor. NRBC increased levels of triglyceride lipases

and agonist-stimulated lipolysis in adipocytes. We observed that expression of RXRγ, an isoform of unknown function, was induced ten-fold after treatment with NRBC. We show that RXRγ is a coactivator bound to the immunoprecipitated PPARγ protein complex from white and beige human adipocytes.

**Discussion:** There is a need for obesity treatments that can be administered long-term without side effects. NRBC increases the abundance and lipolytic response of multiple receptors for hormones released after exercise and cold exposure. Lipolysis provides the fuel for thermogenesis, and these observations suggest that NRBC has therapeutic potential.

KEYWORDS

UCP1, naringenin, carotenoid, PPARγ, RXRγ, PPARα, adiponectin, lipolysis

## Introduction

Adipose tissue is a complex, adaptable organ composed of multiple types of adipocytes which vary in function (1). White adipocytes store triglycerides and expand in number and size under conditions of excess energy intake. Brown and beige adipocytes abound in mitochondria and express uncoupling protein 1 (UCP1), a protein that shifts mitochondrial fat oxidation away from ATP production and towards thermogenesis. Increased density of beige adipocytes and UCP1 in fat depots is associated with elevated energy expenditure and resistance to weight gain and type 2 diabetes (2–4). In rodents, white adipose tissues can adapt to a chronic environmental stimulus such as cold exposure by producing beige adipocytes from precursor cells and by converting white adipocytes into beige cells (5). The adaptive response to cold exposure involves release of norepinephrine by sympathetic nerve fibers to activate β3-adrenergic receptors (β3AR) abundantly expressed in adipocytes (6).

In contrast to rodents, human adipocytes express extremely low levels of the βARs. Humans lack a robust response to systemic infusion of β-adrenergic agonists even when combined with cold exposure (7–9). However, synthetic peroxisome proliferator activator receptor (PPAR)α and PPARɣ ligands have been shown to have potent activity in the conversion of primary human white adipocytes to beige UCP1-expressing cells *in vitro* (10, 11). PPARs are ligand-activated nuclear receptors enriched in metabolic tissues, and they regulate UCP1 and many genes controlling fat oxidation and insulin sensitivity by binding to upstream PPAR responsive elements (PPREs). PPARγ is subject to complex cell-specific post-translational regulatory mechanisms and has multiple ligand binding domains (12). Depending on the binding characteristics of a particular ligand, PPARγ can stimulate adipogenesis, insulin sensitivity, fat oxidation or thermogenesis in adipose tissues (13).

Thiazolidinediones (TZDs) are a class of potent PPARγ agonists that have been approved by the United States Food and Drug Administration (FDA) for the treatment of type 2 diabetes. However, TZDs have multiple adverse effects including weight gain, heart failure, and risk for bladder cancer (14, 15). PPARα agonists primarily upregulate genes for lipolysis and mitochondrial β-oxidation of fatty acids in primary human adipocytes (16). A synthetic PPARα activator, fenofibrate, has been approved for treatment of dyslipidemia (17, 18). At this time, there are no FDA-approved PPARγ or PPARα activators for treatment of obesity (19–21).

Despite the complex regulation of ligand binding to PPARγ, evidence is growing that selective modulators and partial agonists can direct activity toward thermogenesis and away from adipogenesis (12, 22, 23). Naringenin (NR), a polyphenol found in citrus fruit, activates transcriptional activity of PPARγ and PPARα in an expression system with a PPRE linked to a reporter gene (24). In a previous study, we treated human subcutaneous adipocytes with NR and saw induction of UCP1 mRNA as well as increases in basal and maximal oxygen consumption rate (OCR) (25). We used selective inhibitors to demonstrate that upregulation of thermogenesis genes by NR requires activation of both PPARγ and PPARα in adipocytes (26). Data from our clinical studies suggest that naringenin is bioavailable and has potential as a treatment for obesity and type 2 diabetes. Our pharmacokinetic clinical trial showed that naringenin is safe and well-tolerated at doses ranging from 150 mg to 900 mg (27). In a case study of an individual with obesity and untreated type 2 diabetes, we found that body weight and fasting insulin concentrations decreased, and there was a measurable increase in energy expenditure after ingestion of NR for eight weeks (26).

Carotenoids are vitamin A precursors found in fruits and vegetables, and their consumption has been shown to reduce fat mass and insulin resistance in children. Baseline blood concentrations of β-carotene (BC) are inversely correlated with fat mass (28, 29). Most carotenoids are metabolized into retinoid ligands for retinoic acid receptors (RAR) and retinoic-X-receptors (RXR), which are transcriptional coactivators for PPARs. The objective of this study was to determine whether carotenoids could amplify the effects of NR on gene expression and function to convert primary human adipocytes to a beige phenotype. We observed synergistic increases in a subset of mRNAs including UCP1, GLUT4, ATGL and adiponectin with the combination of NR and BC (NRBC). Protein levels of PPARα, PPARγ, PGC-1α and NAMPT were selectively upregulated without increases in mRNA

levels. Whole transcriptome sequencing was conducted, and the results showed that NRBC induced genes for multiple non-UCP1 energy-dissipating futile cycles, beneficial secreted peptides, and adipokines. Importantly, NRBC increased levels of multiple thermogenesis and lipolysis-linked receptors including the β1-adrenergic receptor (β1AR), parathyroid hormone receptor (PTHR), and the stimulatory ratio of natriuretic peptide receptors (NPR1/NPR3). A comprehensive analysis of lipolysis was conducted, and the results showed that the capacity for PTHR and βAR agonist-stimulated lipolysis was substantially higher in NRBC-treated adipocytes compared to untreated cells. Expression of RXRγ, a unique isoform associated with brown adipogenesis, was upregulated ten-fold after treatment. We observed that RXRγ was bound in the PPARγ transcriptional complex immunoprecipitated from human adipocytes. These results suggest that NRBC has potential as a treatment for obesity and type 2 diabetes and is safe primarily because it acts on peripheral tissues, unlike most obesity medications that act on the central nervous system (CNS) (30).

# Materials and methods

## Chemicals and antibodies

Naringenin extract (NR) from whole citrus sinensis oranges (purity ≥ 30%) was purchased from GE Nutrients, Inc. (Gencor, Irvine, CA). BC, lycopene, and lutein were from Cayman Chemical Co. Protease and phosphatase inhibitors were purchased from Cell Signaling Technology (Danvers, MA), TGX protein gels from BIO-RAD (Hercules, CA). Type 1 collagenase, glycerol standard solution, adenosine, estradiol, human pituitary growth hormone, dobutamine hydrochloride, human atrial natriuretic peptide, ACTH, menthol, 8-CPT-cAMP were purchased from Sigma-Aldrich. Isoproterenol, human parathyroid hormone (1–34), CDCA, were purchased from Cayman Chemicals. Glycerol reagent A was from ZenBio (Durham, NC). All other chemicals were purchased from Sigma (St. Louis, Mo) unless otherwise indicated.

Primary antibodies used were UCP1 (#MAB6158, R&D Systems), GLUT4 (Ab654 Abcam), PGC-1α (ST1202, Sigma) and β-Actin (A5316, Sigma), or monoclonals from Santa Cruz against ATGL (sc-365278), adiponectin (sc-136131), PPARα (398394), PPARγ (sc-7273), NAMPT (sc-393444), RXRγ (sc-514134), RXRα (sc-515929). HRP-linked anti-rabbit (12-348, Sigma), anti-mouse (AP130P, Sigma) and anti-IgG kappa light chain (sc-516102, Santa Cruz) were used to detect specific antibody-antigen complexes. Western Lightning Plus-ECL was from PerkinElmer (Waltham, MA).

## Human adipocyte cell culture

Human adipose-derived stem cells from overweight and obese female donors were purchased from LaCell, LLC (New Orleans, Louisiana) or isolated from lipoaspirate waste donated post-surgery from women with obesity using methods as previously described (31). Cells were seeded, maintained until two days after becoming confluent, and differentiated into adipocytes in the presence of rosiglitazone and isobutylmethylxanthine for five days as previously described (25). Treatments of adipocytes with 8μM NR and 2μM carotenoid, dissolved in DMSO at 1000X, started 5 days after the differentiation period and lasted for seven days in adipocyte maintenance medium with heat inactivated serum, before RNA and protein were isolated from adipocyte cultures.

## RNA extraction and transcriptome sequencing

Total RNA was extracted from cells using Tri-reagent and purified with RNeasy (Qiagen) into nuclease-free water with RNAsecure Reagent (Thermo Fisher Scientific). RNA integrity was assessed using an Agilent Bioanalyzer 2100. RNA samples were diluted to 50 ng/μL and libraries were constructed using Lexogen Quant-Seq 3' mRNA-Seq Library Prep Kit (SKU015.96) with oligo(dT) priming. Double-stranded cDNA was purified with magnetic beads, libraries were amplified using PCR, and transcripts were indexed, pooled, and forward-sequenced at 50 bp using NextSeq500 (Illumina). BlueBee software was used to analyze alignment and the DESeq2 V1.32.0 package in R V4.1.0, Rstudio V1.4.1717 and biomaRt V2.48.2 were used for differential expression analysis after estimation of possible outlier counts per gene via the Cook's distance, and their replacement by the trimmed mean over all counts for that gene. Differential gene expression results were computed for 17525 genes of which 3881 genes were differentially regulated at an adjusted p - value¾0.05. Pathway enrichment analysis was carried out via the Gene Set Enrichment Analysis (GSEA) tool (32) by estimating enrichment on pathways present in the Kyoto Encyclopedia of Genes and Genomes (KEGG) database (33) available from the Molecular Signatures Database repository (MSigDb, http://software.broadinstitute.org/gsea/msigdb) (34), and additional custom pathways. Gene-sets with FDR ≤ 5% were considered as significantly enriched (35).

## Quantitative real time polymerase chain reaction

Quantitative reverse transcriptase and real-time PCR were conducted in one reaction with the gene-specific reverse PCR primer also priming the cDNA synthesis as previously described (25). Primer-probe sequences for UCP1, GLUT4, ATGL, adiponectin, PGC-1α and ribosomal RPL13A, used to adjust target gene values for total RNA in each sample, have been previously reported (25). Additional primer and probe oligonucleotide sets used in this study are shown in 5' to 3' orientation: PPARα Forward GTCGATTTCACAAGTGCCTTTC reverse CAGGTAAGAATTTCTGCTTTCAGTT probe AAC GAATCGCGTTGTGTGACATCC; PDK4 forward CTGAGA ATTATTGACCGCCTCT reverse GAAATTGGCAAGCCGTAACC probe TACATACTCCACTGCACCAACGCC; PPARγ forward CCCAAGTTTGAGTTTGCTGTG reverse GCGGTCTCCACTGA GAATAATG probe TGGAATTAGATGACAGCGACTTGGCA; NAMPT forward TGTTCCTTCAAGTGTAGCTATGT reverse TGC TGGCGTCCTATGTAAAG probe AACGTCTTCAAGGACCCAGT TGCT; CKMT1 forward CTTGACCTGTCCATCTAACCTG reverse

ACTCCTCCAGTACCACGTT probe AGATAGCCGCTTCCCAAA GATCCTG. Predesigned human primer and probe sets from Thermofisher Scientific are PM20D1 Hs00399438_m1; ANGPTL4 Hs00211522_m1; GDF11 Hs00195156_m1; S100B Hs00902901_m1.

## Protein extraction, PPARγ immunoprecipitation and Western blotting

Whole cell protein was isolated from differentiated cell cultures after treatment for seven days, lysed with RIPA buffer containing protease and phosphatase inhibitors, and pushed through a 20-gauge needle four times to disrupt organelles. Fifty micrograms of total cell protein were loaded per lane and resolved in 7.5% SDS-PAGE gels, transferred to nitrocellulose membranes, and probed overnight at 4°C with specific primary antibodies. Anti-rabbit or -mouse secondary antibodies conjugated to horseradish peroxidase were used for detection of target proteins. Image J was used to quantify protein bands on Western blots. To adjust for variations in total protein loaded in each lane, β-actin was used.

PPARγ was immunoprecipitated from whole cell lysates with SC-7273 antibody (Santa Cruz) using the Pierce MS-compatible magnetic IP kit with protein A/G beads according to kit directions (Pierce 90409, Thermofisher). Briefly, primary anti-PPARy antibody was incubated with 600 micrograms of adipocyte protein lysate for four hours at 4°C on a tube inverter. The antibody-lysate mixture was then incubated with magnetic protein A/G beads for one hour, and complexes of PPARγ protein attached to beads were isolated, washed and eluted using a magnetic tube holder. Samples were evaporated to dryness under vacuum, resuspended in RIPA buffer and subjected to Western Blot analysis. An HRP-conjugated anti- IgG kappa light chain secondary antibody was used to eliminate primary antibody heavy chain bands from interfering with detection of immunoprecipitated target proteins. Proteins were visualized by chemiluminescence using Western Lightening (Amersham).

## Lipolysis assay

Cells were differentiated in 96-well plates and treated with cell medium (untreated) or NRBC for seven days. On the day of the lipolysis assay, cells were exposed for four hours to buffer (KRB with 1% BSA) or receptor agonists dissolved in buffer. Agonists were used at concentrations shown to give maximum responses and were: 8-Cpt-cAMP 200μM non-hydrolyzable PKA activator of maximum stimulated lipolysis (cAMP) (36), atrial natriuretic peptide 0.1 μM for NPR1 and NPR3 (37), parathyroid hormone (amino acids 1-34) 1 μM for PTHR (38), isoproterenol 1μM all βARs and dobutamine 1μM for β1AR (39), estradiol 1μM for GPER (40), growth hormone 250ng/ml for GHR (41), adrenocorticotropin hormone 1μM for MC1R (42), bile acid chenodeoxycholic acid 30μM for TGR5 (43), adenosine 1μM for ADORA1 and ADORA2B (44), and menthol 100μM for TRPM8 (45). Supernatants were removed for measurement of glycerol released using Glycerol Reagent A, and concentrations were determined using a standard curve. Data are from four or five experiments each with cells from different donors with BMI from 27 to 36.

## Statistical analysis

All statistical analyses were performed using SAS 9.4 (SAS Institute, Cary, North Carolina). The synergistic effect of the combination of NR and BC was investigated by implementing linear mixed effect models including plate as the random effect. The goal was to test if the combination (NRBC) induced a greater response compared to the sum of the individual components' effects. Based on the mixed effect model, an F test was constructed to evaluate the null hypothesis that the additive effect of NR over control and BC over control was no different from that of NRBC over control. We also used linear mixed effect models to test the effects of: 1) NR, BC, and NRBC compared to control for the target variables of mRNA and protein; 2) Agonist stimulated lipolysis in NRBC pre-treated cells v. untreated cells. All experiments were repeated at least three times in primary adipocytes from different donors. Significance was set at $p < 0.05$. Data are reported as least squares means ± standard error unless otherwise specified.

# Results

## Carotenoids act synergistically with NR to amplify UCP1 levels in adipocytes

Metabolites of pro-vitamin A carotenoids are ligands of the retinoid X receptor (RXR) family of nuclear receptors which can heterodimerize with PPARα and PPARγ and recruit coactivators into active transcriptional complexes (46). Our first objective was to evaluate whether treatment of adipocytes with carotenoids could elevate the levels of UCP1, a PPAR target gene known to be upregulated by NR and a marker for beige adipogenesis (25). Three of the most abundant carotenoids in foods and in human serum, BC, lycopene, and lutein were tested (47). Steady state plasma concentrations are approximately 2μM in individuals who eat diets rich in carotenoids, and we used this concentration in experiments (48). Since the mean serum concentration of NR after ingestion of 150mg is 8μM (27), we used this concentration in all assays. Treatment of primary human adipocyte cultures with BC, lutein or lycopene individually for seven days had no effect on gene expression (Figure 1). When BC or lutein were combined with NR for treatment, the increase in UCP1 gene expression was synergistic, greater than the sum of the individual effects of each compound ($P<0.001$). In contrast, lycopene did not alter NR-stimulated UCP1 levels. Unlike lycopene, BC and lutein are pro-vitamin A carotenoids that are metabolized into retinoic acid (49). These data are consistent with a hypothesis that RXR ligands act synergistically with NR to boost thermogenesis gene expression.

## BC elevates the effects of NR on a subset of genes for thermogenesis and insulin sensitivity

We next evaluated the effects of NR, BC and NRBC on expression of additional genes. BC was chosen for the rest of the

10.3389/fendo.2023.1148954

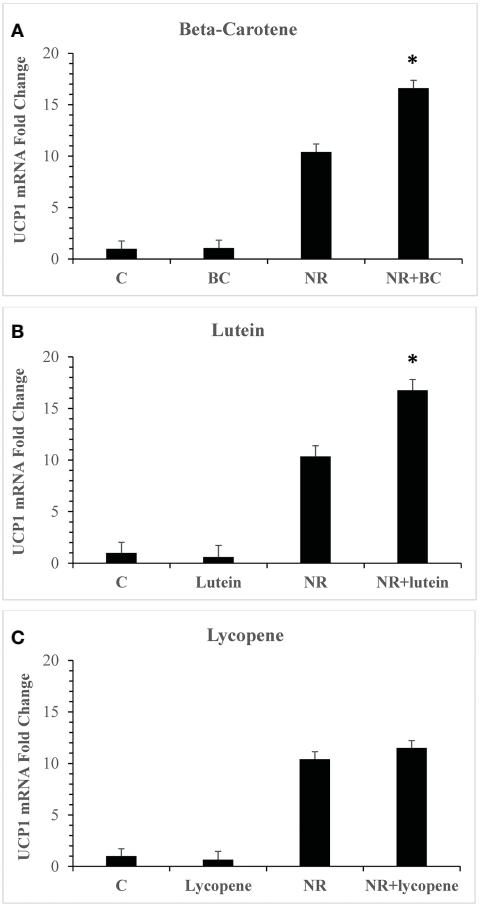


FIGURE 1
Pro-vitamin A carotenoids and NR act synergistically to elevate levels of UCP1 mRNAs Adipocytes from 4 donors with obesity were treated for seven days with vehicle (control) or 8μM NR and 2μM carotenoids. **(A)** NR+BC **(B)** NR+Lutein **(C)** NR+Lycopene mRNA levels were measured using quantitative RTPCR. Data is expressed in least squares means ± standard error. Synergy for mRNA was calculated as: sum of differences ((NR- Control) + (BC - Control)) *vs* (NRBC - Control). *p < 0.001 for synergy, sum of differences versus NRBC. NR, naringenin; BC, beta carotene.

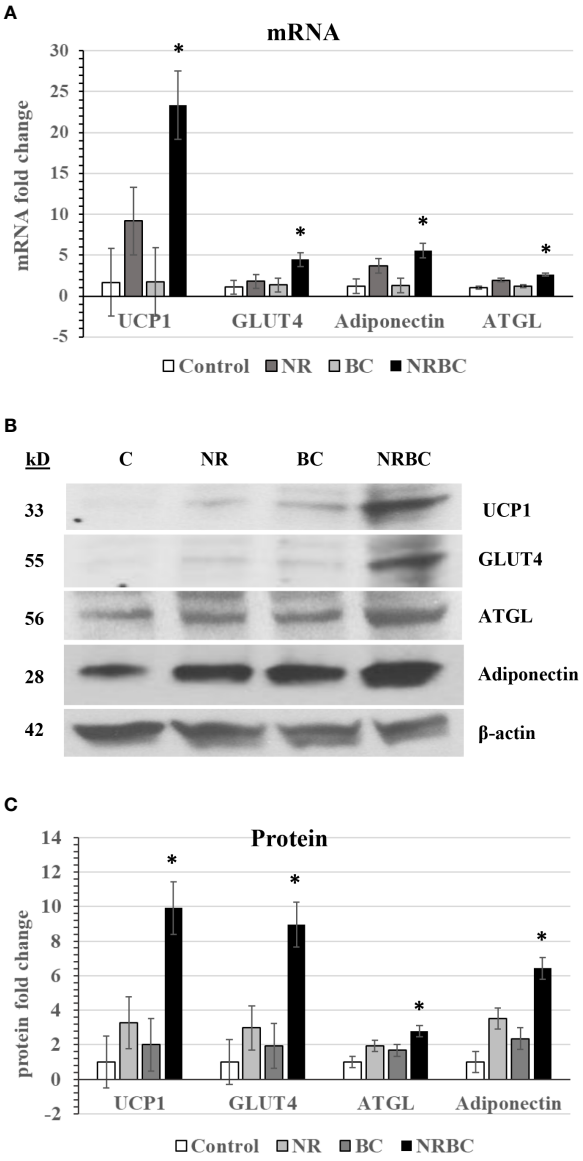


FIGURE 2
NR and BC synergistically induce metabolism genes **(A)** mRNA levels **(B)** Western Blots of Protein levels **(C)** Protein levels were measured with β-actin as loading control. Adipocytes from three or more donors with obesity were treated for seven days. mRNA data are expressed as least squares means ± standard error. Synergy for mRNA was calculated as: sum of differences ((NR- Control) + (BC - Control)) *vs* (NRBC - Control). *p < 0.05 for synergy. NR, Naringenin; BC, beta carotene; NRBC, naringenin and beta carotene.

study because it is safe, stable, bioavailable and has a long half-life in circulation (50). Adipocytes from five donors with body mass index (BMI) ranging from 27 to 36kg/m$^2$ were treated with NRBC for seven days. NRBC synergistically boosted mRNA levels for UCP1 ($p<0.005$), GLUT4 ($p<0.02$), ATGL ($p<0.04$) and adiponectin ($p<0.05$) compared to NR or BC alone (Figure 2A). Protein levels showed a similar trend (Figures 2B, C). Uncropped Western blots are shown in Supplemental Figure 1. ATGL is the rate-limiting lipase for hydrolysis of fatty acids from triglycerides (TGs) (51). GLUT4 is a transporter for glucose uptake, and its upregulation in adipocytes stimulates a cascade of events that reduce insulin resistance (52, 53). Adiponectin is a key circulating factor that acts on muscle and other tissues and improves whole body glucose homeostasis (54). In a previous study we reported induction of CPT1β mRNA in adipocytes after NR treatment (25). We did not see an increase in CPT1β levels with NRBC treatment in comparison to levels induced by NR alone.

NRBC upregulated protein levels of PPARα, PPARγ, PGC-1α, and NAMPT three to six-fold (Figure 3, $p<0.001$) without comparable increases in mRNA levels. Uncropped Western blots are shown in Supplemental Figure 2. PPARα, PPARγ, and PGC-1α proteins have a short half-life and are rapidly degraded by ubiquitin-proteosome systems (55–57). Inhibition of degradation increases protein levels and target gene expression (58). The binding of ligands and coactivators can influence the turnover rates of PPARα and PPARγ (59, 60). Treatment with NR alone did not upregulate protein levels, indicating that RXR ligand is required in addition to PPAR ligand for protein upregulation. The

10.3389/fendo.2023.1148954

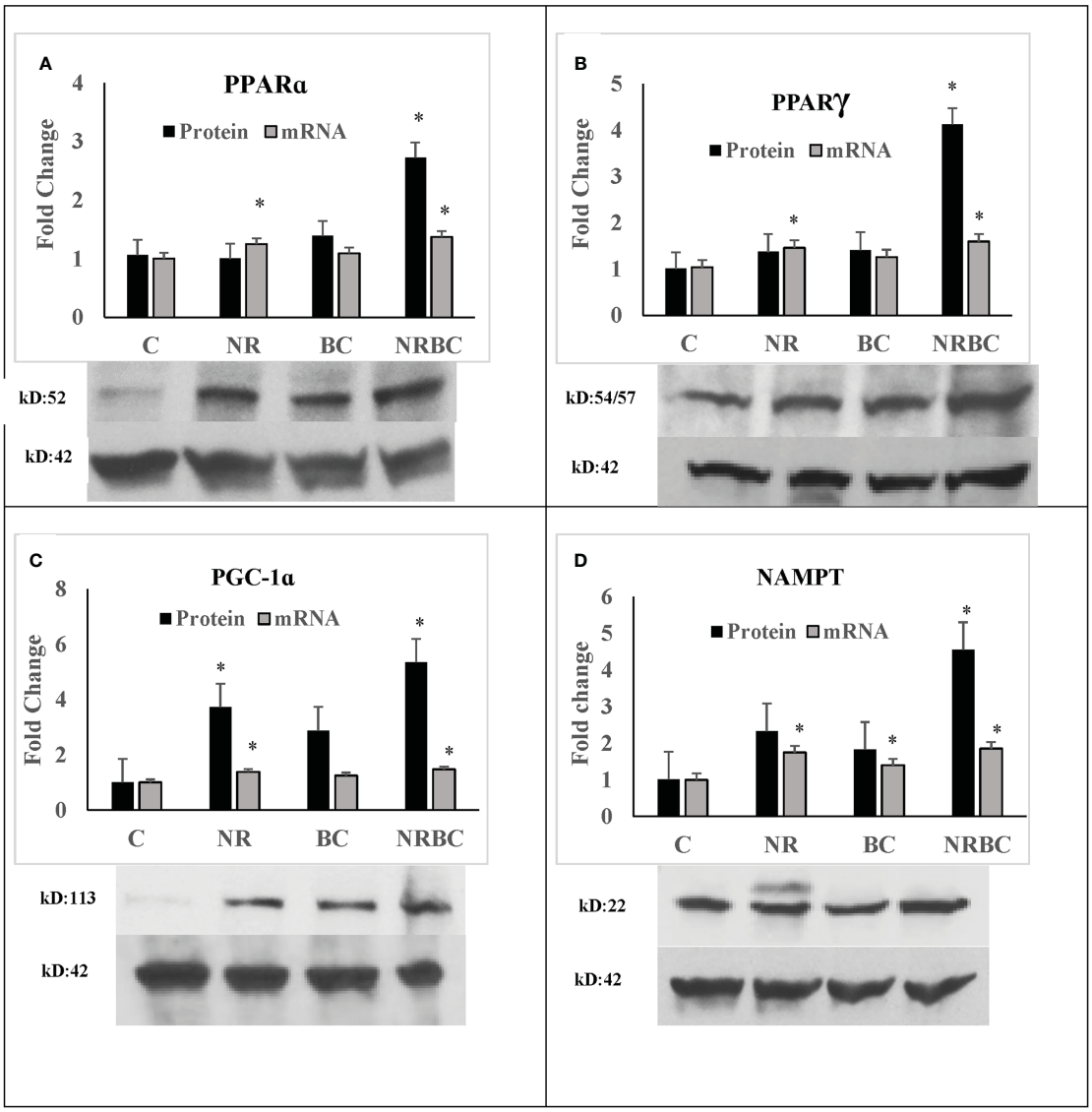


FIGURE 3
NRBC upregulates a subset of key regulatory proteins without mRNA increases **(A)** PPARα; **(B)** PPARγ; **(C)** PGC-1α; and **(D)** NAMPT. Adipocytes from three to five donors with obesity were treated for seven days. Protein was measured by Western Blotting with β-actin used to adjust for loading. mRNA was quantified by real-time PCR. Data are expressed as least squares means ± standard error, *p < 0.001 NR, Naringenin; BC, beta carotene; NRBC, naringenin and beta carotene.

increase in these proteins in the absence of concurrent upregulation of their transcripts suggests that NR and BC act together to stabilize protein levels through post-translational mechanisms.

## Whole transcriptome sequencing for comprehensive analysis of metabolic effects

To expand our understanding of human adipocyte reprogramming by NRBC, we conducted whole transcriptome sequencing. Adipocyte cultures from two female donors with overweight and obesity were treated with cell medium (vehicle control) or NRBC for seven days and RNA samples were processed for library construction. Differential gene expression results were computed for 17525 genes of which 3881 genes were significantly regulated at an adjusted p-value <0.05. Pathway enrichment analysis identified PPAR signaling, adipocyte signaling and insulin signaling pathways to be the most significantly increased after treatment (Figure 4). In addition, the data analysis showed increases in genes for metabolism of pyruvate, fatty acids, glucose, and amino acids. These changes in mRNA levels were validated for selected genes by qRT-PCR (Figure 5, p<0001).

### PPARγ and PPARα target genes

NRBC robustly upregulated a number of classical brown and beige genes that have previously been identified as targets of synthetic PPARα and PPARγ ligands (10) including CIDEA,

10.3389/fendo.2023.1148954

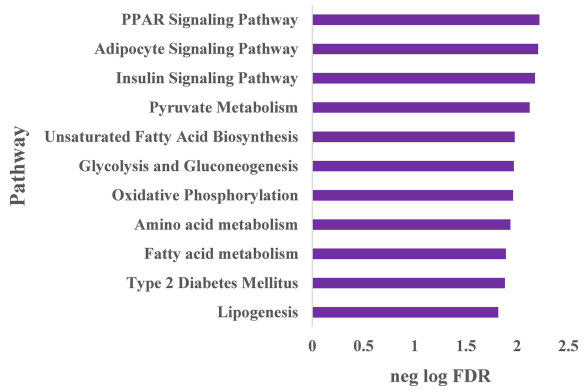


FIGURE 4
Whole transcriptome sequencing analysis of pathways stimulated by naringenin and β-carotene (NRBC) Adipocytes from two donors with BMI of 27 and 36 kg/m$^2$ were treated with cell medium (vehicle control) or NRBC for seven days. cDNA libraries from expressed transcripts were constructed, sequenced and differential gene expression was analyzed. Gene-sets with false discovery rate (FDR) ≤ 5% were considered as significantly enriched, and the top pathways are shown.

CITED, perilipins 2, -4, -5, PDK4, GK, AQP7, fatty acid elongases ELOVL 3, -5, -6, ACSL5 and the fatty acid binding proteins FABP3, FABP4 and FABP7 (Table 1). In addition, FABP5, which delivers retinoic acid to nuclear receptors was significantly upregulated.

## Upregulation of secreted peptides and adipokines

Adipose tissue is an endocrine organ that secretes proteins, hormones, and bioactive lipids with beneficial paracrine effects on whole-body fat and glucose metabolism. NRBC treatment significantly upregulated the expression of a number of these genes including ANGPTL4, FNDC4 and GDF11 (Table 2). ANGPTL4 is produced by adipocytes and promotes lipolysis (Table 2) (61). Both the full-length protein and a truncated form of ANGPTL4 are secreted, and their overexpression in mice stimulates energy expenditure, lowers adiposity, and converts white fat to the beige phenotype (62). FNDC4 induces UCP1 and beige genes and promotes insulin sensitivity in adipocytes (63, 64).

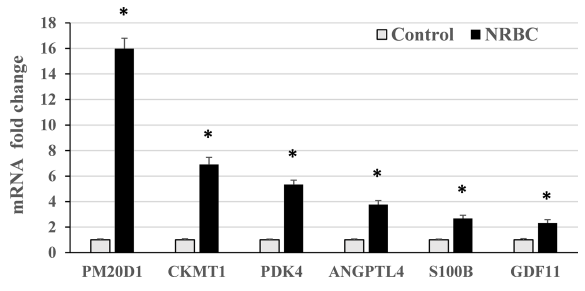


FIGURE 5
RT-PCR validation of genes upregulated by naringenin and beta carotene (NRBC) in RNA sequencing analysis. Adipocytes from three donors with obesity were treated for seven days. mRNA levels were measured using quantitative RT-PCR. Data are expressed as mean ± standard error, *p < 0.001.

GDF11, a circulating cytokine in the transforming growth factor β superfamily, declines with age and has been under investigation as an anti- aging therapeutic (65). Restoration of circulating levels in aged mice promotes adiponectin secretion by fat tissues and reduces adiposity (66).

Hydroxyeicosatetraenoic acids (HETEs) and dihydroxyoctade canoic acids (diHOMEs) are secreted bioactive lipids that are produced from cytochrome P450 metabolites in brown adipocytes after cold exposure and exercise (67, 68). CYP4F11, a cytochrome that produces 20-HETE from arachidonic acid (69), was abundantly increased by NRBC. Circulating levels of 20-HETE correlate with elevated energy expenditure after cold exposure in people with detectable levels of BAT (70), and it is a PPARα activator (71). In addition, NRBC induced epoxide hydrolases EPHX1 and EPHX2, enzymes that utilize HETEs to produce 12,13-diHOME, a lipokine associated with improved insulin sensitivity and reduced triglycerides after exercise (72, 73).

Several circulating CNS-acting proteins were increased by NRBC. Neuromedin B is a peptide that acts on hypothalamic neurons to promote satiety, and a missense mutation is linked to hyperphagia and obesity in genetic studies (74, 75). Pro-opiomelanocortin (POMC), a peptide prohormone that is cleaved by PCSK1 into the hormone α-MSH, is involved in the suppression of food intake (76). POMC and PCSK1 were both elevated by NRBC in adipocytes. The important role of POMC is shown in studies linking severe obesity in humans to rare genetic mutations in POMC or PCSK1 (77). S100b, which has been characterized in brown adipocytes of mice, stimulates neurite outgrowth of sympathetic terminals in adipose tissue following cold exposure (78). The upregulation of genes for CNS-acting circulating factors suggests that appetite reduction could play a role in the physiological response to NRBC.

## Increases in thermogenesis genes for non-UCP1 uncoupling and substrate cycling pathways

Several mechanisms other than uncoupling of mitochondria by UCP1 can yield thermogenic energy expenditure. These mechanisms were originally identified in studies of brown adipose tissue (BAT) from cold exposed Ucp1-knockout mice that are able to maintain their body temperature (79). We found that NRBC induced significant increases in a number of novel thermogenesis genes in human adipocytes (Table 3). RXRγ, a retinoic acid receptor isoform of unknown function, was highly upregulated. This isoform is localized in UCP1 positive cells in human adipose tissues and is expressed at elevated basal levels in adipose-derived stem cells that subsequently differentiate into UCP1-expressing brown adipocytes (80). These observations suggest that RXRγ may be a key transcription factor in the differentiation of human brown and beige adipocytes.

PM20D1 levels were upregulated approximately 15-fold in adipocytes treated with NRBC, and human genetic studies have shown that the PM20D1 gene promoter has a PPRE (81). PM20D1 is a secreted enzyme that regulates synthesis and degradation of N-acyl amino acids (NAAs), molecules that directly uncouple mitochondria and increase energy expenditure (82). High PM20D1 levels in the white adipose tissue of mice correlates with increased respiration, reversal of

10.3389/fendo.2023.1148954

TABLE 1 NRBC-induced genes associated with brown/beige phenotype previously shown as upregulated by synthetic PPARγ and PPARα activators.

| Gene | Description | Fold | Padj* |
|---|---|---|---|
| CIDEA | cell death inducing DFFA like effector a | 12.4 | 4.04E-06 |
| CITED1 | Cbp/p300 interacting transactivator domain 1 | 4.3 | 1.37E-11 |
| PLIN2 | perilipin 2 | 1.8 | 2.56E-13 |
| PLIN4 | perilipin 4 | 4.1 | 4.16E-49 |
| PLIN5 | perilipin 5 | 3.0 | 1.39E-11 |
| AQP7 | aquaporin 7 glycerol channel | 3.5 | 4.26E-20 |
| ELOVL3 | ELOVL fatty acid elongase 3 | 2.4 | 5.38E-07 |
| ELOVL5 | ELOVL fatty acid elongase 5 | 2.2 | 2.46E-26 |
| ELOVL6 | ELOVL fatty acid elongase 6 | 2.3 | 5.71E-13 |
| ACSL5 | acyl-CoA synthetase long chain family member 5 | 1.8 | 0.017 |
| FABP3 | fatty acid binding protein 3 | 2.5 | 2.65E-14 |
| FABP4 | fatty acid binding protein 4 | 5.6 | 2.42E-89 |
| FABP7 | fatty acid binding protein 7 | 6.0 | 2.32E-09 |
| FABP5 | fatty acid binding protein 5 | 1.9 | 1.1E-05 |

*Adjusted p-value.

high fat diet-induced obesity, and reductions in blood glucose (82–84). Creatine phosphate cycling is an enzymatic pathway that contributes to thermogenesis in Ucp1-knockout mice (85). The synthesis and breakdown of creatine phosphate by the mitochondrial creatine kinases CKMT1A, CKMT1B and CKMT2 releases heat and consumes ATP. We found strong upregulation of the genes for all three CKMT isozymes after NRBC treatment of white adipocytes. In humans, CKMT proteins have previously only been detected in primary brown adipocytes (86).

Beige cells favor utilization of fatty acids rather than glucose to fuel thermogenesis and have high lipase activity (87). In addition to ATGL, hormone sensitive lipase (HSL) and protein kinase A regulatory subunit 2A (PRKAR2B) were upregulated by NRBC treatment (Table 3). PRKAR2B is the key PKA subunit regulating activation of lipolysis subsequent to ligand binding of Gs-coupled receptors (88). NRBC significantly upregulated genes for futile cycling of triglycerides, PDK4, GPD1, GK and PCK1. The activities of these enzymes result in shuttling of glycolytic intermediates into pyruvate for the synthesis of glycerol and glycerol-3-phosphate, the precursors for re-esterification of fatty acids during TG synthesis (10). NRBC also stimulated increases in AIFM2, an NADH oxidase (AIFM2) that supports glucose metabolism during thermogenesis in brown adipocytes (89), and UCP2. Elevated UCP2 levels are associated with cells that have high fatty acid oxidation rates, and evidence suggests that UCP2 facilitates fatty acid oxidation to fuel mitochondrial thermogenesis (90–92).

TABLE 2 Genes encoding secreted lipokines and peptides upregulated by NRBC.

| Gene | Description | Fold | Padj* |
|---|---|---|---|
| ANGPTL4 | angiopoietin like 4 | 3.1 | 1.4E-34 |
| FNDC4 | fibronectin type III domain containing 4 | 1.7 | 3.6E-08 |
| GDF11 | growth differentiation factor 11 | 2.2 | 2.6E-24 |
| CYP4F11 | cytochrome P450 family 4 subfamily F member 11 | 14.0 | 3.0E-05 |
| EPHX1 | epoxide hydrolase 1 | 1.7 | 3.2E-06 |
| EPHX2 | epoxide hydrolase 2 | 1.6 | 6.2E-04 |
| NMB | neuromedin B | 2.7 | 1.9E-30 |
| POMC | proopiomelanocortin | 1.7 | 6.0E-06 |
| PCSK1 | proprotein convertase subtilisin/kexin type 1 | 1.7 | 4.4E-03 |
| S100B | S100 calcium binding protein B | 2.5 | 5.0E-11 |

*Adjusted p-value.

10.3389/fendo.2023.1148954

TABLE 3 Thermogenesis genes upregulated by NRBC.

| Gene | Description | Fold | Padj* |
|---|---|---|---|
| RXRG | retinoid X receptor gamma | 10.0 | 8.2E-19 |
| PM20D1 | peptidase M20 domain containing 1 | 15.7 | 2.2E-07 |
| CKMT1A | creatine kinase, mitochondrial 1A | 5.1 | 3.7E-05 |
| CKMT1B | creatine kinase, mitochondrial 1B | 3.9 | 3.5E-06 |
| CKMT2 | creatine kinase, mitochondrial 2 | 3.8 | 5.1E-18 |
| PDK4 | pyruvate dehydrogenase kinase 4 | 4.2 | 1.0E-80 |
| GPD1 | glycerol-3-phosphate dehydrogenase 1 | 3.3 | 1.8E-25 |
| GK | glycerol kinase | 2.4 | 5.4E-03 |
| PCK1 | phosphoenolpyruvate carboxykinase 1 | 3.8 | 6.0E-08 |
| AIFM2 | apoptosis inducing factor mitochondria associated 2 | 2.0 | 1.7E-29 |
| UCP2 | uncoupling protein 2 | 3.4 | 2.5E-31 |
| NAMPT | nicotinamide phosphoribosyltransferase | 2.1 | 3.4E-23 |
| NAPRT | nicotinate phosphoribosyltransferase | 2.4 | 3.1E-22 |
| LIPE | hormone sensitive lipase | 3.2 | 2.5E-31 |
| PRKAR2B | Protein kinase cAMP-dep type II regulatory subunit B | 2.5 | 3.5E-20 |

*Adjusted p-value.

Nicotinamide phosphoribosyltransferase (NAMPT) and nicotinic acid phosphoribosyltransferase (NAPRT) encode enzymes that produce nicotine adenine dinucleotide (NAD) and are upregulated over two-fold. NAD is a key cofactor for cellular metabolism enzymes. Impaired NAD synthesis in adipocytes causes systemic insulin resistance and suppresses lipolysis and thermogenesis in mice (93, 94). In human adipocytes, increasing intracellular NAD induces UCP1 and mitochondrial biogenesis, which are markers of beige cells (95). In summary, these changes in thermogenesis genes suggest that NRBC-treated adipocytes have a higher capacity for uncoupled respiration and thermogenic futile cycling pathways.

## NRBC increases expression of receptors that regulate lipolysis and thermogenesis

There is little comprehensive data available on relative receptor levels or hormone-stimulated lipolysis in human adipocytes. Based on our RNA sequencing data, receptor abundance was estimated from transcript reads per total number of kilobases sequenced (Figures 6A, B). NRBC treatment significantly increased expression of eight receptors potentially capable of driving lipolysis or thermogenesis through various mechanisms including the β1AR, bile acid receptor TGR5, cold receptor TRPM8, adenosine receptor ADORA1, NPR1, G-protein coupled estrogen receptor-1 (GPER1), growth hormone receptor (GHR) and PTHR1 (Padj<0.002). In addition, there were increases in β2AR, β3AR, and melanocortin-1 receptor (MC1R) that did not achieve statistical significance due to variability in the response. The β2AR and β3AR had the lowest expression levels compared to all other receptors in white adipocytes. The β1AR was approximately four times more abundant than the β2AR and β3AR and increased another three-fold after NRBC exposure (Figure 6A). TGR5, TRPM8 and ADORA1 and ADORA2 were also expressed at low levels in untreated white adipocytes.

The ratio of stimulatory NPR1 to the clearance receptor NPR3 determines the magnitude of the response to natriuretic peptides. NRBC treatment increased the NPR1/NPR3 ratio four-fold in NRBC- treated adipocytes, suggesting that adipocytes would be more responsive to natriuretic peptides (Figure 6B). PTHR levels were upregulated over fifty percent by NRBC (Figure 6B). GHR was the most abundant of all receptors upregulated by NRBC, and studies suggest that GH triggers lipolysis by unique mechanisms that occur downstream of receptor signaling in human adipocytes (41, 96). GPER1 is abundantly expressed in adipocytes and estradiol is the endogenous ligand. Little is known about the role of GPER1 in white adipocytes (97). A selective synthetic agonist for GPER stimulates weight loss and energy expenditure in mice (98).

## NRBC-treated adipocytes have higher agonist-stimulated lipolysis than white adipocytes

Thermogenesis is fueled by lipolysis, so we determined whether agonist-stimulated glycerol release, a measure of lipolysis, reflected the increases in receptors and lipolysis machinery in NRBC-treated adipocytes. First, adipocyte cultures from four donors who had obesity were treated with either cell medium (untreated control cells) or NRBC for seven days. On the day of the acute lipolysis assay, cells were exposed to the individual receptor agonists for four hours in buffer and glycerol released into the cell supernatant was

10.3389/fendo.2023.1148954

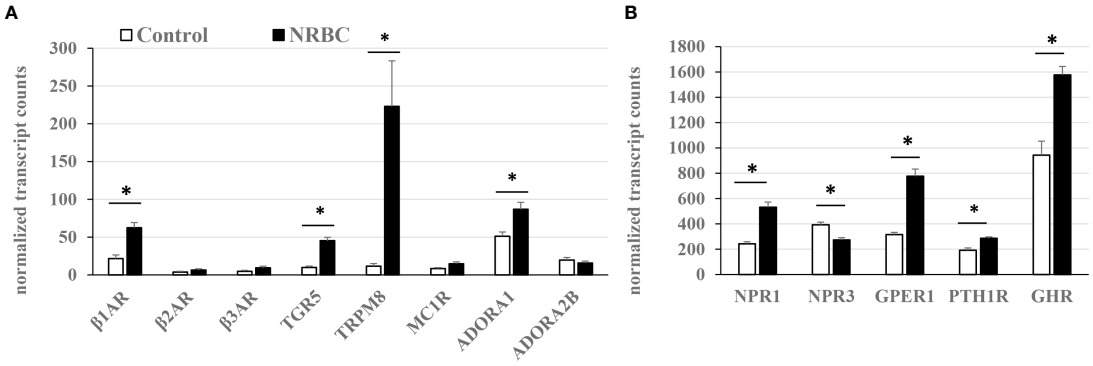


FIGURE 6
Relative receptor levels in white adipocytes (untreated) and NRBC-treated cells. **(A)** Low abundance **(B)** High abundance. Adipocytes from two donors with obesity were treated with cell medium (Control) or NRBC for seven days and transcript sequencing analysis was conducted. Data are expressed as mean normalized transcript counts (DEseq2). * indicates Padj< 0.002 for Control *vs* NRBC. β-adrenergic receptors (β1AR, β2AR, β3AR), G-protein coupled bile acid receptor (TGR5), Transient receptor potential cation channel subfamily M member 8 (TRPM8), Melanocortin-1 receptor (MC1R), Adenosine receptors A1 and A2B (ADORA1, ADORA2B), Natriuretic peptide receptors (NPR1, NPR3), G-protein coupled estrogen receptor 1 (GPER1), Parathyroid hormone receptor 1 (PTHR1), Growth hormone receptor (GHR).

measured. Non-hydrolyzable 8-cpt-cAMP, a potent activator of PKA signaling, was also evaluated in each experiment as a positive control since it bypasses individual receptors and measures the maximum capacity for lipolysis (36). The βARs, PTHR, MC1R, GPER and ADORA2B are all stimulatory G-protein (Gs) coupled receptors and signal through the cAMP-PKA signal transduction mechanism. NPR1 is not a Gs-coupled receptor and signals through an alternate mechanism of guanylate cyclase-cGMP-protein kinase G (PKG).

Of all the hormones tested, PTH- stimulated lipolysis was the highest in control white adipocytes and increased by the greatest magnitude in cultures exposed to NRBC (Figure 7). PTH treatment

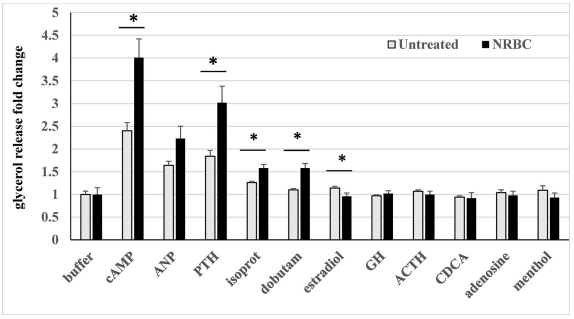


FIGURE 7
Hormone-stimulated lipolysis in white adipocytes (untreated) and NRBC-pretreated cells. After 7d pretreatment with vehicle (untreated) or NRBC, adipocytes were exposed for 4 hours to receptor agonists in KRB buffer. Supernatants were removed for measurement of glycerol. Data are presented as least squares mean ± standard error from experiments using cells from four different donors with BMIs ranging from 27 to 36, each with at least 6 replicates. (*indicates a difference between untreated white adipocytes and NRBC-treated adipocytes p≤ 0.02) cAMP 8-Cpt-cAMP 200μM, ANP atrial natriuretic peptide 0.1 μM, PTH parathyroid hormone (1-34) 1 μM, isoprot isoproterenol 1μM, dobutam dobutamine 1μM, estradiol 1μM, GH growth hormone 250ng/ml, ACTH adrenocorticotropin hormone 1μM, CDCA chenodeoxycholic acid 30μM, adenosine 1μM, menthol 100μM.

of human adipocytes was previously shown to stimulate UCP1 expression and oxygen consumption (99). We tested atrial natriuretic peptide (ANP), one of the key endogenous ligands for NPR1 released from atrial myocytes in response to increases in blood pressure and environmental stimuli such as exercise and cold exposure (100, 101). ANP-stimulated lipolysis increased in NRBC-treated cells, but the overall effect was not statistically significant in adipocytes from four donors.

The collective activity of the βARs was measured using isoproterenol, a non-selective agonist of all three βARs, to evaluate the overall potential for increased sensitivity to sympathetic stimulation. Since the β1AR was 5-fold more abundant than the other βARs, the β1AR-selective ligand dobutamine was also tested. Isoproterenol- and dobutamine- stimulated lipolysis were significantly boosted in NRBC-treated cells, and dobutamine activity was comparable with isoproterenol activity (Figure 7). In NRBC-treated adipocytes, lipolysis stimulated by 8-cpt-cAMP was significantly higher than levels in control cells, showing that maximum capacity for lipolysis was elevated in parallel with the upregulation of the PKA regulatory subunit and lipases.

Agonists for the receptors GHR, MC1R, ADORA1/ADORA2B, TGR5 and TRPM8 did not stimulate detectable increases in lipolysis. In murine white and brown adipocytes adrenocorticotropic hormone (ACTH) and adenosine, endogenous ligands for melanocortin receptors and ADORA2B respectively, stimulate lipolysis and OCR (42, 44, 102). Bile acids activate TGR5 in human brown adipocytes and increase OCR (43). Although GPER activation by estrogen stimulates cAMP production in cancer cells (36), our data showed a small reduction in lipolysis.

## RXRγ is bound to PPARγ complexes before and after treatment

NRBC induced a strong increase in RXRγ mRNA after treatment and RXRα was unchanged. RXRγ is a unique isoform associated with

differentiation of brown adipocytes in human adipose tissue (80). RXRs can form homodimers or heterodimers with multiple nuclear receptors other than PPARγ, so we evaluated whether RXRγ was bound to PPARγ after NRBC treatment. PPARγ was immunoprecipitated from protein lysates of untreated and NRBC-treated adipocytes. The protein complexes pulled down with PPARγ were analyzed on Western Blots (Figure 8). RXRγ protein expression was too low for detection on regular Western Blots of whole cell protein, consistent with our transcriptome sequencing data indicating that it has a low copy number. However, we observed that RXRγ was visible in the immunoprecipitated PPARγ protein complex in control cells (white adipocytes) and in NRBC treated beige adipocytes (Figure 8). RXRα is more abundantly expressed and was readily detected in Western Blots and in PPARγ immunoprecipitates. These results suggest that both isoforms are bound constitutively and that binding of RXRy is independent of the addition of exogenous ligands. RXR isoforms stabilize PPARγ complexes at PPRE promoter elements and direct expression of specific target genes subsequent to ligand binding (46). Therefore, elevated levels of RXRγ may direct expression towards beige genes after the addition of BC.

## Discussion

Thermogenesis is a fundamental component of energy balance. A number of studies have demonstrated that human adipocytes have the functional plasticity to be transformed into thermogenic cells by non-adrenergic stimuli, making adipose tissue a relevant peripheral target tissue for obesity drugs (10, 37, 45) (99). In this report we investigated the potential of carotenoids to intensify the thermogenic response of human adipocytes to NR, a natural activator of PPARα and PPARγ. Pro-vitamin A carotenoids are converted into ligands for RXR nuclear receptors that form heterodimers with PPARs and coordinate expression of metabolism genes. We evaluated adipocytes treated for seven days with NR and carotenoids at concentrations that are reached in serum after oral administration to humans. The two pro-vitamin A carotenoids, BC and lutein, synergistically enhanced levels of UCP1 compared to NR alone. Lycopene, the third carotenoid that we investigated is not converted into an RXR ligand and did not alter the NR response. We used BC for additional experiments and found that NRBC also enhanced expression of ATGL, GLUT4, and adiponectin, which are drivers of lipolysis and insulin sensitivity. The effect of BC was selective. Expression of the PPARα target gene CPT1β, and PM20D1, a PPARγ regulated gene, were not elevated compared to treatment with NR alone.

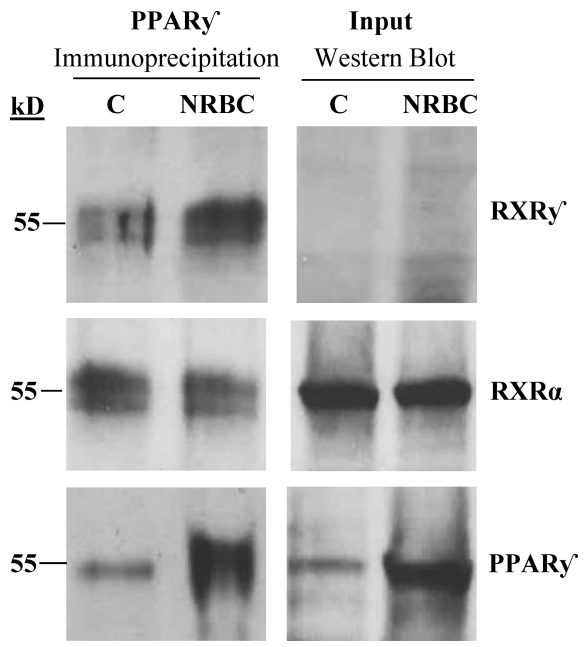


FIGURE 8
Analysis of RXR isoforms bound to immunoprecipitated PPARγ complexes. Adipocytes were treated with vehicle or NRBC for seven days. RXRγ, RXRα and PPARγ protein levels were analyzed by Western blotting. For analysis of whole cell protein levels (input), 50 µg of protein lysate was loaded in each lane. PPARγ was immunoprecipitated from 600 µg of the same whole cell lysate for analysis of PPARγ cofactor binding. An anti-IgGκ light chain secondary antibody was used for detection. This experiment was repeated three times with adipocytes from obese donors.

NRBC upregulated protein levels of PGC-1α, PPARγ, and PPARα without comparable increases in mRNA levels, suggesting that the mechanism does not involve enhanced translation. Pgc-1α is a cold- induced coactivator for PPARγ and PPARα with a short protein half-life, and its transcriptional activity is upregulated in mice by mechanisms that slow degradation (58). When its protein levels increase, Pgc-1α protein associates with the PPARγ/RXR complex and selectively promotes expression of UCP1 and mitochondrial proteins (103). Elevated PGC-1α protein drives the PPARα/RXR complex towards GK expression and TG cycling activity in human adipocytes (104). The half-life of PPARγ and PPARα proteins is regulated by control of degradation rate after binding of ligands and cofactors (56, 57, 59). Since treatment with NR alone did not upregulate protein levels, our data suggest that NR and BC are both required to stabilize PPAR protein levels.

Brown and beige adipocytes release specialized bioactive lipokines and proteins into circulation that activate whole body insulin sensitivity and fatty acid uptake. Transcriptome sequencing showed that NRBC treatment substantially upregulated Cyp4f11, EPDX1 and EPDX2, enzymes that produce HETES and di-HOMEs (69, 72). Secreted HETES and di-HOMEs can signal tissues to increase uptake of fatty acids, and these actions have beneficial effects on lowering blood lipids (73). HETEs are strong PPAR activators (71), and when combined with the increased levels of PPAR proteins observed after NRBC treatment could amplify PPAR target gene expression. NRBC also induced ANGPTL4, a secreted protein that stimulates adipocyte lipolysis, and the insulin sensitizers adiponectin, FNDC4, and GDF11.

ATGL is the rate-limiting lipase for release of fatty acids from TGs, and fatty acids are natural ligands of PPARα and PPARy. In metabolically active beige cells, fatty acids are shuttled into mitochondria to fuel thermogenesis (87). In an energy-wasting futile cycle, fatty acids are also re-esterified onto the glycerol backbone of TGs. Whole transcriptome sequencing showed that NRBC stimulated a number of genes for glyceroneogenesis and TG synthesis, including PDK4, PCK1, GK, and GPD1. When

thermogenesis is activated in adipocytes, PDK4 directs the flow of pyruvate generated by glycolysis into glycerol production (105). The PCK1 gene encodes PEPCK, the rate-limiting enzyme for glycerol synthesis from pyruvate. Studies using radio-labelled pyruvate in human adipocytes showed incorporation of the label into the glycerol backbone and into TGs after induction of PCK1 or PDK4 in human adipocytes (10, 106). In addition, GK and GPD1 encode enzymes that produce glycerol-3-phosphate, the substrate for fatty acid esterification (107, 108). The net result of TG cycling is elevated energy expenditure and a decrease of free fatty acids released into circulation (105).

In addition to UCP1 and TG cycling, we found that NRBC stimulated multiple other uncoupling and ATP-consuming enzymatic pathways. The most highly upregulated gene was PM20D1, encoding an enzyme that reversibly synthesizes NAAs that have potent mitochondrial uncoupling activity (109). In humans, the functional phenotype of PM20D1 is not well defined. In a clinical trial, serum concentrations of PM20D1 were positively correlated with adiposity and biomarkers of glucose metabolism such as glycated hemoglobin and fasting blood glucose (110). Both PM20D1 and NAAs are bound to serum proteins and regulation of circulating levels of NAAs in humans is complex (111). The relationship between adipose tissue PM20D1 and body weight in humans is unclear. Mutations in upstream PPARγ-binding regulatory elements of the PM20D1 gene cause a wide variation in basal expression levels in adipocytes. However, basal levels of PM20D1 in human adipose tissue do not correlate with circulating NAA levels (81). Presently, no clinical studies have been conducted to determine whether a substantial increase PM20D1 expression in thermogenic beige adipose tissue is sufficient to cause an increase in circulating NAA levels and contribute to weight loss.

The mitochondrial creatine kinases CKMT1A, CKMT1B and CKMT2 were highly induced by NRBC. Functional studies in mice showed that creatine kinases are upregulated in brown adipocytes after cold exposure or in the absence of Ucp1 and contribute to whole body energy expenditure (85). Interestingly, ablation of creatine metabolism in white adipose tissues inhibits thermogenesis and drives obesity in mice (112). In primary human brown adipocytes, proteomic analysis of thermogenesis pathways showed that ATP-coupled respiration is stimulated in parallel to uncoupled respiration and contributes half of the total oxygen consumed (86). Cycling of creatine phosphate supports ATP-coupled mitochondrial respiration by increasing the availability of ADP and phosphate to ATP-synthase. The strong induction of creatine kinases by NRBC suggests that ATP-coupled respiration and creatine phosphate cycling could contribute to thermogenesis in human beige adipocytes.

We showed that the enzymes involved in maintaining intracellular NAD levels, including AIFM2, NAMPT and NAPRT, increased after NRBC exposure. AIFM2 converts NADH to NAD to support the high levels required for glycolysis (89). NAMPT and NAPRT both synthesize NAD from intracellular precursors to support cellular needs during conditions of increased metabolic rate and oxidative stress (113). In addition, NAD is a cofactor for the sirtuin enzymes (SIRTs), which are protein deacetylases that regulate the activity of PPARγ, PGC-1α and other transcriptional activators of mitochondrial biogenesis and metabolism genes (114). Increasing NAD levels in human adipocytes can shift the phenotype from white to beige (95).

Our quantitative RNAseq analysis showed that the RXRα transcript is 300-fold more abundant than RXRγ in human white adipocytes, however, only the RXRγ isoform was robustly upregulated by NRBC treatment. We found that both RXRγ and RXRα proteins were bound in immunoprecipitated PPARγ complexes from untreated white adipocytes and in NRBC-treated beige cells. These results indicate that binding of both isoforms to the PPARγ complex is constitutive and ligand independent. In human perirenal adipose tissue, RXRγ expression is enriched in brown adipocyte progenitors and is induced in parallel with UCP1 during conversion of white to beige adipocytes (80). Possible mechanisms for targeting of beige genes could be recruitment of specific coactivators by RXRγ or conformational changes stimulated by BC binding that facilitate and stabilize interaction of this isoform with specific promoter elements (115) (46). In addition, the increase in RXRγ, PGC1α, PPARα and PPARγ proteins after NRBC treatment suggests the existence of a positive feedback loop that upregulates the genes identified in this study.

We used transcriptome sequencing data to estimate relative expression levels of receptors known to activate lipolysis or thermogenesis in adipocytes. In cells treated with NRBC, eight receptors were upregulated and several others trended higher. We evaluated stimulation of lipolysis with agonists for all receptors altered by NRBC and found that only a small subset were lipolytic. ACTH and adenosine stimulate lipolysis in murine white adipocytes and we saw no effect with either (44, 102). TGR5 and TRPM8 agonists induce thermogenesis genes in human adipocytes but did not stimulate lipolysis in our assay. We and others have shown that mild cold exposure of subcutaneous human adipocytes activates UCP1 expression by TRPM8, so the large increase in receptor levels after NRBC treatment has potential to act locally to sensitize adipocytes to cold and stimulate thermogenesis (45, 116). GHR and GPER1 were induced to the highest levels of all receptors after NRBC exposure, but neither growth hormone nor estrogen stimulated lipolysis.

NRBC upregulated PTHR levels. Moreover, PTH stimulated the greatest magnitude of lipolysis of all hormones tested in NRBC pretreated cells. PTH is released from parathyroid glands for regulation of systemic calcium homeostasis and all tissues express the PTHR (117). Evidence is growing that PTH plays an important role in adipose tissue metabolism. PTH stimulates lipolysis in mouse adipocytes and thermogenic gene expression in human adipocytes (99, 118). Cold-induced increases in circulating PTH shift whole-body metabolism toward lipid utilization to fuel energy expenditure in swimmers (119).

NRBC increased the stimulatory ratio of NPR1/NPR3 receptors. ANP is released after cold exposure and exercise and acts additively with adrenergic agonists to stimulate lipolysis and brown adipocyte characteristics in human white adipocytes (37). Although the increase was not statistically significant, our data showed a trend toward increased ANP-activated lipolysis in NRBC-treated cells.

We observed that the β1AR expression level in human adipocytes was substantially higher than the other βARs, and the β1AR was induced an additional three-fold by NRBC. We tested glycerol release with the pan-βAR agonist isoproterenol and the β1AR-selective agonist dobutamine and found that both stimulated a similar

increase in NRBC-exposed cells compared to untreated. These results are in line with other studies showing that the β1AR is the dominant subtype in human white and brown adipocytes (39, 120).

NRBC significantly increased expression of PRKAR2B, the key PKA regulatory subunit linked to insulin sensitivity and resistance to weight gain in humans (88). We used 8-cpt-cAMP to activate PKA downstream of receptors and observed a considerable increase in the maximum capacity for lipolysis in adipocytes pretreated with NRBC. Impaired cAMP-stimulated TG lipolysis in subcutaneous adipose tissue is a characteristic of obesity and insulin resistance (121). A comprehensive analysis of two female cohorts with a ten-year follow-up was conducted to determine adipose tissue characteristics that predict weight gain. Low levels of stimulated lipolysis and PRKAR2B expression predicted weight gain and impaired glucose metabolism (122). Interestingly, there was no correlation with basal lipolysis or fat oxidation.

The human response to cold exposure and exercise involves transient release of ANP and PTH into circulation and sympathetic release of catecholamines in adipose tissues (100, 119) (37, 39, 99). Our data suggest that adipose tissue in an individual consuming NRBC would be more responsive to circulating hormones released after these stimuli. We demonstrate in this report that NRBC reprograms adipocytes by upregulating multiple thermogenic pathways, beneficial secreted factors, receptors and lipolysis, summarized in Figure 9. NR and BC have a good safety profiles and have the potential to be administered long-term without adverse effects (27, 29). A randomized, double blinded placebo-controlled clinical trial will be needed to determine whether the effects of NRBC on adipocytes will translate into weight loss and improvements in insulin sensitivity.

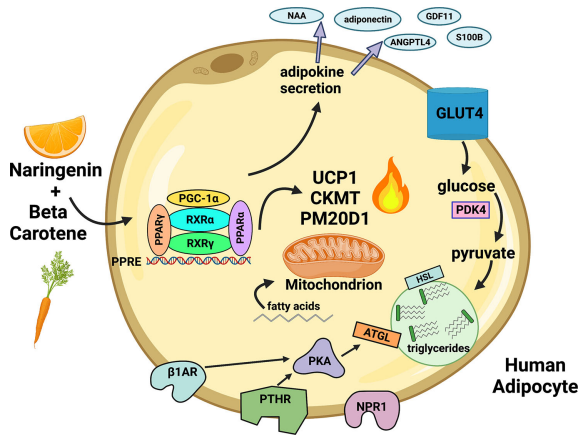


FIGURE 9
Proposed paradigm for remodeling of white adipocytes by NRBC. NR and BC bind nuclear receptors and activate gene expression at PPRE motifs. UCP1 and other uncoupling compounds and mitochondrial proteins mediate multiple energy-wasting enzymatic cycles that generate heat. PM20D1 regulates synthesis and degradation of N-acyl amino acids (NAA), molecules that directly uncouple mitochondria and increase energy expenditure. The synthesis and breakdown of creatine phosphate by the mitochondrial creatine kinases CKMT1A, CKMT1B and CKMT2 facilitates ATP-coupled respiration and enhances oxygen consumption. PDK4 directs pyruvate into synthesis of glycerol, fatty acids, and TGs to promote futile TG recycling. Lipolytic receptors and PKA are upregulated, increasing responsiveness to hormones and lipolysis. Fatty acids are transferred into mitochondria to fuel thermogenesis. Genes are turned on for production of bioactive peptides and lipokines which have autocrine insulin sensitizing effects and are secreted into circulation. NR (Naringenin), BC (β-carotene) Created with Biorender.com.

## Data availability statement

The datasets presented in this study can be found in online repositories. The names of the repository/repositories and accession number(s) can be found below: https://www.ncbi.nlm.nih.gov/geo/, GSE223313.

## Author contributions

Conceptualization, FG, AC and CR. Methodology: FG, AC, LC and CR. Formal analysis: AC, DZ, SG. Conducted research: AC, CC, SJ, CR, SG. Writing—original draft preparation: AC. Writing—review and editing: CR, YH, FG, CC. All authors contributed to the article and approved the submitted version.

## Funding

This work was supported in part by grants from the Brown Foundation of Louisiana, the National Institute on Aging of the National Institutes of Health (R00AG065419), and in part in part by U54 GM104940 from the National Institute of General Medical Sciences of the National Institutes of Health, which funds the Louisiana Clinical and Translational Science Center. The content is solely the responsibility of the authors and does not necessarily represent the official views of the Brown Foundation or the National Institutes of Health.

## Conflict of interest

The authors declare that the research was conducted in the absence of any commercial or financial relationships that could be construed as a potential conflict of interest.

## Publisher's note

All claims expressed in this article are solely those of the authors and do not necessarily represent those of their affiliated organizations, or those of the publisher, the editors and the reviewers. Any product that may be evaluated in this article, or claim that may be made by its manufacturer, is not guaranteed or endorsed by the publisher.

## Supplementary material

The Supplementary Material for this article can be found online at: https://www.frontiersin.org/articles/10.3389/fendo.2023.1148954/full#supplementary-material

# References


1. Kajimura S, Spiegelman BM, Seale P. Brown and beige fat: Physiological roles beyond heat generation. *Cell Metab* (2015) 22(4):546–59. doi: 10.1016/j.cmet.2015.09.007

2. Guerra C, Koza RA, Yamashita H, Walsh K, Kozak LP. Emergence of brown adipocytes in white fat in mice is under genetic control. effects on body weight and adiposity. *J Clin Invest* (1998) 102(2):412–20.

3. Kopecky J, Clarke G, Enerback S, Spiegelman B, Kozak LP. Expression of the mitochondrial uncoupling protein gene from the aP2 gene promoter prevents genetic obesity. *J Clin Invest* (1995) 96(6):2914–23. doi: 10.1172/JCI118363

4. Vallerand AL, Perusse F, Bukowiecki LJ. Stimulatory effects of cold exposure and cold acclimation on glucose uptake in rat peripheral tissues. *Am J Physiol* (1990) 259(5 Pt 2):R1043–9. doi: 10.1152/ajpregu.1990.259.5.R1043

5. Barbatelli G, Murano I, Madsen L, Hao Q, Jimenez M, Kristiansen K, et al. The emergence of cold-induced brown adipocytes in mouse white fat depots is determined predominantly by white to brown adipocyte transdifferentiation. *Am J Physiol Endocrinol Metab* (2010) 298(6):E1244–53. doi: 10.1152/ajpendo.00600.2009

6. Himms-Hagen J, Cui J, Danforth EJr., Taatjes DJ, Lang SS, Waters BL, et al. Effect of CL-316,243, a thermogenic beta 3-agonist, on energy balance and brown and white adipose tissues in rats. *Am J Physiol* (1994) 266(4 Pt 2):R1371–82. doi: 10.1152/ajpregu.1994.266.4.R1371

7. Cypess AM, Chen YC, Sze C, Wang K, English J, Chan O, et al. Cold but not sympathomimetics activates human brown adipose tissue in vivo. *Proc Natl Acad Sci U.S.A.* (2012) 109(25):10001–5. doi: 10.1073/pnas.1207911109

8. Finlin BS, Memetimin H, Zhu B, Confides AL, Vekaria HJ, El Khouli RH, et al. The beta3-adrenergic receptor agonist mirabegron improves glucose homeostasis in obese humans. *J Clin Invest* (2020) 130(5):2319–31. doi: 10.1172/JCI134892

9. Vosselman MJ, van der Lans AA, Brans B, Wierts R, van Baak MA, Schrauwen P, et al. Systemic beta-adrenergic stimulation of thermogenesis is not accompanied by brown adipose tissue activity in humans. *Diabetes* (2012) 61(12):3106–13. doi: 10.2337/db12-0288

10. Barquissau V, Beuzelin D, Pisani DF, Beranger GE, Mairal A, Montagner A, et al. White-to-brite conversion in human adipocytes promotes metabolic reprogramming towards fatty acid anabolic and catabolic pathways. *Mol Metab* (2016) 5(5):352–65. doi: 10.1016/j.molmet.2016.03.002

11. Loft A, Forss I, Siersbaek MS, Schmidt SF, Larsen AS, Madsen JG, et al. Browning of human adipocytes requires KLF11 and reprogramming of PPARgamma superenhancers. *Genes Dev* (2015) 29(1):7–22. doi: 10.1101/gad.250829.114

12. Kaupang A, Hansen TV. The PPAR omega pocket: Renewed opportunities for drug development. *PPAR Res* (2020) 2020:9657380. doi: 10.1155/2020/9657380

13. Tan Y, Muise ES, Dai H, Raubertas R, Wong KK, Thompson GM, et al. Novel transcriptome profiling analyses demonstrate that selective peroxisome proliferator-activated receptor gamma (PPARgamma) modulators display attenuated and selective gene regulatory activity in comparison with PPARgamma full agonists. *Mol Pharmacol* (2012) 82(1):68–79. doi: 10.1124/mol.111.076679

14. Benvenuti S, Cellai I, Luciani P, Deledda C, Baglioni S, Giuliani C, et al. Rosiglitazone stimulates adipogenesis and decreases osteoblastogenesis in human mesenchymal stem cells. *J Endocrinol Invest* (2007) 30(9):RC26–30. doi: 10.1007/BF03350807

15. Soccio RE, Chen ER, Lazar MA. Thiazolidinediones and the promise of insulin sensitization in type 2 diabetes. *Cell Metab* (2014) 20(4):573–91. doi: 10.1016/j.cmet.2014.08.005

16. Ribet C, Montastier E, Valle C, Bezaire V, Mazzucotelli A, Mairal A, et al. Peroxisome proliferator-activated receptor-alpha control of lipid and glucose metabolism in human white adipocytes. *Endocrinology* (2010) 151(1):123–33.

17. Allen LH. How common is vitamin b-12 deficiency? *Am J Clin Nutr* (2009) 89(2):693S–6S.

18. FDA. Tricor fenofibrate. Available at: https://www.accessdata.fda.gov/drugsatfda_docs/label/2010/021656s019lbl.pdf.

19. Cheng HS, Tan WR, Low ZS, Marvalim C, Lee JYH, Tan NS. Exploration and development of PPAR modulators in health and disease: An update of clinical evidence. *Int J Mol Sci* (2019) 20(20).

20. Boeckmans J, Natale A, Rombaut M, Buyl K, Rogiers V, De Kock J, et al. Anti-NASH drug development hitches a lift on PPAR agonism. *Cells* (2019) 9(1).

21. Steele H, Gomez-Duran A, Pyle A, Hopton S, Newman J, Stefanetti RJ, et al. Metabolic effects of bezafibrate in mitochondrial disease. *EMBO Mol Med* (2020) 12(3):e11589.

22. Choi JH, Banks AS, Estall JL, Kajimura S, Bostrom P, Laznik D, et al. Anti-diabetic drugs inhibit obesity-linked phosphorylation of PPARgamma by Cdk5. *Nature* (2010) 466(7305):451–6. doi: 10.1038/nature09291

23. Zhang F, Lavan BE, Gregoire FM. Selective modulators of PPAR-gamma activity: Molecular aspects related to obesity and side-effects. *PPAR Res* (2007) 2007:32696. doi: 10.1155/2007/32696

24. Goldwasser J, Cohen PY, Yang E, Balaguer P, Yarmush ML, Nahmias Y. Transcriptional regulation of human and rat hepatic lipid metabolism by the grapefruit flavonoid naringenin: role of PPARalpha, PPARgamma and LXRalpha. *PloS One* (2010) 5(8):e12399. doi: 10.1371/journal.pone.0012399

25. Rebello CJ, Greenway FL, Lau FH, Lin Y, Stephens JM, Johnson WD, et al. Naringenin promotes thermogenic gene expression in human white adipose tissue. *Obes (Silver Spring)* (2019) 27(1):103–11. doi: 10.1002/oby.22352

26. Murugesan N, Woodard K, Ramaraju R, Greenway FL, Coulter AA, Rebello CJ. Naringenin increases insulin sensitivity and metabolic rate: A case study. *J Med Food* (2020) 23(3):343–8. doi: 10.1089/jmf.2019.0216

27. Rebello CJ, Beyl RA, Lertora JJL, Greenway FL, Ravussin E, Ribnicky DM, et al. Safety and pharmacokinetics of naringenin: A randomized, controlled, single-ascending-dose clinical trial. *Diabetes Obes Metab* (2020) 22(1):91–8. doi: 10.1111/dom.13868

28. Canas JA. Mixed carotenoid supplementation and dysmetabolic obesity: gaps in knowledge. *Int J Food Sci Nutr* (2021) 72(5):653–9. doi: 10.1080/09637486.2020.1852193

29. Canas JA, Lochrie A, McGowan AG, Hossain J, Schettino C, Balagopal PB. Effects of mixed carotenoids on adipokines and abdominal adiposity in children: A pilot study. *J Clin Endocrinol Metab* (2017) 102(6):1983–90. doi: 10.1210/jc.2017-00185

30. Coulter AA, Rebello CJ, Greenway FL. Centrally acting agents for obesity: Past, present, and future. *Drugs* (2018) 78(11):1113–32. doi: 10.1007/s40265-018-0946-y

31. Li J, Curley JL, Floyd ZE, Wu X, Halvorsen YDC, Gimble JM. Isolation of human adipose-derived stem cells from lipoaspirates. *Methods Mol Biol* (2018) 1773:155–65. doi: 10.1007/978-1-4939-7799-4_13

32. Subramanian A, Tamayo P, Mootha VK, Mukherjee S, Ebert BL, Gillette MA, et al. Gene set enrichment analysis: a knowledge-based approach for interpreting genome-wide expression profiles. *Proc Natl Acad Sci U.S.A.* (2005) 102(43):15545–50. doi: 10.1073/pnas.0506580102

33. Ogata H, Goto S, Sato K, Fujibuchi W, Bono H, Kanehisa M. KEGG: Kyoto encyclopedia of genes and genomes. *Nucleic Acids Res* (1999) 27(1):29–34. doi: 10.1093/nar/27.1.29

34. Liberzon A, Birger C, Thorvaldsdottir H, Ghandi M, Mesirov JP, Tamayo P. The molecular signatures database (MSigDB) hallmark gene set collection. *Cell Syst* (2015) 1(6):417–25. doi: 10.1016/j.cels.2015.12.004

35. Reiner A, Yekutieli D, Benjamini Y. Identifying differentially expressed genes using false discovery rate controlling procedures. *Bioinformatics* (2003) 19(3):368–75. doi: 10.1093/bioinformatics/btf877

36. Gettys TW, Blackmore PF, Corbin JD. An assessment of phosphodiesterase activity in situ after treatment of hepatocytes with hormones. *Am J Physiol* (1988) 254(4 Pt 1):E449–53. doi: 10.1152/ajpendo.1988.254.4.E449

37. Bordicchia M, Liu D, Amri EZ, Ailhaud G, Dessi-Fulgheri P, Zhang C, et al. Cardiac natriuretic peptides act *via* p38 MAPK to induce the brown fat thermogenic program in mouse and human adipocytes. *J Clin Invest* (2012) 122(3):1022–36. doi: 10.1172/JCI59701

38. Hoare SR, Gardella TJ, Usdin TB. Evaluating the signal transduction mechanism of the parathyroid hormone 1 receptor. effect of receptor-g-protein interaction on the ligand binding mechanism and receptor conformation. *J Biol Chem* (2001) 276(11):7741–53. doi: 10.1074/jbc.M009395200

39. Riis-Vestergaard MJ, Richelsen B, Bruun JM, Li W, Hansen JB, Pedersen SB. Beta-1 and not beta-3 adrenergic receptors may be the primary regulator of human brown adipocyte metabolism. *J Clin Endocrinol Metab* (2020) 105(4):e994–1005. doi: 10.1210/clinem/dgz298

40. Filardo EJ, Quinn JA, Frackelton ARJr., Bland KI. Estrogen action *via* the G protein-coupled receptor, GPR30: stimulation of adenylyl cyclase and cAMP-mediated attenuation of the epidermal growth factor receptor-to-MAPK signaling axis. *Mol Endocrinol* (2002) 16(1):70–84. doi: 10.1210/mend.16.1.0758

41. Sharma VM, Vestergaard ET, Jessen N, Kolind-Thomsen P, Nellemann B, Nielsen TS, et al. Growth hormone acts along the PPARgamma-FSP27 axis to stimulate lipolysis in human adipocytes. *Am J Physiol Endocrinol Metab* (2019) 316(1):E34–42. doi: 10.1152/ajpendo.00129.2018

42. Schnabl K, Westermeier J, Li Y, Klingenspor M. Opposing actions of adrenocorticotropic hormone and glucocorticoids on UCP1-mediated respiration in brown adipocytes. *Front Physiol* (2018) 9:1931. doi: 10.3389/fphys.2018.01931

43. Broeders EP, Nascimento EB, Havekes B, Brans B, Roumans KH, Tailleux A, et al. The bile acid chenodeoxycholic acid increases human brown adipose tissue activity. *Cell Metab* (2015) 22(3):418–26. doi: 10.1016/j.cmet.2015.07.002

44. Gnad T, Scheibler S, von Kugelgen I, Scheele C, Kilic A, Glode A, et al. Adenosine activates brown adipose tissue and recruits beige adipocytes *via* A2A receptors. *Nature* (2014) 516(7531):395–9. doi: 10.1038/nature13816

45. Rossato M, Granzotto M, Macchi V, Porzionato A, Petrelli L, Calcagno A, et al. Human white adipocytes express the cold receptor TRPM8 which activation induces UCP1 expression, mitochondrial activation and heat production. *Mol Cell Endocrinol* (2014) 383(1-2):137–46. doi: 10.1016/j.mce.2013.12.005

46. IJpenberg A, Tan NS, Gelman L, Kersten S, Seydoux J, Xu J, et al. *In vivo* activation of PPAR target genes by RXR homodimers. *EMBO J* (2004) 23(10):2083–91.

47. Rao AV, Rao LG. Carotenoids and human health. *Pharmacol Res* (2007) 55 (3):207–16. doi: 10.1016/j.phrs.2007.01.012

48. Pierce JP, Natarajan L, Sun S, Al-Delaimy W, Flatt SW, Kealey S, et al. Increases in plasma carotenoid concentrations in response to a major dietary change in the women's healthy eating and living study. *Cancer Epidemiol Biomarkers Prev* (2006) 15(10):1886–92. doi: 10.1158/1055-9965.EPI-05-0928

49. Arballo J, Amengual J, Erdman JWJr. Lycopene: A critical review of digestion, absorption, metabolism, and excretion. *Antioxidants (Basel)* (2021) 10(3). doi: 10.3390/antiox10030342

50. Unlu NZ, Bohn T, Francis D, Clinton SK, Schwartz SJ. Carotenoid absorption in humans consuming tomato sauces obtained from tangerine or high-beta-carotene varieties of tomatoes. *J Agric Food Chem* (2007) 55(4):1597–603. doi: 10.1021/jf062337b

51. Bezaire V, Mairal A, Ribet C, Lefort C, Girousse A, Jocken J, et al. Contribution of adipose triglyceride lipase and hormone-sensitive lipase to lipolysis in hMADS adipocytes. *J Biol Chem* (2009) 284(27):18282–91. doi: 10.1074/jbc.M109.008631

52. Moraes-Vieira PM, Saghatelian A, Kahn BB. GLUT4 expression in adipocytes regulates *De novo* lipogenesis and levels of a novel class of lipids with antidiabetic and anti-inflammatory effects. *Diabetes* (2016) 65(7):1808–15.

53. Carvalho E, Kotani K, Peroni OD, Kahn BB. Adipose-specific overexpression of GLUT4 reverses insulin resistance and diabetes in mice lacking GLUT4 selectively in muscle. *Am J Physiol Endocrinol Metab* (2005) 289(4):E551–61.

54. Achari AE, Jain SK. Adiponectin, a therapeutic target for obesity, diabetes, and endothelial dysfunction. *Int J Mol Sci* (2017) 18(6).

55. Miller KN, Clark JP, Anderson RM. Mitochondrial regulator PGC-1a-Modulating the modulator. *Curr Opin Endocr Metab Res* (2019) 5:37–44.

56. Kilroy GE, Zhang X, Floyd ZE. PPAR-gamma AF-2 domain functions as a component of a ubiquitin-dependent degradation signal. *Obes (Silver Spring)* (2009) 17 (4):665–73.

57. Blanquart C, Barbier O, Fruchart JC, Staels B, Glineur C. Peroxisome proliferator-activated receptor alpha (PPARalpha ) turnover by the ubiquitin-proteasome system controls the ligand-induced expression level of its target genes. *J Biol Chem* (2002) 277(40):37254–9. doi: 10.1074/jbc.M110598200

58. Wei P, Pan D, Mao C, Wang YX. RNF34 is a cold-regulated E3 ubiquitin ligase for PGC-1alpha and modulates brown fat cell metabolism. *Mol Cell Biol* (2012) 32 (2):266–75. doi: 10.1128/MCB.05674-11

59. Blanquart C, Mansouri R, Fruchart JC, Staels B, Glineur C. Different ways to regulate the PPARalpha stability. *Biochem Biophys Res Commun* (2004) 319(2):663–70. doi: 10.1016/j.bbrc.2004.05.035

60. Hauser S, Adelmant G, Sarraf P, Wright HM, Mueller E, Spiegelman BM. Degradation of the peroxisome proliferator-activated receptor gamma is linked to ligand-dependent activation. *J Biol Chem* (2000) 275(24):18527–33. doi: 10.1074/jbc.M001297200

61. Gray NE, Lam LN, Yang K, Zhou AY, Koliwad S, Wang JC. Angiopoietin-like 4 (Angptl4) protein is a physiological mediator of intracellular lipolysis in murine adipocytes. *J Biol Chem* (2017) 292(39):16135. doi: 10.1074/jbc.A111.294124

62. McQueen AE, Kanamaluru D, Yan K, Gray NE, Wu L, Li ML, et al. The c-terminal fibrinogen-like domain of angiopoietin-like 4 stimulates adipose tissue lipolysis and promotes energy expenditure. *J Biol Chem* (2017) 292(39):16122–34. doi: 10.1074/jbc.M117.803973

63. Fruhbeck G, Fernandez-Quintana B, Paniagua M, Hernandez-Pardos AW, Valenti V, Moncada R, et al. FNDC4, a novel adipokine that reduces lipogenesis and promotes fat browning in human visceral adipocytes. *Metabolism* (2020) 108:154261. doi: 10.1016/j.metabol.2020.154261

64. Georgiadi A, Lopez-Salazar V, Merahbi RE, Karikari RA, Ma X, Mourao A, et al. Orphan GPR116 mediates the insulin sensitizing effects of the hepatokine FNDC4 in adipose tissue. *Nat Commun* (2021) 12(1):2999. doi: 10.1038/s41467-021-22579-1

65. Fadini GP, Menegazzo L, Bonora BM, Mazzucato M, Persano S, Vigili de Kreutzenberg S, et al. Effects of age, diabetes, and vascular disease on growth differentiation factor 11: First-in-Human study. *Diabetes Care* (2015) 38(8):e118–9. doi: 10.2337/dc15-0868

66. Katsimpardi L, Kuperwasser N, Camus C, Moigneu C, Chiche A, Tolle V, et al. Systemic GDF11 stimulates the secretion of adiponectin and induces a calorie restriction-like phenotype in aged mice. *Aging Cell* (2020) 19(1):e13038. doi: 10.1111/acel.13038

67. Lynes MD, Leiria LO, Lundh M, Bartelt A, Shamsi F, Huang TL, et al. The cold-induced lipokine 12,13-diHOME promotes fatty acid transport into brown adipose tissue. *Nat Med* (2017) 23(5):631–7. doi: 10.1038/nm.4297

68. Gollasch B, Dogan I, Rothe M, Gollasch M, Luft FC. Maximal exercise and plasma cytochrome P450 and lipoxygenase mediators: a lipidomics study. *Physiol Rep* (2019) 7(13):e14165. doi: 10.14814/phy2.14165

69. Yi M, Cho SA, Min J, Kim DH, Shin JG, Lee SJ. Functional characterization of a common CYP4F11 genetic variant and identification of functionally defective CYP4F11 variants in erythromycin metabolism and 20-HETE synthesis. *Arch Biochem Biophys* (2017) 620:43–51. doi: 10.1016/j.abb.2017.03.010

70. Kulterer OC, Niederstaetter L, Herz CT, Haug AR, Bileck A, Pils D, et al. The presence of active brown adipose tissue determines cold-induced energy expenditure and oxylipin profiles in humans. *J Clin Endocrinol Metab* (2020) 105(7):2203–16. doi: 10.1210/clinem/dgaa183

71. Ng VY, Huang Y, Reddy LM, Falck JR, Lin ET, Kroetz DL. Cytochrome P450 eicosanoids are activators of peroxisome proliferator-activated receptor alpha. *Drug Metab Dispos* (2007) 35(7):1126–34. doi: 10.1124/dmd.106.013839

72. Stanford KI, Lynes MD, Takahashi H, Baer LA, Arts PJ, May FJ, et al. 12,13-diHOME: An exercise-induced lipokine that increases skeletal muscle fatty acid uptake. *Cell Metab* (2018) 27(6):1357.

73. Vasan SK, Noordam R, Gowri MS, Neville MJ, Karpe F, Christodoulides C. The proposed systemic thermogenic metabolites succinate and 12,13-diHOME are inversely associated with adiposity and related metabolic traits: evidence from a large human cross-sectional study. *Diabetologia* (2019) 62(11):2079–87. doi: 10.1007/s00125-019-4947-5

74. Bouchard L, Drapeau V, Provencher V, Lemieux S, Chagnon Y, Rice T, et al. Neuromedin beta: a strong candidate gene linking eating behaviors and susceptibility to obesity. *Am J Clin Nutr* (2004) 80(6):1478–86. doi: 10.1093/ajcn/80.6.1478

75. Blanchet R, Lemieux S, Couture P, Bouchard L, Vohl MC, Perusse L. Effects of neuromedin-beta on caloric compensation, eating behaviours and habitual food intake. *Appetite* (2011) 57(1):21–7. doi: 10.1016/j.appet.2011.04.003

76. Schwartz MW, Woods SC, Porte DJr., Seeley RJ, Baskin DG. Central nervous system control of food intake. *Nature* (2000) 404(6778):661–71. doi: 10.1038/35007534

77. Wabitsch M, Farooqi S, Fluck CE, Bratina N, Mallya UG, Stewart M, et al. Natural history of obesity due to POMC, PCSK1, and LEPR deficiency and the impact of setmelanotide. *J Endocr Soc* (2022) 6(6):bvac057. doi: 10.1210/jendso/bvac057

78. Zeng X, Ye M, Resch JM, Jedrychowski MP, Hu B, Lowell BB, et al. Innervation of thermogenic adipose tissue *via* a calsyntenin 3beta-S100b axis. *Nature* (2019) 569 (7755):229–35. doi: 10.1038/s41586-019-1156-9

79. Chang SH, Song NJ, Choi JH, Yun UJ, Park KW. Mechanisms underlying UCP1 dependent and independent adipocyte thermogenesis. *Obes Rev* (2019) 20(2):241–51. doi: 10.1111/obr.12796

80. Svensson PA, Lindberg K, Hoffmann JM, Taube M, Pereira MJ, Mohsen-Kanson T, et al. Characterization of brown adipose tissue in the human perirenal depot. *Obes (Silver Spring)* (2014) 22(8):1830–7. doi: 10.1002/oby.20765

81. Benson KK, Hu W, Weller AH, Bennett AH, Chen ER, Khetarpal SA, et al. Natural human genetic variation determines basal and inducible expression of PM20D1, an obesity-associated gene. *Proc Natl Acad Sci USA* (2019) 116(46):23232–42.

82. Long JZ, Svensson KJ, Bateman LA, Lin H, Kamenecka T, Lokurkar IA, et al. The secreted enzyme PM20D1 regulates lipidated amino acid uncouplers of mitochondria. *Cell* (2016) 166(2):424–35. doi: 10.1016/j.cell.2016.05.071

83. Long JZ, Roche AM, Berdan CA, Louie SM, Roberts AJ, Svensson KJ, et al. Ablation of PM20D1 reveals n-acyl amino acid control of metabolism and nociception. *Proc Natl Acad Sci U.S.A.* (2018) 115(29):E6937–E45. doi: 10.1073/pnas.1803389115

84. Li D, Liu Y, Gao W, Han J, Yuan R, Zhang M, et al. Inhibition of miR-324-5p increases PM20D1-mediated white and brown adipose loss and reduces body weight in juvenile mice. *Eur J Pharmacol* (2019) 863:172708. doi: 10.1016/j.ejphar.2019.172708

85. Kazak L, Chouchani ET, Jedrychowski MP, Erickson BK, Shinoda K, Cohen P, et al. A creatine-driven substrate cycle enhances energy expenditure and thermogenesis in beige fat. *Cell* (2015) 163(3):643–55. doi: 10.1016/j.cell.2015.09.035

86. Muller S, Balaz M, Stefanicka P, Varga L, Amri EZ, Ukropec J, et al. Proteomic analysis of human brown adipose tissue reveals utilization of coupled and uncoupled energy expenditure pathways. *Sci Rep* (2016) 6:30030. doi: 10.1038/srep30030

87. Braun K, Oeckl J, Westermeier J, Li Y, Klingenspor M. Non-adrenergic control of lipolysis and thermogenesis in adipose tissues. *J Exp Biol* (2018) 221(Pt Suppl 1). doi: 10.1242/jeb.165381

88. Mantovani G, Bondioni S, Alberti L, Gilardini L, Invitti C, Corbetta S, et al. Protein kinase a regulatory subunits in human adipose tissue: decreased R2B expression and activity in adipocytes from obese subjects. *Diabetes* (2009) 58(3):620–6. doi: 10.2337/db08-0585

89. Nguyen HP, Yi D, Lin F, Viscarra JA, Tabuchi C, Ngo K, et al. Aifm2, a NADH oxidase, supports robust glycolysis and is required for cold- and diet-induced thermogenesis. *Mol Cell* (2020) 77(3):600–17.e4. doi: 10.1016/j.molcel.2019.12.002

90. Caron A, Labbe SM, Carter S, Roy MC, Lecomte R, Ricquier D, et al. Loss of UCP2 impairs cold-induced non-shivering thermogenesis by promoting a shift toward glucose utilization in brown adipose tissue. *Biochimie* (2017) 134:118–26. doi: 10.1016/j.biochi.2017.01.006

91. Bouillaud F. UCP2, not a physiologically relevant uncoupler but a glucose sparing switch impacting ROS production and glucose sensing. *Biochim Biophys Acta* (2009) 1787(5):377–83. doi: 10.1016/j.bbabio.2009.01.003

92. Jahansouz C, Xu H, Hertzel AV, Kizy S, Steen KA, Foncea R, et al. Partitioning of adipose lipid metabolism by altered expression and function of PPAR isoforms after bariatric surgery. *Int J Obes (Lond)* (2018) 42(2):139–46. doi: 10.1038/ijo.2017.197

93. Yamaguchi S, Franczyk MP, Chondronikola M, Qi N, Gunawardana SC, Stromsdorfer KL, et al. Adipose tissue NAD(+) biosynthesis is required for regulating adaptive thermogenesis and whole-body energy homeostasis in mice. *Proc Natl Acad Sci U.S.A.* (2019) 116(47):23822–8.

94. Yamaguchi S, Yoshino J. Adipose tissue NAD(+) biology in obesity and insulin resistance: From mechanism to therapy. *Bioessays* (2017) 39(5).

95. Nagy L, Rauch B, Szerafin T, Uray K, Toth A, Bai P. Nicotinamide-riboside shifts the differentiation of human primary white adipocytes to beige adipocytes impacting substrate preference and uncoupling respiration through SIRT1 activation

and mitochondria-derived reactive species production. *Front Cell Dev Biol* (2022) 10:979330.

96. Balaz M, Ukropcova B, Kurdiova T, Vlcek M, Surova M, Krumpolec P, et al. Improved adipose tissue metabolism after 5-year growth hormone replacement therapy in growth hormone deficient adults: The role of zinc-alpha2-glycoprotein. *Adipocyte* (2015) 4(2):113–22.

97. Prossnitz ER, Barton M. Estrogen biology: new insights into GPER function and clinical opportunities. *Mol Cell Endocrinol* (2014) 389(1-2):71–83.

98. Sharma G, Hu C, Staquicini DI, Brigman JL, Liu M, Mauvais-Jarvis F, et al. Preclinical efficacy of the GPER-selective agonist G-1 in mouse models of obesity and diabetes. *Sci Transl Med* (2020) 12(528). doi: 10.1126/scitranslmed.aau5956

99. Hedesan OC, Fenzl A, Digruber A, Spirk K, Baumgartner-Parzer S, Bilban M, et al. Parathyroid hormone induces a browning program in human white adipocytes. *Int J Obes (Lond)* (2019) 43(6):1319–24. doi: 10.1038/s41366-018-0266-z

100. Carper D, Coue M, Nascimento EBM, Barquissau V, Lagarde D, Pestourie C, et al. Atrial natriuretic peptide orchestrates a coordinated physiological response to fuel non-shivering thermogenesis. *Cell Rep* (2020) 32(8):108075. doi: 10.1016/j.celrep.2020.108075

101. Moro C, Crampes F, Sengenes C, De Glisezinski I, Galitzky J, Thalamas C, et al. Atrial natriuretic peptide contributes to physiological control of lipid mobilization in humans. *FASEB J* (2004) 18(7):908–10. doi: 10.1096/fj.03-1086fje

102. Cho KJ, Shim JH, Cho MC, Choe YK, Hong JT, Moon DC, et al. Signaling pathways implicated in alpha-melanocyte stimulating hormone-induced lipolysis in 3T3-L1 adipocytes. *J Cell Biochem* (2005) 96(4):869–78. doi: 10.1002/jcb.20561

103. Puigserver P, Wu Z, Park CW, Graves R, Wright M, Spiegelman BM. A cold-inducible coactivator of nuclear receptors linked to adaptive thermogenesis. *Cell* (1998) 92(6):829–39. doi: 10.1016/S0092-8674(00)81410-5

104. Mazzucotelli A, Viguerie N, Tiraby C, Annicotte JS, Mairal A, Klimcakova E, et al. The transcriptional coactivator peroxisome proliferator activated receptor (PPAR)gamma coactivator-1 alpha and the nuclear receptor PPAR alpha control the expression of glycerol kinase and metabolism genes independently of PPAR gamma activation in human white adipocytes. *Diabetes* (2007) 56(10):2467–75. doi: 10.2337/db06-1465

105. Cadoudal T, Distel E, Durant S, Fouque F, Blouin JM, Collinet M, et al. Pyruvate dehydrogenase kinase 4: regulation by thiazolidinediones and implication in glyceroneogenesis in adipose tissue. *Diabetes* (2008) 57(9):2272–9. doi: 10.2337/db08-0477

106. Cadoudal T, Blouin JM, Collinet M, Fouque F, Tan GD, Loizon E, et al. Acute and selective regulation of glyceroneogenesis and cytosolic phosphoenolpyruvate carboxykinase in adipose tissue by thiazolidinediones in type 2 diabetes. *Diabetologia* (2007) 50(3):666–75. doi: 10.1007/s00125-006-0560-5

107. Iwase M, Tokiwa S, Seno S, Mukai T, Yeh YS, Takahashi H, et al. Glycerol kinase stimulates uncoupling protein 1 expression by regulating fatty acid metabolism in beige adipocytes. *J Biol Chem* (2020) 295(20):7033–45. doi: 10.1074/jbc.RA119.011658

108. Ou X, Ji C, Han X, Zhao X, Li X, Mao Y, et al. Crystal structures of human glycerol 3-phosphate dehydrogenase 1 (GPD1). *J Mol Biol* (2006) 357(3):858–69.

109. Keipert S, Kutschke M, Ost M, Schwarzmayr T, van Schothorst EM, Lamp D, et al. Long-term cold adaptation does not require FGF21 or UCP1. *Cell Metab* (2017) 26(2):437–46.e5.

110. Yang R, Hu Y, Lee CH, Liu Y, Diaz-Canestro C, Fong CHY, et al. PM20D1 is a circulating biomarker closely associated with obesity, insulin resistance and metabolic syndrome. *Eur J Endocrinol* (2021) 186(2):151–61.

111. Kim JT, Jedrychowski MP, Wei W, Fernandez D, Fischer CR, Banik SM, et al. A plasma protein network regulates PM20D1 and n-acyl amino acid bioactivity. *Cell Chem Biol* (2020) 27(9):1130–9.e4.

112. Kazak L, Chouchani ET, Lu GZ, Jedrychowski MP, Bare CJ, Mina AI, et al. Genetic depletion of adipocyte creatine metabolism inhibits diet-induced thermogenesis and drives obesity. *Cell Metab* (2017) 26(4):660–71 e3.

113. Audrito V, Messana VG, Deaglio S. NAMPT and NAPRT: Two metabolic enzymes with key roles in inflammation. *Front Oncol* (2020) 10:358.

114. Qiang L, Wang L, Kon N, Zhao W, Lee S, Zhang Y, et al. Brown remodeling of white adipose tissue by SirT1-dependent deacetylation of ppargamma. *Cell* (2012) 150 (3):620–32.

115. DiRenzo J, Soderstrom M, Kurokawa R, Ogliastro MH, Ricote M, Ingrey S, et al. Peroxisome proliferator-activated receptors and retinoic acid receptors differentially control the interactions of retinoid X receptor heterodimers with ligands, coactivators, and corepressors. *Mol Cell Biol* (1997) 17(4):2166–76.

116. Rebello CJ, Coulter AA, Reaume AG, Cong W, Cusimano LA, Greenway FL. MLR-1023 treatment in mice and humans induces a thermogenic program, and menthol potentiates the effect. *Pharm (Basel)* (2021) 14(11).

117. Wysolmerski JJ, Stewart AF. The physiology of parathyroid hormone-related protein: an emerging role as a developmental factor. *Annu Rev Physiol* (1998) 60:431–60.

118. Larsson S, Jones HA, Goransson O, Degerman E, Holm C. Parathyroid hormone induces adipocyte lipolysis *via* PKA-mediated phosphorylation of hormone-sensitive lipase. *Cell Signal* (2016) 28(3):204–13.

119. Kovanicova Z, Kurdiova T, Balaz M, Stefanicka P, Varga L, Kulterer OC, et al. Cold exposure distinctively modulates parathyroid and thyroid hormones in cold-acclimatized and non-acclimatized humans. *Endocrinology* (2020) 161(7).

120. Mattsson CL, Csikasz RI, Chernogubova E, Yamamoto DL, Hogberg HT, Amri EZ, et al. beta(1)-adrenergic receptors increase UCP1 in human MADS brown adipocytes and rescue cold-acclimated beta(3)-adrenergic receptor-knockout mice *via* nonshivering thermogenesis. *Am J Physiol Endocrinol Metab* (2011) 301(6): E1108–18.

121. Arner P, Bernard S, Salehpour M, Possnert G, Liebl J, Steier P, et al. Dynamics of human adipose lipid turnover in health and metabolic disease. *Nature* (2011) 478 (7367):110–3.

122. Arner P, Andersson DP, Backdahl J, Dahlman I, Ryden M. Weight gain and impaired glucose metabolism in women are predicted by inefficient subcutaneous fat cell lipolysis. *Cell Metab* (2018) 28(1):45–54.e3. doi: 10.1016/j.cmet.2018.05.004

frontiers | Frontiers in Endocrinology

TYPE Original Research
PUBLISHED 02 May 2023
DOI 10.3389/fendo.2023.1176733

Check for updates

OPEN ACCESS

EDITED BY
Rubén Cereijo,
University of Barcelona, Spain

REVIEWED BY
Susanne Keipert,
Stockholm University, Sweden
Erika Monelli,
August Pi i Sunyer Biomedical Research Institute (IDIBAPS), Spain

*CORRESPONDENCE
Alexander Bartelt
alexander.bartelt@med.uni-muenchen.de

†These authors share first authorship

SPECIALTY SECTION
This article was submitted to Cellular Endocrinology, a section of the journal Frontiers in Endocrinology

RECEIVED 28 February 2023
ACCEPTED 14 April 2023
PUBLISHED 02 May 2023

CITATION
Koçberber Z, Willemsen N and Bartelt A (2023) The role of proteasome activators PA28αβ and PA200 in brown adipocyte differentiation and function. *Front. Endocrinol.* 14:1176733. doi: 10.3389/fendo.2023.1176733

COPYRIGHT
© 2023 Koçberber, Willemsen and Bartelt. This is an open-access article distributed under the terms of the Creative Commons Attribution License (CC BY). The use, distribution or reproduction in other forums is permitted, provided the original author(s) and the copyright owner(s) are credited and that the original publication in this journal is cited, in accordance with accepted academic practice. No use, distribution or reproduction is permitted which does not comply with these terms.

# The role of proteasome activators PA28αβ and PA200 in brown adipocyte differentiation and function

Zeynep Koçberber[1†], Nienke Willemsen[1†] and Alexander Bartelt[1,2,3,4*]

[1]Institute for Cardiovascular Prevention (IPEK), Ludwig-Maximilians-University Munich, Munich, Germany, [2]German Center for Cardiovascular Research, Partner Site Munich Heart Alliance, Ludwig-Maximilians-University Hospital, Munich, Germany, [3]Institute for Diabetes and Cancer (IDC), Helmholtz Center Munich, German Research Center for Environmental Health, Neuherberg, Germany, [4]Department of Molecular Metabolism and Sabri Ülker Center for Metabolic Research, Harvard T.H. Chan School of Public Health, Boston, MA, United States

**Introduction:** Brown adipocytes produce heat through non shivering thermogenesis (NST). To adapt to temperature cues, they possess a remarkably dynamic metabolism and undergo substantial cellular remodeling. The proteasome plays a central role in proteostasis and adaptive proteasome activity is required for sustained NST. Proteasome activators (PAs) are a class of proteasome regulators but the role of PAs in brown adipocytes is unknown. Here, we studied the roles of PA28α (encoded by *Psme1*) and PA200 (encoded by *Psme4*) in brown adipocyte differentiation and function.

**Methods:** We measured gene expression in mouse brown adipose tissue. In cultured brown adipocytes, we silenced *Psme1* and/or *Psme4* expression through siRNA transfection. We then assessed impact on the ubiquitin proteasome system, brown adipocyte differentiation and function.

**Results:** We found that *Psme1* and *Psme4* are expressed in brown adipocytes in vivo and in vitro. Through silencing of Psme1 and/or Psme4 expression in cultured brown adipocytes, we found that loss of PAs did not impair proteasome assembly or activity, and that PAs were not required for proteostasis in this model. Loss of *Psme1* and/or *Psme4* did not impair brown adipocyte development or activation, suggesting that PAs are neither required for brown adipogenesis nor NST.

**Discussion:** In summary, we found no role for *Psme1* and *Psme4* in brown adipocyte proteostasis, differentiation, or function. These findings contribute to our basic understanding of proteasome biology and the roles of proteasome activators in brown adipocytes.

KEYWORDS

**BAT, brown adipocytes, proteostasis, ubiquitin-proteasome-system, PA28αβ, *PA200*, *Psme1*, *Psme4***

# 1 Introduction

Thermogenic adipocytes produce heat through non-shivering thermogenesis (NST). Mammals - especially infants, small rodents, and hibernating animals - rely on NST for appropriate thermoregulation as it complements or substitutes shivering- or muscle-generated thermogenesis (1). The main class of thermogenic adipocytes are brown adipocytes, collectively forming brown adipose tissue (BAT) depots. Additionally, beige adipocytes with similar thermogenic capacity to brown adipocytes reside in white adipose tissue (WAT) (2, 3). The common denominator of these thermogenic adipocytes is their (potential) expression of Uncoupling-protein 1 (*Ucp1*), a fatty acid-activated proton carrier that uncouples the electron transport chain from ATP production, which is an exothermic reaction resulting in heat generation (1, 3). Alternatively to Ucp1-mediated uncoupling, futile cycling of creatine, calcium, and fatty acids also lead to heat production in thermogenic adipocytes (4). In response to cold, the central nervous system initiates the release of norepinephrine (NE), which, through β-adrenergic receptors, acutely leads to lipolysis and Ucp1 activation. Over the years, several other thermogenic mediators have been identified to promote adipose tissue browning and NST (5–7). To fuel NST, BAT consumes large amounts of triglycerides and glucose (8, 9), which is associated with a beneficial metabolic profile in mice and humans (8–11). In addition to acute activation, prolonged stimulation of NST results in BAT hyperplasia, mitochondrial biogenesis, as well as the emergence of beige adipocytes within certain white adipose depots (1, 9). This cellular remodeling of oxidative capacity and lipid metabolism is regulated by a complex network of proteostasis mechanisms, including autophagy and the ubiquitin-proteasome system (UPS) (12–17). BAT activation and tissue remodeling are energy and resource costly processes (1, 8), which is probably why thermogenic adipocytes have developed a remarkably dynamic metabolism, allowing them to shift between dormant and active metabolic state depending on the environmental temperature, diet, and hormonal status.

Protein degradation is a major pillar in maintaining proteostasis and metabolism, and appropriate protein turnover is essential for maintaining healthy thermogenic adipocytes (12–14, 17). The proteasome is important both for quality control of misshapen or damaged proteins as well as for determining the lifespan of proteins, and is, therefore, a key player in shaping the cellular proteome in response to nutritional and other environmental changes (18). The proteasome is a multi-meric complex composed of a 28-unit particle (20S, also called CP), which has a 'barrel-shaped' structure with a catalytic core, to which one or two regulatory particles can dock (19). The most common regulatory particle is the 19S particle (also called RP or PA700), which regulates substrate delivery to the 20S in an ubiquitin- and ATP-dependent manner (19, 20). 20S associated with one or two 19S make up the constitutive 26S and 30S proteasome structures, respectively. The abundance of these complexes is partially under the transcriptional control of Nuclear factor erythroid 2-related factor-1 (Nfe2l1, also known as Nrf1 or TCF11) (21). 26S proteasome activity upheld and adapted by the transcriptional activity of Nfe2l1 is required for matching proteasomal activity to the levels of ubiquitinated proteins generated by thermogenic adipocytes during cold and sustained NST (13). In addition to this transcriptional regulation, there are also posttranslational mechanisms regulating proteasome activity. A class of regulatory proteins called proteasome activators (PAs) bind to 20S particles, giving rise to a variety of alternative proteasome complexes, whose functions are less well understood (22, 23). The two cytosolic PAs are PA28αβ (also known as PA28, REG or 11S), and PA200 (also known as Blm10 in yeast). PA28αβ is a heptameric PA composed of four PA28α (encoded by *Psme1*) and three PA28β (encoded by *Psme2*) units (24), and are associated with the immune response and oxidative stress (23, 25, 26). PA200 (encoded by *Psme4*) is a large monomer (circa 200 kDa) that is implicated in the regulation of proteasome activity in the context of DNA repair (23, 27–29). In previous work, we showed that Psme1 expression induces proteasome activity in mice (13). However, the function and importance of PAs for proteasome function and proteostasis in brown adipocyte is currently unknown. As the adaptive regulation of 26S proteasome activity is an essential part of NST and BAT function, we hypothesized that 20S-PAs structures play a role in this process. Here, we systematically investigate the roles of PA28αβ and PA200 in brown adipocytes by manipulating *Psme1* and *Psme4* expression *in vitro*.

**Abbreviations:** BAT, Brown adipose tissue; DMSO, Dimethyl sulfoxide; FCCP, Carbonyl cyanide p trifluoro methoxyphenyl hydrazone; NE, Norepinephrine; Nfe2l1, Nuclear factor erythroid 2 related factor 1; NST, Non shivering thermogenesis; Omy, Oligomycin; ORO, Oil Red O; PA, Proteasome activator; Psm, Proteasome subunit; Psme1-4, Proteasome activator complex subunit 1 4; Rot/AA, Rotenone/Antimycin A; Ucp1, Uncoupling protein 1; UPS, Ubiquitin proteasome system.

# 2 Material and methods

## 2.1 Mice husbandry and tissue collection

All animal experiments were performed with approval of the local authorities (License: ROB-55.2-22532.Vet_02-30-32). Mice were housed in individually ventilated cages at room temperature, with a 12-hour light/dark cycle, and fed chow diet (Sniff) and water ad libitum. For cold exposure, 12-week-old male C57BL/6J mice (purchased from Janvier) were exposed to 4 °C for seven days in a Memmert Climate Chamber HPP750 Life. For tissue collection, the afore-mentioned cold exposed mice and 16-week-old male mice with a C57BL/6J background were injected with a lethal dose of xylazine/ketamine (8/120 mg/kg mouse body weight). For primary cell collection, 6-week-old male C57BL/6J (Janvier) were killed by cervical dislocation. Interscapular and supraclavicular BAT was collected from the animals and freshly used for primary cell isolation.

## 2.2 Primary cell collection and culture

For primary cell culture, the collected BAT was first minced and then digested in DMEM/F-12 (Sigma-Aldrich, supplemented with

1.2 U/mL Dispase (Roche), 1 mg/mL collagenase type 2 (Worthington), 15 mg/mL fatty acid free BSA (Sigma-Aldrich), and 0.1 mg/mL DNase 1 (Roche)) at 37 °C, on a shaker, for 30 minutes. The digestion was stopped by supplementing fetal bovine serum (FBS, Sigma-Aldrich). The suspension was filtered first through a 100 µM filter and then through a 30 µM filter. The stromal vascular fraction (SVF) was plated and cultured in DMEM/F-12 (supplemented with 10% v/v FBS and 1% v/v penicillin/streptomycin (Thermo Fisher Scientific)). The cells were incubated at 37 °C, 5% $CO_2$. After reaching confluency, the pre-adipocytes were differentiated into mature brown adipocytes. From day 0 (confluence) to day 2, the cells received DMEM/F-12 supplemented with 1 µM dexamethasone (Sigma-Aldrich), 340 nM insulin (Sigma-Aldrich), 500 µM isobutylmethylxanthine (Sigma-Aldrich), 2 nM triiodothyronine (Sigma-Aldrich), and 1 µM rosiglitazone (Cayman). From day 2 until day 6, the cell received DMEM/F-12 supplemented with 10 nM insulin, 2 nM triiodothyronine, and 1 uM rosiglitazone. The medium was refreshed every other day.

## 2.3 Immortalized cell culture and treatment

The immortalized WT-1 mouse brown preadipocyte cell-line (kindly provided by Brice Emmanueli, University of Copenhagen) was grown in DMEM Glutamax (Thermo Fisher, supplemented with 10% v/v FBS and 1% v/v penicillin/streptomycin). After the pre-adipocytes reached confluency (day 0), their differentiation was induced with induction medium (DMEM Glutamax, supplemented with 860 nM insulin, 1 µM dexamethasone, 1 µM triiodothyronine, 1 µM rosiglitazone, 500 µM 3-isobutyl-1-methylxanthine, and 125 µM indomethacin (Sigma-Aldrich). After 48 hours, the induction medium was changed to differentiation medium (DMEM Glutamax, 1 µM triiodothyronine, 1 µM rosiglitazone). The differentiation medium was refreshed every other day. Cells were fully differentiated after 5-6 days. For target gene RNA inhibition (RNAi), cells received 30 nM SMARTpool silencing RNA (siRNA, Dharmacon) through reverse transfection with Lipofectamine RNAiMAX transfection reagent (Thermo Fisher) according to manufacturer's protocol. Transfection took place one day before induction (day -1). Cell treatments took place on day 5 of differentiation. Cells were treated with 100 nM Bortezomib (Sellect) for 6 or 24 hours, or 1 µM CL-316,143 (Tocris) for 3 hours, or dimethyl sulfoxide (DMSO) as control. Cells were harvested as pre-adipocytes (day 0), early brown adipocytes (day 3) or mature brown adipocytes (day 5-6). Unless mentioned otherwise, assays were performed on mature (day 5) adipocytes.

## 2.4 Gene expression analysis

RNA was extracted from tissues or cells with NucleoSpin RNA kit (Machery Nagel) according to the manufacturer's instructions, and RNA concentration was determined with NanoDrop (Thermo Fisher). RNA was synthesized into complementary DNA (cDNA) with Maxima H Master Mix (Thermo Fisher) according to the manufacturer's instructions. To measure gene expression, we combined 10 µg cDNA and 0.5 µM DNA primers with 5 µL PowerUp SYBR Green Master Mix (Applied Biosystems). To establish gene expression, the cycles thresholds (Ct) were calculated in Quant-Studio 5 RealTime PCR system (Thermo Fisher, standard conditions: 2 min on 50°C, 10 min on 95°C, 40 cycles of 15 s on 95°C, and 1 min on 60°C). Normalized virtual copy numbers were was calculated by normalizing the Cts of experimental genes to the Cts of the housekeeper gene *TATA-box binding protein* (*Tbp*) (Δ Ct). Relative gene expression was calculated by normalizing delta Ct of the experimental groups to the control groups (ΔΔ Ct). The primer sequences are listed in Supplementary Table 1.

## 2.5 Protein isolation and analysis

The samples were collected in RIPA buffer (50 mM Tris (Merck, pH = 8), 150 mM NaCl (Merck), 0.1% w/v SDS (Carl Roth), 5 mM EDTA (Merck), and 0.5% w/v sodium-deoxycholate (Sigma–Aldrich)) freshly supplemented with a protease inhibitor (Sigma-Aldrich). Samples were lysed in a tissue lyser and then cells were centrifuged twice and tissue lysates were centrifuged three times for 30 min (4°C, 21,000 *g*), to remove lipids and debris. Protein concentrations were determined with Pierce BCA assay (Thermo Fisher). Per sample, 15-30 µg proteins were denatured with 5% v/v 2-mercaptoethanol (Sigma-Aldrich) for 5 min at 95 °C. The denatured samples were loaded in a Bolt 4-12% Bis-Tris gel (Thermo Fisher). After separation, proteins were transferred onto a 0.2 µm PVDF membrane (Bio-Rad) using the Trans-Blot Turbo™ system (Bio-Rad, 25 V, 1.3 A for 7 min). The membrane was blocked in Roti-Block (Roth) for one hour at room temperature. The membranes were incubated overnight in primary antibody dilutions (1:1000 in Roti-block) at 4 °C. The following primary antibodies were used: β-tubulin (Cell Signaling, 2146), Psmb4 (Santa Cruz, sc-390878), Psmd2 (Santa-Cruz, A-11), Psme1 (Abcam, ab3333), Psme4 (Thermo Fisher, PA1-1961), Nfe2l1 (Cell Signaling, 8052), Ubiquitin/P4D1 (Cell Signaling, 3936), Ucp1 (Abcam, ab10983), Hsp90 (Cell Signaling, 4877), and Proteasome 20S alpha 1 + 2 + 3+5 + 6+7 (Abcam, ab22674). The next day, the membrane was washed with TBS-T (200 mM Tris (Merck), 1.36 mM NaCl (Merck), 0.1% v/v Tween 20 (Sigma)), and incubated in secondary antibody (Santa Cruz) (1:10,000 in Roti-block) for 1h at room-temperature. The membranes were developed with SuperSignal West Pico PLUS Chemiluminescent Substrate (Thermo Fisher) in a Chemidoc MP imager (Bio-Rad). Full-size blot images are displayed in Supplementary Figure 2.

## 2.6 Native PAGE: in-gel activity assay and immunoblot

The protocol for Native PAGE in-gel proteasome activity assay and subsequent immunoblotting was previously described in detail (15). Briefly, samples were lysed in OK-lysis buffer (50 mM Tris/HCl, pH = 7.5, 2 mM dithiothreitol, 5 mM $MgCl_2$ 10% v/v glycerol, 2 mM

ATP, 0.05% v/v Digitonin (Thermo Fisher)), kept on ice for 20 minutes, and centrifuged thrice. 15 µg protein, determined with Bio-RAD Protein Assay Kit II, was loaded in a NuPAGE 3-8% Tris-Acetate gel (Thermo Fisher). The gel was run at a constant voltage of 150 V for four hours. The gel was then incubated in a reaction buffer (50 mM Tris, 1 mM $MgCl_2$, 1 mM dithiothreitol) for 30 minutes at 37 °C. The fluorescence signal was measured in ChemiDoc MP. Next, the gel was prepared for protein transfer by 15 minutes incubation in a solubilization buffer (2% w/v SDS, 66 mM $Na_2CO_3$, 1.5% v/v 2-mercaptoethanol. The proteins were transferred to a PVDF membrane by 'wet' tank transfer (40 mA, overnight). The immunoblot was further treated as described above (see **2.5**). Full size blot images can be found in Supplementary Figure 2.

## 2.7 Viability assay

AquaBlueR (MultiTarget Pharmaceuticals) was used to assess cell viability. Cells were incubated in 1:100 AquaBlueR for four hours at 37 °C. Fluorescence was measured at 540/590 nm (excitation/emission) in a Spark 20M Plate reader (Tecan).

## 2.8 Lysate proteasome activity

Cells were lysed in lysis buffer (40 mM Tris (Merck, pH = 7.2), 50 nM NaCl (Merck), 5 mM $MgCl_2(6H_2O)$ (Merck), 10% v/v glycerol (Sigma), 2 mM ATP (Sigma), 2 mM 2-mercaptoethanol (Sigma)). Proteasome Activity Fluorometric Assay II Kit (UBPBio, J41110) was used according to the manufacturer's instructions to measure trypsin-like (T-L), chymotrypsin-like (CT-L), and caspase-like (C-L) proteasome activity. The fluorescent signaling was measured in the plate reader and the results were normalized to DNA with the Quant-iT PicoGreen dsDNA assay kit (Invitrogen, p7589), according to manufacturer's instructions.

## 2.9 Oil-Red-O (ORO) staining

ORO staining was used to measure lipid content. Cells were washed with cold DPBS (Gibco), fixed in zinc formalin solution (Merck) for 15 minutes at room-temperature and again washed with 2-propanol (Merck). The cells were dried, incubated in 60% v/v ORO (Sigma) for 10 minutes at room-temperature followed by washing with water for 3-4 times. A picture of the plate was taken to visualize the lipid content. To measure absorption, ORO was eluted in 100% 2-propanol, and measured in the plate reader.

## 2.10 Free fatty acid release assay

To measure lipolysis in cell culture supernatants, Free Glycerol Reagent (Sigma F6428) and Glycerol standard solution (Sigma G7793) were used. Cell culture medium was collected to measure free glycerol content and the experiment was performed according to the manufacturer's instructions.

## 2.11 Extracellular flux analysis (seahorse)

Oxygen consumption rate (OCR) was measured in a Seahorse XFe24 Analyzer (Agilent) and the assays performed as previously described (30). Briefly, we performed a Seahorse Cell Mito Stress Test (Agilent) largely according to manufacturer's instructions, but with the addition of a NE (1 µM) injection. There was no addition of BSA to the medium at any point. Two days before the assay, 20,000 adipocytes were seeded per well. During the assay, cells were consecutively treated with NE, oligomycin (1 µM), FCCP (4 µM), and Rotenone/Antimycin A (both 0.5 µM). Oxygen consumption was measured in intervals of 3 minutes. The results were normalized to total DNA levels which were measured with CyQuant Cell Proliferation Assay (C7026, Invitrogen) according to manufacturer's instructions. NE-induced respiration was calculated by subtracting maximum baseline OCR from maximum NE-induced OCR. Coupled respiration is baseline OCR minus OCR after oligomycin. Uncoupled respiration is OCR after oligomycin minus OCR after Rot/AA injection. Maximum respiration was calculated by subtracting minimum OCR, measured after Rot/AA injection, from maximum OCR, measured after FCCP injection.

## 2.12 Data analysis and visualization

All data was analyzed with Excel and GraphPad Prism. The raw data from the Seahorse was analyzed with Wave software (Agilent). Immunoblots were quantified with ImageLab (Bio-Rad). Data was visualized in GraphPad Prism. If not otherwise specified, data is represented as mean ± standard error of the mean (SEM). (Multiple) Student's t-test (with Bonferroni post-hoc test) was used to compare two groups with one variable. One-way ANOVA with Tukey post-hoc test was used to compare three groups with one variable. Two-ANOVA with Tukey post-hoc test was used to compare four groups with two different variables, i.e. for the double siRNA transfection experiments. Three-way ANOVA with Dunett's post-hoc test was used to compare more than four groups with more than two different variables, i.e. for the double siRNA transfection plus treatment experiments. P-values lower than 0.05 were considered significant. If groups are significantly different from each other, this is indicated in graphs either with an asterisk (*) or with different letters (a, b). If the same letter is used or if nothing is indicated, the groups are statistically indifferent from each other. The graphics were made in Biorender.com.

# 3 Results

## 3.1 Proteasome activators are expressed in brown adipocytes

The remodeling of the constitutive proteasome is an essential component of brown adipocyte adaptation to sustained activation (13), but PAs are not part of the 26S/30S constitutive proteasome. Instead, they form hybrid shapes with the 20S core particle (22). It is

10.3389/fendo.2023.1176733

unknown if PS are expressed in brown adipocytes, if proteasome hybrids are present in and if so, what their roles are in brown adipocyte biology. Therefore, we first assessed the levels of PAs in BAT ex vivo and found that both *Psme1* and *Psme4* were abundantly expressed in the tissue (Figure 1A). Next, we measured *Psme1* and *Psme4* gene expression before and after brown adipocyte differentiation in primary cells obtained from the interscapular brown adipose tissue derived stromal fraction (SVF). Both genes were expressed in pre-adipocytes and mature brown adipocytes (Figure 1B). Following this, we determined if these genes were differentially expressed during states of BAT inactivity and BAT induction. Mice were exposed to either thermoneutrality (30°C) or to cold (4°C) for one week. Thermoneutrality initiates BAT whitening and cold activates NST and promotes tissue browning. While *Psme1* and *Psme4* were expressed under both conditions, *Psme4* expression was highest in cold-exposed mice (Figure 1C). For the remainder of the experiments in this manuscript, we used an immortalized mouse brown pre-adipocyte cell line (Simplified model in Figure 1D). These pre-adipocytes differentiate into mature brown adipocytes within six days. After three days of induction, there was a marked increase in expression of the adipogenesis markers *Adipoq*, *Cebpa*,

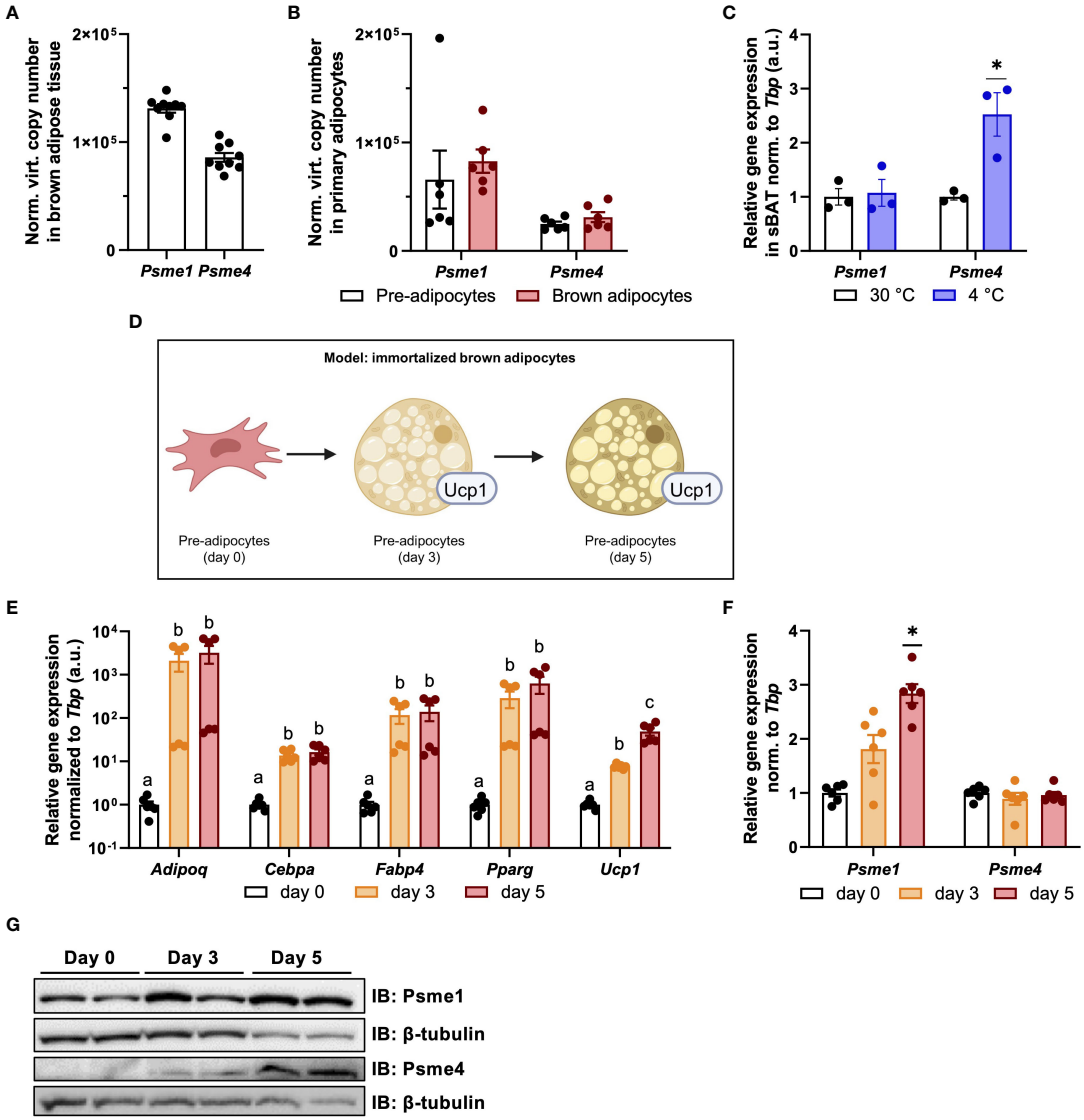


FIGURE 1
Psme1 and Psme4 expression in brown fat and brown adipocytes. **(A, B)** Normalized gene expression of *Psme1* and *Psme4* in **(A)** brown adipose tissue (BAT) (n = 9 biological replicates), and **(B)** primary brown pre-adipocytes and mature adipocytes (n = 6 biological replicates). **(C)** Relative gene expression of Psme1/Psme4 in BAT after cold exposure (1 week at 4 °C) (n = 3 biological replicates). **(D)** Summary of experimental model made in Biorender.com. **(E)** Relative gene expression of *Adipoq, Cebpa, Fabp4, Pparg* and *Ucp1* in immortalized brown adipocytes in different stages of development: pre-adipocytes (day 0), early adipocytes (day 3), and mature adipocytes (day 5). (n = 6 measurements pooled from two independent experiments). **(F)** Relative gene expression of *Psme1* and *Psme4* in immortalized brown adipocytes in different stages of development: pre-adipocytes (day-0), early adipocytes (day 3), and mature adipocytes (day 5). (n = 6 measurements pooled from two independent experiments). **(G)** Representative immunoblots showing Psme1, Psme4 and β-tubulin. Data are represented as mean ± SEM. Data are significant if $P < 0.05$, which is indicated with an asterisk (*) or by different letters (a, b).

*Fabp4*, and *Pparg*, as well as brown adipocyte marker *Ucp1* (Figure 1E). In these cells, we measured both gene expression and protein levels of Psme1 and Psme4 during different stages of cell differentiation. We found increased gene expression of *Psme1* and increased protein level of Psme1 during differentiation (Figures 1F, G). In contrast, *Psme4* expression did not change during differentiation, but protein Psme4 was only detectable in early and mature brown adipocytes, and not in pre-adipocytes. (Figures 1F, G). In summary, Psme1 and Psme4 are constitutively expressed in both pre-adipocytes and brown adipocytes, and Psme1 expression is induced during differentiation whilst Psme4 expression is induced with cold-induced activation *in vivo*.

## 3.2 The effect of loss of PAs on viability, stress, and inflammation

As the PAs Psme1 and Psme4 were present and regulated in brown adipocytes, we hypothesized that they could play a role in brown adipocyte function. In order to study their roles, we silenced *Psme1* and *Psme4* gene expression in brown adipocytes. We transfected cells before differentiation (day -1) with either *Psme1* siRNA, *Psme4* siRNA, or the combination of both. The knockdown successfully led to lower levels of gene expression and kept gene expression low even after differentiation (Figure 2A). This translated into an almost complete ablation of protein levels for both PAs (Figure 2B). First, we checked if silencing of PAs resulted in any impaired cell viability and found no effects of *Psme1* and/or *Psme4* gene silencing (Figure 2C). Additionally, we treated the cells with the chemical proteasome inhibitor bortezomib to measure bortezomib-induced cell death, as impairment of the proteasome or its regulation sensitizes cells to treatment with proteasome inhibitors (21, 31). However, loss of Psme1 or Psme4 did not amplify bortezomib-induced cell death (Figure 2D). Finally, loss of PAs did not alter gene expression of *Ccl2*, a surrogate marker of adipocyte inflammation, nor that of *Atf3, Xbp1s, Herpud2*, or *Hspa5*, all surrogate markers of protein folding stress (Figure 2E) or in the transcription levels of the apoptosis marker *Ddit3*

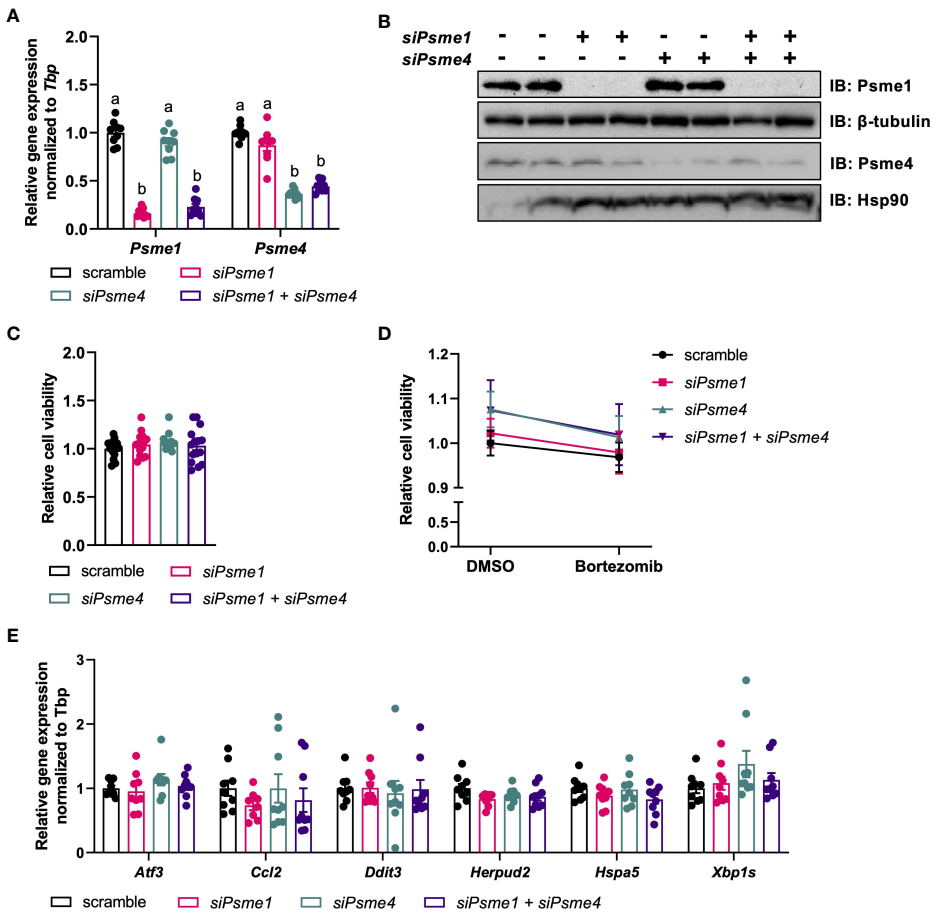


FIGURE 2
Silencing of Psme1 and/or Psme4 had no effect on viability. **(A)** Relative gene expression of *Psme1* and *Psme4* after transfection with si*Psme1* and/or si*Psme4*. **(B)** Representative immunoblots showing Psme1, Psme4, β-tubulin and Hsp90. **(C)** Relative cell viability after transfection measured with AquaBlueR (n = 15 measurements pooled from three independent experiments). **(D)** Relative survival after treatment with DMSO or Bortezomib (100 nM for 16 h) measured with AquaBlueR. (Mean of n = 15 measurements pooled from three independent experiments). **(E)** Relative gene expression of inflammation and stress markers. Genes measured are *Atf3*, *Ccl2*, *Ddit3*, *Herpud2*, *Hspa5*, *Xbp1s*. Graphs show. Unless indicated otherwise, n = 9 measurements pooled from three independent experiments. Data are represented as mean ± SEM. Data are significant if $P < 0.05$, which is indicated with an asterisk (*) or by different letters (a, b).

(Figure 2E). Overall, loss of Psme1 and or Psme4 did neither cause or enhance bortezomib-induced cell death nor provoke an overt stress response in the cells.

## 3.3 Loss of PAs does not impair UPS in brown adipocytes

PAs bind to 20S core particles, forming hybrid proteasomes, and, thus, PAs are implicated in regulating proteasome activity and substrate selection. To determine if manipulation of PAs impacts brown adipocyte proteostasis, we checked if *Psme1* and/or *Psme4* knockdown affected gene expression of proteasome transcription factor *Nfe2l1* or other proteasome subunits. We measured expression of several proteasome subunits to cover the different parts of the proteasome: *Psma3* and *Psmb6* as representative units of the 20S, *Psmd2* as part of the 19S regulatory particle, *Psme2* as part of the PA28αβ complex, and *Psme3* for the nuclear PA28γ. We found no differences in any of these tested transcripts (Figure 3A). Correspondingly, we found no changes in protein levels of the seven α-subunits, ranging from Psma1 to Psma7, and of Psmb4 comparing controls cells and cells with *Psme1* and/or *Psme4* knockdown (Figure 3B). Additionally, both baseline and bortezomib-induced Nfe2l1 protein levels were unchanged, and both full-length and short-length forms were present in the brown adipocytes (Figure 3C). Global ubiquitin levels, as a marker for proteostatic stress and modulation of UPS, were similar between control and experimental groups (Figure 3B). To directly measure proteasome activity, we used two distinct methods. For the first approach, we measured trypsin-like, chymotrypsin-like, and caspase-like activity in whole-cell lysates after gene knockdown (Figure 3D). For the second approach, we loaded non-denatured proteins in a Native PAGE. This allowed us to visualize the 20S, 26S and 30S proteasome with in-gel proteasome activity and then subsequently quantify protein levels by immunoblotting. In line with the unchanged ubiquitin levels, we also found no impairment in proteasome activity, neither in in-gel chymotrypsin-like activity nor in α1-α7 protein levels (Figure 3E). We also investigated if stressing proteostasis with proteasome inhibitor bortezomib under knock-down conditions would result in altered respiration. While

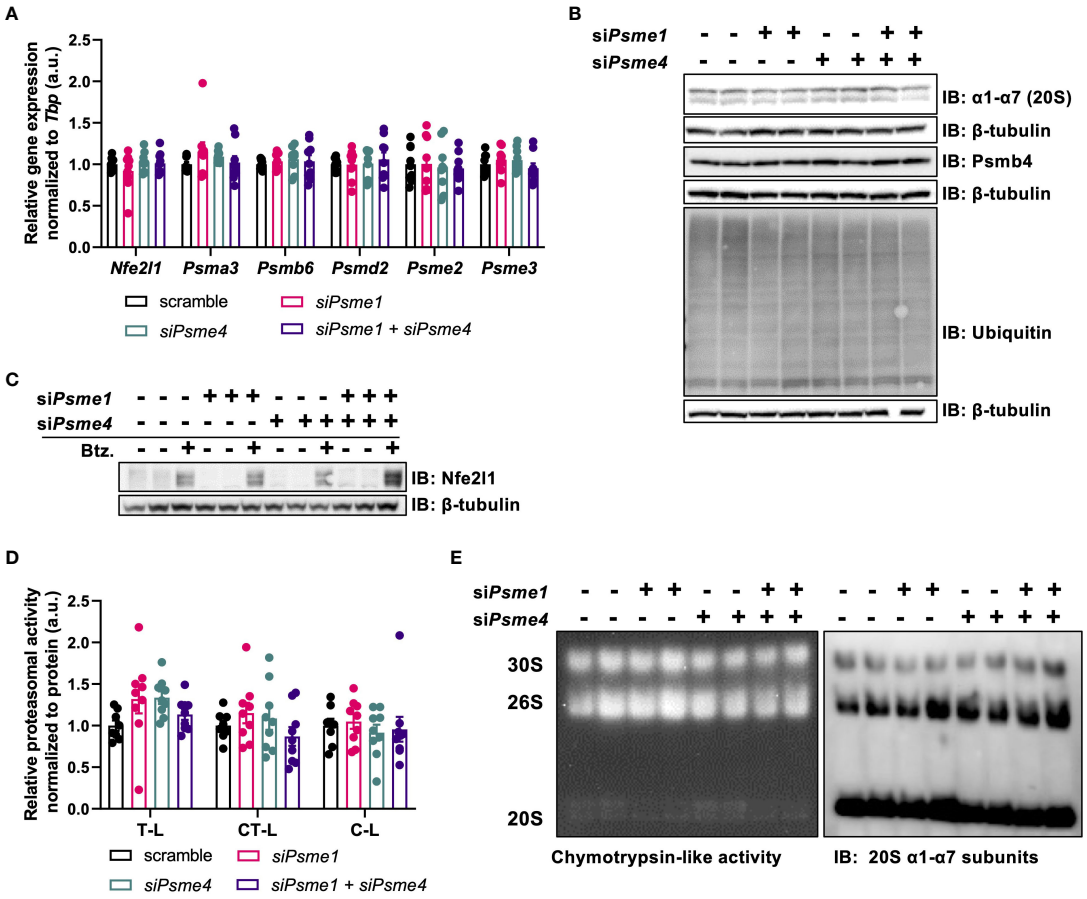


FIGURE 3
The effects of Psme1/Psme4 knockdown on proteasome activity. **(A)** Relative gene expression of *Nfe2l1* and proteasome subunits *Psma3*, *Psmb6*, *Psmd2*, *Psme2*, and *Psme3*, in brown adipocytes after transfection with si*Psme1* and/or si*Psme4*. **(B)** Representative immunoblots with protein levels of Psmb4, α1-α7, ubiquitin and β-tubulin. **(C)** Representative immunoblots with protein levels of Nfe2l1 and β-tubulin after treating cells with DMSO or Bortezomib (100 nM, 6 h). **(D)** Proteasome activity of chymotrypsin-like (CT-L), trypsin-like (T-L) and caspase-like (C-L) activity. **(E)** Representative native PAGE with in-gel CT-L-activity and immunoblot with α1-α7 (20S) staining. Unless indicated otherwise, n = 9 measurements pooled from three independent experiments. Data are represented as mean ± SEM. Data are significant if $P < 0.05$, which is indicated with an asterisk (*).

bortezomib treatment impaired mitochondrial respiration, this effect was not affected by silencing of Psme1 or Psme4 (Supplementary Figures 1A, B). Overall, this set of experiments demonstrated that Psme1 and Psme4 are dispensable for proteasome availability and function in brown adipocytes.

## 3.4 Loss of PAs does not affect adipogenesis or brown adipocyte function

Finally, to determine the effect of PAs on brown adipocyte-specific biology, we studied the effects of loss of PAs on brown adipocyte development and function. *Psme1* and/or *Psme4* knockdown did not affect expression of the adipocyte markers *Adipoq*, *Cebpa, Fabp4*, and *Pparg* (Figure 4A). However, there was a non-significant trend for lower *Ucp1* mRNA expression in cells with si*Psme4* (Figure 4A). Next, lipid content was measured as an indicator for net adipogenesis and lipogenesis. ORO staining showed that lipid content was not lower in the knock-down groups compared to the control groups (Figures 4B, C). As brown adipocytes induce lipolysis to fuel heat production (3), we measured cell culture supernatant glycerol levels before and after stimulation with the β3-adrenergic agonist CL-316,243. The glycerol release assay showed no effects upon loss of Psme1 and/or Psme4 (Figure 4D). Finally, we measured oxygen consumption rate (OCR) to measure sympathetic response and global cellular respiration. NE-induced respiration was used to measure cellular NST-capacity *in vitro*. NE-induced respiration was not different between groups, nor was maximum respiratory capacity, suggesting that there were no significant changes in mitochondrial abundance and health (Figures 4E, F). Even stressing the system with Bortezomib treatment did not differentially affect knock-down groups compared to the control group (Supplementary Figure 1A, B). Taking these results together, we found no evidence that loss of PAs impaired adipocyte function.

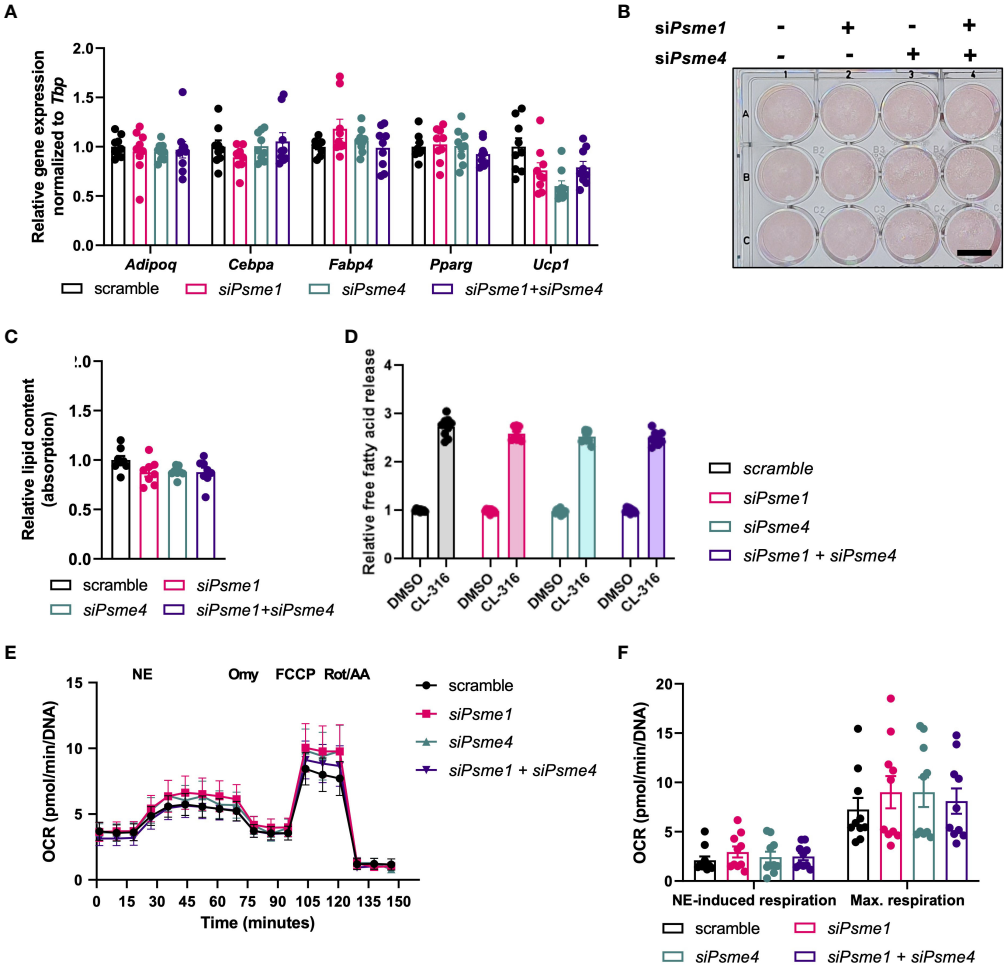


FIGURE 4
Loss of Psme1/Psme4 did not impair adipocyte function. **(A)** Relative gene expression of adipocyte markers in brown adipocytes after transfection with si*Psme1* and/or si*Psme4*. Genes: measured: *Adipoq, Cebpa, Fabp4, Pparg* and *Ucp1*. **(B)** Representative Oil-Red-O staining and **(C)** relative lipid content measured as absorption. Scale bar in image equals 1 cm. **(D)** Relative free fatty acid levels in medium after cell treatment with DMSO or CL-316,243 (CL-316) (1 µM, 3 hours). **(E, F)** Oxygen consumption rate (OCR) during NE treatment and mitochondrial stress test, normalized to DNA levels (n = 8 measurements pooled from two independent experiments). NE: norepinephrine, Omy: oligomycin, FCCP: carbony cyanide p-trifluoro-methoxyphenyl hydrazone, Rot/AA: rotenone/antimycin A Unless indicated otherwise, n = 9 measurements pooled from three independent experiments. Data are represented as mean ± SEM. Data are significant if $P < 0.05$, which is indicated with an asterisk (*).

# 4 Discussion

Brown adipocytes undergo cellular remodeling during thermogenic activation (1), and in order to sustain NST, an appropriate protein turnover is required (14). Although the role of the constitutive 26S proteasome in BAT and NST has been studied previously (13), the role of other proteasome types remains elusive. In this study, we investigated the roles of Psme1/PA28α and Psme4/PA200 in brown adipocyte differentiation and function. We found that *Psme1* and *Psme4* were constitutively expressed in brown pre-adipocytes and mature adipocytes, which alludes to a significant role in brown adipocyte proteostasis. However, in our model of cultured adipocytes, loss of Psme1 and/or Psme4 protein by RNAi did not affect viability or led to a marked stress response in the cells. Moreover, even though we saw minor effects on proteasome activity, UPS and proteostasis remained functional. Finally, neither differentiation nor activation of brown adipocytes was impaired after silencing of *Psme1* and/or *Psme4*. We conclude that in our experimental settings, Psme1 and Psme4 are dispensable for cultured brown adipocytes.

There are limitations to our model and approach that should be noted. Firstly, the experiments were performed in an immortalized brown adipocyte cell line, which cannot mimic the biological complexity and natural regulation of BAT activation or remodeling observed *in vivo* in mice or humans. An adipocyte-specific transgenic deletion mouse model could provide insight into the physiological roles of PAs, but these models have not yet been established. This cell model allowed for basic study of the role of PAs in adipocytes, but did not characterize PAs under different physiological conditions, e.g. nutrient deprivation, inflammation, nor did it take into account cell-cell interactions or systemic effects. Secondly, we limited our study to Psme1 and Psme4, leaving the other proteasome activators subunits Psme2 and Psme3 out of the scope of this study. Admittedly, as PA28αβ consists of Psme1 and Psme2 subunits, it is possible that sole loss of Psme1 would result in an alternative PA28 form with residual activity. However, this PA-variant is thought to be less stable and active, and it is unknown if there is a physiological relevance (24). Furthermore, there could also be compensation mechanism through Psme3 activation, but as Psme3 is a nuclear PA instead of cytosolic, we estimated this chance as low (22). Finally, we used siRNA to knockdown gene expression and this method does not completely ablate protein levels. Even though we observed marked near to complete loss of protein for both Psme1 and Psme4, it is possible that a remaining low expression of *Psme1*/*Psme4* was sufficient to sustain a residual activity. However, we have previously shown that the same experimental strategy resulted in efficient ablation of 20S subunit Psmb4, which disrupted proteostasis, adipocyte differentiation, and thermogenesis (30). In addition, a separate study showed that siRNA-mediated manipulation of Psme4 affected myofibroblast differentiation (32). This indicates that the experimental RNAi strategy is capable of targeting both constitute and adaptive proteasome subunits and investigate their role for brown adipocyte differentiation and activity.

Regardless, the roles of Psme1 and Psme4 in regulating proteasome function and protein degradation are not well-established. Based on their structures, both PA28αβ and PA200 are thought to stimulate the insertion of unfolded proteins or peptides into the 20S proteasomes (22, 23). Also, PA28αβ is associated with the immunoproteasome, a specific type of proteasome that specifically degrades proteins for antigen-presentation (25, 26). However, mice lacking Psme1/Psme2 display no growth abnormalities or obvious health problems (33). In a study with triple-knockout mice, ablation of Psme1, Psme2 and nuclear Psme3/PA28γ (gene: *Psme3*), the researchers found reduced proteasome activity and exacerbated high-fat diet-induced hepatic dysfunction (34), even though the cause of this metabolic phenotype remains unclear. Also, the function of Psme4 is still being debated, but it is associated with the process of DNA repair (27, 28) and was shown to play a role in myofibroblast differentiation (32). Whole-body Psme4 knock-out did not result in an overt phenotype, but showed impaired spermatogenesis and infertility (35, 36). These studies with whole-body knock-out mouse models did not investigate or report any BAT or NST phenotype (32–36), leaving it as an open question if they participate in adipocyte biology *in vivo*. Although we found that Psme1 and Psme4 were not required in brown adipocytes *in vitro* under standard conditions, they may play a role in specific cellular stress responses. Based on its implication of immunoproteasome regulation, Psme1 may play a role in the immune response of the adipocyte, but the role of immunoproteasome formation in adipocytes is unknown, too. Alternatively, Psme1 and or Psme4 could be recruited in response to specific stressors, for example in the adaptive proteasome response against oxidative stress, proteasome autophagy or ferroptosis (37). Interestingly, it was observed that overexpression of Psme1 enhances proteasome activity in obese mouse models when proteasome function was compromised (13). Further scrutiny of the PAs in different contexts will contribute to our understanding of their functions and mechanisms and should determine if and how PAs play a role in adipocytes *in vivo*. In conclusion, our data reveal that, even though expressed high robust levels, Psme1 and Psme4 are dispensable for proteostasis, adipogenesis, and thermogenesis in cultured brown adipocytes.

# Data availability statement

The raw data supporting the conclusions of this article will be made available by the authors, without undue reservation.

# Ethics statement

The animal study was reviewed and approved by Regierung von Oberbayern (ROB) 55.2 22532.Vet_02 30 32.

# Author contributions

AB and NW designed and supervised the study. ZK and NW performed the experiments, analyzed the data, and prepared the figures. AB supervised the study and analyzed the data. The authors wrote the manuscript together. All authors contributed to the article and approved the submitted version.

## Funding

ZK was supported by a DAAD scholarship. AB was funded by the Deutsche Forschungsgemeinschaft Sonderforschungsbereich 1123 (B10) and SPP2306 on ferroptosis, the Deutsches Zentrum für Herz-Kreislauf-Forschung Junior Research Group Grant, and the European Research Council Starting Grant PROTEOFIT.

## Acknowledgments

The authors would like to thank the members of the Bartelt Lab for their support and feedback on the project, Imke Lemmer for assisting with the mouse cold exposure experiment, Henrika Jodeleit for setting up the animal license, Brice Emanuelli for providing the WT-1 cell line, and the group of Silke Meiners for technical assistance with the native PAGE protocol.

## Conflict of interest

The authors declare that the research was conducted in the absence of any commercial or financial relationships that could be construed as a potential conflict of interest.

## Publisher's note

All claims expressed in this article are solely those of the authors and do not necessarily represent those of their affiliated organizations, or those of the publisher, the editors and the reviewers. Any product that may be evaluated in this article, or claim that may be made by its manufacturer, is not guaranteed or endorsed by the publisher.

## Supplementary material

The Supplementary Material for this article can be found online at: https://www.frontiersin.org/articles/10.3389/fendo.2023.1176733/full#supplementary-material

SUPPLEMENTARY FIGURE 1
**(A)** Relative maximum respiratory capacity of Bortezomib treated cells compared to DMSO treated cells. Treatment was either DMSO or 100 nM Bortezomib for 16 hours pre-ceding the mitochondrial stress test. Maximum respiratory capacity is maximum OCR measured after FCCP treatment minus OCR after Rot/A treatment, before DNA normalization (n = 4). **(B)** Oxygen consumption rate (OCR) from mitochondrial stress test, normalized to DNA levels (n = 4). Max. Resp. = Maximum Respiratory capacity. Data are represented as mean ± SEM. Data are significant if $P < 0.05$, which is indicated with an asterisk (*).

SUPPLEMENTARY FIGURE 2
Uncropped pictures from immunoblots.

## References

1. Cannon B, Nedergaard J. Brown adipose tissue: function and physiological significance. *Physiol Rev* (2004) 84(1):277–359. doi: 10.1152/physrev.00015.2003

2. Wu J, Boström P, Sparks LM, Ye L, Choi JH, Giang AH, et al. Beige adipocytes are a distinct type of thermogenic fat cell in mouse and human. *Cell* (2012) 150(2):366–76. doi: 10.1016/j.cell.2012.05.016

3. Giroud M, Jodeleit H, Prentice KJ, Bartelt A. Adipocyte function and the development of cardiometabolic disease. *J Physiol* (2022) 600(5):1189–208. doi: 10.1113/JP281979

4. Roesler A, Kazak L. UCP1-independent thermogenesis. *Biochem J* (2020) 477 (3):709–25. doi: 10.1042/BCJ20190463

5. Li Y, Schnabl K, Gabler SM, Willershäuser M, Reber J, Karlas A, et al. Secretin-activated brown fat mediates prandial thermogenesis to induce satiation. *Cell* (2018) 175(6):1561–74. doi: 10.1016/j.cell.2018.10.016

6. Sveidahl Johansen O, Ma T, Hansen JB, Markussen LK, Schreiber R, Reverte-Salisa L, et al. Lipolysis drives expression of the constitutively active receptor GPR3 to induce adipose thermogenesis. *Cell* (2021) 184(13):3502–18. doi: 10.1016/j.cell.2021.04.037

7. Christen L, Broghammer H, Rapöhn I, Möhlis K, Strehlau C, Ribas-Latre A, et al. Myoglobin-mediated lipid shuttling increases adrenergic activation of brown and white adipocyte metabolism and is as a marker of thermogenic adipocytes in humans. *Clin Transl Med* (2022) 12(12):e1108. doi: 10.1002/ctm2.1108

8. Bartelt A, Bruns OT, Reimer R, Hohenberg H, Ittrich H, Peldschus K, et al. Brown adipose tissue activity controls triglyceride clearance. *Nat Med* (2011) 17(2):200–5. doi: 10.1038/nm.2297

9. Jung SM, Sanchez-Gurmaches J, Guertin DA. Brown adipose tissue development and metabolism. In: Pfeifer A, Klingenspor M, Herzig S, editors. *Brown adipose tissue*. Cham: Springer International Publishing (2018). p. 3–36. Available at: http://link.springer.com/10.1007/164_2018_168.

10. Cypess AM, Lehman S, Williams G, Tal I, Rodman D, Goldfine AB, et al. Identification and importance of brown adipose tissue in adult humans. *N Engl J Med* (2009) 360(15):1509–17. doi: 10.1056/NEJMoa0810780

11. Becher T, Palanisamy S, Kramer DJ, Eljalby M, Marx SJ, Wibmer AG, et al. Brown adipose tissue is associated with cardiometabolic health. *Nat Med* (2021) 27 (1):58–65. doi: 10.1038/s41591-020-1126-7

12. Altshuler-Keylin S, Shinoda K, Hasegawa Y, Ikeda K, Hong H, Kang Q, et al. Beige adipocyte maintenance is regulated by autophagy-induced mitochondrial clearance. *Cell Metab* (2016) 24(3):402–19. doi: 10.1016/j.cmet.2016.08.002

13. Bartelt A, Widenmaier SB, Schlein C, Johann K, Goncalves RLS, Eguchi K, et al. Brown adipose tissue thermogenic adaptation requires Nrf1-mediated proteasomal activity. *Nat Med* (2018) 24(3):292–303. doi: 10.1038/nm.4481

14. Bartelt A, Widenmaier SB. Proteostasis in thermogenesis and obesity. *Biol Chem* (2019) 401(9):1019-10300(0). doi: 10.1515/hsz-2019-0427

15. Foley KP, Chen Y, Barra NG, Heal M, Kwok K, Tamrakar AK, et al. Inflammation promotes adipocyte lipolysis *via* IRE1 kinase. *J Biol Chem* (2021) 296:100440. doi: 10.1016/j.jbc.2021.100440

16. Chen Y, Wu Z, Huang S, Wang X, He S, Liu L, et al. Adipocyte IRE1α promotes PGC1α mRNA decay and restrains adaptive thermogenesis. *Nat Metab* (2022) 4 (9):1166–84. doi: 10.1038/s42255-022-00631-8

17. Madhavan A, Kok BP, Rius B, Grandjean JMD, Alabi A, Albert V, et al. Pharmacologic IRE1/XBP1s activation promotes systemic adaptive remodeling in obesity. *Nat Commun* (2022) 13(1):608. doi: 10.1038/s41467-022-28271-2

18. Goldberg AL. Protein degradation and protection against misfolded or damaged proteins. *Nature* (2003) 426(6968):895–9. doi: 10.1038/nature02263

19. Finley D. Recognition and processing of ubiquitin-protein conjugates by the proteasome. *Annu Rev Biochem* (2009) 78(1):477–513. doi: 10.1146/annurev.biochem.78.081507.101607

20. Martinez-Fonts K, Davis C, Tomita T, Elsasser S, Nager AR, Shi Y, et al. The proteasome 19S cap and its ubiquitin receptors provide a versatile recognition platform for substrates. *Nat Commun* (2020) 11(1):477. doi: 10.1038/s41467-019-13906-8

21. Radhakrishnan SK, Lee CS, Young P, Beskow A, Chan JY, Deshaies RJ. Transcription factor Nrf1 mediates the proteasome recovery pathway after proteasome inhibition in mammalian cells. *Mol Cell* (2010) 38(1):17–28. doi: 10.1016/j.molcel.2010.02.029

22. Stadtmueller BM, Hill CP. Proteasome activators. *Mol Cell* (2011) 41(1):8–19. doi: 10.1016/j.molcel.2010.12.020

23. Coux O, Zieba BA, Meiners S. The proteasome system in health and disease. In: Barrio R, Sutherland JD, Rodriguez MS, editors. *Proteostasis and disease*. Cham: Springer International Publishing (2020). p. 55–100. Available at: http://link.springer.com/10.1007/978-3-030-38266-7_3.

24. Huber EM, Groll M. The mammalian proteasome activator PA28 forms an asymmetric α4β3 complex. *Structure* (2017) 25(10):1473–80. doi: 10.1016/j.str.2017.07.013

25. Pickering AM, Koop AL, Teoh CY, Ermak G, Grune T, Davies KJA. The immunoproteasome, the 20S proteasome and the PA28αβ proteasome regulator are

oxidative-stress-adaptive proteolytic complexes. *Biochem J* (2010) 432(3):585–95. doi: 10.1042/BJ20100878

26. Seifert U, Bialy LP, Ebstein F, Bech-Otschir D, Voigt A, Schröter F, et al. Immunoproteasomes preserve protein homeostasis upon interferon-induced oxidative stress. *Cell* (2010) 142(4):613–24. doi: 10.1016/j.cell.2010.07.036

27. Burris A, Waite KA, Reuter Z, Ockerhausen S, Roelofs J. Proteasome activator Blm10 levels and autophagic degradation directly impact the proteasome landscape. *J Biol Chem* (2021) 296:100468. doi: 10.1016/j.jbc.2021.100468

28. Ustrell V. PA200, a nuclear proteasome activator involved in DNA repair. *EMBO J* (2002) 21(13):3516–25. doi: 10.1093/emboj/cdf333

29. Yazgili AS, Ebstein F, Meiners S. The proteasome activator PA200/PSME4: an emerging new player in health and disease. *Biomolecules* (2022) 12(8):1150. doi: 10.3390/biom12081150

30. Willemsen N, Arigoni I, Studencka-Turski M, Krüger E, Bartelt A. Proteasome dysfunction disrupts adipogenesis and induces inflammation *via* ATF3. *Mol Metab* (2022) 62:101518. doi: 10.1016/j.molmet.2022.101518

31. Sha Z, Goldberg AL. Proteasome-mediated processing of Nrf1 is essential for coordinate induction of all proteasome subunits and p97. *Curr Biol* (2014) 24 (14):1573–83. doi: 10.1016/j.cub.2014.06.004

32. Welk V, Meul T, Lukas C, Kammerl IE, Mulay SR, Schamberger AC, et al. Proteasome activator PA200 regulates myofibroblast differentiation. *Sci Rep* (2019) 9 (1):15224. doi: 10.1038/s41598-019-51665-0

33. Murata S. Immunoproteasome assembly and antigen presentation in mice lacking both PA28alpha and PA28beta. *EMBO J* (2001) 20(21):5898–907. doi: 10.1093/emboj/20.21.5898

34. Otoda T, Takamura T, Misu H, Ota T, Murata S, Hayashi H, et al. Proteasome dysfunction mediates obesity-induced endoplasmic reticulum stress and insulin resistance in the liver. *Diabetes* (2013) 62(3):811–24. doi: 10.2337/db11-1652

35. Khor B, Bredemeyer AL, Huang CY, Turnbull IR, Evans R, Maggi LB, et al. Proteasome activator PA200 is required for normal spermatogenesis. *Mol Cell Biol* (2006) 26(8):2999–3007. doi: 10.1128/MCB.26.8.2999-3007.2006

36. Huang L, Haratake K, Miyahara H, Chiba T. Proteasome activators, PA28γ and PA200, play indispensable roles in male fertility. *Sci Rep* (2016) 6(1):23171. doi: 10.1038/srep23171

37. Kotschi S, Jung A, Willemsen N, Ofoghi A, Proneth B, Conrad M, et al. NFE2L1-mediated proteasome function protects from ferroptosis. *Mol Metab* (2022) 57:101436. doi: 10.1016/j.molmet.2022.101436

frontiers | Frontiers in Endocrinology

TYPE Review
PUBLISHED 24 May 2023
DOI 10.3389/fendo.2023.1175845

Check for updates

OPEN ACCESS

EDITED BY
Endre Károly Kristóf,
University of Debrecen, Hungary

REVIEWED BY
Georgios Paschos,
University of Pennsylvania, United States
Robin Van Eenige,
Leiden University Medical Center (LUMC), Netherlands

*CORRESPONDENCE
Yong Chen
tj.y.chen@vip.163.com

SPECIALTY SECTION
This article was submitted to Obesity, a section of the journal Frontiers in Endocrinology

RECEIVED 28 February 2023
ACCEPTED 06 April 2023
PUBLISHED 24 May 2023

CITATION
Peng X and Chen Y (2023) The emerging role of circadian rhythms in the development and function of thermogenic fat.
*Front. Endocrinol.* 14:1175845.
doi: 10.3389/fendo.2023.1175845

COPYRIGHT
© 2023 Peng and Chen. This is an open-access article distributed under the terms of the Creative Commons Attribution License (CC BY). The use, distribution or reproduction in other forums is permitted, provided the original author(s) and the copyright owner(s) are credited and that the original publication in this journal is cited, in accordance with accepted academic practice. No use, distribution or reproduction is permitted which does not comply with these terms.

# The emerging role of circadian rhythms in the development and function of thermogenic fat

Xuemin Peng[1,2] and Yong Chen[1,2,3]*

[1]Division of Endocrinology, Internal Medicine, Tongji Hospital, Huazhong University of Science and Technology, Wuhan, China, [2]Laboratory of Endocrinology, Tongji Hospital, Huazhong University of Science and Technology, Wuhan, China, [3]Branch of National Clinical Research Center for Metabolic Diseases, Hubei, China

Circadian rhythms regulate many biological processes in response to ambient influences. A disrupted circadian rhythm has been shown to be associated with obesity and obesity-related metabolic disorders. Thermogenic fat, including brown and beige fat, may play an important role in this process since it displays a high capacity to burn fat and release the stored energy as heat, contributing to the combat against obesity and its associated metabolic disorders. In this review, we summarize the relationship between the circadian clock and thermogenic fat and the prominent mechanisms which are involved in the regulation of the development and function of thermogenic fat by circadian rhythms, which may provide novel therapeutics for the prevention and treatment of metabolic diseases by targeting thermogenic fat in a circadian manner.

KEYWORDS

**brown/beige fat, circadian rhythms, obesity, thermogenesis, circadian clock**

## Introduction

Almost every organism exhibits a circadian rhythm in adaptation to environmental changes. These circadian rhythms are self-sustained by an endogenous timekeeping system which is also called circadian clock. The circadian clocks consist of the central circadian clock in the suprachiasmatic nuclei (SCN) and the peripheral clocks in peripheral tissues (1). SCN receives photic information (light signals) from the retina and then regulates the peripheral clocks to coordinate circadian outputs. In addition, other nonphotic signals, such as food, exercise, sleep, and temperature, can also regulate circadian rhythms by central and peripheral clocks (2). Many biological processes such as sleep-wake cycles, blood pressure, core body temperature, hormone secretion, and energy metabolism are rhythmically fluctuate (3, 4). A disruption of circadian system, such as knockout of a circadian gene, altered light/dark cycle, shift work, and jet lag, contributes to obesity and its complications like hyperglycemia and insulin resistance, which brings a huge burden to health and economics (5–7).

Thermogenic fat, including brown adipose tissue (BAT) and beige adipose tissue, has a high capacity to burn fat and dissipate excess energy as heat to resist obesity and its related

metabolic disorders (8). Adipose tissue containing a peripheral clock also shows a diurnal rhythm and is regulated by the circadian system. Brown fat exhibits thermogenic rhythms in nonshivering thermogenesis in C57BL/6J mice (9) despite the fact that such mouse strain is deficient in melatonin, which acts as an important effector of circadian clocks (10). Previous studies support that circadian disruption may lead to obesity by impeding BAT activity. For example, circadian disruption caused by prolonged daily light exposure leads to low activity in brown fat, which contributes to obesity (11). Mice fed on high-fat diet (HFD) gained more weight with the knockout of core clock gene brain and muscle arnt-like 1 (Bmal1) in BAT compared with the wild-type mice due to disrupted rhythms of fatty acid utilization and mildly reduced thermogenesis in BAT (12). Moreover, time-restricted feeding (TRF) can mitigate obesity by increasing rhythmic creatine-mediated thermogenesis (13). Hence, thermogenic fat may play an important role in obesity caused by circadian disruption, while the effect of circadian clock on thermogenic fat has not been fully elucidated. This review will focus on the role of circadian clock in the development and function of thermogenic fat, which might provide novel insights for the prevention and treatment of metabolic diseases by targeting thermogenic fat in a circadian manner.

## Thermogenic fat

Adipocytes in mammals include white adipocytes and thermogenic adipocytes. The white adipocytes are characterized by a large unilocular lipid droplet and few mitochondria. Thermogenic adipocytes have multilocular lipid droplets and large numbers of mitochondria expressing the mitochondrial protein uncoupling protein 1 (UCP1). Thermogenic fat is heterogeneous and consists of BAT and beige adipose tissue. BAT develops in the embryonic period and originates from $Myf5^+$ lineage akin to skeletal muscle, which is mainly distributed in the interscapular region in rodents (14). Unlike BAT, beige adipocytes are derived from $Myf5^-$ but $PDGFR\alpha^+$ non-dermomyotome cells postnatally and are recruited in white adipose tissue (WAT) depots, particularly in the inguinal region (also called browning process), in response to specific signals like cold and β3-adrenergic stimulants (15). Since beige adipocytes are recruited from white adipocytes, they are considered to be of an intermediate color between white and brown adipocytes. The main function of thermogenic fat is turning chemical fuel into physical heat, which is called non-shivering thermogenesis, to maintain the normal body temperature. Besides thermogenesis, thermogenic fat also participates in glucose, lipid, and amino acid metabolism, and thermogenic fat can resist adipose fibrosis (16). The PR domain containing 16 (PRDM16)-GTF2IRD1 complex in thermogenic fat can repress the transcription of TGF-β to inhibit pro-fibrosis genes and improve glucose homeostasis (17). Moreover, beige adipocytes have the ability to secrete β-hydroxybutyrate that acts on precursor cells to reduce fibrosis through the PRDM16-driven transcriptional signal (18). Activation of BAT and beige adipocytes can improve insulin sensitivity and combat obesity (8, 19–21). In recent years, non-shivering thermogenesis has become an attractive target for the therapy of obesity and associated metabolic disorders.

## Circadian rhythms in thermogenic fat

Circadian rhythms are present in thermogenic fat. Circadian genes and circadian-controlled genes show diurnal rhythms in BAT and iWAT (inguinal WAT) (22). Since body temperature shows circadian oscillations and affects many biochemical reactions, the temperature might be the original and universal resetting cue for circadian oscillators in mammals (23, 24). Animal studies suggest that the Ucp1 gene expression in BAT is rhythmical over a period of 24 h and that thermogenesis exhibits a circadian rhythm, which lead to rhythmic body temperature (9). The 24-h rhythm in glucose uptake by BAT is observed by $^{18}$F-FDG uptake imaging in mice (25). In addition, the synthesis of fatty acid shows high-amplitude circadian rhythms in thermogenic BAT during chronic cold in mice, while such rhythms are absent in thermoneutrality (26). Besides those animal studies, human studies also confirm the circadian rhythms in thermogenic fat. Studies suggest that BAT in adult humans shares a number of common features to beige fat (15, 27). Insulin-stimulated glucose uptake was also found to display a circadian rhythm in human BAT (28). In both mice and humans, fatty acid uptake by BAT shows strong rhythms at the onset of wakening, which may explain the rhythmic plasma lipid concentrations at waking (29). Similarly, another study involving healthy humans also confirmed that nonshivering thermogenesis and fat oxidation in BAT are more obvious in the morning than in the evening (30). Collectively, these studies show that thermogenic fat exhibits circadian rhythms in aspects of both genes and functions.

## Circadian disruption contributes to obesity

The central clock SCN and the peripheral clocks in peripheral tissues coordinate with each other in response to environmental cues, such as light, food, and sleep, to maintain circadian rhythms in almost all cells/tissues (1, 29). At the molecular level, the transcriptional–translational feedback loop (TTFL) is mainly involved in the cell-autonomous rhythms. The BMAL1 and Circadian Locomotor Output Cycles Kaput (CLOCK) comprise the key positive arm and bind to E-box sequences to promote the expression of Period (PER) and Cryptochrome (CRY), which then prevent the CLOCK : BMAL1 complexes from driving transcription further (1, 31). Additionally, the expression of nuclear receptors REV-ERB α/β and retinoic acid receptor-related orphan receptors RORs α/β are also driven by the CLOCK : BMAL1 complexes, and then the ROR, in turn, promotes the transcription of BMAL1, while REV-ERB suppresses transcription (32, 33). Thus, the TTFL is mainly composed of the positive arm including BMAL1, CLOCK, and ROR proteins and the negative arm containing PER, CRY, and REV-ERB proteins (31).

A number of biological processes, such as glucose and lipid homeostasis, energy expenditure, and hormone secretion, are regulated by the circadian clock (34, 35). The SCN is mainly entrained by light signals, and the peripheral clocks can be modulated by temperature, food, and sleep as well as hormonal cues (2). The abnormal expression of circadian genes, environmental misalignment like abnormal light/dark cycles, and behavioral misalignment, including feeding, sleep–wake cycles, and activity, can promote circadian disruption, which could contribute to obesity and obesity-related metabolic disorders (36, 37). For example, animals with a genetic circadian disruption, such as the mutation of CLOCK and the deletion of BMAL1, are prone to obesity and metabolic syndrome (38–40). Animals gained more weight under the altered light/dark cycle including shortened period and prolonged light as well as blue light (11, 41, 42). Behavioral misalignments, such as shift work, jet lag, and sleep disruption, can accelerate the occurrence and development of obesity and its associated metabolic disorders in both animal models and humans (7, 43–45), in which the inactivation of thermogenic fat may be involved (11, 13, 46, 47). The existence of circadian rhythms in thermogenic fat also suggested that it may participate in circadian disruption-associated obesity and relevant metabolic complications.

The circadian rhythms in thermogenic fat and the related obesity under circadian disruption are shown in Figure 1. As thermogenic fat is becoming a promising target for treating obesity and metabolic disease, it is very important to figure out how thermogenic fat is regulated by the circadian clock to provide more accurate anti-obesity therapy.

## Circadian clock regulates the development of thermogenic fat

The development of brown and beige adipocytes is controlled by transcriptional regulation. Many clock genes encode transcription factors that impact adipogenesis and regulate the development of thermogenic fat. The deficiency of Bmal1 in both brown preadipocytes and mesenchymal precursors contributed to the formation of brown adipocytes by reducing TGF-β pathway activity and enhancing BMP signaling (48). The Bmal1-null mouse also had increased thermogenesis and adipogenesis in BAT (48).

Enhanced Ucp1 expression, more multilocular lipid droplets, and mitochondria were observed in the BAT and subcutaneous WAT in Rorα-deficient mice, and primary brown adipocytes with

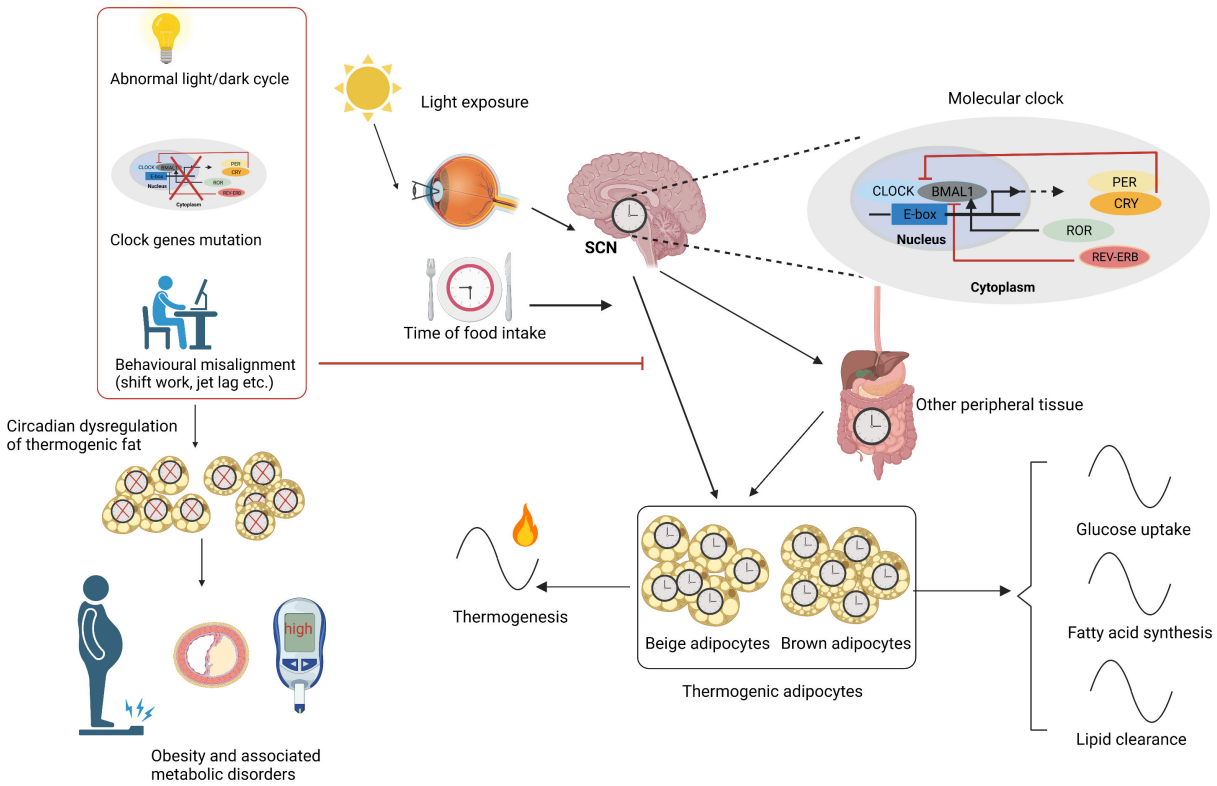


FIGURE 1
Circadian rhythms in thermogenic fat. SCN is mainly entrained by light signals and synchronizes the circadian rhythms of thermogenic fat and other peripheral tissues. SCN and other factors like time of food intake and peripheral tissues carefully regulate the thermogenic adipocyte clock. The molecular mechanism lies in TTFL including a positive arm such as CLOCK, BMAL1, and ROR and a negative arm like PER, CRY, and REV-ERB. Circadian rhythms including glucose uptake, fatty acid synthesis, lipid clearance, and thermogenesis are present in thermogenic fat. Circadian disruptions caused by abnormal light/dark cycle, clock gene mutation, and behavioral misalignments like shift work and jet lag cause circadian dysregulation of thermogenic fat, contributing to obesity and related metabolic disorders. SCN, suprachiasmatic nuclei; TTFL, transcriptional–translational feedback loop. Figures were created with BioRender (https://biorender.com/).

Rorα deficiency also showed a higher metabolic rate. Rorα deficiency promotes brown/beige adipogenesis by enhancing histone-lysine N-methyltransferase enzyme 1, which contributes to the development of thermogenic fat by stabilizing PRDM 16 transcriptional complex (49). Moreover, the RORα inverse-agonist SR3335 was confirmed to activate BAT and increase beige fat and adaptive thermogenesis in *in vivo* mice models and *in vitro* experiments. Human adipocytes also presented increasing beige characteristics after RORα inhibition, while the RORα agonist exerted an opposite effect (50). With respect to Rev-erbα, Gerhart-Hines et al. found that Rev-erbα could reduce thermogenic capacity by the transcriptional inhibition of Ucp1 in BAT so as to regulate circadian thermogenic plasticity in adult mice (9). However, Rev-erbα was found to promote BAT development in another study. The formation, structural integrity, and characteristics of BAT were impaired by the loss of Rev-erbα in neonatal mice. The Rev-erbα knockdown also diminished the brown fat-specific features in brown adipogenic differentiation, while its overexpression promoted brown adipogenesis by suppressing TGF-β signaling (51). The former study mainly focused on the role of Rev-erbα in Ucp1 expression levels in adult mice at thermoneutrality (9), while the latter study investigated its role in BAT development in neonatal mice at 22°C and *in vitro* experiments (51). The age of mice and ambient temperature may account for the differences in these two studies. The specific role of Rev-erbα in BAT development needs to be further explored by tissue-selective ablation models in future studies. Moreover, CRY1/2 was reported to increase brown fat-specific gene expressions and enhance brown adipocyte differentiation, in which the repression of BMAL1 and the interaction with PPARγ may be involved (52).

## Circadian clock controls the function of thermogenic fat

Early studies showed that excitation of the SCN by glutamate leads to an increase in BAT temperature (53). The SCN promotes fatty acid uptake from triglyceride-rich lipoproteins in the skeletal muscle as well as BAT, which maintains the day–night variations in plasma triglycerides (54). The diurnal rhythms are present in both thermogenesis and lipid clearance in BAT (9, 29). As a result, the function of thermogenic fat may be closely related to the circadian clock. As components of the TTFL, many key clock genes play vital roles in the function of thermogenic fat. The peroxisome-proliferator-activated receptor α (PPARα), as a distinctive marker of BAT, is widely considered to enhance lipid catabolism, activate the thermogenic function in BAT, and promote a white-to-beige conversion in WAT (55, 56). The CLOCK protein was also found to regulate the circadian expression of PPARα by combining its E-box-rich region (34). These studies suggest a possible role of CLOCK in the regulation of thermogenic fat.

The role of BMAL1 in thermogenic fat seems to be inconsistent in BAT. Global Bmal1-null mice had higher Ucp1 expression levels and could maintain core body temperature upon cold exposure, although having large lipid droplets (57). Another study also confirmed the increased thermogenesis and adipogenesis in BAT when Bmal1 was globally absent (48). The deficiency of BMAL1 in adipocyte was shown to contribute to obesity, although increased Ucp1 expression levels were observed (5). Moreover, the specific deletion of Bmal1 in BAT was also used to explore the relationship between BAT and thermogenic fat. The core body temperature was lower in brown adipocyte-selective Bmal1-deficient mice at 22°C, and the locomotor activity was similar compared with the control mice, while higher levels of thermogenic genes, such as Ucp1, Cidea, and Elovl3, were observed in BAT when Bmal1 was deficient (58). A recent study also found increased Ucp1 mRNA and UCP1 protein levels in BAT, with Bmal1 specifically deleted. Although the mice with Bmal1 KO in BAT had decreased UCP1-independent futile creatine cycling and mildly impaired thermogenesis, the cold tolerance was comparable to the control mice with increased shivering thermogenesis (12). The paradoxical results of the role of Bmal1 in core body temperature may be explained by the different Bmal1-floxed alleles (12, 58). REV-ERBα's role in repressing Ucp1 may be involved in the effect of Bmal1 on Ucp1 expression levels (9). Recently, Xiong et al. reported that the overexpression of Bmal1 in beige fat inhibited beige adipogenesis and thermogenesis by regulating MRTF/SRF signaling in *in vivo* mice model. Correspondingly, the selective ablation of Bmal1 enhanced iWAT browning and improved glucose homeostasis (59).

Rev-erbα regulates circadian thermogenic plasticity by repressing Ucp1 gene expression (9). Additionally, during chronic cold exposure, circadian lipid synthesis in BAT was mediated by the circadian regulation of SREBP by Rev-erbα. Similarly, the specific absence of REV-ERBα in BAT led to increased Ucp1 after de-repression (26). Furthermore, Rorα-deficient mice induced increased thermogenic genes in BAT and iWAT, which might contribute to the resistance to diet-induced obesity (7, 60). Another study also confirmed that the deletion of RORα induced iWAT browning process by increasing the PGC-1A and PRDM16 levels in staggerer mice (61). However, the Per2 mutant mice were cold-sensitive due to impaired adaptive thermogenesis. PER2 could act as a co-activator of PPARα and upregulated fatty acid binding protein 3, which thus led to increased and activated Ucp1 (62).

Moreover, the factors regulating circadian rhythms also have an impact on the function of thermogenic fat—for example, as light is an important zeitgeber for SCN, constant light caused abnormal rhythms and reduced the UCP1 expression levels in BAT (63). Both constant light and dark conditions led to the absence of diet-induced thermogenesis in humans (64). Prolonged light decreased the uptake of fatty acids and the transcription of Ucp1 of BAT in mice (11). A study also reported that advanced light phase shifts led to a brown-to-white transformation and reduced the Ucp1 levels in BAT (65). Thermogenic fat is also regulated by the photoperiod with a short 8:16 light/dark cycle, causing higher expression levels of Ucp1 in both BAT and retroperitoneal WAT compared with the long 16:8 light/dark cycle in Siberian hamsters (66). Consistent with this, another study also confirmed that short photoperiod stimulated lipid mobilization and the browning of WAT (67). Opsin 3, a blue-light-responsive opsin, was found to enhance adaptive thermogenesis in mice through adipocyte light sensing (68). A more recent study figured out the neuroregulatory mechanism of light-modulating glucose metabolism in BAT (69).

The SCN is mainly entrained by light signals, while many peripheral clocks could be entrained by food signals (70). Temporally restricted food access entrained phase shifts of the circadian gene of BAT in mice (71). The impact of TRF under HFD was also explored in another study. HFD in mice disrupted the normal metabolic cycle, and TRF considered to restore rhythms increased the rhythmic Ucp1 and PPARα expression, which enhanced thermogenesis and resisted obesity (72). Time-restricted feeding during the inactive (light) period also increased thermogenesis in BAT and iWAT by controlling the adipocyte creatine metabolism in a circadian manner in mice (13). In a word, the abovementioned studies suggest that the functions of thermogenic fat, including thermogenesis and improvement of glucose and lipid metabolism, are all regulated by a circadian clock.

## Mechanism involving the circadian regulation of thermogenic fat

The factors regulating circadian rhythms also influence thermogenic fat function, while the exact mechanism remains to be illuminated. β3-adrenergic signaling is a classic beiging signal that induces adaptive thermogenesis in brown and beige adipocytes by promoting cAMP production in mice (73, 74). In addition, many hormones vary across the day and night and participate in the regulation of thermogenic fat (75, 76). Most clock genes, as transcription factors, directly regulate the transcription of thermogenic genes and genes involving glucose and lipid metabolism as mentioned above. Besides the direct effect of clock genes, circadian sympathetic innervation and hormones are also involved in the circadian regulation of thermogenic fat. The circadian regulation of thermogenic fat is shown in Figure 2.

## Circadian regulation of thermogenic fat by the sympathetic nervous system

The activity of thermogenic fat is largely controlled by the sympathetic nervous system (SNS). There are neuroanatomical connections between SCN and BAT, and SCN neurons cooperate with other neurons in controlling sympathetic activity in BAT (77). Glutamate injection into the SCN enhanced BAT thermogenesis and increased the core temperature in rats, which was mediated by the ipsilateral ventromedial hypothalamic (VMH) nucleus (53). Light inputs entrain the circadian clocks *via* the light-sensitive ganglion cells in the retina, and disruption of the light–dark cycles causes the inactivation of thermogenic fat. The reduced β3-adrenergic intracellular signaling input accounts for the impaired BAT activity in mice under prolonged daily light (11). The uptake of fatty acid in BAT presents circadian rhythms, which were lost after the sympathetic denervation of BAT (29). A short photoperiod could resist obesity in Siberian hamsters by increasing SNS-stimulated lipid mobilization and inducing WAT browning (67). Interestingly, Meng et al. recently found that hypothalamic

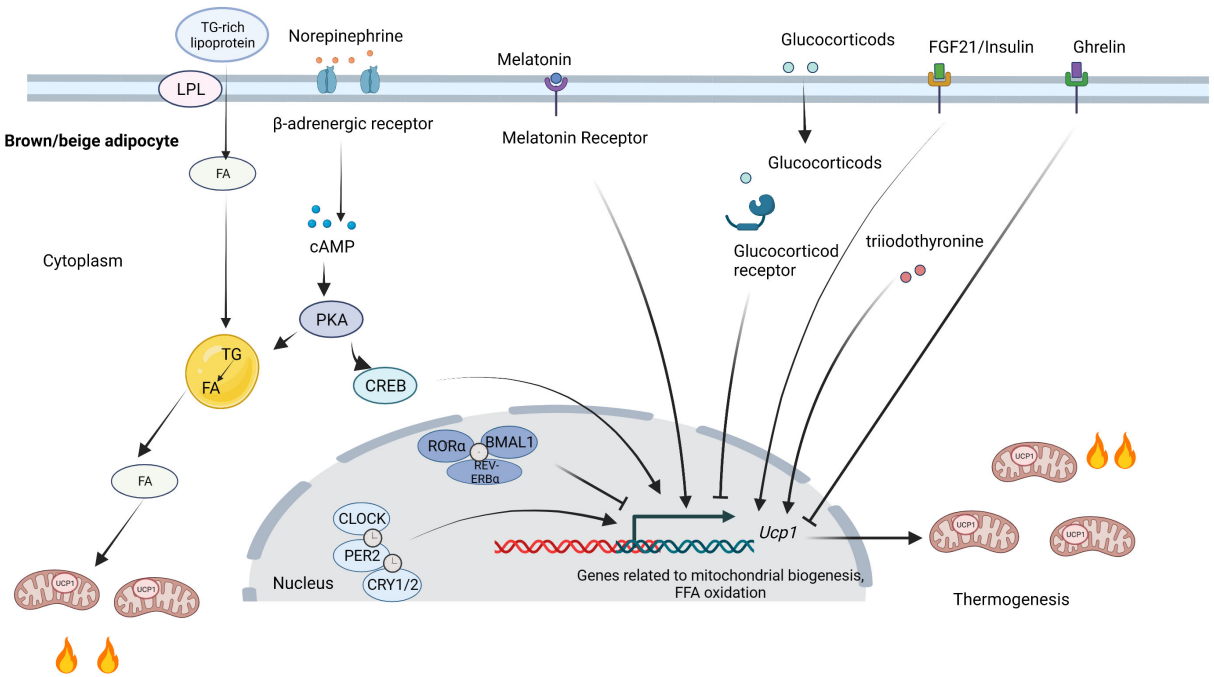


FIGURE 2
Circadian regulation of thermogenic fat. Clock proteins directly influence thermogenic fat function by regulating transcription. CLOCK, PER2, and CRY1/2 positively regulate thermogenesis, while RORα, BMAL1, and REV-ERBα inhibit thermogenesis. SNS activates thermogenic fat by releasing norepinephrine. FA released from lipid droplets can activate UCP1. The TG-rich lipoproteins promote FA uptake by LPL and replenish intracellular lipid stores. Melatonin, FGF21, and insulin bind to their receptors and contribute to thermogenesis, while glucocorticoids and ghrelin suppress thermogenesis. SNS, sympathetic nervous system; TG, triglyceride; FA, fatty acids; UCP1, uncoupling protein 1; LPL, lipoprotein lipase; FGF21; fibroblast growth factor 21. Figures were created with BioRender (https://biorender.com/).

supraoptic nucleus (SON) collects light signals by intrinsically photosensitive retinal ganglion cells and then passes signals to paraventricular nucleus neurons, which caused the activated GABAergic neurons in the solitary tract nucleus. This process finally led to impaired adaptive thermogenesis in BAT and decreased glucose tolerance through β3-adrenergic signaling. This study revealed a novel neural circuit of SON modulating light-mediated glucose tolerance independent of SCN (69). These results indicate that light signals may modulate lipid metabolism and thermogenic activity in thermogenic fat by SNS.

Besides light signals, Orozco-Solis et al. investigated how nutrition signals regulate circadian energetics. As VMH is involved in nutrient sensing, the deletion of core-clock gene Bmal1 specifically in Sf1-neurons of the VMH resulted in increased energy expenditure and enhanced thermogenic capacity mainly in BAT *via* adrenergic signaling, which suggested that the VMH clock can regulate circadian thermogenesis independent of the SCN and the endogenous BAT clock by receiving inputs from environmental zeitgebers (78).

However, Razzoli et al. reported that mice lacking β-adrenergic receptors maintained the circadian rhythmicity of Ucp1 and clock genes of BAT despite the low Ucp1 expressions at room temperature and cold challenge. This indicates that β-adrenergic receptors modulated Ucp1 during cold challenge without influencing its circadian rhythmicity (79). Similarly, thermogenesis still exhibited circadian rhythms at thermoneutrality when the sympathetic outflow to BAT was minimal (9). These further confirm that other factors, like clock genes and the following hormones, also participate in the circadian regulation of thermogenic fat apart from circadian sympathetic innervation.

## Circadian regulation of thermogenic fat by hormones

When referring to the circadian releases of hormones, melatonin is one of the most important circadian hormones as it rises as light fades and peaks during darkness (80). The circadian rhythms of melatonin are produced by the pineal gland under the control of SCN. Circadian disruptions like abnormal light, shift work, and jet lag could lead to impaired rhythms of melatonin (80). Even low-intensity light like LED in the evening can delay the phase and reduce melatonin secretion (81). Besides in the brain, melatonin receptors were also observed in adipocytes (82). Melatonin has been shown to promote circadian rhythm-mediated proliferation in WAT (83). The association between melatonin and thermogenic fat has also been reported. Ryu et al. reported that a short photoperiod increased the iWAT browning and BAT activity and thus reversed obesity compared with a long photoperiod, in which melatonin was involved in stimulating a sympathetic activity (67). In addition, pinealectomized rats with melatonin absence were overweight with reduced UCP1 levels in BAT and showed intolerance to cold, which was reversed by melatonin treatment (84). Melatonin is also reported to induce iWAT browning and promote BAT activity in other studies, while the exact mechanism remains to be investigated, and the increased sympathetic drive by SCN and the direct effects of its receptors in fat might be involved (85–88). In view of the role of melatonin in circadian rhythms and thermogenic fat, melatonin is considered to participate in the circadian regulation of thermogenic fat.

Glucocorticoids also show robust daily variation under the regulation of the hypothalamus–pituitary–adrenal gland. The rhythmic secretion of glucocorticoid is controlled by SCN as the diurnal rhythms were completely blunted after the destruction of the SCN (89). Many clock proteins can regulate the activity of glucocorticoids. CLOCK can directly repress the transcriptional activity of the glucocorticoid receptor (GR) (90). Another study showed that CRYs mediated the rhythmic repression of GRs (91). In turn, glucocorticoid signaling can also reset the phase of circadian time in peripheral tissues (92). Many clock genes like *Per1* and *Per2* that contain GR-responsive elements can be regulated by glucocorticoids (93). Blue light increased the expression of circadian genes in the WAT partly by increasing plasma corticosterone (42). The constant light causes blunted corticosterone rhythm in mice (94). These further confirm the close relationship between circadian rhythms and glucocorticoids. Genes associated with BAT function are also modulated by glucocorticoids in a GR-dependent fashion (95). Glucocorticoid signaling activation has been shown to inhibit BAT thermogenesis and induce the whitening of beige adipocytes (96, 97). The disruption of glucocorticoid diurnal rhythms could lead to the dysregulation of thermogenic fat—for example, the diurnal range of corticosterone concentration increases lipid storage and suppresses nonshivering thermogenesis in BAT (98). The flattening of circadian glucocorticoid oscillations similar to jet lag causes adipocyte hypertrophy and reduced UCP1 levels in BAT (99). Moreover, another study also reported that flattened corticosterone rhythm led to the loss of circadian rhythm in BAT-mediate triglyceride-derived fatty acid uptake possibly by reducing sympathetic innervation (100). As glucocorticoid is tightly regulated by circadian rhythms and its dysregulation can impair thermogenic fat function, the circadian regulation of thermogenic fat is at least partly mediated by glucocorticoid.

Apart from melatonin and glucocorticoid, some other hormones are also involved in the circadian regulation of thermogenic fat. Mistimed feeding was shown to disrupt the rhythms of serum melatonin, fibroblast growth factor 21 (FGF21), and ghrelin in growing pigs (101). FGF21, mainly secreted by the liver, exhibits a circadian oscillation, and its induction can activate thermogenesis in BAT and increase iWAT browning (102–104). The circadian expression levels of FGF21 can be regulated by clock genes such as REV-ERBα and RORα (105, 106). FGF21 signaling also feeds back SCN and regulates circadian behavior (107), which may indicate its circadian regulation in thermogenic fat. Furthermore, ghrelin, as a hunger-inducing hormone, also shows daily oscillations (108, 109). Circadian misalignment by a 12-h behavioral cycle inversion elevated the postprandial ghrelin levels (110). Ghrelin has been shown to inhibit BAT function by noradrenaline, and the suppression of ghrelin receptors activates BAT function (111, 112). Moreover, insulin and triiodothyronine are considered to enhance thermogenic fat activity (113, 114) and present circadian rhythms under the regulation of the circadian

clock (115). Despite the fact that the studies about these abovementioned hormones and the circadian regulation of thermogenic fat are relatively scarce, they may be more or less involved in the regulation of thermogenic fat through circadian rhythmicity. Further investigations are needed to explore the exact associations and mechanisms.

## Conclusion and perspective

Collectively, almost all organs and tissues are under the control of circadian clock to adapt to environmental changes. Lots of cases of obesity and its associated diseases are accelerated by circadian disruption such as clock deficiency, prolonged light, and other ways. Like most other tissues, thermogenic fat shows strong circadian oscillation by a complex interplay of local clocks and a central clock. Circadian factors like light, feeding, and clock genes have an impact on the thermogenic clock. The differentiation and development of thermogenic fat are well orchestrated by a circadian clock. Most aspects of thermogenic fat function, including thermogenesis and glucose and lipid metabolism, are all under circadian control to promote metabolic homeostasis. The adipocyte clock genes, SNS, and some rhythmic hormones appear to be involved in the circadian regulation of thermogenic fat.

Several questions involving the circadian clock and thermogenic fat still remain. Firstly, the association between BAT and circadian rhythms has been reported in many previous studies, while studies on beige fat are relatively few. The late discovery of beige fat may partly explain this, and more research need to be made. Secondly, despite the role of clock genes, SNS, and some hormones that have been found to participate in the circadian modulation of thermogenic fat, other unknown mechanisms also need to be explored as circadian regulation is coordinated by many molecules both in transcription and posttranslational modification levels. Moreover, emerging studies also show that human BAT exhibits circadian rhythms. Chronotherapy targeting thermogenic fat like TRF seems promising, while relevant studies are not enough, especially in humans. Further studies are needed to resist obesity and metabolic disorders by therapeutically targeting circadian rhythms in thermogenic fat. Lastly, the exact contribution of dysfunction in thermogenic fat to the obesity phenotype is unclear and difficult to explain. A deeper understanding of the extent and exact mechanisms may offer novel avenues for combating metabolic disease.

## Author contributions

XP and YC wrote the manuscript. YC edited the manuscript. All authors contributed to the article and approved the submitted version.

## Funding

This study was supported by the National Natural Science Foundation of China (Grant No. 82270910 and 82070859 to YC) and a grant from Tongji Hospital in Huazhong University of Science and Technology (Grant No. 2201103295 to YC).

## Conflict of interest

The authors declare that the research was conducted in the absence of any commercial or financial relationships that could be construed as a potential conflict of interest.

## Publisher's note

All claims expressed in this article are solely those of the authors and do not necessarily represent those of their affiliated organizations, or those of the publisher, the editors and the reviewers. Any product that may be evaluated in this article, or claim that may be made by its manufacturer, is not guaranteed or endorsed by the publisher.

## References

1. Schibler U, Sassone-Corsi P. A web of circadian pacemakers. *Cell* (2002) 111 (7):919–22. doi: 10.1016/s0092-8674(02)01225-4

2. Challet E, Pévet P. Interactions between photic and nonphotic stimuli to synchronize the master circadian clock in mammals. *Front Biosci* (2003) 8:s246–57. doi: 10.2741/1039

3. Arendt J. Biological rhythms during residence in polar regions. *Chronobiol Int* (2012) 29(4):379–94. doi: 10.3109/07420528.2012.668997

4. Hor CN, Yeung J, Jan M, Emmenegger Y, Hubbard J, Xenarios I, et al. Sleep-wake-driven and circadian contributions to daily rhythms in gene expression and chromatin accessibility in the murine cortex. *Proc Natl Acad Sci U.S.A.* (2019) 116 (51):25773–83. doi: 10.1073/pnas.1910590116

5. Paschos GK, Ibrahim S, Song WL, Kunieda T, Grant G, Reyes TM, et al. Obesity in mice with adipocyte-specific deletion of clock component arntl. *Nat Med* (2012) 18 (12):1768–77. doi: 10.1038/nm.2979

6. Poggiogalle E, Jamshed H, Peterson CM. Circadian regulation of glucose, lipid, and energy metabolism in humans. *Metabolism* (2018) 84:11–27. doi: 10.1016/j.metabol.2017.11.017

7. Parsons MJ, Moffitt TE, Gregory AM, Goldman-Mellor S, Nolan PM, Poulton R, et al. Social jetlag, obesity and metabolic disorder: investigation in a cohort study. *Int J Obes (Lond)* (2015) 39(5):842–8. doi: 10.1038/ijo.2014.201

8. Pan R, Zhu X, Maretich P, Chen Y. Combating obesity with thermogenic fat: current challenges and advancements. *Front Endocrinol (Lausanne)* (2020) 11:185. doi: 10.3389/fendo.2020.00185

9. Gerhart-Hines Z, Feng D, Emmett MJ, Everett LJ, Loro E, Briggs ER, et al. The nuclear receptor rev-erbα controls circadian thermogenic plasticity. *Nature* (2013) 503 (7476):410–3. doi: 10.1038/nature12642

10. Roseboom PH, Namboodiri MA, Zimonjic DB, Popescu NC, Rodriguez IR, Gastel JA, et al. Natural melatonin 'knockdown' in C57BL/6J mice: rare mechanism truncates serotonin n-acetyltransferase. *Brain Res Mol Brain Res* (1998) 63(1):189–97. doi: 10.1016/s0169-328x(98)00273-3

11. Kooijman S, van den Berg R, Ramkisoensing A, Boon MR, Kuipers EN, Loef M, et al. Prolonged daily light exposure increases body fat mass through attenuation of brown adipose tissue activity. *Proc Natl Acad Sci U.S.A.* (2015) 112(21):6748–53. doi: 10.1073/pnas.1504239112

12. Hasan N, Nagata N, Morishige JI, Islam MT, Jing Z, Harada KI, et al. Brown adipocyte-specific knockout of Bmal1 causes mild but significant thermogenesis impairment in mice. *Mol Metab* (2021) 49:101202. doi: 10.1016/j.molmet.2021.101202

13. Hepler C, Weidemann BJ, Waldeck NJ, Marcheva B, Cedernaes J, Thorne AK, et al. Time-restricted feeding mitigates obesity through adipocyte thermogenesis. *Science* (2022) 378(6617):276–84. doi: 10.1126/science.abl8007

14. Seale P, Bjork B, Yang W, Kajimura S, Chin S, Kuang S, et al. PRDM16 controls a brown fat/skeletal muscle switch. *Nature* (2008) 454(7207):961–7. doi: 10.1038/nature07182

15. Wu J, Boström P, Sparks LM, Ye L, Choi JH, Giang AH, et al. Beige adipocytes are a distinct type of thermogenic fat cell in mouse and human. *Cell* (2012) 150(2):366–76. doi: 10.1016/j.cell.2012.05.016

16. Cohen P, Kajimura S. The cellular and functional complexity of thermogenic fat. *Nat Rev Mol Cell Biol* (2021) 22(6):393–409. doi: 10.1038/s41580-021-00350-0

17. Hasegawa Y, Ikeda K, Chen Y, Alba DL, Stifler D, Shinoda K, et al. Repression of adipose tissue fibrosis through a PRDM16-GTF2IRD1 complex improves systemic glucose homeostasis. *Cell Metab* (2018) 27(1):180–194.e6. doi: 10.1016/j.cmet.2017.12.005

18. Wang W, Ishibashi J, Trefely S, Shao M, Cowan AJ, Sakers A, et al. A PRDM16-driven metabolic signal from adipocytes regulates precursor cell fate. *Cell Metab* (2019) 30(1):174–189.e5. doi: 10.1016/j.cmet.2019.05.005

19. Jeong MY, Park J, Youn DH, Jung Y, Kang J, Lim S, et al. Albiflorin ameliorates obesity by inducing thermogenic genes *via* AMPK and PI3K/AKT in vivo and *in vitro*. *Metabolism* (2017) 73:85–99. doi: 10.1016/j.metabol.2017.05.009

20. Yoneshiro T, Aita S, Matsushita M, Kayahara T, Kameya T, Kawai Y, et al. Recruited brown adipose tissue as an antiobesity agent in humans. *J Clin Invest* (2013) 123(8):3404–8. doi: 10.1172/jci67803

21. Wu T, Liu Q, Li Y, Li H, Chen L, Yang X, et al. Feeding-induced hepatokine, manf, ameliorates diet-induced obesity by promoting adipose browning *via* p38 MAPK pathway. *J Exp Med* (2021) 218(6):e20201203. doi: 10.1084/jem.20201203

22. Zvonic S, Ptitsyn AA, Conrad SA, Scott LK, Floyd ZE, Kilroy G, et al. Characterization of peripheral circadian clocks in adipose tissues. *Diabetes* (2006) 55 (4):962–70. doi: 10.2337/diabetes.55.04.06.db05-0873

23. Refinetti R. The circadian rhythm of body temperature. *Front Biosci (Landmark Ed)* (2010) 15(2):564–94. doi: 10.2741/3634

24. Buhr ED, Yoo SH, Takahashi JS. Temperature as a universal resetting cue for mammalian circadian oscillators. *Science* (2010) 330(6002):379–85. doi: 10.1126/science.1195262

25. van der Veen DR, Shao J, Chapman S, Leevy WM, Duffield GE. A diurnal rhythm in glucose uptake in brown adipose tissue revealed by *in vivo* PET-FDG imaging. *Obes (Silver Spring)* (2012) 20(7):1527–9. doi: 10.1038/oby.2012.78

26. Adlanmerini M, Carpenter BJ, Remsberg JR, Aubert Y, Peed LC, Richter HJ, et al. Circadian lipid synthesis in brown fat maintains murine body temperature during chronic cold. *Proc Natl Acad Sci U.S.A.* (2019) 116(37):18691–9. doi: 10.1073/pnas.1909883116

27. Shinoda K, Luijten IH, Hasegawa Y, Hong H, Sonne SB, Kim M, et al. Genetic and functional characterization of clonally derived adult human brown adipocytes. *Nat Med* (2015) 21(4):389–94. doi: 10.1038/nm.3819

28. Lee P, Bova R, Schofield L, Bryant W, Dieckmann W, Slattery A, et al. Brown adipose tissue exhibits a glucose-responsive thermogenic biorhythm in humans. *Cell Metab* (2016) 23(4):602–9. doi: 10.1016/j.cmet.2016.02.007

29. van den Berg R, Kooijman S, Noordam R, Ramkisoensing A, Abreu-Vieira G, Tambyrajah LL, et al. A diurnal rhythm in brown adipose tissue causes rapid clearance and combustion of plasma lipids at wakening. *Cell Rep* (2018) 22(13):3521–33. doi: 10.1016/j.celrep.2018.03.004

30. Matsushita M, Nirengi S, Hibi M, Wakabayashi H, Lee SI, Domichi M, et al. Diurnal variations of brown fat thermogenesis and fat oxidation in humans. *Int J Obes (Lond)* (2021) 45(11):2499–505. doi: 10.1038/s41366-021-00927-x

31. Takahashi JS. Transcriptional architecture of the mammalian circadian clock. *Nat Rev Genet* (2017) 18(3):164–79. doi: 10.1038/nrg.2016.150

32. Preitner N, Damiola F, Lopez-Molina L, Zakany J, Duboule D, Albrecht U, et al. The orphan nuclear receptor REV-ERBalpha controls circadian transcription within the positive limb of the mammalian circadian oscillator. *Cell* (2002) 110(2):251–60. doi: 10.1016/s0092-8674(02)00825-5

33. Guillaumond F, Dardente H, Giguère V, Cermakian N. Differential control of Bmal1 circadian transcription by REV-ERB and ROR nuclear receptors. *J Biol Rhythms* (2005) 20(5):391–403. doi: 10.1177/0748730405277232

34. Oishi K, Shirai H, Ishida N. CLOCK is involved in the circadian transactivation of peroxisome-proliferator-activated receptor alpha (PPARalpha) in mice. *Biochem J* (2005) 386(Pt 3):575–81. doi: 10.1042/bj20041150

35. Bartness TJ, Song CK, Demas GE. SCN efferents to peripheral tissues: implications for biological rhythms. *J Biol Rhythms* (2001) 16(3):196–204. doi: 10.1177/074873040101600302

36. Li Y, Ma J, Yao K, Su W, Tan B, Wu X, et al. Circadian rhythms and obesity: timekeeping governs lipid metabolism. *J Pineal Res* (2020) 69(3):e12682. doi: 10.1111/jpi.12682

37. Fonken LK, Nelson RJ. The effects of light at night on circadian clocks and metabolism. *Endocr Rev* (2014) 35(4):648–70. doi: 10.1210/er.2013-1051

38. Turek FW, Joshu C, Kohsaka A, Lin E, Ivanova G, McDearmon E, et al. Obesity and metabolic syndrome in circadian clock mutant mice. *Science* (2005) 308 (5724):1043–5. doi: 10.1126/science.1108750

39. Marcheva B, Ramsey KM, Buhr ED, Kobayashi Y, Su H, Ko CH, et al. Disruption of the clock components CLOCK and BMAL1 leads to hypoinsulinaemia and diabetes. *Nature* (2010) 466(7306):627–31. doi: 10.1038/nature09253

40. Jouffe C, Weger BD, Martin E, Atger F, Weger M, Gobet C, et al. Disruption of the circadian clock component BMAL1 elicits an endocrine adaption impacting on insulin sensitivity and liver disease. *Proc Natl Acad Sci U.S.A.* (2022) 119(10): e2200083119. doi: 10.1073/pnas.2200083119

41. Karatsoreos IN, Bhagat S, Bloss EB, Morrison JH, McEwen BS. Disruption of circadian clocks has ramifications for metabolism, brain, and behavior. *Proc Natl Acad Sci U.S.A.* (2011) 108(4):1657–62. doi: 10.1073/pnas.1018375108

42. Guan Q, Li Y, Wang Z, Cao J, Dong Y, Ren F, et al. Monochromatic light pollution exacerbates high-fat diet-induced adipocytic hypertrophy in mice. *Cells* (2022) 11(23). doi: 10.3390/cells11233808

43. Christie S, Vincent AD, Li H, Frisby CL, Kentish SJ, O'Rielly R, et al. A rotating light cycle promotes weight gain and hepatic lipid storage in mice. *Am J Physiol Gastrointest Liver Physiol* (2018) 315(6):G932–g942. doi: 10.1152/ajpgi.00020.2018

44. Xiong X, Lin Y, Lee J, Paul A, Yechoor V, Figueiro M, et al. Chronic circadian shift leads to adipose tissue inflammation and fibrosis. *Mol Cell Endocrinol* (2021) 521:111110. doi: 10.1016/j.mce.2020.111110

45. Chaput JP, McHill AW, Cox RC, Broussard JL, Dutil C, da Costa BGG, et al. The role of insufficient sleep and circadian misalignment in obesity. *Nat Rev Endocrinol* (2023) 19(2):82–97. doi: 10.1038/s41574-022-00747-7

46. Heyde I, Begemann K, Oster H. Contributions of white and brown adipose tissues to the circadian regulation of energy metabolism. *Endocrinology* (2021) 162(3). doi: 10.1210/endocr/bqab009

47. Straat ME, Hogenboom R, Boon MR, Rensen PCN, Kooijman S. Circadian control of brown adipose tissue. *Biochim Biophys Acta Mol Cell Biol Lipids* (2021) 1866 (8):158961. doi: 10.1016/j.bbalip.2021.158961

48. Nam D, Guo B, Chatterjee S, Chen MH, Nelson D, Yechoor VK, et al. The adipocyte clock controls brown adipogenesis through the TGF-β and BMP signaling pathways. *J Cell Sci* (2015) 128(9):1835–47. doi: 10.1242/jcs.167643

49. Lau P, Tuong ZK, Wang SC, Fitzsimmons RL, Goode JM, Thomas GP, et al. Rorα deficiency and decreased adiposity are associated with induction of thermogenic gene expression in subcutaneous white adipose and brown adipose tissue. *Am J Physiol Endocrinol Metab* (2015) 308(2):E159–71. doi: 10.1152/ajpendo.00056.2014

50. Auclair M, Roblot N, Capel E, Fève B, Antoine B. Pharmacological modulation of RORα controls fat browning, adaptive thermogenesis, and body weight in mice. *Am J Physiol Endocrinol Metab* (2021) 320(2):E219–e233. doi: 10.1152/ajpendo.00131.2020

51. Nam D, Chatterjee S, Yin H, Liu R, Lee J, Yechoor VK, et al. Novel function of rev-erbα in promoting brown adipogenesis. *Sci Rep* (2015) 5:11239. doi: 10.1038/srep11239

52. Miller S, Son YL, Aikawa Y, Makino E, Nagai Y, Srivastava A, et al. Isoform-selective regulation of mammalian cryptochromes. *Nat Chem Biol* (2020) 16(6):676–85. doi: 10.1038/s41589-020-0505-1

53. Amir S, Shizgal P, Rompré PP. Glutamate injection into the suprachiasmatic nucleus stimulates brown fat thermogenesis in the rat. *Brain Res* (1989) 498(1):140–4. doi: 10.1016/0006-8993(89)90409-5

54. Moran-Ramos S, Guerrero-Vargas NN, Mendez-Hernandez R, Basualdo MDC, Escobar C, Buijs RM. The suprachiasmatic nucleus drives day-night variations in postprandial triglyceride uptake into skeletal muscle and brown adipose tissue. *Exp Physiol* (2017) 102(12):1584–95. doi: 10.1113/ep086026

55. Hondares E, Rosell M, Díaz-Delfín J, Olmos Y, Monsalve M, Iglesias R, et al. Peroxisome proliferator-activated receptor α (PPARα) induces PPARγ coactivator 1α (PGC-1α) gene expression and contributes to thermogenic activation of brown fat: involvement of PRDM16. *J Biol Chem* (2011) 286(50):43112–22. doi: 10.1074/jbc.M111.252775

56. Kroon T, Harms M, Maurer S, Bonnet L, Alexandersson I, Lindblom A, et al. PPARγ and PPARα synergize to induce robust browning of white fat in vivo. *Mol Metab* (2020) 36:100964. doi: 10.1016/j.molmet.2020.02.007

57. Li S, Yu Q, Wang GX, Lin JD. The biological clock is regulated by adrenergic signaling in brown fat but is dispensable for cold-induced thermogenesis. *PloS One* (2013) 8(8):e70109. doi: 10.1371/journal.pone.0070109

58. Chang L, Xiong W, Zhao X, Fan Y, Guo Y, Garcia-Barrio M, et al. Bmal1 in perivascular adipose tissue regulates resting-phase blood pressure through transcriptional regulation of angiotensinogen. *Circulation* (2018) 138(1):67–79. doi: 10.1161/circulationaha.117.029972

59. Xiong X, Li W, Liu R, Saha P, Yechoor V, Ma K. Circadian clock control of MRTF/SRF pathway suppresses beige adipocyte thermogenic recruitment. *J Mol Cell Biol* (2022). doi: 10.1093/jmcb/mjac079

60. Lau P, Fitzsimmons RL, Raichur S, Wang SC, Lechtken A, Muscat GE. The orphan nuclear receptor, RORalpha, regulates gene expression that controls lipid metabolism: staggerer (SG/SG) mice are resistant to diet-induced obesity. *J Biol Chem* (2008) 283(26):18411–21. doi: 10.1074/jbc.M710526200

61. Monnier C, Auclair M, Le Cam G, Garcia MP, Antoine B. The nuclear retinoid-related orphan receptor RORα controls circadian thermogenic programming in white fat depots. *Physiol Rep* (2018) 6(8):e13678. doi: 10.14814/phy2.13678

62. Chappuis S, Ripperger JA, Schnell A, Rando G, Jud C, Wahli W, et al. Role of the circadian clock gene Per2 in adaptation to cold temperature. *Mol Metab* (2013) 2 (3):184–93. doi: 10.1016/j.molmet.2013.05.002

63. Palanivel R, Vinayachandran V, Biswal S, Deiuliis JA, Padmanabhan R, Park B, et al. Exposure to air pollution disrupts circadian rhythm through alterations in chromatin dynamics. *iScience* (2020) 23(11):101728. doi: 10.1016/j.isci.2020.101728

64. Fukuda Y, Morita T. Effects of the light-dark cycle on diurnal rhythms of diet-induced thermogenesis in humans. *Chronobiol Int* (2017) 34(10):1465–72. doi: 10.1080/07420528.2017.1362422

65. Herrero L, Valcarcel L, da Silva CA, Albert N, Diez-Noguera A, Cambras T, et al. Altered circadian rhythm and metabolic gene profile in rats subjected to advanced light phase shifts. *PloS One* (2015) 10(4):e0122570. doi: 10.1371/journal.pone.0122570

66. Demas GE, Bowers RR, Bartness TJ, Gettys TW. Photoperiodic regulation of gene expression in brown and white adipose tissue of Siberian hamsters (Phodopus sungorus). *Am J Physiol Regul Integr Comp Physiol* (2002) 282(1):R114–21. doi: 10.1152/ajpregu.2002.282.1.R114

67. Ryu V, Zarebidaki E, Albers HE, Xue B, Bartness TJ. Short photoperiod reverses obesity in Siberian hamsters via sympathetically induced lipolysis and browning in adipose tissue. *Physiol Behav* (2018) 190:11–20. doi: 10.1016/j.physbeh.2017.07.011

68. Nayak G, Zhang KX, Vemaraju S, Odaka Y, Buhr ED, Holt-Jones A, et al. Adaptive thermogenesis in mice is enhanced by opsin 3-dependent adipocyte light sensing. *Cell Rep* (2020) 30(3):672–686.e8. doi: 10.1016/j.celrep.2019.12.043

69. Meng JJ, Shen JW, Li G, Ouyang CJ, Hu JX, Li ZS, et al. Light modulates glucose metabolism by a retina-hypothalamus-brown adipose tissue axis. *Cell* (2023) 186 (2):398–412.e17. doi: 10.1016/j.cell.2022.12.024

70. Green CB, Takahashi JS, Bass J. The meter of metabolism. *Cell* (2008) 134 (5):728–42. doi: 10.1016/j.cell.2008.08.022

71. Goh BC, Wu X, Evans AE, Johnson ML, Hill MR, Gimble JM. Food entrainment of circadian gene expression altered in PPARalpha-/- brown fat and heart. *Biochem Biophys Res Commun* (2007) 360(4):828–33. doi: 10.1016/j.bbrc.2007.06.136

72. Hatori M, Vollmers C, Zarrinpar A, DiTacchio L, Bushong EA, Gill S, et al. Time-restricted feeding without reducing caloric intake prevents metabolic diseases in mice fed a high-fat diet. *Cell Metab* (2012) 15(6):848–60. doi: 10.1016/j.cmet.2012.04.019

73. Dallner OS, Chernogubova E, Brolinson KA, Bengtsson T. Beta3-adrenergic receptors stimulate glucose uptake in brown adipocytes by two mechanisms independently of glucose transporter 4 translocation. *Endocrinology* (2006) 147 (12):5730–9. doi: 10.1210/en.2006-0242

74. Jiang Y, Berry DC, Graff JM. Distinct cellular and molecular mechanisms for β3 adrenergic receptor-induced beige adipocyte formation. *Elife* (2017) 6. doi: 10.7554/eLife.30329

75. Morris CJ, Aeschbach D, Scheer FA. Circadian system, sleep and endocrinology. *Mol Cell Endocrinol* (2012) 349(1):91–104. doi: 10.1016/j.mce.2011.09.003

76. Emont MP, Yu H, Wu J. Transcriptional control and hormonal response of thermogenic fat. *J Endocrinol* (2015) 225(2):R35–47. doi: 10.1530/joe-15-0026

77. Bamshad M, Song CK, Bartness TJ. CNS origins of the sympathetic nervous system outflow to brown adipose tissue. *Am J Physiol* (1999) 276(6):R1569–78. doi: 10.1152/ajpregu.1999.276.6.R1569

78. Orozco-Solis R, Aguilar-Arnal L, Murakami M, Peruquetti R, Ramadori G, Coppari R, et al. The circadian clock in the ventromedial hypothalamus controls cyclic energy expenditure. *Cell Metab* (2016) 23(3):467–78. doi: 10.1016/j.cmet.2016.02.003

79. Razzoli M, Emmett MJ, Lazar MA, Bartolomucci A. β-adrenergic receptors control brown adipose UCP-1 tone and cold response without affecting its circadian rhythmicity. *FASEB J* (2018) 32(10):5640–6. doi: 10.1096/fj.201800452R

80. Vasey C, McBride J, Penta K. Circadian rhythm dysregulation and restoration: the role of melatonin. *Nutrients* (2021) 13(10). doi: 10.3390/nu13103480

81. Chang AM, Aeschbach D, Duffy JF, Czeisler CA. Evening use of light-emitting eReaders negatively affects sleep, circadian timing, and next-morning alertness. *Proc Natl Acad Sci U.S.A.* (2015) 112(4):1232–7. doi: 10.1073/pnas.1418490112

82. Brydon L, Petit L, Delagrange P, Strosberg AD, Jockers R. Functional expression of MT2 (Mel1b) melatonin receptors in human PAZ6 adipocytes. *Endocrinology* (2001) 142(10):4264–71. doi: 10.1210/endo.142.10.8423

83. Liu Z, Gan L, Luo D, Sun C. Melatonin promotes circadian rhythm-induced proliferation through clock/histone deacetylase 3/c-myc interaction in mouse adipose tissue. *J Pineal Res* (2017) 62(4):e12383. doi: 10.1111/jpi.12383

84. Buonfiglio D, Parthimos R, Dantas R, Cerqueira Silva R, Gomes G, Andrade-Silva J, et al. Melatonin absence leads to long-term leptin resistance and overweight in rats. *Front Endocrinol (Lausanne)* (2018) 9:122. doi: 10.3389/fendo.2018.00122

85. Agil A, Navarro-Alarcon M, Ali FAZ, Albrakati A, Salagre D, Campoy C, et al. Melatonin enhances the mitochondrial functionality of brown adipose tissue in obese-diabetic rats. *Antioxidants (Basel)* (2021) 10(9):1482. doi: 10.3390/antiox10091482

86. Fernández Vázquez G, Reiter RJ, Agil A. Melatonin increases brown adipose tissue mass and function in zücker diabetic fatty rats: implications for obesity control. *J Pineal Res* (2018) 64(4):e12472. doi: 10.1111/jpi.12472

87. Jiménez-Aranda A, Fernández-Vázquez G, Campos D, Tassi M, Velasco-Perez L, Tan DX, et al. Melatonin induces browning of inguinal white adipose tissue in zucker diabetic fatty rats. *J Pineal Res* (2013) 55(4):416–23. doi: 10.1111/jpi.12089

88. Salagre D, Chayah M, Molina-Carballo A, Oliveras-López MJ, Munoz-Hoyos A, Navarro-Alarcón M, et al. Melatonin induces fat browning by transdifferentiation of white adipocytes and *de novo* differentiation of mesenchymal stem cells. *Food Funct* (2022) 13(6):3760–75. doi: 10.1039/d1fo04360a

89. Abe K, Kroning J, Greer MA, Critchlow V. Effects of destruction of the suprachiasmatic nuclei on the circadian rhythms in plasma corticosterone, body temperature, feeding and plasma thyrotropin. *Neuroendocrinology* (1979) 29(2):119–31. doi: 10.1159/000122913

90. Nader N, Chrousos GP, Kino T. Circadian rhythm transcription factor CLOCK regulates the transcriptional activity of the glucocorticoid receptor by acetylating its hinge region lysine cluster: potential physiological implications. *FASEB J* (2009) 23 (5):1572–83. doi: 10.1096/fj.08-117697

91. Lamia KA, Papp SJ, Yu RT, Barish GD, Uhlenhaut NH, Jonker JW, et al. Cryptochromes mediate rhythmic repression of the glucocorticoid receptor. *Nature* (2011) 480(7378):552–6. doi: 10.1038/nature10700

92. Balsalobre A, Brown SA, Marcacci L, Tronche F, Kellendonk C, Reichardt HM, et al. Resetting of circadian time in peripheral tissues by glucocorticoid signaling. *Science* (2000) 289(5488):2344–7. doi: 10.1126/science.289.5488.2344

93. Yamamoto T, Nakahata Y, Tanaka M, Yoshida M, Soma H, Shinohara K, et al. Acute physical stress elevates mouse period1 mRNA expression in mouse peripheral tissues *via* a glucocorticoid-responsive element. *J Biol Chem* (2005) 280(51):42036–43. doi: 10.1074/jbc.M509600200

94. Coomans CP, van den Berg SA, Houben T, van Klinken JB, van den Berg R, Pronk AC, et al. Detrimental effects of constant light exposure and high-fat diet on circadian energy metabolism and insulin sensitivity. *FASEB J* (2013) 27(4):1721–32. doi: 10.1096/fj.12-210898

95. Luijten IHN, Cannon B, Nedergaard J. Glucocorticoids and brown adipose tissue: do glucocorticoids really inhibit thermogenesis? *Mol Aspects Med* (2019) 68:42–59. doi: 10.1016/j.mam.2019.07.002

96. Zeng X, Jedrychowski MP, Chen Y, Serag S, Lavery GG, Gygi SP, et al. Lysine-specific demethylase 1 promotes brown adipose tissue thermogenesis *via* repressing glucocorticoid activation. *Genes Dev* (2016) 30(16):1822–36. doi: 10.1101/gad.285312.116

97. Roh HC, Tsai LTY, Shao M, Tenen D, Shen Y, Kumari M, et al. Warming induces significant reprogramming of beige, but not brown, adipocyte cellular identity. *Cell Metab* (2018) 27(5):1121–1137.e5. doi: 10.1016/j.cmet.2018.03.005

98. Strack AM, Bradbury MJ, Dallman MF. Corticosterone decreases nonshivering thermogenesis and increases lipid storage in brown adipose tissue. *Am J Physiol* (1995) 268(1 Pt 2):R183–91. doi: 10.1152/ajpregu.1995.268.1.R183

99. Tholen S, Patel R, Agas A, Kovary KM, Rabiee A, Nicholls HT, et al. Flattening of circadian glucocorticoid oscillations drives acute hyperinsulinemia and adipocyte hypertrophy. *Cell Rep* (2022) 39(13):111018. doi: 10.1016/j.celrep.2022.111018

100. Kroon J, Schilperoort M, In Het Panhuis W, van den Berg R, van Doeselaar L, Verzijl CRC, et al. A physiological glucocorticoid rhythm is an important regulator of brown adipose tissue function. *Mol Metab* (2021) 47:101179. doi: 10.1016/j.molmet.2021.101179

101. Wang QJ, Guo Y, Yao CY, Zhang KH, Li Q, Shan CH, et al. Loss of diurnal behavioral rhythms and impaired lipid metabolism in growing pigs with mistimed feeding. *FASEB J* (2021) 35(11):e21972. doi: 10.1096/fj.202100768R

102. Yu H, Xia F, Lam KS, Wang Y, Bao Y, Zhang J, et al. Circadian rhythm of circulating fibroblast growth factor 21 is related to diurnal changes in fatty acids in humans. *Clin Chem* (2011) 57(5):691–700. doi: 10.1373/clinchem.2010.155184

103. Chartoumpekis DV, Habeos IG, Ziros PG, Psyrogiannis AI, Kyriazopoulou VE, Papavassiliou AG. Brown adipose tissue responds to cold and adrenergic stimulation by induction of FGF21. *Mol Med* (2011) 17(7-8):736–40. doi: 10.2119/molmed.2011.00075

104. Fisher FM, Kleiner S, Douris N, Fox EC, Mepani RJ, Verdeguer F, et al. FGF21 regulates PGC-1α and browning of white adipose tissues in adaptive thermogenesis. *Genes Dev* (2012) 26(3):271–81. doi: 10.1101/gad.177857.111

105. Chavan R, Preitner N, Okabe T, Strittmatter LM, Xu C, Ripperger JA, et al. REV-ERBα regulates Fgf21 expression in the liver *via* hepatic nuclear factor 6. *Biol Open* (2017) 6(1):1–7. doi: 10.1242/bio.021519

106. Hirai T, Nomura K, Ikai R, Nakashima KI, Inoue M. Baicalein stimulates fibroblast growth factor 21 expression by up-regulating retinoic acid receptor-related orphan receptor α in C2C12 myotubes. *BioMed Pharmacother* (2019) 109:503–10. doi: 10.1016/j.biopha.2018.10.154

107. Bookout AL, de Groot MH, Owen BM, Lee S, Gautron L, Lawrence HL, et al. FGF21 regulates metabolism and circadian behavior by acting on the nervous system. *Nat Med* (2013) 19(9):1147–52. doi: 10.1038/nm.3249

108. LeSauter J, Hoque N, Weintraub M, Pfaff DW, Silver R. Stomach ghrelin-secreting cells as food-entrainable circadian clocks. *Proc Natl Acad Sci U.S.A.* (2009) 106(32):13582–7. doi: 10.1073/pnas.0906426106

109. Natalucci G, Riedl S, Gleiss A, Zidek T, Frisch H. Spontaneous 24-h ghrelin secretion pattern in fasting subjects: maintenance of a meal-related pattern. *Eur J Endocrinol* (2005) 152(6):845–50. doi: 10.1530/eje.1.01919

110. Qian J, Morris CJ, Caputo R, Garaulet M, Scheer F. Ghrelin is impacted by the endogenous circadian system and by circadian misalignment in humans. *Int J Obes (Lond)* (2019) 43(8):1644–9. doi: 10.1038/s41366-018-0208-9

111. Mano-Otagiri A, Ohata H, Iwasaki-Sekino A, Nemoto T, Shibasaki T. Ghrelin suppresses noradrenaline release in the brown adipose tissue of rats. *J Endocrinol* (2009) 201(3):341–9. doi: 10.1677/joe-08-0374

112. Mano-Otagiri A, Iwasaki-Sekino A, Nemoto T, Ohata H, Shuto Y, Nakabayashi H, et al. Genetic suppression of ghrelin receptors activates brown adipocyte function and decreases fat storage in rats. *Regul Pept* (2010) 160(1-3):81–90. doi: 10.1016/j.regpep.2009.11.010

113. Mullur R, Liu YY, Brent GA. Thyroid hormone regulation of metabolism. *Physiol Rev* (2014) 94(2):355–82. doi: 10.1152/physrev.00030.2013

114. Golic I, Kalezic A, Jankovic A, Jonic S, Korac B, Korac A. Insulin modulates the bioenergetic and thermogenic capacity of rat brown adipocytes *In Vivo* by modulating mitochondrial mosaicism. *Int J Mol Sci* (2020) 21(23):9204. doi: 10.3390/ijms21239204

115. Kim BH, Joo Y, Kim MS, Choe HK, Tong Q, Kwon O. Effects of intermittent fasting on the circulating levels and circadian rhythms of hormones. *Endocrinol Metab (Seoul)* (2021) 36(4):745–56. doi: 10.3803/EnM.2021.405

frontiers | Frontiers in Cell and Developmental Biology

TYPE Original Research
PUBLISHED 14 June 2023
DOI 10.3389/fcell.2023.1155673

Check for updates

OPEN ACCESS

EDITED BY
Etienne Audet-Walsh,
Laval University, Canada

REVIEWED BY
Amandine Girousse,
Centre National de la Recherche Scientifique (CNRS), France
Hai-Bin Ruan,
University of Minnesota, United States

*CORRESPONDENCE
Endre Kristóf,
kristof.endre@med.unideb.hu

†These authors have contributed equally to this work and share first authorship

RECEIVED 31 January 2023
ACCEPTED 26 May 2023
PUBLISHED 14 June 2023

CITATION
Vámos A, Arianti R, Vinnai BÁ, Alrifai R, Shaw A, Póliska S, Guba A, Csősz É, Csomós I, Mocsár G, Lányi C, Balajthy Z, Fésüs L and Kristóf E (2023), Human abdominal subcutaneous-derived active beige adipocytes carrying *FTO* rs1421085 obesity-risk alleles exert lower thermogenic capacity.
*Front. Cell Dev. Biol.* 11:1155673.
doi: 10.3389/fcell.2023.1155673

COPYRIGHT
© 2023 Vámos, Arianti, Vinnai, Alrifai, Shaw, Póliska, Guba, Csősz, Csomós, Mocsár, Lányi, Balajthy, Fésüs and Kristóf. This is an open-access article distributed under the terms of the Creative Commons Attribution License (CC BY). The use, distribution or reproduction in other forums is permitted, provided the original author(s) and the copyright owner(s) are credited and that the original publication in this journal is cited, in accordance with accepted academic practice. No use, distribution or reproduction is permitted which does not comply with these terms.

# Human abdominal subcutaneous-derived active beige adipocytes carrying *FTO* rs1421085 obesity-risk alleles exert lower thermogenic capacity

Attila Vámos[1,2†], Rini Arianti[1,3†], Boglárka Ágnes Vinnai[1,2], Rahaf Alrifai[1,2], Abhirup Shaw[1], Szilárd Póliska[4], Andrea Guba[2,5], Éva Csősz[5], István Csomós[6], Gábor Mocsár[6], Cecilia Lányi[7], Zoltán Balajthy[1], László Fésüs[1] and Endre Kristóf[1]*

[1]Laboratory of Cell Biochemistry, Department of Biochemistry and Molecular Biology, Faculty of Medicine, University of Debrecen, Debrecen, Hungary, [2]Doctoral School of Molecular Cell and Immune Biology, University of Debrecen, Debrecen, Hungary, [3]Universitas Muhammadiyah Bangka Belitung, Pangkalanbaru, Indonesia, [4]Genomic Medicine and Bioinformatics Core Facility, Department of Biochemistry and Molecular Biology, Faculty of Medicine, University of Debrecen, Debrecen, Hungary, [5]Proteomics Core Facility, Department of Biochemistry and Molecular Biology, Faculty of Medicine, University of Debrecen, Debrecen, Hungary, [6]Department of Biophysics and Cell Biology, Faculty of Medicine, University of Debrecen, Debrecen, Hungary, [7]Laser Clinic, Budapest, Hungary

**Introduction:** White adipocytes store lipids, have a large lipid droplet and few mitochondria. Brown and beige adipocytes, which produce heat, are characterized by high expression of uncoupling protein (UCP) 1, multilocular lipid droplets, and large amounts of mitochondria. The rs1421085 T-to-C single-nucleotide polymorphism (SNP) of the human *FTO* gene interrupts a conserved motif for ARID5B repressor, resulting in adipocyte type shift from beige to white.

**Methods:** We obtained abdominal subcutaneous adipose tissue from donors carrying *FTO* rs1421085 TT (risk-free) or CC (obesity-risk) genotypes, isolated and differentiated their preadipocytes into beige adipocytes (driven by the PPARγ agonist rosiglitazone for 14 days), and activated them with dibutyryl-cAMP for 4 hours. Then, either the same culture conditions were applied for additional 14 days (active beige adipocytes) or it was replaced by a white differentiation medium (inactive beige adipocytes). White adipocytes were differentiated by their medium for 28 days.

**Results and Discussion:** RNA-sequencing was performed to investigate the gene expression pattern of adipocytes carrying different *FTO* alleles and found that active beige adipocytes had higher brown adipocyte content and browning capacity compared to white or inactive beige ones when the cells were obtained from risk-free TT but not from obesity-risk CC genotype carriers. Active beige adipocytes carrying *FTO* CC had lower thermogenic gene (e.g., *UCP1, PM20D1, CIDEA*) expression and thermogenesis measured by proton leak respiration as compared to TT carriers. In addition, active beige adipocytes with CC alleles exerted lower expression of ASC-1 neutral amino acid transporter (encoded by *SLC7A10*) and less consumption of Ala, Ser, Cys, and Gly as compared to risk-free carriers. We did not observe any influence of the *FTO* rs1421085 SNP

on white and inactive beige adipocytes highlighting its exclusive and critical effect when adipocytes were activated for thermogenesis.

KEYWORDS

adipocytes, beige, obesity, FTO rs1421085, thermogenesis, UCP 1, *SLC7A10*

## 1 Introduction

In the last few decades, the prevalence of obesity dramatically increased across the world. Chronic obesity can lead to various cancers, type 2 diabetes, and cardiovascular disease. Therefore, obesity has been identified as one of the globally leading causes of mortality and disability, and is responsible for 10%–13% of deaths in different regions worldwide (Frühbeck et al., 2013). Imbalance of energy homeostasis, when energy intake is significantly greater than energy expenditure, has been identified as the main pathophysiological cause of obesity (Heymsfield and Wadden, 2017). However, obesity is a multifactorial disease which can be the result of factors including social, lifestyle, behavioral networks, and genetic background of the individuals (Christakis and Fowler, 2007; Frühbeck et al., 2018; Lin and Li, 2021).

In rodents, adipocytes are classified into three types. The energy storing white adipocytes have one large unilocular lipid droplet and low mitochondrial density. The brown adipocytes located in the brown adipose tissue (BAT) are active thermogenic cells with high mitochondrial abundance, fragmentation, and uncoupling protein (UCP) 1 expression, as well as numerous small lipid droplet content in the cytoplasm. The "brown-like-in-white" (brite) or beige cells have cold-inducible thermogenic potential and multilocular lipid droplets (Sanchez-Gurmaches et al., 2016). Beige adipocytes are interspersed in the white adipose tissue (WAT). In basal state, their gene expression pattern is similar to the white adipocytes, but upon extended stimuli (cold exposure, β-adrenergic stimulation, peroxisome proliferator-activated receptor (PPAR)-γ activation) they exhibit a brown-like phenotype acquired in a process called browning (Petrovic et al., 2010; Wu et al., 2012). Inguinal WAT has been discovered as a natural beige adipocyte depot, in which the adipocytes possess multilocular morphology and thermogenic gene expression profile in response to thermogenic cues (Chan et al., 2019).

In humans, BAT was primarily regarded as a tissue which is only present in infants and located at anatomical sites that are difficult to reach (Heaton, 1972). Several studies using positron emission tomography (PET) provided evidence that adults have significant amounts of BAT, most commonly the cervical-supraclavicular depot was marked by high labeled glucose uptake especially after cold exposure (Cypess et al., 2009; Virtanen et al., 2009). Using an elegant approach of the PET-Computed Tomography (CT) method, brownable adipose tissue could be found interspersed in several areas, such as cervical, supraclavicular, axillary, mediastinal, paraspinal, and abdominal (Leitner et al., 2017). However, unlike in rodents, the molecular characteristics of human BAT remain elusive. Several studies reported that human BAT isolated from cervical-supraclavicular depots (Cypess et al., 2013) and primary adipocytes derived from fetal interscapular adipose tissue (Seiler et al., 2015) possess classical brown adipocyte characteristics marked by high expression of zinc finger protein-1 (ZIC1), whereas other studies using clonally derived human brown adipocytes isolated from supraclavicular depot reported the existence of a population of UCP1-positive cells displaying beige adipocyte features (Shinoda et al., 2015). Another study using total RNA isolated from fat biopsies from various anatomical locations, including subcutaneous (SC) supraclavicular, posterior mediastinal, retroperitoneal, intra-abdominal, or mesenteric depots reported that beige-selective markers, such as *HOXC8*,

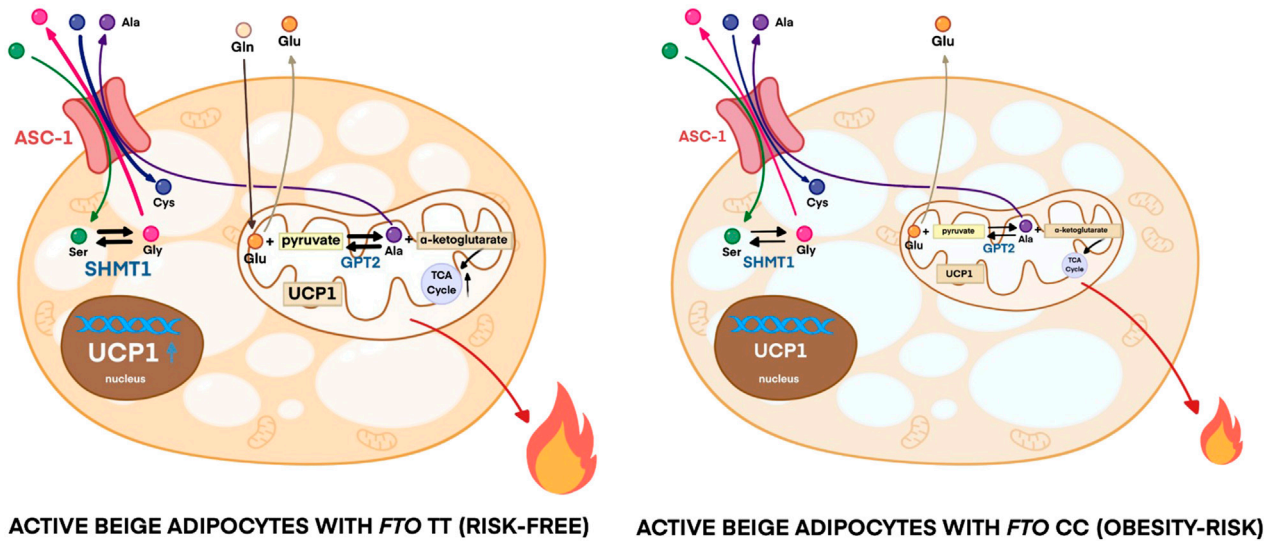


GRAPHICAL ABSTRACT

*HOXC9*, and *CITED1* were highly expressed in human thermogenic adipose tissue, whereas classical BAT markers were not detectable (Sharp et al., 2012).

The activation of UCP1 to generate heat by brown/beige adipocytes drives a higher uptake of fuels, such as glucose and fatty acids, to sustain the metabolic substrates for tricarboxylic acid (TCA) cycle and generate NADH and $FADH_2$ that subsequently enter the electron transport chain. Active brown/beige adipocytes also take up large amounts of TCA cycle intermediates, e.g., succinate, to enhance their proton leak respiration (Mills et al., 2018). A recent study reported that the labeled glucose consumed by murine BAT during cold exposure is converted to pyruvate, which is further oxidized to acetyl-CoA catalyzed by pyruvate dehydrogenase (Panic et al., 2020). In addition to glucose and fatty acids, active brown/beige adipocytes also catabolize branched-chain amino acids to fulfill the high demand of energy (Yoneshiro et al., 2019). Our previous study also underlined the importance of alanine-serine-cysteine transporter 1 (ASC-1)-mediated consumption of serine, cysteine, and glycine for efficient thermogenic response upon adrenergic stimulation in deep neck derived adipocytes (Arianti et al., 2021). The capability of active brown/beige adipocytes as metabolic sink may contribute to the clearance of blood glucose and lipids, which indirectly improves glucose tolerance and insulin sensitivity (Cheng et al., 2021). High rate of metabolic substrate utilization by active brown/beige adipocytes enhances the energy expenditure, therefore it may promote weight loss and become a potential pharmaceutical target to treat obesity and related metabolic diseases.

Recent publications reported the involvement of autophagy in the downregulation of beige adipocyte thermogenesis. In rodents, parkin-dependent selective mitochondrial clearance (mitophagy) drives the generation of inactive–morphologically white, but reactivation capable–masked beige adipocytes (Altshuler-Keylin et al., 2016). In human abdominal SC adipocytes, both parkin-dependent and parkin-independent mitophagy related genes were upregulated upon *ex vivo* beige to white transition (Vámos et al., 2022). In contrast, in differentiated human primary SC and Simpson–Golabi–Behmel syndrome (SGBS) adipocytes, cAMP-induced thermogenic activation downregulated mitophagy blocking beige to white transition (Szatmári-Tóth et al., 2020). Preventing entry into this conversion might be a potential way to maintain elevated thermogenesis for combatting obesity.

Individual susceptibility to obesity is determined by interactions between genetic background and behavior. Genome-wide association studies identified the strong association between obesity and the Fat mass and obesity-associated (*FTO*) gene (Wang et al., 2011; Dina et al., 2007; Frayling et al., 2007; Scuteri et al., 2007). Among several identified single-nucleotide polymorphisms (SNPs) of *FTO*, an intronic rs1421085 T-to-C SNP has recently attracted attention. Studies in European and Japanese populations reported that the presence of the obesity-risk C allele increased the susceptibility for obesity, elevated fat mass and food intake (Wheeler et al., 2013; Felix et al., 2016; Imamura et al., 2016; Tanaka et al., 2013). Claussnitzer et al. (2015) elucidated the molecular background for the association between *FTO* rs1421085 SNP and increased fat storage. In the presence of the risk-free allele (T), the AT-Rich Interaction Domain 5B (ARID5B) repressor protein can bind to the enhancer region of Iroquois Homeobox (IRX) 3 and 5, therefore the expression of IRX3 and 5 is suppressed (Claussnitzer et al., 2015). When the obesity-risk allele is present, the conserved motif for ARID5B repressor is disrupted resulting in elevated expression of IRX3 and 5. As the consequence, the differentiation program is shifted from energy dissipation by beige adipocytes to lipid storage into white adipocytes (Claussnitzer et al., 2015; Herman and Rosen, 2015). $IRX5^{-/-}$ mice possessed reduced fat mass and did not develop obesity when fed on a high-fat diet. In addition, *IRX5* silencing increased the mitochondrial respiration in isolated mouse adipocytes (Bjune et al., 2019). $IRX3^{-/-}$ ME3 murine embryonic fibroblast line failed to differentiate to beige adipocytes, however, increased their capacity for chondrogenesis (Bjune et al., 2020). On the other hand, it was also reported that IRX3 promotes the browning of white adipocytes as it can directly bind to the promoter of *UCP1* (Zou et al., 2017).

In this study, we employed transcriptomic and metabolomic data to investigate the effect of *FTO* rs1421085 SNP on the thermogenic capacity of three types of adipocytes: white, active and inactive beige, which were derived from human adipose-derived stromal cells (hASCs) isolated from abdominal SC fat of donors carrying *FTO* risk-free (TT) or obesity-risk (CC) genotypes (4 individuals of each genotype). RNA-sequencing (RNA-seq) analysis was performed to screen the global transcriptomic profiles of the differentiated adipocytes and we found that active beige adipocytes carrying risk-free alleles had higher brown adipocyte content, browning capacity, mitochondrial complex I, II, and IV subunit amount, proton leak respiration, extracellular acidification, expression of thermogenic markers (*UCP1*, *PM20D1*, *CITED1*, *CIDEA*, *CKMT1*, and *CKMT2*), and ASC-1-mediated amino acid consumption, as compared to white or inactive beige adipocytes carrying the same genotypes. Intriguingly, we found that active beige adipocytes carrying *FTO* obesity-risk genotypes have less distinguishable characteristics as compared to white or inactive beige adipocytes. Our findings underline the critical effect of *FTO* rs1421085 SNP in human abdominal SC adipocytes when they are activated for thermogenesis.

# 2 Materials and methods

## 2.1 Materials

All chemicals and reagents were obtained from Sigma-Aldrich (Munich, Germany) unless stated otherwise.

## 2.2 Ethical statement and obtained hASCs

The human SC abdominal adipose tissue collection was approved by the Medical Research Council of Hungary (20571-2/2017/EKU) followed by the EU Member States' Directive 2004/23/EC on presumed consent practice for tissue collection. All experiments were implemented in accordance with the Helsinki Declaration. All participants were informed about the experiments and written informed consent was obtained from them. hASCs were obtained and isolated from stromal vascular fractions (SVFs) of human SC abdominal adipose tissue of healthy donors undergoing plastic surgery, as previously described (Kristóf et al., 2019; Szatmári-Tóth et al., 2020). Briefly, the tissue samples were immediately transported to the laboratory following plastic surgery. Adipose tissue specimens were dissected from fibrous material and blood vessels, minced into small pieces and digested in phosphate buffered

saline (PBS) with 120 U/mL collagenase for 120 min in a 37°C water bath with gentle agitation. The completely disaggregated tissue was filtered (pore size 140 μm) to remove any remaining tissue. The cell suspension was centrifuged for 10 min at 1,300 rpm and the pellet of SVF was suspended and maintained. Floating cells were washed away with PBS after 3 days of isolation and the remaining cells were cultured as described in 2.3. Data of the donors included in the study are listed in Supplementary Table S1.

## 2.3 Maintenance and differentiation of hASCs

hASCs were seeded in 6-well plates and cultured in Dulbecco's Modified Eagle's Medium/Nutrient F-12 Ham (DMEM-F12) medium containing 17 μM pantothenic acid, 33 μM biotin, 100 U/mL penicillin/streptomycin, and 10% fetal bovine serum (Thermo Fisher Scientific, Waltham, MA, United States) at 37°C in 5% $CO_2$ until they reach complete confluence. The absence of *mycoplasma* was verified by polymerase chain reaction (PCR) analysis (PCR *Mycoplasma* Test Kit I/C, PromoKine, PromoCell, Heidelberg, Germany).

White adipogenic differentiation was induced for 3 days with serum-free DMEM-F12 medium supplemented with 17 μM pantothenic acid, 33 μM biotin, 100 U/mL penicillin/streptomycin, 100 nM cortisol, 10 μg/mL human apo-transferrin, 200 pM triiodothyronine, 20 nM human insulin, 2 μM rosiglitazone (Cayman Chemicals, Ann Arbor, MI, United States), 25 nM dexamethasone, and 500 μM 3-isobutyl-l-methylxantine. After the third day, rosiglitazone, dexamethasone, and 3-isobutyl-l-methylxantine were removed from the medium during the remaining 25 days of the differentiation. The medium was exchanged in every third day.

The active beige differentiation was induced for 3 days with serum-free DMEM-F12 medium supplemented with 17 μM pantothenic acid, 33 μM biotin, 100 U/mL penicillin/streptomycin, 10 μg/mL human apo-transferrin, 200 pM triiodothyronine, 20 nM human insulin, 2 μM rosiglitazone, 25 nM dexamethasone, and 500 μM 3-isobutyl-l-methylxantine. After the third day, dexamethasone and 3-isobutyl-l-methylxantine were removed and 500 nM rosigliazone was added to the medium for the remaining 25 days of differentiation. On the 14th day, a 4 h long 500 μM dibutyryl-cAMP treatment was carried out to mimic the *in vivo* cold-induced thermogenesis (Szatmári-Tóth et al., 2020). After the treatment, the aforementioned beige differentiation medium was applied until the end of the differentiation.

The inactive beige differentiation was induced in the first 14 days as in the case of the active beige adipocytes, but after the dibutyryl-cAMP treatment, the medium was replaced to the white cocktail without rosiglitazone, dexamethasone, and 3-isobutyl-l-methylxantine for additional 14 days.

## 2.4 RNA isolation, reverse-transcription PCR (RT-PCR), quantitative PCR (qPCR), and RNA-Seq analysis

Adipocytes were collected in TRIzol reagent (Thermo Fisher Scientific), followed by manual RNA isolation by chloroform extraction and isopropanol precipitation. The RNA quality was evaluated by Nanodrop (Thermo Fisher Scientific). cDNA generation was carried out by TaqMan reverse transcription reagent kit (Thermo Fisher Scientific) and followed by qPCR analysis (Szatmári-Tóth et al., 2020; Shaw et al., 2021). Gene expressions were normalized to the geometric mean of β-actin (*ACTB*) and *GAPDH*. All TaqMan assays are listed in Supplementary Table S2.

Total RNA sample quality was checked on Agilent BioAnalyzer using Eukaryotic Total RNA Nano Kit according to the Manufacturer's protocol. Samples with RNA integrity number (RIN) value >7 were accepted for the library preparation process. RNA-Seq libraries were prepared from total RNA using MGIEasy RNA Library Prep Set V3.0 (MGI, Shenzhen, China) according to the manufacturer's protocol. Briefly, poly-A RNAs were captured by oligo-dT conjugated magnetic beads then the mRNAs were eluted and fragmented at 94°C. First-strand cDNA was generated by random priming reverse transcription, then in the second strand synthesis step, double-stranded cDNA was generated. After repairing ends, A-tailing and adapter ligation steps, adapter-ligated fragments were amplified in enrichment PCR and finally sequencing libraries were generated. In the next step double-stranded libraries were denatured and single strand circularization was performed, after enzymatic digestion step circularized single-stranded library was generated for DNA nano ball (DNB) generation. After making DNB step, single-end 100 cycles sequencing run was executed on MGI DNBSEQ G400 instrument. After sequencing, the reads were aligned to the GRCh38 reference genome (with EnsEMBL 95 annotation) using STAR aligner (version 2.7.0a). FeatureCounts was used to quantify our reads to genes. Significantly differentially expressed genes (DEGs) were defined based on adjusted $p$ values <0.05 and log2 fold change threshold >0.85. Heatmap was generated by using GraphPad 8.0 Software and interactome map was constructed by using Gephi 0.9 based on interaction from STRING (https://string-db.org/). Pathway analysis was performed by subjecting the list of DEGs to STRING and overrepresented KEGG pathways were selected based on the false discovery rate (FDR) < 0.05. Brown adipocyte content and browning capacity was estimated by BATLAS and ProFAT webtools, respectively, by subjecting the transcriptomic data of both groups of markers (Perdikari et al., 2018; Cheng et al., 2018).

## 2.5 *FTO* allele genotyping

DNA isolation was performed as previously described (Klusóczki et al., 2019). Rs1421085 SNP was genotyped by qPCR using TaqMan SNP Genotyping assay (Thermo Fisher Scientific, 4351379) according to the Manufacturer's instructions.

## 2.6 Antibodies and immunoblotting

The separation of investigated proteins was performed by SDS-PAGE, followed by transfer to a PVDF membrane, which was blocked by 5% skimmed milk solution (Szatmári-Tóth et al., 2020; Shaw et al., 2021). The primary antibodies were utilized in the following dilutions: anti-β-actin (1:5000, A2066), anti-UCP1 (1:750, R&D Systems, Minneapolis, MN, United States,

MAB6158), anti-OXPHOS (1:1,000, Abcam, Cambridge, MA, United States, ab110411), anti-SLC7A10 (1:500, Abnova, Taipei City, Taiwan, H00056301-B01P), anti-PGC1α (1:1,000, Novus Biologicals, Centennial, CO, United States, NBP1-04676) anti-GPT2 (1:2000, Thermo Fisher Scientific, PA5-62426), and anti-SHMT1 (1:2000, Thermo Fisher Scientific, PA5-88581). The following species corresponding secondary antibodies were used: HRP-conjugated goat anti-mouse (1:5000, Advansta, San Jose, CA, United States, R-05071-500) or anti-rabbit (1: 5000, Advansta, R-05072-500) IgG. The expression of the visualized immunoreactive proteins were quantified by densitometry using the FIJI ImageJ software (National Institutes of Health (NIH), Bethesda, MD, United States) as previously described (Szatmári-Tóth et al., 2020).

## 2.7 Immunofluorescent staining

hASCs were seeded and differentiated on Ibidi eight-well μ-slides as described in Section 2.3. Cells were washed once with PBS and fixed by 4% paraformaldehyde, followed by permeabilization with 0.1% saponin and blocking with 5% skimmed milk. Primary antibody incubations were kept overnight with anti-TOM20 (1:75, WH0009804M1) and anti-LC3 (1:200, Novus Biologicals, NB100-2220). Secondary antibody incubation was for 3 h with Alexa Fluor 647 goat anti-mouse IgG (1: 1,000, Thermo Fisher Scientific, A21236) and Alexa Fluor 488 goat anti-rabbit IgG (1:1,000, Thermo Fisher Scientific, A11034). Propidium iodide (PI, 1.5 μg/mL, 1 h) was used for nuclei labeling. Images were obtained with an Olympus FluoView 1,000 (Olympus Scientific Solutions, Tokyo, Japan) confocal microscope and FluoView10-ASW (Olympus Scientific Solutions) software version 3.0, as previously described (Szatmári-Tóth et al., 2020; Vámos et al., 2022). LC3 and TOM20 immunostaining images were converted to binary form, followed by processing with FIJI. The LC3 punctae count was determined by size (pixel$^2$) 50–infinity AU with circularity 0–1 AU. Fragmented mitochondria were analyzed from the binary TOM20 immunostaining images with size (pixel$^2$) 0–100 AU and circularity 0–1 AU. The optimum size values for the LC3 punctae and fragmented mitochondria were determined based on an analysis of all immunostaining images and manual verification of the counting accuracy by checking the outlines of counts. Both LC3 punctae and fragmented mitochondria content were normalized to per nucleus for individual images. Co-localization of LC3 and TOM20 was evaluated by calculation of the Pearson correlation coefficient (PCC) (Szatmári-Tóth et al., 2020; Vámos et al., 2022). 30 cells per three donors were recorded and analyzed.

## 2.8 Quantification of amino acid fluxes of adipocytes

Supernatants of the cells were collected at the end of the differentiation process and examined as previously described (Guba et al., 2022; Nokhoijav et al., 2022). Briefly, the media were filtered using a 3 kDa filter (Pall Corporation, Port Washington, NY, United States) and 10 μL of this filtrate was derivatized with AccQ Tag Ultra Derivatization Kit (Waters, Milford, MA, United States). Chromatographic separation was executed on H-class UPLC (Waters) using AccQ Tag Ultra Column (2.1 × 100 mm), AccQ Tag Eluent A and B, and gradient was ensured by the AccQ Tag Ultra Chemistry Kit (Waters). Amino acid (both L and D enantiomers) derivatives were detected at 260 nm in the PDA detector of the UPLC. Detection of the amino acid concentrations were calculated by Empower software (Waters) using a 7-point calibration curve. Flux of amino acids into or from adipocytes was calculated by comparing concentration differences measured in the conditioned media, which was administered to the cells at day 25 and collected at the end point of 28 days differentiation, and the unconditioned medium. The concentration of amino acids was normalized to the number of cells as described previously (Arianti et al., 2021).

## 2.9 Determination of real-time cellular oxygen consumption (OCR) and extracellular acidification rate (ECAR)

Cells were seeded and differentiated on XF96 assay plates (Seahorse Biosciences, North Billerica, MA, United States) to white, active beige, or inactive beige using the protocols as described in Section 2.3. The OCR and ECAR were measured with XF96 oximeter (Seahorse Biosciences). Dibutyryl-cAMP stimulated OCR and ECAR, etomoxir-resistant (ETO-R) OCR, and stimulated proton leak OCR were quantified using previously utilized protocols (Kristóf et al., 2015; Arianti et al., 2021; Nagy et al., 2022). 10 μM antimycin A was used for baseline collection (measuring non-mitochondrial respiration). The OCR was normalized to protein content of each well.

## 2.10 Statistical analysis

All results are expressed as mean ± SD. The normality of the obtained data was tested by Shapiro-Wilk test. Datasets with a normal distribution was analyzed using one-way ANOVA with a Tukey's *post hoc* test. Data was analyzed and visualized by GraphPad Prism 8 Software.

# 3 Results

## 3.1 Active beige adipocytes derived from abdominal SC exert high browning capacity

Primarily, we aimed to investigate the global gene expression patterns of the three types of differentiated SC adipocytes, white, active, and inactive beige (see Methods for their differentiation protocol) by performing RNA-seq analysis. We found that general adipocyte markers, such as *SLC2A4*, *FABP4*, *LPL*, *ADIPOQ*, *AGPAT2*, *PLIN1*, *LEP*, and *LEPR* were not expressed differentially among the three types of adipocytes (Figure 1A) suggesting that their differentiation rate was similar. The thermogenic markers, such as *UCP1*, *ELOVL3*, *PGC1a*, *CIDEA*, *CITED1*, *AQP3*, *GK*, *CKMT1a/b*, and *PM20D1* had higher expression in active beige as compared to white or inactive beige adipocytes (Figure 1B). Next, we subjected our transcriptomic data from RNA-seq analysis to open source webtools

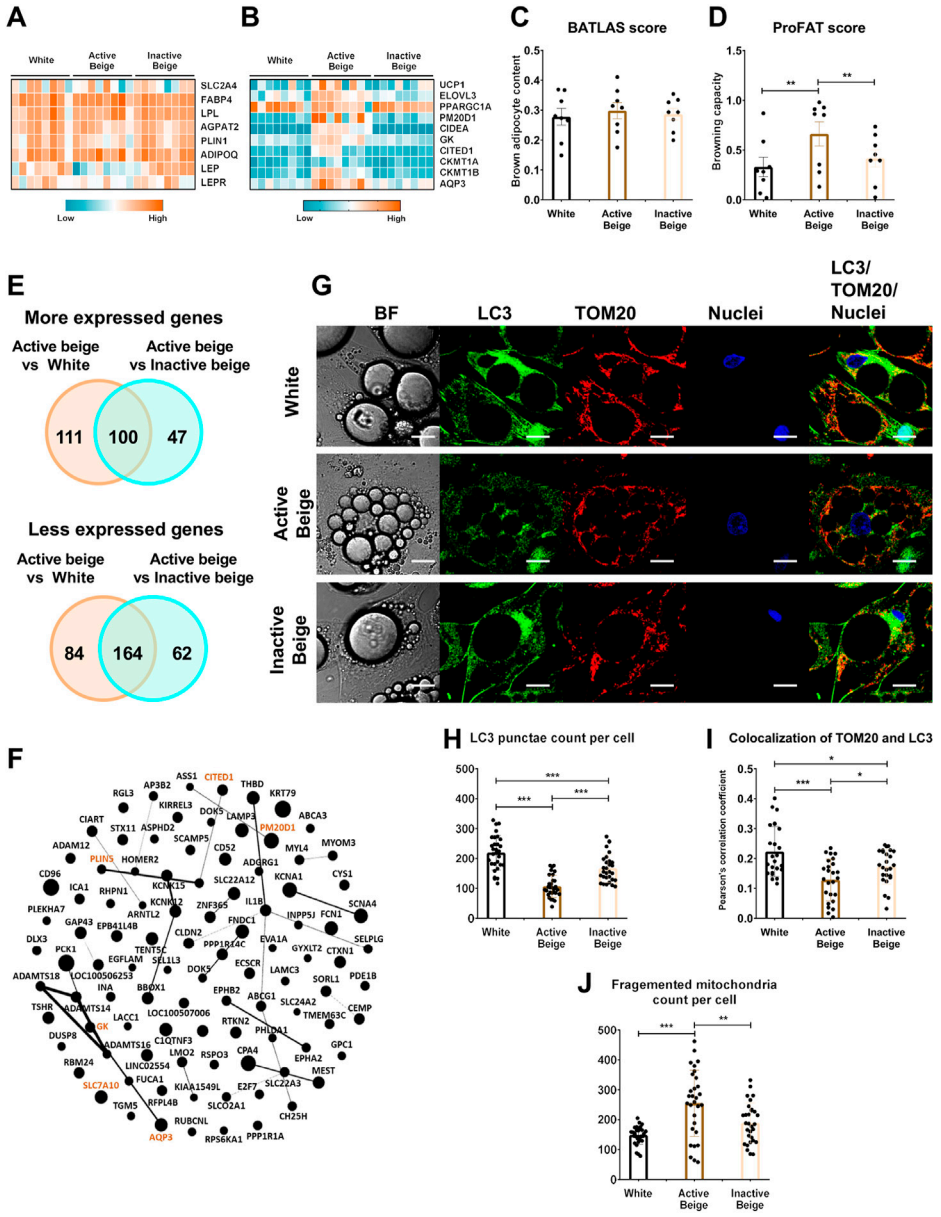


FIGURE 1
Differentially expressed genes and thermogenic capacity of human abdominal subcutaneous adipocytes. **(A)** Heatmap displaying the expression of general markers of adipocytes. **(B)** Heatmap displaying the expression of brown/beige adipocyte markers. **(C)** Brown adipocyte content quantified by BATLAS open source webtool, $n = 8$. **(D)** Browning capacity quantified by ProFAT open source webtool, $n = 8$. **(E)** Venn diagram displaying the numbers of more (top panel) and less (bottom panel) expressed genes in comparison of active beige vs. white and active beige vs. inactive beige adipocytes. **(F)** Overlapping upregulated genes between active beige vs. white and active beige vs. inactive beige in interactome map generated by Gephi. The size of the nodes correlates with fold change in the expression values. Gene names marked in brown are known thermogenic markers. **(G)** Representative confocal microscopy images of microtubule-associated protein 1 light chain 3 (LC3) and Translocase of outer mitochondrial membrane (TOM) 20 immunostaining of white, active beige, and inactive beige adipocytes. BF: bright field, scale bars represent 10 µm. **(H)** Quantification of LC3 punctae, $n = 30$ cells of three donors. **(I)** Co-localization of TOM20 and LC3, $n = 25$ per cells cells of three donors. **(J)** Quantification of fragmented mitochondria count per cell, $n = 30$ cells of three donors. Statistical analysis by ANOVA. $^*p < 0.05$, $^{**}p < 0.01$, and $^{***}p < 0.001$.

to estimate brown adipocyte content by BATLAS (Perdikari et al., 2018) and browning capacity by ProFAT (Cheng et al., 2018) based on the expression levels of well-defined marker genes. We did not find significant differences in brown adipocyte content (Figure 1C), however, active beige adipocytes showed higher browning capacity score as compared to white or inactive beige ones (Figure 1D). According to our RNA-seq analysis data, we found that 211 and 147 genes had higher expression in the comparison of active beige vs. white and active beige vs. inactive beige, respectively; out of those, 100 genes were common (Figure 1E, top panel; Supplementary Tables S3, S4). Among the commonly highly expressed 100 genes, thermogenic markers, such as *GK*, *PM20D1*, *PLIN5*, *CITED1*, and *AQP3* were found (Figure 1F). Interestingly, *SLC7A10*, encoding ASC-1, which was described as an important transporter during

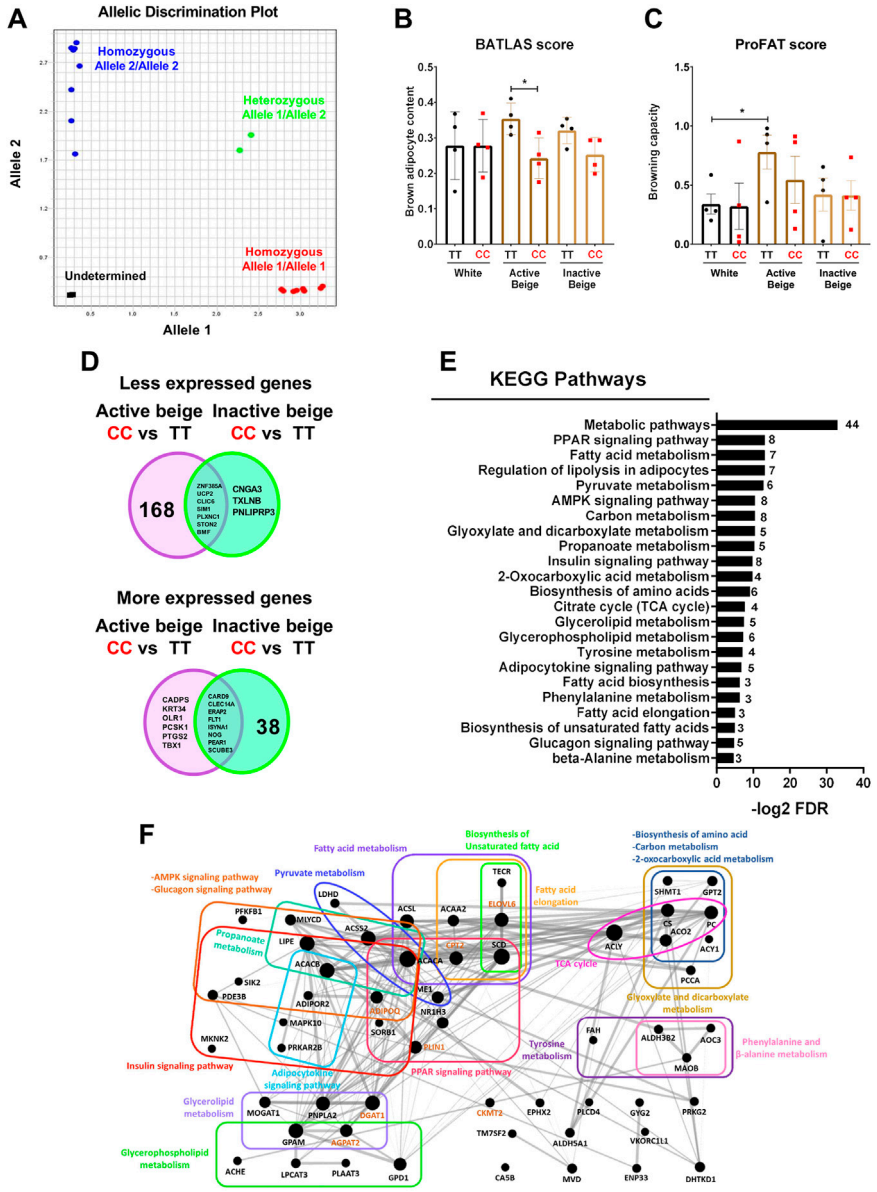


FIGURE 2
The effect of *FTO* rs1421085 SNP on the thermogenic capacity and gene expression pattern of differentiated abdominal subcutaneous (SC) adipocytes. **(A)** Allelic distribution of *FTO* rs1421085 SNP. Blue: SC progenitors with TT alleles, red: SC progenitors with CC alleles, green: heterozygous SGBS adipocytes, black: no template negative control. **(B)** Brown adipocyte content quantified by BATLAS, $n = 4$ of each genotype. **(C)** Browning capacity quantified by ProFAT, $n = 4$ of each genotype, $^{*}p < 0.05$, $^{**}p < 0.01$, statistical analysis by ANOVA. **(D)** Venn diagram displaying the numbers of less (top panel) and more (bottom panel) expressed genes in comparison of *FTO* rs1421085 CC vs. TT in both active and inactive beige differentiated adipocytes. **(E)** Overrepresented pathways which are less expressed in active beige differentiated adipocytes carrying *FTO* CC/obesity-risk variant as compared to TT/risk-free variant. Numbers on the right side indicate the number of genes involved in the pathways. **(F)** Genes involved in less expressed pathways shown in figure **(E)** in interactome map generated by Gephi. The size of the nodes correlates with fold change of the expression values. Gene names marked in brown are known thermogenic markers.

thermogenic activation (Arianti et al., 2021; Jersin et al., 2021) was also commonly upregulated in both comparisons (Figure 1F). 248 and 226 genes had lower expression in the comparison of active beige vs. white and active beige vs. inactive beige, respectively, and 164 genes had commonly lower expression (Figure 1E, bottom panel; Supplementary Tables S3, S4). We did not find any DEGs when we compared the gene expression profile of white and inactive beige adipocytes. We also analyzed the mitophagy rate and mitochondrial morphology by co-immunostaining of microtubule-associated protein 1 light chain 3 (LC3) and translocase of outer mitochondrial membrane 20 (TOM20) [Szatmári-Tóth et al., 2020] (Figure 1G). Confocal images were used to quantify the co-localization of LC3 and TOM20 by measuring the correlation between pixel intensities of two detection channels [Szatmári-Tóth et al., 2020]. We observed lower LC3 punctae counts per cell (Figure 1H) and PCC values in active beige as compared to white

or inactive beige adipocytes (Figure 1I). We also found that active beige adipocytes had higher amounts of fragmented mitochondria, which were shown to support uncoupled respiration and enhanced energy expenditure (Pisani et al., 2018), as compared to white or inactive beige cells (Figure 1J). Altogether, these data suggests that thermogenesis-related genes were upregulated, the mitophagy rate was lowered, and mitochondria were more fragmented when human abdominal SC adipocytes were activated for thermogenesis.

## 3.2 Active beige adipocytes carrying *FTO* rs1421085 obesity-risk alleles had lower brown adipocyte content and expressed lower level of genes involved in metabolic pathways

Next, we intended to investigate whether *FTO* rs1421085 SNP affected the browning capacity of human abdominal SC adipocytes, which were differentiated into white, active, or inactive beige. Therefore, we genotyped the hASCs for *FTO* rs1421085 SNP by using SNP genotyping assay and obtained the allelic discrimination plot (Figure 2A). Then, we selected samples from 4 individuals with homozygous TT (risk-free) and from 4 individuals with homozygous CC (obesity-risk) genotypes for further analysis. We found that active beige adipocytes carrying *FTO* obesity-risk alleles exerted lower brown adipocyte content estimated by BATLAS (Perdikari et al., 2018), but no effect of the allelic distribution was observed in case of white or inactive beige adipocytes (Figure 2B). We also found that the risk-free genotype carrier active beige adipocytes had higher tendency of BATLAS and significantly higher ProFAT (Cheng et al., 2018) scores as compared to white ones that carried the same TT genotype (Figures 2B, C). Interestingly, active beige adipocytes carrying *FTO* obesity-risk genotype showed similar estimated brown adipocyte content and browning capacity as compared to white adipocytes (Figures 2B, C) suggesting that active beige differentiation could not overcome the browning inhibitory effect of the CC alleles. Active beige adipocytes with *FTO* risk-free genotype expressed the BATLAS marker genes at the highest level, whereas ones with the obesity-risk allele carriers expressed them at a level similar to those observed in the white or inactive beige adipocytes (Supplementary Figure S1). The expression of ProFAT markers was high in risk-free carrier active beige adipocytes and showed large donor variability in the obesity-risk allele carrier ones (Supplementary Figure S2).

A total of 175 genes including thermogenic markers (*UCP2*, *CKMT2*, and *CITED1*) and 5 BATLAS markers (*PPARGC1B*, *ACO2*, *ACSF2*, *NNAT*, and *DMRT2*) were expressed less in active beige adipocytes carrying *FTO* obesity-risk variant as compared to risk-free carriers (Figure 2D, top panel; Supplementary Table S5). Only 10 genes (7 of them were common in both comparisons) were expressed at a lower extent in CC as compared to TT carrier inactive beige adipocytes (Figure 2D, top panel; Supplementary Table S6). We found only 14 and 46 genes (8 of them were common in both comparisons) which were expressed more in active or inactive beige adipocytes, respectively, carrying the *FTO* obesity-risk as compared to the risk-free variant (Figure 2D, bottom panel; Supplementary Tables S5, S6). In white adipocytes, we did not find any DEGs which was affected by the *FTO* rs1421085 SNP. Next, we investigated the gene expression pathways affected by the *FTO* rs1421085 SNP and found that genes, which were less expressed in active beige adipocytes that carried the obesity-risk genotype, were overrepresented in several pathways, such as metabolic, PPAR signaling, lipolysis, fatty acid metabolism, or TCA cycle (Figures 2E, F). More expressed genes in active beige adipocytes with CC alleles were not significantly overrepresented in any of the pathways. We did not find any overrepresented pathway with respect to the DEGs found in inactive beige adipocytes either.

Because we observed significant effects of *FTO* rs1421085 SNP on the gene expression pattern of active beige SC adipocytes, we also compared the transcriptomic data of active beige and white or inactive beige adipocytes that carried *FTO* risk-free or obesity-risk genotypes, respectively. We found a total of 226 genes that were expressed more in active beige as compared to white adipocytes with *FTO* risk-free genotype, whereas only 54 higher expressed genes were found between the two types of differentiations in obesity-risk carriers; 25 genes were overlapping in the two comparisons (Supplementary Figure S3A; Supplementary Tables S7, S8). There were 93 and 130 genes which were expressed less in active beige as compared to white adipocytes carrying *FTO* risk-free or obesity-risk alleles, respectively. Out of those, 46 were common (Supplementary Figure S3B; Supplementary Tables S7, S8). The PPAR signaling pathway was the only one in which more expressed genes in active beige as compared to white adipocytes carrying *FTO* risk-free variant were overrepresented. The less expressed genes in active beige adipocytes as compared to white ones were overrepresented in several pathways, such as axon guidance or longevity regulating only in *FTO* obesity-risk genotype carriers (Supplementary Figure S3C). When adipocytes carried the risk-free alleles, no overrepresented pathway was found in this comparison.

We found a total of 172 genes that were expressed more in active as compared to inactive beige adipocytes carrying *FTO* risk-free variant, whereas only 18 genes were found in the same comparison with obesity-risk genotype carrier cells; nine genes were overlapping in the two comparisons (Supplementary Figure S3D; Supplementary Tables S9, S10). There were 116 and 158 genes (61 common), which were expressed less in active as compared to inactive beige adipocytes carrying *FTO* risk-free or obesity-risk alleles, respectively (Supplementary Figure S3E; Supplementary Tables S9, S10). Genes expressed in a lower extent in active beige adipocytes as compared to white ones were overrepresented in several pathways, such as AMPK signaling and TGF-beta signaling only in *FTO* obesity-risk allele carriers (Supplementary Figure S3F). When adipocytes carried the risk-free genotype, we did not find any overrepresented pathway in comparison of active with white or inactive beige adipocytes. These results suggest that *FTO* rs1421085 SNP only affects the gene expression profile, particularly that of the thermogenesis-related genes, in active beige but not in white or inactive beige adipocytes. In addition, the applied differentiation protocols resulted in more pronounced differences in the gene expression patterns of adipocytes with *FTO* risk-free alleles which suggest their significant browning potential when thermogenic cues are constantly present.

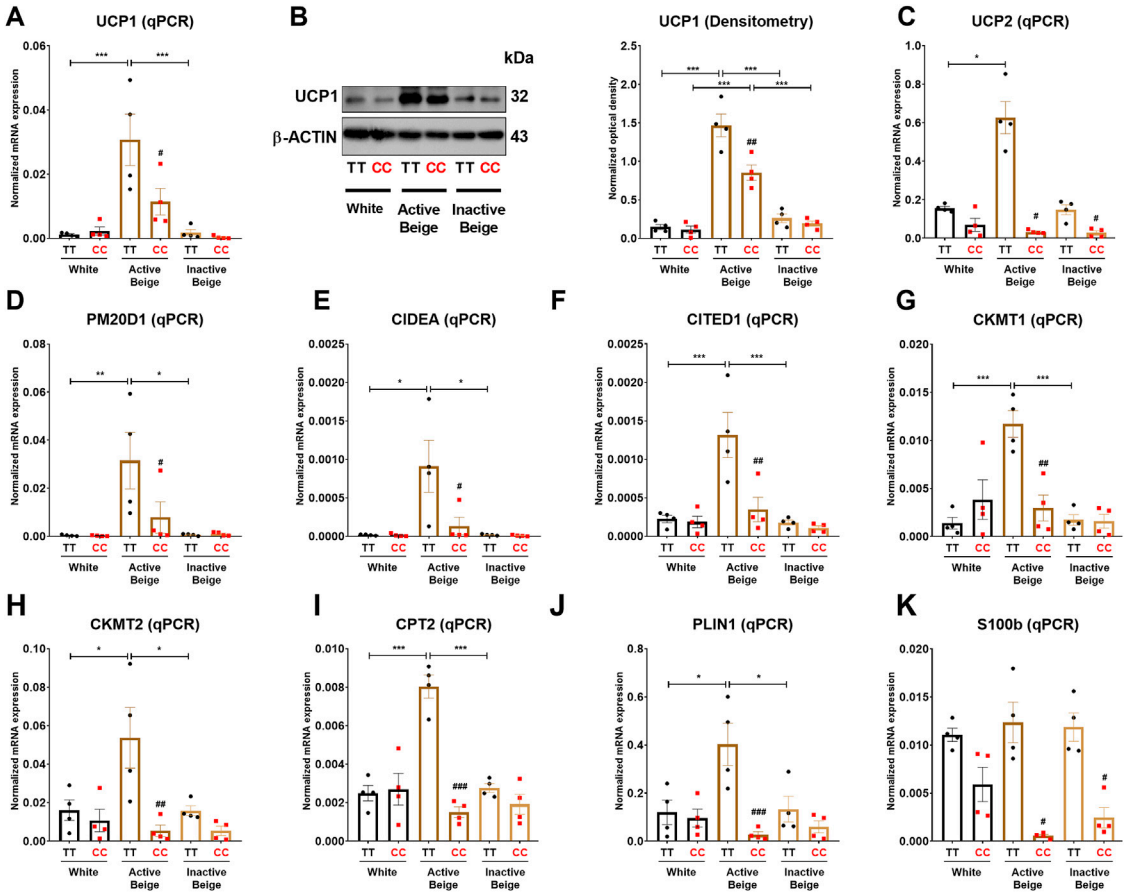


FIGURE 3
The effect of the differentiation protocols and alleles at *FTO* rs1421085 on the expression of thermogenesis markers in differentiated abdominal subcutaneous adipocytes. **(A, B)** The mRNA **(A)** and protein **(B)** expression of UCP1 measured by qPCR or immunoblotting. **(C–K)** The mRNA expression of *UCP2, PM20D1, CIDEA, CITED1, CKMT1* and *2, CPT2, PLIN1*, and *S100B* was analyzed by RT-qPCR. Statistical analysis was performed by ANOVA, n = 4 of each genotypes, */#$p < 0.05$, **/##$p < 0.01$, and ***/###$p < 0.001$. *analysis was performed to compare the effect of the applied differentiation protocol in the same genotype. #analysis was performed to compare *FTO* rs1421085 TT and CC genotypes within the same differentiation protocol.

## 3.3 Thermogenic marker genes were less expressed in active beige adipocytes carrying *FTO* obesity-risk alleles

Since we observed that the allelic discrimination at *FTO* rs1421085 SNP influences the expression of thermogenic and BATLAS markers, we went further to investigate the expression of thermogenic genes at mRNA and protein levels in abdominal SC adipocytes. Our results showed that the mRNA expression of *UCP1* was higher in active beige as compared to white or inactive beige adipocytes with *FTO* risk-free alleles, however, this difference was not observed in obesity-risk carriers (Figure 3A). At the protein level, we observed that active beige adipocytes expressed more UCP1 as compared to white or inactive beige adipocytes regardless the *FTO* rs1421085 genotypes, however, less UCP1 protein amount was detected in obesity-risk than in risk-free allele carrier active beige adipocytes (Figure 3B). Other thermogenic genes, such as *UCP2*, *PM20D1*, *CIDEA*, *CITED1*, *CKMT1* and *2*, *CPT2*, and *PLIN1* were also expressed higher in active beige adipocytes carrying risk-free alleles as compared to white or inactive beige adipocytes with the same TT variant, however, we did not observe these differences in *FTO* obesity-risk carrier samples (Figures 3D–J). As compared to risk-free carriers, active beige adipocytes with *FTO* obesity-risk genotype had lower expression of these thermogenic genes and also that of the neurotrophic factor *S100b*, which was postulated to stimulate sympathetic axon growth and to play an important role in BAT innervation (Zeng et al., 2019) (Figures 3A–K). These results are in accordance with our RNA-seq data suggesting the critical importance of *FTO* rs1421085 SNP in active beige adipocytes and the compromised effect of active beige differentiation protocol in the presence of obesity-risk alleles.

## 3.4 Active beige adipocytes with *FTO* obesity-risk genotype expressed less amount of mitochondrial complex subunits and had lower proton leak respiration

Having observed that *FTO* rs1421085 SNP affected the expression of thermogenic genes, our next aim was to investigate whether the expression of mitochondrial complex subunits and cellular respiration were also suppressed in adipocytes with obesity-risk alleles. We found that active beige adipocytes carrying *FTO* risk-free genotype had higher

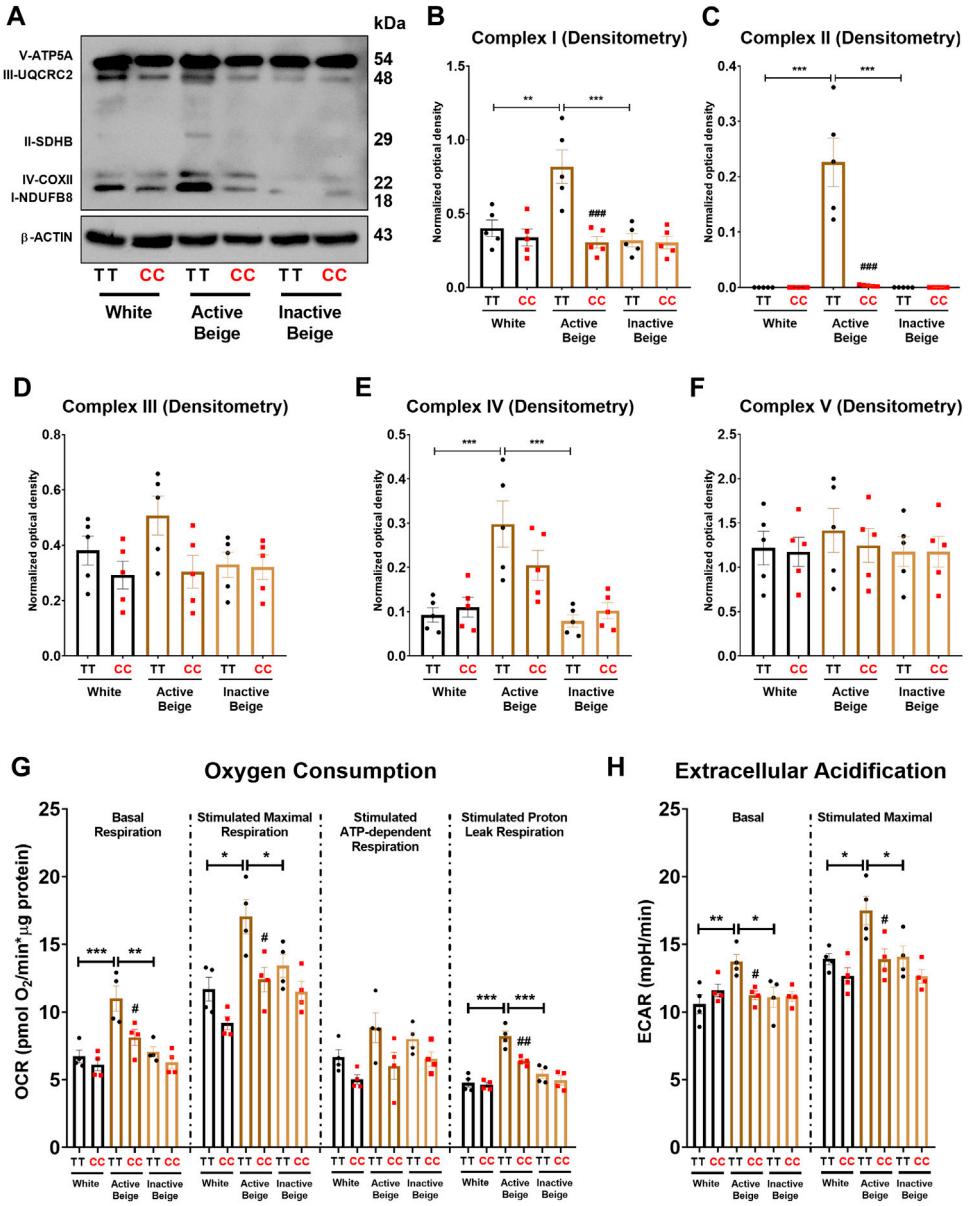


FIGURE 4
The effect of the differentiation protocols and alleles at *FTO* rs1421085 on the expression of mitochondrial complex subunits, oxygen consumption, and extracellular acidification. **(A–F)** Protein expression of mitochondrial complex subunits detected by immunoblotting. **(G, H)** Oxygen consumption at basal, dibutyryl-cAMP stimulated maximal, and stimulated proton leak respiration **(G)** and extracellular acidification **(H)** were quantified in white, active beige, and inactive beige adipocytes carrying *FTO* risk-free or obesity-risk genotypes by Seahorse extracellular flux analysis. Statistical analysis was performed by ANOVA, $n = 4$ of each genotypes, */#$p < 0.05$, **/##$p < 0.01$, and ***/###$p < 0.001$. *analysis was performed to compare the effect of the applied differentiation protocol in the same genotype. #analysis was performed to compare *FTO* rs1421085 TT and CC genotypes within the same differentiation protocol.

amounts of mitochondrial complex subunits I, II, and IV as compared to white or inactive beige adipocytes carrying the same TT genotype (Figures 4A–C, E). However, no difference was found between the three types of differentiation programs when adipocytes carried the obesity-risk variant (Figures 4A–C, E). Active beige adipocytes with *FTO* obesity-risk alleles had lower expression of mitochondrial complex subunits I, II, and IV as compared to the risk-free carriers (Figures 4A–C,E). We observed a similar but statistically not significant trend in the case of mitochondrial complex subunit III (Figure 4D), while the expression of complex V subunit was similar for all types of adipocytes regardless the *FTO* rs1421085 genotype (Figure 4F). Next, we measured the cellular respiration of the three types of adipocytes carrying *FTO* risk-free or obesity-risk alleles. In accordance with the mitochondrial complex subunit expression, we found that active beige adipocytes carrying risk-free genotype had higher respiration (at both basal and maximal stimulated conditions), stimulated proton leak respiration, and extracellular acidification as compared to white or inactive beige adipocytes, but this difference was not pronounced when the adipocytes carried the risk variant (Figures 4G, H). Stimulated ATP-dependent respiration was not affected significantly by either the

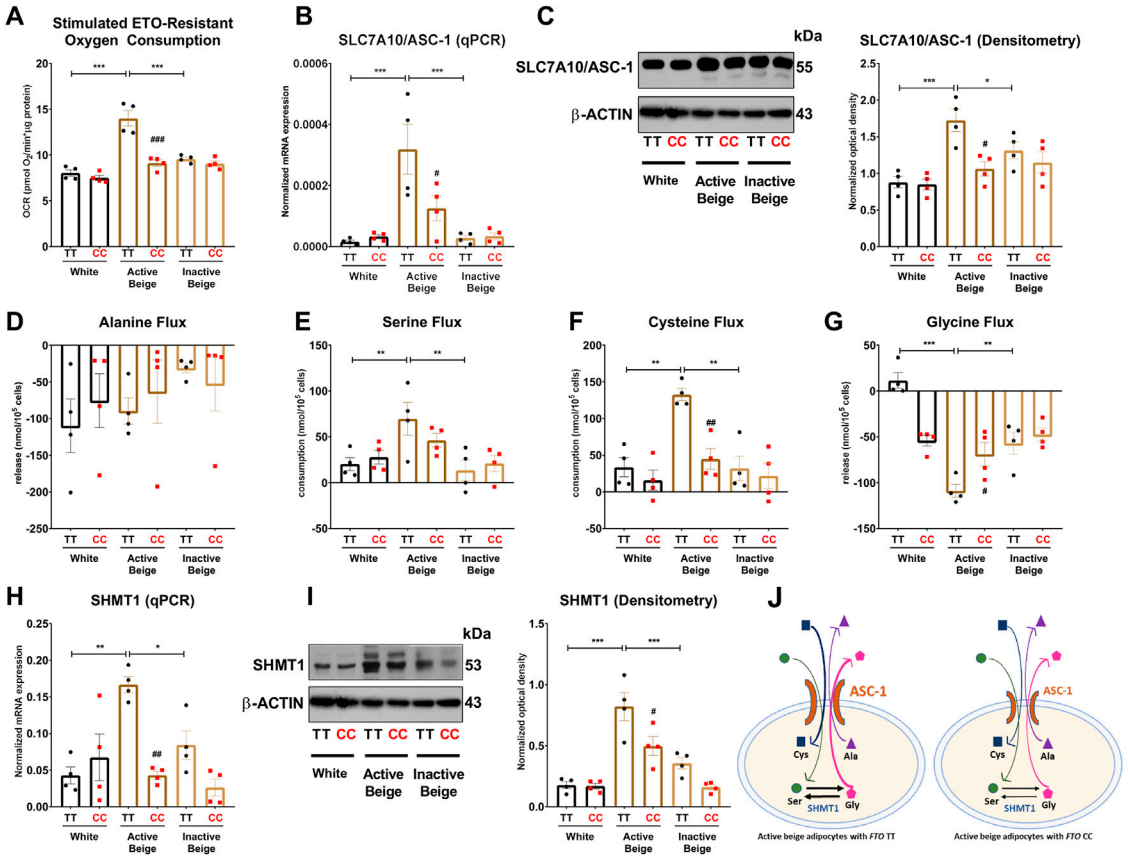


FIGURE 5
The effect of the differentiation protocols and alleles at *FTO* rs1421085 on the ASC-1-mediated amino acid flux and the expression of SHMT1 of differentiated abdominal subcutaneous adipocytes. **(A)** Etomoxir-resistant oxygen consumption was quantified in white, active beige, and inactive beige adipocytes carrying risk-free or obesity-risk genotypes by Seahorse extracellular flux analysis. **(B, C)** mRNA **(B)** and protein **(C)** expression of *SLC7A10*/ASC-1 by RT-qPCR and immunoblotting, $n = 4$ of each genotype. **(D–G)** Amino acids flux measured in the conditioned media of differentiated abdominal subcutaneous adipocytes, $n = 4$ of each genotype. **(H, I)** mRNA **(H)** and protein **(I)** expression of SHMT1 by RT-qPCR and immunoblotting, $n = 4$ of each genotype. **(J)** Graphical representation of ASC-1-mediated amino acid flux and SHMT1 enzyme activity in active beige adipocytes with *FTO* TT (left panel) and CC (right panel) alleles. Statistical analysis was performed by ANOVA. */#$p < 0.05$, **/##$p < 0.01$, and ***/###$p < 0.001$. *analysis was performed to compare the effect of the applied differentiation protocol in the same genotype. #analysis was performed to compare *FTO* rs1421085 TT and CC genotypes within the same differentiation protocol.

applied differentiation protocols or the *FTO* rs1421085 genotype (Figure 4G). Active beige adipocytes with *FTO* obesity-risk variant showed lower cellular respiration, especially stimulated proton leak respiration which reflects UCP1-dependent heat production, and extracellular acidification, which associates with glycolytic activity, as compared to risk-free carriers (Figures 4G, H). Intriguingly, the effect of *FTO* obesity-risk alleles on cellular respiration was observed in active beige but not in white or inactive beige adipocytes highlighting its exclusive effect in human abdominal SC adipocytes only when they are activated for thermogenesis.

## 3.5 Adipocytes carrying *FTO* obesity-risk genotype consume lower amounts of neutral amino acids when activated for thermogenesis

Active thermogenic adipocytes utilize metabolic substrates, such as carbohydrates, fatty acids, or amino acids to generate heat (Onogi and Ussar, 2022). Therefore, we aimed to investigate the fuel utilization by abdominal SC adipocytes with distinct *FTO* genotypes in three types of differentiation programs. Fatty acids are primarily released from lipid droplets via lipolysis (Cannon and Nedergaard, 2004; Townsend and Tseng, 2014). We found that the regulation of lipolysis in adipocytes and fatty acid metabolism gene expression pathways were downregulated in active beige adipocytes with *FTO* CC as compared to TT allele carriers (Figure 2E). Although murine brown adipocytes can compensate the lack of lipid droplets-derived fatty acids (Chitraju et al., 2020), our *ex vivo* model did not include fatty acids in the applied differentiation media. Furthermore, stimulated etomoxir-sensitive oxygen consumption, which correlates with the activity of fatty acid oxidation (Nagy et al., 2022), was not affected significantly by either the differentiation programs or the *FTO* genotypes (Supplementary Figure S4). ASC-1, which is encoded by *SLC7A10*, plays an important role in mediating alanine, serine, cysteine, and glycine consumption in human adipocytes derived from abdominal SC and deep neck regions (Jersin et al., 2021; Arianti et al., 2021). To

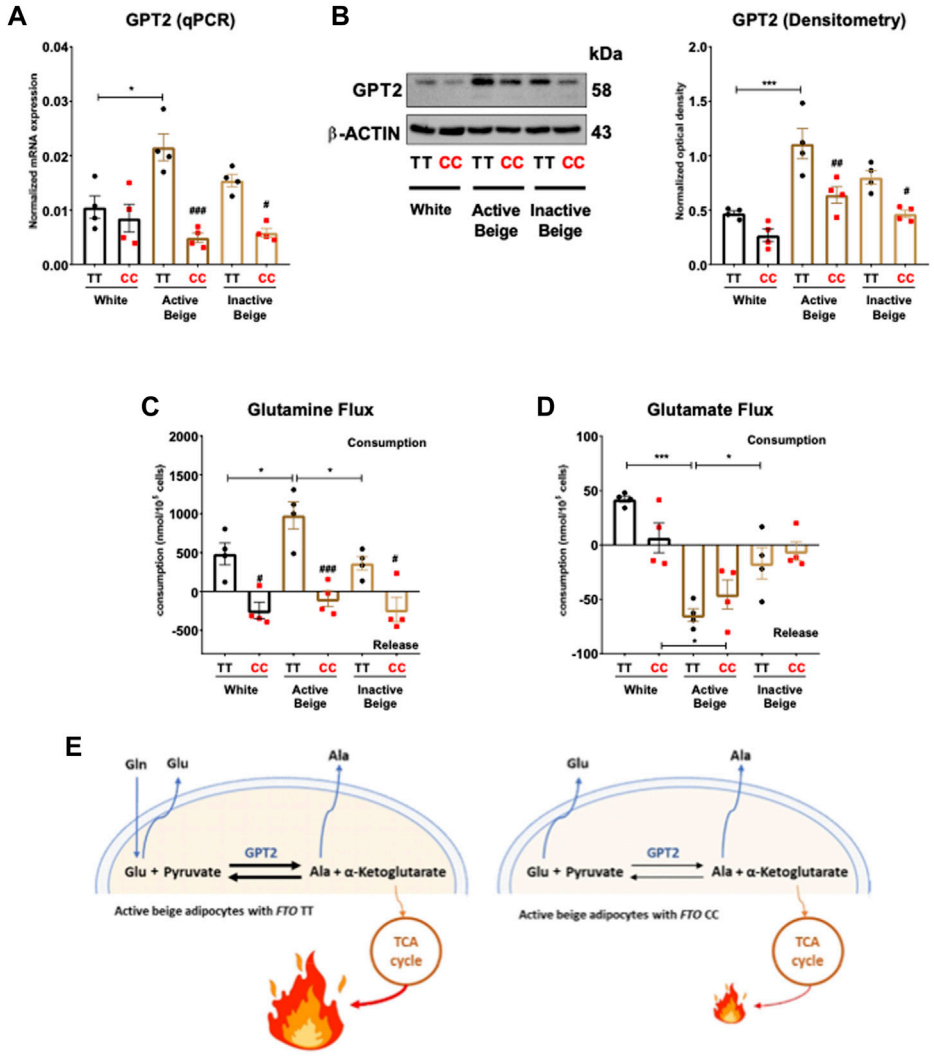


FIGURE 6
The effect of differentiation protocols and alleles at *FTO* rs1421085 on the expression of GPT2 and glutamine-glutamate flux of differentiated abdominal subcutaneous adipocytes. **(A, B)** mRNA **(A)** and protein **(B)** expression of GPT2 by RT-qPCR and immunoblotting, $n = 4$ of each genotype. **(C, D)** Glutamine **(C)** and glutamate **(D)** flux measured in the conditioned media of differentiated abdominal subcutaneous adipocytes, $n = 4$ of each genotypes. **(E)** Graphical representation of glutamine-glutamate flux and GPT2 enzyme activity in active beige adipocytes with *FTO* TT (left panel) and CC (right panel) alleles. Statistical analysis was performed by ANOVA. */#$p < 0.05$, **/##$p < 0.01$, and ***/###$p < 0.001$. *analysis was performed to compare the effect of the applied differentiation protocol in the same genotype. #analysis was performed to compare *FTO* rs1421085 TT and CC genotypes within the same differentiation protocol.

evaluate the preferable energy sources during thermogenic activation, we monitored the oxygen consumption of adipocytes upon etomoxir (inhibitor of carnitine palmitoyltransferase-1) administration. ETO-R respiration, which reflects the activity of carbohydrate and amino acid oxidation (Nagy et al., 2022), was higher in active beige adipocytes with *FTO* risk-free genotype than in white or inactive beige adipocytes carrying the same TT genotype (Figure 5A). Active beige adipocytes with *FTO* obesity-risk alleles had lower level of ETO-R oxygen consumption as compared to risk-free carriers (Figure 5A). These observations suggest less pronounced carbohydrate and/or amino acid utilization in active beige adipocytes of CC carriers at *FTO* rs1421085.

Because we found *SLC7A10* (encoding alanine-serine-cysteine transporter, ASC-1) as a DEG among the most abundantly expressed genes in active beige adipocytes with *FTO* risk-free genotype (Figure 1H; Supplementary Table S7), we decided to investigate the effect of the applied differentiation protocols and *FTO* rs1421085 SNP on the expression of ASC-1 and the consumption of ASC-1 cargos by the adipocytes. We found that active beige adipocytes with risk-free alleles expressed higher mRNA level of *SLC7A10* as compared to white or inactive beige ones that carried the same TT variant (Figure 5B), which could be confirmed at ASC-1 protein level (Figure 5C). The presence of the *FTO* rs1421085 SNP resulted in lower expression of *SLC7A10* in active beige adipocytes; this effect was statistically significant at protein level but not at mRNA level (Figures 5B,C). Next, we measured the consumption of amino acids in the conditioned media obtained from the three types of differentiated adipocytes with CC or TT

alleles, respectively. The applied differentiation programs did not affect the release of alanine regardless of the *FTO* allele status (Figure 5D). In the case of adipocytes with *FTO* risk-free genotype, we found that active beige ones consumed higher amounts of serine (Figure 5E) and cysteine (Figure 5F) and released more glycine as compared to white or inactive beige adipocytes (Figure 5G). In accordance with the aforementioned gene expression and ETO-R oxygen consumption results, we did not observe any differences in the fluxes of these amino acids between the three types of differentiation protocols in adipocytes with obesity-risk alleles. Active beige adipocytes with obesity-risk genotype consumed lower amount of cysteine as compared to risk-free carriers (Figure 5F), but significant effect of the SNP was not observed on serine consumption (Figure 5E) suggesting that other amino acid transporters might compensate for the reduced expression of ASC-1.

Our RNA-seq data showed that serine hydroxymethyltransferase (SHMT) 1, which catalyzes the conversions of L-serine and tetrahydrofolate (THF) to glycine and 5,10-methylene-THF (5,10-$CH_2$-THF), was expressed lower in active beige adipocytes with *FTO* obesity-risk as compared to risk-free carriers (Supplementary Table S5). We validated our RNA-seq data of SHMT1 expression by RT-qPCR (Figure 5H) and immunoblotting (Figure 5I). We also found that active beige adipocytes had higher protein content of SHMT1 as compared to white or inactive beige adipocytes in the presence of the *FTO* risk-free variant, but this difference was not observed in obesity-risk carrier samples (Figure 5I). The proposed model of ASC-1 mediated amino acid flux and possible interconversion of serine and glycine by SHMT1 are summarized in Figure 5J.

According to the RNA-seq data, active beige adipocytes carrying obesity-risk genotype expressed lower mRNA level of glutamic pyruvic transaminase (GPT) 2 as compared to risk-free allele carriers (Supplementary Table S5). In the case of adipocytes with *FTO* risk-free alleles, active beige cells expressed more GPT2 both at mRNA (Figure 6A) and protein level (Figure 6B) as compared to white ones. We also observed lower expression of GPT2 in active and inactive beige adipocytes with *FTO* obesity-risk genotype as compared to risk-free allele carriers (Figures 6A, B). Active beige adipocytes carrying risk-free genotypes also consumed higher amount of glutamine as compared to white or inactive beige adipocytes carrying the same TT genotype, but no difference was observed among the three types of differentiation protocols in the case of the samples with obesity-risk alleles. On the contrary to risk-free carrier cells, adipocytes with *FTO* obesity-risk genotype did not consume glutamine irrespective to the applied differentiation protocols (Figure 6C). In contrast, we found that active beige adipocytes released higher amount of glutamate as compared to inactive ones, while white adipocytes rather consumed that amino acid. The consumption of glutamate did not depend on the allelic discrimination at *FTO* rs1421085 locus (Figure 6D). In the case of adipocytes with TT alleles, active beige cells consumed less aspartate and more leucine than white or inactive beige ones, however, the consumption of asparagine, isoleucine, threonine, valine, histidine, lysine, tyrosine, tryptophan, proline, methionine, phenylalanine, and arginine was not significantly affected by the applied protocols. Histidine was consumed by adipocytes with risk-free alleles, however, it was released by obesity-risk allele carrier ones irrespective of the applied differentiation. The same trend was found in the case of lysine without observing statistically significant differences. Adipocytes with CC genotype tended to consume valine, however, it was released by the adipocytes with TT genotype. The *FTO* alleles did not affect the consumption of aspartate, asparagine, leucine, isoleucine, threonine, tyrosine, tryptophan, proline, methionine, phenylalanine, and arginine at a statistically significant level (Supplementary Figure S5). These results suggest that active beige adipocytes with *FTO* TT alleles utilize higher amounts of glutamine, which can be converted to glutamate, presumably to generate more of the TCA cycle intermediate, α-ketoglutarate which may contribute to elevated heat generation (Figure 6E).

# 4 Discussion

Abdominal fat is classified into SC and intraabdominal fat, which is mainly composed of visceral or intraperitoneal WAT (Mårin et al., 1992; Wajchenberg, 2000). Several studies reported that accumulation of visceral WAT is strongly associated with the risk of metabolic disorders (Matsuzawa et al., 1995; Fujimoto et al., 1994; Banerji et al., 1999), whereas other studies claimed that abdominal SC WAT may possess a protective role (McLaughlin et al., 2011; Patel and Abate, 2013). A more recent study using an elegant PET/CT technique, Leitner et al. (2017) reported that human BAT or brownable adipose tissue can be found in cervical, supraclavicular, axillary, mediastinal, paraspinal, and abdominal depots. In this study, we performed RNA-seq on human abdominal SC derived adipocytes with *FTO* rs1421085 risk-free or obesity-risk genotypes, which were differentiated by applying three types of protocols: white, active, or inactive beige. Irrespective to the *FTO* genotypes, we found that active beige adipocytes exerted greater thermogenic potential, marked by higher expression of thermogenic genes and browning capacity quantified by ProFAT, as compared to white or inactive beige cells. Our results suggest that human abdominal SC adipocytes have a significant thermogenic potential when they are activated using active beige differentiation protocol driven by a PPARγ agonist and adrenergic stimulation. However, this potential subsides when adipocytes are inactivated through beige to white transition. This is in line with our previous study which has reported that beige to white transition leads to increased mitophagy resulting in the appearance of white-like phenotype and reduced thermogenesis (Vámos et al., 2022). Other studies also revealed that beige adipocytes in mice gradually lose their thermogenic morphology and capacity after the external stimuli, such as β-adrenergic agonist or cold exposure, were withdrawn (Altshuler-Keylin et al., 2016; Rosenwald et al., 2013). The loss of thermogenic characteristics in murine beige adipocytes was coupled with increased mitophagy, which was mediated by parkin (Lu et al., 2018; Sarraf and Youle, 2018). The comparison of active beige and white or inactive beige adipocytes found 100 and 164 genes, which were commonly more and less expressed, respectively, in active beige adipocytes. Notably, several well-known thermogenesis markers, such as *CITED1*, *PM20D1*, *PLIN5*, *GK*, and *AQP3* were commonly upregulated in active beige as compared to white or inactive beige adipocytes. No DEGs were found in the comparison of white and inactive beige

adipocytes indicating a high similarity of the gene expression profiles in these two differentiation programs.

Dibutyryl-cAMP is extensively used to mimic *in vivo* thermogenesis due to its ability to penetrate the cell membrane (Cypess et al., 2013). In contrast to cAMP, which can be hydrolyzed by phosphodiesterase (PDE), dibutyryl-cAMP is resistant to degradation by PDE (Jarett and Smith, 1974; Blecher, 1971). cAMP activates protein kinase A (PKA), which phosphorylates various proteins and initiate consecutive cascades of additional protein kinases (Daniel et al., 1998). More recently, a role has emerged for PKA in the regulation of gene transcription (Daniel et al., 1998; London and Stratakis, 2022). When we administered dibutyryl-cAMP in the middle of active and inactive beige differentiation programs (at day 14 for 4 h) we found that the effect of the compound on the thermogenic gene expression was sustained until the end of the differentiation of active beige, but not in inactive beige (undergoing beige to white transition) adipocytes. This suggests that the effect of dibutyryl-cAMP can be maintained for a long period of time in beige adipocytes. Activation of cAMP response element binding protein (CREB) is one of the most studied links between PKA and gene expression regulation (Daniel et al., 1998). Daniel et al. (1998) described that cAMP increased the mRNA level of PDE, although the molecular mechanism of this regulation remained elusive. We also found that the expression of *PDE1B* was high in active beige adipocytes suggesting active cAMP-driven signaling. In another set of experiments, we found that the mRNA expression of *UCP1* was higher in active beige as compared to regularly differentiated beige adipocytes (28 days differentiation driven by rosiglitazone without dibutyryl-cAMP administration at day 14) (Supplementary Figure S6) suggesting that dibutytyl-cAMP treatment at the middle of beige differentiation program further enhances the thermogenic capacity of abdominal SC adipocytes at a sustained manner.

We also evaluated the effect of rs1421085 T-to-C SNP of the *FTO* gene, which interrupts a conserved motif for ARID5B repressor, resulting in elevated expression of IRX3 and IRX5 during the early stage of adipocyte differentiation. As the consequence, the commitment of the cells diverts from beige towards the white program and lipid storage increases (Claussnitzer et al., 2015). When the gene expression profiles of the three types of adipocytes were analyzed by segregating the *FTO* rs1421085 risk-free (TT) and obesity-risk (CC) allele carrier samples, intriguingly, we found that the SNP affected the gene expression profile, in particular the expression of thermogenic markers (*CITED1*, *CIDEC*, *PLIN1*, *LIPE, CKMT2*, and *S100b*), in active beige adipocytes, but not in white or inactive beige adipocytes. CIDEC, PLIN1, and LIPE are lipid droplet-associated proteins, which regulate triglyceride accumulation and lipolysis (Wolins et al., 2006; Puri et al., 2008). Decreased expression of these genes in active beige adipocytes with *FTO* obesity-risk alleles may contribute to the downregulation of lipolysis in the SC adipose tissue of affected individuals. CKMT1a/b and CKMT2 mitochondrial creatine kinases phosphorylate creatine generating phosphocreatine and contribute to UCP1-independent heat generation via creatine futile cycle (Kazak et al., 2015). S100b protein was proposed to play a role in the sympathetic innervation of thermogenic adipose tissue by stimulating neurite outgrowth from sympathetic neurons through calsyntenin (CLSTN) 3β axis (Zeng et al., 2019). Reduced expression or loss of function of S100b resulted in disrupted sympathetic innervation leading to reduced thermogenesis in brown or beige adipocytes. Of note, recently, it was shown that adipose tissue specific CLSTN3$\beta^{-/-}$ mice did not have defects in the sympathetic innervation and adrenergic signaling of BAT (Qian et al., 2023). Decreased expression of S100b in abdominal SC adipocytes with *FTO* obesity-risk carriers, however, might partially contribute to lower thermogenic capacity in abdominal SC WAT even when the adipocytes are activated for heat production. Importantly, genes overrepresented in metabolic, especially in energy metabolism-related pathways, such as TCA cycle, lipolysis, pyruvate metabolism, and PPAR signaling were downregulated in active beige adipocytes with obesity-risk genotypes as compared to risk-free allele carriers, indicating lower energy dissipation in active beige adipocytes with CC alleles. Our findings suggest that C alleles at *FTO* rs1421085 suppress the thermogenic activation of human abdominal SC adipocytes; even long-term rosiglitazone treatment could not compensate for the effect of the obesity-risk genotype. In addition, we also observed that active beige adipocytes carrying *FTO* obesity-risk alleles exerted similar transcriptomic profiles as white or inactive beige adipocytes. This is in association with our previous study, which reported that the thermogenically prone human neck derived adipocytes carrying *FTO* obesity-risk genotype had lower expression of thermogenic genes, such as *CKMT1A/B*, *CITED1*, *PPARGC1A/B*, and *CPT1B* and genes involved in respiratory electron transport, fatty acid metabolism, and the signaling by retinoic acid pathways (Tóth et al., 2020).

Active heat producing adipocytes utilize higher amounts of nutrients, such as glucose, fatty acids, and amino acids to provide sufficient fuel for thermogenesis and solute carrier (SLC) transporters play a crucial role in mediating the transport of these molecules (Cypess et al., 2009; Virtanen et al., 2009; Wu et al., 2006; Yoneshiro et al., 2019). Our data showed that active beige adipocytes carrying risk-free genotype had higher ETO-R oxygen consumption that reflects carbohydrate and amino acid utilization and expressed higher level of the neutral amino acid transporter, ASC-1 (encoded by *SLC7A10*) as compared to white or inactive beige adipocytes with the same TT genotypes, whereas there was no difference when the three types of adipocytes with *FTO* obesity-risk alleles were compared. ASC-1 has been recently identified as a novel regulator of energy metabolism in human SC adipose tissue elevating mitochondrial respiration and preventing development of adipocyte hypertrophy and insulin resistance (Jersin et al., 2021). Our previous study reported that ASC-1-mediated uptake of serine, cysteine, and glycine is essential for efficient thermogenic response upon adrenergic stimulation in human neck derived adipocytes (Arianti et al., 2021). The role of ASC-1 in adipose tissue has been comprehensively reviewed by Jersin et al. (2022) highlighting its beneficial effects in enhancing mitochondrial activity and lowering reactive oxygen species production in white adipocytes. We also found that the consumption of serine and cysteine was higher in active beige as compared to white or inactive beige adipocytes with *FTO* risk-free genotype. Lower consumption of these amino acids was observed in active beige adipocytes with *FTO* obesity-risk genotype as compared to risk-free allele carriers. In addition, we observed release of less glycine by active beige adipocytes carrying obesity-risk genotypes as compared to those with risk-free alleles. Serine is an important

metabolic source to generate one-carbon units in mammalian cells (de Koning et al., 2003), which are produced by both isoforms of SHMT enzymes, SHMT1 (cytosolic) and SHMT2 (mitochondrial), resulting in glycine. Our data showed that active beige adipocytes carrying *FTO* obesity-risk genotype expressed lower level of SHMT1 as compared to risk-free allele carrier ones suggesting lower generation of one-carbon units in thermogenic adipocytes with *FTO* obesity-risk genotype. We also revealed that one-carbon metabolism pathway, in which SHMT1 and GPT2 participate, was less expressed in active beige adipocytes with *FTO* obesity-risk alleles. One-carbon unit metabolism forms a functional interaction with mitochondrial oxidative phosphorylation that is crucial for ATP or heat generation in mammalian cells (Lucas et al., 2018). Lower serine influx that can result in the decrease of one-carbon unit levels may lead to lower amounts of mitochondrial complex subunits I, II, and IV in active beige adipocytes carrying *FTO* obesity-risk genotype. As a consequence, stimulated maximal and proton leak respiration, which positively correlates with UCP1 activity, and extracellular acidification were suppressed in active beige adipocytes originated from *FTO* obesity-risk genotype carriers.

Active beige adipocytes with risk-free genotype also consumed higher amounts of glutamine as compared to white or inactive beige adipocytes carrying the same alleles. The *FTO* obesity-risk carrier adipocytes did not consume glutamine irrespective of the differentiation protocol used. Glutamine is the most abundant free amino acid in the circulation (Hall et al., 1996) and in the applied DMEM-F12 cell culture medium. It is one of the main fuel resources for cells supplying carbon atoms to drive the TCA cycle and generate ATP (or heat) (Scalise et al., 2016). Lower expression of *GPT2* and glutamine consumption may contribute to the downregulation of pyruvate metabolism and TCA cycle pathway in active beige adipocytes with obesity-risk alleles. In addition, sodium-dependent neutral amino acid transporter type 2 (ASCT2)/SLC1A5-mediated glutamine uptake is important for histone acetylation and methylation in murine WAT. Downregulation of ASCT2 as the consequence of disrupted PPAR-γ expression in WAT of obese mice led to reduced glutamine uptake and correlated with decreased H3K27ac and H3K4me3 at the *Bmal1* promoter (Wang et al., 2022). A recent publication reported that disrupted function of adipocyte ASC-1 led to the elevation of lipid storage and diverted adipocytes from releasing to consuming glutamate and aspartate (Jersin et al., 2023). Our data showed that active beige adipocytes with risk-free *FTO* genotype, which expressed the highest level of ASC-1, consumed less aspartate as compared to white or inactive beige adipocytes. In contrast to white adipocytes that consumed glutamate, active beige adipocytes released it into the extracellular space. Altogether, our findings suggest that adipocytes derived from abdominal SC tissues of *FTO* obesity-risk carriers exert lower uptake of several amino acids as substrates of cellular metabolic processes contributing to compromised energy dissipation.

The positive correlation between *FTO* rs1421085 SNP and obesity or increased body mass index has been reported in several populations such as Estonian children (Katus et al., 2020), Chinese children (Wang et al., 2013), Iranian adults (Najd-Hassan-Bonab et al., 2022), Arabic (Hebbar et al., 2020), Pakistani (Rana and Bhatti, 2020), Balinese (Priliani et al., 2020), and Mexican Mayan girls (González-Herrera et al., 2019). Through genome-wide association meta-analyses of more than 100000 individuals of European ancestry without diabetes, *FTO* rs1421085 SNP was found to be significantly associated with fasting insulin levels (Scott et al., 2012). A recently published study by Laber et al. (2021) showed that an engineered deletion of the rs1421085 conserved cis-regulatory module in mice prevented high fat diet-induced obesity, decreased whole-body fat mass, and elevated the number of mitochondria in WAT. Our presented data highlight the critical effect of *FTO* rs1421085 SNP on human abdominal SC adipocytes only when they are activated for thermogenesis. Leitner *et al.* (2017) reported that large amounts of brownable adipocytes can be found in abdominal SC fat whose *in vivo* relevance in humans is still unrevealed. Furthermore, the activation of these adipocytes in humans to reduce adiposity remains challenging. Although these cells can be potentially activated, our previous (Tóth et al., 2020) and present results have pointed to a strong effect of obesity-risk genotype at *FTO* rs1421085 SNP, which has a high prevalence in the European population (Dina et al., 2007; Babenko et al., 2019; Huđek et al., 2017) and Mexican children (12.93%–18.67%) (González-Herrera et al., 2019) that must be overcome to enable efficient thermogenesis and weight loss. Our findings further support the importance of genetic background not only in the pathogenesis of obesity but also in the potential effectivity of novel therapeutic approaches which target thermogenesis-related energy dissipation.

## Data availability statement

The RNA-seq datasets generated and analyzed for this study can be found in the Sequence Read Archive (SRA) database [https://www.ncbi.nlm.nih.gov/sra] under accession number PRJNA928240.

## Ethics statement

The studies involving human participants were reviewed and approved by Medical Research Council of Hungary (20571-2/2017/EKU). The patients/participants provided their written informed consent to participate in this study.

## Author contributions

AV, RiA, BV, RaA, AS performed the experiments. EK, RiA, and AV conceptualized the research, with inputs from LF. SP performed the RNA-seq. AG and ÉC carried out measurements of amino acid concentration. IC and GM acquired and analyzed confocal microscopy images. CL and ZB provided adipose tissue samples. EK and LF supervised the research and acquired funding. RiA and AV wrote the original draft of the manuscript. EK and LF edited the final version of the manuscript. All authors contributed to the article and approved the submitted version.

## Funding

This research was funded by the National Research, Development and Innovation Office (NKFIH-FK131424 and K129139) of Hungary. AV and BV was supported by the ÚNKP-22-3-II and ÚNKP-22-3-I New National Excellence Program of the

Ministry for Culture and Innovation from the source of the National Research, Development and Innovation Fund.

## Acknowledgments

We thank Zsuzsa Szondy for her exceptional help in reviewing the manuscript before its submission and Jennifer Nagy for technical assistance.

## Conflict of interest

The authors declare that the research was conducted in the absence of any commercial or financial relationships that could be construed as a potential conflict of interest.

## Publisher's note

All claims expressed in this article are solely those of the authors and do not necessarily represent those of their affiliated organizations, or those of the publisher, the editors and the reviewers. Any product that may be evaluated in this article, or claim that may be made by its manufacturer, is not guaranteed or endorsed by the publisher.

## Supplementary material

The Supplementary Material for this article can be found online at: https://www.frontiersin.org/articles/10.3389/fcell.2023.1155673/full#supplementary-material

## References

Altshuler-Keylin, S., Shinoda, K., Hasegawa, Y., Ikeda, K., Hong, H., Kang, Q., et al. (2016). Beige adipocyte maintenance is regulated by autophagy-induced mitochondrial clearance. *Cell Metab.* 24 (3), 402–419. doi:10.1016/j.cmet.2016.08.002

Arianti, R., Vinnai, B. Á., Tóth, B. B., Shaw, A., Csősz, É., Vámos, A., et al. (2021). ASC-1 transporter-dependent amino acid uptake is required for the efficient thermogenic response of human adipocytes to adrenergic stimulation. *FEBS Lett.* 595 (16), 2085–2098. doi:10.1002/1873-3468.14155

Babenko, V., Babenko, R., Gamieldien, J., and Markel, A. (2019). FTO haplotyping underlines high obesity risk for European populations. *BMC Med. Genomics* 12 (Suppl. 2), 46. doi:10.1186/s12920-019-0491-x

Banerji, M. A., Faridi, N., Atluri, R., Chaiken, R. L., and Lebovitz, H. E. (1999). Body composition, visceral fat, leptin, and insulin resistance in Asian Indian men. *J. Clin. Endocrinol. Metab.* 84 (1), 137–144. doi:10.1210/jcem.84.1.5371

Bjune, J. I., Haugen, C., Gudbrandsen, O., Nordbø, O. P., Nielsen, H. J., Våge, V., et al. (2019). IRX5 regulates adipocyte amyloid precursor protein and mitochondrial respiration in obesity. *Int J Obes (Lond).*, 43 (11), 2151–2162. doi:10.1038/s41366-018-0275-y

Bjune, J. I., Dyer, L., Røsland, G. V., Tronstad, K. J., Njølstad, P. R., Sagen, J. V., et al. (2020). The homeobox factor Irx3 maintains adipogenic identity. *Metab. Clin. Exp.* 103, 154014. doi:10.1016/j.metabol.2019.154014

Blecher, M. (1971). Biological effects and catabolic metabolism of 3',5'-cyclic nucleotides and derivatives in rat adipose tissue and liver. *Metab. Clin. Exp.* 20 (1), 63–77. doi:10.1016/0026-0495(71)90060-6

Cannon, B., and Nedergaard, J. (2004). Brown adipose tissue: Function and physiological significance. *Physiol. Rev.* 84 (1), 277–359. doi:10.1152/physrev.00015.2003

Chan, M., Lim, Y. C., Yang, J., Namwanje, M., Liu, L., and Qiang, L. (2019). Identification of a natural beige adipose depot in mice. *J. Biol. Chem.* 294 (17), 6751–6761. doi:10.1074/jbc.RA118.006838

Cheng, L., Wang, J., Dai, H., Duan, Y., An, Y., Shi, L., et al. (2021). Brown and beige adipose tissue: A novel therapeutic strategy for obesity and type 2 diabetes mellitus. *Adipocyte* 10 (1), 48–65. doi:10.1080/21623945.2020.1870060

Cheng, Y., Jiang, L., Keipert, S., Zhang, S., Hauser, A., Graf, E., et al. (2018). Prediction of adipose browning capacity by systematic integration of transcriptional profiles. *Cell Rep.* 23 (10), 3112–3125. doi:10.1016/j.celrep.2018.05.021

Chitraju, C., Fischer, A. W., Farese, R. V., Jr, and Walther, T. C. (2020). Lipid droplets in Brown adipose tissue are dispensable for cold-induced thermogenesis. *Cell Rep.* 33 (5), 108348. doi:10.1016/j.celrep.2020.108348

Christakis, N. A., and Fowler, J. H. (2007). The spread of obesity in a large social network over 32 years. *N. Engl. J. Med.* 357 (4), 370–379. doi:10.1056/NEJMsa066082

Claussnitzer, M., Dankel, S. N., Kim, K. H., Quon, G., Meuleman, W., Haugen, C., et al. (2015). FTO obesity variant circuitry and adipocyte browning in humans. *N. Engl. J. Med.* 373 (10), 895–907. doi:10.1056/NEJMoa1502214

Cypess, A. M., Lehman, S., Williams, G., Tal, I., Rodman, D., Goldfine, A. B., et al. (2009). Identification and importance of Brown adipose tissue in adult humans. *N. Engl. J. Med.* 360 (15), 1509–1517. doi:10.1056/NEJMoa0810780

Cypess, A. M., White, A. P., Vernochet, C., Schulz, T. J., Xue, R., Sass, C. A., et al. (2013). Anatomical localization, gene expression profiling and functional characterization of adult human neck Brown fat. *Nat. Med.* 19 (5), 635–639. doi:10.1038/nm.3112

Daniel, P. B., Walker, W. H., and Habener, J. F. (1998). Cyclic AMP signaling and gene regulation. *Annu. Rev. Nutr.* 18, 353–383. doi:10.1146/annurev.nutr.18.1.353

de Koning, T. J., Snell, K., Duran, M., Berger, R., Poll-The, B. T., and Surtees, R. (2003). L-serine in disease and development. *Biochem. J.* 371 (Pt 3), 653–661. doi:10.1042/BJ20021785

Dina, C., Meyre, D., Gallina, S., Durand, E., Körner, A., Jacobson, P., et al. (2007). Variation in FTO contributes to childhood obesity and severe adult obesity. *Nat. Genet.* 39 (6), 724–726. doi:10.1038/ng2048

Felix, J. F., Bradfield, J. P., Monnereau, C., van der Valk, R. J., Stergiakouli, E., Chesi, A., et al. Bone Mineral Density in Childhood Study BMDCS (2016). Genome-wide association analysis identifies three new susceptibility loci for childhood body mass index. *Hum. Mol. Genet.* 25(2), 389–403. doi:10.1093/hmg/ddv472

Frayling, T. M., Timpson, N. J., Weedon, M. N., Zeggini, E., Freathy, R. M., Lindgren, C. M., et al. (2007). A common variant in the FTO gene is associated with body mass index and predisposes to childhood and adult obesity. *Sci. (New York, N.Y.)* 316 (5826), 889–894. doi:10.1126/science.1141634

Frühbeck, G., Kiortsis, D. N., and Catalán, V. (2018). Precision medicine: Diagnosis and management of obesity. *Diabetes and Endocrinol.* 6 (3), 164–166. doi:10.1016/S2213-8587(17)30312-1

Frühbeck, G., Toplak, H., Woodward, E., Yumuk, V., Maislos, M., Oppert, J. M., et al. (2013). Obesity: The gateway to ill health - an EASO position statement on a rising public health, clinical and scientific challenge in europe. *Obes. facts*, 6(2), 117–120. doi:10.1159/000350627

Fujimoto, W. Y., Abbate, S. L., Kahn, S. E., Hokanson, J. E., and Brunzell, J. D. (1994). The visceral adiposity syndrome in Japanese-American men. *Obes. Res.* 2 (4), 364–371. doi:10.1002/j.1550-8528.1994.tb00076.x

González-Herrera, L., Zavala-Castro, J., Ayala-Cáceres, C., Pérez-Mendoza, G., López-González, M. J., Pinto-Escalante, D., et al. (2019). Genetic variation of FTO: rs1421085 T>C, rs8057044 G>A, rs9939609 T>A, and copy number (CNV) in Mexican mayan school-aged children with obesity/overweight and with normal weight. *Am. J. Hum. Biol. Off. J. Hum. Biol. Counc.* 31 (1), e23192. doi:10.1002/ajhb.23192

Guba, A., Bába, O., Tőzsér, J., Csősz, É., and Kalló, G. (2022). Fast and sensitive quantification of AccQ-tag derivatized amino acids and biogenic amines by UHPLC-UV analysis from complex biological samples. *Metabolites* 12 (3), 272. doi:10.3390/metabo12030272

Hall, J. C., Heel, K., and McCauley, R. (1996). Glutamine. *Br. J. Surg.* 83 (3), 305–312. doi:10.1002/bjs.1800830306

Heaton, J. M. (1972). The distribution of Brown adipose tissue in the human. *J. Anat.* 112 (Pt 1), 35–39.

Hebbar, P., Abu-Farha, M., Mohammad, A., Alkayal, F., Melhem, M., Abubaker, J., et al. (2020). FTO variant rs1421085 associates with increased body weight, soft lean mass, and total body water through interaction with ghrelin and apolipoproteins in arab population. *Front. Genet.* 10, 1411. doi:10.3389/fgene.2019.01411

Herman, M. A., and Rosen, E. D. (2015). Making biological sense of GWAS data: Lessons from the FTO locus. *Cell metab.* 22 (4), 538–539. doi:10.1016/j.cmet.2015.09.018

Heymsfield, S. B., and Wadden, T. A. (2017). Mechanisms, pathophysiology, and management of obesity. *N. Engl. J. Med.* 376 (3), 254–266. doi:10.1056/NEJMra1514009

Huđek, A., Škara, L., Smolkovič, B., Kazazić, S., Ravlić, S., Nanić, L., et al. (2017). Higher prevalence of FTO gene risk genotypes AA rs9939609, CC rs1421085, and GG

rs17817449 and saliva containing *Staphylococcus aureus* in obese women in Croatia. *Nutr. Res. (New York, N.Y.)* 50, 94–103. doi:10.1016/j.nutres.2017.12.005

Imamura, M., Takahashi, A., Yamauchi, T., Hara, K., Yasuda, K., Grarup, N., et al. (2016). Genome-wide association studies in the Japanese population identify seven novel loci for type 2 diabetes. *Nat. Commun.* 7, 10531. doi:10.1038/ncomms10531

Jarett, L., and Smith, R. M. (1974). Mode of action of N6-O2'-dibutyryl cyclic 3',5' AMP on fat cell metabolism. *Diabetes* 23 (1), 29–40. doi:10.2337/diab.23.1.29

Jersin, R. Å., Jonassen, L. R., and Dankel, S. N. (2022). The neutral amino acid transporter SLC7A10 in adipose tissue, obesity and insulin resistance. *Front. Cell Dev. Biol.* 10, 974338. doi:10.3389/fcell.2022.974338

Jersin, R. Å., Tallapragada, D. S. P., Madsen, A., Skartveit, L., Fjære, E., McCann, A., et al. (2021). Role of the neutral amino acid transporter SLC7A10 in adipocyte lipid storage, obesity, and insulin resistance. *Diabetes* 70 (3), 680–695. doi:10.2337/db20-0096

Jersin, R. Å., Tallapragada, D. S. P., Skartveit, L., Bjune, M. S., Muniandy, M., Lee-Ødegård, S., et al. (2023). Impaired adipocyte SLC7A10 promotes lipid storage in association with insulin resistance and altered BCAA metabolism. *J. Clin. Endocrinol. metabolism*, dgad148. Advance online publication. doi:10.1210/clinem/dgad148

Katus, U., Villa, I., Ringmets, I., Vaht, M., Mäestu, E., Mäestu, J., et al. (2020). Association of FTO rs1421085 with obesity, diet, physical activity, and socioeconomic status: A longitudinal birth cohort study. *Nutr. Metab. Cardiovasc. Dis.* 30 (6), 948–959. doi:10.1016/j.numecd.2020.02.008

Kazak, L., Chouchani, E. T., Jedrychowski, M. P., Erickson, B. K., Shinoda, K., Cohen, P., et al. (2015). A creatine-driven substrate cycle enhances energy expenditure and thermogenesis in beige fat. *Cell* 163 (3), 643–655. doi:10.1016/j.cell.2015.09.035

Klusóczki, Á., Veréb, Z., Vámos, A., Fischer-Posovszky, P., Wabitsch, M., Bacso, Z., et al. (2019). Differentiating SGBS adipocytes respond to PPARγ stimulation, irisin and BMP7 by functional browning and beige characteristics. *Sci. Rep.* 9 (1), 5823. doi:10.1038/s41598-019-42256-0

Kristóf, E., Doan-Xuan, Q. M., Bai, P., Bacso, Z., and Fésüs, L. (2015). Laser-scanning cytometry can quantify human adipocyte browning and proves effectiveness of irisin. *Sci. Rep.* 5, 12540. doi:10.1038/srep12540

Kristóf, E., Klusóczki, Á., Veress, R., Shaw, A., Combi, Z. S., Varga, K., et al. (2019). Interleukin-6 released from differentiating human beige adipocytes improves browning. *Exp. Cell Res.* 377 (1-2), 47–55. doi:10.1016/j.yexcr.2019.02.015

Laber, S., Forcisi, S., Bentley, L., Petzold, J., Moritz, F., Smirnov, K. S., et al. (2021). Linking the FTO obesity rs1421085 variant circuitry to cellular, metabolic, and organismal phenotypes *in vivo*. *Sci. Adv.* 7 (30), eabg0108. doi:10.1126/sciadv.abg0108

Leitner, B. P., Huang, S., Brychta, R. J., Duckworth, C. J., Baskin, A. S., McGehee, S., et al. (2017). Mapping of human Brown adipose tissue in lean and obese young men. *Proc. Natl. Acad. Sci. U. S. A.* 114 (32), 8649–8654. doi:10.1073/pnas.1705287114

Lin, X., and Li, H. (2021). Obesity: Epidemiology, pathophysiology, and therapeutics. *Front. Endocrinol.* 12, 706978. doi:10.3389/fendo.2021.706978

London, E., and Stratakis, C. A. (2022). The regulation of PKA signaling in obesity and in the maintenance of metabolic health. *Pharmacol. Ther.* 237, 108113. doi:10.1016/j.pharmthera.2022.108113

Lu, X., Altshuler-Keylin, S., Wang, Q., Chen, Y., Henrique Sponton, C., Ikeda, K., et al. (2018). Mitophagy controls beige adipocyte maintenance through a Parkin-dependent and UCP1-independent mechanism. *Sci. Signal.* 11 (527), eaap8526. doi:10.1126/scisignal.aap8526

Lucas, S., Chen, G., Aras, S., and Wang, J. (2018). Serine catabolism is essential to maintain mitochondrial respiration in mammalian cells. *Life Sci. Alliance* 1 (2), e201800036. doi:10.26508/lsa.201800036

Mårin, P., Andersson, B., Ottosson, M., Olbe, L., Chowdhury, B., Kvist, H., et al. (1992). The morphology and metabolism of intraabdominal adipose tissue in men. *Metab. Clin. Exp.* 41 (11), 1242–1248. doi:10.1016/0026-0495(92)90016-4

Matsuzawa, Y., Shimomura, I., Nakamura, T., Keno, Y., Kotani, K., and Tokunaga, K. (1995). Pathophysiology and pathogenesis of visceral fat obesity. *Obes. Res.* 3 (Suppl. 2), 187S–194S. doi:10.1002/j.1550-8528.1995.tb00462.x

McLaughlin, T., Lamendola, C., Liu, A., and Abbasi, F. (2011). Preferential fat deposition in subcutaneous versus visceral depots is associated with insulin sensitivity. *J. Clin. Endocrinol. Metab.* 96 (11), E1756–E1760. doi:10.1210/jc.2011-0615

Mills, E. L., Pierce, K. A., Jedrychowski, M. P., Garrity, R., Winther, S., Vidoni, S., et al. (2018). Accumulation of succinate controls activation of adipose tissue thermogenesis. *Nature* 560 (7716), 102–106. doi:10.1038/s41586-018-0353-2

Nagy, L., Rauch, B., Szerafin, T., Uray, K., Tóth, A., and Bai, P. (2022). Nicotinamide-riboside shifts the differentiation of human primary white adipocytes to beige adipocytes impacting substrate preference and uncoupling respiration through SIRT1 activation and mitochondria-derived reactive species production. *Front. Cell Dev. Biol.* 10, 979330. doi:10.3389/fcell.2022.979330

Najd-Hassan-Bonab, L., Safarpour, M., Moazzam-Jazi, M., Azizi, F., and Daneshpour, M. S. (2022). The role of FTO variant rs1421085 in the relationship with obesity: A systematic review and meta-analysis. *Eat. Weight Disord.* 27, 3053–3062. Advance online publication. doi:10.1007/s40519-022-01509-0

Nokhoijav, E., Guba, A., Kumar, A., Kunkli, B., Kalló, G., Káplár, M., et al. (2022). Metabolomic analysis of serum and tear samples from patients with obesity and type 2 diabetes mellitus. *Int. J. Mol. Sci.* 23 (9), 4534. doi:10.3390/ijms23094534

Onogi, Y., and Ussar, S. (2022). Regulatory networks determining substrate utilization in Brown adipocytes. *Trends Endocrinol. Metab.* 33 (7), 493–506. doi:10.1016/j.tem.2022.04.001

Panic, V., Pearson, S., Banks, J., Tippetts, T. S., Velasco-Silva, J. N., Lee, S., et al. (2020). Mitochondrial pyruvate carrier is required for optimal Brown fat thermogenesis. *eLife* 9, e52558. doi:10.7554/eLife.52558

Patel, P., and Abate, N. (2013). Body fat distribution and insulin resistance. *Nutrients* 5 (6), 2019–2027. doi:10.3390/nu5062019

Perdikari, A., Leparc, G. G., Balaz, M., Pires, N. D., Lidell, M. E., Sun, W., et al. (2018). BATLAS: Deconvoluting Brown adipose tissue. *Cell Rep.* 25 (3), 784–797. doi:10.1016/j.celrep.2018.09.044

Petrovic, N., Walden, T. B., Shabalina, I. G., Timmons, J. A., Cannon, B., and Nedergaard, J. (2010). Chronic peroxisome proliferator-activated receptor gamma (PPARgamma) activation of epididymally derived white adipocyte cultures reveals a population of thermogenically competent, UCP1-containing adipocytes molecularly distinct from classic Brown adipocytes. *J. Biol. Chem.* 285 (10), 7153–7164. doi:10.1074/jbc.M109.053942

Pisani, D. F., Barquissau, V., Chambard, J. C., Beuzelin, D., Ghandour, R. A., Giroud, M., et al. (2018). Mitochondrial fission is associated with UCP1 activity in human brite/beige adipocytes. *Mol. Metab.* 7, 35–44. doi:10.1016/j.molmet.2017.11.007

Priliani, L., Oktavianthi, S., Hasnita, R., Nussa, H. T., Inggriani, R. C., Febinia, C. A., et al. (2020). Obesity in the Balinese is associated with FTO rs9939609 and rs1421085 single nucleotide polymorphisms. *PeerJ* 8, e8327. doi:10.7717/peerj.8327

Puri, V., Ranjit, S., Konda, S., Nicoloro, S. M., Straubhaar, J., Chawla, A., et al. (2008). Cidea is associated with lipid droplets and insulin sensitivity in humans. *Proc. Natl. Acad. Sci. U. S. A.* 105 (22), 7833–7838. doi:10.1073/pnas.0802063105

Qian, K., Tol, M. J., Wu, J., Uchiyama, L. F., Xiao, X., Cui, L., et al. (2023). CLSTN3β enforces adipocyte multilocularity to facilitate lipid utilization. *Nature* 613 (7942), 160–168. doi:10.1038/s41586-022-05507-1

Rana, S., and Bhatti, A. A. (2020). Association and interaction of the FTO rs1421085 with overweight/obesity in a sample of Pakistani individuals. *Eat Weight Disord.* 25 (5), 1321–1332. doi:10.1007/s40519-019-00765-x

Rosenwald, M., Perdikari, A., Rülicke, T., and Wolfrum, C. (2013). Bi-directional interconversion of brite and white adipocytes. *Nat. Cell Biol.* 15 (6), 659–667. doi:10.1038/ncb2740

Sanchez-Gurmaches, J., Hung, C. M., and Guertin, D. A. (2016). Emerging complexities in adipocyte origins and identity. *Trends Cell Biol.* 26 (5), 313–326. doi:10.1016/j.tcb.2016.01.004

Sarraf, S. A., and Youle, R. J. (2018). Parkin mediates mitophagy during beige-to-white fat conversion. *Sci. Signal.* 11 (527), eaat1082. doi:10.1126/scisignal.aat1082

Scalise, M., Pochini, L., Galluccio, M., and Indiveri, C. (2016). Glutamine transport. From energy supply to sensing and beyond. *Biochim. Biophys. acta* 1857 (8), 1147–1157. doi:10.1016/j.bbabio.2016.03.006

Scott, R. A., Lagou, V., Welch, R. P., Wheeler, E., Montasser, M. E., Luan, J., et al. (2012). Large-scale association analyses identify new loci influencing glycemic traits and provide insight into the underlying biological pathways. *Nat. Genet.* 44 (9), 991–1005. doi:10.1038/ng.2385

Scuteri, A., Sanna, S., Chen, W. M., Uda, M., Albai, G., Strait, J., et al. (2007). Genome-wide association scan shows genetic variants in the FTO gene are associated with obesity-related traits. *PLoS Genet.* 3 (7), e115. doi:10.1371/journal.pgen.0030115

Seiler, S. E., Xu, D., Ho, J. P., Lo, K. A., Buehrer, B. M., Ludlow, Y. J., et al. (2015). Characterization of a primary Brown adipocyte culture system derived from human fetal interscapular fat. *Adipocyte* 4 (4), 303–310. doi:10.1080/21623945.2015.1042192

Sharp, L. Z., Shinoda, K., Ohno, H., Scheel, D. W., Tomoda, E., Ruiz, L., et al. (2012). Human BAT possesses molecular signatures that resemble beige/brite cells. *PloS one* 7 (11), e49452. doi:10.1371/journal.pone.0049452

Shaw, A., Tóth, B. B., Király, R., Arianti, R., Csomós, I., Póliska, S., et al. (2021). Irisin stimulates the release of CXCL1 from differentiating human subcutaneous and deep-neck derived adipocytes via upregulation of NFκB pathway. *Front. Cell Dev. Biol.* 9, 737872. doi:10.3389/fcell.2021.737872

Shinoda, K., Luijten, I. H., Hasegawa, Y., Hong, H., Sonne, S. B., Kim, M., et al. (2015). Genetic and functional characterization of clonally derived adult human Brown adipocytes. *Nat. Med.* 21 (4), 389–394. doi:10.1038/nm.3819

Szatmári-Tóth, M., Shaw, A., Csomós, I., Mocsár, G., Fischer-Posovszky, P., Wabitsch, M., et al. (2020). Thermogenic activation downregulates high mitophagy rate in human masked and mature beige adipocytes. *Int. J. Mol. Sci.* 21 (18), 6640. doi:10.3390/ijms21186640

Tanaka, T., Ngwa, J. S., van Rooij, F. J., Zillikens, M. C., Wojczynski, M. K., Frazier-Wood, A. C., et al. (2013). Genome-wide meta-analysis of observational studies shows common genetic variants associated with macronutrient intake. *Am. J. Clin. Nutr.* 97 (6), 1395–1402. doi:10.3945/ajcn.112.052183

Tóth, B. B., Arianti, R., Shaw, A., Vámos, A., Veréb, Z., Póliska, S., et al. (2020). FTO intronic SNP strongly influences human neck adipocyte browning determined by tissue and PPARγ specific regulation: A transcriptome analysis. *Cells* 9 (4), 987. doi:10.3390/cells9040987

Townsend, K. L., and Tseng, Y. H. (2014). Brown fat fuel utilization and thermogenesis. *Trends Endocrinol. Metab.* 25 (4), 168–177. doi:10.1016/j.tem.2013.12.004

Vámos, A., Shaw, A., Varga, K., Csomós, I., Mocsár, G., Balajthy, Z., et al. (2022). Mitophagy mediates the beige to white transition of human primary subcutaneous adipocytes *ex vivo*. *Pharm. (Basel, Switz.)* 15 (3), 363. doi:10.3390/ph15030363

Virtanen, K. A., Lidell, M. E., Orava, J., Heglind, M., Westergren, R., Niemi, T., et al. (2009). Functional Brown adipose tissue in healthy adults. *N. Engl. J. Med.* 360 (15), 1518–1525. doi:10.1056/NEJMoa0808949

Wajchenberg, B. L. (2000). Subcutaneous and visceral adipose tissue: Their relation to the metabolic syndrome. *Endocr. Rev.* 21 (6), 697–738. doi:10.1210/edrv.21.6.0415

Wang, K., Li, W. D., Zhang, C. K., Wang, Z., Glessner, J. T., Grant, S. F., et al. (2011). A genome-wide association study on obesity and obesity-related traits. *PloS one* 6 (4), e18939. doi:10.1371/journal.pone.0018939

Wang, L., Yu, Q., Xiong, Y., Liu, L., Zhang, X., Zhang, Z., et al. (2013). Variant rs1421085 in the FTO gene contribute childhood obesity in Chinese children aged 3-6 years. *Obes. Res. Clin. Pract.* 7 (1), e14–e22. doi:10.1016/j.orcp.2011.12.007

Wang, S., Lin, Y., Gao, L., Yang, Z., Lin, J., Ren, S., et al. (2022). PPAR-γ integrates obesity and adipocyte clock through epigenetic regulation of Bmal1. *Theranostics* 12 (4), 1589–1606. doi:10.7150/thno.69054

Wheeler, E., Huang, N., Bochukova, E. G., Keogh, J. M., Lindsay, S., Garg, S., et al. (2013). Genome-wide SNP and CNV analysis identifies common and low-frequency variants associated with severe early-onset obesity. *Nat. Genet.* 45 (5), 513–517. doi:10.1038/ng.2607

Wolins, N. E., Quaynor, B. K., Skinner, J. R., Tzekov, A., Croce, M. A., Gropler, M. C., et al. (2006). OXPAT/PAT-1 is a PPAR-induced lipid droplet protein that promotes fatty acid utilization. *Diabetes* 55 (12), 3418–3428. doi:10.2337/db06-0399

Wu, J., Boström, P., Sparks, L. M., Ye, L., Choi, J. H., Giang, A. H., et al. (2012). Beige adipocytes are a distinct type of thermogenic fat cell in mouse and human. *Cell* 150 (2), 366–376. doi:10.1016/j.cell.2012.05.016

Wu, Q., Ortegon, A. M., Tsang, B., Doege, H., Feingold, K. R., and Stahl, A. (2006). FATP1 is an insulin-sensitive fatty acid transporter involved in diet-induced obesity. *Mol. Cell. Biol.* 26 (9), 3455–3467. doi:10.1128/MCB.26.9.3455-3467.2006

Yoneshiro, T., Wang, Q., Tajima, K., Matsushita, M., Maki, H., Igarashi, K., et al. (2019). BCAA catabolism in Brown fat controls energy homeostasis through SLC25A44. *Nature* 572 (7771), 614–619. doi:10.1038/s41586-019-1503-x

Zeng, X., Ye, M., Resch, J. M., Jedrychowski, M. P., Hu, B., Lowell, B. B., et al. (2019). Innervation of thermogenic adipose tissue via a calsyntenin 3β-S100b axis. *Nature* 569 (7755), 229–235. doi:10.1038/s41586-019-1156-9

Zou, Y., Lu, P., Shi, J., Liu, W., Yang, M., Zhao, S., et al. (2017). IRX3 promotes the browning of white adipocytes and its rare variants are associated with human obesity risk. *EBioMedicine* 24, 64–75. doi:10.1016/j.ebiom.2017.09.010

frontiers | Frontiers in Endocrinology

TYPE Systematic Review
PUBLISHED 16 June 2023
DOI 10.3389/fendo.2023.1132342

Check for updates

OPEN ACCESS

EDITED BY
Endre Károly Kristóf,
University of Debrecen, Hungary

REVIEWED BY
Naresh Chandra Bal,
KIIT University, India
Amaia Rodríguez,
University of Navarra, Spain

*CORRESPONDENCE
Hongya Yang
yhy6018@163.com
Weijun Ding
dingweijun@cdutcm.edu.cn

RECEIVED 27 December 2022
ACCEPTED 24 May 2023
PUBLISHED 16 June 2023

CITATION
Zheng Y, Yang N, Pang Y, Gong Y, Yang H, Ding W and Yang H (2023) Mitochondria-associated regulation in adipose tissues and potential reagents for obesity intervention.
*Front. Endocrinol.* 14:1132342.
doi: 10.3389/fendo.2023.1132342

COPYRIGHT
© 2023 Zheng, Yang, Pang, Gong, Yang, Ding and Yang. This is an open-access article distributed under the terms of the Creative Commons Attribution License (CC BY). The use, distribution or reproduction in other forums is permitted, provided the original author(s) and the copyright owner(s) are credited and that the original publication in this journal is cited, in accordance with accepted academic practice. No use, distribution or reproduction is permitted which does not comply with these terms.

# Mitochondria-associated regulation in adipose tissues and potential reagents for obesity intervention

Yali Zheng[1], Ni Yang[1], Yueshan Pang[1], Yanju Gong[1], Hong Yang[1,2], Weijun Ding[1*] and Hongya Yang[1*]

[1]Department of Fundamental Medicine, Chengdu University of Traditional Chinese Medicine, Chengdu, China, [2]School of Medical and Life Sciences/Reproductive & Women-Children Hospital, Chengdu University of Traditional Chinese Medicine, Chengdu, China

**Introduction:** A systematic review analysis was used to assess the profile of mitochondrial involvement in adipose tissue regulation and potential reagents to intervene in obesity through the mitochondrial pathway.

**Methods:** Three databases, PubMed, Web of Science, and Embase, were searched online for literature associated with mitochondria, obesity, white adipose tissue, and brown adipose tissue published from the time of their creation until June 22, 2022, and each paper was screened.

**Results:** 568 papers were identified, of which 134 papers met the initial selection criteria, 76 were selected after full-text review, and 6 were identified after additional searches. A full-text review of the included 82 papers was performed.

**Conclusion:** Mitochondria play a key role in adipose tissue metabolism and energy homeostasis, including as potential therapeutic agents for obesity.

KEYWORDS

**obesity, mitochondria, white adipose tissue (WAT), brown adipose tissue (BAT), UCP1**

## 1 Introduction

Adipose tissue, as a major energy storage site, is involved in physiological regulation of the whole body, including energy maintenance, insulin sensitivity, and food intake. Adipose tissue includes white adipose tissue (WAT), brown adipose tissue (BAT), and beige adipose tissue. Distinct fat depots have very unique biochemical properties and association with metabolic diseases (1). WAT stores excess energy as triglycerides (TG) and secretes adipokines such as leptin, TNF-α, and lipocalin, which contribute to the regulation of energy homeostasis (2), white adipocytes consist of single-compartment lipid droplets. BAT and beige adipose tissue are characterized by multi-compartment lipid droplets, high mitochondrial density and expression of uncoupling protein 1 (UCP1), and BAT consumes

energy through non-fibrillatory thermogenesis by mitochondria (3). Adipose tissue is highly plastic and its restriction can drive pathological consequences such as obesity and metabolic diseases. As a risk factor for several metabolic diseases, obesity contributes to inflammation, insulin resistance, type 2 diabetes, non-alcoholic fatty liver disease and cardiovascular disease (4).

Mitochondria are organelles found in eukaryotes that are essential for energy metabolism and cellular homeostasis. Mitochondria have unique enzymes and systems that contribute to the citric acid cycle, fatty acid oxidation and oxidative phosphorylation (5). The mitochondria are essential to the differentiation of adipocytes (adipogenesis) and to major adipocyte functions (6). White adipocyte mitochondria are elongated and thin, which are involved in the production of ATP. Mitochondria of brown adipocytes have more quantity and larger body size compared to white adipocytes, and UCP1 located in the inner mitochondrial membrane can cause proton leakage across the inner membrane of the mitochondria, thus transforming the electrochemical energy into heat (7). The pathological expansion of the adipose tissue expansion is accompanied by the downregulation of mitochondrial oxidative pathways and changes in mitochondrial shape and number, ultimately leading to cell death (8–10). Mitochondrial dysfunction has deleterious effects on important adipocyte biology processes (lipid metabolism, adipocyte differentiation, insulin sensitivity, and thermogenesis), leading to metabolic diseases such as obesity and type 2 diabetes (11). Recent studies have shown that mitochondrial function can be improved by adding some herbal extracts and natural compounds in the diet, thereby inducing browning of WAT and adaptive thermogenesis of BAT to maintain metabolic homeostasis.

In this review, we focus on the specific role of mitochondria in adipocytes, summarize the mechanisms of mitochondrial regulation of adipose tissue, and discuss potential therapeutic agents from the perspective of treating obesity, which provide new insights for clinical treatment.

# 2 Research methods

## 2.1 Search strategy

The reporting items were created in strict accordance with the systematic review statement. All articles were retrieved from the PubMed, Embase and Web of Science databases. We used search words such as ‘Mitochondria’, ‘Obesity’, ‘Adipose Tissue, White’, and ‘Adipose Tissue, Brown’ in conjunction with Boolean operators. Within each concept, we combined subject words and free words with the ‘OR’ Boolean operator, and the four concepts were combined with the ‘AND’ Boolean operator. The specific search process can be found in the supplementary materials.

## 2.2 Study selection

We screened the titles and abstracts of each paper, and articles that were repeated and irrelevant were removed. The inclusion criteria were the mechanism of mitochondrial regulation of adipose tissue and potential reagents for obesity intervention through the mitochondrial pathway. Articles were excluded according to the following criteria: review articles, editorials, commentaries, conference abstracts, case reports, articles written in other languages, letters to the editor and articles not relevant to the main topic. A ‘PRISMA’ flow chart was used to document the selection process (Figure 1) (12).

# 3 Results

## 3.1 Mitochondria regulate adipocyte thermogenesis

Adipose tissue is one of the significant features in maintaining systemic energy homeostasis and insulin sensitivity, not only as a storehouse of excess energy substrates but also as a metabolic health sensor and regulator of energy storage and expenditure. Thermogenesis in adipose tissue is activated in a state of metabolic overload to rapidly utilize excess nutrients. BAT disrupt electron transport in the respiratory chain by activating UCP1 on the mitochondria, thereby preventing the production of ATP and converting energy into heat (13). In addition, mitochondria provide energy for thermogenesis due to efficient proton gradient generation during catabolic processes and electron transport chain (ETC) function (14). It has been reported that

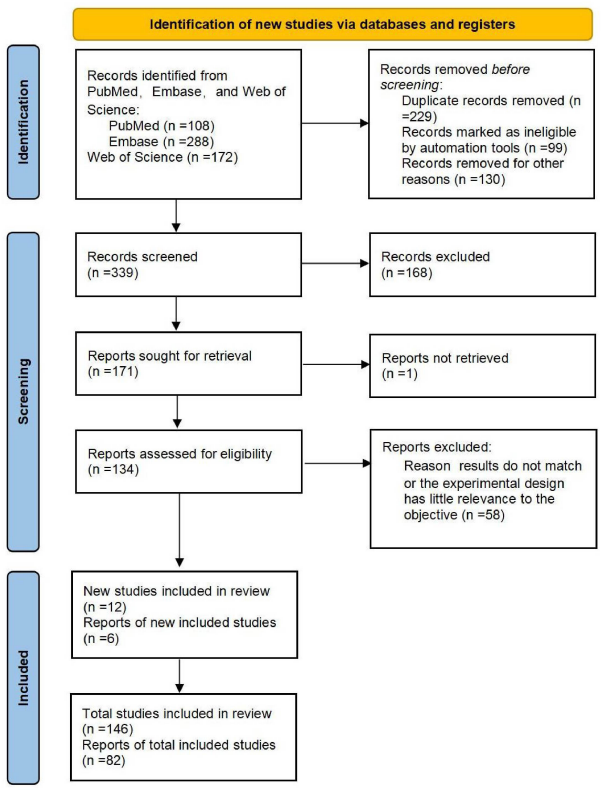


FIGURE 1
The flow of the literature retrieval.

individuals with obesity have reduced adipocyte UCP1 expression and that activation of UCP1 improves obesity and metabolic complications. Therefore, targeting mitochondria to activate UCP1 is a strategy to treat obesity (15).

Sirtuin 3 (SIRT3) is a mitochondrially localized deacetylase (16) that belongs to the sirtuin family. Sirtuins are evolutionarily conserved deacetylases whose activity is dependent on NAD+ and have a variety of physiological functions, including the regulation of cell proliferation, DNA repair, antioxidant activity and mitochondrial energy homeostasis. One study reported that caloric restriction activated SIRT3 expression in WAT and BAT, and in BAT from genetically obese mice, SIRT3 was downregulated along with genes related to mitochondrial function, suggesting that SIRT3 activates mitochondrial function and contributes to adaptive thermogenesis in BAT (17, 18). The peroxisome biogenesis factor Pex16 (19), the angiogenic factor VEGF-A (20), disulfide-bond-A oxidoreductase-like protein (DsbA-L) (21), and PR domain-containing 16 (PRDM16) (22) may also regulate thermogenesis by regulating mitochondrial function.

The overexpression of hypoxia-inducible factor-1α (HIF-1α) in adipose tissue inhibits thermogenesis and cellular respiration in BAT and promotes weight gain in mice, which is associated with a reduction in oxygen consumption in BAT, while the decrease in oxygen consumption may be mediated by a reduction in mitochondria (23). Carbohydrate response element-binding protein (ChREBP) is one of the major transcription factors regulating lipogenesis (24). One study showed that overexpression of ChREBP-β reduced the expression of genes involved in mitochondrial biogenesis, autophagy and respiration, leading to a bleached phenotype of BAT (25), which suggested that ChREBP-β is a negative regulator of thermogenesis in BAT. Bone morphogenetic protein 7 (BMP7) has also been shown to upregulate UCP1 and increase adipocyte thermogenesis (26). The absence of the membrane-associated estrogen receptor G protein-coupled receptor 30 (GPR30) may promote BAT mitochondrial uncoupling of respiration (27), suggesting that it is a negative regulator of thermogenesis and contributes to reduced obesity. Optic atrophy protein 1 (OPA1) (28), Brain-derived neurotrophic factor (BDNF) (29), also plays an important role in the adaptive thermogenesis of BAT.

Fat burning relying on adaptive thermogenesis has emerged as a viable strategy to reduce obesity, and the activation of mitochondrial-localized UCP1 and related molecules targeting mitochondria becomes a potential driving force to execute this strategy. Therefore, mitochondria are an essential organelle for maintaining adipocyte metabolic homeostasis.

## 3.2 Activation of WAT browning and BAT whitening

Some WATs exhibit a BAT phenotype when exposed to certain stimuli, which is called “the browning of WAT”. WAT browning produces beige adipocytes, which exhibit UCP1-dependent thermogenesis, and fibroblast growth factor 21 (FGF21) was shown to play an important role in this thermogenesis (30). WAT browning has been found to suppress diet-induced obesity and improve systemic energy metabolism in many animal models (31, 32). Therefore, WAT browning has been investigated as an alternative therapy to BAT thermogenesis. Exercise is a major driver of fat browning. In this sense, the impact of myokines, which are factors secreted by the contracting muscle, on fat browning has provided a molecular mechanism to explain the benefits of exercise on weight loss and metabolic disease prevention. In this sense, several myokines act as positive (FNDC5/irisin, FNDC4, BAIBA and meteorin-like) and negative (myostatin) regulators of fat browning (33–37).

The role of mitochondria in WAT browning cannot be ignored. As an important factor of mitochondrial function, the expression of peroxisome prolileratorsactivated receptor γ coactivator l α (PGC1α) was significantly increased in WAT of protein kinase Cβ (PKCβ) deficiency on profound obesity, double knockout (DBKO) mice (38). OPA1, a key protein for mitochondrial fusion, promotes browning of white adipocytes (39).Human white adipocyte mitochondrial activity is regulated by the ubiquitin carrier protein 9/microRNA-30a axis, which is involved in controlling white adipocyte browning (40). MiR-337-3p in adipocytes inhibits Twist1, a negative feedback regulator of BAT metabolism, and enhances adipocyte browning (41). It has also been found that the small molecule compounds RepSox (42), Endonuclease G (EndoG) (43), milk fat globule membrane (MFGM) and its components phosphatidylcholine (PC) (44), bone morphogenetic protein-4 (MBP4) (45), cannabinoid receptor type 1 (CB1R) (46), and E2F transcription factor 1(E2F1) (47) can be involved in the induction of WAT browning. Electroacupuncture (EA) has also been shown to remodel WAT to BAT by deacetylating SIRT-1-dependent peroxisome proliferator-activated receptor gamma (PPARγ) and regulating the PGC1α-TFAM-UCP1 pathway in order to induce mitochondrial biogenesis (48). These appears to be potential strategies for the treatment of obesity through WAT browning.

The “whitening” of BAT is closely related to obesity-related BAT dysfunction. It is worth mentioning that the process of BAT whitening associated with obesity is reversible by cold exposure and bariatric surgery (49, 50). It is possible that inflammation in whitened BAT contributes to the typical inflammatory state found in obesity (49). Shimizu, I et al. (51) showed that vascular rarefaction results in mitochondrial dysfunction and loss in BAT, which is a noteworthy causal factor in the whitening of BAT in mice models and could affect obesity and obesity-linked diseases. Activation of mTOR signaling downregulated PGC1α, a key activator of mitochondrial biosynthesis, and nuclear respiratory factor 1 (NRF1), an important transcriptional regulator, and downregulated Mitofusin 2 (Mfn2) and OPA1, genes involved in mitochondrial dynamics (52), which may have led to the “whitening” of BAT, suggesting that inhibition of the mTOR signaling pathway is a potential therapeutic avenue for obesity.

Obesity is associated with reduced WAT browning and BAT thermogenesis, and some transcriptional regulators and signaling pathways can regulate WAT browning and BAT thermogenesis by improving mitochondrial quality control, suggesting that targeting mitochondrial regulation is an important entry point for obesity prevention and treatment (Figure 2).

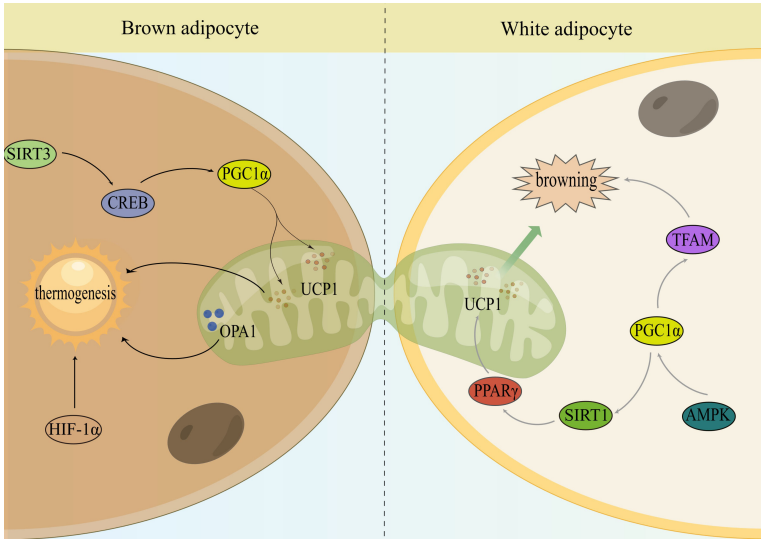


FIGURE 2
Mitochondria monitor the thermogenesis of brown and activate the browning of WAT. Sirtuin 3 (SIRT3); cAMP response element-binding protein (CREB); peroxisome proliferator-activated receptor-γ cofactor 1α (PGC1α); uncoupling protein-1 (UCP1); optic atrophy 1 (OPA1); hypoxia-inducible factor-1α (HIF-1α); peroxisome proliferator-activated receptor gamma (PPARγ); sirtuin 1 (SIRT1); AMP-activated protein kinase (AMPK); mitochondrial transcription factor A (TFAM).

## 3.3 Mitochondrial regulation of glucolipid metabolism in subjects with obesity

Mitochondrial dynamics in adipocytes may play a key role in initiating systemic metabolic dysregulation. Nutrient overload promotes hypoxia in BAT, which leads to whitening through mitochondrial dysfunction and loss, subsequently leading to impaired systemic glucose metabolism (53). Bean and coworkers (54) identified that the OPA1 gene regulates insulin sensitivity and adipose tissue functions, and controlled OPA1 overexpression in mice could reduce body weight, improve glucose metabolism and insulin sensitivity, reduce fat accumulation and promote browning of white adipocytes. Mfn2 is a gene that promotes mitochondrial fusion and mitochondrial-endoplasmic reticulum interactions. When Mfn2 is knocked down in adipocytes, adult mice consume more food, gain more fat, and have impaired glucose metabolism in standard diets (55). Mfn2 also plays a key role in the regulation of brown adipose tissue thermogenesis favouring mitochondria to lipid droplet interactions (56).

A dysfunctional mitochondrial system in WAT is implicated in obesity-related insulin resistance. OPA1 deletion completely prevented the increase in adiposity and improved insulin fate sensitivity in mice fed a high-fat diet (57). MLX interacting protein-like (MLXIPL) is a transcriptional regulator. MLXIPL-deficient mice are resistant to excessive lipid accumulation and heat-induced mitochondrial degradation in brown adipocytes (58). This result suggested that knockout of MLXPIL may be a potential therapeutic target for obesity-related metabolic diseases. Takaya et al. (59) found that the expression of UCP1 was increased in BAT-derived cultured preadipocytes and their local transplantation reduced inguinal fat pad weight. This finding suggests that local transplantation of BAT-derived preadipocytes may increase energy expenditure and thus reduce obesity. In the tricarboxylic acid cycle, pyruvate is transported to mitochondria by pyruvate carrier 1 (MPC1) to be oxidized to acetyl coenzyme A. Inhibition of MPC1 inhibits pyruvate transport and thus activates fatty acid oxidation (60), this suggests that MPC1 may be an important regulator of mitochondrial energy metabolism.

Mitochondria play a key role in the regulation of glucose utilization and lipid metabolism in adipocytes. By regulating mitochondrial biogenesis and mitochondrial dynamics in adipocytes, the development of obesity and metabolic diseases can be improved.

## 3.4 Other mitochondrial regulation approaches in obesity

Mitophagy is a process that selectively removes damaged mitochondria through a specialized form of autophagy and is essential for mitochondrial quality control (mitochondrial QC) and metabolic homeostasis. The mitochondrial autophagy receptor Fundc1 is a newly defined mitophagy receptor, and mice lacking Fundc1 develop more severe obesity and insulin resistance when fed a high-fat diet (HFD), and disruption of Fundc1 leads to impaired mitophagy and mitochondrial quality in WAT (61). PGC1α is essential for maintaining energy homeostasis. Overexpression of PGC1α in epicardial adipose tissue induces mitosis and improves mitochondrial function, resulting in improved adipose tissue quality (62). The deletion of mitochondrial transcription factor A (TFAM) in adipose tissue results in reduced mtDNA copy number, mitochondrial dysfunction, increased mitochondrial oxidation and positive metabolic effects (63, 64), suggesting that adipose tissue

mitochondrial biosynthesis regulation may be a potential therapeutic target for the treatment of obesity.

The expression of PTEN-induced kinase 1 (PINK1), a protein involved in mitochondrial autophagic clearance, was upregulated in the WAT of HFD mice (65). Deletion of PINK1 induced BAT dysfunction, suggesting that the regulation of mitochondrial autophagy contributes to the "whitening" of adipose tissue during the development of obesity (66). The transition from beige to white adipocytes was associated with decreased mitochondria and increased autophagy (67), uncovering a mechanism by which autophagy-mediated mitochondrial clearance controls the maintenance of beige adipocytes, thus providing an opportunity to combat obesity.

Intercellular mitochondrial transfer can support the survival of cells with impaired metabolism. Rohatgi et al. (68) found that adipocytes and macrophages employ intercellular mitochondrial transfer as an immunometabolic crosstalk mechanism to regulate metabolic homeostasis, which is impaired in obesity. Borcherding et al. (69) showed the existence of a potential direct dietary mechanism on the basis of the above studies that could largely ameliorate mitochondrial translocation.

## 3.5 Mitochondrial targeting as a strategy to treat obesity

### 3.5.1 Herbal extracts and natural compounds

Increasing energy expenditure is a common approach to obesity prevention, and activating BAT may be a potential strategy against obesity. Beta vulgaris has been shown to have an anti-obesity effect by increasing UCP1 during nonshivering thermogenesis in brown adipocytes (70). Liu Z et al. (71) studied the effects of sesamol on disorders of adiposity and fat-related metabolism in mice fed a Western diet. They found that sesamol reduced WAT and BAT mass and adipocyte size by improving the expression of mitochondria-related genes, including PGC1α and UCP1. Jung Y et al. (72) investigated the anti-obesity effects of vanillic acid (VA) *in vivo* and *in vitro* and found that VA increased mitochondrial and thermogenesis-related factors such as UCP1 and PPARγ-1 in BAT and primary cultured brown adipocytes from mice, suggesting the potential of VA as a thermogenesis-activated anti-obesity agent.

Stimulating browning of white adipose cells helps to limit obesity and related metabolic disorders. Lactobacillus plantarum dy-1 (LFBE) can suppress obesity by enhancing thermogenic processes in BAT and browning of adipose tissue in the epithelium using a UCP1-dependent mechanism of activation (73). Averrhoa bilimbi can also induce adipocyte browning and enhance mitochondrial activity due to upregulation of UCP1 (74). Kang J et al. (75) studied the effects of secoisolariciresinol diglucoside (SDG) on WAT browning and found that SDG increased UCP1, PGC1α and PRDM16 in WAT and BAT in mice, as well as mitochondrial biogenesis and activation, suggesting that SDG is a potential candidate for ameliorating obesity and other metabolic disorders. Lycopene (LYC), one of the major carotenoids in tomatoes, has been used preclinically and clinically in the treatment of obesity and type 2 diabetes. LYC can induce browning and enhance mitochondrial respiration in white adipocytes and improve glucose and lipid metabolism by upregulating PPARγ (76).

The whitening of BAT during obesity and aging promotes metabolic disorders and related diseases. Gao P et al. (77) determined that the inhibitory effect of capsaicin on HFD-induced obesity and BAT whitening was dependent on the involvement of SIRT3, which could mediate the beneficial effects of capsaicin on attenuating reactive oxygen species production, increasing mitochondrial activity and limiting HFD-induced mitochondrial calcium overload.

Regulation of mitochondrial biogenesis is also a potential avenue for the treatment of obesity. The ethanolic extracts of both rutin and Platycodon grandiflorum (PG) can provide benefits for obesity by increasing the expression of genes involved in mitochondrial biogenesis (78, 79). α-Lipoic acid (α-LIP) is a naturally occurring antioxidant that promotes mitochondrial biogenesis and brown-like remodeling in cultured white subcutaneous adipocytes from donors with obesity (80). Marqués and colleagues (81) found that resveratrol has potential therapeutic effects in improving mitochondrial biogenesis (Table 1).

Some compounds can also activate mitochondrial biogenesis in skeletal muscle. Resveratrol was shown in 2006 to affect skeletal muscle mitochondrial biogenesis and thus metabolic homeostasis by decreasing PGC1α acetylation and increasing PGC1α activity (88). As a thermogenic tissue, skeletal muscle is also capable of regulating energy expenditure. When UCP1 is absent or non-shivering thermogenesis is affected, skeletal muscle generates heat through shivering and is supplied with energy by carbohydrates and lipids (89). Thermogenesis in skeletal muscle is dependent on the homologue of UCP1, uncoupling protein 3 (UCP3). 5,3'-Triiodo-L-thyronine (T3) was reported to induce UCP3 expression to regulate skeletal muscle thermogenesis (90). It is interesting to note that these compounds also work through similar pathways in BAT. Recruitment of BAT and skeletal muscle bear very high degree of similarities (91). Both organs are highly vascularized, neuralized, and contain abundant mitochondria (92). Studies by Bal et al. (93) have shown that skeletal muscle thermogenesis can be activated to compensate for the absence of BAT, suggesting that the two thermogenic systems can be functionally complementary. It has been shown that PRDM16 can control the bidirectional transformation of brown adipocytes and skeletal muscle cells (94), which may represent two different potential therapeutic targets to expand the thermogenic capacity of adipose tissue.

### 3.5.2 Traditional Chinese medicine and other alternative medicines

Zhang et al. (95) found that the natural antioxidant Lycium could enhance UCP1 expression, upregulate PGC1α and induce browning in white adipocytes, as well as enhance glucose uptake and oxidative utilization, lipolysis and fatty acid oxidation in 3T3-L1 adipocytes, and the application of Lycium is a promising strategy to combat obesity and obesity-related metabolic disorders. Huangqi San (HQS) is a traditional Chinese medicine formula, and Hao M et al. (96) found that it could significantly increase the number of mitochondria, increase the expression of UCP1 and PGC1α in

TABLE 1 Key factors in herbal extracts and natural compounds.

| Name | Key factors | Function | Reference |
|---|---|---|---|
| **Beta vulgaris** | *UCP1, PPARγ* | Adaptive thermogenesis | (70) |
| **VA** | UCP1, *PPARγ-1α, PPARγ, C/EBPα, AMPKα* | Adaptive thermogenesis | (72) |
| **LFBE** | *UCP1, PPARγ, C/EBPα, SREBP-1c, aP2, Cidea* | Adaptive thermogenesis | (73) |
| **Averrhoa bilimbi** | *UCP1, PPARγ*, PRDM16 | WAT browning | (74) |
| **SDG** | UCP1, PGC1α, PRDM16, AMPK*α* | WAT browning and mitochondrial biogenesis | (75) |
| **LYC** | *UCP1, PPARγ, PPARγ-1α*, PRDM16 | WAT browning | (76) |
| **Capsaicin** | SIRT3, AMPK, MCU, H3K27ac | Mitochondrial biogenesis | (77) |
| **Rutin** | UCP2, PGC1α, *PPARγ, SREBP-1c, aP2* | Mitochondrial biogenesis | (78) |
| **PG** | UCP1, PGC1α, *PPARγ*, PRDM16, SIRT3, NRF, Cyto C, SIRT1, *C/EBPα, AMPKα* | Mitochondrial biogenesis | (79) |
| **α-Lip** | PGC1α, SIRT1, PRDM16, NRF1, TFAM, Cidea, Tbx1 | WAT browning and mitochondrial biogenesis | (80) |
| **Resveratrol** | UCP1, *PPARγ*, PRDM16, Cidea, CD137, TMEM26, COX4α, NRF, TFAM, IGFBP3 | Mitochondrial biogenesis and WAT browning | (81) (82) |
| **Sesamol** | UCP1, PGC1α | Mitochondrial biogenesis | (83) |
| **Phytol** | UCP1, PGC1α, Cyto C, Cidea, PRDM16, AMPK*α, CD137, TMEM26* | Adipocyte differentiation | (84) |
| **Ursodeoxycholic Acid** | PGC1α, STAT3, CD36, SREBP-1 | WAT browning and mitochondrial biogenesis | (85) |
| **Multi-Ingredient Supplement** | UCP1, PGC1α, *PRDM16, Cidea* | WAT browning and mitochondrial biogenesis | (86) |
| **T3** | UCP1, PGC1α, *PRDM16*, TOMM20, VDAC1 | WAT browning and mitochondrial autophagy | (87) |

BAT, and improve metabolic disorders and lipid deposition in hyperlipidemia in obese rats after 13 W intravenous injection of HQS, suggesting that HSQ is an effective drug for the treatment of hyperlipidemia with obesity. Tanshinone IIA (TAN2A) is a major active ingredient of the traditional Chinese medicine tanshinone, and tanshinone 20 (TAN20) is a derivative of TAN2A. Ma L et al. (97) showed that both TAN2A and TAN20 were able to increase mitochondrial content in adipose tissue, increase energy expenditure and reduce body weight, thereby improving insulin sensitivity and metabolic homeostasis in mouse models of obesity and diabetes. It has also been shown (98) that administration of tanshinone 1 (TAN1) prevents HFD-induced obesity in mice, which was associated with enhanced expression of brown adipocyte-related genes in WAT and BAT, and that TAN1 also led to increased mtDNA content and lipolysis.

Drugs with therapeutic potential can combat obesity by affecting the differentiation of white adipocytes. Ravaud C et al. (99) showed that HIV protease inhibitors (PIs) can reduce the expression of UCP1, improve mitochondrial function in brown adipocytes and regulate thermogenesis and are promising potential drugs against obesity. Empagliflozin can increase mitochondrial biogenesis and fusion, improve their function and promote browning of 3T3-L1 adipocytes (100), FAM134B improves adipocyte differentiation by enhancing mitophagy (101), and melatonin drives WAT browning (102), which are also promising anti-obesity treatments.

Targeting mitochondria as a therapeutic strategy for metabolic diseases is being extensively investigated as a new potential approach. In conclusion, the possibility of reducing obesity and metabolic diseases by mediating mitochondrial biogenesis or mitochondrial dynamics to increase thermogenesis, activate WAT brownout, and promote lipid metabolism and fatty acid oxidation is being progressively demonstrated.

## 3.6 Conclusion

The importance of mitochondria in energy metabolism and cellular homeostasis has been extensively noted and studied. Since the rediscovery of active brown and beige adipocytes in humans a decade ago, more and more research has focused on the regulation of adipocyte function by mitochondria. We summarized the searched articles and showed that mitochondria are involved in regulating the thermogenesis of BAT and increasing energy expenditure; in lipid homeostasis of adipose tissue and regulating glucose metabolism; and are also able to participate in inducing browning of WAT while promoting the whitening of BAT. These are key therapeutic targets for obesity-related metabolic diseases. The regulation of mitochondrial biogenesis, mitochondrial autophagy and mitochondrial translocation are also potential therapeutic opportunities for obesity. In fact, a series of studies

are working on the interpretation of drugs or potential drugs for the treatment of obesity through these mitochondrial pathways.

In conclusion, mitochondria-targeted drugs for adipocytes are very promising. Therefore, understanding the molecular mechanisms underlying adipocyte mitochondrial dysfunction and the pathogenesis of obesity-related metabolic diseases is crucial for the development of new therapeutic approaches. However, future studies need to elucidate the mechanisms by which mitochondria undergo metabolic disorders to better account for their pathogenic role in metabolic diseases.

## Data availability statement

The original contributions presented in the study are included in the article/Supplementary Material. further inquiries can be directed to the corresponding authors.

## Author contributions

YZ and HongyaY conceived the research question. YZ wrote the first draft of the manuscript with the support of WD, YP and YG. HongY and NY discussed the results. All authors contributed to the article and approved the submitted version.

## Funding

This research received the Natural Science Foundation of China (No. 82074151).

## Acknowledgments

Ying Ning, Yan He, Yingxiu Mei and Yue Jin are acknowledged for their assistance in the writing of this article.

## Conflict of interest

The authors declare that the research was conducted in the absence of any commercial or financial relationships that could be construed as a potential conflict of interest.

## Publisher's note

All claims expressed in this article are solely those of the authors and do not necessarily represent those of their affiliated organizations, or those of the publisher, the editors and the reviewers. Any product that may be evaluated in this article, or claim that may be made by its manufacturer, is not guaranteed or endorsed by the publisher.

## Supplementary material

The Supplementary Material for this article can be found online at: https://www.frontiersin.org/articles/10.3389/fendo.2023.1132342/full#supplementary-material

## References

1. Sahu B, Tikoo O, Pati B, Senapati U, Bal NC. Role of distinct fat depots in metabolic regulation and pathological implications. *Rev Physiol Biochem Pharmacol* (2023) 186:135–76. doi: 10.1007/112_2022_73

2. Bartelt A, Heeren J. Adipose tissue browning and metabolic health. *Nat Rev Endocrinol* (2014) 10(1):24–36. doi: 10.1038/nrendo.2013.204

3. Betz MJ, Enerback S. Human brown adipose tissue: what we have learned so far. *Diabetes* (2015) 64(7):2352–60. doi: 10.2337/db15-0146

4. Ali Khan A, Hansson J, Weber P, Foehr S, Krijgsveld J, Herzig S, et al. Comparative secretome analyses of primary murine white and brown adipocytes reveal novel adipokines*. *Mol Cell Proteomics* (2018) 17(12):2358–70. doi: 10.1074/mcp.RA118.000704

5. Ernster L, Schatz G. Mitochondria: a historical review. *J Cell Biol* (1981) 91(3 Pt 2):227s–55s. doi: 10.1083/jcb.91.3.227s

6. Li Q, Gao Z, Chen Y, Guan MX. The role of mitochondria in osteogenic, adipogenic and chondrogenic differentiation of mesenchymal stem cells. *Protein Cell* (2017) 8(6):439–45. doi: 10.1007/s13238-017-0385-7

7. Shabalina IG, Petrovic N, de Jong JM, Kalinovich AV, Cannon B, Nedergaard J. UCP1 in brite/beige adipose tissue mitochondria is functionally thermogenic. *Cell Rep* (2013) 5(5):1196–203. doi: 10.1016/j.celrep.2013.10.044

8. Heinonen S, Saarinen L, Naukkarinen J, Rodriguez A, Fruhbeck G, Hakkarainen A, et al. Adipocyte morphology and implications for metabolic derangements in acquired obesity. *Int J Obes (Lond)* (2014) 38(11):1423–31. doi: 10.1038/ijo.2014.31

9. Heinonen S, Muniandy M, Buzkova J, Mardinoglu A, Rodriguez A, Fruhbeck G, et al. Mitochondria-related transcriptional signature is downregulated in adipocytes in obesity: a study of young healthy MZ twins. *Diabetologia* (2017) 60(1):169–81. doi: 10.1007/s00125-016-4121-2

10. Ejarque M, Ceperuelo-Mallafre V, Serena C, Maymo-Masip E, Duran X, Diaz-Ramos A, et al. Adipose tissue mitochondrial dysfunction in human obesity is linked to a specific DNA methylation signature in adipose-derived stem cells. *Int J Obes (Lond)* (2019) 43(6):1256–68. doi: 10.1038/s41366-018-0219-6

11. Boudina S, Graham TE. Mitochondrial function/dysfunction in white adipose tissue. *Exp Physiol* (2014) 99(9):1168–78. doi: 10.1113/expphysiol.2014.081414

12. Page MJ, McKenzie JE, Bossuyt PM, et al. The PRISMA 2020 statement: An updated guideline for reporting systematic reviews. *J Clin Epidemiol.* (2021) 134:178–89. doi: 10.1016/j.jclinepi.2021.03.001

13. Zafrir B. Brown adipose tissue: research milestones of a potential player in human energy balance and obesity. *Horm Metab Res* (2013) 45(11):774–85. doi: 10.1055/s-0033-1348264

14. Hankir MK, Klingenspor M. Brown adipocyte glucose metabolism: a heated subject. *EMBO Rep* (2018) 19(9):1–13. doi: 10.15252/embr.201846404

15. Cypess AM, Kahn CR. Brown fat as a therapy for obesity and diabetes. *Curr Opin Endocrinol Diabetes Obes* (2010) 17(2):143–9. doi: 10.1097/MED.0b013e328337a81f

16. Lahiri T, Brambilla L, Andrade J, Askenazi M, Ueberheide B, Levy DE. Mitochondrial STAT3 regulates antioxidant gene expression through complex I-derived NAD in triple negative breast cancer. *Mol Oncol* (2021) 15(5):1432–49. doi: 10.1002/1878-0261.12928

17. Shi T, Wang F, Stieren E, Tong Q. SIRT3, a mitochondrial sirtuin deacetylase, regulates mitochondrial function and thermogenesis in brown adipocytes. *J Biol Chem* (2005) 280(14):13560–7. doi: 10.1074/jbc.M414670200

18. Giralt A, Hondares E, Villena JA, Ribas F, Díaz-Delfín J, Giralt M, et al. Sirt3, a mitochondrial sirtuin controlling brown adipose thermogenic activation. *Obes Facts* (2012) 5:23. doi: 10.1159/000171026

19. Park H, He A, Tan M, Johnson JM, Dean JM, Pietka TA, et al. Peroxisome-derived lipids regulate adipose thermogenesis by mediating cold-induced mitochondrial fission. *J Clin Invest* (2019) 129(2):694–711. doi: 10.1172/JCI120606

20. Mahdaviani K, Chess D, Wu Y, Shirihai O, Aprahamian TR. Autocrine effect of vascular endothelial growth factor-a is essential for mitochondrial function in brown adipocytes. *Metabolism: Clin Exp* (2016) 65(1):26–35. doi: 10.1016/j.metabol.2015.09.012

21. Bai J, Su X, Chen H, Cervantes C, Zhang C, Hu D, et al. Identification of DSBA-l as a key regulator of mitochondrial function, thermogenesis, and energy homeostasis. *Diabetes* (2015) 64:A88. doi: 10.2337/db151385

22. Kissig M, Ishibashi J, Harms MJ, Lim HW, Stine RR, Won KJ, et al. PRDM16 represses the type I interferon response in adipocytes to promote mitochondrial and thermogenic programing. *EMBO J* (2017) 36(11):1528–42. doi: 10.15252/embj.201695588

23. Jun JC, Devera R, Unnikrishnan D, Shin MK, Bevans-Fonti S, Yao Q, et al. Adipose HIF-1alpha causes obesity by suppressing brown adipose tissue thermogenesis. *J Mol Med (Berl)* (2017) 95(3):287–97. doi: 10.1007/s00109-016-1480-6

24. Tsai PJ, Chang ML, Hsin CM, Chuang CC, Chuang LT, Wu WH. Antilipotoxicity activity of osmanthus fragrans and chrysanthemum morifolium flower extracts in hepatocytes and renal glomerular mesangial cells. *Mediators Inflammation* (2017) 2017:4856095. doi: 10.1155/2017/4856095

25. Wei C, Ma X, Su K, Qi S, Zhu Y, Lin J, et al. ChREBP-beta regulates thermogenesis in brown adipose tissue. *J Endocrinol* (2020) 245(3):343–56. doi: 10.1530/JOE-19-0498

26. Shaw A, Tóth BB, Arianti R, Csomós I, Póliska S, Vámos A, et al. Bmp7 increases ucp1-dependent and independent thermogenesis with a unique gene expression program in human neck area derived adipocytes. *Pharmaceuticals* (2021) 14(11). doi: 10.3390/ph14111078

27. Luo J, Wang Y, Gilbert E, Liu D. Deletion of GPR30 drives the activation of mitochondrial uncoupling respiration to induce adipose thermogenesis in female mice. *Front Endocrinol* (2022) 13:877152. doi: 10.3389/fendo.2022.877152

28. Jiménez B, García G, Marqués P, González Blanco C, Burillo J, Guillén C, et al. Essential role of OPA-1 in the functionality of thermogenesis in the brown adipose tissue. *Obes Facts* (2021) 14(SUPPL 1):158. doi: 10.1159/000516203

29. Colitti M, Montanari T. Brain-derived neurotrophic factor modulates mitochondrial dynamics and thermogenic phenotype on 3T3-L1 adipocytes. *Tissue Cell* (2020) 66. doi: 10.1016/j.tice.2020.101388

30. Fisher FM, Kleiner S, Douris N, Fox EC, Mepani RJ, Verdeguer F, et al. FGF21 regulates PGC-1alpha and browning of white adipose tissues in adaptive thermogenesis. *Genes Dev* (2012) 26(3):271–81. doi: 10.1101/gad.177857.111

31. Vegiopoulos A, Muller-Decker K, Strzoda D, Schmitt I, Chichelnitskiy E, Ostertag A, et al. Cyclooxygenase-2 controls energy homeostasis in mice by *de novo* recruitment of brown adipocytes. *Science* (2010) 328(5982):1158–61. doi: 10.1126/science.1186034

32. Seale P, Conroe HM, Estall J, Kajimura S, Frontini A, Ishibashi J, et al. Prdm16 determines the thermogenic program of subcutaneous white adipose tissue in mice. *J Clin Invest* (2011) 121(1):96–105. doi: 10.1172/JCI44271

33. Bostrom P, Wu J, Jedrychowski MP, Korde A, Ye L, Lo JC, et al. A PGC1-alpha-dependent myokine that drives brown-fat-like development of white fat and thermogenesis. *Nature* (2012) 481(7382):463–8. doi: 10.1038/nature10777

34. Shan T, Liang X, Bi P, Kuang S. Myostatin knockout drives browning of white adipose tissue through activating the AMPK-PGC1alpha-Fndc5 pathway in muscle. *FASEB J* (2013) 27(5):1981–9. doi: 10.1096/fj.12-225755

35. Knudsen JG, Murholm M, Carey AL, Bienso RS, Basse AL, Allen TL, et al. Role of IL-6 in exercise training- and cold-induced UCP1 expression in subcutaneous white adipose tissue. *PloS One* (2014) 9(1):e84910. doi: 10.1371/journal.pone.0084910

36. Roberts LD, Bostrom P, O'Sullivan JF, Schinzel RT, Lewis GD, Dejam A, et al. Beta-aminoisobutyric acid induces browning of white fat and hepatic beta-oxidation and is inversely correlated with cardiometabolic risk factors. *Cell Metab* (2014) 19(1):96–108. doi: 10.1016/j.cmet.2013.12.003

37. Fruhbeck G, Fernandez-Quintana B, Paniagua M, Hernandez-Pardos AW, Valenti V, Moncada R, et al. FNDC4, a novel adipokine that reduces lipogenesis and promotes fat browning in human visceral adipocytes. *Metabolism* (2020) 108:154261. doi: 10.1016/j.metabol.2020.154261

38. Huang W, Bansode RR, Bal NC, Mehta M, Mehta KD. Protein kinase cbeta deficiency attenuates obesity syndrome of ob/ob mice by promoting white adipose tissue remodeling. *J Lipid Res* (2012) 53(3):368–78. doi: 10.1194/jlr.M019687

39. Bean C, Audano M, Varanita T, Favaretto F, Medaglia M, Gerdol M, et al. The mitochondrial protein Opa1 promotes adipocyte browning that is dependent on urea cycle metabolites. *Nat Metab* (2021) 3(12):1633–47. doi: 10.1038/s42255-021-00497-2

40. Koh EH, Chen Y, Bader DA, Hamilton MP, He B, York B, et al. Mitochondrial activity in human white adipocytes is regulated by the ubiquitin carrier protein 9/microRNA-30a axis. *J Biol Chem* (2016) 291(47):24747–55. doi: 10.1074/jbc.M116.749408

41. Vonhogen I, El AH, Olieslagers S, Vasilevich A, de Boer J, Tinahones FJ, et al. MiR-337-3p promotes adipocyte browning by inhibiting TWIST1. *Cells* (2020) 9(4):1–16. doi: 10.3390/cells9041056

42. Tu WZ, Fu YB, Xie X. RepSox, a small molecule inhibitor of the TGFbeta receptor, induces brown adipogenesis and browning of white adipocytes. *Acta Pharmacol Sin* (2019) 40(12):1523–31. doi: 10.1038/s41401-019-0264-2

43. Pardo R, Blasco N, Vila M, Beiroa D, Nogueiras R, Canas X, et al. EndoG knockout mice show increased brown adipocyte recruitment in white adipose tissue and improved glucose homeostasis. *Endocrinology* (2016) 157(10):3873–87. doi: 10.1210/en.2015-1334

44. Li T, Du M, Wang H, Mao X. Milk fat globule membrane and its component phosphatidylcholine induce adipose browning both *in vivo* and *in vitro*. *J Nutr Biochem* (2020) 81:108372. doi: 10.1016/j.jnutbio.2020.108372

45. Gustafson B, Hammarstedt A, Hedjazifar S, Hoffmann JM, Svensson PA, Grimsby J, et al. BMP4 and BMP antagonists regulate human white and beige adipogenesis. *Diabetes* (2015) 64(5):1670–81. doi: 10.2337/db14-1127

46. Perwitz N, Wenzel J, Wagner I, Büning J, Drenckhan M, Zarse K, et al. Cannabinoid type 1 receptor blockade induces transdifferentiation towards a brown fat phenotype in white adipocytes. *Diabetes Obes Metab* (2010) 12(2):158–66. doi: 10.1111/j.1463-1326.2009.01133.x

47. Xiong M, Hu W, Tan Y, Yu H, Zhang Q, Zhao C, et al. Transcription factor E2F1 knockout promotes mice white adipose tissue browning through autophagy inhibition. *Front IN Physiol* (2021) 12:748040. doi: 10.3389/fphys.2021.748040

48. Tang Q, Lu M, Xu B, Wang Y, Lu S, Yu Z, et al. Electroacupuncture regulates inguinal white adipose tissue browning by promoting sirtuin-1-Dependent PPARgamma deacetylation and mitochondrial biogenesis. *Front Endocrinol (Lausanne)* (2020) 11:607113. doi: 10.3389/fendo.2020.607113

49. Kotzbeck P, Giordano A, Mondini E, Murano I, Severi I, Venema W, et al. Brown adipose tissue whitening leads to brown adipocyte death and adipose tissue inflammation. *J Lipid Res* (2018) 59(5):784–94. doi: 10.1194/jlr.M079665

50. Fruhbeck G, Mendez-Gimenez L, Becerril S, Ramirez B, Hernandez-Pardos AW, Cienfuegos JA, et al. Increased aquaporin-7 expression is associated with changes in rat brown adipose tissue whitening in obesity: impact of cold exposure and bariatric surgery. *Int J Mol Sci* (2023) 24(4):1–17. doi: 10.3390/ijms24043412

51. Shimizu I, Walsh K. The whitening of brown fat and its implications for weight management in obesity. *Curr Obes Rep* (2015) 4(2):224–9. doi: 10.1007/s13679-015-0157-8

52. Huwatibieke B, Yin W, Liu L, Jin Y, Xiang X, Han J, et al. Mammalian target of rapamycin signaling pathway regulates mitochondrial quality control of brown adipocytes in mice. *Front Physiol* (2021) 12:638352. doi: 10.3389/fphys.2021.638352

53. Shimizu I, Aprahamian T, Kikuchi R, Shimizu A, Papanicolaou KN, MacLauchlan S, et al. Vascular rarefaction mediates whitening of brown fat in obesity. *J Clin Invest* (2014) 124(5):2099–112. doi: 10.1172/JCI71643

54. Bean C, Varanita T, Favaretto F, Vettor R. The mitochondria and cristae shaping protein Opa1 impinges on fat browning to control insulin sensitivity. *Obes Rev* (2016) 17:15. doi: 10.1111/obr.12398

55. Mancini G, Pirruccio K, Yang X, Bluher M, Rodeheffer M, Horvath TL. Mitofusin 2 in mature adipocytes controls adiposity and body weight. *Cell Rep* (2019) 26(11):2849–2858.e4. doi: 10.1016/j.celrep.2019.02.039

56. Boutant M, Kulkarni SS, Joffraud M, Ratajczak J, Valera-Alberni M, Combe R, et al. Mfn2 is critical for brown adipose tissue thermogenic function. *EMBO J* (2017) 36(11):1543–58. doi: 10.15252/embj.201694914

57. Pereira RO, White J, Fang S, Olvera A, Hewezi R, McGlauflin R, et al. Mice lacking OPA1 in adipose tissue are resistant to diet-induced obesity and insulin resistance. *Circulation* (2017) 136.

58. Schlein C, Fischer AW, Worthmann A, Schaltenberg N, John C, Lynes M, et al. Mlxipl controls brown adipose tissue whitening. *Med Genet.-Berlin* (2019) 31(1):106. doi: 10.1007/s11825-019-0234-6

59. Takaya K, Matsuda N, Asou T, Kishi K. Brown preadipocyte transplantation locally ameliorates obesity. *Arch Plast Surg* (2021) 48(4):440–7. doi: 10.5999/aps.2020.02257

60. Zou S, Zhu L, Huang K, Luo H, Xu W, He X. Adipose tissues of MPC1± mice display altered lipid metabolism-related enzyme expression levels. *PeerJ* (2021) 6:e5799. doi: 10.7717/peerj.5799

61. Wu H, Wang Y, Li W, Chen H, Du L D, Wang X, et al. Chen: Deficiency of mitophagy receptor FUNDC1 impairs mitochondrial quality and aggravates dietary-induced obesity and metabolic syndrome. *Autophagy* (2019) 15(11):1882–98. doi: 10.1080/15548627.2019.1596482

62. Waldman M, Alex R, Kornowski R, Hochhauser E, Arad M, Abraham NG. Adipocyte pgc1-α and nov/ccn3: novel targets in the management of obesity-linked cardiomyopathy. *Circulation* (2021) 144(SUPPL 1). doi: 10.1161/circ.144.suppl-1.13903

63. Vernochet C, Mourier A, Bezy O, MacOtela Y, Boucher J, Rardin MJ, et al. Adipose-specific deletion of TFAM increases mitochondrial oxidation and protects mice against obesity and insulin resistance. *Cell Metab* (2012) 16(6):765–76. doi: 10.1016/j.cmet.2012.10.016

64. Vernochet C, Bezy O, Macotela Y, Emanuelli B, Larson NG, Kahn CR. Deletion of the mitochondrial transcription factor a (Tfam) in adipose tissue protects mice from age-and diet-induced obesity and insulin resistance. *Endocr Rev* (2011) 32(3). doi: 10.1210/endo-meetings.2011.PART4.OR3.OR31-3

65. Hill BG, Cummins TD, Sansbury BE, Holden CR, Bhatnagar A. Metabolic remodeling of white adipose tissue in obesity. *Free Radical Bio Med* (2012) 53:S93. doi: 10.1016/j.freeradbiomed.2012.10.167

66. Ko MS, Yun JY, Baek IJ, Jang JE, Hwang JJ, Lee SE, et al. Mitophagy deficiency increases NLRP3 to induce brown fat dysfunction in mice. *Autophagy* (2021) 17 (5):1205–21. doi: 10.1080/15548627.2020.1753002

67. Altshuler-Keylin S, Shinoda K, Hasegawa Y, Ikeda K, Hong H, Kang Q, et al. Beige adipocyte maintenance is regulated by autophagy-induced mitochondrial clearance. *Cell Metab* (2016) 24(3):402–19. doi: 10.1016/j.cmet.2016.08.002

68. Brestoff JR, Wilen CB, Moley JR, Li Y, Zou W, Malvin NP, et al. Intercellular mitochondria transfer to macrophages regulates white adipose tissue homeostasis and is impaired in obesity. *Cell Metab* (2021) 33(2):270–282.e8. doi: 10.1016/j.cmet.2020.11.008

69. Borcherding N, Moley J, Field R, Brestoff JR. Mapping cell-to-cell mitochondria transfer in obesity using high-dimensional spectral flow cytometry. *Am J Clin Pathol* (2021) 156(SUPPL 1):S3–4. doi: 10.1093/ajcp/aqab189.005

70. Otieno D, Lee SG, Kang HW. Beetroot extract increases the expression of uncoupling protein 1 in primary brown adipocytes in vitro. *FASEB J* (2016) 30. doi: 10.1096/fasebj.30.1_supplement.691.36

71. Lin C, Chen J, Hu M, Zheng W, Song Z, Qin H. Sesamol promotes browning of white adipocytes to ameliorate obesity by inducing mitochondrial biogenesis and inhibition mitophagy *via* beta 3-AR/PKA signaling pathway. *Food Nutr Res* (2021) 65:1–12. doi: 10.29219/fnr.v65.7577

72. Jung Y, Park J, Kim HL, Sim JE, Youn DH, Kang J, et al. Vanillic acid attenuates obesity *via* activation of the AMPK pathway and thermogenic factors *in vivo* and in vitro. *FASEB J* (2018) 32(3):1388–402. doi: 10.1096/fj.201700231RR

73. Xiao X, Bai J, Li MS, Zhang JY, Sun XJ, Dong Y. Supplementation of fermented barley extracts with lactobacillus plantarum dy-1 inhibits obesity *via* a UCP1-dependent mechanism. *Biomed Environ sciences: BES* (2019) 32(8):578–91. doi: 10.3967/bes2019.076

74. Lau WK, Noruddin NAA, Ariffin AH, Mahmud MZ, Noor MHM, Amanah A, et al. Novel discovery of averrhoa bilimbi ethanolic leaf extract in the stimulation of brown fat differentiation program in combating diet-induced obesity. *BMC Complem Altern M* (2019) 19(1):243. doi: 10.1186/s12906-019-2640-3

75. Kang J, Park J, Park WY, Jiao W, Lee S, Jung Y, et al. A phytoestrogen secoisolariciresinol diglucoside induces browning of white adipose tissue and activates non-shivering thermogenesis through AMPK pathway. *Pharmacol Res* (2020) 158:104852. doi: 10.1016/j.phrs.2020.104852

76. Zhu R, Wei J, Liu H, Liu C, Wang L, Chen B, et al. Lycopene attenuates body weight gain through induction of browning *via* regulation of peroxisome proliferator-activated receptor γ in high-fat diet-induced obese mice. *J Nutr Biochem* (2020) 78:1–13. doi: 10.1016/j.jnutbio.2019.108335

77. Gao P, Jiang Y, Wu H, Sun F, Li Y, He H, et al. Inhibition of mitochondrial calcium overload by SIRT3 prevents obesity-or age-related whitening of brown adipose tissue. *Diabetes* (2020) 69(2):165–80. doi: 10.2337/db19-0526

78. Seo S, Oh S, Shin Y, Jung S, Kim Y. Reduction of body weight by rutin is associated with an increase of brown adipose tissue mitochondrial biogenesis in high-fat diet induced obese rat. *FASEB J* (2014) 28(1). doi: 10.1096/fasebj.28.1_supplement.lb430

79. Kim H, Park J, Park H, Jung Y, Youn D, Kang J, et al. Platycodon grandiflorum a. de candolle ethanolic extract inhibits adipogenic regulators in 3T3-L1 cells and induces mitochondrial biogenesis in primary brown preadipocytes. *J Agr Food Chem* (2015) 63(35):7721–30. doi: 10.1021/acs.jafc.5b01908

80. Fernández-Galilea M, Pérez-Matute P, Prieto-Hontoria PL, Houssier M, Burrell MA, Langin D, et al. α-lipoic acid treatment increases mitochondrial biogenesis and promotes beige adipose features in subcutaneous adipocytes from overweight/obese subjects. *Biochim Biophys Acta - Mol Cell Biol Lipids* (2015) 1851(3):273–81. doi: 10.1016/j.bbalip.2014.12.013

81. Marqués P, Martínez H, Jiménez B, Burillo J, González-Blanco C, García G, et al. Resveratrol enhanced cold-induced thermogenesis through a differential browning effect on the adipose organ in a mouse model showing atrophied interscapular adipose tissue: a therapeutic approach. *Obes Rev* (2020) 21(SUPPL 1). doi: 10.1111/obr.13115

82. Overby H, Zu Y, Wang S, Zhao L. Nanoparticles encapsulated with resveratrol induce browning of white adipocytes. *FASEB J* (2017) 31(1).

83. Liu Z, Qiao Q, Sun Y, Chen Y, Ren B, Liu X. Sesamol ameliorates diet-induced obesity in C57BL/6J mice and suppresses adipogenesis in 3T3-L1 cells *via* regulating mitochondria-lipid metabolism. *Mol Nutr Food Res* (2017) 61(8). doi: 10.1002/mnfr.201600717

84. Zhang F, Ai W, Hu X, Meng Y, Yuan C, Su H, et al. Phytol stimulates the browning of white adipocytes through the activation of AMP-activated protein kinase (AMPK) α in mice fed high-fat diet. *Food Funct* (2018) 9(4):2043–50. doi: 10.1039/C7FO01817G

85. Chen Y, Liu H, Lee T. Ursodeoxycholic acid regulates hepatic energy homeostasis and white adipose tissue macrophages polarization in leptin-deficiency obese mice. *CELLS* (2019) 8(3):1–24. doi: 10.3390/cells8030253

86. Nederveen JP, Manta K, Bujak AL, Simone AC, Fuda MR, Nilsson MI, et al. A novel multi-ingredient supplement activates a browning program in white adipose tissue and mitigates weight gain in high-fat diet-fed mice. *Nutrients* (2021) 13(11):1–22. doi: 10.3390/nu13113726

87. Yau WW, Singh BK, Lesmana R, Zhou J, Sinha RA, Wong KA, et al. Thyroid hormone (T3) stimulates brown adipose tissue activation *via* mitochondrial biogenesis and MTOR-mediated mitophagy. *Autophagy* (2019) 15(1):131–50. doi: 10.1080/15548627.2018.1511263

88. Lagouge M, Argmann C, Gerhart-Hines Z, Meziane H, Lerin C, Daussin F, et al. Resveratrol improves mitochondrial function and protects against metabolic disease by activating SIRT1 and PGC-1alpha. *Cell* (2006) 127(6):1109–22. doi: 10.1016/j.cell.2006.11.013

89. Rowland LA, Bal NC, Kozak LP, Periasamy M. Uncoupling protein 1 and sarcolipin are required to maintain optimal thermogenesis, and loss of both systems compromises survival of mice under cold stress. *J Biol Chem* (2015) 290(19):12282–9. doi: 10.1074/jbc.M115.637603

90. Lombardi A, Moreno M, de Lange P, Iossa S, Busiello RA, Goglia F. Regulation of skeletal muscle mitochondrial activity by thyroid hormones: focus on the "old" triiodothyronine and the "emerging" 3,5-diiodothyronine. *Front Physiol* (2015) 6:237. doi: 10.3389/fphys.2015.00237

91. Gorrell E, Shemery A, Kowalski J, Bodziony M, Mavundza N, Titus AR, et al. Skeletal muscle thermogenesis induction by exposure to predator odor. *J Exp Biol* (2020) 223(Pt 8). doi: 10.1242/jeb.218479

92. Pani S, Dey S, Pati B, Senapati U, Bal NC. Brown to white fat transition overlap with skeletal muscle during development of larger mammals: is it a coincidence? *J Endocr Soc* (2022) 6(12):bvac151. doi: 10.1210/jendso/bvac151

93. Bal NC, Singh S, Reis F, Maurya SK, Pani S, Rowland LA, et al. Both brown adipose tissue and skeletal muscle thermogenesis processes are activated during mild to severe cold adaptation in mice. *J Biol Chem* (2017) 292(40):16616–25. doi: 10.1074/jbc.M117.790451

94. Seale P, Bjork B, Yang W, Kajimura S, Chin S, Kuang S, et al. PRDM16 controls a brown fat/skeletal muscle switch. *Nature* (2008) 454(7207):961–7. doi: 10.1038/nature07182

95. Zhang HQ, Chen SY, Wang AS, Yao AJ, Fu JF, Zhao JS, et al. Sulforaphane induces adipocyte browning and promotes glucose and lipid utilization. *Mol Nutr Food Res* (2016) 60(10):2185–97. doi: 10.1002/mnfr.201500915

96. Hao M, Guan Z, Gao Y, Xing J, Zhou X, Wang C, et al. Huang-Qi San ameliorates hyperlipidemia with obesity rats *via* activating brown adipocytes and converting white adipocytes into brown-like adipocytes. *Phytomedicine* (2020) 78. doi: 10.1016/j.phymed.2020.153292

97. Ma L, Zhao Z, Guo X, Li J, Xu L, Mei W, et al. Tanshinone IIA and its derivative activate thermogenesis in adipocytes and induce "beiging" of white adipose tissue. *Mol Cell Endocrinol* (2022) 544. doi: 10.1016/j.mce.2022.111557

98. Jung DY, Suh N, Jung MH. Tanshinone 1 prevents high fat diet-induced obesity through activation of brown adipocytes and induction of browning in white adipocytes. *Life Sci* (2022) 298. doi: 10.1016/j.lfs.2022.120488

99. Ravaud C, Paré M, Yao X, Azoulay S, Mazure NM, Dani C, et al. Resveratrol and HIV-protease inhibitors control UCP1 expression through opposite effects on p38 MAPK phosphorylation in human adipocytes. *J Cell Physiol* (2020) 235(2):1184–96. doi: 10.1002/jcp.29032

100. Xu L, Xu C, Liu X, Li X, Li T, Yu X, et al. Empagliflozin induces white adipocyte browning and modulates mitochondrial dynamics in KK cg-Ay/J mice and mouse adipocytes. *Front Physiol* (2021) 12:745058. doi: 10.3389/fphys.2021.745058

101. Cai M, Zhao J, Liu Q, Wang X, Wang Y. FAM134B improves preadipocytes differentiation by enhancing mitophagy. *Biochim Biophys Acta - Mol Cell Biol Lipids* (2019) 1864(12). doi: 10.1016/j.bbalip.2019.08.004

102. Jiménez-Aranda A, Fernández-Vázquez G, Campos D, Tassi M, Velasco-Perez L, Tan DX, et al. Melatonin induces browning of inguinal white adipose tissue in zucker diabetic fatty rats. *J Pineal Res* (2013) 55(4):416–23. doi: 10.1111/jpi.12089

frontiers | Frontiers in Endocrinology

TYPE Review
PUBLISHED 03 July 2023
DOI 10.3389/fendo.2023.1215772

Check for updates

OPEN ACCESS

EDITED BY
Endre Károly Kristóf,
University of Debrecen, Hungary

REVIEWED BY
Monica Colitti,
University of Udine, Italy
Rosemari Otton,
Universidade Cruzeiro do Sul, Brazil

*CORRESPONDENCE
Wenxiang Hu
hu_wenxiang@gzlab.ac.cn

†These authors have contributed equally to this work

RECEIVED 02 May 2023
ACCEPTED 14 June 2023
PUBLISHED 03 July 2023

CITATION
Wang C, Wang X and Hu W (2023) Molecular and cellular regulation of thermogenic fat.
*Front. Endocrinol.* 14:1215772.
doi: 10.3389/fendo.2023.1215772

COPYRIGHT
© 2023 Wang, Wang and Hu. This is an open-access article distributed under the terms of the Creative Commons Attribution License (CC BY). The use, distribution or reproduction in other forums is permitted, provided the original author(s) and the copyright owner(s) are credited and that the original publication in this journal is cited, in accordance with accepted academic practice. No use, distribution or reproduction is permitted which does not comply with these terms.

# Molecular and cellular regulation of thermogenic fat

Cuihua Wang[1,2†], Xianju Wang[1†] and Wenxiang Hu[1*]

[1]GMU-GIBH Joint School of Life Sciences, The Guangdong-Hong Kong-Macau Joint Laboratory for Cell Fate Regulation and Diseases, Guangzhou Laboratory, Guangzhou Medical University, Guangzhou, China, [2]Zhongshan School of Medicine, Sun Yat-Sen University, Guangdong, China

Thermogenic fat, consisting of brown and beige adipocytes, dissipates energy in the form of heat, in contrast to the characteristics of white adipocytes that store energy. Increasing energy expenditure by activating brown adipocytes or inducing beige adipocytes is a potential therapeutic strategy for treating obesity and type 2 diabetes. Thus, a better understanding of the underlying mechanisms of thermogenesis provides novel therapeutic interventions for metabolic diseases. In this review, we summarize the recent advances in the molecular regulation of thermogenesis, focusing on transcription factors, epigenetic regulators, metabolites, and non-coding RNAs. We further discuss the intercellular and inter-organ crosstalk that regulate thermogenesis, considering the heterogeneity and complex tissue microenvironment of thermogenic fat.

KEYWORDS

**thermogenic fat, energy expenditure, transcription factor, epigenetic modification, intercellular regulation, inter-organ crosstalk**

## Introduction

Obesity is a chronic and complex condition resulting from an imbalance of excessive energy intake and insufficient energy expenditure, and it is tightly associated with type 2 diabetes, cardiovascular disease, nonalcoholic fatty liver disease (NAFLD), and other metabolic diseases (1). Adipose tissue is a metabolically active organ with significant roles in regulating whole-body energy homeostasis, whose dysfunction causes obesity and related metabolic disorders. Mammals have been shown to possess two classes of fat cells—white and thermogenic adipocytes. White adipocyte contains a large lipid droplet and a few mitochondria and plays an essential role in energy storage in triglycerides. In contrast, thermogenic adipocytes possess multilocular lipid droplets and higher amounts of mitochondria and dissipate energy in the form of heat.

Thermogenic adipocytes consist of brown adipocytes and beige adipocytes. Brown adipocytes are characterized by marker gene *uncoupling protein 1* (*Ucp1*), which uncouples oxidative respiration from ATP synthesis, resulting in energy dissipation as heat (2). The brown adipose tissue (BAT) is predominantly located in the interscapular region of infants and rodents. UCP1-positive multilocular adipocytes were also found in cervical and supraclavicular regions in human adults using positron-emission tomography and

computed tomography (PET/CT) imaging (3, 4). Importantly, BAT activity is inversely correlated with body mass index (BMI) and age in humans (5, 6). Moreover, *Ucp1*-deficient mice gain more weight than wild-type mice under thermoneutral conditions (7, 8), while transplantation of mouse BAT or CRISPR-enhanced human or mouse brown-like adipocytes improves glucose tolerance and insulin sensitivity in recipient mice (9, 10). These data suggest the importance of BAT in regulating energy metabolism and homeostasis both in mice and humans. In regard to beige adipocytes, they are predominantly spread in inguinal white adipose tissue (iWAT), and induced in response to cold environment, exercise training or activation of β-adrenergic receptors (β-AR) in mice (11). Intriguingly, the gene profile of mouse beige adipocyte is very similar to that of human BAT in the supraclavicular region during cold exposure (12). Induction of browning in iWAT by transgenic expression of PR domain-containing 16 (Prdm16) increases *Ucp1* mRNA level and protects the mice from diet-induced obesity (13). Therefore, inducing the formation of beige adipocytes may serve as an alternative therapeutic strategy for combating obesity and metabolic diseases.

In this review, we summarize the cell autonomous and non-cell autonomous regulation of the biogenesis and function of thermogenic fat, which will facilitate the development of new therapies for metabolic diseases.

## Molecular regulations of thermogenesis of brown and beige adipocytes

Brown adipocyte and beige adipocyte share similar functions in energy expenditure and thermogenesis, and various molecular events involve in the cell fate determination of thermogenic fat and thermogenesis, including transcriptional regulation, epigenetic modulation, non-coding RNA regulation and metabolic reprogramming (Figure 1).

### Transcriptional regulation of thermogenesis in brown and beige adipocytes

The cell fate determination of thermogenic fat is regulated by various adipocyte-specific lineage-determining transcription factors and co-factors as shown in Table 1. There are three core regulators in the regulation of thermogenesis of beige and brown adipocyte, proliferator-activated receptor γ(PPARγ), PRDM16 and peroxisome proliferator-activated receptor γ coactivator 1 α (PGC1α). PPARγ was indispensable for the function of both

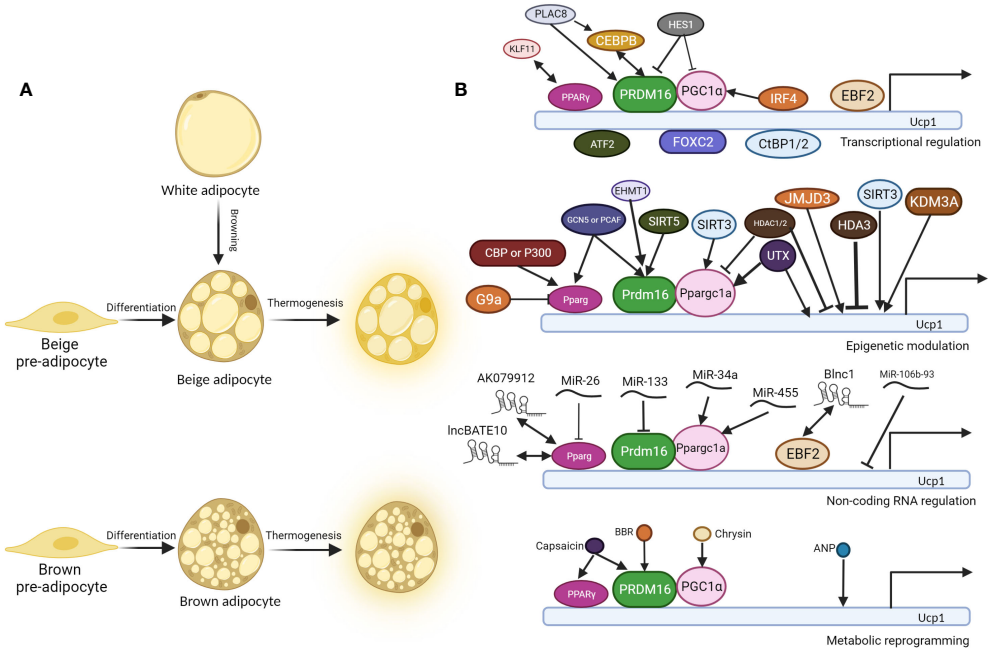


FIGURE 1
Molecular regulation of thermogenesis of brown and beige adipocytes. **(A)**. Beige pre-adipocyte and brown pre-adipocyte differentiate into beige adipocyte and brown adipocyte respectively. In specific conditions, white adipocytes convert into beige adipocytes, a process called "browning". Under cold exposure or other signal induction, differentiated brown and beige adipocytes undergo thermogenesis, accompanied by higher glucose and fatty acid uptake, *UCP1* expression, and uncoupled respiration. **(B)**. Regulatory mechanisms behind thermogenesis of brown and beige adipocytes including the following 4 parts: 1. Transcriptional regulation; 2. Epigenetic modulation; 3. Non-coding RNA regulation; 4. Metabolic reprogramming. *UCP1* is one of the most critical thermogenic genes, and its expression is critical for uncoupled cellular respiration. There are three core regulators in the thermogenesis program regulation: PPARγ, PRDM16, and PGC1α, and most other regulators regulate thermogenesis through them. Double-headed arrows indicate protein interaction and complex formation, while arrow-headed and bar-headed lines show inducing and inhibiting effects.

white and brown adipocytes. PPARγ ligands induce the browning of white adipocytes with the cooperation of PRDM16 (30). PRDM16 is highly expressed in brown adipocyte cells, and overexpression of PRDM16 leads to the browning of white adipocytes. Consistently, knock down of PRDM16 causes to the loss of brown fat cell identity (32). PGC1α also plays essential roles in energy metabolism and homeostasis. Although mice without PGC1α underwent normal brown fat differentiation, it accompanied with decreased thermogenic genes induction (25).

As will discussed in more details below, there are more than 30 transcriptional regulators identified to positively or negatively regulate the formation and function of beige and brown adipocytes, and most of them function through the above three core regulators. CCAAT enhancer-binding protein beta (C/EBPβ) forms a

TABLE 1 Transcription regulators behind thermogenesis of brown and beige adipocytes.

| Factors | Type | Model system | Function | Ref. |
|---|---|---|---|---|
| **ATF2** | TF (+) | Interscapular BAT (IBAT) | Phosphorylated form promotes UCP1 expression | (14) |
| **C/EBPα** | TF (+) | 3T3-L1 preadipocytes | Inhibits the expression of white fat genes and promotes the expression of brown-specific genes | (15) |
| **C/EBPβ** | TF (+) | Skin fibroblasts from mouse and man | Form complex with PRDM16 to switch myoblastic precursors to brown fat cells | (16) |
| **CtBP1/2** | Coregulator (+) | 3T3-L1 adipocytes | Interacts with C/EBPα to inhibit the expression of white adipocyte genes | (15) |
| **EBF2 (COE2)** | TF (+) | Primary brown and white preadipocytes | Recruits PPARγ to BAT specific genes | (17) |
| **FoxC2** | TF (+) | Transgenic mice with FoxC2 overexpression in fat | Transcription activates UCP1 | (18) |
| **HES1** | TF (-) | Mouse model | Binds promoters of *Prdm16* and *Ppargc1a* to inhibit their expression | (19) |
| **IRF4** | TF (+) | Mouse model | Interacts with PGC1α to drive *Ucp1* expression | (20) |
| **IRX3, IRX5** | TF (-) | Primary human adipose–derived progenitor cell cultures | Knockdown of IRX3 or IRX5 restore thermogenesis induced by risk allele | (21, 22) |
| **KLF11** | TF (+) | hMADS-3 cells were differentiated into mature adipocytes | Cooperates with PPARγ to activate and maintain brite selective gene program | (23) |
| **MRTFA** | TF (-) | White adipose tissue from MRTFA(-/-) mice | Under the control of BMP7-ROCK signaling axis and inhibits brown-selective genes' expression in white adipose tissue | (24) |
| **PGC1α** | Coregulator (+) | Immortal preadipocyte lines from mice lacking PGC1α | Plays essential roles in brown fat thermogenesis | (25–28) |
| **PLAC8** | Coregulator (+) | Brown preadipocyte lines | Induces the expression of *C/EBPβ* and *Prdm16* | (29) |
| **PPARγ** | TF* (+) | White adipocytes and mouse model | Acts collaboratively with PRDM16 to induce brown fat gene program | (30, 31) |
| **PRDM16** | Coregulator (+) | Brown fat precursors, white fat cell progenitors and white fat depots | Activates expression of PGC1α, UCP1 and Dio2 | (30–33) |
| **PRDM3** | Coregulator (+) | Mouse model with PRDM16/PRDM3 double-knockout | Reduces BAT specific genes' expression in the knockout mice | (34) |
| **Rb and p107** | TF (-) | p107-/- mice and adult primary preadipocytes | Repress the expression of PGC1α and UCP1 | (35) |
| **RIP140** | Coregulator (-) | 3T3-L1 adipocytes, RIP140-null mice | Suppresses adipocyte oxidative metabolism and mitochondrial biogenesis | (36–38) |
| **SIRT1** | Coregulator (+) | 3T3-L1 cells and mouse model | Catalyzes deacetylation of PPAR γ Lys268 and Lys293, and recruits PRDM16 to Pparγ, to induce BAT genes | (31) |
| **SMAD3** | TF (-) | Smad3-deficient mice | Represses PGC1α expression | (39) |
| **SRC1** | TF (+) | SRC-1-/- mice | Reduces energy expenditure | (40) |
| **TBX15** | TF (+) | Adipose tissue in 129/Sv mouse pups | Induces expression of brown phenotypic marker genes | (41) |
| **TFAM** | mitochondrial TF (+) | TFAM floxed (TFAMf/f) mice | Knocking down TFAM decreases mtDNA copy number and Complex I activity | (42) |

*(Continued)*

TABLE 1 Continued

| Factors | Type | Model system | Function | Ref. |
|---|---|---|---|---|
| **TIF2** | TF (-) | TIF2-/- mice | Enhances adaptive thermogenesis in the KO mice | (40) |
| **TLE3** | TF (-) | Brown Preadipocytes, mice lacking TLE3 | Disrupts interaction between Prdm16 and PPARγ, and suppresses brown-selective genes | (43) |
| **TWIST1** | TF (-) | Mouse model | Interacts with PGC1α to suppress brown thermogenesis gene | (44) |
| **USF1** | TF (-) | Mice lacking Usf1 | Increases BAT-facilitated thermogenesis in the *Usf1* knockout mice | (45) |
| **ZFP423** | TF (+) | 3T3-L1, 3T3 and Zfp423 knockout mice | Activates *Pparg* expression and increases adipocyte differentiation | (46–48) |
| **ZFP516** | TF (+) | Zfp516 knockout embryos | Activates UCP1 and PGC1α, to promote a BAT program | (49) |

transcriptional complex with PRDM16 to induce brown fat cell determination and differentiation (16). In contrast, CCAAT enhancer-binding protein alpha (C/EBPα) acts collaboratively with other corepressors C-terminal-binding protein 1/2 (CtBP1/2) to repress the expression of white fat genes (15). Early B-cell factor 2 (EBF2), a selective marker of brown and beige precursors (50), regulates the cell fate determination of brown fat precursor cells and the expression of thermogenic genes (17). Brown adipocytes isolated from mice with *Ebf2* deficiency exhibit diminished mitochondrial density and larger lipid droplets (51). Interferon regulatory factor 4 (IRF4), which is induced by cold and cAMP, interacts with PGC1α to promote the expression of PRDM16 and then drive the expression of thermogenic genes (20). Claussnitzer et al. found that rs1421085 T-to-C single-nucleotide variant disrupts the function of AT-rich interative domain-containing protein 5B (ARID5B) that repress the expression of Iroquois homeobox protein 3 (IRX3) and Iroquois homeobox protein 5 (IRX5), which further result in a shift from beige adipocytes to white adipocytes (21). Loft et al. reported that kruepple-like factor 11 (KLF11), which is induced by PPARγ agonists, acts in cooperation with PPARγ to activate beige-selective gene program (23). Zinc finger transcription factors also play important roles in thermogenesis. Gupta et al. reported that zinc finger protein 423 (Zfp423) expression is enriched in white adipocytes compared to brown adipocytes and is repressed upon cold exposure (46). Zfp423 inhibits the activity of EBF2 and suppress PRDM16 activation to maintain white adipocyte identity, and loss of adipocyte Zfp423 induces an EBF2 NuRD-to-BAF coregulator switch and promotes thermogenic genes (47). Dempersmier et al. stated that zinc finger protein 516 (Zfp516) directly binds to the proximal region of the *Ucp1* promoter and activates its expression to induce white fat cell browning and the development of brown fat cells (49). Taken together, the formation and function of thermogenic fat greatly rely on a complex transcriptional network coordinated by a set of core transcriptional factors.

## Epigenetic modulation behind thermogenesis of brown and beige adipocytes

Adipogenesis is involved with complicated epigenetic remodeling that mainly include histone modification and DNA methylation, the two fundamental processes that play crucial roles in the regulation of gene expression and genome stability. In general, Histone modifications modulate chromatin structure, influencing gene accessibility and transcriptional activity, while DNA methylation directly modifies the DNA sequence, leading to gene silencing. A lot of studies have demonstrated the roles of epigenetic modulators in regulating the formation and function of thermogenic adipocytes (Table 2). In this review, we specifically focused on the role of histone modification, including histone acetylation, histone deacetylation, histone methylation, and histone demethylation.

Epigenetic modulators catalyze the formation of active epigenetic markers in the regulatory regions of corresponding genes to positively regulate their expression. CREB binding protein (CBP) and histone acetyltransferase p300 (P300), which catalyze histone acetylation of H3K27, improve the expression of *PPARγ* and then promote adipocyte differentiation and white adipocyte browning (52). General control of amino acid synthesis 5-like 2 (GCN5) and P300/CBP-associated factor (PCAF), which acetylate histone H3K9, also facilitate brown adipogenesis through positively regulating the expression of *Pparγ*and *Prdm16* (53).

In regard to histone deacetylation, epigenetic modulators erase pre-settled active epigenetic marker at the regulatory regions of thermogenic genes to negatively regulate their expression. Histone deacetylases (HDAC1, HDAC2, HDAC3, HDAC9 and HDAC11) exert their influences on thermogenesis through deacetylation of H3K27ac (79). HDAC1 and HDAC2 negatively regulate brown adipocyte thermogenic program through decreasing acetylation of histone H3 lysine 27, an active epigenetic marker, on the promoter regions of *Ucp1* and *Pgc1α* to inhibit their expression (54). Ferrari et al. showed HDAC3 deletion induce WAT browning through increased H3K27ac modification at the enhancer region of *Pparγ* and *Ucp1* (55). However, other study revealed that HDAC3 primes *Ucp1* and the thermogenic transcriptional program to maintain the brown adipose tissue identity through deacetylation of PGC1α by HDAC3 (80). Bagchi et al. reported that HDAC11 suppresses WAT browning through physical association with bromodomain-containing protein 2 (BRD2) (57). Other histone deacetylases, including NAD-dependent protein deacetylases-SIRT1, SIRT2, SIRT3, SIRT5, SIRT6, and SIRT7, catalyze the deacetylation of H3K9ac, and/or H4K16ac (58, 81, 82). Shi et al. found that SIRT3 positively correlated with the expression of *Pgc1α* and *Ucp1*, and

TABLE 2 Epigenetic regulators behind thermogenesis of brown and beige adipocytes.

| Histone modification | Epigenetic regulators | Influenced gene | Roles | Ref. |
|---|---|---|---|---|
| **Histone acetylation** | CBP and P300 | *Pparγ* | Promotes adipocyte differentiation | (52) |
| | GCN5 and PCAF | *Pparγ* and *Prdm16* | Facilitates brown adipogenesis | (53) |
| **Histone deacetylation** | HDAC1 and HDAC2 | *Ucp1* and *Pgc1α* | Negatively regulates thermogenic program in brown adipocytes | (54) |
| | HDAC3 | *Pparg*, *Ucp1* and *Ppara* | Inhibits WAT browning | (55) |
| | HDAC9 | *C/EBPα* | Negative regulates adipogenic differentiation | (56) |
| | HDAC11 | *Brd2* | Suppresses brown adipocyte differentiation | (57) |
| | SIRT1 | *Pparγ*, *sFRP1*, *sFRP2*, and *Dact1* | Induces browning of WAT and enhances BAT function | (31, 58, 59) |
| | SIRT2 | *Foxo1* and *Pparγ* | Suppresses adipocyte differentiation | (60) |
| | SIRT3 | *CREB* and *PGC1α* | Activates mitochondria functions and adaptive thermogenesis in brown adipose | (61) |
| | SIRT5 | *Pparγ* and *Prdm16* | Promotes subcutaneous white adipose tissue browning | (62) |
| | TET | *Ucp1* and *Pgc1α* | Inhibits thermogenic genes' expression | (63) |
| **Histone Methylation** | MLL3 | *aP2* | Promotes brown and white adipocytes differentiation | (64) |
| | MLL4 | *C/EBPs* and *Pparγ* | Promotes brown and white adipocytes differentiation | (65, 66) |
| | EHMT1 | *Prdm16* | Promotes BAT-mediated adaptive thermogenesis | (67) |
| | G9A | *Pparγ* | Inhibits brown and white adipocytes differentiation | (68) |
| | KMT5c | *Trp53* | Activates thermogenic program in adipocytes | (69) |
| | DOT1L | *Ucp1* and *Prdm16* | Inhibits thermogenic adipocyte differentiation and function | (70) |
| **Histone Demethylation** | LSD1 | *Ppara* | Promotes white adipocyte browning | (71) |
| | LSD2 | Brown adipogenesis genes, such as *Ucp1* | Promotes brown adipocyte differentiation | (72) |
| | KDM5A | *C/EBPβ* and *Wnt6* | Promotes preadipocyte differentiation | (73) |
| | Kdm3a | *Ppara* and *Ucp1* | Promotes white adipocyte browning | (74–76) |
| | Jmjd3 | *Rreb1*, *Ucp1* and *Cidea* | Promotes browning of WAT | (77) |
| | UTX | *Ucp1* and *PGC1α* | Regulates brown adipocyte thermogenic program | (78) |

SIRT3 activates mitochondria functions and adaptive thermogenesis in brown adipose (61). Shuai et al. found SIRT5 promoted the browning of subcutaneous white adipose tissue through regulating H3K9me2 and H3K9me3 modification at the promoter regions of *Pparγ* and *Prdm16* (62). Moreover, ten-eleven translocation (TET) proteins, oxidize 5-methylcytosines and promote specific DNA demethylation (83), were found to inhibit β3-AR dependent thermogenic genes' expression and white fat browning through indirectly recruiting histone deacetylases to the promoter regions of concerning genes (63).

Histone methylation exerts essential roles in regulating chromatin functional states and usually includes two types of amino acids modification, lysine methyl-transferation and arginine methyl-transferation. Several studies have linked histone methylation with thermogenesis (79). Euchromatic histone methyltransferase 1 (EHMT1), which could catalyze methylation of histone 3 lysine 9 (H3K9me2 and me3), promotes adaptive thermogenesis through stabilizing PRDM16 protein (67). Lysine methyltransferase 5C (KMT5C), a H4K20 methyltransferase, positively regulates thermogenesis through regulating the expression of *transformation related protein 53* (*Trp53*), a repressor of thermogenic program (69). DOT1-like (DOT1L), a lysine 79 of histone H3 (H3K79) methyltransferase, inhibits thermogenic adipocyte differentiation and function through repressing the expression of brown adipocyte tissue-selective genes (70).

Histone demethylases catalyze histone demethylation that usually correlates with enhanced adipogenesis and white adipocyte browning. LSD1, lysine-specific demethylase 1, increases the content of beige adipocytes in aging inguinal white adipose tissue through activating the expression of *proliferator-activated receptor alpha* (*Pparα*) (71). Similarly, lysine-specific demethylase 2 (LSD2) plays its vital roles primarily at the early stage of brown adipocyte differentiation, and its deletion *in vivo* was accompanied with compromised expression of thermogenic genes (72). Tateishi et al. demonstrated lysine-specific demethylase 3A

(KDM3A) positively regulates *Pparα* and *Ucp1* expression, and KDM3A-deficient mice developed obesity and hyperlipidemia (74). Pan et al. revealed that JmjC domain-containing protein 3 (JMJD3) demethylases repressive mark H3K27me3 at the promoter regions of *Ucp1* and *Cell death-inducing DFFA-like effector a* (*Cidea*) in order to activate thermogenic program and induce white adipocyte browning (77). Moreover, UTX, ubiquitously transcribed tetratricopeptide repeat on chromosome X, catalyzes demethylation of H3K27me2/3 at the promoter region of *Ucp1* and *Pgc1α* to positively regulate their expression and promote brown adipocyte thermogenic genes expression (78). Altogether, various epigenetic remodelers act through altering histone acetylation and methylation dynamics to regulate the thermogenic program in response to the external stimuli.

## Non-coding RNAs regulation of thermogenesis of brown and beige adipocytes

Non-coding RNAs, including microRNAs (miRNAs) and long non-coding RNAs (lncRNAs), play important roles in the development and physiology of white, brown and beige adipocytes, and non-coding RNAs themselves can serve as markers of different adipocyte tissue depots (Table 3).

miRNAs usually exert their functions on regulating thermogenesis through complementary reaction with the UTR regions of mRNA transcripts of effector genes. MiR-26 is upregulated during human adipogenesis and induces brown adipocyte differentiation through directly targeting ADAM metallopeptidase domain 17 (ADAM17) (84). MiR-30b/c target 3'UTR of receptor-interacting protein 140 (RIP140), a negative regulator of thermogenic genes, to promote brown adipose tissue function and the development of beige fat (91). MiR-32 is highly expressed during cold exposure, and increases *fibroblast growth factor 21* (*Fgf21*) expression through repressing the expression of *transducer of ErbB-2.1* (*Tob1*), which further promotes white fat cell browning and BAT thermogenesis (92). Ge et al. showed miR-34a inhibits white adipocytes browning through targeting *fibronectin type III domain-containing protein 5* (*Fndc5*) expression (93), while Fu et al. demonstrated miR-34a promotes the deacetylation of PGC1α and its activation by targeting fibroblast growth factor receptor 1 (FGFR1), klotho beta-like protein (βKL) and NAD-dependent protein deacetylase sirtuin-1 (SIRT1) (94). MiR-106b-93 cluster negatively regulate the expression of *Ucp1* and promote the lipid content in differentiated brown adipocytes (95). Giroud et al. reported miR-125b prevents beige adipocyte formation through decreasing mitochondrial biogenesis (96). miR-133 targets 3' UTR of *Prdm16* to repress its expression that lead to impaired brown fat differentiation and WAT browning (97, 98). MicroRNA 155 is down-regulated during brown preadipocyte differentiation and inhibition of miR-155 enhances brown adipocyte differentiation and white adipocytes browning. Mechanistically, miR-155 forms a bistable feedback loop with CEBP-β (99). MiR-193b–365, referred to as miR-193b and miR-365, showed two contradictory results, that Sun et al. found that blocking of miR-193b–365 impair brown adipocyte adipogenesis by upregulating the expression of *runt-related transcriptional factor 1 translocation partner 1* (*Runx1t1*) (102), while Feuermann et al. reported that miR-193b–365 are not required for the differentiation and development of BAT (103). The detailed roles of miR-193b–365 *in vivo* and *in vitro* need to be further clarified.

The regulation of lncRNAs in the thermogenesis of brown and beige adipocytes are mainly through interacting with other important transcription factors such as PGC1α, EBF2, and PPARγ (113). Recent study identified Blnc1 as a vital lncRNA in promoting the function of brown and beige adipocytes, and then further experiments demonstrated Blnc1 acts synergistically with EBF2 to drive thermogenic gene program (108). Similarly, lncRNA-AK079912 was also reported to play a positive role in brown preadipocyte differentiation and white adipocytes browning, which is mediated by PPARγ (109). A brown adipose tissue-enriched lncRNA, lncBATE10, was found to be differently regulated in cold or exercise conditions, and it regulates brown adipose tissue gene program through decoying the repressor factor-CUGBP Elav-like family member 1 (CELF1) from *Pgc1α*'s mRNA elements (110). In together, the influences of lncRNAs on the regulatory network of brown and beige adipocytes differentiation remain elusive, and especially their direct roles in affecting core transcriptional factors of thermogenic program need to be further elucidated. In summary, miRNAs and lncRNAs, the tight regulators of gene expression, play an indispensable role in regulating brown and beige adipogenesis, which further complicates the regulatory network of thermogenesis.

## Metabolic reprogramming behind thermogenesis of brown and beige adipocytes

The development and function of thermogenic fat involves intensive metabolic reprogramming (114). Table 4 summarized the nutrients and metabolites that regulates thermogenesis. Notably, most of the studies were conducted in rodent models and their implications in human need to be further explored.

Wu et al. reported that NAFLD patients treated with Berberine (BBR) for 1 month exhibited increased brown adipocyte mass and activity in mice, since BBR promotes the DNA demethylation of *Prdm16* promoter to activate its expression (117). Dietary capsaicin induces white adipocyte browning through facilitating the interaction and activation of PPARγ and PRDM16, depending on transient receptor potential vanilloid 1 (TRPV1) channels (119). Chlorogenic acid (CGA), a Chinese traditional medicine, induces brown adipocyte thermogenesis through promoting mitochondria function and glucose uptake (121). Lone et al. and Wang et al. demonstrated that curcumin promotes browning of white adipocytes through upregulating *Ucp1* expression (125, 126). Ellagic Acid (EA), located mainly in fruits and plant extracts, also increases iWAT browning through decreasing the expression of *Zfp423* and *aldehyde dehydrogenase family 1 member a1* (*Aldh1a1*) and increasing thermogenic genes expression (128). Epicatechin (Epi), a cacao flavanol, can induce white adipose tissue browning

TABLE 3 Non-coding RNAs behind thermogenesis of brown and beige adipocytes.

| Non-coding RNAs | Regulation | Model system | Roles | Ref |
|---|---|---|---|---|
| **miR-26** | + | Human multipotent adipose-derived stem (hMADS) cells | Represses activity of ADAM17 to increase white adipocytes browning | (84) |
| **miR-27** | – | Human adipose-derived stem cells, Male C57BL/6J mice, 3T3-L1 cells … | Suppresses PPARγ and CEBPα, targets prohibitin (PHB) to inhibit adipogenesis, and upregulates UCP1, PRDM16 and PGC1α | (85–90) |
| **miR-30** | + | Brown preadipocyte cell line, SVFs, and C57BL/6 male mice | Upregulates thermogenic genes' expression | (91) |
| **miR-32** | + | WT-1, iWAT SVF cells and C57BL6/J mice | Promotes BAT thermogenesis and WAT browning | (92) |
| **miR-34a** | – | Male C57BL/6 mice and SVF cells | Suppresses FGF21 and sirtuin1 (SIRT1) and fat browning | (93, 94) |
| **miR-106b-93** | – | Mouse brown preadipocyte cell line, primary mouse stromal vascular fraction (SVF) cells, and C57BL/6J mice | Knockdown of miR-106b-93 increases brown fat-specific genes' expression | (95) |
| **miR-125-5p** | – | C57Bl/6J mice | Inhibits WAT browning | (96) |
| **miR-133** | – | BAT and SAT to mature brown adipocytes, and mouse model | Impairs *Prdm16*, *Ucp1*, *Pparα* and *Pparγ* expression | (97, 98) |
| **miR-155** | – | miR-155-/- mice, BAT and igWAT cells isolated from C57BL/6J mice | Targets CEBPβ to impair *Ucp1* and *Pgc1α* expression | (99, 100) |
| **miR-182 and miR-203** | + | Dgcr8 KO mice and primary brown adipocytes | Knockdown of miR-182 or miR-203 causes reduction of BAT markers | (101) |
| **miR-193b-365** | + | Primary brown preadipocytes and C2C12 myoblasts | Promotes brown adipocyte adipogenesis by inhibiting *Runx1t1* expression, but its roles were controversial | (102, 103) |
| **miR-196a** | + | Human WAT-progenitor cells, fat progenitor cells, and C57Bl/6 mice | Suppresses expression of white-fat gene *Hoxc8* | (104) |
| **miR-328** | + | Mouse model | Inhibition of miR-328 decreases thermogenic genes' expression | (105) |
| **miR-378** | +- | C57BL6 mice, and isolated BAT and gonadal WAT | Promotes brown adipogenesis, and inhibits WAT browning | (106) |
| **miR-455** | + | C3H10T1/2 cells | Activates expression of PPARγ and PGC1α and promotes iWAT browning | (107) |
| **Blnc1** | + | 10T1/2 fibroblasts, 3T3-L1 fibroblasts and mouse model | Form complex with EBF2 to stimulate thermogenic gene program | (108) |
| **AK079912** | + | Primary SVF cells | Drives thermogenic gene program in white adipocytes | (109) |
| **LncBATE10** | + | Primary preadipocytes, 3T3-L1 cells and mouse model | Protects PGC1α from degradation | (110) |
| **NONMMUG024827 lncRNA** | + | Mouse model | Positively regulates adiponectin mRNA levels | (111) |
| **lncRNA H19** | | Mouse model | Binds MBD1 and regulates *Igf2*, *Slc38a4* and *Mest*'s expression | (112) |

through improving mitochondrial function and upregulating the expression of key thermogenic genes (131).

Apart from the aforementioned nutrients and small molecules that regulate thermogenesis of brown and beige adipocytes, there are other metabolites performing the similar functions, including flavan-3-Alcohol, fucoxanthin, irisin, leptin, luteolin, Menthol Neuregulin 4 (Nrg4), Prostaglandin (PG), Purple Sweet Potato (PSP), Quercetin, Resveratrol, Rice Bran, Sesamol, Taurine, Telmisartan, and 3-Hydroxydaidzein (134, 135, 137–140, 142–153, 155), which will be discussed in details in the below sections.

## Intercellular communications within thermogenic fat

As extensively discussed in a recent review (156), thermogenic fat consists of various cell types or cell states in stromal vascular fractions (SVFs) and mature adipocytes, identified by state-of-art single-cell RNA-sequencing (scRNA-seq) or single nuclei RNA-sequencing (snRNA-seq) in mice (157–165) and humans (157, 162, 165–168). These subpopulations of thermogenic fat, including immune cells, endothelial cells, neurons, smooth muscle cells,

TABLE 4 Metabolic reprogramming behind thermogenesis of brown and beige adipocytes.

| Name | Regulation | Model system | Roles | Ref. |
|---|---|---|---|---|
| **Atrial Natriuretic Peptide (ANP)** | + | Mouse model | Increases browning of fat cells and upregulates expression of *Ucp1* | (115, 116) |
| **Berberine** | + | db/db mice | Increases thermogenic genes' expression | (117) |
| **Bone Morphogenetic Protein 9 (BMP-9)** | + | Obese mice | Enhances expression of FGF21 | (118) |
| **Capsaicin** | + | TRPV1(-/-) mouse models | Promotes interaction between PPARγ and PRDM16 to induce WAT browning | (119) |
| **Catecholamine** | + | Mouse model | Binds to β3-AR and promotes white fat browning | (120) |
| **Chlorogenic Acid** | + | Mouse brown adipocytes and human Adipocytes | Upregulates AMPK expression to enhance PPARγ, PRDM16, and PGC1α expression | (121, 122) |
| **Chrysin** | + | 3T3-L1 cells | Activates AMPK and then upregulates browning proteins' expression | (123) |
| **Cinnamicaldehyde** | + | Male C57BL/6J mice | Induces WAT browning and UCP1 expression | (124) |
| **Curcumin** | + | C57BL/6J mice, and 3T3-L1 and primary white adipocytes | Promotes beige fat cells production and induces white fat browning process | (125–127) |
| **Ellagic Acid** | + | Rats and hamsters | Upregulates expression of UCP1 and inhibits lipid accumulation | (128, 129) |
| **Emodin** | + | Obese Mice | Increases expression of beige adipocyte markers | (130) |
| **Epicatechin** | + | High-fat diet mouse model and cultured human adipocytes | Increases mitochondrial biogenesis-related proteins expression and activates browning of fat cells and WATs | (131) |
| **Fibroblast Growth Factor 21** | + | *C57BL/6J Fgf21-null and wild-type mice* | Upregulates thermogenic genes expression and regulates PGC1α at post-transcription level | (132, 133) |
| **Flavan-3-Alcohol** | + | 3T3-L1 cells and mice | Increases mRNA expression of UCP1 | (134) |
| **Fucoxanthin** | + | White adipose tissues from mice | Increases β3-AR expression and then stimulates UCP1 expression | (135) |
| **Glucocorticoids** | – | Murine brown adipocytes | Downregulates UCP1 expression in BATs | (136) |
| **Irisin** | + | Mouse model | Activates ERK and p38MAPK signalling pathways to induce white fat browning | (137) |
| **Leptin** | + | Wild type mice and UCP1 deficient mice | Promotes expression of UCP1 and UCP2 in the WATs to reduces white adipose tissue | (138) |
| **Luteolin** | + | male C57BL/6 mice | Activates browning and thermogenesis | (139) |
| **Mammalian Target of Rapamycin Complex 1 (mTORC1)** | + | Mouse and human adipocytes, and mice with mTORC1 impairment | Activates browning of fat cells | (140) |
| **Menthol** | + | Mice and primary white adipocytes | Activates TRPM8 which can upregulate UCP1 and PGC1α expression | (141) |
| **Neuregulin 4 (NRG4)** | + | Mouse model | Has the potential to promote white fat browning | (142, 143) |
| **Prostaglandin (PG)** | + | Mouse model | Induces the formation of BAT and white fat browning | (144, 145) |
| **Purple Sweet Potato (PSP)** | + | Mouse model | Upregulates browning-related genes' expression | (146) |
| **Quercetin** | + | Mouse model | Increases brown fat marker genes *Ucp1* and *Elovl3* expression | (147) |
| **Resveratrol** | + | db/db mice | Promotes lithocholic acid (LCA) in the plasma and faeces | (148) |
| **Rice Bran** | + | High-fat diet-induced obese mice | Upregulates UCP1 expression and downregulates WAT-specific proteins | (149) |
| **Sesamol** | + | Mouse system and 3T3-L1 model cells | Inhibits white adipogenic genes and promotes expression of brown fat marker genes | (150, 151) |

*(Continued)*

TABLE 4 Continued

| Name | Regulation | Model system | Roles | Ref. |
|---|---|---|---|---|
| **Taurine** | + | C3H10T1/2 white adipocytes and mouse model | Induces the browning of WAT | (152) |
| **Telmisartan** | + | 3T3/L1 adipocytes and mouse model | Increases expression of white fat browning key factors | (153, 154) |
| **3-Hydroxydaidzein** | + | Mouse model | Stimulates the browning of WAT | (155) |

Schwann cells, and a few other cell types, create a unique adipose niche and regulate adipose tissue function, such as thermogenic fat turnover, expansion, and remodeling (156). Here we focus on the intercellular crosstalk between thermogenic fat cells and endothelial cells, immune cells, and neurons (Figure 2).

## Endothelial cells in the thermogenic adipose tissue

Adipose tissue, especially BAT, is one of the most vascularized tissues in the body (169). A lot of stimuli, including cold, diet, exercise, and nutrition state, modulate angiogenesis and vascular remodeling in adipose tissue. Vascular Endothelial Growth Factor A (VEGFA) and Vascular Endothelial Growth Factor B (VEGFB) are two important angiogenic factors in adipose tissue in response to cold or β3-AR activation. BAT-specific overexpression of VEGFA increases vascularization and improves thermogenesis in mice after cold exposure, and protects mice against diet-induced obesity (170). Similarly, VEGFB promotes the proliferation of endothelial cells and fatty lipid oxidation in thermogenic fat in mice, providing a novel cure strategy for obesity and diabetes diseases (171). Besides, Seki et al. revealed that endothelial-specific *Vegfr2*$^{-/-}$ mice showed impaired angiogenesis as well as

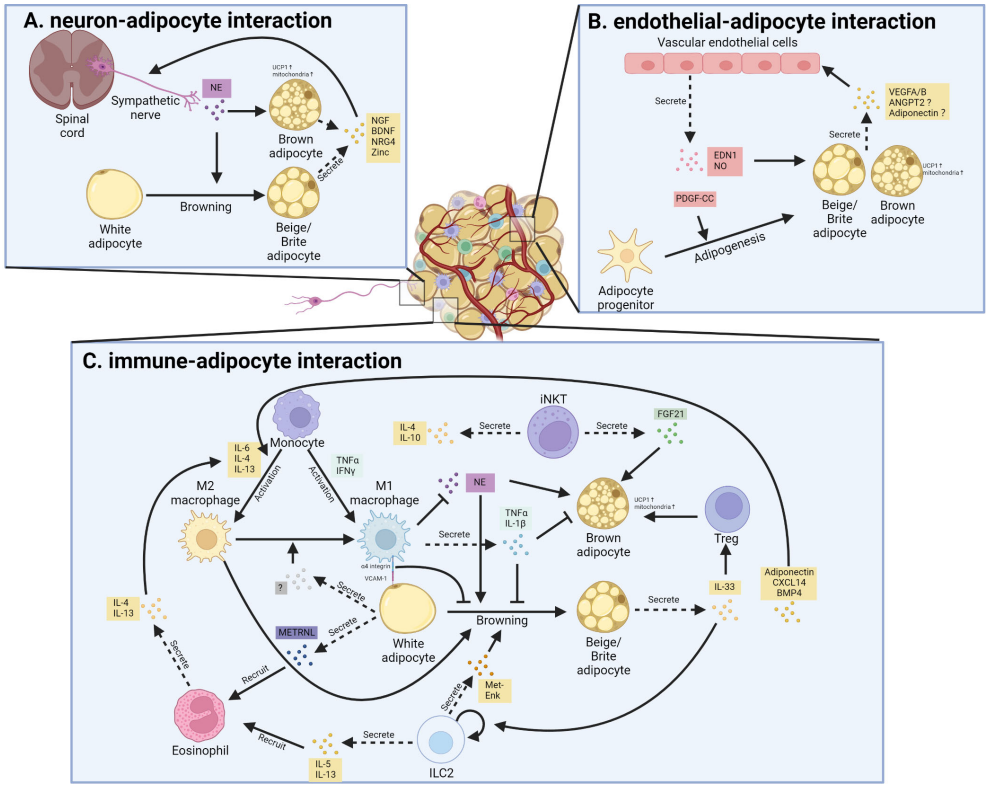


FIGURE 2
Cellular interaction between thermogenic adipocytes and resident cells. **(A)**. Interaction between sympathetic nerve and thermogenic adipocyte. Sympathetic nerve secretes norepinephrine (NE) that promotes white adipocyte browning and brown adipocyte activation; in turn, beige adipocytes and brown adipocytes promote nerve remodeling through secreting neurotrophic factor, including nerve growth factor (NGF), brain-derived neurotrophic factor (BDNF), neuregulin-4 (NRG4) as well as Zinc. **(B)**. Interaction between vascular endothelial cells and thermogenic adipocyte. Vascular endothelial cells secrete endothelin 1 (EDN1) and nitric oxide (NO) to promote the thermogenic function of brown and beige adipocytes. Besides, the secreted EDN1 and platelet-derived growth factor C (PDGF-C) also regulate the adipogenesis of preadipocytes. Reciprocally, thermogenic adipocytes and their progenitors secrete several factors that promote angiogenesis in adipose tissue. ANGPT2, angiopoietin 2; VEGF, vascular endothelial growth factor. **(C)**. Interaction between resident immune cells and thermogenic adipocytes. Various cytokines and signals mediate the bi-directional communication between thermogenic fat and different kinds of immune cells.

reduced browning of iWAT, which is modulated through the endothelial cells-derived platelet-derived growth factor-CC (PDGF-CC)-induced signaling pathway, since administration of PDGF-CC upregulated the expression level of *Ucp1* and promoted browning of iWAT both in mice and humans (172). Endothelial cells-secreted endothelin 1 (EDN1) and nitric oxide inhibit biogenesis and the function of brown and beige adipocytes *in vitro* (173, 174). In contrast, endothelial deficiency of lysosomal acid lipase (LAL) impairs vascularization and thermogenesis in BAT and WAT (175). The decreased production of vasodilatory factors and increased vasoconstricting factors production, due to dysfunction of endothelial cells, lead to insulin resistance and diabetes (176). The diverse functions of endothelial cells suggest the existence of different subpopulations. Indeed, Sun et al. observed two distinct types of endothelial cells in human deep-neck BAT using scRNA-seq (162). Vijay et al. also identified three types of endothelial cells in human WAT, with the largest population of endothelial cells defined as fatty-acid-handling microvascular endothelial cells and another subpopulation was lymphatic-derived (167). However, delineating the exact role of each subpopulation of endothelial cells in thermogenic fat needs further investigation. Taken together, these bidirectional communications between thermogenic fat and endothelial cells maintain the adipose homeostasis, and dysfunction of them cause metabolic disorders.

## Immune cells in the thermogenic adipose tissue

Several types of immune cells reside in adipose tissue, including macrophages, natural killer (NK) cells, lymphocytes, dendritic cells, neutrophils, eosinophils, T cells, and mast cells, which play an important role in regulating metabolic homeostasis (177, 178). The adipose immune cells composition is highly variable in response to the nutritional status, as well as environmental stimuli (179).

Among the immune cells that infiltrate into obese adipose tissue, macrophages are functionally and numerically dominant. Activated macrophages are divided into two main categories, M1 macrophages and M2 macrophages. M1 macrophages produce pro-inflammatory cytokines and chemokines, while M2 macrophages secrete anti-inflammatory cytokines that alleviate inflammation. Several studies show that activated M1-like macrophages facilitate the infiltration of other immune cells into obese adipose tissues and impairs insulin sensitivity (180). In detail, studies identified TNFα as a pro-inflammatory cytokine produced from M1 macrophages that suppresses the emergence of thermogenic adipocytes in mice (181). It was also reported that the direct contact between M1 macrophage and white adipocyte could inhibit the browning process as well as *Ucp1* expression in iWAT of mice, mainly though the direct adhesion between α4-integrin in activated M1 macrophage and vascular cell adhesion molecule 1 (Vcam-1) in adipocytes (182). In contrast to M1 macrophages, M2 macrophages exert positive effects on brown adipocyte activity and WAT browning (183). *Signal transducer and activator of transcription 6* (*Stat6*)-deficient or macrophage-specific *interleukin-4 receptor α* (*Il4rα*) knockout mice exhibited impaired BAT thermogenic response, suggesting the positive role of M2 macrophages in BAT thermogenesis, which is further supported by the specific depletion of *Il4rα* in myeloid cells of mice (184, 185). M2 macrophages could produce catecholamine to sustain adaptive thermogenesis, which may also reflect the situations in WAT browning, as similar recruitment of M2 macrophages were also found in iWAT of cold-induced mice (185, 186). Another study demonstrated that a fraction of M1 macrophages were concentrated around the sympathetic nerve endings in the adipose tissue of obese people (187). Such macrophages are called sympathetic neuron-associated macrophages (SAM), which can transport catecholamine released from sympathetic nerve endings into the cell body and degrade it through monoamine oxidase A, thereby inhibiting the browning of iWAT induced by sympathetic nerve in obese mice (187, 188). Mutually, thermogenic fat could also secrete batokines to regulate the activation and function of macrophages. CXC Motif Chemokine Ligand 14 (CXCL14), one of the batokines secreted by brown adipocytes, promotes the M2 macrophage phenotype in adipose tissue and leads to WAT browning, and *Cxcl14*-deficient mice show impaired BAT activity and altered glucose homeostasis in response to cold exposure (189). Adiponectin is another adipokine that promotes the activation of M2 macrophages and then results in cold-induced browning of WAT in mice (190). Adipose-secreted bone morphogenetic protein 4 (BMP4) also increase the accumulation of M2 macrophages and induce beige fat biogenesis in iWAT of mice (191). Moreover, adipocytes deficient in fatty acid synthase (iAdFASNKO) show increased macrophage polarization, and ablation of macrophage from iWAT in iAdFASNKO mice inhibit beige adipogenesis (161).

Innate lymphoid type 2 cells (ILC2s), another group of adipose resident immune cells, also activate M2 macrophage and regulate thermogenesis in brown and beige adipocytes (192). Activation of ILC2s in the iWAT of mice strongly stimulates the biogenesis of beige fat (193). Mechanistically, ILC2 activation leads to the proliferation of adipocyte precursors and their commitment to the beige fat lineage in mice (193). ILC2 cells also secrete peptide methionine-enkephalin (Met-Enk), which directly targets subcutaneous white adipocytes to induce their browning (194). Moreover, ILC2s respond to the stimulation of interleukin (IL)-33 and produce IL-13 and IL-4 to promote the browning of iWAT in mice, although the cellular origin and signal pathways involved in the endogenous IL-33 production in adipose tissue remain unidentified (193). Consistent with this, *Il-33* deficient mice in iWAT have fewer beige adipocyte formations and larger white adipocyte compared to control mice (194). In a recent study, the unique ILC populations were profiled in human WAT (168), which suggests ILC3s may play a similar role as ILC2 in adipose homeostasis, but function as a more important mediator of adipose tissue inflammation and obesity (168, 194).

Eosinophils are the main IL-4-producing cells in iWAT of mice, and play a key role in the thermogenesis and metabolic homeostasis (195). METRNL, a circulating factor meteorin-like hormone, is induced after exercise and cold exposure in the skeletal muscle and adipose tissue of mice, respectively (196). METRNL promotes alternative activation of adipose tissue macrophages and

thermogenic and anti-inflammatory gene programs in iWAT through an eosinophil-dependent increased *Il-4* expression, and blocking IL4/IL13 signaling abrogates METRNL-induced browning of iWAT in mice (196). Moreover, eosinophils-derived IL-4 directly work on PDGFRα$^+$ adipocyte precursors to induce beige adipogenesis both *in vitro* and *in vivo* (193). In response to chemokine ligand 11 (CCL11) stimulation, eosinophils are recruited to iWAT and promote type 2 immune responses and beige adipogenesis in mice (197).

## Neurons in the thermogenic adipose tissue

BAT is highly innervated by the complex sympathetic nervous system, which can transmit signals from the central nervous system to BAT (198). BAT thermogenesis is triggered by the release of norepinephrine from its sympathetic nerve terminals, which binds to β3-AR that result in the activation of UCP1 (198). Sympathetic innervation increases after cold exposure in BAT and subcutaneous WAT both in mice and human adults (199). More detailed analysis revealed that sympathetic arborizations in iWAT cover 90% of individual adipocytes, and the sympathetic arborizations are important for the cold-induced browning of iWAT in mice (200). Mutually, the thermogenic fat also regulates the sympathetic innervation and neuron activity. Overexpression of PRDM16 in mice significantly increase the number of sympathetic parenchymal nerve fibers infiltrating the iWAT compared with that in wild-type mice, although the exact mechanism of the recruitment of sympathetic nerves in iWAT remain elusive (200). A recent study revealed that mice lack of fatty acid synthase in fat (iAdFASNKO) activated the sympathetic nerve fiber to result in browning in iWAT of mice (161). Zeng et al. reported that thermogenic adipocytes express mammal-specific endoplasmic reticulum membrane protein (Calsyntenin-3β), which promotes the secretion of S100b from brown adipocytes and stimulates neurite outgrowth in mice (201). Luan group further demonstrated that thermogenic adipocytes secrete zinc that promotes sympathetic innervation, and administration of zinc ameliorates obesity by promoting sympathetic neuron-induced thermogenesis in mice (202). These studies revealed the beneficial and critical role of sympathetic innervation in maintenance of thermogenic fat in response to cold exposure and other environmental challenge.

# Inter-organ communications around thermogenic fat

The coordination of multiple tissues and organs is very important for maintaining systemic homeostasis and responding to nutritional and environmental challenges, and its dysregulation leads to various metabolic disorders (203–205). The thermogenic fat function as an endocrine organ by secreting specific factors (brown adipokines or batokines) and interact with distant organs that express the corresponding receptors, and *vice versa* (Figure 3).

## Brain-thermogenic fat communication

Besides the local effects of nerve on the thermogenic fat, the brain-thermogenic fat communication axis plays an important role in regulating systemic energy balance. Adipose tissue transmits the message to the brain *via* secreted factors and sensory innervation (206, 207). Leptin, an adipokine, is mainly produced by the *obese* (*ob*) gene in adipocytes, and regulates the balance of energy *via* decreasing food intake and inducing energy expenditure (208, 209). Although the role of leptin in regulating energy balance is well known, the underlying mechanism is still elusive. Recent work has shown that leptin target the melanocortin receptor 4 (MC4R) and melanocortin receptor 3 (MC3R) in the brain of mice (210, 211). *Mc4r*-deficient mice exhibit reduced upregulation of *Ucp1* in BAT exposed to cold condition or high-fat food (212). In contrast, central administration of MC3/4-R agonists MTII promote *Ucp1* mRNA expression in mice (213), suggesting the role of MC4R-expressing neuronal populations in regulating BAT thermogenesis. It was also shown that leptin and insulin act synergically on hypothalamic neurons to promote iWAT browning in mice (214). Bone morphogenetic protein 8b (BMP8b), a factor induced by nutritional and thermogenic stimuli in mature BAT and hypothalamus, is also involved in central control of BAT thermogenesis, and central BMP8B treatment increases sympathetic activation of BAT in mice, depending on the hypothalamic AMP-activated protein kinase (AMPK) activation (215).

Central control could also inhibit the browning process, as fasting and chemical-genetic activation of orexigenic agouti-related protein (AgRP) neurons in the hypothalamus suppress iWAT browning in mice (216). Mechanistically, the levels of O-linked β-N-acetylglucosamine (O-GlcNAc) transferase and O-GlcNAc modification in AgRP neurons are increased after fasting in mice, thus promoting neuronal excitability and inhibiting iWAT browning (216). It was also reported that glucocorticoids, a class of steroid hormones synthesized in the adrenal cortex, also suppress *Ucp1* expression and BAT thermogenesis in mice (217). In contrast, the glucocorticoids promote *UCP1* expression in human brown adipocytes and increase glucose uptake and energy expenditure in response to mild cold condition (218). Understanding the species-specific action of glucocorticoid on BAT thermogenesis will provide not only the understanding for BAT-brain axis, but also new therapeutic strategy for maintaining energy homeostasis. Overall, these studies show the differential effects of central control of function of thermogenic fat, mainly depending on the different types of neurons.

## Liver-thermogenic fat communication

The liver is a metabolic organ important for glucose and lipid metabolism, whose dysfunction leads to many kinds of metabolic diseases. The interaction between the liver and thermogenic fat are mainly mediated by peptide hormones, lipokines as well as bile acids. Fibroblast growth factor 21 (FGF21) is a circulating peptide hormone, which is mainly expressed in the liver in response to

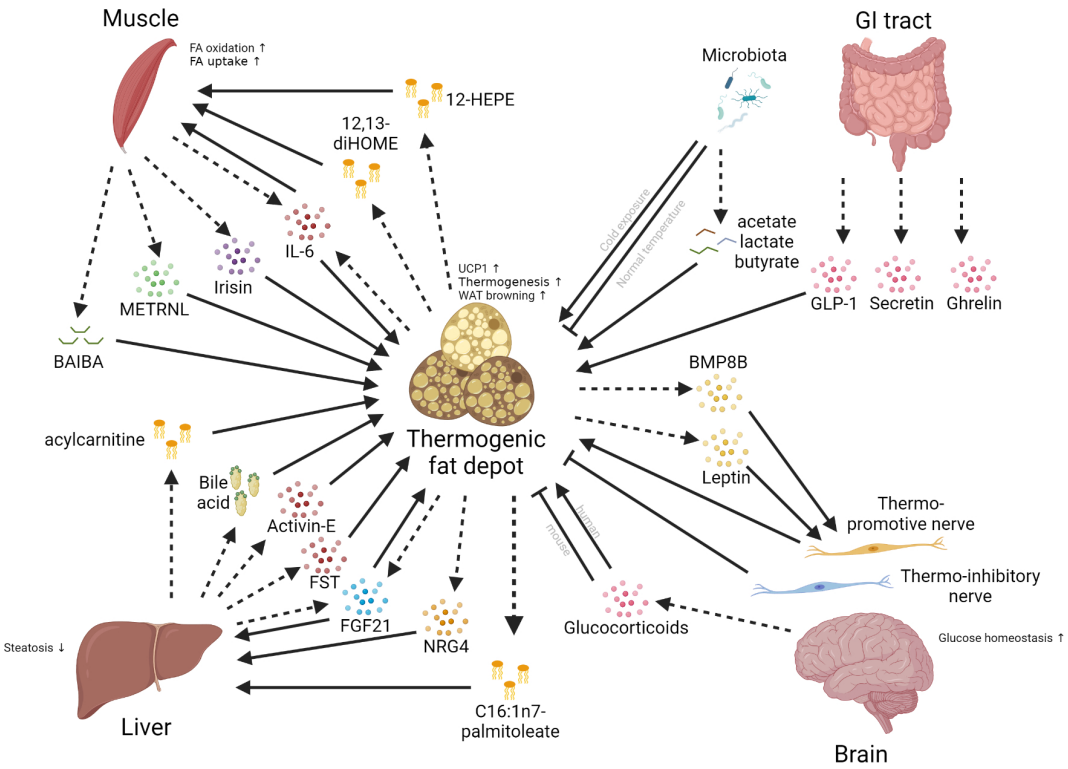


FIGURE 3
Inter-organ communications between thermogenic fat depots and different organs. Multiple organs, such as the brain, liver, muscle, and gut, can have crosstalk with thermogenic fat depots. The communications between these organs and the thermogenic fat depot mainly involve the secretion of different kinds of molecules, including peptide hormones, lipokines, glucocorticoids, and bile acids. Dashed arrows mean the secretion of factors; solid arrows mean positive effects; blunt-end lines mean inhibitory effects.

starvation or exercise and induced in BAT and WAT when fasted or exposed to cold environment both in mice and humans (219). FGF21 not only acts locally in an endocrine and autocrine manner, but also travels to distant organs to exert its role by secreting into the bloodstream (220). Studies showed that administration of FGF21 increases energy expenditure and improves insulin sensitivity in mice (221). Owen et al. further revealed that FGF21 improves energy expenditure through enhanced sympathetic nerve activity in BAT of mice (222). Moreover, the administration of recombinant FGF21 for 6 weeks in diabetic rhesus monkeys lead to a significant decline in glucose level, body weight, and circulating lipids levels (223). Similarly, Activin-E, a member of transforming growth factor beta (TGFβ) superfamily, is primarily produced by the liver and functions as a hepatokine to activate thermogenesis both in iWAT and BAT of mice (224, 225). Follistatin (Fst), which binds and neutralizes the activity of TGFβ superfamily, is secreted by the liver and promotes brown preadipocyte differentiation and cold-induced brown thermogenesis in mice, although the autocrine effect could not be excluded, since *Fst* is also induced in brown adipocytes in response to cold (226–228).

On the other hand, brown adipocytes secrete batokines to regulate the functions of the liver. As discussed above, FGF21 mediate the bi-directional crosstalk between BAT and the liver in mice (204, 221, 222). Besides, brown adipocyte-derived Neuregulin 4 (Nrg4), a member of the epidermal growth factor (EGF) family of ligands, attenuates hepatic lipogenic signaling and protects mice against diet-induced insulin resistance and hepatic steatosis (142). In mice, acute psychological stress induces IL6 secretion from brown adipocytes and then promotes hyperglycemia through hepatic enhanced gluconeogenesis (229). Other reports revealed that some adipokines, such as adiponectin, suppress hepatic injury induced by alcohol intake in mice model (230).

Another class of molecules that mediate the communication between the liver and thermogenic fat are lipokines, which can be secreted both by the adipose tissue and the liver (231, 232). Through quantitative and systemic lipidomic analyses, Cao et al. identified C16:1n7-palmitoleate as an adipose tissue-derived lipid hormone that functions as an important regulator of metabolic homeostasis, such as suppression of hepatosteatosis in mice (231). Similarly, using non-targeted liquid chromatography-mass spectrometry-based lipidomics, Simcox et al. identified that acylcarnitine,produced by the mouse liver in response to cold exposure, transports to BAT to induce UCP1-dependent uncoupling respiration and heat production (232). Bile acids also participate in the communication between the liver and thermogenic fat. TGR5, a G-protein-coupled receptor, could bind to the bile acids transported to brown or beige adipocytes from the liver and induce cold-induced thermogenesis in mice (233–235). BAT also regulate liver inflammation, although the exact pathway governing this crosstalk remains unclear. Previous studies showed that *Ucp1*$^{-/-}$ mice exhibits decreased capacity to clear succinate from both the liver and the circulation, thus driving liver inflammation through the interaction with stellate cells and macrophages (236,

237). Collectively, these studies show that the intensive crosstalk between the liver and thermogenic fat mediated by various circulating factors, including peptide hormones, lipokines as well as bile acids.

## Skeletal muscle-thermogenic fat communication

Upon muscle contraction, skeletal muscles produce and release circulating cytokines and other peptides, known as myokines, which exert endocrine effects and mediate the communication between muscle and other organs (238–240). In reciprocal, cold- or exercise-induced batokines from thermogenic fat also regulate the function of skeletal muscle.

The earliest identified and most studied myokine is IL-6, which can increase up to 100 folds in circulation during physical exercise (241). Daily injection of IL-6 for 1 week significantly increases *Ucp1* mRNA levels in iWAT of mice (242). Moreover, administration of recombinant human IL-6 enhances lipolysis as well as fatty acid oxidation both in healthy young and elderly humans (243, 244). Consistent with this, elevated IL-6 secretion is also observed in differentiating human beige adipocytes, and blockage of IL-6 receptor by specific antibody inhibits human brown adipocyte differentiation (245). Irisin is another myokine that mediates the communication between skeletal muscle and thermogenic fat, which is secreted from skeletal muscle in a PGC1α-dependent manner and stimulates *Ucp1* expression and thermogenesis both *in vitro* and *in vivo* (246). Irisin is also induced by cold exposure in human and promotes brown fat thermogenesis in collaboration with FGF21, representing a cold-activated endocrine axis regulating both shivering and non-shivering thermogenesis (247). METRNL is released by skeletal muscle and adipose tissue after exercise or upon cold exposure respectively, and significantly promotes browning of WAT depots (183), stimulates energy expenditure and improves glucose tolerance, which is mediated by the recruitment of resident eosinophil in WAT depots of mice (196). Roberts et al. identified β-aminoisobutyric acid (BAIBA), a myokine secreted after exercise, increases the expression of brown adipocyte marker genes and induces a brown adipocyte-like phenotype both in human iPSC-derived white adipocytes and in white adipose depot of mice (248).

Meanwhile, batokines from thermogenic fat also regulate the function of skeletal muscle. 12,13-dihydroxy-9Z-octadecenoic acid (12,13-diHOME), a lipokine secreted from BAT when exposed to cold or exercise in mice and human, increases skeletal muscle fatty acid oxidation and uptake (249, 250). 12-hydroxyeicosapentaenoic acid (12-HEPE), a 12-lipoxygenase-derived lipokine that is secreted in response to cold exposure and β-AR signaling, also promotes glucose uptake in muscle as well as BAT in mice (251). These studies clearly show the mutually regulatory network between skeletal muscle and thermogenic fat to maintain thermogenic fat homeostasis.

## GI tract-thermogenic fat communication

The gastrointestinal tract (GI tract) plays a very important role in thermogenesis through gut microbiota or directly secreting factors from intestinal cells (252). In a study that compared the metabolic profiling between germ-free mice and conventional mice, Mestdagh et al. revealed increased lipolysis while reduced lipogenesis in BAT of germ-free mice (253). Suarez et al. also showed that depletion of microbiota, either by antibiotic treatment or in germ-free mice, promote the browning of iWAT and perigonadal visceral adipose tissue in lean mice, obese mice and high-fat diet-fed mice (254). However, Zietak et al. found cold exposure markedly alter the microbiome composition, and cold-adapted microbiota improved energy metabolism (255). Transplantation of the gut microbiota from cold-induced mice to germ-free mice increase insulin sensitivity, cold tolerance, and browning of WAT (256). Other study revealed that acetate and lactate from the gut microbiota promote the browning of iWAT of mice after intermittent fasting, although the underlying mechanism remains unclear (257). Of note, administration of the bacterial metabolite butyrate also increases the thermogenic capacity of the germ-free mice (258).

Besides gut microbiota, the GI tract also secrete various factors to regulate thermogenesis. Secretin, secreted by the gut and upregulated during fasting, increases lipolysis and inhibits glucose uptake in mice (259). Li et al. revealed that secretin mediates a gut-BAT-brain axis, which stimulates brown fat thermogenesis and satiation in mice (260). The similar role of secretin is also observed in human (261). Glucagon-like peptide 1 (GLP-1), a peptide released from enteroendocrine cells in the gut, increases insulin secretion in beta cells and activates BAT thermogenesis in mice (262). GLP-1 has also been proved to increase satiety and reduce energy intake in human (263). GLP-1 agonists significantly induce BAT thermogenesis and promote browning of iWAT in mice (264). Numerous evidences support that GLP-1 agonists decrease the risk of developing cardiovascular disease in diabetes and obesity both in mice and humans (265). Ghrelin, another growth-hormone-releasing acylated peptide from stomach, also modulates thermogenesis in BAT as well as lipid utilization in WAT, possibly through the gut-brain-BAT axis, as this occurs when ghrelin was centrally administered in mice (266–269). Further studies need to investigate whether and how thermogenic fat could influence the gut homeostasis, as this has not been explored in depth so far.

# Conclusion

Understanding of the development route of thermogenic fat will provides novel therapeutic interventions for metabolic diseases. In this review, we discussed the regulatory network of thermogenic fat at the molecular and cellular levels, respectively. The molecular regulation of thermogenic fat mainly involves transcriptional regulation, epigenetic regulation, non-coding RNA regulation and metabolic reprogramming. Among these regulators, PPARγ, PRDM16 and PGC1α represent the core regulators, as most of the other regulators regulate the thermogenesis depending on them. Besides, thermogenic fat is also educated by other cell types within adipose depots or other organs. These complex and comprehensive regulatory networks help to maintain the functionality of

thermogenic fat in response to kinds of changes of the environment. This holds a promising strategy for inducing artificial thermogenesis to counteract obesity *in vivo*. For example, recent study has shown that thermogenesis could be induced through local hyperthermia therapy, mainly through the HSF1-A2B1 transcriptional axis (270). However, whether this kind of induced thermogenesis represents a new specific regulatory network or converges on the core regulators still needs to be identified. In future, more advanced technology, such as spatial transcriptomics and epigenomics methodologies, should be applied to this field to better delineate the development route of thermogenic fat.

## Author contributions

All authors listed have made a substantial, direct, and intellectual contribution to the work and approved it for publication.

## Funding

WH was supported by the Natural Science Foundation of China (82270868).

## Acknowledgments

The authors thank the members of the laboratory of WH for valuable discussions and proofreading. The authors also acknowledge the many investigators who have contributed to this area of research and whose work, in many cases, could not be cited owing to the limitation of references allowed in this Review. The figures were created by Biorender.

## Conflict of interest

The authors declare that the research was conducted in the absence of any commercial or financial relationships that could be construed as a potential conflict of interest.

## Publisher's note

All claims expressed in this article are solely those of the authors and do not necessarily represent those of their affiliated organizations, or those of the publisher, the editors and the reviewers. Any product that may be evaluated in this article, or claim that may be made by its manufacturer, is not guaranteed or endorsed by the publisher.

## References

1. Tomiyama AJ. Stress and obesity. *Annu Rev Psychol* (2019) 70:703–18. doi: 10.1146/annurev-psych-010418-102936

2. Cannon B, Nedergaard J. Brown adipose tissue: function and physiological significance. *Physiol Rev* (2004) 84(1):277–359. doi: 10.1152/physrev.00015.2003

3. Cypess AM, Lehman S, Williams G, Tal I, Rodman D, Goldfine AB, et al. Identification and importance of brown adipose tissue in adult humans. *N Engl J Med* (2009) 360(15):1509–17. doi: 10.1056/NEJMoa0810780

4. Virtanen KA, Lidell ME, Orava J, Heglind M, Westergren R, Niemi T, et al. Functional brown adipose tissue in healthy adults. *N Engl J Med* (2009) 360(15):1518–25. doi: 10.1056/NEJMoa0808949

5. Yoneshiro T, Aita S, Matsushita M, Kayahara T, Kameya T, Kawai Y, et al. Recruited brown adipose tissue as an antiobesity agent in humans. *J Clin Invest* (2013) 123(8):3404–8. doi: 10.1172/JCI67803

6. Saito M, Okamatsu-Ogura Y, Matsushita M, Watanabe K, Yoneshiro T, Nio-Kobayashi J, et al. High incidence of metabolically active brown adipose tissue in healthy adult humans: effects of cold exposure and adiposity. *Diabetes* (2009) 58 (7):1526–31. doi: 10.2337/db09-0530

7. Zhang Z, Funcke JB, Zi Z, Zhao S, Straub LG, Zhu Y, et al. Adipocyte iron levels impinge on a fat-gut crosstalk to regulate intestinal lipid absorption and mediate protection from obesity. *Cell Metab* (2021) 33(8):1624–39 e9. doi: 10.1016/j.cmet.2021.06.001

8. Feldmann HM, Golozoubova V, Cannon B, Nedergaard J. UCP1 ablation induces obesity and abolishes diet-induced thermogenesis in mice exempt from thermal stress by living at thermoneutrality. *Cell Metab* (2009) 9(2):203–9. doi: 10.1016/j.cmet.2008.12.014

9. Tsagkaraki E, Nicoloro SM, DeSouza T, Solivan-Rivera J, Desai A, Lifshitz LM, et al. CRISPR-enhanced human adipocyte browning as cell therapy for metabolic disease. *Nat Commun* (2021) 12(1):6931. doi: 10.1038/s41467-021-27190-y

10. Stanford KI, Middelbeek RJ, Townsend KL, An D, Nygaard EB, Hitchcox KM, et al. Brown adipose tissue regulates glucose homeostasis and insulin sensitivity. *J Clin Invest* (2013) 123(1):215–23. doi: 10.1172/JCI62308

11. Peres Valgas da Silva C, Hernandez-Saavedra D, White JD, Stanford KI. Cold and exercise: therapeutic tools to activate brown adipose tissue and combat obesity. *Biol (Basel)* (2019) 8(1):9-37. doi: 10.3390/biology8010009

12. Sharp LZ, Shinoda K, Ohno H, Scheel DW, Tomoda E, Ruiz L, et al. Human BAT possesses molecular signatures that resemble beige/brite cells. *PloS One* (2012) 7 (11):e49452. doi: 10.1371/journal.pone.0049452

13. Seale P, Conroe HM, Estall J, Kajimura S, Frontini A, Ishibashi J, et al. Prdm16 determines the thermogenic program of subcutaneous white adipose tissue in mice. *J Clin Invest* (2011) 121(1):96–105. doi: 10.1172/JCI44271

14. Cao W, Daniel KW, Robidoux J, Puigserver P, Medvedev AV, Bai X, et al. p38 mitogen-activated protein kinase is the central regulator of cyclic AMP-dependent transcription of the brown fat uncoupling protein 1 gene. *Mol Cell Biol* (2004) 24 (7):3057–67. doi: 10.1128/MCB.24.7.3057-3067.2004

15. Vernochet C, Peres SB, Davis KE, McDonald ME, Qiang L, Wang H, et al. C/EBPalpha and the corepressors CtBP1 and CtBP2 regulate repression of select visceral white adipose genes during induction of the brown phenotype in white adipocytes by peroxisome proliferator-activated receptor gamma agonists. *Mol Cell Biol* (2009) 29 (17):4714–28. doi: 10.1128/MCB.01899-08

16. Kajimura S, Seale P, Kubota K, Lunsford E, Frangioni JV, Gygi SP, et al. Initiation of myoblast to brown fat switch by a PRDM16-C/EBP-beta transcriptional complex. *Nature* (2009) 460(7259):1154–8. doi: 10.1038/nature08262

17. Rajakumari S, Wu J, Ishibashi J, Lim HW, Giang AH, Won KJ, et al. EBF2 determines and maintains brown adipocyte identity. *Cell Metab* (2013) 17(4):562–74. doi: 10.1016/j.cmet.2013.01.015

18. Cederberg A, Grønning LM, Ahrén B, Taskén K, Carlsson P, Enerbäck S. FOXC2 is a winged helix gene that counteracts obesity, hypertriglyceridemia, and diet-induced insulin resistance. *Cell* (2001) 106(5):563–73. doi: 10.1016/S0092-8674(01)00474-3

19. Bi P, Shan T, Liu W, Yue F, Yang X, Liang XR, et al. Inhibition of notch signaling promotes browning of white adipose tissue and ameliorates obesity. *Nat Med* (2014) 20 (8):911–8. doi: 10.1038/nm.3615

20. Kong X, Banks A, Liu T, Kazak L, Rao Rajesh R, Cohen P, et al. IRF4 is a key thermogenic transcriptional partner of PGC-1α. *Cell* (2014) 158(1):69–83. doi: 10.1016/j.cell.2014.04.049

21. Claussnitzer M, Dankel SN, Kim KH, Quon G, Meuleman W, Haugen C, et al. FTO obesity variant circuitry and adipocyte browning in humans. *N Engl J Med* (2015) 373(10):895–907. doi: 10.1056/NEJMoa1502214

22. Laber S, Cox RD. Commentary: FTO obesity variant circuitry and adipocyte browning in humans. *Front Genet* (2015) 6:318. doi: 10.3389/fgene.2015.00318

23. Loft A, Forss I, Siersbaek MS, Schmidt SF, Larsen AS, Madsen JG, et al. Browning of human adipocytes requires KLF11 and reprogramming of PPARgamma superenhancers. *Genes Dev* (2015) 29(1):7–22. doi: 10.1101/gad.250829.114

24. McDonald ME, Li C, Bian H, Smith BD, Layne MD, Farmer SR. Myocardin-related transcription factor a regulates conversion of progenitors to beige adipocytes. *Cell* (2015) 160(1-2):105–18. doi: 10.1016/j.cell.2014.12.005

25. Uldry M, Yang W, St-Pierre J, Lin J, Seale P, Spiegelman BM. Complementary action of the PGC-1 coactivators in mitochondrial biogenesis and brown fat differentiation. *Cell Metab* (2006) 3(5):333–41. doi: 10.1016/j.cmet.2006.04.002

26. Lin J, Wu PH, Tarr PT, Lindenberg KS, St-Pierre J, Zhang CY, et al. Defects in adaptive energy metabolism with CNS-linked hyperactivity in PGC-1alpha null mice. *Cell* (2004) 119(1):121–35. doi: 10.1016/j.cell.2004.09.013

27. Puigserver P, Wu Z, Park CW, Graves R, Wright M, Spiegelman BM. A cold-inducible coactivator of nuclear receptors linked to adaptive thermogenesis. *Cell* (1998) 92(6):829–39. doi: 10.1016/S0092-8674(00)81410-5

28. Tiraby C, Tavernier G, Lefort C, Larrouy D, Bouillaud F, Ricquier D, et al. Acquirement of brown fat cell features by human white adipocytes. *J Biol Chem* (2003) 278(35):33370–6. doi: 10.1074/jbc.M305235200

29. Jimenez-Preitner M, Berney X, Uldry M, Vitali A, Cinti S, Ledford JG, et al. Plac8 is an inducer of C/EBPβ required for brown fat differentiation, thermoregulation, and control of body weight. *Cell Metab* (2011) 14(5):658–70. doi: 10.1016/j.cmet.2011.08.008

30. Ohno H, Shinoda K, Spiegelman BM, Kajimura S. PPARγ agonists induce a white-to-brown fat conversion through stabilization of PRDM16 protein. *Cell Metab* (2012) 15(3):395–404. doi: 10.1016/j.cmet.2012.01.019

31. Qiang L, Wang L, Kon N, Zhao W, Lee S, Zhang Y, et al. Brown remodeling of white adipose tissue by SirT1-dependent deacetylation of ppargamma. *Cell* (2012) 150 (3):620–32. doi: 10.1016/j.cell.2012.06.027

32. Seale P, Kajimura S, Yang W, Chin S, Rohas LM, Uldry M, et al. Transcriptional control of brown fat determination by PRDM16. *Cell Metab* (2007) 6(1):38–54. doi: 10.1016/j.cmet.2007.06.001

33. Seale P, Bjork B, Yang W, Kajimura S, Chin S, Kuang S, et al. PRDM16 controls a brown fat/skeletal muscle switch. *Nature* (2008) 454(7207):961–7. doi: 10.1038/nature07182

34. Harms MJ, Ishibashi J, Wang W, Lim HW, Goyama S, Sato T, et al. Prdm16 is required for the maintenance of brown adipocyte identity and function in adult mice. *Cell Metab* (2014) 19(4):593–604. doi: 10.1016/j.cmet.2014.03.007

35. Scimè A, Grenier G, Huh MS, Gillespie MA, Bevilacqua L, Harper ME, et al. Rb And p107 regulate preadipocyte differentiation into white versus brown fat through repression of PGC-1alpha. *Cell Metab* (2005) 2(5):283–95. doi: 10.1016/j.cmet.2005.10.002

36. Powelka AM, Seth A, Virbasius JV, Kiskinis E, Nicoloro SM, Guilherme A, et al. Suppression of oxidative metabolism and mitochondrial biogenesis by the transcriptional corepressor RIP140 in mouse adipocytes. *J Clin Invest* (2006) 116 (1):125–36.

37. Christian M, Kiskinis E, Debevec D, Leonardsson G, White R, Parker MG. RIP140-targeted repression of gene expression in adipocytes. *Mol Cell Biol* (2005) 25 (21):9383–91. doi: 10.1128/MCB.25.21.9383-9391.2005

38. Leonardsson G, Steel JH, Christian M, Pocock V, Milligan S, Bell J, et al. Nuclear receptor corepressor RIP140 regulates fat accumulation. *Proc Natl Acad Sci USA* (2004) 101(22):8437–42. doi: 10.1073/pnas.0401013101

39. Yadav H, Quijano C, Kamaraju AK, Gavrilova O, Malek R, Chen W, et al. Protection from obesity and diabetes by blockade of TGF-beta/Smad3 signaling. *Cell Metab* (2011) 14(1):67–79. doi: 10.1016/j.cmet.2011.04.013

40. Picard F, Géhin M, Annicotte J-S, Rocchi S, Champy M-F, O'Malley BW, et al. SRC-1 and TIF2 control energy balance between white and brown adipose tissues. *Cell* (2002) 111(7):931–41. doi: 10.1016/S0092-8674(02)01169-8

41. Gburcik V, Cawthorn WP, Nedergaard J, Timmons JA, Cannon B. An essential role for Tbx15 in the differentiation of brown and "brite" but not white adipocytes. *Am J Physiol Endocrinol Metab* (2012) 303(8):E1053–60. doi: 10.1152/ajpendo.00104.2012

42. Vernochet C, Mourier A, Bezy O, Macotela Y, Boucher J, Rardin MJ, et al. Adipose-specific deletion of TFAM increases mitochondrial oxidation and protects mice against obesity and insulin resistance. *Cell Metab* (2012) 16(6):765–76. doi: 10.1016/j.cmet.2012.10.016

43. Villanueva CJ, Vergnes L, Wang J, Drew BG, Hong C, Tu Y, et al. Adipose subtype-selective recruitment of TLE3 or Prdm16 by PPARgamma specifies lipid storage versus thermogenic gene programs. *Cell Metab* (2013) 17(3):423–35. doi: 10.1016/j.cmet.2013.01.016

44. Pan D, Fujimoto M, Lopes A, Wang Y-X. Twist-1 is a PPARδ-inducible, negative-feedback regulator of PGC-1α in brown fat metabolism. *Cell* (2009) 137 (1):73–86. doi: 10.1016/j.cell.2009.01.051

45. Laurila PP, Soronen J, Kooijman S, Forsstrom S, Boon MR, Surakka I, et al. USF1 deficiency activates brown adipose tissue and improves cardiometabolic health. *Sci Transl Med* (2016) 8(323):323ra13. doi: 10.1126/scitranslmed.aad0015

46. Gupta RK, Arany Z, Seale P, Mepani RJ, Ye L, Conroe HM, et al. Transcriptional control of preadipocyte determination by Zfp423. *Nature* (2010) 464(7288):619–23. doi: 10.1038/nature08816

47. Shao M, Zhang Q, Truong A, Shan B, Vishvanath L, Li L, et al. ZFP423 controls EBF2 coactivator recruitment and PPARgamma occupancy to determine the thermogenic plasticity of adipocytes. *Genes Dev* (2021) 35(21-22):1461–74. doi: 10.1101/gad.348780.121

48. Shao M, Ishibashi J, Kusminski CM, Wang QA, Hepler C, Vishvanath L, et al. Zfp423 maintains white adipocyte identity through suppression of the beige cell thermogenic gene program. *Cell Metab* (2016) 23(6):1167–84. doi: 10.1016/j.cmet.2016.04.023

49. Dempersmier J, Sambeat A, Gulyaeva O, Paul SM, Hudak CS, Raposo HF, et al. Cold-inducible Zfp516 activates UCP1 transcription to promote browning of white fat and development of brown fat. *Mol Cell* (2015) 57(2):235–46. doi: 10.1016/j.molcel.2014.12.005

50. Wang W, Kissig M, Rajakumari S, Huang L, Lim HW, Won KJ, et al. Ebf2 is a selective marker of brown and beige adipogenic precursor cells. *Proc Natl Acad Sci USA* (2014) 111(40):14466–71. doi: 10.1073/pnas.1412685111

51. Angueira AR, Shapira SN, Ishibashi J, Sampat S, Sostre-Colon J, Emmett MJ, et al. Early b cell factor activity controls developmental and adaptive thermogenic gene programming in adipocytes. *Cell Rep* (2020) 30(9):2869–78 e4. doi: 10.1016/j.celrep.2020.02.023

52. Takahashi N, Kawada T, Yamamoto T, Goto T, Taimatsu A, Aoki N, et al. Overexpression and ribozyme-mediated targeting of transcriptional coactivators CREB-binding protein and p300 revealed their indispensable roles in adipocyte differentiation through the regulation of peroxisome proliferator-activated receptor gamma. *J Biol Chem* (2002) 277(19):16906–12. doi: 10.1074/jbc.M200585200

53. Jin Q, Wang C, Kuang X, Feng X, Sartorelli V, Ying H, et al. Gcn5 and PCAF regulate PPARgamma and Prdm16 expression to facilitate brown adipogenesis. *Mol Cell Biol* (2014) 34(19):3746–53. doi: 10.1128/MCB.00622-14

54. Haberland M, Carrer M, Mokalled MH, Montgomery RL, Olson EN. Redundant control of adipogenesis by histone deacetylases 1 and 2. *J Biol Chem* (2010) 285 (19):14663–70. doi: 10.1074/jbc.M109.081679

55. Ferrari A, Longo R, Fiorino E, Silva R, Mitro N, Cermenati G, et al. HDAC3 is a molecular brake of the metabolic switch supporting white adipose tissue browning. *Nat Commun* (2017) 8(1):93. doi: 10.1038/s41467-017-00182-7

56. Chatterjee TK, Idelman G, Blanco V, Blomkalns AL, Piegore MGJr., Weintraub DS, et al. Histone deacetylase 9 is a negative regulator of adipogenic differentiation. *J Biol Chem* (2011) 286(31):27836–47. doi: 10.1074/jbc.M111.262964

57. Bagchi RA, Ferguson BS, Stratton MS, Hu T, Cavasin MA, Sun L, et al. HDAC11 suppresses the thermogenic program of adipose tissue *via* BRD2. *JCI Insight* (2018) 3 (15):e120159-74. doi: 10.1172/jci.insight.120159

58. Zhou Y, Song T, Peng J, Zhou Z, Wei H, Zhou R, et al. SIRT1 suppresses adipogenesis by activating wnt/beta-catenin signaling *in vivo* and *in vitro*. *Oncotarget* (2016) 7(47):77707–20. doi: 10.18632/oncotarget.12774

59. Mayoral R, Osborn O, McNelis J, Johnson AM, Oh DY, Izquierdo CL, et al. Adipocyte SIRT1 knockout promotes PPARgamma activity, adipogenesis and insulin sensitivity in chronic-HFD and obesity. *Mol Metab* (2015) 4(5):378–91. doi: 10.1016/j.molmet.2015.02.007

60. Wang F, Tong Q. SIRT2 suppresses adipocyte differentiation by deacetylating FOXO1 and enhancing FOXO1's repressive interaction with PPARgamma. *Mol Biol Cell* (2009) 20(3):801–8. doi: 10.1091/mbc.e08-06-0647

61. Shi T, Wang F, Stieren E, Tong Q. SIRT3, a mitochondrial sirtuin deacetylase, regulates mitochondrial function and thermogenesis in brown adipocytes. *J Biol Chem* (2005) 280(14):13560–7. doi: 10.1074/jbc.M414670200

62. Shuai L, Zhang LN, Li BH, Tang CL, Wu LY, Li J, et al. SIRT5 regulates brown adipocyte differentiation and browning of subcutaneous white adipose tissue. *Diabetes* (2019) 68(7):1449–61. doi: 10.2337/db18-1103

63. Byun S, Lee CH, Jeong H, Kim H, Kwon HM, Park S, et al. Loss of adipose TET proteins enhances beta-adrenergic responses and protects against obesity by epigenetic regulation of beta3-AR expression. *Proc Natl Acad Sci USA* (2022) 119(26): e2205626119.

64. Lee J, Saha PK, Yang QH, Lee S, Park JY, Suh Y, et al. Targeted inactivation of MLL3 histone H3-Lys-4 methyltransferase activity in the mouse reveals vital roles for MLL3 in adipogenesis. *Proc Natl Acad Sci USA* (2008) 105(49):19229–34. doi: 10.1073/pnas.0810100105

65. Lee J-E, Wang C, Xu S, Cho Y-W, Wang L, Feng X, et al. H3K4 mono- and di-methyltransferase MLL4 is required for enhancer activation during cell differentiation. *eLife* (2013) 2:e01503. doi: 10.7554/eLife.01503.027

66. Jang Y, Broun A, Wang C, Park YK, Zhuang L, Lee JE, et al. H3.3K4M destabilizes enhancer H3K4 methyltransferases MLL3/MLL4 and impairs adipose tissue development. *Nucleic Acids Res* (2019) 47(2):607–20.

67. Ohno H, Shinoda K, Ohyama K, Sharp LZ, Kajimura S. EHMT1 controls brown adipose cell fate and thermogenesis through the PRDM16 complex. *Nature* (2013) 504 (7478):163–7. doi: 10.1038/nature12652

68. Wang L, Xu S, Lee JE, Baldridge A, Grullon S, Peng W, et al. Histone H3K9 methyltransferase G9a represses PPARgamma expression and adipogenesis. *EMBO J* (2013) 32(1):45–59.

69. Zhao Q, Zhang Z, Rong W, Jin W, Yan L, Jin W, et al. KMT5c modulates adipocyte thermogenesis by regulating Trp53 expression. *Proc Natl Acad Sci USA* (2020) 117(36):22413–22. doi: 10.1073/pnas.1922548117

70. Shuai L, Li BH, Jiang HW, Yang L, Li J, Li JY. DOT1L regulates thermogenic adipocyte differentiation and function *via* modulating H3K79 methylation. *Diabetes* (2021) 70(6):1317–33. doi: 10.2337/db20-1110

71. Duteil D, Tosic M, Willmann D, Georgiadi A, Kanouni T, Schule R. Lsd1 prevents age-programed loss of beige adipocytes. *Proc Natl Acad Sci USA* (2017) 114 (20):5265–70. doi: 10.1073/pnas.1702641114

72. Takase R, Hino S, Nagaoka K, Anan K, Kohrogi K, Araki H, et al. Lysine-specific demethylase-2 is distinctively involved in brown and beige adipogenic differentiation. *FASEB J* (2019) 33(4):5300–11. doi: 10.1096/fj.201801422RR

73. Guo L, Guo YY, Li BY, Peng WQ, Tang QQ. Histone demethylase KDM5A is transactivated by the transcription factor C/EBPβ and promotes preadipocyte differentiation by inhibiting wnt/β-catenin signaling. *J Biol Chem* (2019) 294 (24):9642–54. doi: 10.1074/jbc.RA119.008419

74. Tateishi K, Okada Y, Kallin EM, Zhang Y. Role of Jhdm2a in regulating metabolic gene expression and obesity resistance. *Nature* (2009) 458(7239):757–61. doi: 10.1038/nature07777

75. Inagaki T, Tachibana M, Magoori K, Kudo H, Tanaka T, Okamura M, et al. Obesity and metabolic syndrome in histone demethylase JHDM2a-deficient mice. *Genes Cells* (2009) 14(8):991–1001. doi: 10.1111/j.1365-2443.2009.01326.x

76. Abe Y, Rozqie R, Matsumura Y, Kawamura T, Nakaki R, Tsurutani Y, et al. JMJD1A is a signal-sensing scaffold that regulates acute chromatin dynamics *via* SWI/SNF association for thermogenesis. *Nat Commun* (2015) 6:7052. doi: 10.1038/ncomms8052

77. Pan D, Huang L, Zhu LJ, Zou T, Ou J, Zhou W, et al. Jmjd3-mediated H3K27me3 dynamics orchestrate brown fat development and regulate white fat plasticity. *Dev Cell* (2015) 35(5):568–83. doi: 10.1016/j.devcel.2015.11.002

78. Zha L, Li F, Wu R, Artinian L, Rehder V, Yu L, et al. The histone demethylase UTX promotes brown adipocyte thermogenic program *Via* coordinated regulation of H3K27 demethylation and acetylation. *J Biol Chem* (2015) 290(41):25151–63. doi: 10.1074/jbc.M115.662650

79. Nanduri R. Epigenetic regulators of white adipocyte browning. *Epigenomes* (2021) 5(1):3-21. doi: 10.3390/epigenomes5010003

80. Emmett MJ, Lim HW, Jager J, Richter HJ, Adlanmerini M, Peed LC, et al. Histone deacetylase 3 prepares brown adipose tissue for acute thermogenic challenge. *Nature* (2017) 546(7659):544–8. doi: 10.1038/nature22819

81. Rifai K, Judes G, Idrissou M, Daures M, Bignon YJ, Penault-Llorca F, et al. SIRT1-dependent epigenetic regulation of H3 and H4 histone acetylation in human breast cancer. *Oncotarget* (2018) 9(55):30661–78. doi: 10.18632/oncotarget.25771

82. Vaquero A, Scher MB, Lee DH, Sutton A, Cheng HL, Alt FW, et al. SirT2 is a histone deacetylase with preference for histone H4 lys 16 during mitosis. *Genes Dev* (2006) 20(10):1256–61. doi: 10.1101/gad.1412706

83. Kohli RM, Zhang Y. TET enzymes TDG. And the dynamics of DNA demethylation. *Nature* (2013) 502(7472):472–9. doi: 10.1038/nature12750

84. Karbiener M, Pisani DF, Frontini A, Oberreiter LM, Lang E, Vegiopoulos A, et al. MicroRNA-26 family is required for human adipogenesis and drives characteristics of brown adipocytes. *Stem Cells* (2014) 32(6):1578–90. doi: 10.1002/stem.1603

85. Kim SY, Kim AY, Lee HW, Son YH, Lee GY, Lee JW, et al. miR-27a is a negative regulator of adipocyte differentiation *via* suppressing PPARgamma expression. *Biochem Biophys Res Commun* (2010) 392(3):323–8. doi: 10.1016/j.bbrc.2010.01.012

86. Kang T, Lu W, Xu W, Anderson L, Bacanamwo M, Thompson W, et al. MicroRNA-27 (miR-27) targets prohibitin and impairs adipocyte differentiation and mitochondrial function in human adipose-derived stem cells. *J Biol Chem* (2013) 288 (48):34394–402. doi: 10.1074/jbc.M113.514372

87. Kang T, Lu W, Xu W, Anderson L, Bacanamwo M, Thompson W, et al. Correction: MicroRNA-27 (miR-27) targets prohibitin and impairs adipocyte differentiation and mitochondrial function in human adipose-derived stem cells. *J Biol Chem* (2020) 295(48):16468. doi: 10.1074/jbc.AAC120.016601

88. Sun L, Trajkovski M. MiR-27 orchestrates the transcriptional regulation of brown adipogenesis. *Metabolism* (2014) 63(2):272–82. doi: 10.1016/j.metabol.2013.10.004

89. Lin Q, Gao Z, Alarcon RM, Ye J, Yun Z. A role of miR-27 in the regulation of adipogenesis. *FEBS J* (2009) 276(8):2348–58. doi: 10.1111/j.1742-4658.2009.06967.x

90. Kong X, Yu J, Bi J, Qi H, Di W, Wu L, et al. Glucocorticoids transcriptionally regulate miR-27b expression promoting body fat accumulation *via* suppressing the browning of white adipose tissue. *Diabetes* (2015) 64(2):393–404. doi: 10.2337/db14-0395

91. Hu F, Wang M, Xiao T, Yin B, He L, Meng W, et al. miR-30 promotes thermogenesis and the development of beige fat by targeting RIP140. *Diabetes* (2015) 64(6):2056–68. doi: 10.2337/db14-1117

92. Ng R, Hussain NA, Zhang Q, Chang C, Li H, Fu Y, et al. miRNA-32 drives brown fat thermogenesis and trans-activates subcutaneous white fat browning in mice. *Cell Rep* (2017) 19(6):1229–46. doi: 10.1016/j.celrep.2017.04.035

93. Ge X, Sathiakumar D, Lua BJ, Kukreti H, Lee M, McFarlane C. Myostatin signals through miR-34a to regulate Fndc5 expression and browning of white adipocytes. *Int J Obes (Lond)* (2017) 41(1):137–48. doi: 10.1038/ijo.2016.110

94. Fu T, Seok S, Choi S, Huang Z, Suino-Powell K, Xu HE, et al. MicroRNA 34a inhibits beige and brown fat formation in obesity in part by suppressing adipocyte fibroblast growth factor 21 signaling and SIRT1 function. *Mol Cell Biol* (2014) 34 (22):4130–42. doi: 10.1128/MCB.00596-14

95. Wu Y, Zuo J, Zhang Y, Xie Y, Hu F, Chen L, et al. Identification of miR-106b-93 as a negative regulator of brown adipocyte differentiation. *Biochem Biophys Res Commun* (2013) 438(4):575–80. doi: 10.1016/j.bbrc.2013.08.016

96. Giroud M, Pisani DF, Karbiener M, Barquissau V, Ghandour RA, Tews D, et al. miR-125b affects mitochondrial biogenesis and impairs brite adipocyte formation and function. *Mol Metab* (2016) 5(8):615–25. doi: 10.1016/j.molmet.2016.06.005

97. Trajkovski M, Ahmed K, Esau CC, Stoffel M. MyomiR-133 regulates brown fat differentiation through Prdm16. *Nat Cell Biol* (2012) 14(12):1330–5. doi: 10.1038/ncb2612

98. Liu W, Bi P, Shan T, Yang X, Yin H, Wang YX, et al. miR-133a regulates adipocyte browning *in vivo*. *PloS Genet* (2013) 9(7):e1003626. doi: 10.1371/journal.pgen.1003626

99. Chen Y, Siegel F, Kipschull S, Haas B, Frohlich H, Meister G, et al. miR-155 regulates differentiation of brown and beige adipocytes *via* a bistable circuit. *Nat Commun* (2013) 4:1769. doi: 10.1038/ncomms2742

100. Ignotz RA, Massagué J. Type beta transforming growth factor controls the adipogenic differentiation of 3T3 fibroblasts. *Proc Natl Acad Sci USA* (1985) 82 (24):8530–4. doi: 10.1073/pnas.82.24.8530

101. Kim HJ, Cho H, Alexander R, Patterson HC, Gu M, Lo KA, et al. MicroRNAs are required for the feature maintenance and differentiation of brown adipocytes. *Diabetes* (2014) 63(12):4045–56. doi: 10.2337/db14-0466

102. Sun L, Xie H, Mori MA, Alexander R, Yuan B, Hattangadi SM, et al. Mir193b-365 is essential for brown fat differentiation. *Nat Cell Biol* (2011) 13(8):958–65. doi: 10.1038/ncb2286

103. Feuermann Y, Kang K, Gavrilova O, Haetscher N, Jang SJ, Yoo KH, et al. MiR-193b and miR-365-1 are not required for the development and function of brown fat in the mouse. *RNA Biol* (2013) 10(12):1807–14. doi: 10.4161/rna.27239

104. Mori M, Nakagami H, Rodriguez-Araujo G, Nimura K, Kaneda Y. Essential role for miR-196a in brown adipogenesis of white fat progenitor cells. *PloS Biol* (2012) 10(4):e1001314. doi: 10.1371/journal.pbio.1001314

105. Oliverio M, Schmidt E, Mauer J, Baitzel C, Hansmeier N, Khani S, et al. Dicer1-miR-328-Bace1 signalling controls brown adipose tissue differentiation and function. *Nat Cell Biol* (2016) 18(3):328–36. doi: 10.1038/ncb3316

106. Pan D, Mao C, Quattrochi B, Friedline RH, Zhu LJ, Jung DY, et al. MicroRNA-378 controls classical brown fat expansion to counteract obesity. *Nat Commun* (2014) 5:4725. doi: 10.1038/ncomms5725

107. Zhang H, Guan M, Townsend KL, Huang TL, An D, Yan X, et al. MicroRNA-455 regulates brown adipogenesis *via* a novel HIF1an-AMPK-PGC1alpha signaling network. *EMBO Rep* (2015) 16(10):1378–93. doi: 10.15252/embr.201540837

108. Zhao XY, Li S, Wang GX, Yu Q, Lin JD. A long noncoding RNA transcriptional regulatory circuit drives thermogenic adipocyte differentiation. *Mol Cell* (2014) 55 (3):372–82. doi: 10.1016/j.molcel.2014.06.004

109. Xiong Y, Yue F, Jia Z, Gao Y, Jin W, Hu K, et al. A novel brown adipocyte-enriched long non-coding RNA that is required for brown adipocyte differentiation and sufficient to drive thermogenic gene program in white adipocytes. *Biochim Biophys Acta Mol Cell Biol Lipids* (2018) 1863(4):409–19. doi: 10.1016/j.bbalip.2018.01.008

110. Bai Z, Chai XR, Yoon MJ, Kim HJ, Lo KA, Zhang ZC, et al. Dynamic transcriptome changes during adipose tissue energy expenditure reveal critical roles for long noncoding RNA regulators. *PloS Biol* (2017) 15(8):e2002176. doi: 10.1371/journal.pbio.2002176

111. Liu J, Zhang C, Zhang B, Sheng Y, Xu W, Luo Y, et al. Comprehensive analysis of the characteristics and differences in adult and newborn brown adipose tissue (BAT): newborn BAT is a more Active/Dynamic BAT. *Cells* (2020) 9(1):201. doi: 10.3390/cells9010201

112. Schmidt E, Dhaouadi I, Gaziano I, Oliverio M, Klemm P, Awazawa M, et al. LincRNA H19 protects from dietary obesity by constraining expression of monoallelic genes in brown fat. *Nat Commun* (2018) 9(1):3622. doi: 10.1038/s41467-018-05933-8

113. Zhang B, Xu S, Liu J, Xie Y, Xiaobo S. Long noncoding RNAs: novel important players in adipocyte lipid metabolism and derivative diseases. *Front Physiol* (2021) 12:691824. doi: 10.3389/fphys.2021.691824

114. Zhang P, He Y, Wu S, Li X, Lin X, Gan M, et al. Factors associated with white fat browning: new regulators of lipid metabolism. *Int J Mol Sci* (2022) 23(14):7641-70. doi: 10.3390/ijms23147641

115. Kimura H, Nagoshi T, Oi Y, Yoshii A, Tanaka Y, Takahashi H, et al. Treatment with atrial natriuretic peptide induces adipose tissue browning and exerts thermogenic actions *in vivo*. *Sci Rep* (2021) 11(1):17466. doi: 10.1038/s41598-021-96970-9

116. Schlueter N, de Sterke A, Willmes DM, Spranger J, Jordan J, Birkenfeld AL. Metabolic actions of natriuretic peptides and therapeutic potential in the metabolic syndrome. *Pharmacol Ther* (2014) 144(1):12–27. doi: 10.1016/j.pharmthera.2014.04.007

117. Wu L, Xia M, Duan Y, Zhang L, Jiang H, Hu X, et al. Berberine promotes the recruitment and activation of brown adipose tissue in mice and humans. *Cell Death Dis* (2019) 10(6):468. doi: 10.1038/s41419-019-1706-y

118. Kim S, Choe S, Lee DK. BMP-9 enhances fibroblast growth factor 21 expression and suppresses obesity. *Biochim Biophys Acta* (2016) 1862(7):1237–46. doi: 10.1016/j.bbadis.2016.04.006

119. Baskaran P, Krishnan V, Ren J, Thyagarajan B. Capsaicin induces browning of white adipose tissue and counters obesity by activating TRPV1 channel-dependent mechanisms. *Br J Pharmacol* (2016) 173(15):2369–89. doi: 10.1111/bph.13514

120. Fischer K, Ruiz HH, Jhun K, Finan B, Oberlin DJ, van der Heide V, et al. Alternatively activated macrophages do not synthesize catecholamines or contribute to adipose tissue adaptive thermogenesis. *Nat Med* (2017) 23(5):623–30. doi: 10.1038/nm.4316

121. Han X, Zhang Y, Guo J, You Y, Zhan J, Huang W. Chlorogenic acid stimulates the thermogenesis of brown adipocytes by promoting the uptake of glucose and the function of mitochondria. *J Food Sci* (2019) 84(12):3815–24. doi: 10.1111/1750-3841.14838

122. Vasileva LV, Savova MS, Amirova KM, Balcheva-Sivenova Z, Ferrante C, Orlando G, et al. Caffeic and chlorogenic acids synergistically activate browning program in human adipocytes: implications of AMPK- and PPAR-mediated pathways. *Int J Mol Sci* (2020) 21(24):9740-55. doi: 10.3390/ijms21249740

123. Choi JH, Yun JW. Chrysin induces brown fat-like phenotype and enhances lipid metabolism in 3T3-L1 adipocytes. *Nutrition* (2016) 32(9):1002–10. doi: 10.1016/j.nut.2016.02.007

124. Zuo J, Zhao D, Yu N, Fang X, Mu Q, Ma Y, et al. Cinnamaldehyde ameliorates diet-induced obesity in mice by inducing browning of white adipose tissue. *Cell Physiol Biochem* (2017) 42(4):1514–25. doi: 10.1159/000479268

125. Lone J, Choi JH, Kim SW, Yun JW. Curcumin induces brown fat-like phenotype in 3T3-L1 and primary white adipocytes. *J Nutr Biochem* (2016) 27:193–202. doi: 10.1016/j.jnutbio.2015.09.006

126. Wang S, Wang X, Ye Z, Xu C, Zhang M, Ruan B, et al. Curcumin promotes browning of white adipose tissue in a norepinephrine-dependent way. *Biochem Biophys Res Commun* (2015) 466(2):247–53. doi: 10.1016/j.bbrc.2015.09.018

127. Song Z, Revelo X, Shao W, Tian L, Zeng K, Lei H, et al. Dietary curcumin intervention targets mouse white adipose tissue inflammation and brown adipose tissue UCP1 expression. *Obes (Silver Spring)* (2018) 26(3):547–58. doi: 10.1002/oby.22110

128. Wang L, Wei Y, Ning C, Zhang M, Fan P, Lei D, et al. Ellagic acid promotes browning of white adipose tissues in high-fat diet-induced obesity in rats through suppressing white adipocyte maintaining genes. *Endocr J* (2019) 66(10):923–36. doi: 10.1507/endocrj.EJ18-0467

129. Liu R, Li J, Cheng Y, Huo T, Xue J, Liu Y, et al. Effects of ellagic acid-rich extract of pomegranates peel on regulation of cholesterol metabolism and its molecular mechanism in hamsters. *Food Funct* (2015) 6(3):780–7. doi: 10.1039/C4FO00759J

130. Cheng L, Zhang S, Shang F, Ning Y, Huang Z, He R, et al. Emodin improves glucose and lipid metabolism disorders in obese mice *via* activating brown adipose tissue and inducing browning of white adipose tissue. *Front Endocrinol (Lausanne)* (2021) 12:618037. doi: 10.3389/fendo.2021.618037

131. Varela CE, Rodriguez A, Romero-Valdovinos M, Mendoza-Lorenzo P, Mansour C, Ceballos G, et al. Browning effects of (-)-epicatechin on adipocytes and white adipose tissue. *Eur J Pharmacol* (2017) 811:48–59. doi: 10.1016/j.ejphar.2017.05.051

132. Tanaka N, Takahashi S, Zhang Y, Krausz KW, Smith PB, Patterson AD, et al. Role of fibroblast growth factor 21 in the early stage of NASH induced by methionine- and choline-deficient diet. *Biochim Biophys Acta* (2015) 1852(7):1242–52. doi: 10.1016/j.bbadis.2015.02.012

133. Fisher FM, Maratos-Flier E. Understanding the physiology of FGF21. *Annu Rev Physiol* (2016) 78:223–41. doi: 10.1146/annurev-physiol-021115-105339

134. Yamashita Y, Mitani T, Wang L, Ashida H. Methylxanthine derivative-rich cacao extract suppresses differentiation of adipocytes through downregulation of PPARγ and C/EBPs. *J Nutr Sci Vitaminol (Tokyo)* (2018) 64(2):151–60. doi: 10.3177/jnsv.64.151

135. Maeda H, Hosokawa M, Sashima T, Funayama K, Miyashita K. Fucoxanthin from edible seaweed, undaria pinnatifida, shows antiobesity effect through UCP1 expression in white adipose tissues. *Biochem Biophys Res Commun* (2005) 332(2):392–7. doi: 10.1016/j.bbrc.2005.05.002

136. Rodríguez AM, Palou A. UCP1 mRNA induction by RU486 in brown adipocytes is followed by marked induction of UCP1 protein levels. *Genes Nutr* (2007) 2(1):133–4. doi: 10.1007/s12263-007-0035-4

137. Zhang Y, Li R, Meng Y, Li S, Donelan W, Zhao Y, et al. Irisin stimulates browning of white adipocytes through mitogen-activated protein kinase p38 MAP kinase and ERK MAP kinase signaling. *Diabetes* (2014) 63(2):514–25. doi: 10.2337/db13-1106

138. Commins SP, Watson PM, Frampton IC, Gettys TW. Leptin selectively reduces white adipose tissue in mice *via* a UCP1-dependent mechanism in brown adipose tissue. *Am J Physiol Endocrinol Metab* (2001) 280(2):E372–7. doi: 10.1152/ajpendo.2001.280.2.E372

139. Zhang X, Zhang QX, Wang X, Zhang L, Qu W, Bao B, et al. Dietary luteolin activates browning and thermogenesis in mice through an AMPK/PGC1α pathway-mediated mechanism. *Int J Obes (Lond)* (2016) 40(12):1841–9. doi: 10.1038/ijo.2016.108

140. Liu D, Bordicchia M, Zhang C, Fang H, Wei W, Li JL, et al. Activation of mTORC1 is essential for β-adrenergic stimulation of adipose browning. *J Clin Invest* (2016) 126(5):1704–16. doi: 10.1172/JCI83532

141. Jiang C, Zhai M, Yan D, Li D, Li C, Zhang Y, et al. Dietary menthol-induced TRPM8 activation enhances WAT "browning" and ameliorates diet-induced obesity. *Oncotarget* (2017) 8(43):75114–26. doi: 10.18632/oncotarget.20540

142. Wang GX, Zhao XY, Meng ZX, Kern M, Dietrich A, Chen Z, et al. The brown fat-enriched secreted factor Nrg4 preserves metabolic homeostasis through attenuation of hepatic lipogenesis. *Nat Med* (2014) 20(12):1436–43. doi: 10.1038/nm.3713

143. Pfeifer A. NRG4: an endocrine link between brown adipose tissue and liver. *Cell Metab* (2015) 21(1):13–4. doi: 10.1016/j.cmet.2014.12.008

144. Ali AT, Hochfeld WE, Myburgh R, Pepper MS. Adipocyte and adipogenesis. *Eur J Cell Biol* (2013) 92(6-7):229–36. doi: 10.1016/j.ejcb.2013.06.001

145. Paschos GK, Tang SY, Theken KN, Li X, Verginadis I, Lekkas D, et al. Cold-induced browning of inguinal white adipose tissue is independent of adipose tissue cyclooxygenase-2. *Cell Rep* (2018) 24(4):809–14. doi: 10.1016/j.celrep.2018.06.082

146. Lee SG, Chae J, Kim DS, Lee JB, Kwon GS, Kwon TK, et al. Enhancement of the antiobesity and antioxidant effect of purple sweet potato extracts and enhancement of the effects by fermentation. *Antioxidants (Basel)* (2021) 10(6):888-900. doi: 10.3390/antiox10060888

147. Pei Y, Otieno D, Gu I, Lee SO, Parks JS, Schimmel K, et al. Effect of quercetin on nonshivering thermogenesis of brown adipose tissue in high-fat diet-induced obese mice. *J Nutr Biochem* (2021) 88:108532. doi: 10.1016/j.jnutbio.2020.108532

148. Hui S, Liu Y, Huang L, Zheng L, Zhou M, Lang H, et al. Resveratrol enhances brown adipose tissue activity and white adipose tissue browning in part by regulating bile acid metabolism *via* gut microbiota remodeling. *Int J Obes (Lond)* (2020) 44(8):1678–90. doi: 10.1038/s41366-020-0566-y

149. Zou Y, Ju X, Chen W, Yuan J, Wang Z, Aluko RE, et al. Rice bran attenuated obesity *via* alleviating dyslipidemia, browning of white adipocytes and modulating gut microbiota in high-fat diet-induced obese mice. *Food Funct* (2020) 11(3):2406–17. doi: 10.1039/C9FO01524H

150. Lee DH, Chang SH, Yang DK, Song NJ, Yun UJ, Park KW. Sesamol increases Ucp1 expression in white adipose tissues and stimulates energy expenditure in high-fat diet-fed obese mice. *Nutrients* (2020) 12(5):1459-73. doi: 10.3390/nu12051459

151. Lin C, Chen J, Hu M, Zheng W, Song Z, Qin H. Sesamol promotes browning of white adipocytes to ameliorate obesity by inducing mitochondrial biogenesis and inhibition mitophagy *via* beta3-AR/PKA signaling pathway. *Food Nutr Res* (2021) 65:7577-88.

152. Guo YY, Li BY, Peng WQ, Guo L, Tang QQ. Taurine-mediated browning of white adipose tissue is involved in its anti-obesity effect in mice. *J Biol Chem* (2019) 294(41):15014–24. doi: 10.1074/jbc.RA119.009936

153. Jeon EJ, Kim DY, Lee NH, Choi HE, Cheon HG. Telmisartan induces browning of fully differentiated white adipocytes *via* M2 macrophage polarization. *Sci Rep* (2019) 9(1):1236. doi: 10.1038/s41598-018-38399-1

154. Jeon EJ, Kim DY, Lee NH, Choi HE, Cheon HG. Author correction: telmisartan induces browning of fully differentiated white adipocytes *via* M2 macrophage polarization. *Sci Rep* (2020) 10(1):2165. doi: 10.1038/s41598-020-58948-x

155. Tung Y-C, Chou R-F, Nagabhushanam K, Ho C-T, Pan M-H. 3'-hydroxydaidzein improves obesity through the induced browning of beige adipose and modulation of gut microbiota in mice with obesity induced by a high-fat diet. *J Agric Food Chem* (2020) 68(49):14513–22. doi: 10.1021/acs.jafc.0c06138

156. Sun W, Modica S, Dong H, Wolfrum C. Plasticity and heterogeneity of thermogenic adipose tissue. *Nat Metab* (2021) 3(6):751–61. doi: 10.1038/s42255-021-00417-4

157. Emont MP, Jacobs C, Essene AL, Pant D, Tenen D, Colleluori G, et al. A single-cell atlas of human and mouse white adipose tissue. *Nature* (2022) 603(7903):926–33. doi: 10.1038/s41586-022-04518-2

158. Song A, Dai W, Jang MJ, Medrano L, Li Z, Zhao H, et al. Low- and high-thermogenic brown adipocyte subpopulations coexist in murine adipose tissue. *J Clin Invest* (2020) 130(1):247–57.

159. Rajbhandari P, Arneson D, Hart SK, Ahn IS, Diamante G, Santos LC, et al. Single cell analysis reveals immune cell-adipocyte crosstalk regulating the transcription of thermogenic adipocytes. *Elife* (2019) 8:e49501-26. doi: 10.7554/eLife.49501

160. Oguri Y, Shinoda K, Kim H, Alba DL, Bolus WR, Wang Q, et al. CD81 controls beige fat progenitor cell growth and energy balance *via* FAK signaling. *Cell* (2020) 182(3):563–77 e20. doi: 10.1016/j.cell.2020.06.021

161. Henriques F, Bedard AH, Guilherme A, Kelly M, Chi J, Zhang P, et al. Single-cell RNA profiling reveals adipocyte to macrophage signaling sufficient to enhance thermogenesis. *Cell Rep* (2020) 32(5):107998. doi: 10.1016/j.celrep.2020.107998

162. Sun W, Dong H, Balaz M, Slyper M, Drokhlyansky E, Colleluori G, et al. snRNA-seq reveals a subpopulation of adipocytes that regulates thermogenesis. *Nature* (2020) 587(7832):98–102. doi: 10.1038/s41586-020-2856-x

163. Karlina R, Lutter D, Miok V, Fischer D, Altun I, Schottl T, et al. Identification and characterization of distinct brown adipocyte subtypes in C57BL/6J mice. *Life Sci Alliance* (2021) 4(1):e202000924-42. doi: 10.26508/lsa.202000924

164. Shamsi F, Piper M, Ho LL, Huang TL, Gupta A, Streets A, et al. Vascular smooth muscle-derived Trpv1(+) progenitors are a source of cold-induced thermogenic adipocytes. *Nat Metab* (2021) 3(4):485–95. doi: 10.1038/s42255-021-00373-z

165. Angueira AR, Sakers AP, Holman CD, Cheng L, Arbocco MN, Shamsi F, et al. Defining the lineage of thermogenic perivascular adipose tissue. *Nat Metab* (2021) 3(4):469–84. doi: 10.1038/s42255-021-00380-0

166. Ramirez AK, Dankel SN, Rastegarpanah B, Cai W, Xue R, Crovella M, et al. Single-cell transcriptional networks in differentiating preadipocytes suggest drivers associated with tissue heterogeneity. *Nat Commun* (2020) 11(1):2117. doi: 10.1038/s41467-020-16019-9

167. Vijay J, Gauthier MF, Biswell RL, Louiselle DA, Johnston JJ, Cheung WA, et al. Single-cell analysis of human adipose tissue identifies depot and disease specific cell types. *Nat Metab* (2020) 2(1):97–109.

168. Hildreth AD, Ma F, Wong YY, Sun R, Pellegrini M, O'Sullivan TE. Single-cell sequencing of human white adipose tissue identifies new cell states in health and obesity. *Nat Immunol* (2021) 22(5):639–53. doi: 10.1038/s41590-021-00922-4

169. Cao Y. Angiogenesis and vascular functions in modulation of obesity, adipose metabolism, and insulin sensitivity. *Cell Metab* (2013) 18(4):478–89. doi: 10.1016/j.cmet.2013.08.008

170. Sun K, Kusminski CM, Luby-Phelps K, Spurgin SB, An YA, Wang QA, et al. Brown adipose tissue derived VEGF-a modulates cold tolerance and energy expenditure. *Mol Metab* (2014) 3(4):474–83. doi: 10.1016/j.molmet.2014.03.010

171. Hagberg CE, Falkevall A, Wang X, Larsson E, Huusko J, Nilsson I, et al. Vascular endothelial growth factor b controls endothelial fatty acid uptake. *Nature* (2010) 464(7290):917–21. doi: 10.1038/nature08945

172. Seki T, Hosaka K, Lim S, Fischer C, Honek J, Yang Y, et al. Endothelial PDGF-CC regulates angiogenesis-dependent thermogenesis in beige fat. *Nat Commun* (2016) 7:12152. doi: 10.1038/ncomms12152

173. Bhattacharya I, Ullrich A. Endothelin-1 inhibits adipogenesis: role of phosphorylation of akt and ERK1/2. *FEBS Lett* (2006) 580(24):5765–71. doi: 10.1016/j.febslet.2006.09.032

174. Engeli S, Janke J, Gorzelniak K, Böhnke J, Ghose N, Lindschau C, et al. Regulation of the nitric oxide system in human adipose tissue. *J Lipid Res* (2004) 45 (9):1640–8. doi: 10.1194/jlr.M300322-JLR200

175. Fischer AW, Jaeckstein MY, Gottschling K, Heine M, Sass F, Mangels N, et al. Lysosomal lipoprotein processing in endothelial cells stimulates adipose tissue thermogenic adaptation. *Cell Metab* (2021) 33(3):547–64 e7. doi: 10.1016/j.cmet.2020.12.001

176. Rask-Madsen C, King GL. Mechanisms of disease: endothelial dysfunction in insulin resistance and diabetes. *Nat Clin Pract Endocrinol Metab* (2007) 3(1):46–56. doi: 10.1038/ncpendmet0366

177. Lumeng CN, Saltiel AR. Inflammatory links between obesity and metabolic disease. *J Clin Invest* (2011) 121(6):2111–7. doi: 10.1172/JCI57132

178. Olefsky JM, Glass CK. Macrophages, inflammation, and insulin resistance. *Annu Rev Physiol* (2010) 72:219–46. doi: 10.1146/annurev-physiol-021909-135846

179. Ferrante AWJr. The immune cells in adipose tissue. *Diabetes Obes Metab* (2013) 15 Suppl 3(0 3):34–8. doi: 10.1111/dom.12154

180. Liu R, Nikolajczyk BS. Tissue immune cells fuel obesity-associated inflammation in adipose tissue and beyond. *Front Immunol* (2019) 10:1587. doi: 10.3389/fimmu.2019.01587

181. Sakamoto T, Nitta T, Maruno K, Yeh YS, Kuwata H, Tomita K, et al. Macrophage infiltration into obese adipose tissues suppresses the induction of UCP1 level in mice. *Am J Physiol Endocrinol Metab* (2016) 310(8):E676–E87. doi: 10.1152/ajpendo.00028.2015

182. Chung KJ, Chatzigeorgiou A, Economopoulou M, Garcia-Martin R, Alexaki VI, Mitroulis I, et al. A self-sustained loop of inflammation-driven inhibition of beige adipogenesis in obesity. *Nat Immunol* (2017) 18(6):654–64. doi: 10.1038/ni.3728

183. Villarroya F, Cereijo R, Villarroya J, Gavalda-Navarro A, Giralt M. Toward an understanding of how immune cells control brown and beige adipobiology. *Cell Metab* (2018) 27(5):954–61. doi: 10.1016/j.cmet.2018.04.006

184. Ricardo-Gonzalez RR, Red Eagle A, Odegaard JI, Jouihan H, Morel CR, Heredia JE, et al. IL-4/STAT6 immune axis regulates peripheral nutrient metabolism and insulin sensitivity. *Proc Natl Acad Sci USA* (2010) 107(52):22617–22. doi: 10.1073/pnas.1009152108

185. Nguyen KD, Qiu Y, Cui X, Goh YP, Mwangi J, David T, et al. Alternatively activated macrophages produce catecholamines to sustain adaptive thermogenesis. *Nature* (2011) 480(7375):104–8. doi: 10.1038/nature10653

186. Qiu Y, Nguyen KD, Odegaard JI, Cui X, Tian X, Locksley RM, et al. Eosinophils and type 2 cytokine signaling in macrophages orchestrate development of functional beige fat. *Cell* (2014) 157(6):1292–308. doi: 10.1016/j.cell.2014.03.066

187. Pirzgalska RM, Seixas E, Seidman JS, Link VM, Sánchez NM, Mahú I, et al. Sympathetic neuron-associated macrophages contribute to obesity by importing and metabolizing norepinephrine. *Nat Med* (2017) 23(11):1309–18. doi: 10.1038/nm.4422

188. Camell CD, Sander J, Spadaro O, Lee A, Nguyen KY, Wing A, et al. Inflammasome-driven catecholamine catabolism in macrophages blunts lipolysis during ageing. *Nature* (2017) 550(7674):119–23. doi: 10.1038/nature24022

189. Cereijo R, Gavalda-Navarro A, Cairo M, Quesada-Lopez T, Villarroya J, Moron-Ros S, et al. CXCL14, a brown adipokine that mediates brown-Fat-to-Macrophage communication in thermogenic adaptation. *Cell Metab* (2018) 28 (5):750–63 e6. doi: 10.1016/j.cmet.2018.07.015

190. Hui X, Gu P, Zhang J, Nie T, Pan Y, Wu D, et al. Adiponectin enhances cold-induced browning of subcutaneous adipose tissue *via* promoting M2 macrophage proliferation. *Cell Metab* (2015) 22(2):279–90. doi: 10.1016/j.cmet.2015.06.004

191. Qian SW, Wu MY, Wang YN, Zhao YX, Zou Y, Pan JB, et al. BMP4 facilitates beige fat biogenesis *via* regulating adipose tissue macrophages. *J Mol Cell Biol* (2019) 11 (1):14–25. doi: 10.1093/jmcb/mjy011

192. Molofsky AB, Nussbaum JC, Liang HE, Van Dyken SJ, Cheng LE, Mohapatra A, et al. Innate lymphoid type 2 cells sustain visceral adipose tissue eosinophils and alternatively activated macrophages. *J Exp Med* (2013) 210(3):535–49. doi: 10.1084/jem.20121964

193. Lee MW, Odegaard JI, Mukundan L, Qiu Y, Molofsky AB, Nussbaum JC, et al. Activated type 2 innate lymphoid cells regulate beige fat biogenesis. *Cell* (2015) 160(1-2):74–87. doi: 10.1016/j.cell.2014.12.011

194. Brestoff JR, Kim BS, Saenz SA, Stine RR, Monticelli LA, Sonnenberg GF, et al. Group 2 innate lymphoid cells promote beiging of white adipose tissue and limit obesity. *Nature* (2015) 519(7542):242–6. doi: 10.1038/nature14115

195. Wu D, Molofsky AB, Liang HE, Ricardo-Gonzalez RR, Jouihan HA, Bando JK, et al. Eosinophils sustain adipose alternatively activated macrophages associated with glucose homeostasis. *Science* (2011) 332(6026):243–7. doi: 10.1126/science.1201475

196. Rao RR, Long JZ, White JP, Svensson KJ, Lou J, Lokurkar I, et al. Meteorin-like is a hormone that regulates immune-adipose interactions to increase beige fat thermogenesis. *Cell* (2014) 157(6):1279–91. doi: 10.1016/j.cell.2014.03.065

197. Huang Z, Zhong L, Lee JTH, Zhang J, Wu D, Geng L, et al. The FGF21-CCL11 axis mediates beiging of white adipose tissues by coupling sympathetic nervous system to type 2 immunity. *Cell Metab* (2017) 26(3):493–508.e4. doi: 10.1016/j.cmet.2017.08.003

198. Bartness TJ, Vaughan CH, Song CK. Sympathetic and sensory innervation of brown adipose tissue. *Int J Obes (Lond)* (2010) 34 Suppl 1(0 1):S36–42. doi: 10.1038/ijo.2010.182

199. Muzik O, Mangner TJ, Leonard WR, Kumar A, Granneman JG. Sympathetic innervation of cold-activated brown and white fat in lean young adults. *J Nucl Med* (2017) 58(5):799–806. doi: 10.2967/jnumed.116.180992

200. Jiang H, Ding X, Cao Y, Wang H, Zeng W. Dense intra-adipose sympathetic arborizations are essential for cold-induced beiging of mouse white adipose tissue. *Cell Metab* (2017) 26(4):686–92 e3. doi: 10.1016/j.cmet.2017.08.016

201. Zeng X, Ye M, Resch JM, Jedrychowski MP, Hu B, Lowell BB, et al. Innervation of thermogenic adipose tissue *via* a calsyntenin 3β-S100b axis. *Nature* (2019) 569 (7755):229–35. doi: 10.1038/s41586-019-1156-9

202. Jiang J, Zhou D, Zhang A, Yu W, Du L, Yuan H, et al. Thermogenic adipocyte-derived zinc promotes sympathetic innervation in male mice. *Nat Metab* (2023) 5 (3):481-94. doi: 10.1038/s42255-023-00751-9

203. Priest C, Tontonoz P. Inter-organ cross-talk in metabolic syndrome. *Nat Metab* (2019) 1(12):1177–88. doi: 10.1038/s42255-019-0145-5

204. Shamsi F, Wang CH, Tseng YH. The evolving view of thermogenic adipocytes - ontogeny, niche and function. *Nat Rev Endocrinol* (2021) 17(12):726–44. doi: 10.1038/s41574-021-00562-6

205. Yin X, Chen Y, Ruze R, Xu R, Song J, Wang C, et al. The evolving view of thermogenic fat and its implications in cancer and metabolic diseases. *Signal Transduct Target Ther* (2022) 7(1):324. doi: 10.1038/s41392-022-01178-6

206. Bartness TJ, Liu Y, Shrestha YB, Ryu V. Neural innervation of white adipose tissue and the control of lipolysis. *Front Neuroendocrinol* (2014) 35(4):473–93. doi: 10.1016/j.yfrne.2014.04.001

207. Morrison SF, Nakamura K. Central mechanisms for thermoregulation. *Annu Rev Physiol* (2019) 81:285–308. doi: 10.1146/annurev-physiol-020518-114546

208. Picó C, Palou M, Pomar CA, Rodríguez AM, Palou A. Leptin as a key regulator of the adipose organ. *Rev Endocr Metab Disord* (2022) 23(1):13–30. doi: 10.1007/s11154-021-09687-5

209. Friedman JM, Halaas JL. Leptin and the regulation of body weight in mammals. *Nature* (1998) 395(6704):763–70. doi: 10.1038/27376

210. Begriche K, Sutton GM, Butler AA. Homeostastic and non-homeostatic functions of melanocortin-3 receptors in the control of energy balance and metabolism. *Physiol Behav* (2011) 104(4):546–54. doi: 10.1016/j.physbeh.2011.04.007

211. Kishi T, Aschkenasi CJ, Lee CE, Mountjoy KG, Saper CB, Elmquist JK. Expression of melanocortin 4 receptor mRNA in the central nervous system of the rat. *J Comp Neurol* (2003) 457(3):213–35. doi: 10.1002/cne.10454

212. Voss-Andreae A, Murphy JG, Ellacott KL, Stuart RC, Nillni EA, Cone RD, et al. Role of the central melanocortin circuitry in adaptive thermogenesis of brown adipose tissue. *Endocrinology* (2007) 148(4):1550–60. doi: 10.1210/en.2006-1389

213. Williams DL, Bowers RR, Bartness TJ, Kaplan JM, Grill HJ. Brainstem melanocortin 3/4 receptor stimulation increases uncoupling protein gene expression in brown fat. *Endocrinology* (2003) 144(11):4692–7. doi: 10.1210/en.2003-0440

214. Dodd GT, Decherf S, Loh K, Simonds SE, Wiede F, Balland E, et al. Leptin and insulin act on POMC neurons to promote the browning of white fat. *Cell* (2015) 160(1-2):88–104. doi: 10.1016/j.cell.2014.12.022

215. Whittle AJ, Carobbio S, Martins L, Slawik M, Hondares E, Vazquez MJ, et al. BMP8B increases brown adipose tissue thermogenesis through both central and peripheral actions. *Cell* (2012) 149(4):871–85. doi: 10.1016/j.cell.2012.02.066

216. Ruan HB, Dietrich MO, Liu ZW, Zimmer MR, Li MD, Singh JP, et al. O-GlcNAc transferase enables AgRP neurons to suppress browning of white fat. *Cell* (2014) 159(2):306–17. doi: 10.1016/j.cell.2014.09.010

217. Soumano K, Desbiens S, Rabelo R, Bakopanos E, Camirand A, Silva JE. Glucocorticoids inhibit the transcriptional response of the uncoupling protein-1 gene to adrenergic stimulation in a brown adipose cell line. *Mol Cell Endocrinol* (2000) 165 (1-2):7–15. doi: 10.1016/S0303-7207(00)00276-8

218. Ramage LE, Akyol M, Fletcher AM, Forsythe J, Nixon M, Carter RN, et al. Glucocorticoids acutely increase brown adipose tissue activity in humans, revealing

species-specific differences in UCP-1 regulation. *Cell Metab* (2016) 24(1):130–41. doi: 10.1016/j.cmet.2016.06.011

219. Staiger H, Keuper M, Berti L, Hrabe de Angelis M, Haring HU. Fibroblast growth factor 21-metabolic role in mice and men. *Endocr Rev* (2017) 38(5):468–88. doi: 10.1210/er.2017-00016

220. Cheong LY, Xu A. Intercellular and inter-organ crosstalk in browning of white adipose tissue: molecular mechanism and therapeutic complications. *J Mol Cell Biol* (2021) 13(7):466–79. doi: 10.1093/jmcb/mjab038

221. Bookout AL, de Groot MH, Owen BM, Lee S, Gautron L, Lawrence HL, et al. FGF21 regulates metabolism and circadian behavior by acting on the nervous system. *Nat Med* (2013) 19(9):1147–52. doi: 10.1038/nm.3249

222. Owen BM, Ding X, Morgan DA, Coate KC, Bookout AL, Rahmouni K, et al. FGF21 acts centrally to induce sympathetic nerve activity, energy expenditure, and weight loss. *Cell Metab* (2014) 20(4):670–7. doi: 10.1016/j.cmet.2014.07.012

223. Kharitonenkov A, Wroblewski VJ, Koester A, Chen YF, Clutinger CK, Tigno XT, et al. The metabolic state of diabetic monkeys is regulated by fibroblast growth factor-21. *Endocrinology* (2007) 148(2):774–81. doi: 10.1210/en.2006-1168

224. Chabicovsky M, Herkner K, Rossmanith W. Overexpression of activin beta(C) or activin beta(E) in the mouse liver inhibits regenerative deoxyribonucleic acid synthesis of hepatic cells. *Endocrinology* (2003) 144(8):3497–504. doi: 10.1210/en.2003-0388

225. Hashimoto O, Funaba M, Sekiyama K, Doi S, Shindo D, Satoh R, et al. Activin e controls energy homeostasis in both brown and white adipose tissues as a hepatokine. *Cell Rep* (2018) 25(5):1193–203. doi: 10.1016/j.celrep.2018.10.008

226. Braga M, Reddy ST, Vergnes L, Pervin S, Grijalva V, Stout D, et al. Follistatin promotes adipocyte differentiation, browning, and energy metabolism. *J Lipid Res* (2014) 55(3):375–84. doi: 10.1194/jlr.M039719

227. Singh R, Braga M, Reddy ST, Lee SJ, Parveen M, Grijalva V, et al. Follistatin targets distinct pathways to promote brown adipocyte characteristics in brown and white adipose tissues. *Endocrinology* (2017) 158(5):1217–30. doi: 10.1210/en.2016-1607

228. Hansen JS, Rutti S, Arous C, Clemmesen JO, Secher NH, Drescher A, et al. Circulating follistatin is liver-derived and regulated by the glucagon-to-Insulin ratio. *J Clin Endocrinol Metab* (2016) 101(2):550–60. doi: 10.1210/jc.2015-3668

229. Qing H, Desrouleaux R, Israni-Winger K, Mineur YS, Fogelman N, Zhang C, et al. Origin and function of stress-induced IL-6 in murine models. *Cell* (2020) 182(2):372–87 e14.

230. Shen H, Jiang L, Lin JD, Omary MB, Rui L. Brown fat activation mitigates alcohol-induced liver steatosis and injury in mice. *J Clin Invest* (2019) 129(6):2305–17. doi: 10.1172/JCI124376

231. Cao H, Gerhold K, Mayers JR, Wiest MM, Watkins SM, Hotamisligil GS. Identification of a lipokine, a lipid hormone linking adipose tissue to systemic metabolism. *Cell* (2008) 134(6):933–44. doi: 10.1016/j.cell.2008.07.048

232. Simcox J, Geoghegan G, Maschek JA, Bensard CL, Pasquali M, Miao R, et al. Global analysis of plasma lipids identifies liver-derived acylcarnitines as a fuel source for brown fat thermogenesis. *Cell Metab* (2017) 26(3):509–22 e6. doi: 10.1016/j.cmet.2017.08.006

233. Velazquez-Villegas LA, Perino A, Lemos V, Zietak M, Nomura M, Pols TWH, et al. TGR5 signalling promotes mitochondrial fission and beige remodelling of white adipose tissue. *Nat Commun* (2018) 9(1):245. doi: 10.1038/s41467-017-02068-0

234. Broeders EP, Nascimento EB, Havekes B, Brans B, Roumans KH, Tailleux A, et al. The bile acid chenodeoxycholic acid increases human brown adipose tissue activity. *Cell Metab* (2015) 22(3):418–26. doi: 10.1016/j.cmet.2015.07.002

235. Watanabe M, Houten SM, Mataki C, Christoffolete MA, Kim BW, Sato H, et al. Bile acids induce energy expenditure by promoting intracellular thyroid hormone activation. *Nature* (2006) 439(7075):484–9. doi: 10.1038/nature04330

236. Mills EL, Pierce KA, Jedrychowski MP, Garrity R, Winther S, Vidoni S, et al. Accumulation of succinate controls activation of adipose tissue thermogenesis. *Nature* (2018) 560(7716):102–6. doi: 10.1038/s41586-018-0353-2

237. Mills EL, Harmon C, Jedrychowski MP, Xiao H, Garrity R, Tran NV, et al. UCP1 governs liver extracellular succinate and inflammatory pathogenesis. *Nat Metab* (2021) 3(5):604–17. doi: 10.1038/s42255-021-00389-5

238. Iizuka K, Machida T, Hirafuji M. Skeletal muscle is an endocrine organ. *J Pharmacol Sci* (2014) 125(2):125–31. doi: 10.1254/jphs.14R02CP

239. Florin A, Lambert C, Sanchez C, Zappia J, Durieux N, Tieppo AM, et al. The secretome of skeletal muscle cells: a systematic review. *Osteoarthr Cartil Open* (2020) 2 (1):100019. doi: 10.1016/j.ocarto.2019.100019

240. Severinsen MCK, Pedersen BK. Muscle-organ crosstalk: the emerging roles of myokines. *Endocr Rev* (2020) 41(4):594–609. doi: 10.1210/endrev/bnaa016

241. Pedersen BK, Febbraio MA. Muscle as an endocrine organ: focus on muscle-derived interleukin-6. *Physiol Rev* (2008) 88(4):1379–406. doi: 10.1152/physrev.90100.2007

242. Knudsen JG, Murholm M, Carey AL, Bienso RS, Basse AL, Allen TL, et al. Role of IL-6 in exercise training- and cold-induced UCP1 expression in subcutaneous white adipose tissue. *PloS One* (2014) 9(1):e84910. doi: 10.1371/journal.pone.0084910

243. van Hall G, Steensberg A, Sacchetti M, Fischer C, Keller C, Schjerling P, et al. Interleukin-6 stimulates lipolysis and fat oxidation in humans. *J Clin Endocrinol Metab* (2003) 88(7):3005–10. doi: 10.1210/jc.2002-021687

244. Petersen EW, Carey AL, Sacchetti M, Steinberg GR, Macaulay SL, Febbraio MA, et al. Acute IL-6 treatment increases fatty acid turnover in elderly humans *in vivo* and in tissue culture *in vitro*. *Am J Physiol Endocrinol Metab* (2005) 288(1):E155–62. doi: 10.1152/ajpendo.00257.2004

245. Kristof E, Klusoczki A, Veress R, Shaw A, Combi ZS, Varga K, et al. Interleukin-6 released from differentiating human beige adipocytes improves browning. *Exp Cell Res* (2019) 377(1-2):47–55. doi: 10.1016/j.yexcr.2019.02.015

246. Bostrom P, Wu J, Jedrychowski MP, Korde A, Ye L, Lo JC, et al. A PGC1-alpha-dependent myokine that drives brown-fat-like development of white fat and thermogenesis. *Nature* (2012) 481(7382):463–8. doi: 10.1038/nature10777

247. Lee P, Linderman JD, Smith S, Brychta RJ, Wang J, Idelson C, et al. Irisin and FGF21 are cold-induced endocrine activators of brown fat function in humans. *Cell Metab* (2014) 19(2):302–9. doi: 10.1016/j.cmet.2013.12.017

248. Roberts LD, Bostrom P, O'Sullivan JF, Schinzel RT, Lewis GD, Dejam A, et al. Beta-aminoisobutyric acid induces browning of white fat and hepatic beta-oxidation and is inversely correlated with cardiometabolic risk factors. *Cell Metab* (2014) 19 (1):96–108. doi: 10.1016/j.cmet.2013.12.003

249. Lynes MD, Leiria LO, Lundh M, Bartelt A, Shamsi F, Huang TL, et al. The cold-induced lipokine 12,13-diHOME promotes fatty acid transport into brown adipose tissue. *Nat Med* (2017) 23(5):631–7. doi: 10.1038/nm.4297

250. Stanford KI, Lynes MD, Takahashi H, Baer LA, Arts PJ, May FJ, et al. 12,13-diHOME: an exercise-induced lipokine that increases skeletal muscle fatty acid uptake. *Cell Metab* (2018) 27(5):1111–20 e3. doi: 10.1016/j.cmet.2018.03.020

251. Leiria LO, Wang CH, Lynes MD, Yang K, Shamsi F, Sato M, et al. 12-lipoxygenase regulates cold adaptation and glucose metabolism by producing the omega-3 lipid 12-HEPE from brown fat. *Cell Metab* (2019) 30(4):768–83 e7. doi: 10.1016/j.cmet.2019.07.001

252. Clarke G, Stilling RM, Kennedy PJ, Stanton C, Cryan JF, Dinan TG. Minireview: gut microbiota: the neglected endocrine organ. *Mol Endocrinol* (2014) 28(8):1221–38. doi: 10.1210/me.2014-1108

253. Mestdagh R, Dumas ME, Rezzi S, Kochhar S, Holmes E, Claus SP, et al. Gut microbiota modulate the metabolism of brown adipose tissue in mice. *J Proteome Res* (2012) 11(2):620–30. doi: 10.1021/pr200938v

254. Suarez-Zamorano N, Fabbiano S, Chevalier C, Stojanovic O, Colin DJ, Stevanovic A, et al. Microbiota depletion promotes browning of white adipose tissue and reduces obesity. *Nat Med* (2015) 21(12):1497–501. doi: 10.1038/nm.3994

255. Zietak M, Kovatcheva-Datchary P, Markiewicz LH, Stahlman M, Kozak LP, Backhed F. Altered microbiota contributes to reduced diet-induced obesity upon cold exposure. *Cell Metab* (2016) 23(6):1216–23. doi: 10.1016/j.cmet.2016.05.001

256. Chevalier C, Stojanovic O, Colin DJ, Suarez-Zamorano N, Tarallo V, Veyrat-Durebex C, et al. Gut microbiota orchestrates energy homeostasis during cold. *Cell* (2015) 163(6):1360–74. doi: 10.1016/j.cell.2015.11.004

257. Li G, Xie C, Lu S, Nichols RG, Tian Y, Li L, et al. Intermittent fasting promotes white adipose browning and decreases obesity by shaping the gut microbiota. *Cell Metab* (2017) 26(4):672–85.e4. doi: 10.1016/j.cmet.2017.08.019

258. Li B, Li L, Li M, Lam SM, Wang G, Wu Y, et al. Microbiota depletion impairs thermogenesis of brown adipose tissue and browning of white adipose tissue. *Cell Rep* (2019) 26(10):2720–37 e5. doi: 10.1016/j.celrep.2019.02.015

259. Sumara G, Sumara O, Kim JK, Karsenty G. Gut-derived serotonin is a multifunctional determinant to fasting adaptation. *Cell Metab* (2012) 16(5):588–600. doi: 10.1016/j.cmet.2012.09.014

260. Li Y, Schnabl K, Gabler SM, Willershauser M, Reber J, Karlas A, et al. Secretin-activated brown fat mediates prandial thermogenesis to induce satiation. *Cell* (2018) 175(6):1561–74 e12. doi: 10.1016/j.cell.2018.10.016

261. Laurila S, Sun L, Lahesmaa M, Schnabl K, Laitinen K, Klen R, et al. Secretin activates brown fat and induces satiation. *Nat Metab* (2021) 3(6):798–809. doi: 10.1038/s42255-021-00409-4

262. Krieger JP, Santos da Conceição EP, Sanchez-Watts G, Arnold M, Pettersen KG, Mohammed M, et al. Glucagon-like peptide-1 regulates brown adipose tissue thermogenesis via the gut-brain axis in rats. *Am J Physiol Regul Integr Comp Physiol* (2018) 315(4):R708–r20. doi: 10.1152/ajpregu.00068.2018

263. Gutzwiller JP, Drewe J, Göke B, Schmidt H, Rohrer B, Lareida J, et al. Glucagon-like peptide-1 promotes satiety and reduces food intake in patients with diabetes mellitus type 2. *Am J Physiol* (1999) 276(5):R1541–4. doi: 10.1152/ajpregu.1999.276.5.R1541

264. Beiroa D, Imbernon M, Gallego R, Senra A, Herranz D, Villarroya F, et al. GLP-1 agonism stimulates brown adipose tissue thermogenesis and browning through hypothalamic AMPK. *Diabetes* (2014) 63(10):3346–58. doi: 10.2337/db14-0302

265. Drucker DJ. The cardiovascular biology of glucagon-like peptide-1. *Cell Metab* (2016) 24(1):15–30. doi: 10.1016/j.cmet.2016.06.009

266. Kojima M, Hosoda H, Date Y, Nakazato M, Matsuo H, Kangawa K. Ghrelin is a growth-hormone-releasing acylated peptide from stomach. *Nature* (1999) 402 (6762):656–60. doi: 10.1038/45230

267. Tschöp M, Smiley DL, Heiman ML. Ghrelin induces adiposity in rodents. *Nature* (2000) 407(6806):908–13. doi: 10.1038/35038090

268. Yasuda T, Masaki T, Kakuma T, Yoshimatsu H. Centrally administered ghrelin suppresses sympathetic nerve activity in brown adipose tissue of rats. *Neurosci Lett* (2003) 349(2):75–8. doi: 10.1016/S0304-3940(03)00789-4

269. Theander-Carrillo C, Wiedmer P, Cettour-Rose P, Nogueiras R, Perez-Tilve D, Pfluger P, et al. Ghrelin action in the brain controls adipocyte metabolism. *J Clin Invest* (2006) 116(7):1983–93. doi: 10.1172/JCI25811

270. Li Y, Wang D, Ping X, Zhang Y, Zhang T, Wang L, et al. Local hyperthermia therapy induces browning of white fat and treats obesity. *Cell* (2022) 185(6):949–66 e19. doi: 10.1016/j.cell.2022.02.004

# Frontiers in Endocrinology

**Explores the endocrine system to find new therapies for key health issues**

The second most-cited endocrinology and metabolism journal, which advances our understanding of the endocrine system. It uncovers new therapies for prevalent health issues such as obesity, diabetes, reproduction, and aging.

---

## Discover the latest Research Topics

See more →

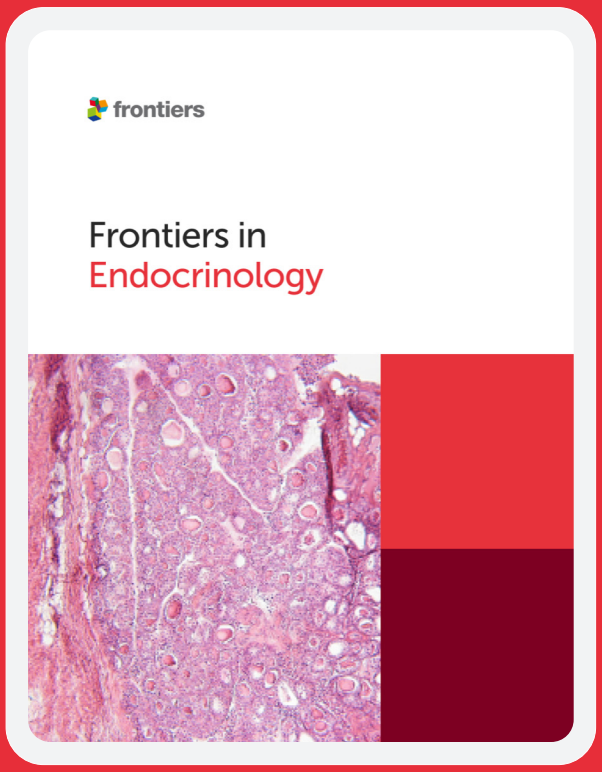


**Frontiers**

Avenue du Tribunal-Fédéral 34
1005 Lausanne, Switzerland
frontiersin.org

**Contact us**

+41 (0)21 510 17 00
frontiersin.org/about/contact